Secondary Metabolites from Endophytic Fungi: Isolation, Structure Elucidation, Bioactivity and Expanding the Chemical Diversity

Inaugural dissertation

for the attainment of the title of doctor
in the Faculty of Mathematics and Natural Sciences
at the Heinrich Heine University Düsseldorf

presented by

Ni Putu Ariantari
from Tabanan, Indonesia

Düsseldorf, 12. 2019

from the Institute for Pharmaceutical Biology and Biotechnology
at the Heinrich Heine University Düsseldorf

Published by permission of the
Faculty of Mathematics and Natural Sciences at
Heinrich Heine University Düsseldorf

Supervisor: Prof. Dr. Dres. h.c. Peter Proksch
Co-supervisor: Prof. Dr. Rainer Kalscheuer

Date of the oral examination: 12/03/2020

Declaration of academic honesty/Erklärung

Hiermit erkläre ich ehrenwörtlich, dass ich die vorliegende Dissertation mit dem Titel "Sekundärmetaboliten aus endophytischen Pilzen: Isolierung, Strukturaufklärung, Bioaktivität und Erweiterung des Metabolitenmusters" selbst angefertigt habe. Außer den angegebenen Quellen und Hilfsmitteln wurden keine weiteren verwendet. Diese Dissertation wurde weder in gleicher noch in abgewandelter Form in einem anderen Prüfungsverfahren vorgelegt. Weiterhin erkläre ich, dass ich früher weder akademische Grade erworben habe, noch dies versucht habe.

Düsseldorf, den 12. 12. 2019

Ni Putu Ariantari

Contents

Abstract

Fungi are recognized as sources of many important drugs and lead structures. Particularly, endophytic fungi that colonize plant tissues without causing any harmful effects during their life cycle, are known as producers of numerous structurally novel natural products, possessing a wide range of bioactivities. Each plant is believed to harbor their own endophytes, which emphasizes the broad distribution of these microorganisms in nature. Among the culturable endophytes, many gene clusters responsible for the biosynthetic pathways of their metabolites are frequently silent under standard laboratory conditions, indicating their biosynthetic capacity to be far larger than previously reported. As only a small portion of these microorganisms has been investigated so far and their biosynthetic potential remains largely hidden, endophytes are considered as a promising source for diversifying scaffolds for the discovery of new drug leads.

In this dissertation, the study on the three endophytes *Penicillium* sp., *Bulgaria inquinans* and *Didymella* sp. led to the isolation of several structurally diverse metabolites, including indole diterpenoids, azaphilones, butyrolactones and decahydrofluorene-class of natural products. Some of these metabolites showed potent cytotoxicity and antibacterial activities. Moreover, upon utilization of the "One Strain, MAny Compounds" (OSMAC) approach on the endophyte *B. inquinans* several new metabolites were obtained. This result highlights the usefulness of the OSMAC strategy for triggering particular biosynthetic pathways leading to structural diversity produced by this strain. The structures of the isolated natural products were elucidated by means of spectroscopic techniques (NMR and MS). The absolute configuration of the new compounds was established through the application of x-ray crystallography analysis, Mosher's method and the TDDFT-ECD approach, as well as by comparison of their specific optical rotations to those reported in the literature. Accordingly, this dissertation reflects the result of the following three published or submitted manuscripts, from which the following abstracts are taken as direct quotations.

Indole diterpenoids from an endophytic Penicillium sp.

A chemical investigation of the endophyte *Penicillium* sp. (strain ZO-R1-1), isolated from roots of the medicinal plant *Zingiber officinale*, yielded nine new indole diterpenoids (**1**−**9**), together with 13 known congeners (**10**−**22**). The structures of the new compounds were elucidated by 1D and 2D NMR analysis in combination with HRESIMS data. The absolute configuration of the new natural products **1**, **3** and **7** was determined using the TDDFT-ECD approach and confirmed for **1** by single-crystal x-ray determination through anomalous dispersion. The isolated compounds were tested for cytotoxicity against L5178Y, A2780, J82, and HEK-293 cell lines. Compound **1** was the most active metabolite towards L5178Y cells, with an IC_{50} value of 3.6 μM, and an IC_{50} against A2780 cells of 8.7 μM. Interestingly, **1** features a new type of indole diterpenoid scaffold with a rare 6/5/6/6/6/6/5 heterocyclic system bearing an aromatic ring C, which is suggested to be important for the cytotoxic activity of this natural product against L5278Y and A2780 cells.

Expanding the chemical diversity of an endophytic fungus Bulgaria inquinans, an ascomycete associated with mistletoe, through an OSMAC approach.

An endophytic fungus *Bulgaria inquinans* (isolate MSp3-1), isolated from mistletoe (*Viscum album*), was subjected to fermentation on solid Czapek medium. Chromatographic workup of the crude EtOAc extract yielded five new natural products (**1**–**5**). Subsequent application of the "One Strain, MAny Compounds" (OSMAC) strategy on this strain by the addition of a mixture of salts ($MgSO_4$, $NaNO_3$ and NaCl) to solid Czapek medium induced the accumulation of nine additional new secondary metabolites (**6**–**13**, **16**), with most of them (**8**, **10**–**12**) not detectable in cultures lacking the salt mixture. The structures of the new compounds were established on the basis of the 1D/2D NMR and HRESIMS data. The TDDFT-ECD method was applied to determine the absolute configurations of the new compounds **1**, **4** and **6** as well as of the previously reported bulgarialactone B (**14**), for which the absolute configuration was unknown so far. The modified Mosher's method was performed to assign

the absolute configurations of **12** and **13**. TDDFT-ECD analysis also allowed determining the absolute configuration of (+)-epicocconone, which had an enantiomeric absolute configuration in the tricyclic moiety compared to that of bulgarialactone B (**14**). All the isolated metabolites were evaluated for their cytotoxic activity. Compound **2** was found to possess strong cytotoxic activity against the murine lymphoma cell line L5178Y with an IC_{50} value of 1.8 μM, while the remaining metabolites were shown to be inactive.

Didymellanosine, a new decahydrofluorene analogue, and ascolactone C from Didymella sp. IEA-3B.1 an endophyte of Terminalia catappa

Didymellanosine (**1**), the first analogue of the decahydrofluorene-class of natural products bearing a 13-membered macrocyclic alkaloid conjugated with adenosine, and a new benzolactone derivative, ascolactone C (**4**) along with eight known compounds (**2**, **3**, **5**−**10**), were isolated from a solid rice fermentation of the endophytic fungus *Didymella* sp. IEA-3B.1 derived from the host plant *Terminalia catappa*. In addition, ascochitamine (**11**) was obtained when $(NH_4)_2SO_4$ was added to rice medium and is reported here for the first time as a natural product. The structures of the new compounds were established through extensive analysis of one- and two-dimensional NMR data as well as HRESIMS data. Didymellanosine (**1**) displayed strong to moderate activity against the murine lymphoma cell line L5178Y, Burkitt's lymphoma B cells (Ramos) and adult lymphoblastic leukemia T cells (Jurkat J16), with IC_{50} values of 2.2, 7.6 and 11.0 μM, respectively. Moreover, when subjected to a NFκB inhibition assay, compounds **1** and phomapyrrolidone A (**2**) efficiently blocked NFκB activation. In an antimicrobial assay, ascomylactam C (**3**) was the most active compound when tested against a panel of Gram-positive bacteria including drug-resistant strains with MICs of 3.1−6.3 μM, while **1** revealed weaker activity. Interestingly, both compounds were also found active against Gram-negative *Acinetobacter baumannii* with MICs of 3.1 μM, in the presence of a sublethal concentration (0.1 μM) of colistin.

Zusammenfassung

Pilze leisten als Quelle von Naturstoffen einen erheblichen Beitrag zur Entdeckung von Arzneistoffen und Leitstrukturen. Insbesondere die als Endophyten bekannten Pilze, welche Pflanzengewebe besiedeln ohne innerhalb ihres Lebenzyklus am Wirt einen ersichtlichen Schaden zu verursachen, sind dafür bekannt eine Vielzahl strukturell neuartiger Naturstoffe zu produzieren, welche ein breites Spektrum biologischer Aktivitäten zeigen. Es wird angenommen, dass jede Pflanze Endophyten beherbergt, was die weite Verbreitung von Mikroorganismen in der Natur verdeutlicht. Unter Standard Laborbedingungen liegen bei den kultivierbaren Endophyten ein großteil der für die Sekundärmetabolitsynthese verantwortlichen Gencluster still. Dies zeigt, dass die Biosynthesemöglichkeiten in diesen Organismen deutlich größer sein müssen als aus den Veröffentlichungen der letzen Jahrzehnte hervorgeht. Da bisher nur ein Bruchteil dieser Organismengruppe untersucht wurde und das Biosynthesepotential größtenteils unerkannt blieb, sind Endophyten nach wie vor als vielversprechende Quelle strukturdiverser Molekülgerüste für die Entdeckung neuer Arzneistoffleitstrukturen anzusehen.

Diese Dissertation stellt die Untersuchungen an den drei Endophyten *Penicillium* sp., *Bulgaria inquinans* und *Didymella* sp. vor, in deren Umfang es zur Isolation strukturdiverser Sekundärmetaboliten aus den Naturstoffklassen Indolditerpenoide, Azaphilone, Butyrolaktone und Decahydrofluorene kam. Einige dieser Metaboliten zeigten starke zytotoxische oder antibakterielle Aktivitäten. Außerdem wurden durch den Einsatz der OSMAC-Methode (One Strain Many Compounds) aus einem Kulturansatz von *B. inquinans* neue Metaboliten isoliert. Dieses Ergebnis verdeutlicht die Nützlichkeit der OSMAC-Methode beim Versuch Biosynthesewege zu aktivieren um die Strukturdiversität eines Produktionsstammes zu erhöhen. Die Struktur aller isolierten Naturstoffe wurde durch den Einsatz von Kernspinresonanzspektroskopie (NMR) und Massenspetrometrie (MS) aufgeklärt. Die absolute Konfiguration der neuen Verbindungen wurde durch den Einsatz von Röntgenbeugungskristallographie, Mosher Ester Analyse, Circulardichroismus Berechnungen

(TDDFT-ECD) und Literaturdatenvergleich der spezifischen optischen Rotation bestimmt. Diese Dissertation ist in Kapitel gegliedert, welche die Ergebnisse der Projekte in Form von veröffentlichten oder eingereichten Manuskripten wiederspiegeln, aus denen die folgenden Zusammenfassungen als wörtliche Zitate übernommen wurden.

Indolditerpenoide aus einem endophytischen Penicillium sp.

Eine Untersuchung des chemischen Profils des Endophyten *Penicillium* sp. (Stamm ZO-R1-1), welcher aus der Wurzel der Arzneipflanze *Zingiber officinale* isoliert wurde, lieferte neun neue Indolditerpenoide (**1**−**9**) und dreizehn bekannte Verbindungen (**10**−**22**). Die Struktur der neuen Verbindungen wurde durch die Analyse ein- und zweidimensionaler NMR Spektren und Ergebnissen der hochauflösenden Massenspektrometrie (HRESIMS) aufgeklärt. Die absolute Konfiguration der neuen Naturstoffe **1**, **3** und **7** wurde durch TDDFT-ECD Berechnungen bestimmt und durch die Kristallstrukturanalyse von **1** mittels anormaler Dispersion am Einzelkristall unabhängig bestätigt. Die isolierten Verbindungen wurden auf Zytotoxizität gegenüber den Zelllinien L5178Y, A2780, J82 und HEK-293 geprüft. Verbindung **1** war der am stärksten aktive Metabolit gegenüber L5178Y Zellen mit einem IC_{50} Wert von 3.6 μM und einem IC_{50} Wert von 8.7 μM gegenüber A2780 Zellen. Interessanterweise weist **1** ein neues diterpenoides Grundgerüst mit einem seltenen 6/5/6/6/6/6/5 verknüpftem heterozyklischen Ringsystem und einem aromatischen C-Ring auf. Dies scheint essentiell für die zytotoxische Aktivität dieses Naturstoffes gegenüber L5278Y und A2780 Zellen zu sein.

Erweiterung der chemischen Diversität des endophytischen Pilzes Bulgaria inquinans, einem mistelassozierten Schlauchpilz, durch den Einsatz der OSMAC-Methode.

Der endophytische Pilz *Bulgaria inquinans* (Isolat MSp3-1), isoliert aus einer Mistel (*Viscum album*), wurde auf festem Czapek Medium fermentiert. Die chromatographische Aufarbeitung des Ethylacetat Rohextraktes lieferte fünf neue Naturstoffe (**1**−**5**). Die anschließende Anwendung der OSMAC Strategie durch Zusatz verschiedener Salzmischungen ($MgSO_4$, $NaNO_3$ und NaCl) zum Czapek Medium induzierte die Akkumulation von neun

zusätzlichen, neuen Sekundärmetaboliten (**6**−**13**, **16**), von denen die meisten (**8**, **10**−**12**) in Kulturen ohne Salzmischungen nicht detektierbar waren. Die Struktur der neuen Verbindungen wurde anhand ihrer 1D/2D-NMR Spektren und HRESIMS Daten bestimmt. Die TDDFT-ECD Berechnungen wurden benutzt um die absolute Konfiguration der neuen Verbindungen **1**, **4** und **6** zu bestimmen und zusätzlich von Bulgarialakton B (**14**) für welches die absolute Konfiguration noch unbeschrieben war. Um die absolute Konfiguration von **12** und **13** erfolgreich zu bestimmen wurden modifizierte Mosher Ester Analysen durchgeführt. Die TDDFT-ECD Berechnungen ließen außerdem die bestimmung der absoluten Konfiguration von (+)-Epicocconon zu, welches in seiner trizyklischen Substruktur das Enantiomer zu Bulgarialakton B (**14**) darstellt. Alle isolierten Metaboliten wurden auf ihre zytotoxische Aktivität untersucht. Verbindung **2** zeigte starke zytotoxische Aktivität gegenüber Mauslymphom Zelllinie L5178Y mit einem IC_{50} Wert von 1.8 μM, während sich die übrigen Verbindungen als inaktiv erwiesen.

Didymellanosin, ein neues Decahydrofluorenanalogon, und Ascolakton C aus Didymella sp. IEA-3B.1, einem Endophyten aus Terminalia catappa.

Didymellanosin (**1**), der erste Vertreter der Naturstoffklasse Decahydrofluorene, welcher ein 13-gliedriges makrozyklisches Alkaloidgrundgerüst besitzt, das mit Adenosin konjugiert ist und das neue Benzolaktonderivat Ascolakton C (**4**) wurden zusammen mit acht bekannten Verbindungen (**2**−**3**, **5**−**10**) aus einer Reisfermentation des endophytischen Pilzes *Didymella* sp. IEA-3B-1, welcher mit der Wirtspflanze *Terminalia catappa* assoziiert ist, isoliert. Zusätzlich lies sich das neue Ascochitamin (**11**) isolieren, nachdem $(NH_4)_2SO_4$ dem Reismedium zugesetzt wurde. Die Struktur der neuen Verbindungen wurde durch ausgiebige Analyse der ein- und zweidimensionalen NMR Daten und HRESIMS Daten ermittelt. Bei der Untersuchung der Zytotoxizität zeigte Didymellanosin (**1**) starke bis mäßige Aktivität gegenüber der murinen Lymphomzelllinie L5178Y, der Burkitt B-Lymphom Zelllinie (Ramos) und der T-Zell Leukämiezelllinie (Jurkat J16) mit IC_{50} Werten von jeweils 2.2, 7.6 und

11.0 μM. Außerdem wurde mit den Substanzen ein NFκB-Inhibitionsassay durchgeführt, bei dem Verbindung **1** und Phomapyrrolidon A (**2**) effizient die Aktivierung von NFκB blockierten. Bei der Untersuchung der antibakteriellen Aktivität stellte sich Ascomylaktam C (**3**) als aktivste Verbindung heraus. Beim Test gegen eine Auswahl grampositiver Bakterien, einschließlich therapieresistenter Stämme, wurden hierbei MIC zwischen 3.1 und 6.3 μM ermittelt, während **1** deutlich weniger aktiv war. Interessanterweise waren beide Verbindungen gegenüber dem gramnegativen Bakterium *Acinetobacter baumannii* aktiv, mit einer MIC von 3.1 μM, wenn zusätzlich 0.1 μM Colistin hinzugefügt wurden.

Chapter 1

Introduction

1.1. Natural products in drug discovery

Natural products are produced by plants, animals and microorganisms to improve their fitness against competitors, predators and pathogens (Kellenberger *et al*., 2011). Based on the structural classes, natural products can be categorized as polyketides, non-ribosomal peptides (NRPs), alkaloids, terpenoids and others. These reflect the main biosynthetic pathways which are employed in organisms (Clardy and Walsh, 2004). These metabolites are remarkable for a wide array of biological activities that significantly contribute to the treatment of many diseases since ancient times (Dias *et al*., 2012).

The idea of isolating pure natural products as therapeutic substances can be traced back to the beginning of the 19th century. One early successful story is the isolation of morphine from opium (*Papaver somniferum*) in 1806 by the German pharmacist Friedrich Wilhelm Adam Sertürner, which was later produced and commercialized by E. Merck in 1826 for the first time (Newman *et al*., 2000; Klockgether-Radke, 2002). Further examples include the discovery of the antimalarial drugs quinine and artemisinin, the antibiotics penicillin and erythromycin, the anticancer agents paclitaxel and camptothecin, the cholesterol-lowering agents compactin and lovastatin, among many other remarkable drugs and lead structures of natural products origin (Butler, 2004; Cragg and Newman, 2013).

In general, natural products are utilized as drugs in three distinct ways, including the direct application of molecules, the serving as starting material for further chemical modifications and acting as lead structures that enable the synthesis of a series of analogues or as templates for generating drug-like compound libraries (Berdy, 2005; Grabowski *et al*., 2008). Thus far, with the growing advance in synthetic and combinatorial chemistry, natural products continuously contribute as an invaluable source of novel scaffolds for drug candidates (Butler,

2004; Clardy and Walsh, 2004; Grabowski *et al*., 2008). Natural products offer several advantages in the search for new therapeutic agents. Firstly, natural compounds can go straightforward from "hit" to drug, without involving any modifications beforehand. Secondly, natural product-derived scaffolds are unique, particularly those representing privileged structures bearing the property of "drug-likeness", that place them as legitimate starting points for lead optimization in rational drug design. Eventually, natural products can lead to the elucidation and better understanding of targets or pathways involved in disease processes (Lam, 2007; Amedei and D'Elios, 2012; Lachance *et al*., 2012).

Natural products or molecules inspired by their structures contribute to around one quarter of small molecules as new chemical entities (NCEs) approved by the FDA in 2014. This indicates that this field is still growing, in spite of a decreasing interest of pharmaceutical companies in natural product-based research programs (Newman and Cragg, 2016). Even in 2018, 10 out of 59 drugs approved by the FDA fell within this category (de la Torre and Albericio, 2019). Among the licensed therapeutic agents thus far, anti-infective and anticancer drugs are still strongly influenced by natural products and most of them are of microbial origin (Lam, 2007; Newman and Cragg, 2016).

1.2. Therapeutic molecules of fungal origin

Secondary metabolites of fungal origin are an important part of natural products that historically have made substantial contributions to the discovery of drugs and leads (Berdy, 2005). The milestone of antibiotic research was started by the discovery of penicillin, the first therapeutically used antibiotic, by Sir Alexander Fleming in 1928 (Lobanovska and Pilla, 2017). Penicillin was produced by the filamentous fungus, *Penicillium notatum*, which was initially found as a contaminant of a Petri dish containing a culture of *Staphylococcus aureus*. Its structure was fully characterized in 1945 as penicillin G, which contains a characteristic *β*-lactam moiety. The latter is the most essential part of the molecule regarding its activity. It

covalently binds to the penicillin-binding proteins (PBPs) of bacteria to exert its killing action (Bentley, 2009; Lobanovska and Pilla, 2017). Another member of the *β*-lactam family was firstly isolated in 1948 from *Acremonium chrysogenum* (formerly known as *Cephalosporium acremonium*) by Giuseppe Brotzu and identified as cephalosphorin C (Amedei and D'Elios, 2012). Nowadays, a number of *β*-lactam antibiotics inspired by penicillins and cephalosporins are in clinical use and are produced through a semi-synthesis approach or large-scale fermentation of the highly productive strains derived from genetic engineering (Elander, 2003).

The earliest antifungal agent, griseofulvin, was discovered in 1939 and defined as a metabolite product of *Penicillium griseofulvum* (Oxford *et al*., 1939). Griseofulvin is especially active against dermatophytes and used for the treatment of ringworm disease in humans and animals. Yet, the exact antifungal mode-of-action is not completely understood, but the preferred explanation is its interference with the microtubule assembly and resulting mitotic arrest (Odds *et al*., 2003). Griseofulvin also drew attention due to its antimitotic and antiproliferative activities towards mammalian cancer cells (Rathinasamy *et al*., 2010). However, the mode-of-action in both fungi and mammalian cells was proposed to be different and required further detailed investigation (Rønnest *et al*., 2012). Moreover, a number of griseofulvin analogues were prepared synthetically for the purpose of improving its antifungal and anticancer properties (Petersen *et al*., 2014).

Furthermore, the discovery of echinocandins, a group of cyclic hexapeptides bearing a lipid side chain, represents yet a new class of antifungal drugs. They are used especially for the treatment of invasive candidiasis and aspergillosis (Chen *et al*., 2011). Caspofungin became the first clinically approved analogue by the FDA in 2001, followed by micafungin in 2005 and anidulafungin in the following year (Hashimoto, 2009). These echinocandins were semi-synthesized upon structure modification of the fungal products pneumocandin B_0 from *Glarea lozoyensis* (Wichmann *et al*. 1989), FR901379 from *Coleophoma empetri* (Iwamoto *et al*., 1994) and echinocandin B from *Aspergillus nidulans var. echinulatus* (Benz *et al*., 1974),

respectively. All echinocandins act as non-competitive inhibitors of 1,3-*β*-glucan synthase and hinder the synthesis of fungal cell walls (Hashimoto, 2009).

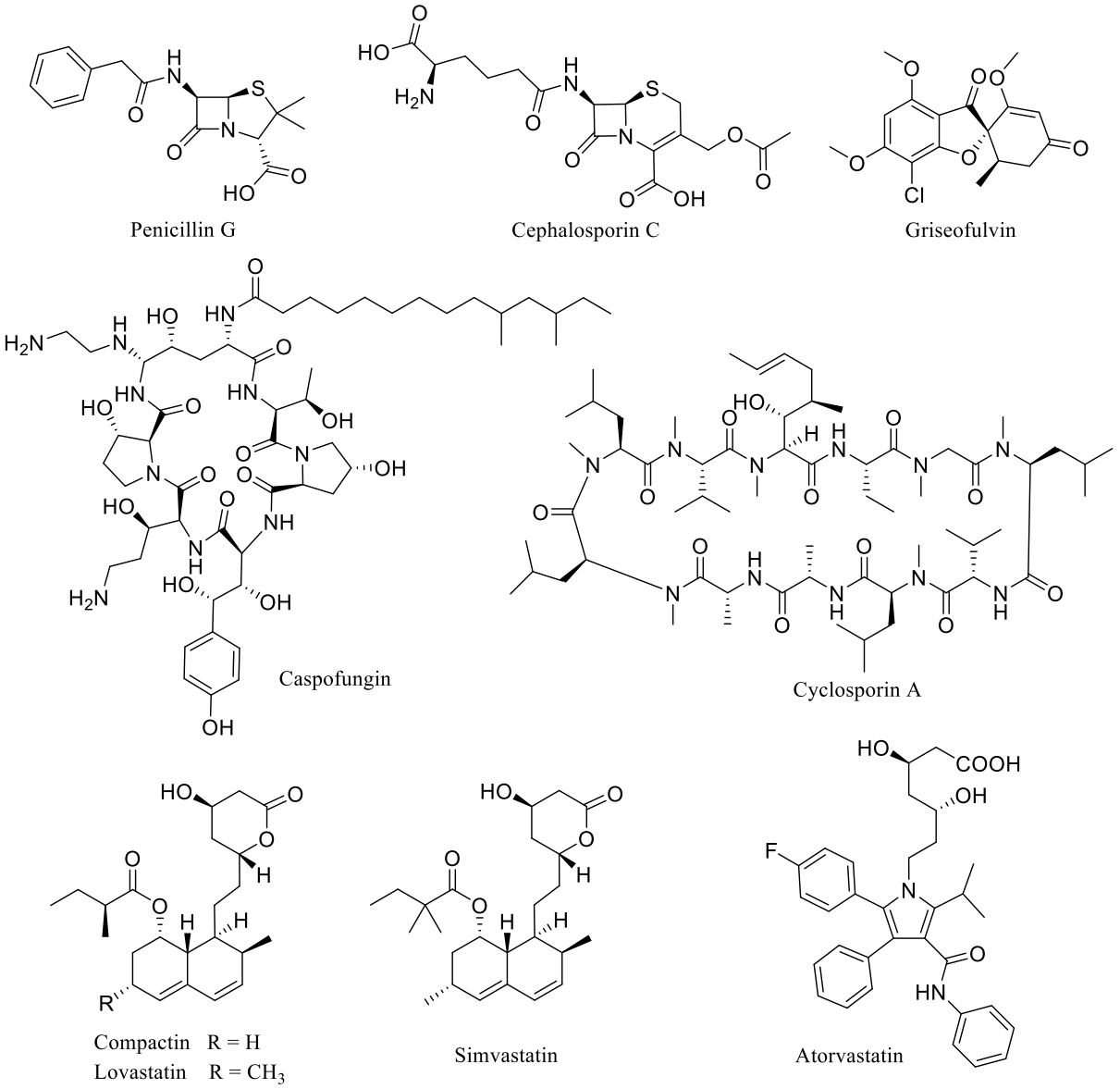

Figure 1.2.1. Drugs and leads derived from fungi.

Cyclosporin A is a clinically important immunosuppressant agent used to prevent organ transplantation rejection. Interaction of cyclosporin A with a specific cytosolic binding protein, cyclophilin, results in a novel complex that further inhibits the function of the calcineurin enzyme and leads to a disruption of the signal transduction process in T cells activation (Jørgensen *et al*., 2003). It was first isolated from *Tolypocladium inflatum* (formerly identified as *Trichoderma polysporum*) and initially studied for its antifungal activity (Demain, 2014).

Cyclosporin A has been reported also for its antiviral activity against the hepatitis C virus (HCV), however the immunosuppressive action limited further applications (Nakagawa *et al*., 2004). Many analogues of cyclosporin A have been afforded through total synthesis, semi-synthesis after chemical modification or a biosynthetic approach, allowing for the investigation of less toxic derivatives and other potential uses (Lazarova and Weng, 2003). Interestingly, the synthetic non-immunosuppressive analogue Debio-025 was found to be superior against HCV infection to cyclosporin A itself. Additionally, it showed impressive activity against human immunodeficiency virus type 1 (HIV-1), rendering it a potential option for the therapy of HCV/HIV co-infection (Chatterji *et al*., 2005; Paeshuyse *et al*., 2006). Moreover, several analogues were evaluated in clinical trials for the treatment of asthma and have demonstrated promising effects (Eckstein and Fung, 2003).

Lovastatin is the first commercially available cholesterol-lowering agent from the statin class of metabolites, initially isolated from a filamentous fungus *Aspergillus terreus* (Alberts *et al*., 1980). Prior to lovastatin, compactin was obtained as a product of *Penicillium brevicompactum* (Brown *et al*., 1976), but it has never entered the market. Nonetheless, biotransformation of compactin yielded pravastatin, while simvastatin was produced after chemical modification of lovastatin. Newer statins (*e.g.* fluvastatin and atorvastatin) were derived from total chemical synthesis. All statins bind to the active site of the 3-hydroxy-3-methylglutaryl coenzyme A (HMG-CoA) reductase, the first rate-limiting step in the cholesterol biosynthesis pathway (Tobert, 2003). Besides their main application field, subsequent clinical studies reported the potential therapeutic effects of lovastatin for the treatment of cancer (Hindler *et al*., 2006), multiple sclerosis (Sena *et al*., 2003), and Alzheimer's disease (Friedhoff *et al*., 2001). Similarly, some drugs were found to have new pharmacological effects during their licensed clinical uses, which led to drug repurposing of the current uses for their new therapeutic applications (Cragg *et al*., 2014).

A number of approaches have been introduced to capture a wider structural diversity and hence more potentially therapeutic compounds from fungi. Those include the extensive exploration of biological sources from diverse geographical areas and untapped ecosystems to enhance the genetic diversity, as well as efforts to induce the expression of "silent" gene clusters in the strains under study conditions (Knight *et al*., 2003; Lam, 2007; Brakhage and Schroeckh, 2011). Useful tools to overcome the major challenge of re-discovery of known metabolites, include dereplication strategies such as the combination of chromatographic and spectroscopic techniques as well as utilization of in-house libraries and natural product databases, such as the Dictionary of Natural Products (DNPs), AntiBase, and MarinLit (Lam, 2007; Nielsen and Larsen, 2015). An appreciated number of valuable metabolites has been discovered from fungal resources and is used for various clinical applications so far. Nevertheless, the need for new and better drugs is likely at pace with the rapidly emerging cases of resistance to the existing drugs, especially in the field of antimicrobial and anticancer agents (Cragg *et al*., 2014; Harvey *et al*., 2015).

1.3. Endophytic fungi as a reservoir of biologically active secondary metabolites

Endophytic fungi are a diverse polyphyletic group of microorganisms that can be found in each part of plant tissues, from less accessible roots to the inner tissue of stems, leaves, flowers and fruits (Aly *et al*., 2010). To date, only around 1–2% of 300.000 known plant species have been investigated for their endophyte composition, which makes them largely unexplored in comparison with their pathogenetic counterparts or soil-borne fungi (Chandra, 2012; Strobel, 2018). Plants derived from tropical and temperate rainforests, which harbor more than 60% of the world's terrestrial biodiversity, and those which were traditionally used as medicinal plants, are considered as rich sources of endophytes. These microorganisms are capable of producing a myriad of bioactive secondary metabolites (Strobel *et al*., 2004).

Basically, endophytes synthesize secondary metabolites to compete with epiphytes or pathogens for colonization of the host as well as to maintain host metabolism in balance (Chandra, 2012). On the plant side, the occurrence of endophytes enhances the growth and increases adaptation to abiotic and biotic stress. The latter is relevant in regard to the finding that the majority of compounds derived from endophytes possess antimicrobial activity and in many cases, these have been involved in protecting the host plants towards phytopathogenic microorganisms (Gunatilaka, 2006; Aly *et al*., 2011; Jia *et al*., 2016). Thus, natural products produced by endophytes are shaped through an evolutionary unique relationship with the host plants and many of them display unprecedented structures and various biological impacts that are promising for pharmaceutical and agricultural applications (Gunatilaka, 2006, Aly *et al*., 2010).

Cryptocandin is a unique lipopeptide related to echinocandins that revealed excellent antifungal activity against either human pathogenic (*Candida albicans*, *Trichophyton mentagrophytes* and *Trichophyton rubrum*) and plant pathogenic fungi (*Botrytis cinerea* and *Sclerotinia sclerotiorum*). The compound was isolated from the fungal endophyte *Cryptosporiopsis cf. quercina*, harbored in the inner bark of the stems of *Triptergyium wilfordii* (Strobel *et al*., 1999). Another metabolite from this endophyte, namely cryptocin, contains an unusual tetramic acid moiety and was found active against some species of plant pathogenic fungi belonging to oomycetes and ascomycetes, including *Pyricularia oryzae*, the most economically important pathogen as a causal agent of rice blast disease (Li *et al*., 2000).

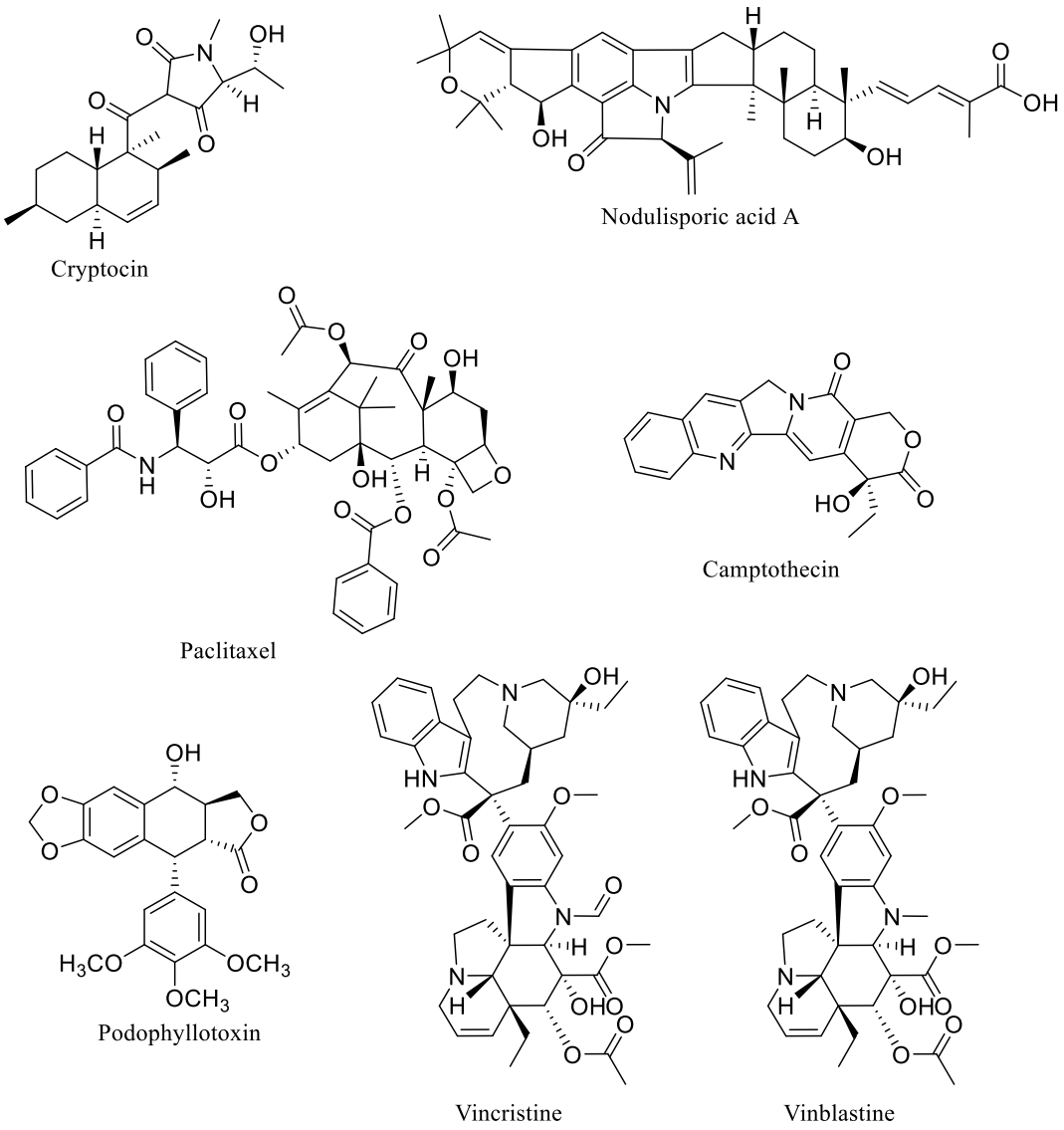

Figure 1.3.1. Bioactive metabolites isolated from endophytic fungi.

A novel compound of indole diterpenoids with potent insecticidal activity, nodulisporic acid A, was obtained after chemical investigation of *Nodulisporium* sp. cultures. The fungus was isolated from woody tissue of *Bontia daphnoides*, collected in Hawaii (Ondeyka *et al*., 1997). Nodulisporic acid A itself further showed impressive activity against blood-feeding ectoparasites *Cimex lectularius* and *Ctenocephalides felis*. Its mode-of-action in parasite killing is similar to that of ivermectin. However, unlike ivermectin it selectively inhibits a glutamate-gated chloride channel in invertebrates which is lacking in mammals. The lack of effects to the GABA-gated chloride channel, renders this an orally active compound that is safe in mammals at a dosage not possible for ivermectin. A number of analogues thereof have been produced

through semisynthetic and total synthetic efforts after structure modifications, to improve the spectrum of its biological activity (Meinke *et al*., 2002).

Intriguingly, endophytic fungi are found to be capable of producing natural products originally considered exclusive to the host plants. They have gained much attention since first noticed for their capability to produce the remarkable anticancer agent, paclitaxel from *Taxomyces andreanae*, a fungal endophyte of *Taxus brevifolia*, the latter being the original source of the compound (Stierle *et al*., 1993). In the years to follow, some wonder molecules were isolated from endophytic fungi, such as the anticancer agent camptothecin, a precursor of semisynthetic derivatives, topotecan and irinotecan (Puri *et al*., 2005), as well as podophyllotoxin, a precursor of three current anticancer drugs etoposide, teniposide and etoposide phosphate (Eyberger *et al*., 2006; Puri *et al*., 2006). Further examples include the microtubule-targeting anticancer agents, vincristine and vinblastine, isolated from *Fusarium solani*, a fungus associated with *Catharanthus roseus* (Kumar *et al*., 2013).

These findings have raised the prospect of the utilization of such endophytes as alternative sources for those pharmaceutically valuable metabolites (Priti *et al*., 2009). On the other hand, substantial reduction in metabolite production upon repeated sub-culturing of endophytes was encountered, thus far preventing the industrial applications of using endophytes (Kusari *et al*., 2009,; Kusari and Spiteller, 2011). Various hypotheses have been proposed to explain this attenuation process, including the absence of host-specific stimuli after laboratory cultivation, gene silencing and the loss of essential elements in gene clusters that are required for metabolite biosynthesis (Deepika *et al*., 2016). Nevertheless, recent progress on genome analysis of the paclitaxel-producing endophyte *Penicillium aurantiogriseum* revealed that the fungus and the *Taxus* genus have evolved independently in the paclitaxel biosynthetic pathway, thereby ruling out the possibility of horizontal gene transfer between endophyte and the host plant or *vice versa* as suggested before. Hence, this finding provides new insight into the evolutionary origin of their biosynthetic genes (Yang *et al*., 2014). Owing to the broad diversity

in nature along with the great biosynthetic potential, endophytic fungi remain as an inexhaustible resource of bioactive and structurally novel natural products (Kusari *et al*., 2012; Deepika *et al*., 2016).

1.4. Strategies to unlock silent gene clusters in fungal biosynthetic pathway

The enzymes involved in the biosynthetic pathways of fungal secondary metabolites are encoded by genes arranged as clusters in the genome and are collectively called biosynthetic gene clusters (BGCs) (Pfannenstiel and Keller, 2019). As favored by the advance of genome mining, a growing number of BGCs controlling the biosynthetic pathways of fungal natural products are being identified. This effort indicated that the actual biosynthetic capacity of endophytic fungi as producers of secondary metabolites is much greater than known today, thus a plethora of novel and bioactive natural products from fungi await to be discovered (Kusari *et al*., 2012; Brakhage, 2013; Harvey *et al*., 2015).

In fact, many of these BGCs remain not expressed under laboratory culture conditions, thus limiting the chemical diversity of compounds afforded from the standard fermentation (Wakefield *et al*., 2017). This challenge has prompted the development of numerous strategies to activate the silent BGCs and characterize their cryptic metabolites. These included the "One Strain MAny Compounds" (OSMAC) approach, the co-cultivation technique of two or more different microorganisms (either fungus and fungus or fungus and bacterium co-cultures) and epigenetic modulation (Wakefield *et al*., 2017; Pfannenstiel and Keller, 2019).

1.4.1. OSMAC approach

It is well established that each biosynthetic step in metabolic processes of endophytic fungi can be influenced by general ecological factors (Aly *et al*., 2010; Kusari *et al*., 2012). The term OSMAC was introduced by Zeeck and co-workers to describe the systematic modification on easily accessible culture parameters such as media composition, pH, light, temperature, aeration, the shape of culture vessels or addition of enzyme inhibitors/inducers (Bode *et al*.,

2002; Daletos *et al*., 2017). As shown by Paranagama *et al*. (2007), even simple differences such as exchanging tap water to distilled water in preparing potato-dextrose broth (PDB) as culture medium shifted the main metabolites production of an endophytic *Paraphaeosphaeria quadriseptata*. These changes were attributed to the presence of trace amount of metal ions (Cu^{2+}, Cd^{2+}, and Cr^{3+}) in tap water. When cultivated on PDB medium prepared with tap water, the fungus mainly produced monicillin I, whereas cytosporone F and aposphearine B were afforded as major metabolites upon culturing the fungus on PDB prepared with distilled water. Further studies on a mangrove endophyte, *Penicillium brocae*, revealed that the fungus when cultured on PDB medium was capable of producing a series of new disulfide-bridged diketopiperazines, brocazines A–F, which exhibited potent cytotoxic activities towards a panel of cancer cells (Meng *et al*., 2014). On the other hand, several additional diketopiperazines lacking a disulfide-bridge, penicibrocazines F–I, were obtained following fermentation of the respective fungus on Czapek medium (Meng *et al*., 2017). This result indicated the sensitivity of biosynthetic process of the suited strains to the changes of medium composition.

1.4.2. Co-cultivation

Co-cultivation involving two or more different microorganisms in the same confined environment is inspired by their omnipresence in the natural microbe communities (Bertrand *et al*., 2014). This technique is considered as an experimental imitation of the microbial interactions occurring in nature at the laboratory scale, either to enhance the accumulation of the constitutively present metabolites or to provoke the production of new metabolites missing in discrete fungal or bacterial cultures (Daletos *et al*., 2017; Wakefield *et al*., 2017). Take *Fusarium tricinctum* as an example, co-cultivation of this endophyte with *Bacillus subtilis* resulted in a significant enhancement of the constitutive fungal metabolites, such as enniatins, lateropyrone and fusaristatin A compared to those in axenically grown culture. In addition, the accumulation of three new cryptic metabolites, such as macrocarpon C, 2-(carboxymethyl-amino) benzoic acid and (−)-citreoisocoumarinol was detected only in co-cultures (Ola *et al*.,

2013). When challenged with *Streptomyces lividans*, this fungus was able to produce several new further cryptic naphthoquinone dimers, fusatricinones A–D, along with dihydrolateropyrone (Moussa *et al*., 2019). These results suggested that the fungus responds differently during their interaction with different microorganisms.

Even though the precise mechanism of this microbial interaction remains unclear, direct contact between microorganisms or secretion of signaling molecules may unlock silent gene clusters and lead them to produce new secondary metabolites for communication, competition and defense purposes (Scherlach and Hertweck, 2009; Wakefield *et al*., 2017; Tomm *et al*., 2019). An interesting result was shown in a recent study by the treatment of an endophytic *Chaetomium* sp. with autoclaved culture of *Pseudomonas aeruginosa* that resulted in the accumulation of new butenolides, chaetobutenolides A–C (Ancheeva *et al*., 2017). Further chemical investigation of the resulting extract also led to the isolation of two additional cryptic metabolites bearing an unprecedented alkaloid scaffold, chaetolines A and B, thereby suggesting the fungal response to be related to exposure to the conserved microbe-specific molecules that may be released upon autoclaving *P. aeruginosa*, regardless of the absence of physical interaction between the studied microorganisms (Ancheeva *et al*., 2018).

1.4.3. Epigenetic modulation

Epigenetic modifiers are capable of changing microbial characteristics in correspondence to alteration of their epigenetic status, without involving any changes in the DNA sequence (Pan *et al*., 2019). There are two main groups of chemicals used as epigenetic modifiers such as histone deacetylase (HDAC) and DNA methyltransferase (DNMT) inhibitors. Suberoylanilide hydroxamic acid (SAHA), suberoyl bishydroxamic acid (SBHA) and nicotinamide are some common HDAC chemicals to inhibit the removal of acetyl groups in epigenetic machinery, while 5-azacytidine (5-AC) is the most commonly used DNMT inhibitor (Pan *et al*., 2019; Pfannenstiel and Keller, 2019). Among other successful applications of this approach, cultivation of *Chaetomium indicum* in the presence of SBHA particularly promoted

the expression of two silent genes (*pksCH-1* and *pksCH-2*) for nonreducing PKSs in chaetophenol biosynthesis, leading to the isolation of structurally diverse polyketides, chaetophenols A–F (Asai *et al*., 2013). Furthermore, epigenetic stimulation by addition of nicotinamide, a NAD^+-dependent HDAC inhibitor, in the cultures of the endophytic fungus *Eupenicillium* sp., derived from the Chinese medicinal plant *Xanthium sibiricum* led to an increased production of two new polyketides containing a decalin motif, eupenicinicols C and D. The latter compound showed strong antibacterial activity against *Staphylococcus aureus*, in addition to its pronounced cytotoxicity towards human acute monocytic leukemia cells (THP-1) (Li *et al*., 2017).

1.5. Aims and significance of this study

The capability of endophytic fungi to produce various types of secondary metabolites bearing unique structural features and a vast array of bioactivities, combined with their potential biosynthetic capacity, have continuously inspired many studies in natural products. This study is aimed at affording secondary metabolites derived from endophytes with anticancer and antibacterial properties. Moreover, OSMAC approaches were utilized to maximize the chemical diversity of metabolites of the producing strains. Thus, three species of endophytic fungi such as *Penicillium* sp., *Bulgaria inquinans* and *Didymella* sp., were used as biological sources, guided by the intriguing chromatographic profiles of their crude EtOAc extracts through HPLC-DAD analysis, in combination with in-house UV spectra library.

A total of 22 indole diterpenoids, of which nine are new natural products were obtained following chromatographic workup on a rice culture of *Penicillium* sp., an endophyte isolated from roots of *Zingiber officinale.* When tested for cytotoxicity, a series of analogues showed potent to moderate activity against L5178Y and A2780 cells. The structure-activity relationship (SAR) of this type of analogues is proposed (Chapter 2 Publication 1).

The study of the mistletoe-associated fungus, *Bulgaria inquinans* cultured on solid Czapek medium yielded a series of butyrolactones and an azaphilone pigment, of which one butyrolactone analogue was found to be cytotoxic towards L5178Y cells. In order to influence the biosynthetic capacity of this strain, the OSMAC strategy was applied by supplementing the media with a mixture of salts ($MgSO_4$, $NaNO_3$, and NaCl), resulting in the accumulation of other types of new compounds including a 1,3-oxazine containing metabolites and a series of α-pyrones (Chapter 3 Publication 2).

The fermentation of an endophytic *Didymella* sp. derived from the host plant *Terminalia catappa* on rice medium led to the isolation of azaphilones, isocoumarins and decahydrofluorene-class of compounds. The latter revealed significant activities as antibacterial agents against Gram-positive bacteria (*Staphylococcus aureus*, *Enterococcus faecalis,* and *Enterococcus faecium*) including drug-resistant strains and Gram-negative bacterium (*Acinetobacter baumannii*). Furthermore, didymellanosine revealed NFκB inhibitory activity, in addition to its strong to weak cytotoxicities against L5178Y, Jurkat, Ramos and MDA-MB-231 cells. The utilization of the OSMAC approach by addition of $(NH_4)_2SO_4$ to the rice medium influenced the metabolite profile of this fungus and led to the isolation of a nitrogen-containing azaphilone, presumably derived from conversion of oxygen to nitrogen of the corresponding azaphilone (Chapter 4 Publication 3).

Chapter 2

Publication 1

Indole diterpenoids from an endophytic *Penicillium* sp.

Published in : "Journal of Natural Products"

Impact factor : 4.257

Research contribution: first authorship, contributed to 60% of this publication. The first author conducted most of the laboratory work including isolation and structure elucidation of secondary metabolites, as well as preparation of the manuscript.

JOURNAL OF NATURAL PRODUCTS

Article

Cite This: J. Nat. Prod. 2019, 82, 1412−1423

pubs.acs.org/jnp

Indole Diterpenoids from an Endophytic *Penicillium* sp.

Ni P. Ariantari,[†,‡] Elena Ancheeva,[*,†] Chenyin Wang,[§] Attila Mándi,[⊥] Tim-O. Knedel,[#] Tibor Kurtán,[⊥] Chaidir Chaidir,[∥] Werner E. G. Müller,[○] Matthias U. Kassack,[§] Christoph Janiak,[#] Georgios Daletos,[*,†] and Peter Proksch[*,†]

[†]Institute of Pharmaceutical Biology and Biotechnology, Heinrich Heine University Düsseldorf, Universitätsstrasse 1, 40225 Düsseldorf, Germany

[‡]Department of Pharmacy, Faculty of Mathematic and Natural Sciences, Udayana University, 80361 Bali, Indonesia

[§]Institute of Pharmaceutical and Medicinal Chemistry, Heinrich Heine University Düsseldorf, Universitätsstrasse 1, 40225 Düsseldorf, Germany

[⊥]Department of Organic Chemistry, University of Debrecen, P.O.B. 400, 4002 Debrecen, Hungary

[#]Institute of Inorganic Chemistry and Structural Chemistry, Heinrich Heine University Düsseldorf, Universitätsstraße 1, 40225 Düsseldorf, Germany

[∥]Center for Pharmaceutical and Medical Technology, Agency for the Assessment and Application Technology, 10340 Jakarta, Indonesia

[○]Institute of Physiological Chemistry, Universitätsmedizin der Johannes Gutenberg-Universität Mainz, Duesbergweg 6, 55128 Mainz, Germany

Supporting Information

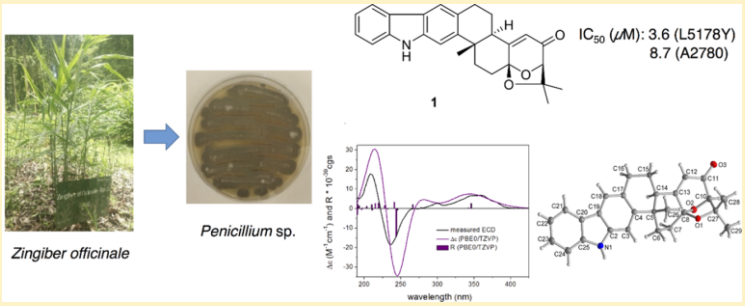

ABSTRACT: A chemical investigation of the endophyte *Penicillium* sp. (strain ZO-R1-1), isolated from roots of the medicinal plant *Zingiber officinale*, yielded nine new indole diterpenoids (**1**−**9**), together with 13 known congeners (**10**−**22**). The structures of the new compounds were elucidated by 1D and 2D NMR analysis in combination with HRESIMS data. The absolute configuration of the new natural products **1**, **3**, and **7** was determined using the TDDFT-ECD approach and confirmed for **1** by single-crystal X-ray determination through anomalous dispersion. The isolated compounds were tested for cytotoxicity against L5178Y, A2780, J82, and HEK-293 cell lines. Compound **1** was the most active metabolite toward L5178Y cells, with an IC_{50} value of 3.6 μM, and an IC_{50} against A2780 cells of 8.7 μM. Interestingly, **1** features a new type of indole diterpenoid scaffold with a rare 6/5/6/6/6/6/5 heterocyclic system bearing an aromatic ring C, which is suggested to be important for the cytotoxic activity of this natural product against L5278Y and A2780 cells.

Filamentous fungi (e.g., *Penicillium*, *Aspergillus*, and *Fusarium* sp.) are important producers of structurally unusual natural products with pharmaceutical potential.[1] Since the discovery of the antibiotic penicillin G from *Penicillium notatum*, fungi belonging to this genus have gained considerable attention with regard to their secondary metabolites and proved to be prolific sources of bioactive compounds. The discovery of the antifungal compound griseofulvin from *P. griseofulvum*, of the cholesterol-lowering agent compactin produced by *P. citrinum*, and of the immunosuppressant agent mycophenolic acid, isolated from *P. brevicompactum*, represents further success stories leading to important therapeutically used molecules from this genus.[1−5]

In our search for new bioactive compounds from fungal sources, we investigated *Penicillium* sp. (strain ZO-R1-1), an endophytic fungus isolated from the medicinal plant *Zingiber officinale* (Zingiberaceae) collected in Indonesia. Rhizomes of

Received: August 26, 2018
Published: May 22, 2019

DOI: 10.1021/acs.jnatprod.8b00723
J. Nat. Prod. 2019, 82, 1412−1423

Chart 1

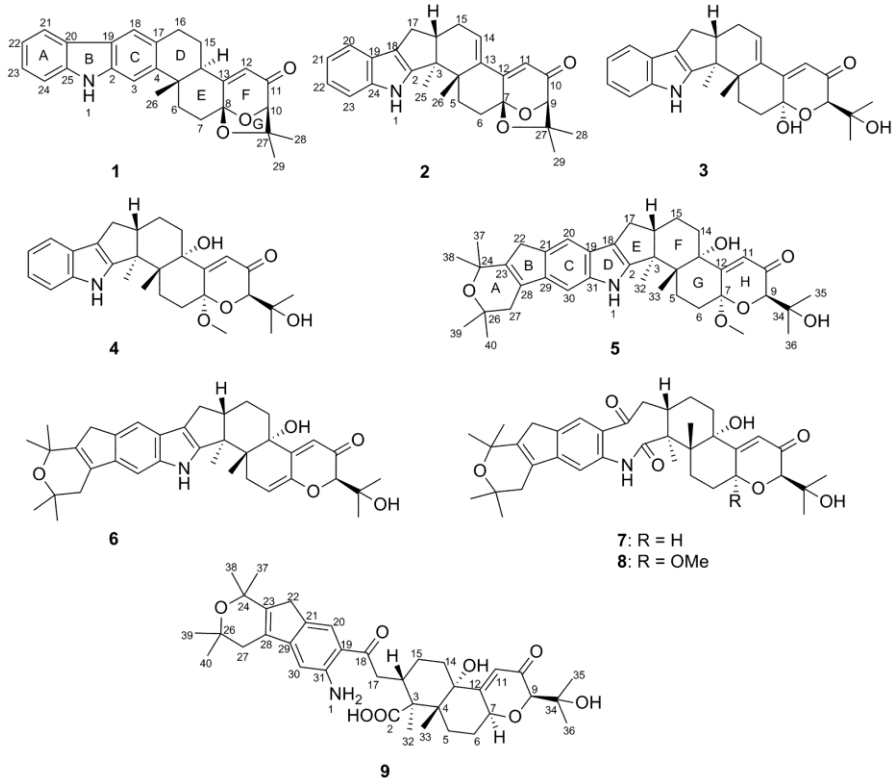

Z. officinale have been widely used in traditional medicine systems among Asian countries to treat numerous ailments, such as vertigo, common cold, cough, anorexia, and rheumatism.[6−8] A number of studies have reported antioxidant,[9] antiemetic,[10] anticancer,[7,8,11] antiarthritic,[12] and anti-inflammatory[9,11] activities, attributed to the main bioactive metabolites, gingerols and shogaols.

The HPLC-PDA analysis of the EtOAc extract of *Penicillium* sp., in combination with an in-house UV spectra library, demonstrated a series of peaks with similar UV absorptions at around 228 and 280 nm, which suggested the presence of indole diterpenoids.[13−15] Indole diterpenoids are a large class of structurally diverse fungal secondary metabolites, featuring an indole moiety fused to a diterpene skeleton.[16−18] Among them, lolitrem B,[19] paxilline,[20] paspalitrems A and B,[21] janthitrems B and C,[22−24] penitrems A−F,[25] aflatrem,[26] and paspalinine[27] are known as tremorgenic mycotoxins, causing neurological disorders in farm animals. These compounds are produced by species of fungi from the genera *Penicillium*, *Aspergillus*, *Epichloë*, and *Claviceps*[16,19,28,29] and are also known for their insecticidal properties.[16,30] Moreover, indole diterpenoids were found to be antibacterial,[31,32] inhibitors of *Candida albicans* biofilm formation,[33] antiviral (against H1N1 influenza A virus)[14] and antiproliferative with activities against human glioblastoma[34] and breast cancer cell lines.[35] Paxilline has been shown to inhibit high-conductance Ca^{2+}-activated K^+ (Maxi-K) channels,[36] which was associated with its anticonvulsant effect.[37] Synthetic derivatives of indole diterpenoids were patented as Maxi-K channel blockers for treatment of glaucoma.[38] The complex structures of these natural products and the broad range of their biological activities have inspired numerous studies, which focused on their total synthesis and on the elucidation of the biosynthetic pathways and enzymes leading to the rich chemical diversity of these intriguing secondary metabolites.[39−41]

In the present study, we describe the isolation and structure elucidation of nine new indole diterpenoid analogues (**1**−**9**) from the endophyte *Penicillium* sp. ZO-R1-1. A plausible biosynthetic pathway leading to the formation of the uncommon alkaloid diterpenoid skeleton of **1** is proposed. Furthermore, we discuss the cytotoxicity of the new and known indole diterpenoids isolated in this study.

RESULTS AND DISCUSSION

The HRESIMS spectrum of shearilicine (**1**) exhibited a prominent pseudomolecular ion peak at *m*/*z* 414.2063 $[M + H]^+$ attributed to the molecular formula $C_{27}H_{27}NO_3$ and accounting for 15 degrees of unsaturation. Investigation of the ^{1}H NMR data (Table 1) revealed the presence of one isolated NH signal, three methyl groups, four sets of methylene signals, nine methines including six aromatic, one olefinic and two further aliphatic protons. Four characteristic aromatic proton signals resonating at δ_H 8.00 (H-21), 7.19 (H-22), and 7.38 (H-23, H-24), along with the NH signal (δ_H 7.90), hinted at the presence of an indole moiety containing a 1,2-disubstituted benzene (ring A). The observed HMBC correlations from H-

DOI: 10.1021/acs.jnatprod.8b00723
J. Nat. Prod. 2019, 82, 1412−1423

Table 1. ^{1}H and ^{13}C NMR Data for 1−4

	1[a]		2[b]		3[b]		4[c]	
position	δ_C, type[d]	δ_H (J in Hz)	δ_C, type[d]	δ_H (J in Hz)	δ_C, type	δ_H (J in Hz)	δ_C, type	δ_H (J in Hz)
1-NH		7.90, s		10.84, s		10.85, s		10.76, s
2	139.8, C		148.4, C		148.8, C		152.7, C	
3	107.8, CH	7.28, s	48.7, C		47.8, C		50.4, C	
4	147.6, C		38.8, C		42.0, C		42.4, C	
5	35.9, C		28.4, CH_2	2.45, m; 1.98, ov	28.1, CH_2	2.20, m; 2.08, ov	24.9, CH_2	2.42, m; 1.81, m
6	34.5, CH_2	2.53, m	30.4, CH_2	1.98, ov; 1.84, m	32.9, CH_2	2.08, ov	27.3, CH_2	2.47, m; 1.83, ov
7	27.7, CH_2	2.24, ddd (14.0, 11.9, 9.2); 2.04, br dd (14.0, 6.3)	103.8, C		93.5, C		97.1, C	
8	103.9, C							
9			87.4, CH	4.43, d (1.2)	78.3, CH	4.13, s	78.5, CH	3.92, s
10	88.1, CH	4.35, d (1.2)	195.1, C		198.7, C		197.2, C	
11	197.5, C		117.3, CH	6.16, s	120.7, CH	5.86, s	121.3, CH	5.79, s
12	120.4, CH	5.94, br s	163.8, C		161.4, C		160.3, C	
13	171.0, C		138.4, C		140.7, C		75.7, C	
14	43.3, CH	3.04, dt (12.0, 2.6)	132.5, CH	6.52, dd (5.2, 2.7)	130.4, CH	6.07, dd (5.2, 2.4)	32.7, CH_2	1.83, m; 1.68, m
15	19.9, CH_2	2.18, m; 1.85, qd (12.0, 6.1)	27.9, CH_2	2.39, ov; 2.34, dt (19.3, 5.2)	27.5, CH_2	2.30, m; 2.26, m	21.0, CH_2	1.94, dd (11.8, 3.0); 1.64, ov
16	29.5, CH_2	3.14, m	44.5, CH	2.90, m	45.0, CH	2.82, m	49.5, CH	2.75, m
17	125.6, C		26.7, CH_2	2.74, dd (13.2, 6.7); 2.39, ov	26.5, CH_2	2.76, dd (13.1, 6.7); 2.39, dd (13.1, 10.1)	26.9, CH_2	2.62, dd (13.0, 6.0); 2.34, ov
18	119.7, CH	7.75, s	116.1, C		116.1, C		114.9, C	
19	122.2, C		124.2, C		124.2, C		124.5, C	
20	123.1, C		117.6, CH	7.32, ov	117.9, CH	7.31, d (8.0)	117.7, CH	7.27, ov
21	120.2, CH	8.00, d (7.7)	118.4, CH	6.93, ddd (8.1, 7.0, 1.2)	118.5, CH	6.92, td (8.0, 1.2)	118.4, CH	6.90, td (7.0, 1.1)
22	119.1, CH	7.19, m	119.5, CH	6.98, ddd (8.1, 7.0, 1.2)	119.7, CH	6.97, td (8.0, 1.2)	119.3, CH	6.92, td (7.0, 1.3)
23	125.8, CH	7.38, ov[e]	111.7, CH	7.32, ov	111.8, CH	7.29, d (8.0)	111.8, CH	7.27, ov
24	110.7, CH	7.38, ov	140.4, C		140.4, C		139.7, C	
25	140.1, C		14.2, CH_3	0.97, s	15.0, CH_3	0.92, s	16.3, CH_3	1.26, s
26	30.8, CH_3	1.39, s	27.2, CH_3	1.17, s	22.4, CH_3	1.09, s	19.1, CH_3	0.96, s
27	78.7, C		77.6, C		71.4, C		71.0, C	
28	22.8, CH_3	1.26, s	22.6, CH_3	1.14, s	25.8, CH_3	1.18, s	25.7, CH_3	1.20, s
29	28.7, CH_3	1.47, s	28.5, CH_3	1.39, s	26.7, CH_3	1.18, s	26.2, CH_3	1.23, s
7-OH						6.54, s		
7-OMe							49.0, CH_3	3.38, s
13-OH								4.58, s
27-OH						4.31, s		4.45, s

[a]Recorded at 600 MHz (^{1}H) and 150 MHz (^{13}C) in $CDCl_3$. [b]Recorded at 600 MHz (^{1}H) and 150 MHz (^{13}C) in DMSO-d_6. [c]Recorded at 300 MHz (^{1}H) and 75 MHz (^{13}C) in DMSO-d_6. [d]Chemical shifts extracted from HSQC and HMBC spectra. [e]ov stands for overlapped signals.

21 to C-19, C-23, and C-25, from H-23 to C-21 and C-25, and from NH to C-2 and C-20 confirmed this substructure. Two further aromatic protons appearing at δ_H 7.28 (H-3) and 7.75 (H-18) afforded HMBC correlations to C-17 and C-19 and to C-2 and C-4, respectively. These correlations suggested an additional aromatic ring C fused to the indole part at positions C-2 and C-19, thus forming a carbazole unit, which was previously described for indole sesquiterpenes from bacteria.[42,43] Detailed analysis of the COSY spectrum revealed two further spin systems, H_2-6/H_2-7 and H_2-16/H_2-15/H-14, which were connected based on the detected HMBC correlations from H_2-6 to C-14, from H_2-7 to C-5 and C-13, and from H-14 to C-5 and C-6 (Figure 1). Further HMBC correlations from H_2-6 and H_2-7 to C-8 and from H-14 to C-13 confirmed the structure of rings D and E in **1**. Furthermore, the methyl group CH_3-26 was placed at position C-5, as confirmed by the HMBC spectrum. The connection of ring D to the carbazole substructure was established by HMBC correlations from H_2-16 to C-4, C-17, and C-18, as well as

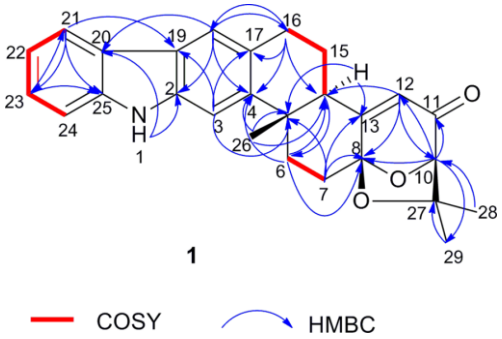

Figure 1. COSY and selected HMBC correlations of **1**.

from H_2-6 to C-4. The olefinic proton H-12 displayed correlations to the sp^3 carbons C-8 and C-10, which together with the correlations from H-10 to the ketone C-11 and to C-8

DOI: 10.1021/acs.jnatprod.8b00723
J. Nat. Prod. 2019, 82, 1412−1423

hinted at the presence of an α,β-unsaturated pyranone moiety (ring F) in **1**. Moreover, the HMBC correlations of the two methyl signals H_3-28 and H_3-29 to C-27 and C-10, in addition to the remaining degree of unsaturation, allowed the deduction of a dioxolane moiety (ring G) fused to the pyranone at C-8 and C-10. The HMBC correlations from H-10 to C-8, C-11, C-12, and C-29 confirmed the assignments of rings F and G in **1**, which were in accordance with the NMR data of the well-described indole diterpene paspalicine (**12**),[44,45] containing the same partial structure of rings D−G. The absence of a ROESY correlation between H-14 and H_3-26, together with similarity of NMR data for rings E−G of **1** with those of paspalicine, suggested that the two compounds shared the same relative configuration. Accordingly, the structure of **1** was established as a new indole diterpenoid containing a rare carbazole unit forming an unprecedented 6/5/6/6/6/5 heterocyclic system.

In order to elucidate the absolute configuration of **1**, the solution time-dependent density functional theory−electronic circular dichroism (TDDFT-ECD) method was applied. While ECD is mostly used to efficiently distinguish enantiomers and determine absolute configuration, it is also capable of distinguishing more than two stereoisomers in molecules with multiple chirality centers when the relative configuration is not available or obvious from NMR measurements.[46−49] In compound **1**, the two blocks of chirality, C-5/C-14 and C-8/C-10, could not be correlated by NMR, although the trans relative configuration of C-5 and C-14 and the cis relationship of the C-8 and C-10 centers of the bridged ring F were determined. Therefore, ECD calculations were carried out for the (5*S*,8*R*,10*S*,14*R*) and (5*S*,8*S*,10*R*,14*R*) stereoisomers to correlate C-5 and C-14 with ring F. The initial Merck molecular force field (MMFF) conformational search yielded two low-energy conformers for (5*S*,8*R*,10*S*,14*R*)-**1** and one low-energy conformer for (5*S*,8*S*,10*R*,14*R*)-**1** in a 21 kJ/mol energy window, which were reoptimized at the B3LYP/6-31+G(d,p) and the CAM-B3LYP/TZVP[50] PCM/MeCN levels. ECD spectra were than computed at various levels of theory (B3LYP, BH&HLYP, CAM-B3LYP, and PBE0 functionals and TZVP basis set) for all sets of conformers, which reproduced the experimental ECD spectrum for (5*S*,8*S*,10*R*,14*R*)-**1** (Figure 2) and resulted in a mirror-image spectrum for (5*S*,8*R*,10*S*,14*R*)-**1** (Figure 3). This suggests that the ECD spectrum is mainly governed by the α,β-unsaturated carbonyl chromophore and hence the C-8 and C-10 chirality centers, and the absolute configuration of **1** could not be assigned by only considering the ECD calculations. However, if the (5*S*,14*R*) absolute configuration, the same as that of paxilline, is assumed for **1**, the ECD calculation affords the (8*S*,10*R*) configuration for ring F. In order to elucidate the absolute configuration, ^{13}C NMR DFT calculations were performed on the two diastereomers above at the mPW1PW91/6-311+G(2d,p)[51] and the mPW1PW91/6-311+G(2d,p) SMD/$CHCl_3$ levels. Substantially lower average deviations at both applied levels of theory were found from the experimental data for the (5*S*,8*S*,10*R*,14*R*) stereoisomer than for the other diastereomer, allowing elucidation of the relative configuration as (5*S**,8*S**,10*R**,14*R**). This result in combination with the ECD calculation of (5*S*,8*S*,10*R*,14*R*)-**1** allowed the unambiguous configurational assignment of **1** as (5*S*,8*S*,10*R*,14*R*). Moreover, the absolute structure of compound **1** was confirmed by anomalous dispersion of Cu Kα radiation to (5*S*,8*S*,10*R*,14*R*) (Figure 4), thus unequivocally

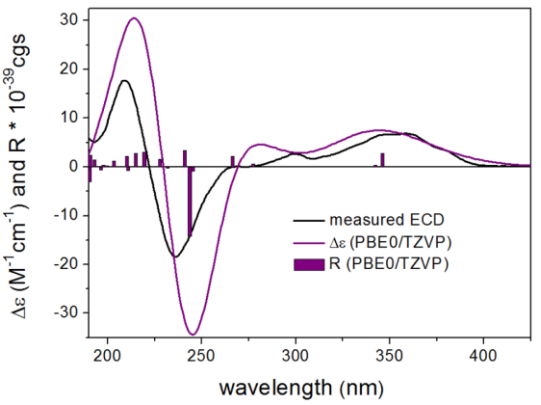

Figure 2. Experimental ECD spectrum of **1** in MeCN compared with the PBE0/TZVP PCM/MeCN ECD spectrum of (5*S*,8*S*,10*R*,14*R*)-**1** computed for the single CAM-B3LYP/TZVP PCM/MeCN conformer. Bars represent the rotational strength values.

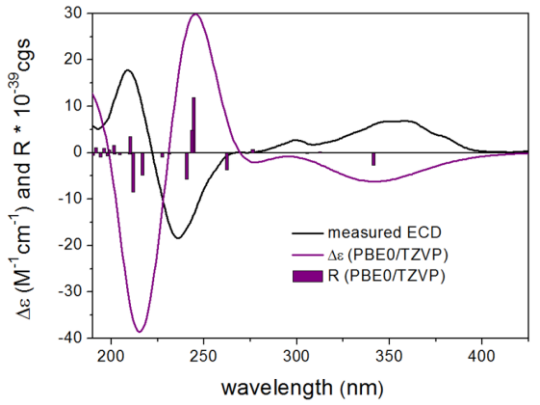

Figure 3. Experimental ECD spectrum of **1** in MeCN compared with the PBE0/TZVP PCM/MeCN ECD spectrum of (5*S*,8*R*,10*S*,14*R*)-**1** computed for the single low-energy CAM-B3LYP/TZVP PCM/MeCN conformer. Bars represent the rotational strength values.

supporting the predicted configuration. Further crystal data are listed in Table S75 (Supporting Information).

The molecular formula of paspalinine-13-ene (**2**) was established as $C_{27}H_{29}NO_3$ on the basis of the pseudomolecular ion peak at m/z 416.2215 $[M + H]^+$ in the HRESIMS spectrum, accounting for 14 degrees of unsaturation. The ^{1}H NMR data of **2** (Table 1) were similar to those of the known indole diterpenoid paspalicine,[44,45] except for an additional olefinic proton resonating at δ_H 6.52 (H-14) and the absence of the aliphatic signal at H-13, suggesting a double bond at $\Delta^{13(14)}$. The HMBC correlations from H_2-15 to two olefinic carbons C-13 and C-14 as well as to C-3 and C-16, together with correlations from H-14 to C-4, C-12, and C-16, confirmed the proposed structure of **2**. The relative configuration of **2** was deduced from the NOESY spectrum, which revealed a correlation between H-16 and H_3-26 and no correlation between H_3-25 and H-16. Compound **2** is known as a synthetic product described in a patent application together with a series of other synthetic paspalinine derivatives with

DOI: 10.1021/acs.jnatprod.8b00723
J. Nat. Prod. 2019, 82, 1412−1423

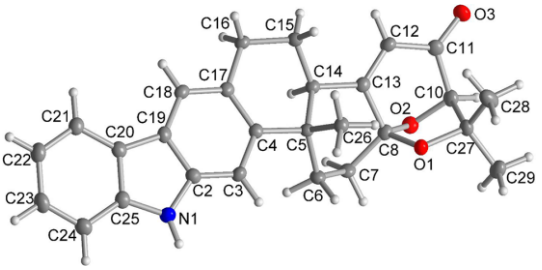

Figure 4. Molecular structure of one of the two symmetry-independent molecules in the crystal of **1** (50% thermal ellipsoids). For an image of both independent molecules in the asymmetric unit and their hydrogen-bonding interaction, see Figure S74 in the Supporting Information.

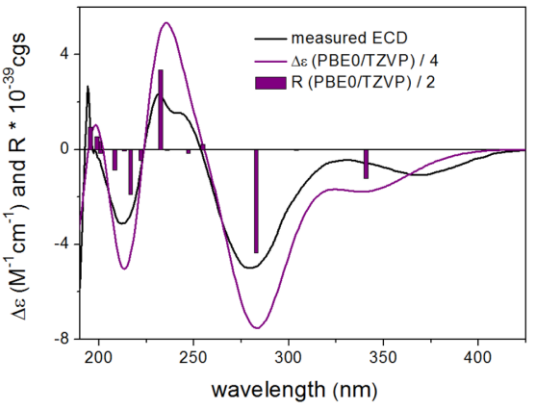

Figure 5. Experimental ECD spectrum of **3** in MeCN compared with the Boltzmann-averaged PBE0/TZVP PCM/MeCN ECD spectrum of (3*S*,4*S*,7*S*,9*R*,16*S*)-**3** computed for the low-energy (≥1%) CAM-B3LYP/TZVP PCM/MeCN conformers. Bars represent the rotational strength values of conformer A.

potent potassium channel blocking activity for use in the treatment of glaucoma.[38] In this paper, we report **2** as a new natural product for the first time and provide complete NMR data of this compound.

The HRESIMS spectrum of 7-hydroxypaxilline-13-ene (**3**) showed a prominent pseudomolecular ion peak at *m*/*z* 434.2325 $[M + H]^+$ consistent with the molecular formula $C_{27}H_{31}NO_4$, indicating 13 degrees of unsaturation. The ^1H and ^{13}C NMR data of **3** (Table 1) closely resembled those of **2**, apart from an additional hydroxy signal resonating at δ_H 6.54. The HMBC correlations from the extra hydroxy function to C-6, C-7, and C-12 suggested cleavage of the 1,3-dioxolane ring in the structure of **3**, which was in agreement with the loss of one degree of unsaturation in comparison with **2**. The cross-peak 7-OH/H-9 in the ROESY spectrum indicated the α-orientation of the hydroxy group. Moreover, the ROESY correlation H-16/H_3-26 implied a trans-3,16-ring junction as observed in former congeners.[20,52]

For the configurational assignment of **3**, the same solution TDDFT-ECD computational protocol was applied as for **1**. MMFF conformational search of (3*S*,4*S*,7*S*,9*R*,16*S*)-**3** resulted in 12 conformer clusters in a 21 kJ/mol energy window, the DFT reoptimization of which yielded three low-energy conformers over 1% population at both applied levels. ECD spectra computed at various levels for both sets of conformers reproduced the experimental ECD spectrum (Figure 5), allowing elucidation of the absolute configuration as (3*S*,4*S*,7*S*,9*R*,16*S*), which was in accordance with that of **1** and of paxilline.

The molecular formula of **4** was established on the basis of the HRESIMS as $C_{28}H_{35}NO_5$, accounting for 12 degrees of unsaturation. The ^1H and ^{13}C NMR data of **4** (Table 1) were similar to those of **3**, with additional signals of a methoxy group resonating at δ_H 3.38/δ_C 49.0 and of a hydroxy group at δ_H 4.58 in addition to the methylene protons at δ_H 1.64/1.83 (H_2-14). The methoxy group was assigned based on the observed HMBC correlation from 7-OMe to C-7. Furthermore, HMBC correlations from the hydroxy proton 13-OH to C-4, C-12, C-13, and C-14 confirmed its attachment to C-13. Accordingly, the planar structure of **4** was elucidated as 7-methoxypaxilline. The ROESY data suggested that **4** adopts the same relative configuration as **3**, and based on the displayed cross-peaks 7-OMe/H-9 and 13-OH/H_3-25, the hydroxy group 13-OH and 7-OMe are suggested to have a cofacial orientation.

The molecular formulas of 7-methoxypyrapaxilline (**5**) and pyrapaxilline-6-ene (**6**) were determined as $C_{38}H_{49}NO_6$ and $C_{37}H_{45}NO_5$, respectively, on the basis of prominent pseudomolecular ion peaks in the HRESIMS spectra. The ^1H and ^{13}C NMR data of these two metabolites (Table 2) were in good agreement with those of pyrapaxilline (**21**)[53] isolated in this study, indicating that both compounds share the same eight-membered ring skeleton characteristic of the janthitremane group of indole diterpenoids isolated from *Eupenicillium shearii*.[54] Compound **5** differed from pyrapaxilline by the presence of a methoxy group attached to C-7, instead of the oxymethine proton in the known analogue. This was confirmed by the respective HMBC correlation from 7-OMe to C-7. Further comparison of NMR data of derivatives **5** and **6** revealed that **6** displays an olefinic signal (δ_H 5.64/δ_C 110.9 and a sp^2 carbon at δ_C 145.1), instead of a 7-OMe group, that were assigned to the double bond at $\Delta^{6(7)}$, accounting for the additional degree of unsaturation of compound **6**. The NMR chemical shift data were in accordance with the recently reported shearinines L and M, bearing double bonds at the same position as well.[55] Based on the similarity of the NMR data with regard to signals of rings D−H of compounds **5** and **6**, including the NOE correlations with those of **4** and pyrapaxilline and considering their common biosynthetic origin, **5** and **6** are suggested to share the same relative configuration that is characteristic for shearinine/paspalinine derivatives. Consequently, the structures of **5** and **6** were established as new shearinine derivatives, and shearinine N and O were proposed as their trivial names, respectively.

The molecular formula of shearinine P (**7**) was determined as $C_{37}H_{47}NO_7$ on the basis of the prominent pseudomolecular ion peak at *m*/*z* 618.3416 $[M + H]^+$ in the HRESIMS spectrum. The ^1H and ^{13}C NMR data of **7** (Table 2) showed close similarity to those of pyrapaxilline.[53] However, the olefinic signals at C-18 and C-2 of pyrapaxilline were replaced by two carbonyl signals at δ_C 174.6 (C-2) and δ_C 204.6 (C-18), respectively. These signals suggested the presence of a keto-amide ring in the structure of **7**, as described for shearinine C,[54] which is presumably formed via oxidation of the indole moiety at the C-2−C-18 double bond. The presence

DOI: 10.1021/acs.jnatprod.8b00723
J. Nat. Prod. 2019, 82, 1412−1423

Table 2. ^{1}H and ^{13}C NMR Data for 5–9

	5[a]		6[b]		7[a]		8[a]		9[a]	
position	δ_C type	δ_H (J in Hz)	δ_C type	δ_H (J in Hz)	δ_C type[c]	δ_H (J in Hz)	δ_C type[c]	δ_H (J in Hz)	δ_C type[c]	δ_H (J in Hz)
1-NH		10.60, s		10.59, s		9.09, s		9.09, s		7.28, br s (NH_2)
2	151.8, C		151.7, C		174.6, C		174.5, C		176.5, C	12.30, br s (COOH)
3	50.5, C		50.3, C		56.6, C		56.4, C		52.7, C	
4	42.5, C		42.8, C		43.3, C		43.4, C		41.7, C	
5	25.0, CH_2	2.41 m; 1.79, m	30.4, CH_2	3.01, br d (17.5); 2.43, m	24.9, CH_2	2.34, ov; 1.70, m	23.5, CH_2	2.19, td (14.1, 4.5); 1.73, m	25.0, CH_2	2.38, m; 1.53, ov
6	27.3, CH_2	2.47, m; 1.88, m	110.9, CH	5.64, br dt (6.4, 2.4)	27.8, CH_2	2.07, m; 1.54, m	26.7, CH_2	2.35, td (14.9, 3.3); 1.62, td (14.9, 4.7)	27.7, CH_2	2.06, m; 1.53, ov
7	97.2, C		145.1, C		71.9, CH	4.67, ddt (10.3, 8.0, 2.2)	96.6, C		72.1, CH	4.69, br ddt (10.0, 7.7, 2.1)
9	78.5, CH	3.92, s	85.9, CH	4.02, s	82.9, CH	3.60, d (1.9)	78.0, CH	3.86, s	82.9, CH	3.63, d (1.9)
10	197.2, C		195.1, C		197.6, C		197.1, C		197.5, C	
11	121.3, CH	5.76, s	115.9, CH	5.80, s	119.3, CH	5.66, br d (1.9)	121.7, CH	5.68, s	119.3, CH	5.77, br d (2.0)
12	160.3, C		154.5, C		168.4, C		159.7, C		168.7, C	
13	75.8, C		73.9, C		75.1, C		75.0, C		75.2, C	
14	32.6, CH_2	1.71, m; 1.64, m	31.8, CH_2	1.94, ov; 1.85, m	30.3, CH_2	1.59, m; 1.44, m	30.1, CH_2	1.51, td (13.0, 3.7); 1.45, m	29.2, CH_2	1.72, br td (13.4, 4.2); 1.53, ov
15	21.0, CH_2	1.89, m; 1.60, m	21.1, CH_2	1.94, ov; 1.66, m	24.9, CH_2	1.74, m; 1.30, br dt (9.8, 3.4)	24.9, CH_2	1.73, m; 1.30, m	22.2, CH_2	1.53, ov; 148 m
16	49.2, CH	2.68, m	49.1, CH	2.72, m	35.2, CH	2.88, ov	35.0, CH	2.92, m	33.4, CH	2.89, m
17	27.0, CH_2	2.61, dd (12.8, 6.1); 2.29, dd (12.8, 10.9)	26.8, CH_2	2.62, dd (12.8, 6.2); 2.29, dd (12.8, 11.0)	47.8, CH_2	2.88, ov; 2.34, ov	47.7, CH_2	2.88, dd (17.5, 6.6); 2.35, ov	42.6, CH_2	2.76, dd (14.9, 2.1); 2.58, m
18	114.9, C		114.8, C		204.6, C		204.8, C		200.4, C	
19	122.4, C		122.4, C		130.8, C		130.9, C		113.7, C	
20	113.0, CH	7.31, s	113.0, CH	7.31, s	122.0, CH	7.47, s	121.9, CH	7.45, s	125.0, CH	7.91, s
21	133.5, C		133.6, C		140.5, C		140.5, C		127.9, C	
22	35.6, CH_2	3.28, ov[d]	35.6, CH_2	3.29, ov	36.4, CH_2	3.44, dt (22.8, 2.5); 3.49 dt (22.8, 2.5)	36.4, CH_2	3.43, d (22.8); 3.49, d (22.8)	35.5, CH_2	3.30, ov
23	141.8, C		141.8, C		149.3, C		149.0, C		151.0, C	
24	72.9, C		73.0, C		72.9, C		72.9, C		73.0, C	
26	70.8, C		70.8, C		70.5, C		70.8, C		70.8, C	
27	33.9, CH_2	2.38, m	33.9, CH_2	2.37, t (2.8)	33.4, CH_2	2.34, m	33.4, CH_2	2.35, ov	33.3, CH_2	2.29, t (2.5)
28	131.5, C		131.5, C		130.5, C		130.7, C		130.8, C	
29	138.0, C		138.1, C		148.2, C		148.0, C		150.7, C	
30	101.3, CH	7.05, br d (0.8)	101.4, CH	7.06, d (0.8)	116.5, CH	6.88, s	116.2, CH	6.88, s	105.4, CH	6.56, s
31	139.1, C		139.3, C		136.4, C		136.2, C		150.7, C	
32	16.2, CH_3	1.23, s	16.4, CH_3	1.27, s	16.0, CH_3	1.46, s	16.1, CH_3	1.44, s	14.4, CH_3	1.38, s
33	19.1, CH_3	0.91, s	19.7, CH_3	1.01, s	19.2, CH_3	0.82, s	19.5, CH_3	0.85, s	19.4, CH_3	0.83, s
34	71.0, C		72.9, C		70.9, C		70.9, C		70.8, C	
35	25.8, CH_3	1.21, s	26.8, CH_3	1.14, s	25.6, CH_3	1.12, s	25.5, CH_3	1.15, s	25.6, CH_3	1.14, s
36	26.2, CH_3	1.23, s	27.1, CH_3	1.25, s	25.4, CH_3	1.16, s	25.8, CH_3	1.18, s	25.5, CH_3	1.18, s
37	30.4, CH_3	1.35, s	30.5, CH_3	1.35, s	30.0, CH_3	1.36, s	30.1, CH_3	1.35, s	29.8, CH_3	1.34, s
38	30.4, CH_3	1.35, s	30.6, CH_3	1.35, s	30.0, CH_3	1.36, s	30.1, CH_3	1.36, s	29.8, CH_3	1.34, s
39	29.4, CH_3	1.24, s	29.4, CH_3	1.25, s	28.8, CH_3	1.20, s	28.7, CH_3	1.20, s	28.9, CH_3	1.22, s

DOI: 10.1021/acs.jnatprod.8b00723
J. Nat. Prod. 2019, 82, 1412−1423

Table 2. continued

	5[a]		6[b]		7[a]		8[a]		9[a]	
position	δ_C type	δ_H (J in Hz)	δ_C type	δ_H (J in Hz)	δ_C type[c]	δ_H (J in Hz)	δ_C type[c]	δ_H (J in Hz)	δ_C type[c]	δ_H (J in Hz)
40	29.5, CH_3	1.24, s	29.5, CH_3	1.25, s	29.2, CH_3	1.24, s	29.2, CH_3	1.24, s	28.9, CH_3	1.22, s
7-OMe	49.0, CH_3	3.38, s					48.6, CH_3	3.32, s		
13-OH		4.56, s		4.88, s		4.92, s		4.47, s		4.90, s
34-OH		4.45, s		4.53, s		4.28, s		4.38, s		4.30, s

[a]Recorded at 600 MHz (^{1}H) and 300 MHz (^{13}C) in DMSO-d_6. [b]Recorded at 300 MHz (^{1}H) and 75 MHz (^{13}C) in DMSO-d_6. [c]Chemical shifts extracted from HSQC and HMBC spectra. [d]ov stands for overlapped signals.

of this substructure in **7** was further corroborated by HMBC correlations from H_2-17 to C-18, from H-20 to C-18, from H-30 to C-18 (long-range correlation), and from NH and H_3-32 to C-2. Moreover, **7** exhibited the same molecular formula as shearinine C.[47] The double bond in ring A, however, was switched from $\Delta^{27(28)}$ to $\Delta^{23(28)}$ for compound **7**, which was supported by HMBC correlations from H_3-37/H_3-38 to C-23, as well as from H_2-22 and H_2-27 to both olefinic carbons C-23 and C-28. Thus, the planar structure of **7** was identified as the ring-opened 7-desmethoxy derivative of **5**, in which the C-2−C-18 bond of the indole moiety was oxidized and cleaved.

The MMFF search of (3*S*,4*R*,7*S*,9*R*,13*S*,16*S*)-7 resulted in 18 conformer clusters in a 21 kJ/mol window, the DFT reoptimization of which yielded five and six low-energy conformers above 1% at the B3LYP/6-31+G(d,p) and the CAM-B3LYP/TZVP PCM/MeCN levels, respectively. ECD spectra computed at various levels gave moderate agreement with the experimental ECD spectrum (see Figure S73). While the B3LYP and the PBE0 functionals resembled well the 197 and the 290 nm transitions, they failed to reproduce the 249 nm transition. The BH&HLYP and CAM-B3LYP functionals on the other hand gave better results for this transition but were not successful in the low-wavelength region.[48] It is possible that the real conformational distribution is somewhat different from the estimated one (results not shown). Based on the approximate overall ECD agreement, the absolute configuration was determined as (3*S*,4*R*,7*S*,9*R*,13*S*,16*S*).

The pseudomolecular ion peak of **8** was 30 amu larger than that of **7**, as evident from the HRESIMS spectrum, which was consistent with the molecular formula $C_{38}H_{49}NO_8$. The ^{1}H and ^{13}C NMR data of **8** (Table 2) were almost identical to those of **7**, with the exception of an additional methoxy signal at δ_H 3.32/δ_C 48.6 instead of the methine at position 7. The connection of this group to δ_C 96.6 (C-7) was verified by the respective HMBC correlation. Therefore, the structure of **8** was determined as a new shearinine congener, and the name 7-methoxyshearinine P was suggested. The ^{1}H and ^{13}C NMR data of shearinine Q (**9**) (Table 2) closely resembled those of **7**. Compound **9**, however, displayed an increase in the molecular weight of 18 amu compared to **7**, which together with the loss of one degree of unsaturation indicated cleavage of the keto-amide ring in the structure of **9**. This was further corroborated by the presence of free amino and carboxylic acid groups resonating at δ_H 7.28 and 12.30, respectively. Thus, the planar structure of **9** was elucidated. Based on biosynthetic considerations and on the similarity of NOESY data of **7**−**9** it is assumed that **8** and **9** share the same relative stereochemistry as **7**.

The structures of the remaining 13 known compounds were established based on their spectroscopic data, as well as by comparison with the literature. These natural products were identified as emindole SB (**10**),[14,56] shearinine F (**11**),[52,57] paspalicine (**12**),[44,45] 21-isopentenylpaxilline (**13**),[54] paxilline (**14**),[14,20,56] dehydroxypaxilline (**15**),[56] paspalinine (**16**),[27,58] 6,7-dehydropaxilline (**17**),[59] paspaline (**18**),[44,60] 7-hydroxy-13-dehydroxypaxilline (**19**),[54,61] 10β-hydroxy-13-desoxypaxilline (**20**),[61] pyrapaxilline (**21**),[53] and paspalitrem A (**22**),[62] as shown in Figure S80.

An additional experiment was performed to exclude the possibility that **4**, **5**, and **8** are artifacts arising from their corresponding analogues (paxilline, pyrapaxilline, and **7**, respectively) during the isolation process. For this purpose, 1 mg of paxilline, pyrapaxilline, or **7** was each dissolved in 1.0 mL

DOI: 10.1021/acs.jnatprod.8b00723
J. Nat. Prod. 2019, 82, 1412−1423

of MeOH, exposed to light for 72 h at room temperature, and then analyzed by HPLC and LC-MS. The results showed no additional peak in the HPLC chromatograms nor in the MS spectra, indicating that the new methoxylated analogues **4**, **5**, and **8** are true natural products and not artifacts formed through methylation when using MeOH.

The biosynthetic pathway leading to indole diterpenoids has been widely discussed in the literature. These compounds are suggested to be formed through a common intermediate, 3-geranylgeranylindole, followed by a series of epoxidation, oxidation, cyclization, and prenylation reactions, which provide their large chemical diversity.[16,18,40,41] Interestingly, compound **1** bears a rare carbazole motif, which has previously been reported for xiamycin A,[43,63] an uncommon indole sesquiterpene isolated from the bacterial endophyte *Streptomyces* sp. Following characterization of the corresponding biosynthetic gene cluster, it was suggested that a flavoprotein-catalyzed hydroxylation of the indole moiety takes place forming an indole C-3-hydroxyiminium species. Subsequently, the resulting C-2 carbanion equivalent is attacked by the C-23 olefinic function, leading to a cyclization reaction.[63] Finally, dehydration and proton loss followed by spontaneous oxidative aromatization would lead to the formation of the carbazole moiety of xiamycin A.[63] Accordingly, compound **1** is proposed to undergo a similar cyclization mechanism for geranylgeranylindole, as described for xiamycin A (Figure S81). However, considering that xiamycin A is a bacterial compound, the cyclization mechanism for geranylgeranylindole in **1** might be novel and warrants further investigation. Additional oxidation steps followed by cyclization would yield the keto function at C-11 and ketal formation at C-8, thus forming the rings F and G in **1**, which is related to paspalicine.

All isolated compounds were evaluated for their cytotoxic activity toward the murine L5178Y cell line (Table 3). Among the tested natural products, compound **1** exhibited the most pronounced activity, with an IC_{50} value of 3.6 μM, which was stronger than that of the positive control kahalalide F (IC_{50} 4.3 μM). Compounds **2**, **3**, **6**, **7**, and 7-hydroxy-13-dehydroxypaxilline (**19**) displayed cytotoxicity with IC_{50} values in the range of 5.3−8.1 μM. In addition, the cytotoxicity of the isolated compounds toward the A2780 human ovarian cancer cell line was determined (Table 3). Compounds **1**, **6**, emindole SB (**10**), and paspaline (**18**) showed pronounced activity with IC_{50} values of 5.3−8.7 μM. The remaining compounds were found to be inactive against both cell lines. The unusual motif of the indole diterpenoid scaffold in **1**, bearing an aromatic ring C, is suggested to be determinant of its strong cytotoxicity [**1** vs paspalicine (**12**)]. A double bond at $\Delta^{13(14)}$ increases the activity of paspalinine derivatives [**2** vs paspalicine (**12**)], whereas it has little influence on the cytotoxicity of paxilline derivatives [**3** vs 7-hydroxy-13-dehydroxypaxilline (**19**)]. Furthermore, a double bond at $\Delta^{6(7)}$ slightly enhances the cytotoxicity of janthitremane derivatives [**6** vs pyrapaxilline (**21**)]. Cleavage of the keto-amide ring in the seven-membered ring skeleton of indole diterpenoid leads to loss of activity, as observed in **9** vs **7**. Meanwhile, the replacement of a proton at C-7 by a methoxy group tends to attenuate the activity [pyrapaxilline (**21**) vs **5**, and **7** vs **8**]. Interestingly, Sallam et al. demonstrated the antiproliferative and antimigratory activities of emindole SB (**10**) and paspaline (**18**) against human breast cancer cells, showing no BK channel inhibitory effect, which renders these compounds interesting pharmacophores for further biological studies.[35]

Table 3. Cytotoxicity (IC_{50} in μM) of 1−10, 13, 15, 18−22 toward L5178Y, A2780, J82, and HEK-293 Cell Lines

	1	2	3	4	5	6	7	8	9	10	13	15	18	19	20	21	22
L5178Y[a]	3.6	5.3	5.3	–[f]	–[f]	8.1	7.6	–[f]	–[f]	18.3	12.9	–[f]	–[f]	6.2	–[f]	10.9	–[f]
A2780[b]	8.7 (3.3)[e]	12.2 (1.8)[e]	–[f]	12.2	32.2	7.8 (4.8)[e]	11.9 (2.4)[e]	19.4	51.5	8.2 (5.4)[e]	–[f]	17.1	5.3 (8.1)[e]	–[f]	28.5	12.8	19.8
J82[c]	40.6	42.1	–[g]	55.3	96.7	31.7	29.4	73.0	–[f]	–[g]	–[g]	–[g]	–[g]	–[g]	–[g]	–[g]	–[g]
HEK-293[d]	28.5	21.7	27.9	–[g]	–[g]	37.4	28.3	–[g]	–[g]	44.6	–[g]	–[g]	43.0	39.8	–[g]	–[g]	–[g]

[a]Kahalalide F (IC_{50} 4.3 μM) as positive control. Cisplatin (IC_{50} 1.2 μM,[b] 0.8 μM,[c] and 6.2 μM[d]) as positive control. [e]Selectivity index (SI): IC_{50} values against HEK-293 cells divided by IC_{50} value against the A2780 cell line. [f]Inactive. [g]Not tested.

DOI: 10.1021/acs.jnatprod.8b00723
J. Nat. Prod. 2019, 82, 1412−1423

A high-content analysis-based fluorescent live/dead assay of the new compounds was applied to the human urothelial bladder cancer cell line J82 (Table 3). Bladder cancer is known to rapidly develop chemoresistance. Thus, compounds active against bladder cancer cell lines are of high scientific interest. In the fluorescent live/dead assay, direct counts of live and dead cells were acquired by the fluorescent imaging system. Most of the tested compounds gave IC_{50} values between 30 and 100 μM toward J82 cells, thus showing considerably lower potency compared to their activity against L5178Y or A2780 cells (Figures S86 and S87).

Furthermore, active compounds with IC_{50} values of <10 μM against L5178Y or A2780 cells [**1**–**3**, **6**, **7**, emindole SB (**10**), paspaline (**18**), and 7-hydroxy-13-dehydroxypaxilline (**19**)] were tested against the human embryonic kidney cell line HEK-293 for preliminary estimation of their selectivity index (SI). Compounds **1**, **6**, emindole SB (**10**), and paspaline (**18**) showed the highest selectivity among tested compounds with SI values in the range from 3.3 to 8.1, comparable to that of the positive control cisplatin (SI = 5.2), which merits further pharmacological investigation.

EXPERIMENTAL SECTION

General Experimental Procedures. Optical rotations were determined with a Jasco P-2000 polarimeter. ^{1}H (600 and 300 MHz), ^{13}C (150 and 75 MHz), and 2D NMR were recorded on Bruker AVANCE DMX 600 or 300 NMR spectrometers. The chemical shifts (δ) were referred to the residual solvent peaks at δ_H 2.50 (DMSO-d_6) and δ_H 7.26 ($CDCl_3$) ppm for ^{1}H, and δ_C 39.5 (DMSO-d_6) and δ_C 77.2 ($CDCl_3$) ppm for ^{13}C. Mass spectra (ESI) were measured with a Finnigan LCQ Deca mass spectrometer, and HRMS (ESI) spectra were recorded with an FTHRMS-Orbitrap (Thermo-Finnigan) mass spectrometer. HPLC analysis was performed with a Dionex UltiMate 3000 HPLC system with an UltiMate 3000 pump coupled to a photodiode array detector (DAD 3000 RS), with the detection wavelength set at 235, 254, 280, and 340 nm. The column was prefilled with Eurospher 100-10 C_{18}, 125 × 4 mm (Knauer, Germany). The following gradient was used for routine analysis (MeOH: 0.1% HCOOH in H_2O): 0 min (65% MeOH); 2 min (65% MeOH); 25.5 min (100% MeOH); 35.5 min (100% MeOH). Semipreparative HPLC was performed with a Merck Hitachi Chromaster HPLC system (UV detector 5410; pump 5110; column Eurospher 100-10 C_{18}, 300 × 8 mm, Knauer, Germany; flow rate 5 mL/min). Column chromatography was performed on silica 60 M (0.040–0.063 mm; Macherey-Nagel, Germany) and on Sephadex LH-20 stationary phases. TLC plates precoated with silica gel 60 F_{254} (Macherey-Nagel, Germany) were used for analysis; detection was under UV 254 and 366 nm. ECD spectra were recorded on a J-810 spectropolarimeter.

Fungal Material. The fungus *Penicillium* sp. (strain ZO-R1-1) was isolated[64] from healthy roots of *Zingiber officinale*, collected in May 2016 at Banyumas, the Central Java Province, Indonesia. The taxonomic identification of the fungus was conducted according to a molecular biology protocol by DNA amplification and gene sequencing in the ITS region as previously described,[64] followed by BlastN search in the NCBI database. The sequence was submitted to GenBank (accession no. MH602299). The fungus strain was deposited in one of the author's laboratory (P.P.).

Fermentation, Extraction, and Isolation. The fungus was inoculated on solid rice medium, which was prepared by autoclaving 100 g of rice in 100 mL of demineralized water in a 1 L Erlenmeyer flask. The fermentation was performed in 5 flasks under static conditions at room temperature for 3 weeks. The fungal culture was extracted with 500 mL of ethyl acetate added to each flask, and the extract was subsequently dried under vacuum to afford 7.6 g. Fat was removed from the extract by liquid–liquid separation between *n*-hexane and 90% aqueous MeOH. The MeOH fraction (4.6 g) was subjected to vacuum liquid chromatography over silica gel 60 using a step gradient elution, employing mixtures of *n*-hexane–EtOAc followed by CH_2Cl_2–MeOH to yield 16 fractions. Fractions 80HEA, 70HEA, 60HEA, and 50HEA eluted with *n*-hexane–EtOAc (8:2), (7:3), (6:4), and (5:5), respectively, were selected for further separation according to their HPLC chromatograms. Separation of fraction 80HEA (173.2 mg) was carried out on Sephadex LH-20 employing CH_2Cl_2–MeOH as mobile phase, followed by purification using semipreparative HPLC with MeOH–H_2O as mobile phase to yield the new compounds **1** (2.4 mg) and **2** (1.3 mg), along with known compounds shearinine F (1.1 mg), paspalicine (4.1 mg), paspalinine (11.7 mg), and paspalitrem A (3.0 mg). Following the same procedure, emindole SB (3.5 mg), dehydroxypaxilline (1.9 mg), and paspaline (1.9 mg) were obtained from fraction 70HEA (398.2 mg). The new compounds **3** (3.7 mg), **4** (7.0 mg), **5** (10.9 mg), **6** (4.5 mg), **7** (4.5 mg), **8** (1.4 mg), and **9** (2.5 mg), as well as known analogues 21-isopentenylpaxilline (11.2 mg), paxilline (38.0 mg), 6,7-dehydropaxilline (1.8 mg), 7-hydroxy-13-dehydroxypaxilline (3.2 mg), and pyrapaxilline (19.8 mg), were afforded from fraction 60HEA (513.9 mg). In the same manner, chromatographic separation of fraction 50HEA (133.9 mg), yielded the known compound 10β-hydroxy-13-desoxypaxilline (6.7 mg).

*Shearilicine (**1**):* colorless, crystal; $[\alpha]_D^{20}$ +201 (*c* 0.27, $CHCl_3$); UV (MeOH, photodiode array) λ_{max} 301, 261, 239 nm; ECD (MeCN, λ [nm] ($\Delta\varepsilon$), *c* 0.121 mM) 379sh (+3.57), 358 (+6.87), 345sh (+6.54), 332sh (+4.43), 300 (+2.69), 246sh (−11.68), 236 (−18.43), 208 (+17.70); ^{1}H and ^{13}C NMR data, see Table 1; HRESIMS *m*/*z* 414.2063 $[M + H]^+$ (calcd for $C_{27}H_{28}NO_3$, 414.2064).

*Paspalinine-13-ene (**2**):* colorless, crystal; $[\alpha]_D^{20}$ −63 (*c* 0.10, $CHCl_3$); UV (MeOH, photodiode array) λ_{max} 299, 229 nm; ECD (MeCN, λ [nm] ($\Delta\varepsilon$), *c* 0.175 mM) 369 (+4.59), 302sh (−12.62), 294 (−13.17), 249 (+0.72), 227sh (+2.72), 215sh (+3.20), 204 (+3.35); ^{1}H and ^{13}C NMR data, see Table 1; HRESIMS *m*/*z* 416.2215 $[M + H]^+$ (calcd for $C_{27}H_{30}NO_3$, 416.2220).

*7-Hydroxypaxilline-13-ene (**3**):* white, amorphous powder; $[\alpha]_D^{20}$ −365 (*c* 0.10, $CHCl_3$); UV (MeOH, photodiode array) λ_{max} 287, 229 nm; ECD (MeCN, λ [nm] ($\Delta\varepsilon$), *c* 0.346 mM) 402sh (−0.34), 369 (−1.07), 290sh (−4.24), 279 (−5.00), 244sh (+1.51), 231 (+2.34), 219sh (−2.12), 212 (−3.12); ^{1}H and ^{13}C NMR data, see Table 1; HRESIMS *m*/*z* 434.2325 $[M + H]^+$ (calcd for $C_{27}H_{32}NO_4$, 434.2326).

*7-Methoxypaxilline (**4**):* yellow, amorphous powder; $[\alpha]_D^{20}$ +11 (*c* 0.10, MeOH); UV (MeOH, photodiode array) λ_{max} 281, 230 nm; ECD (MeCN, λ [nm] ($\Delta\varepsilon$), *c* 0.054 mM) 368 (−0.62), 300 (+1.00), 247 (+3.42), 233 (−3.57), 223 (+2.57), 205 (−12.00); ^{1}H and ^{13}C NMR data, see Table 1; HRESIMS *m*/*z* 466.2587 $[M + H]^+$ (calcd for $C_{28}H_{36}NO_5$, 466.2588).

*Shearinine N (**5**):* yellow, amorphous powder; $[\alpha]_D^{20}$ +5 (*c* 0.10, MeOH); UV (MeOH, photodiode array) λ_{max} 306, 238 nm; ECD (MeCN, λ [nm] ($\Delta\varepsilon$), *c* 0.162 mM) 359 (−0.30), 303 (+1.20), 264 (−2.11), 240 (+3.82), 212 (−8.49); ^{1}H and ^{13}C NMR data, see Table 2; HRESIMS *m*/*z* 616.3620 $[M + H]^+$ (calcd for $C_{38}H_{50}NO_6$, 616.3633).

*Shearinine O (**6**):* yellow, amorphous powder; $[\alpha]_D^{20}$ −5 (*c* 0.10, MeOH); UV (MeOH, photodiode array) λ_{max} 308, 257, 241 nm; ECD (MeCN, λ [nm] ($\Delta\varepsilon$), *c* 0.128 mM) 375 (−3.99), 318 (+6.15), 254sh (−3.49), 248 (−3.54), 220 (+1.69), 203 (−2.59); ^{1}H and ^{13}C NMR data, see Table 2; HRESIMS *m*/*z* 584.3361 $[M + H]^+$ (calcd for $C_{37}H_{46}NO_5$, 584.3370).

*Shearinine P (**7**):* white, amorphous powder; $[\alpha]_D^{20}$ −76 (*c* 0.20, $CHCl_3$); UV (MeOH, photodiode array) λ_{max} 309, 243 nm; ECD (MeCN, λ [nm] ($\Delta\varepsilon$), *c* 0.081 mM) 341 (−2.46), 294 (+9.42), 250 (−30.80), 231sh (−19.32), 213sh (+1.82); ^{1}H and ^{13}C NMR data, see Table 2; HRESIMS *m*/*z* 618.3416 $[M + H]^+$ (calcd for $C_{37}H_{48}NO_7$, 618.3425).

*7-Methoxyshearinine P (**8**):* white, amorphous powder; $[\alpha]_D^{20}$ −19 (*c* 0.05, MeOH); UV (MeOH, photodiode array) λ_{max} 309, 224 nm; ECD (MeCN, λ [nm] ($\Delta\varepsilon$), *c* 0.077 mM) 367sh (−0.88), 340 (−1.12), 292 (+3.12), 256 (−8.17), 212 (−8.86); ^{1}H and ^{13}C NMR

DOI: 10.1021/acs.jnatprod.8b00723
J. Nat. Prod. 2019, 82, 1412–1423

data, see Table 2; HRESIMS m/z 648.3523 $[M + H]^+$ (calcd for $C_{38}H_{50}NO_8$, 648.3531).

*Shearinine Q (**9**):* yellow, amorphous powder; $[\alpha]_D^{20}$ −33 (c 0.20, $CHCl_3$); UV (MeOH, photodiode array) λ_{max} 381, 306, 245 nm; ^1H and ^{13}C NMR data, see Table 2; HRESIMS m/z 636.3530 $[M + H]^+$ (calcd for $C_{37}H_{50}NO_8$, 636.3531).

Cytotoxicity Assay. Cytotoxicity toward the murine lymphoma cell line L5178Y was tested by the MTT method with kahalalide F as positive control and media with 0.1% DMSO as negative control as described earlier.[65] The rate of cell survival of the ovarian cancer cell line A2780 and of the human embryonic kidney cell line HEK-293 under the action of test substances was evaluated by an improved MTT assay as previously described.[66] The A2780 and HEK-293 cells were seeded into 96-well plates (Sarstedt, Germany) and incubated overnight. Then, cells were exposed to increasing concentrations of compounds in phosphate-buffered saline (PBS) and positive control cisplatin. After 72 h treatment, 25 μL of MTT solution (5 mg/mL) was added into each well and incubated for 15 min. The formazan precipitate was dissolved in 75 μL of DMSO per well. Absorbance was then measured at 544 and 690 nm using the BMG FLUOstar microplate reader (BMG Labtechnologies Offenburg, Germany).

High Content Analysis Based Fluorescent Live/Dead Assay. Live and dead cells were assayed by high content analysis (HCA). Briefly, the urothelial bladder cancer cell line J82 was treated with increasing concentrations of compounds in 96-well plates (Sarstedt, Germany). After 72 h treatment, cells were stained with a mixture of Hoechst 33342 (Sigma-Aldrich, St. Louis, MO, USA), calcein AM (Merck Millipore, Germany), and propidium iodide (Santa Cruz Biotechnology, Heidelberg) for cell nuclei and live and dead cells, respectively. The staining solution was replaced by PBS after 20 min. Images were acquired with the ArrayScan XTI Live High Content Platform (Thermo Fisher Scientific Inc., USA) using excitation filters of 386 nm (Hoechst 33342), 485 nm (calcein AM), and 560 nm (propidium iodide), respectively. Results were analyzed using HCS Studio: Cellomics Scan (Thermo Fisher Scientific Inc., USA).

Computational Section. Mixed torsional/low-frequency mode conformational searches were carried out by means of the Macromodel 10.8.011 software by using the MMFF with an implicit solvent model for $CHCl_3$.[67] Geometry reoptimizations were carried out at the B3LYP/6-31+G(d,p) level in vacuo and CAM-B3LYP/TZVP[50] levels with the PCM solvent model for MeCN with the Gaussian 09 package.[68] TDDFT-ECD calculations were run with various functionals (B3LYP, BH&HLYP, CAM-B3LYP, and PBE0) and the TZVP basis set with the same or no solvent model as in the preceding DFT optimization step. ECD spectra were generated as sums of Gaussians with 2400−3600 cm^{-1} half-height widths using dipole-velocity-computed rotational strength values.[69] NMR shift values were computed at the mPW1PW91/6-311+G(2d,p) and the mPW1PW91/6-311+G(2d,p) SMD/$CHCl_3$ levels. Computed ^{13}C NMR data were corrected with I = 185.4855 and S = −1.0306 in the gas phase and I = 186.5242 and S = −1.0533 in the SMD calculations.[70,71] Boltzmann distributions were estimated from the B3LYP and the CAM-B3LYP energies. The MOLEKEL software package was used for visualization of the results.[72]

X-ray Crystallographic Analysis of 1. Crystals were afforded by slow evaporation from methanol solution. Data Collection: Compound **1** was measured with a Bruker Kappa APEX2 CCD diffractometer with a microfocus tube and Cu Kα radiation (λ = 0.710 73 Å). For data collection APEX2, for cell refinement and data reduction SAINT,[73] and for experimental absorption correction SADABS were used.[74] The structure was solved by intrinsic phasing using SHELXT,[75] and refinement was done by full-matrix least-squares on F^2 using SHELXL-2016/6.[76] The hydrogen atoms were positioned geometrically (with C−H = 0.95 Å for aromatic CH, 1.00 Å for aliphatic CH, 0.99 Å for CH_2, and 0.98 Å for CH_3) and refined using riding models (AFIX 43, 13, 23, 137, respectively), with $U_{iso}(H)$ = 1.2U_{eq}(CH, CH_2), and 1.5U_{eq}(CH_3). The hydrogen atoms in amine groups were refined with $U_{iso}(H)$ = 1.5U_{eq}.

The absolute structure configuration of **1** was solved using anomalous dispersion from Cu Kα, resulting in a Flack parameter of x = −0.01(7) using Parsons quotient method. All graphics were drawn using DIAMOND.[77] The structural data have been deposited in the Cambridge Crystallographic Data Center (CCDC No. 1862565).

■ ASSOCIATED CONTENT

Supporting Information

The Supporting Information is available free of charge on the ACS Publications website at DOI: 10.1021/acs.jnatprod.8b00723.

HPLC chromatograms, UV, HRESIMS, NMR spectra of **1**−**9**, structure of the single conformer of **1**, results of ^{13}C NMR DFT calculations of **1**, structure and population of the low-energy conformers of **3**, ECD spectrum of **7**, results of the X-ray analysis of **1** as well as results of the cell viability assay of **1**, **2**, and **4**−**9** (PDF)

Crystallographic data of **1** (CIF)

■ AUTHOR INFORMATION

Corresponding Authors

*Tel: +49 211 81 14175. E-mail: Elena.Ancheeva@uni-duesseldorf.de.

*Tel: +49 211 81 14173. E-mail: Georgios.Daletos@uni-duesseldorf.de.

*Tel: +49 211 81 14163. Fax: +49 211 81 11923. E-mail: proksch@uni-duesseldorf.de.

ORCID

Elena Ancheeva: 0000-0002-2440-4427

Attila Mándi: 0000-0002-7867-7084

Christoph Janiak: 0000-0002-6288-9605

Georgios Daletos: 0000-0002-1636-6424

Present Address

G. Daletos: Department of Chemical Engineering, Massachusetts Institute of Technology, 25 Ames Street, Cambridge, Massachusetts 02139, United States.

Notes

The authors declare no competing financial interest.

■ ACKNOWLEDGMENTS

The scholarship granted to N.P.A. by DAAD under the Program Biodiversity and Health is gratefully acknowledged. This study was supported by the Bundesministerium für Bildung und Forschung (BMBF, Germany, project BALIPEND, grant number 16GW0107K to P.P. and grant number 16GW0108 to M.U.K.) and by the Deutsche Forschungsgemeinschaft (DFG, Germany) for funding the ThermoFisher Arrayscan XTI (Grant INST 208/690-1-FUGG) to M.U.K. The research of the Hungarian authors was supported by the EU and cofinanced by the European Regional Development Fund under the project GINOP-2.3.2-15-2016-00008. The Governmental Information-Technology Development Agency (KIFÜ) is acknowledged for CPU time. We wish to thank Harwoko (Institute of Pharmaceutical Biology and Biotechnology, Heinrich Heine University Düsseldorf, Germany) for collection of the plant material.

■ REFERENCES

(1) Berdy, J. *J. Antibiot.* **2005**, *58*, 1−26.

(2) Finkelstein, E.; Amichai, B.; Grunwald, M. H. *Int. J. Antimicrob. Agents* **1996**, *6*, 189−194.

(3) Demain, A. L. *J. Ind. Microbiol. Biotechnol.* **2014**, *41*, 185−201.

DOI: 10.1021/acs.jnatprod.8b00723
J. Nat. Prod. 2019, 82, 1412−1423

(4) Cragg, G. M.; Newman, D. J. *Biochim. Biophys. Acta, Gen. Subj.* **2013**, *1830*, 3670−3695.
(5) Dias, D. A.; Urban, S.; Roessner, U. *Metabolites* **2012**, *2*, 303−336.
(6) Elfahmi; Woerdenbag, H. J.; Kayser, O. *J. Herb. Med.* **2014**, *4*, 51−73.
(7) Chen, C. Y.; Yang, Y. H.; Kuo, S. Y. *J. Nat. Prod.* **2010**, *73*, 1370−1374.
(8) Zhang, F.; Thakur, K.; Hu, F.; Zhang, J. G.; Wei, Z. J. *J. Agric. Food Chem.* **2017**, *65*, 2089−2099.
(9) Dugasani, S.; Pichika, M. R.; Nadarajah, V. D.; Balijepalli, M. K.; Tandra, S.; Korlakunta, J. N. *J. Ethnopharmacol.* **2010**, *127*, 515−520.
(10) Yang, Y.; Kinoshita, K.; Koyama, K.; Takahashi, K.; Kondo, S.; Watanabe, K. *Phytomedicine* **2002**, *9*, 146−152.
(11) Sang, S.; Hong, J.; Wu, H.; Liu, J.; Yang, C. S.; Pan, M. H.; Badmaev, V.; Ho, C. T. *J. Agric. Food Chem.* **2009**, *57*, 10645−10650.
(12) Funk, J. L.; Frye, J. B.; Oyarzo, J. N.; Timmermann, B. N. *J. Nat. Prod.* **2009**, *72*, 403−407.
(13) Selala, M. I.; Musuku, A.; Schepens, P. J. C. *Anal. Chim. Acta* **1991**, *244*, 1−8.
(14) Fan, Y.; Wang, Y.; Liu, P.; Fu, P.; Zhu, T.; Wang, W.; Zhu, W. *J. Nat. Prod.* **2013**, *76*, 1328−1336.
(15) Uhlig, S.; Egge-Jacobsen, W.; Vrålstad, T.; Miles, C. O. *Rapid Commun. Mass Spectrom.* **2014**, *28*, 1621−1634.
(16) Saikia, S.; Nicholson, M. J.; Young, C.; Parker, E. J.; Scott, B. *Mycol. Res.* **2008**, *112*, 184−199.
(17) Matsuda, Y.; Abe, I. *Nat. Prod. Rep.* **2016**, *33*, 26−53.
(18) Xu, W.; Gavia, D. J.; Tang, Y. *Nat. Prod. Rep.* **2014**, *31*, 1474−1487.
(19) Philippe, G. *Toxins* **2016**, *8*, 47.
(20) Springer, J. P.; Clardy, J.; Wells, J. M.; Cole, R. J.; Kirksey, J. W. *Tetrahedron Lett.* **1975**, *16*, 2531−2534.
(21) Cole, R. J.; Dorner, J. W.; Lansden, J. A.; Cox, R. H.; Pape, C.; Cunfer, B.; Nicholson, S. S.; Bedell, D. M. *J. Agric. Food Chem.* **1977**, *25*, 1197−1201.
(22) Gallagher, R. T.; Latch, G. C. M.; Keogh, R. G. *Appl. Environ. Microbiol.* **1980**, *39*, 272−273.
(23) Wilkins, A. L.; Miles, C. O.; Ede, R. M.; Gallagher, R. T.; Munday, S. C. *J. Agric. Food Chem.* **1992**, *40*, 1307−1309.
(24) Penn, J.; Swift, R.; Wigley, L. J.; Mantle, P. G.; Bilton, J. N.; Sheppard, R. N. *Phytochemistry* **1993**, *32*, 1431−1434.
(25) González, M. C.; Lull, C.; Moya, P.; Ayala, I.; Primo, J.; Yufera, E. P. *J. Agric. Food Chem.* **2003**, *51*, 2156−2160.
(26) Gallagher, R. T.; Clardy, J.; Wilson, B. J. *Tetrahedron Lett.* **1980**, *21*, 239−242.
(27) Gallagher, R. T.; Finer, J.; Clardy, J.; Leutwiler, A.; Weibel, F.; Acklin, W.; Arigoni, D. *Tetrahedron Lett.* **1980**, *21*, 235−238.
(28) Mantle, P. G. *Phytochemistry* **2009**, *70*, 7−10.
(29) Bennett, J. W.; Klich, M. *Clin. Microbiol. Rev.* **2003**, *16*, 497−516.
(30) Singh, S. B.; Ondeyka, J. G.; Jayasuriya, H.; Zink, D. L.; Ha, S. N.; Dahl-Roshak, A.; Greene, J.; Kim, J. A.; Smith, M. M.; Shoop, W.; Tkacz, J. S. *J. Nat. Prod.* **2004**, *67*, 1496−1506.
(31) Qiao, M. F.; Ji, N. Y.; Liu, X. H.; Li, K.; Zhu, Q. M.; Xue, Q. Z. *Bioorg. Med. Chem. Lett.* **2010**, *20*, 5677−5680.
(32) Ogata, M.; Ueda, J. Y.; Hoshi, M.; Hashimoto, J.; Nakashima, T.; Anzai, K.; Takagi, M.; Shin-ya, K. *J. Antibiot.* **2007**, *60*, 645−648.
(33) You, J.; Du, L.; King, J. B.; Hall, B. E.; Cichewicz, R. H. *ACS Chem. Biol.* **2013**, *8*, 840−848.
(34) Abdullaev, I. F.; Rudkouskaya, A.; Mongin, A. A.; Kuo, Y. H. *PLoS One* **2010**, *5*, e12304.
(35) Sallam, A. A.; Houssen, W. E.; Gissendanner, C. R.; Orabi, K. Y.; Foudah, A. I.; El Sayed, K. A. *MedChemComm* **2013**, *4*, 1360−1369.
(36) Knaus, H. G.; McManus, O. B.; Lee, S. H.; Schmalhofer, W. A.; Garcia-Calvo, M.; Helms, L. M.; Sanchez, M.; Giangiacomo, K.; Reuben, J. P.; Smith, A. B., III; Kaczorowski, G. J.; Garcia, M. L. *Biochemistry* **1994**, *33*, 5819−5828.
(37) Sheehan, J. J.; Benedetti, B. L.; Barth, A. L. *Epilepsia* **2009**, *50*, 711−720.
(38) Brnardic, E.; Doherty, J. B.; Dorsey, J.; Ellwood, C.; Fillmore, M.; Malaska, M.; Nelson, K.; Soukri, M. Maxi-K channel blockers and methods of use. Patent WO2009/048559 A1, 2009.
(39) Corsello, M. A.; Kim, J.; Garg, N. K. *Chem. Sci.* **2017**, *8*, 5836−5844.
(40) Tang, M. C.; Lin, H. C.; Li, D.; Zou, Y.; Li, J.; Xu, W.; Cacho, R. A.; Hillenmeyer, M. E.; Garg, N. K.; Tang, Y. *J. Am. Chem. Soc.* **2015**, *137*, 13724−13727.
(41) Liu, C.; Minami, A.; Dairi, T.; Gomi, K.; Scott, B.; Oikawa, H. *Org. Lett.* **2016**, *18*, 5026−5029.
(42) Ding, L.; Münch, J.; Goerls, H.; Maier, A.; Fiebig, H. H.; Lin, W. H.; Hertweck, C. *Bioorg. Med. Chem. Lett.* **2010**, *20*, 6685−6687.
(43) Ding, L.; Maier, A.; Fiebig, H. H.; Lin, W. H.; Hertweck, C. *Org. Biomol. Chem.* **2011**, *9*, 4029−4031.
(44) Fehr, T.; Acklin, W. *Helv. Chim. Acta* **1966**, *49*, 1907−1910.
(45) Springer, J. P.; Clardy, J. P. *Tetrahedron Lett.* **1980**, *21*, 231−234.
(46) Ancheeva, E.; Küppers, L.; Akone, S. H.; Ebrahim, W.; Liu, Z.; Mándi, A.; Kurtán, T.; Lin, W.; Orfali, R.; Rehberg, N.; Kalscheuer, R.; Daletos, G.; Proksch, P. *Eur. J. Org. Chem.* **2017**, *2017*, 3256−3264.
(47) Liu, Y.; Kurtán, T.; Mándi, A.; Weber, H.; Wang, C.; Hartmann, R.; Lin, W.; Daletos, G.; Proksch, P. *Tetrahedron Lett.* **2018**, *59*, 632−636.
(48) Tóth, L.; Mándi, A.; Váradi, D.; Kovács, T.; Szabados, A.; Kiss-Szikszai, A.; Gong, Q.; Zhang, H.; Mátyus, P.; Antus, S.; Kurtán, T. *Chirality* **2018**, *30*, 866−874.
(49) Zhang, P.; Meng, L. H.; Mándi, A.; Kurtán, T.; Li, X. M.; Liu, Y.; Li, X.; Li, C. S.; Wang, B. G. *Eur. J. Org. Chem.* **2014**, *2014*, 4029−4036.
(50) Yanai, T.; Tew, D. P.; Handy, N. C. *Chem. Phys. Lett.* **2004**, *393*, 51−57.
(51) Adamo, C.; Barone, V. *J. Chem. Phys.* **1998**, *108*, 664−675.
(52) Smetanina, O. F.; Kalinovsky, A. I.; Khudyakova, Y. V.; Pivkin, M. V.; Dmitrenok, P. S.; Fedorov, S. N.; Ji, H.; Kwak, J. Y.; Kuznetsova, T. A. *J. Nat. Prod.* **2007**, *70*, 906−909.
(53) Matsui, C.; Ikeda, Y.; Iinuma, H.; Kushida, N.; Kunisada, T.; Simizu, S.; Umezawa, K. *J. Antibiot.* **2014**, *67*, 787−790.
(54) Belofsky, G. N.; Gloer, J. B.; Wicklow, D. T.; Dowd, P. F. *Tetrahedron* **1995**, *51*, 3959−3968.
(55) Dhodary, B.; Schilg, M.; Wirth, R.; Spiteller, D. *Chem. - Eur. J.* **2018**, *24*, 4445−4452.
(56) Nozawa, K.; Nakajima, S.; Kawai, K. I.; Udagawa, S. I. *J. Chem. Soc., Perkin Trans. 1* **1988**, 2607−2610.
(57) Xu, M.; Gessner, G.; Groth, I.; Lange, C.; Christner, A.; Bruhn, T.; Deng, Z.; Li, X.; Heinemann, S. H.; Grabley, S.; Bringmann, G.; Sattler, I.; Lin, W. *Tetrahedron* **2007**, *63*, 435−444.
(58) Smith, A. B., III; Kingery-Wood, J.; Leenay, T. L.; Nolen, E. G.; Sunazuka, T. *J. Am. Chem. Soc.* **1992**, *114*, 1438−1449.
(59) Gao, N.; Shang, Z. C.; Yu, P.; Luo, J.; Jian, K. L.; Kong, L. Y.; Yang, M. H. *Chin. Chem. Lett.* **2017**, *28*, 1194−1199.
(60) Munday-Finch, S. C.; Wilkins, A. L.; Miles, C. O. *Phytochemistry* **1996**, *41*, 327−332.
(61) Mantle, P. G.; Weedon, C. M. *Phytochemistry* **1994**, *36*, 1209−1217.
(62) Bills, G. F.; Giacobbe, R. A.; Lee, S. H.; Peláez, F.; Tkacz, J. S. *Mycol. Res.* **1992**, *96*, 977−983.
(63) Li, H.; Zhang, Q.; Li, S.; Zhu, Y.; Zhang, G.; Zhang, H.; Tian, X.; Zhang, S.; Ju, J.; Zhang, C. *J. Am. Chem. Soc.* **2012**, *134*, 8996−9005.
(64) Kjer, J.; Debbab, A.; Aly, A. H.; Proksch, P. *Nat. Protoc.* **2010**, *5*, 479−490.
(65) Chen, H.; Daletos, G.; Abdel-Aziz, M. S.; Thomy, D.; Dai, H.; Brötz-Oesterhelt, H.; Lin, W.; Proksch, P. *Phytochem. Lett.* **2015**, *12*, 35−41.
(66) Rönsberg, D.; Debbab, A.; Mandi, A.; Vasylyeva, V.; Böhler, P.; Stork, B.; Engelke, L.; Hamacher, A.; Sawadogo, R.; Diederich, M.;

DOI: 10.1021/acs.jnatprod.8b00723
J. Nat. Prod. 2019, 82, 1412−1423

Wray, V.; Lin, W.; Kassack, M. U.; Janiak, C.; Scheu, S.; Wesselborg, S.; Kurtán, T.; Aly, A. H.; Proksch, P. *J. Org. Chem.* **2013**, *78*, 12409−12425.
(67) *MacroModel*; Schrödinger, LLC, 2015; http://www.schrodinger.com/MacroModel.
(68) Frisch, M. J.; Trucks, G. W.; Schlegel, H. B.; Scuseria, G. E.; Robb, M. A.; Cheeseman, J. R.; Scalmani, G.; Barone, V.; Mennucci, B.; Petersson, G. A.; Nakatsuji, H.; Caricato, M.; Li, X.; Hratchian, H. P.; Izmaylov, A. F.; Bloino, J.; Zheng, G.; Sonnenberg, J. L.; Hada, M.; Ehara, M.; Toyota, K.; Fukuda, R.; Hasegawa, J.; Ishida, M.; Nakajima, T.; Honda, Y.; Kitao, O.; Nakai, H.; Vreven, T.; Montgomery, J. A., Jr.; Peralta, J. E.; Ogliaro, F.; Bearpark, M.; Heyd, J. J.; Brothers, E.; Kudin, K. N.; Staroverov, V. N.; Kobayashi, R.; Normand, J.; Raghavachari, K.; Rendell, A.; Burant, J. C.; Iyengar, S. S.; Tomasi, J.; Cossi, M.; Rega, N.; Millam, J. M.; Klene, M.; Knox, J. E.; Cross, J. B.; Bakken, V.; Adamo, C.; Jaramillo, J.; Gomperts, R.; Stratmann, R. E.; Yazyev, O.; Austin, A. J.; Cammi, R.; Pomelli, C.; Ochterski, J. W.; Martin, R. L.; Morokuma, K.; Zakrzewski, V. G.; Voth, G. A.; Salvador, P.; Dannenberg, J. J.; Dapprich, S.; Daniels, A. D.; Farkas, O.; Foresman, J. B.; Ortiz, J. V.; Cioslowski, J.; Fox, D. J. *Gaussian 09*, Revision E.01; Gaussian, Inc.: Wallingford, CT, 2013.
(69) Stephens, P. J.; Harada, N. *Chirality* **2009**, *22*, 229−233.
(70) CHESHIRE CCAT, *the Chemical Shift Repository for computed NMR scaling factors*, http://cheshirenmr.info/index.htm.
(71) Lodewyk, M. W.; Siebert, M. R.; Tantillo, D. J. *Chem. Rev.* **2012**, *112*, 1839−1862.
(72) Varetto, U. *MOLEKEL* 5.4; Swiss National Supercomputing Centre: Manno, Switzerland, 2009.
(73) *Apex2*, Data Collection Program for the CCD Area-Detector System; *SAINT*, Data Reduction and Frame Integration Program for the CCD Area-Detector System; Bruker Analytical X-ray Systems: Madison, WI, USA, 1997−2012.
(74) Sheldrick, G. M. *SADABS: Area-detector absorption correction*; University of Goettingen: Germany, 1996.
(75) Sheldrick, G. M. *Acta Crystallogr., Sect. A: Found. Adv.* **2015**, *71*, 3−8.
(76) Sheldrick, G. M. *Acta Crystallogr., Sect. C: Struct. Chem.* **2015**, *71*, 3−8.
(77) Brandenburg, K. *Diamond (Version 3.2), Crystal and Molecular Structure Visualization, Crystal Impact − K*; Brandenburg & H. Putz Gbr: Bonn, Germany, 2009.

DOI: 10.1021/acs.jnatprod.8b00723
J. Nat. Prod. 2019, 82, 1412−1423

Supporting Information

Indole Diterpenoids from an Endophytic *Penicillium* sp.

Ni P. Ariantari,[†,‡] Elena Ancheeva,[*,†] Chenyin Wang,[§] Attila Mándi,[⊥], Tim-O. Knedel,[#] Tibor Kurtán,[⊥] Chaidir Chaidir, [▽] Werner E. G. Müller,[○] Matthias U. Kassack,[§] Christoph Janiak,[#] Georgios Daletos,[*,†] Peter Proksch[*,†]

[†]Institute of Pharmaceutical Biology and Biotechnology, Heinrich Heine University Düsseldorf, Universitätsstrasse 1, 40225 Düsseldorf, Germany

[‡]Department of Pharmacy, Faculty of Mathematic and Natural Sciences, Udayana University, 80361 Bali, Indonesia

[§]Institute of Pharmaceutical and Medicinal Chemistry, Heinrich Heine University Düsseldorf, Universitätsstrasse 1, 40225 Düsseldorf, Germany

[⊥]Department of Organic Chemistry, University of Debrecen, P.O.B. 400, 4002 Debrecen, Hungary

[#]Institute of Inorganic Chemistry and Structural Chemistry, Heinrich Heine University Düsseldorf, Universitätsstraße 1, 40225 Düsseldorf, Germany

[▽]Center for Pharmaceutical and Medical Technology, Agency for the Assessment and Application Technology, 10340 Jakarta, Indonesia

[○]Institute of Physiological Chemistry, Universitätsmedizin der Johannes Gutenberg-Universität Mainz, Duesbergweg 6, 55128 Mainz, Germany

[*]Corresponding author

Table of Contents

(A)

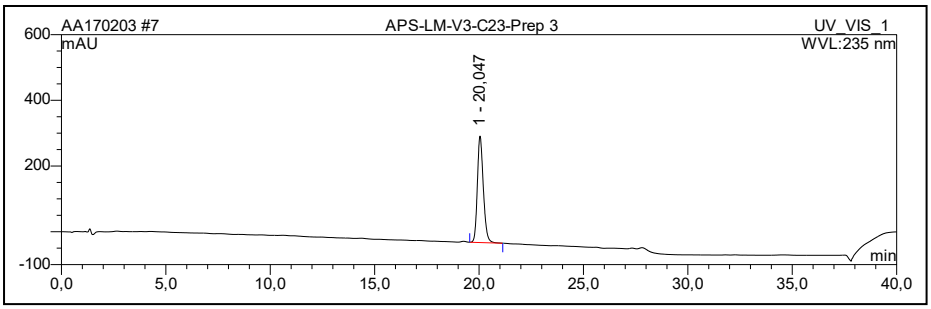

(B)

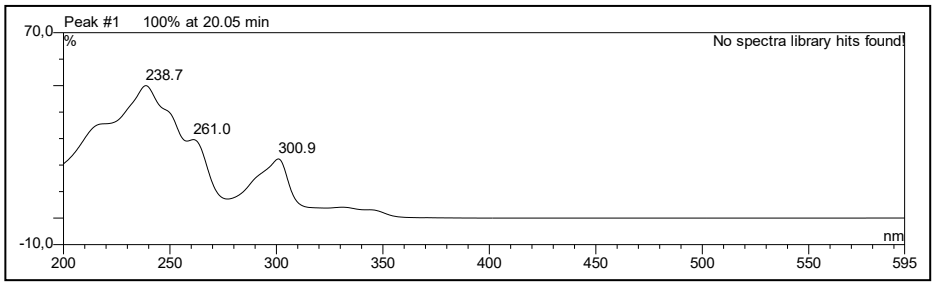

Figure S1. HPLC chromatogram (A) and UV spectrum (B) of compound **1**.

Acquisition Parameter

Source Type	ESI	Ion Polarity	Positive	Set Nebulizer	0.3 Bar
Focus	Not active	Set Capillary	4000 V	Set Dry Heater	180 °C
Scan Begin	50 m/z	Set End Plate Offset	-500 V	Set Dry Gas	4.0 l/min
Scan End	1500 m/z	Set Collision Cell RF	600.0 Vpp	Set Divert Valve	Source

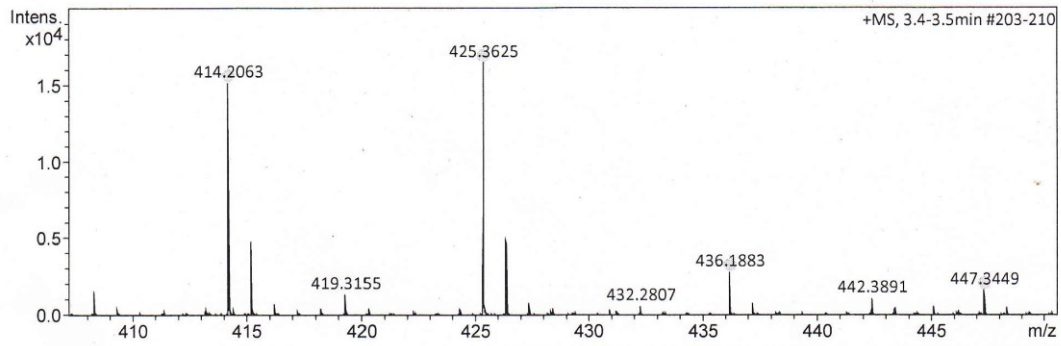

Meas. m/z	#	Ion Formula	m/z	err [ppm]	mSigma	# mSigma	Score	rdb	e⁻ Conf	N-Rule
414.2063	1	C27H28NO3	414.2064	0.1	10.3	1	100.00	14.5	even	ok
425.3625	1	C26H49O4	425.3625	-0.0	5.6	1	100.00	2.5	even	ok
	2	C27H45N4	425.3639	3.1	8.1	2	48.83	7.5	even	ok
436.1883	1	C27H27NNaO3	436.1883	0.1	29.3	1	100.00	14.5	even	ok
447.3449	1	C27H44N4Na	447.3458	2.1	27.3	1	79.45	7.5	even	ok
	2	C26H48NaO4	447.3445	-0.9	29.9	2	100.00	2.5	even	ok

Figure S2. HRESIMS spectrum of compound **1**.

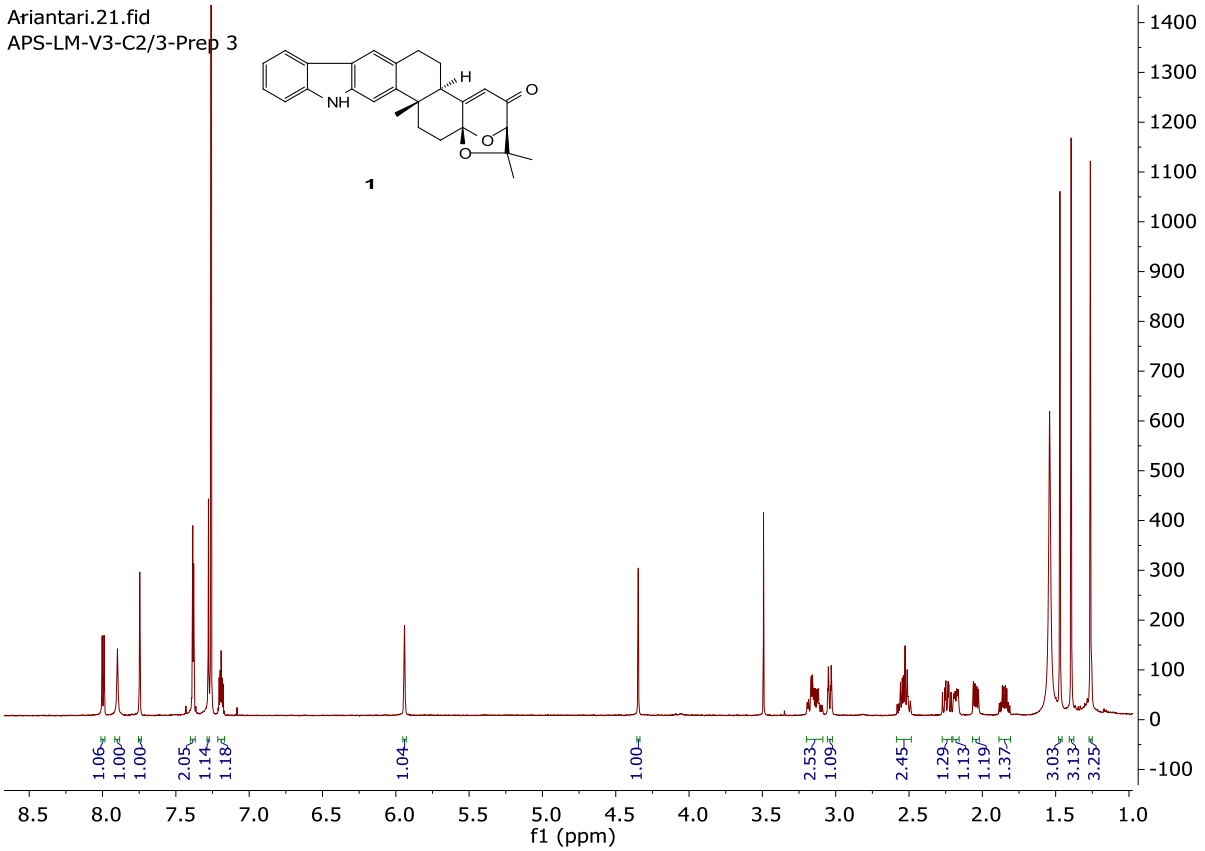

Figure S3. ^{1}H NMR (600 MHz, $CDCl_3$) spectrum of compound **1**.

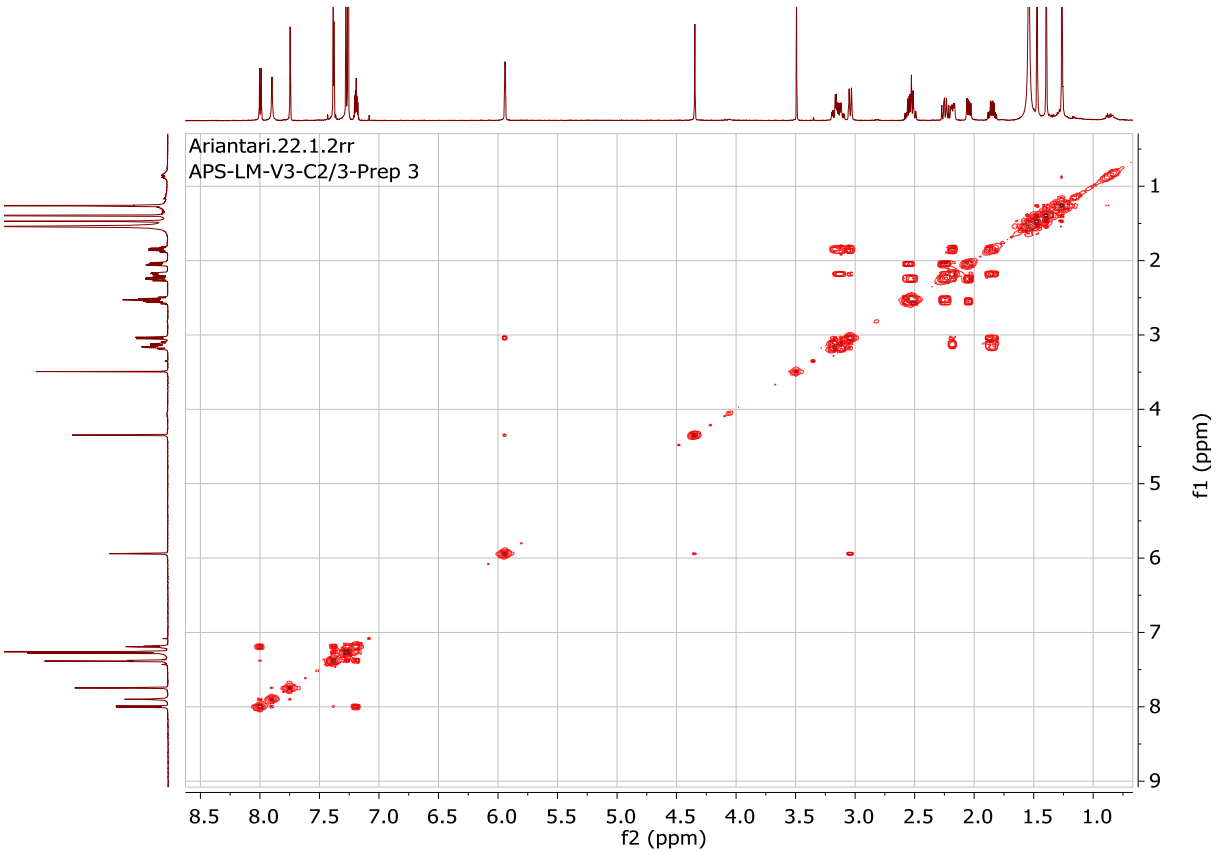

Figure S4. ^{1}H-^{1}H COSY (600 MHz, $CDCl_3$) spectrum of compound **1**.

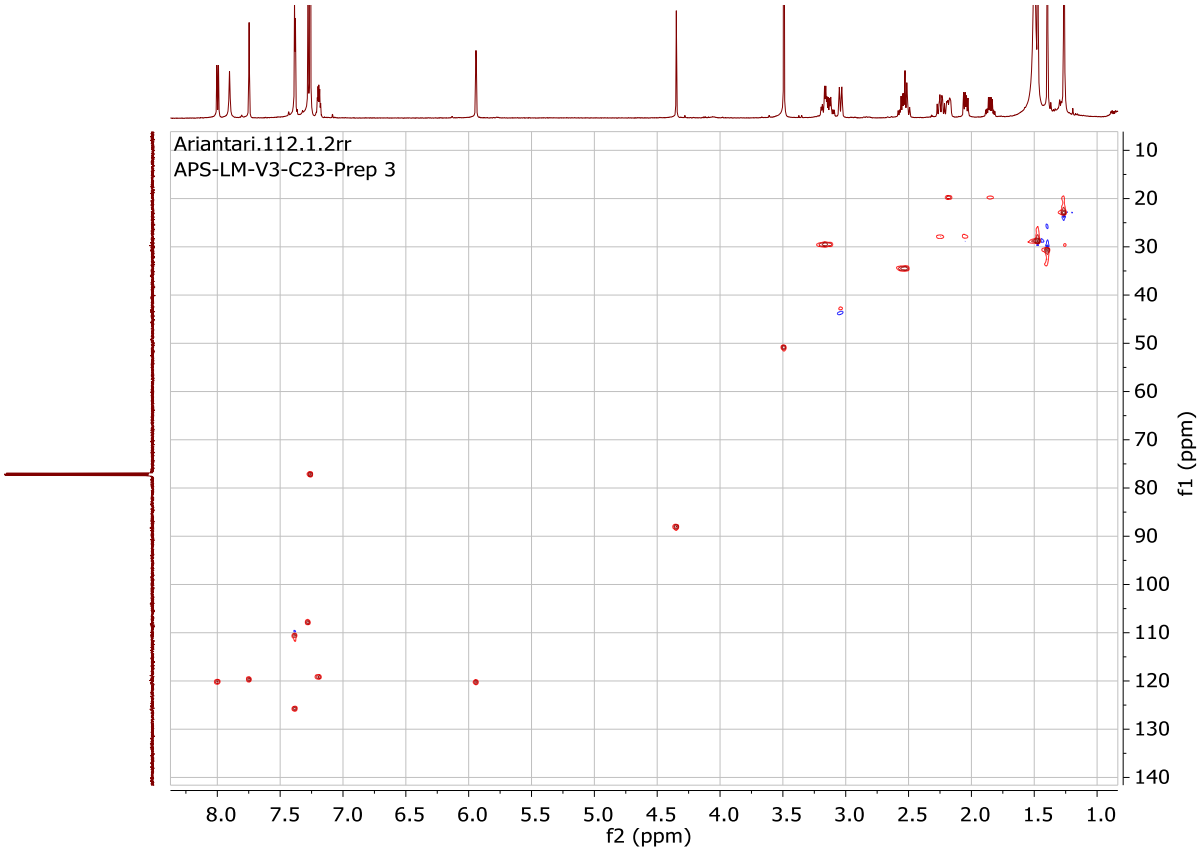

Figure S5. HSQC (600 and 150 MHz, $CDCl_3$) spectrum of compound **1**.

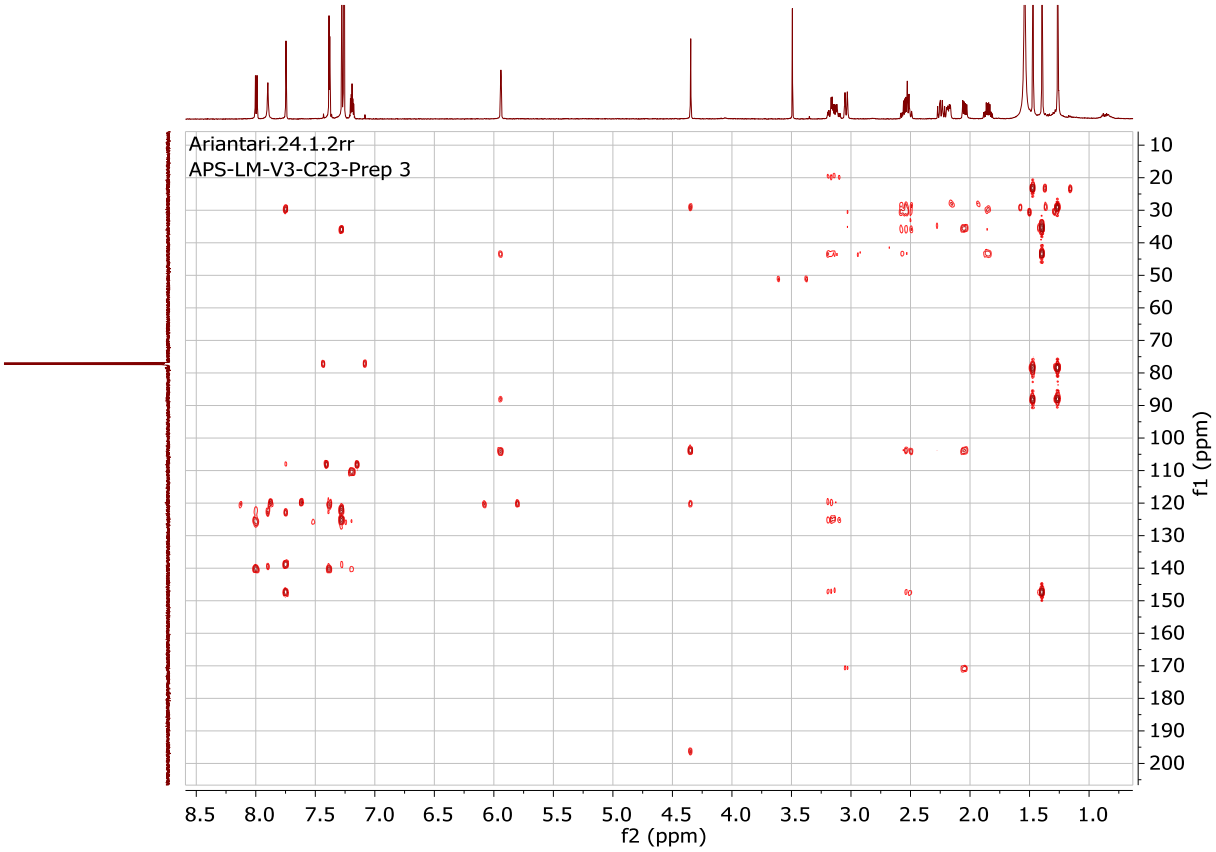

Figure S6. HMBC (600 and 150 MHz, $CDCl_3$) spectrum of compound **1**.

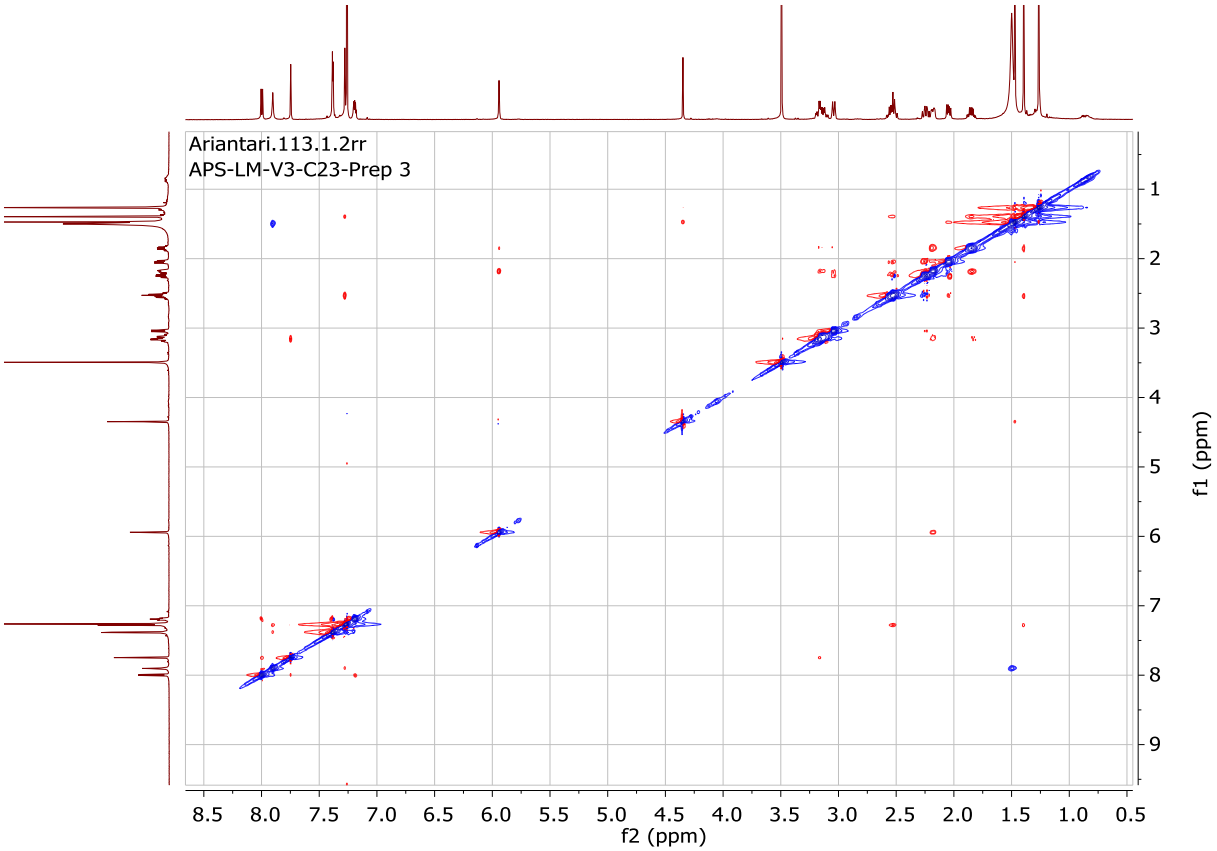

Figure S7. ROESY (600 MHz, $CDCl_3$) spectrum of compound **1**.

(A)

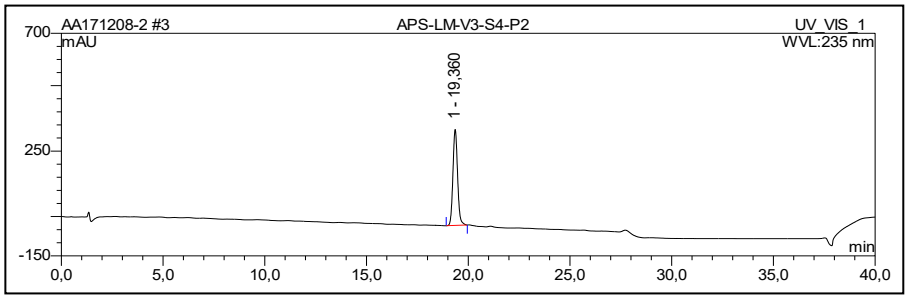

(B)

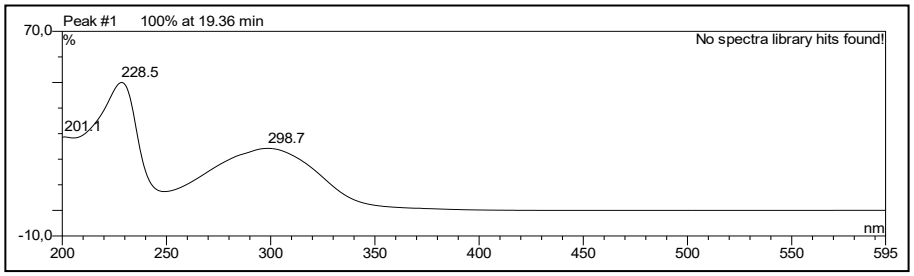

Figure S8. HPLC chromatogram (A) and UV spectrum (B) of compound **2**.

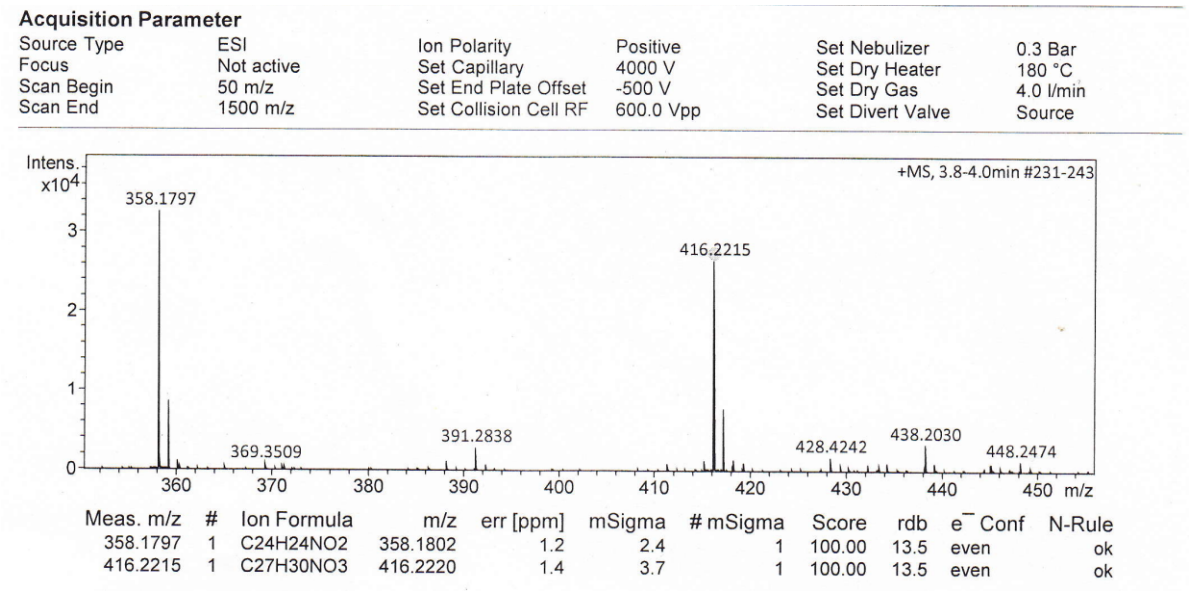

Figure S9. HRESIMS spectrum of compound **2**.

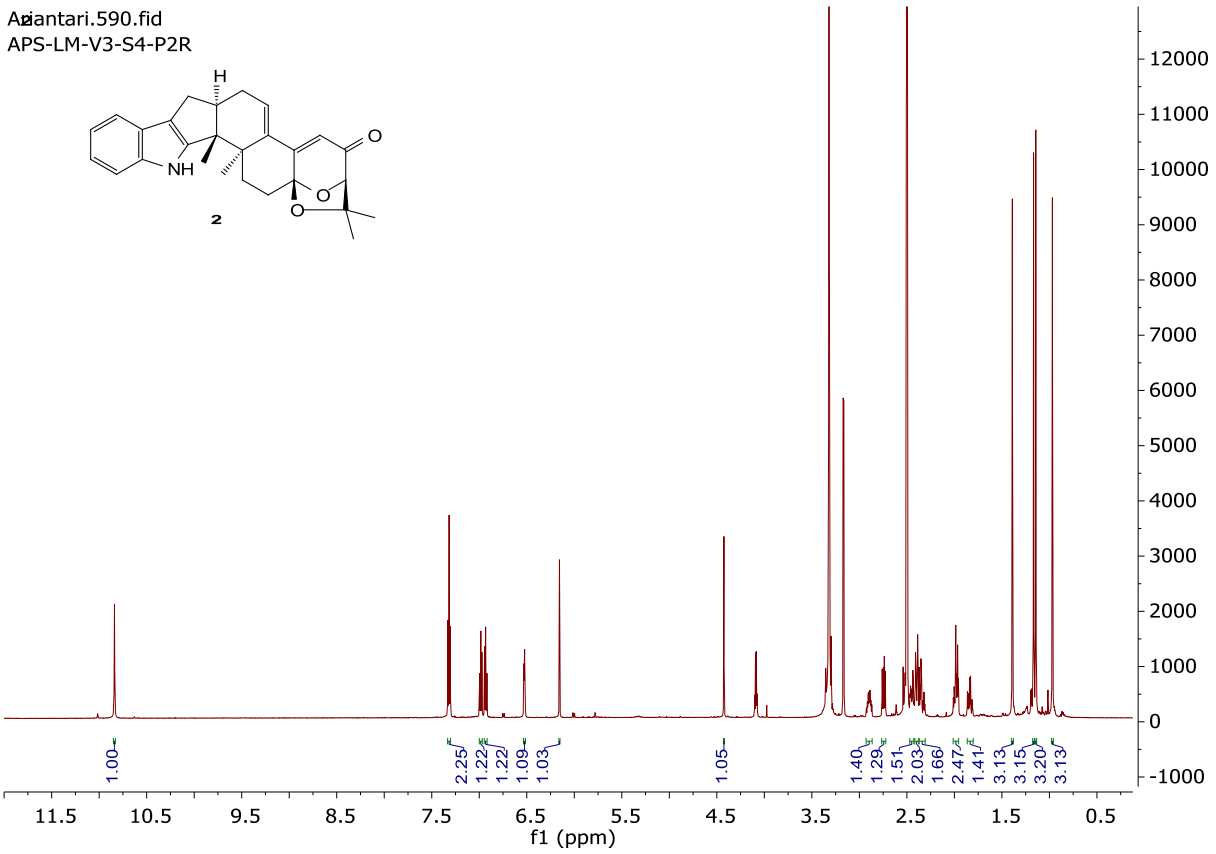

Figure S10. ^{1}H NMR (600 MHz, DMSO-d_6) spectrum of compound **2**.

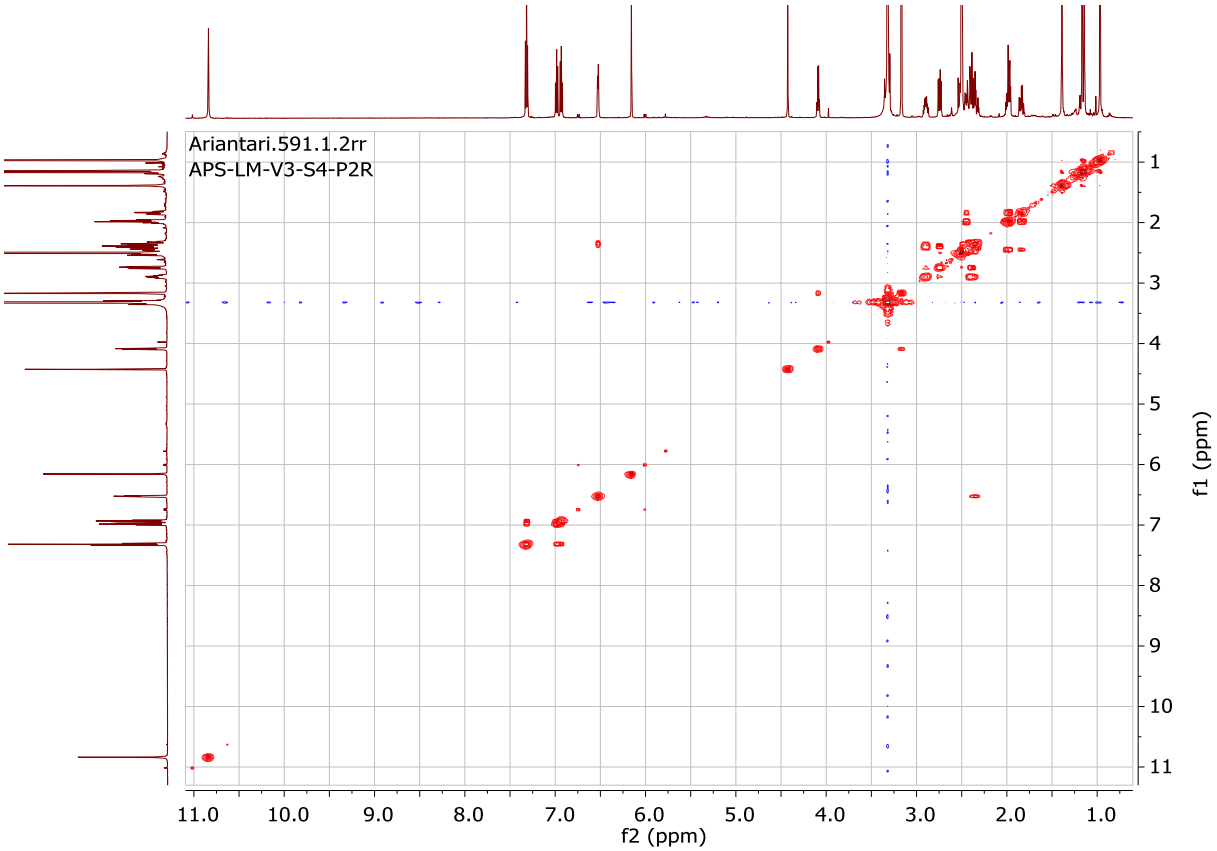

Figure S11. ^{1}H-^{1}H COSY (600 MHz, DMSO-d_6) spectrum of compound **2**.

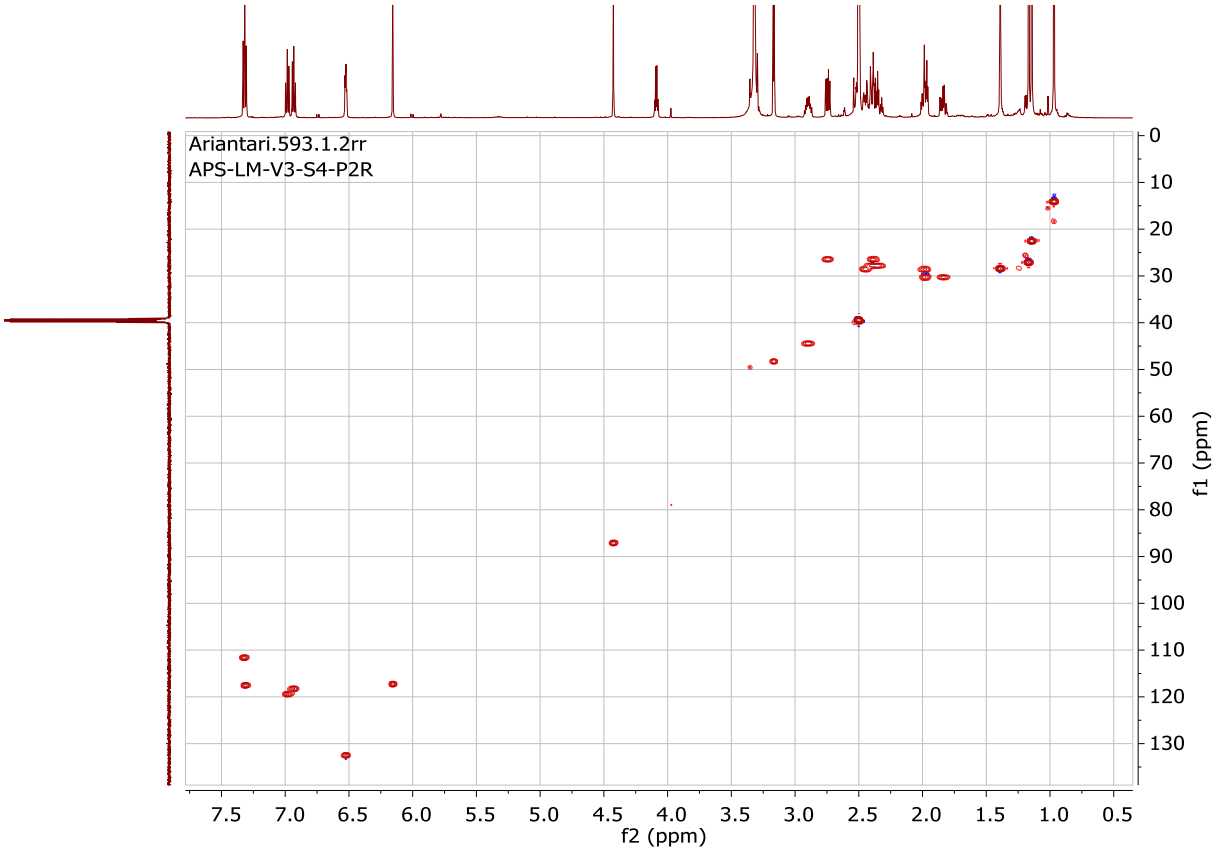

Figure S12. HSQC (600 and 150 MHz, DMSO-d_6) spectrum of compound **2**.

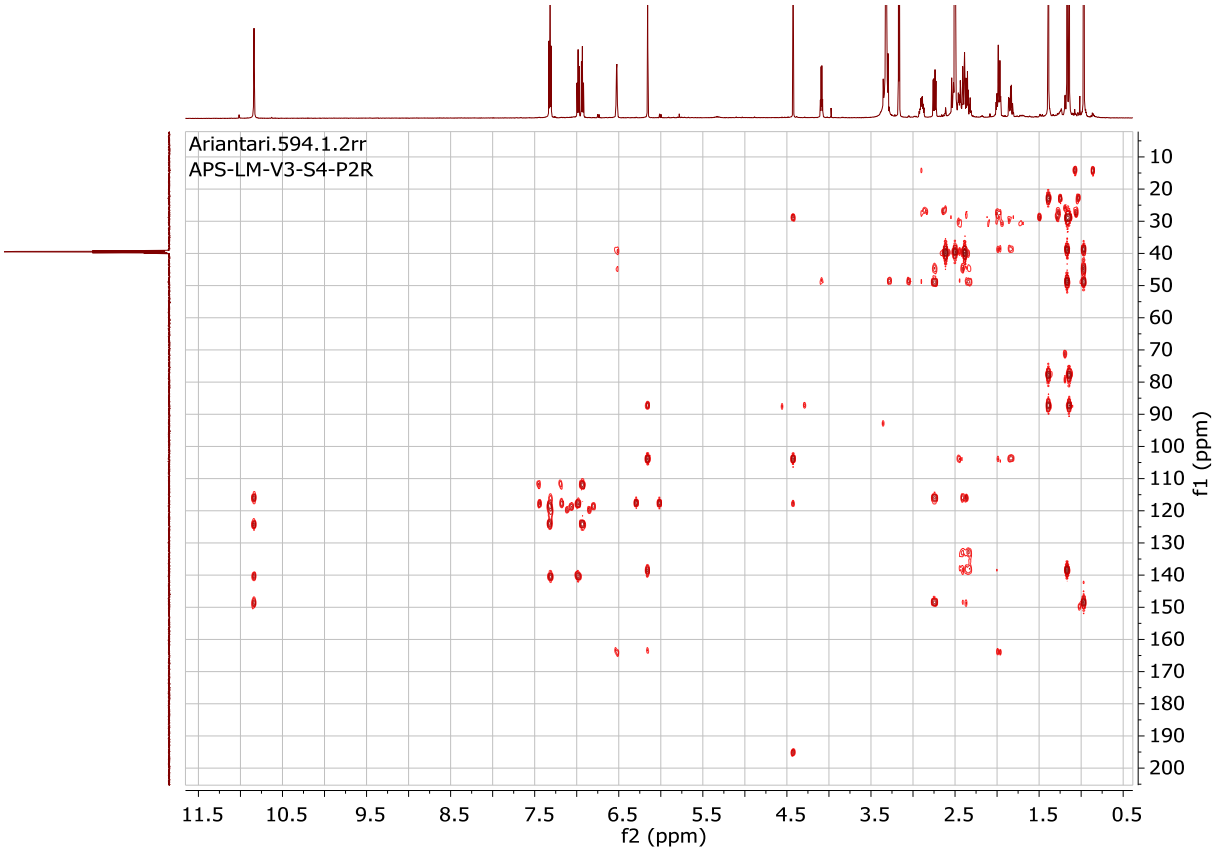

Figure S13. HMBC (600 and 150 MHz, DMSO-d_6) spectrum of compound **2**.

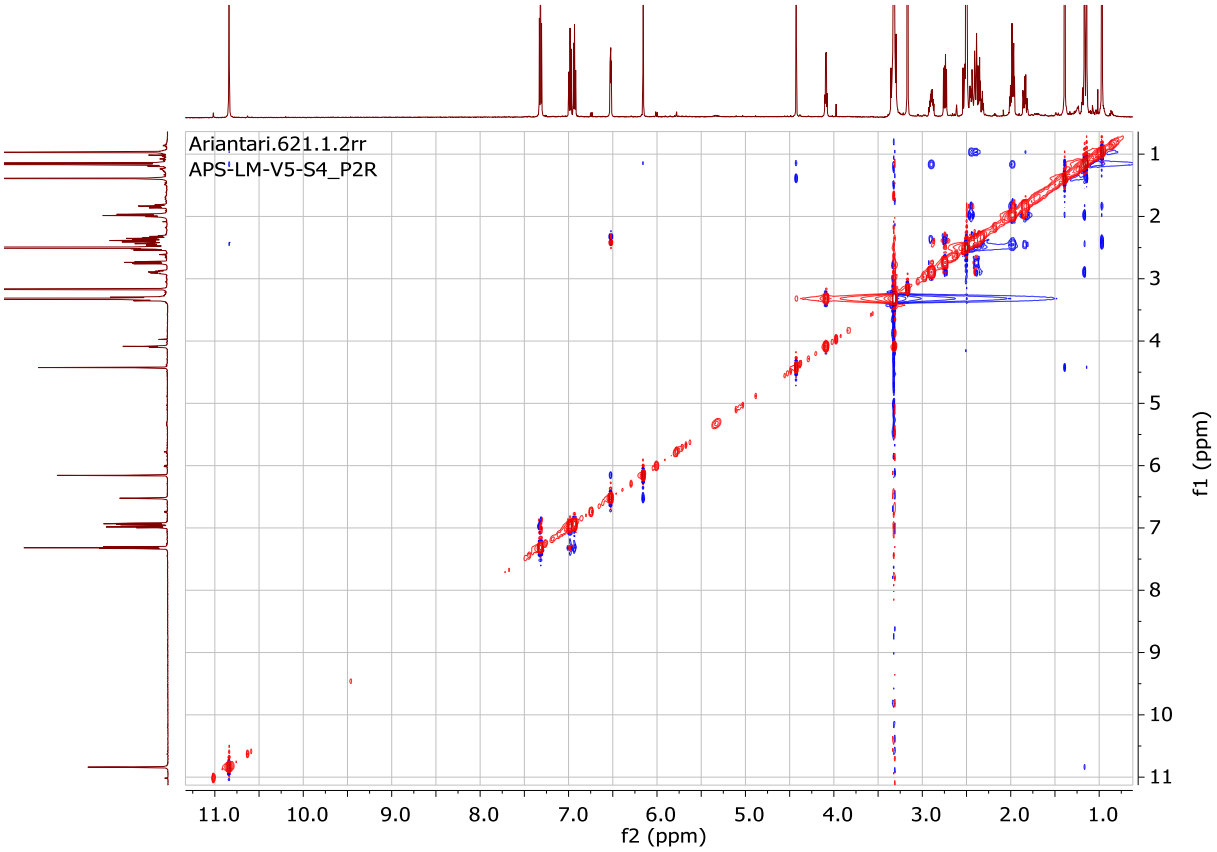

Figure S14. NOESY (600 MHz, DMSO-d_6) spectrum of compound **2**.

(A)

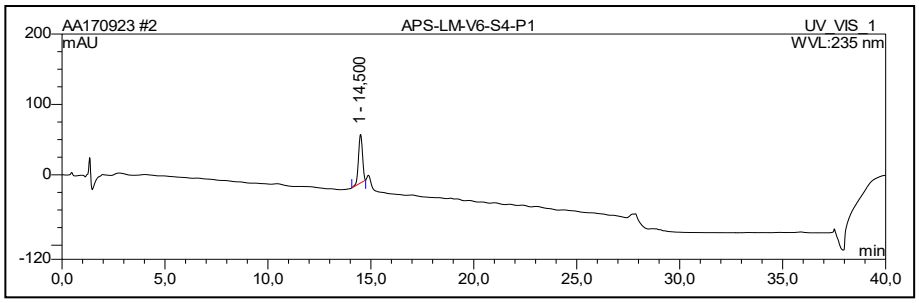

(B)

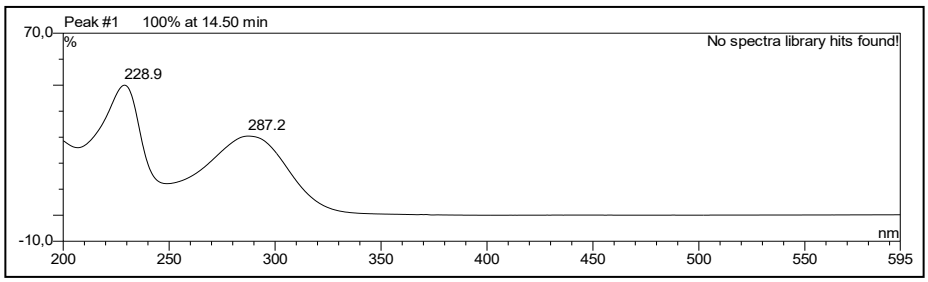

Figure S15. HPLC chromatogram (A) and UV spectrum (B) of compound **3**.

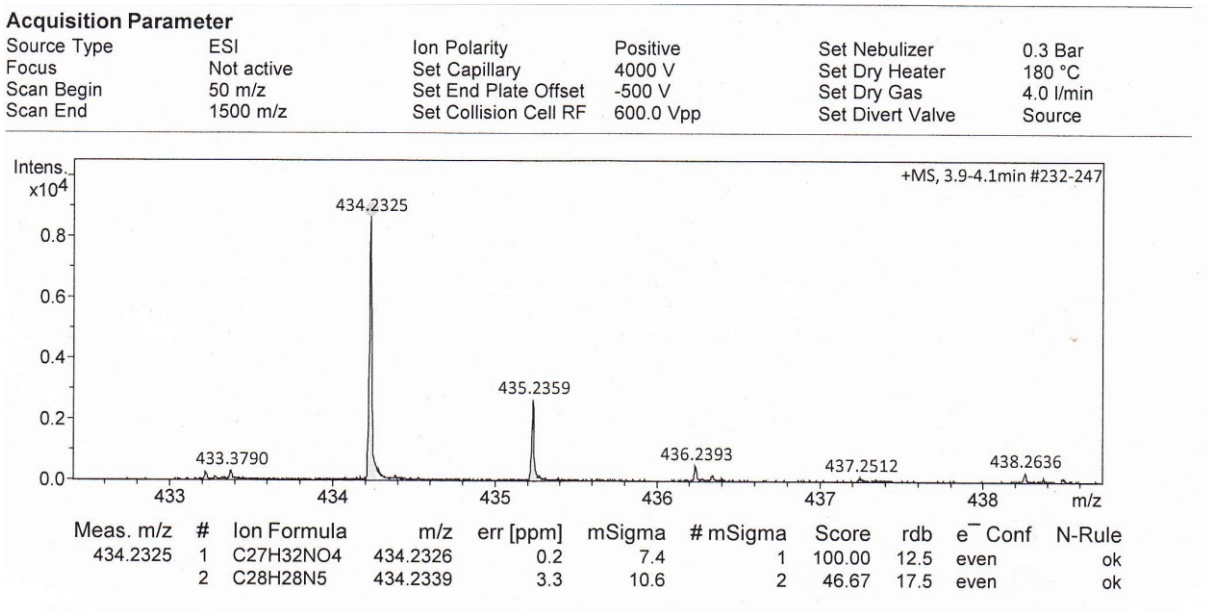

Figure S16. HRESIMS spectrum of compound **3**.

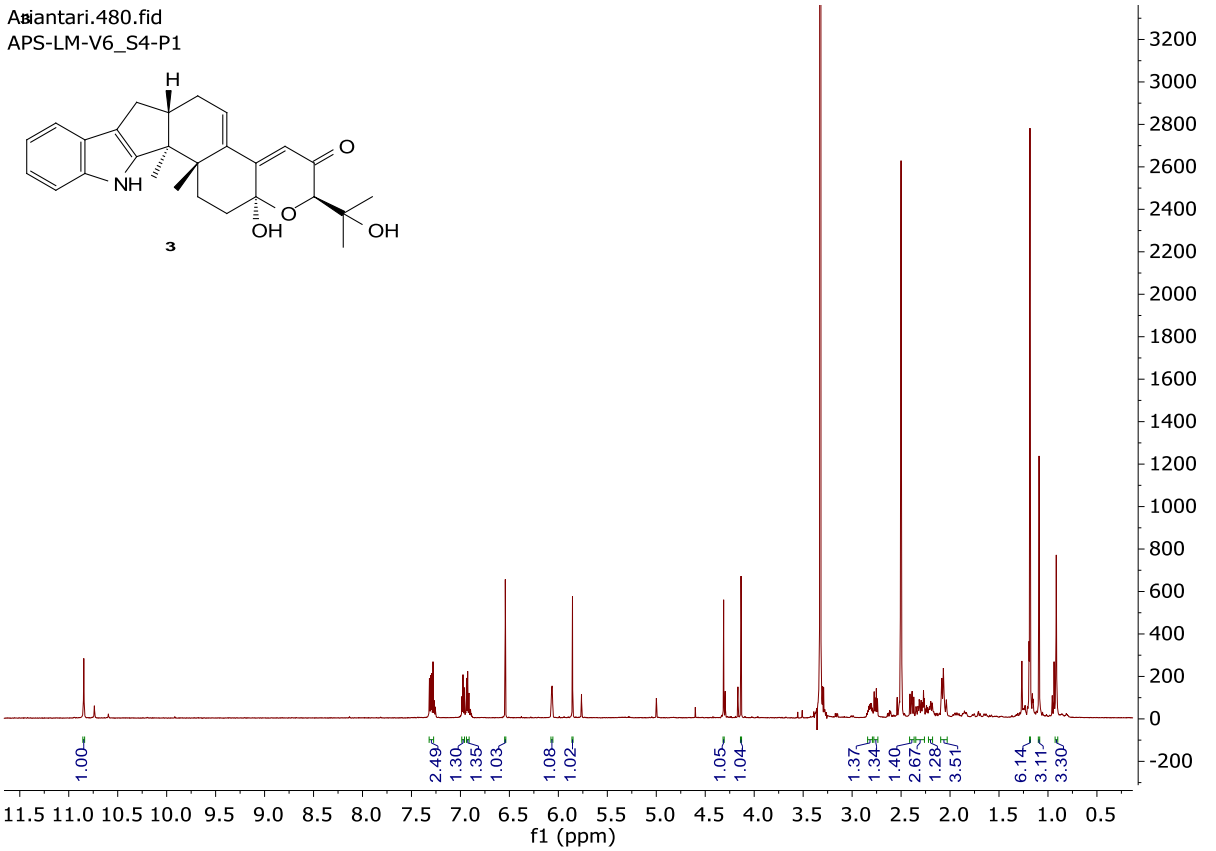

Figure S17. ^{1}H NMR (600 MHz, DMSO-d_6) spectrum of compound **3**.

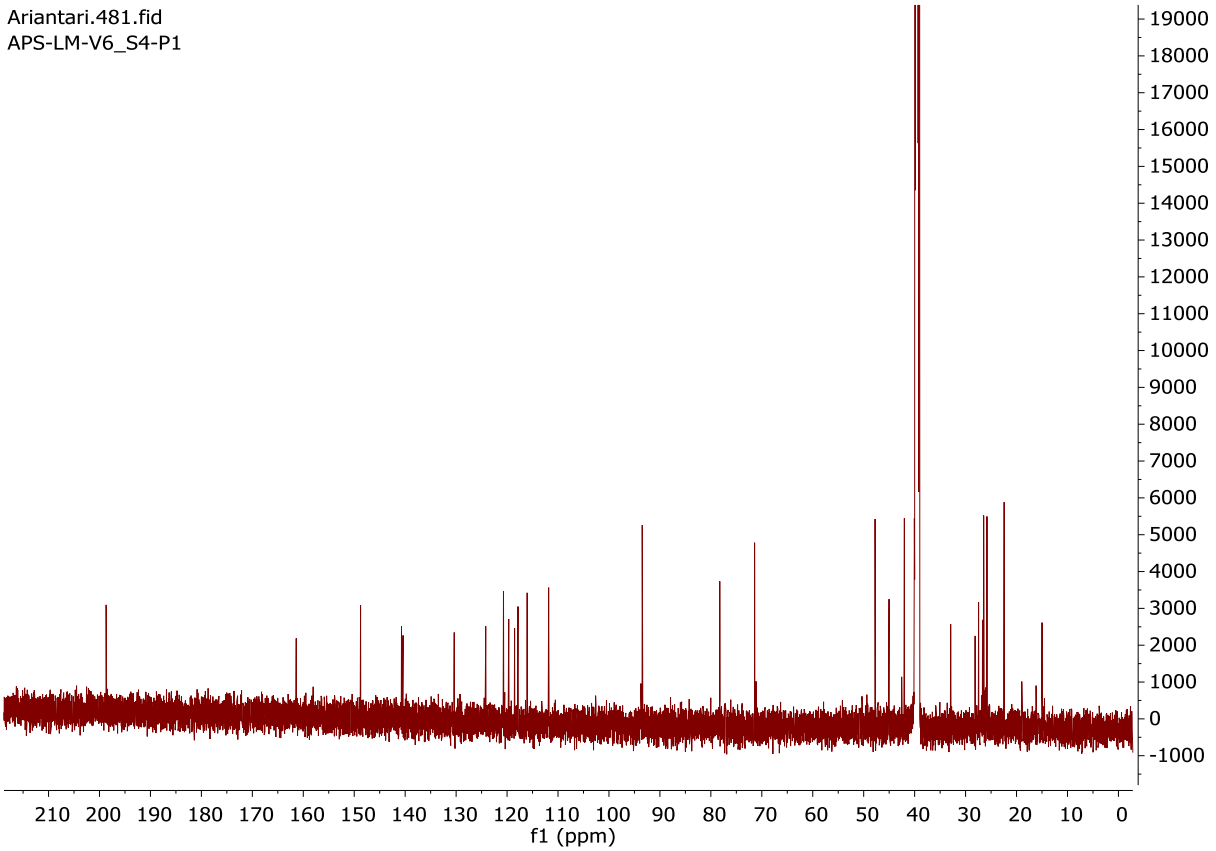

Figure S18. ^{13}C NMR (150 MHz, DMSO-d_6) spectrum of compound **3**.

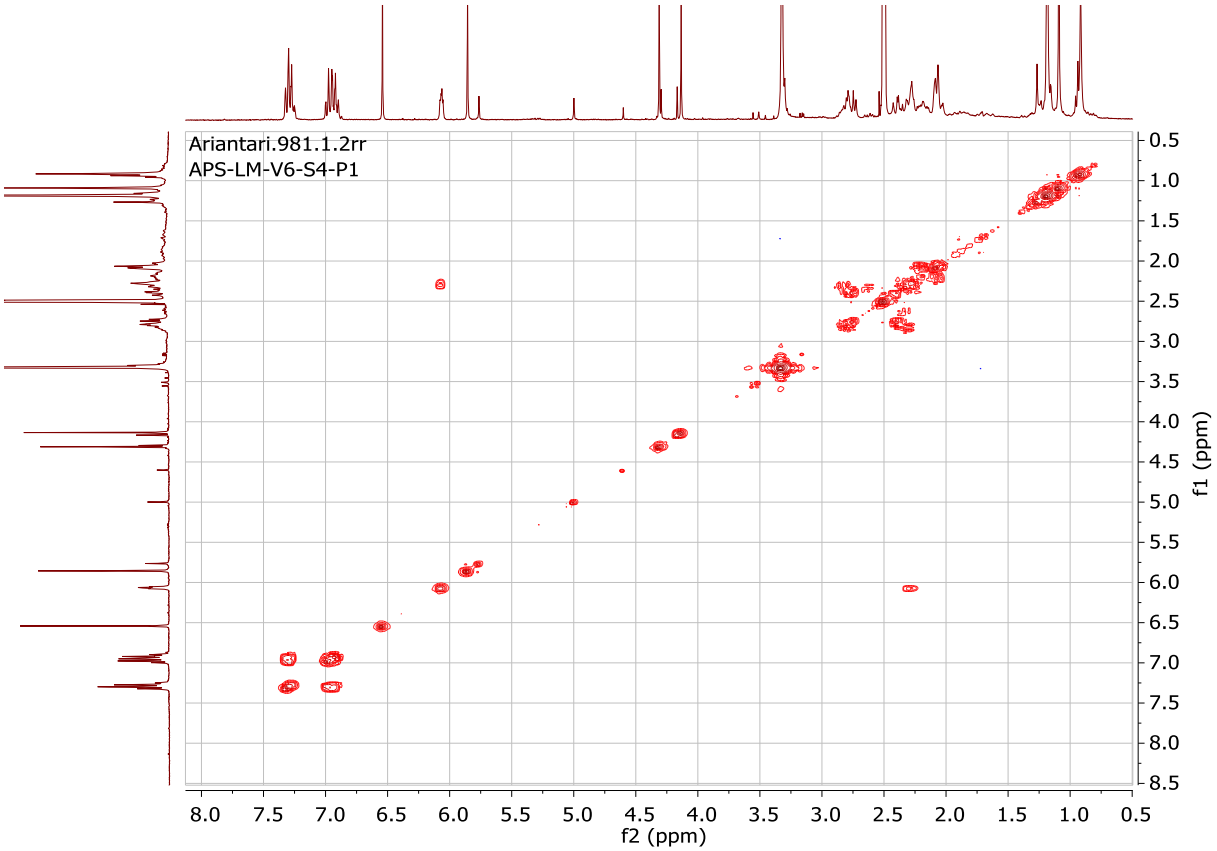

Figure S19. ^{1}H-^{1}H COSY (300 MHz, DMSO-d_6) spectrum of compound **3**.

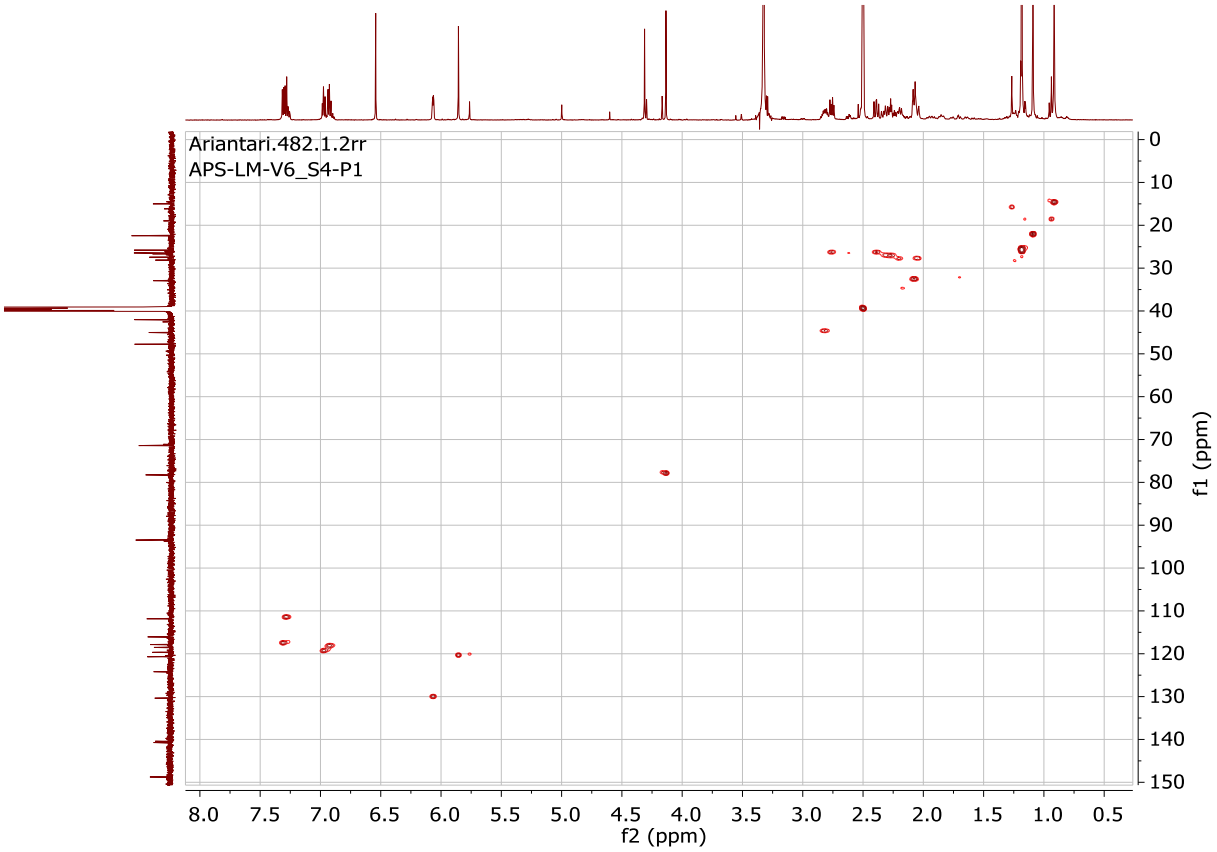

Figure S20. HSQC (600 and 150 MHz, DMSO-d_6) spectrum of compound **3**.

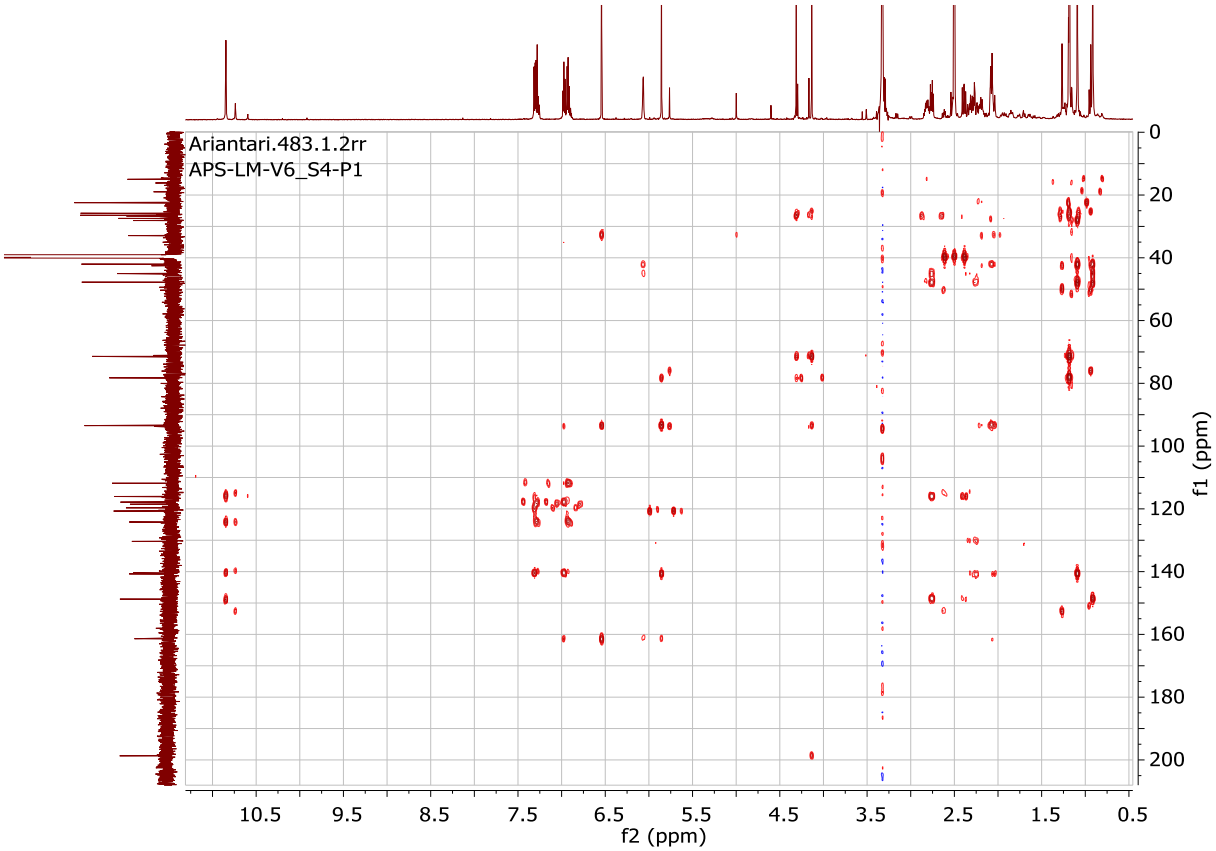

Figure S21. HMBC (600 and 150 MHz, DMSO-d_6) spectrum of compound **3**.

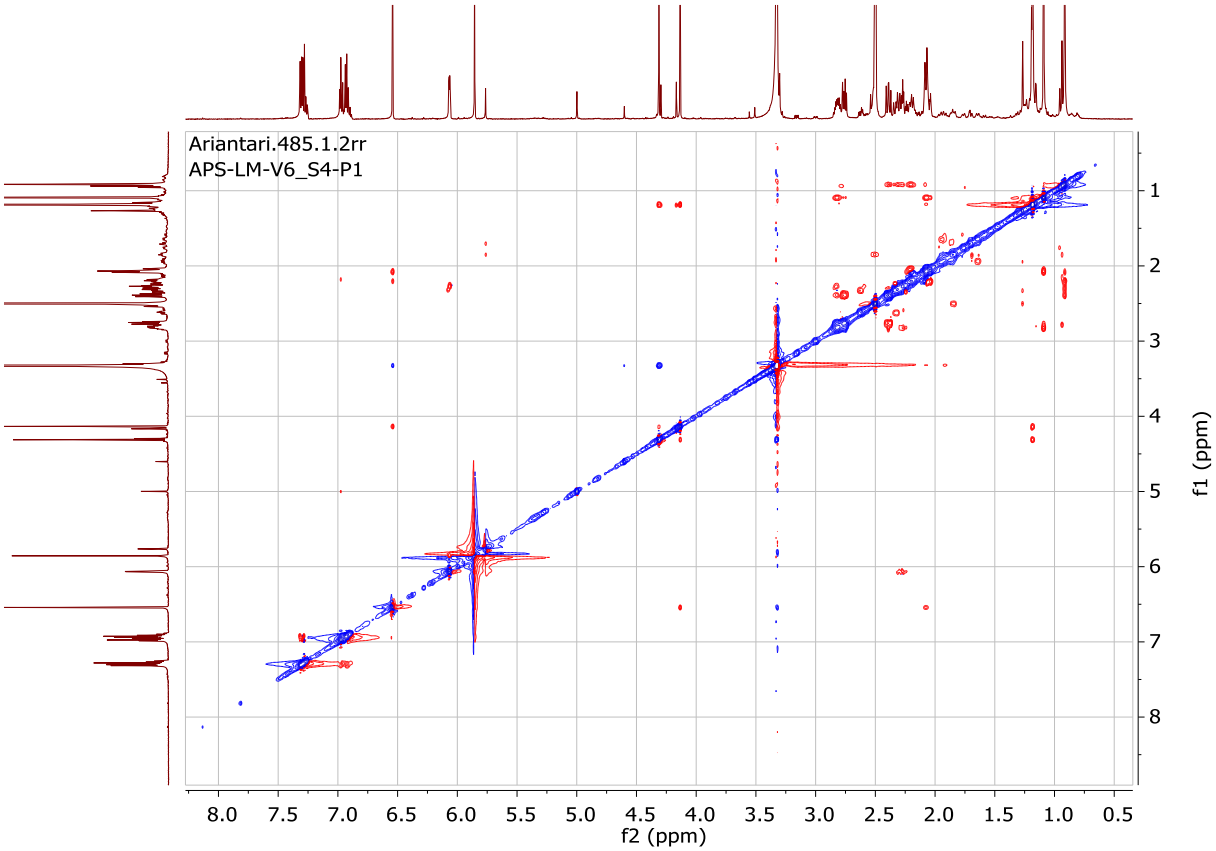

Figure S22. ROESY (600 MHz, DMSO-d_6) spectrum of compound **3**.

(A)

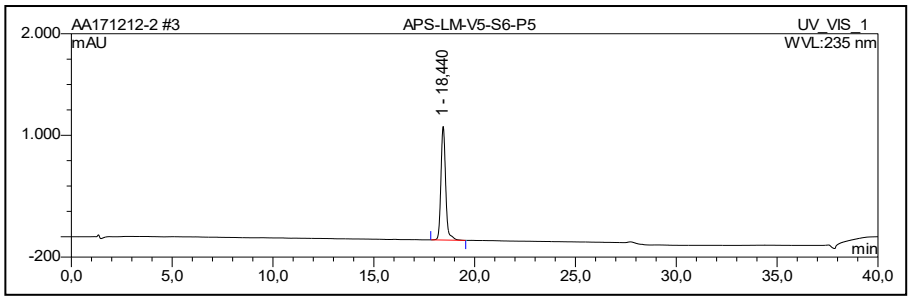

(B)

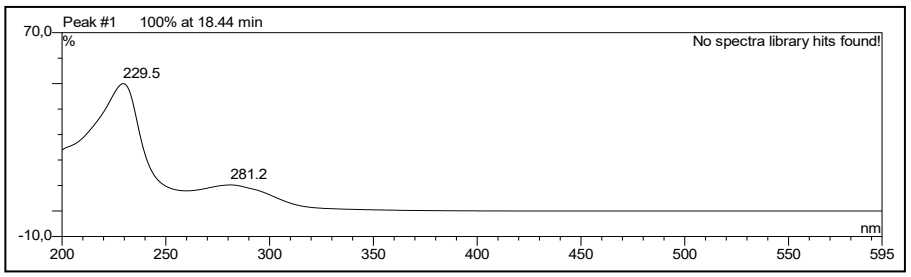

Figure S23. HPLC chromatogram (A) and UV spectrum (B) of compound **4**.

Acquisition Parameter

Source Type	ESI	Ion Polarity	Positive	Set Nebulizer	0.3 Bar
Focus	Not active	Set Capillary	4000 V	Set Dry Heater	180 °C
Scan Begin	50 m/z	Set End Plate Offset	-500 V	Set Dry Gas	4.0 l/min
Scan End	1500 m/z	Set Collision Cell RF	600.0 Vpp	Set Divert Valve	Source

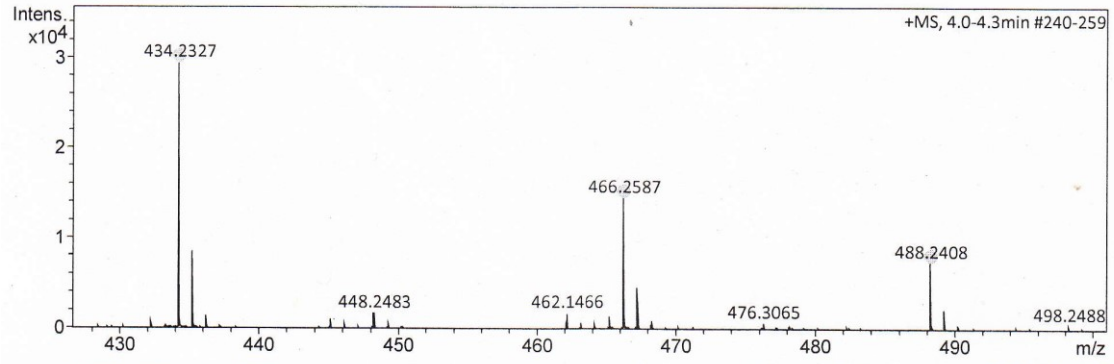

Meas. m/z	#	Ion Formula	m/z	err [ppm]	mSigma	# mSigma	Score	rdb	e⁻ Conf	N-Rule
434.2327	1	C27H32NO4	434.2326	-0.3	6.2	1	100.00	12.5	even	ok
466.2587	1	C28H36NO5	466.2588	0.3	4.4	1	100.00	11.5	even	ok
488.2408	1	C28H35NNaO5	488.2407	-0.1	10.3	1	100.00	11.5	even	ok

Figure S24. HRESIMS spectrum of compound **4**.

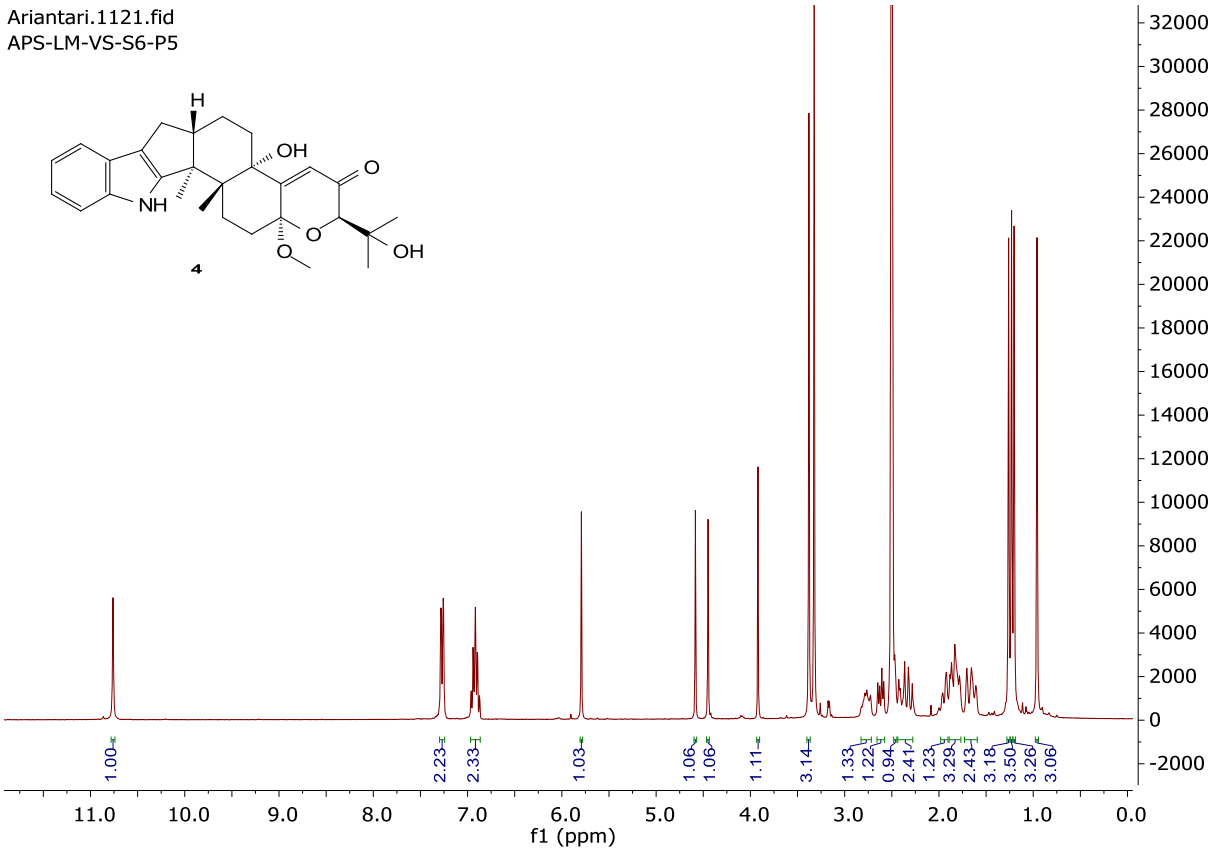

Figure S25. ^{1}H NMR (300 MHz, DMSO-d_6) spectrum of compound **4**.

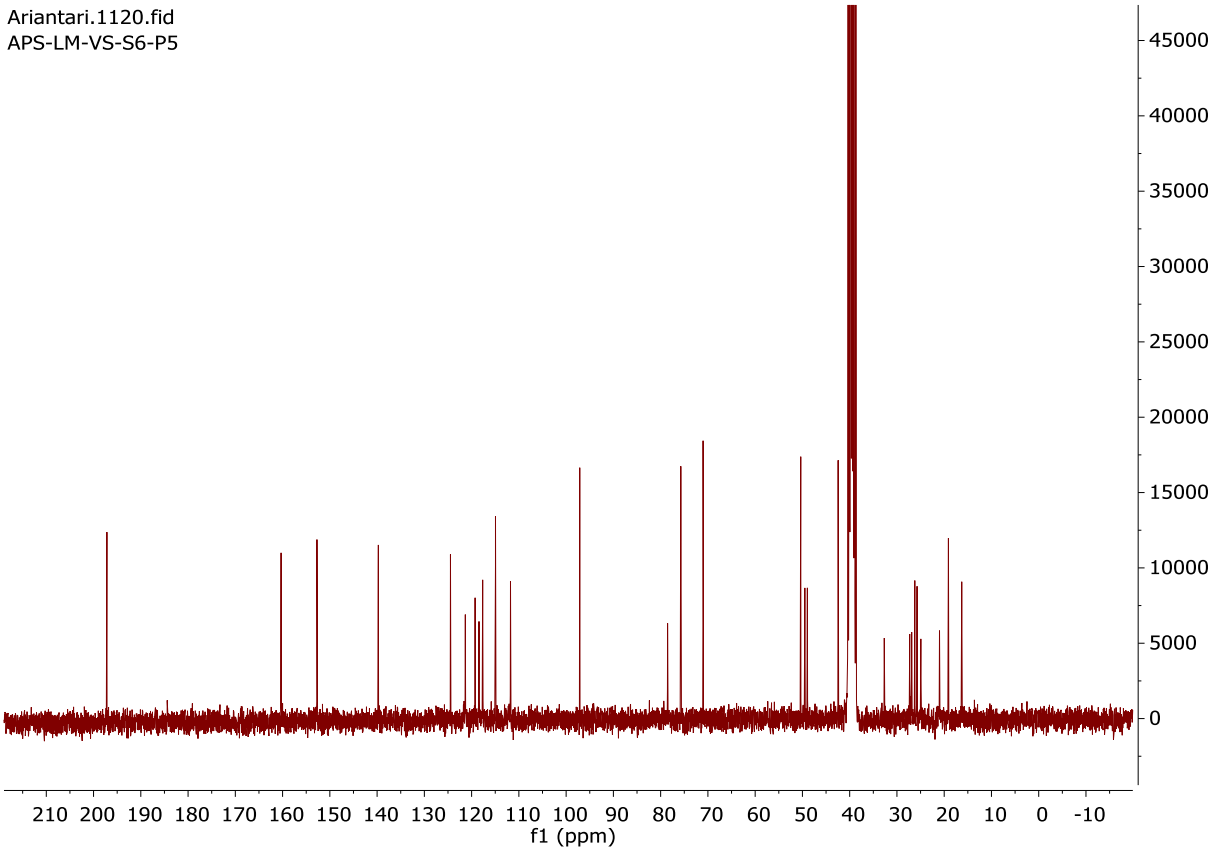

Figure S26. ^{13}C NMR (75 MHz, DMSO-d_6) spectrum of compound **4**.

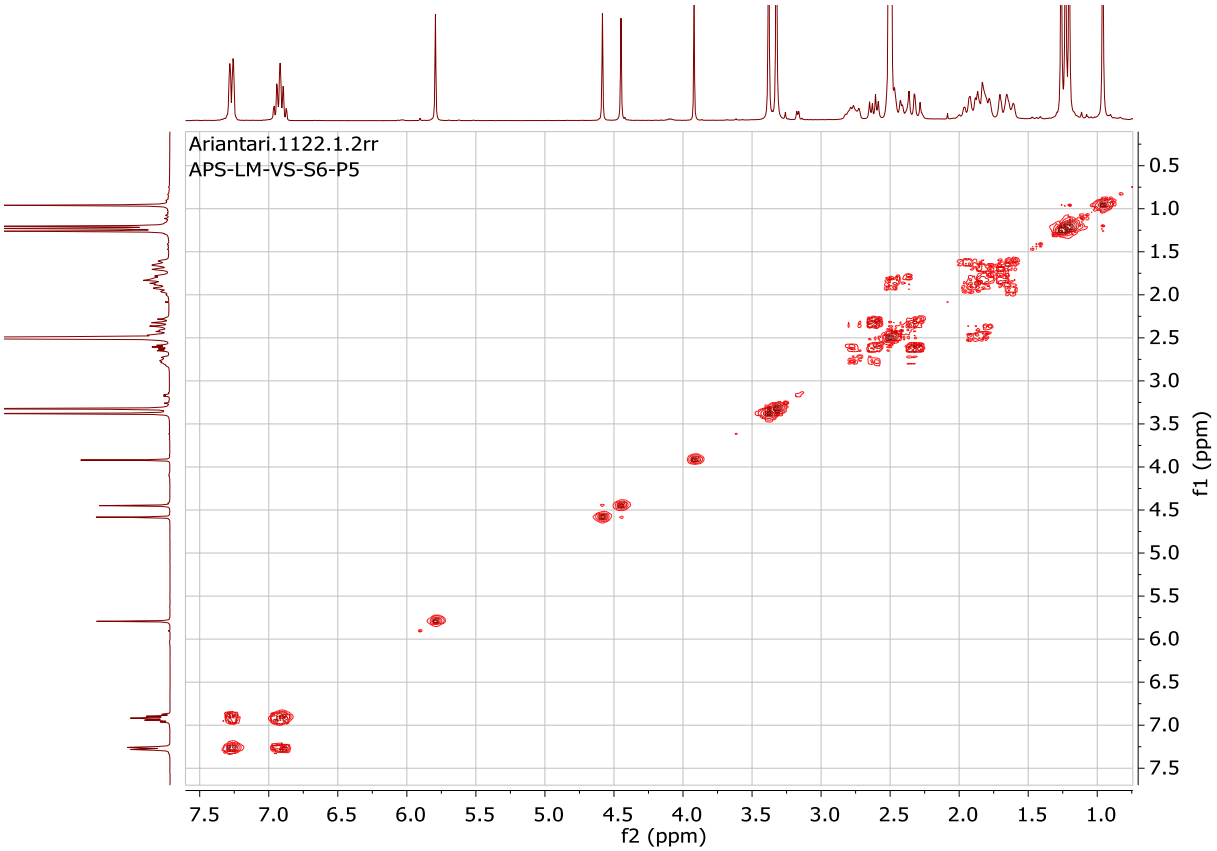

Figure S27. ^{1}H-^{1}H COSY (300 MHz, DMSO-d_6) spectrum of compound **4**.

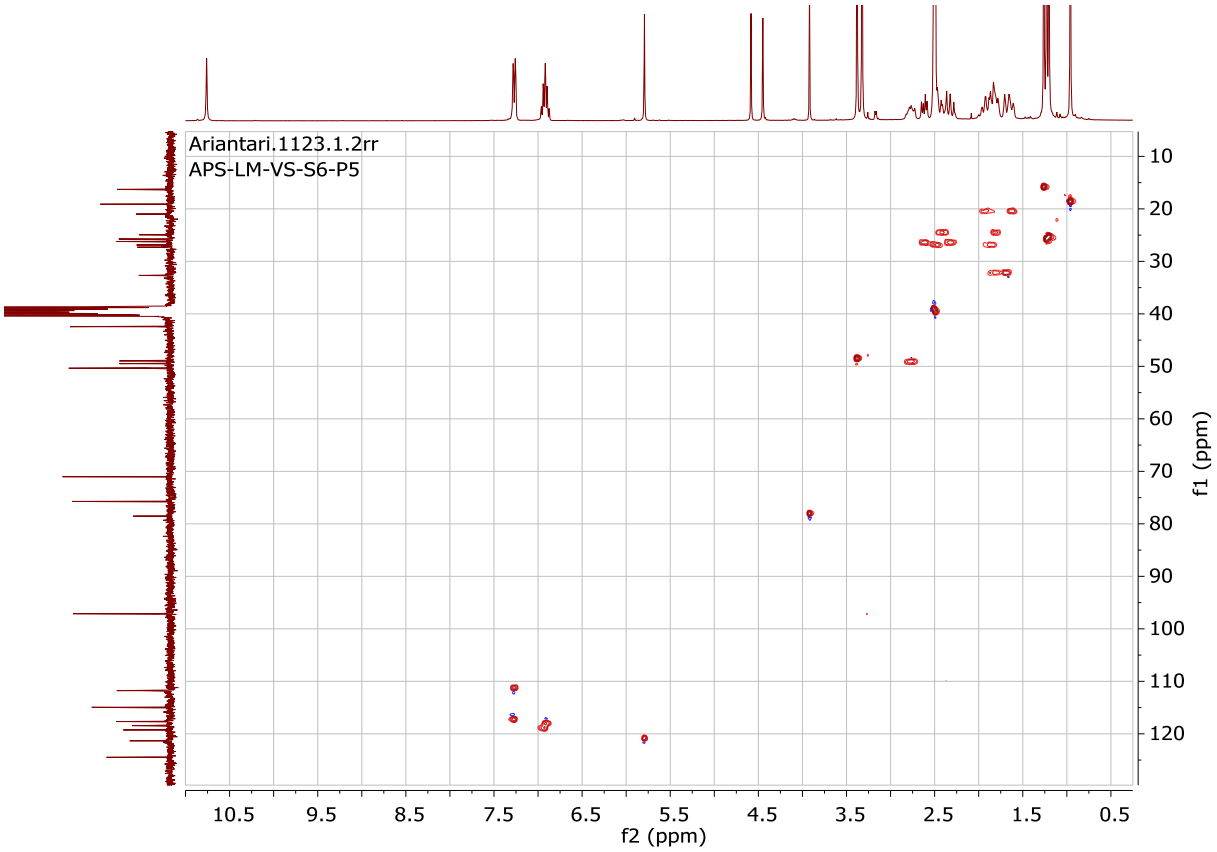

Figure S28. HSQC (300 and 75 MHz, DMSO-d_6) spectrum of compound **4**.

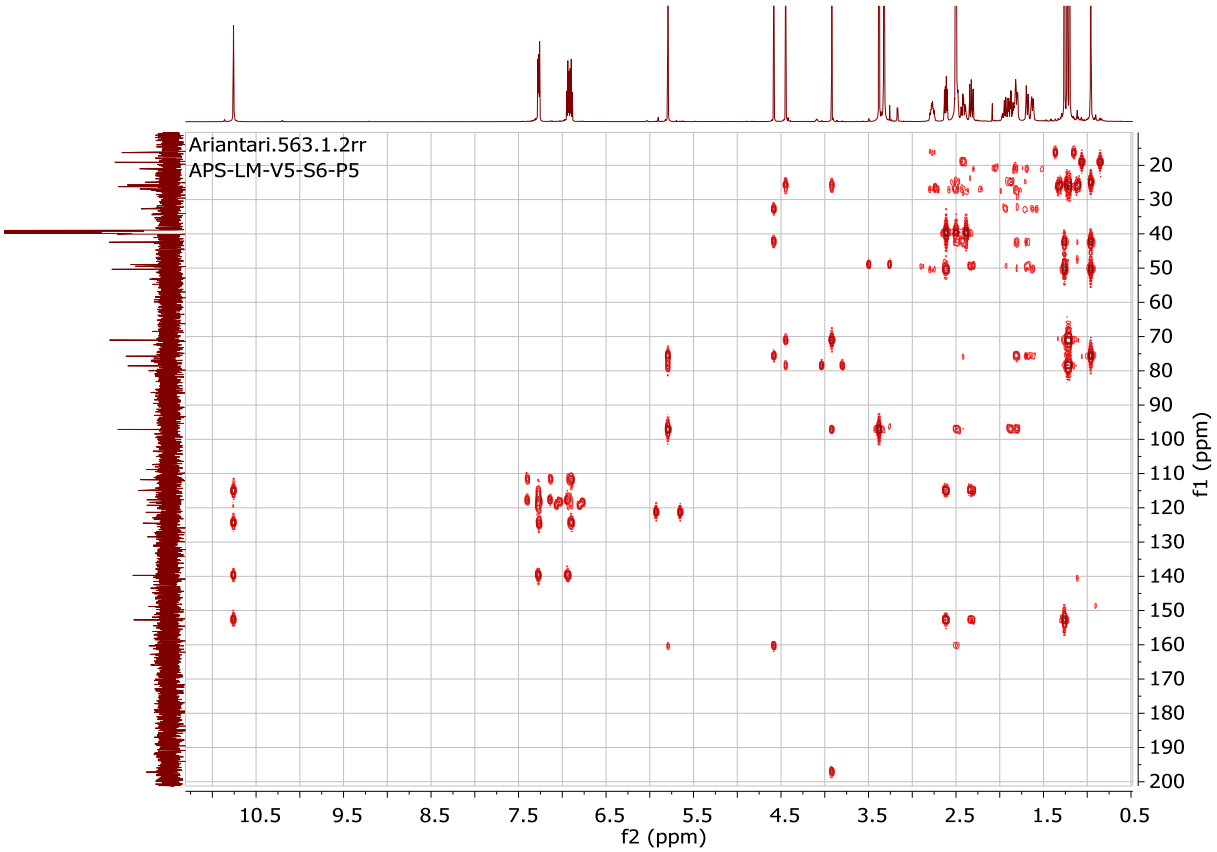

Figure S29. HMBC (600 and 150 MHz, DMSO-d_6) spectrum of compound **4**.

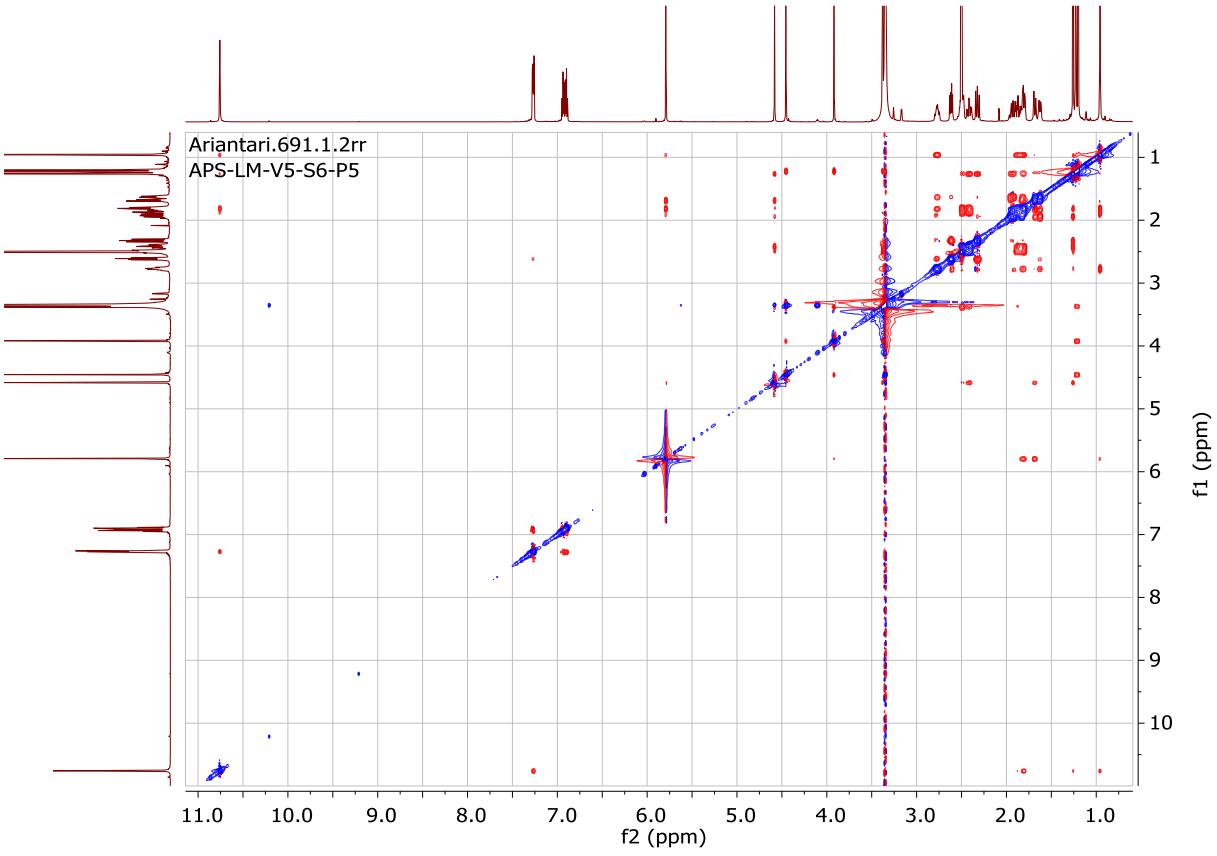

Figure S30. NOESY (600 MHz, DMSO-d_6) spectrum of compound **4**.

(A)

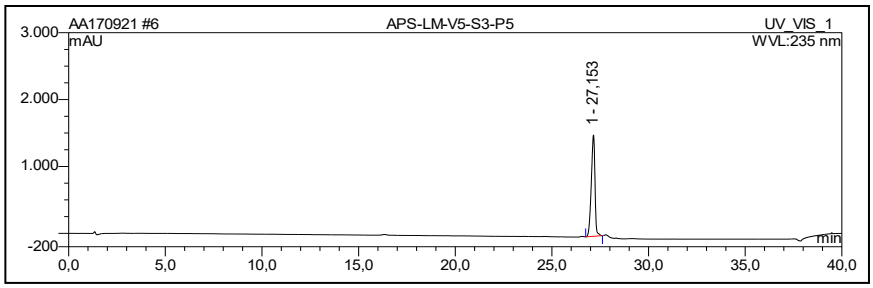

(B)

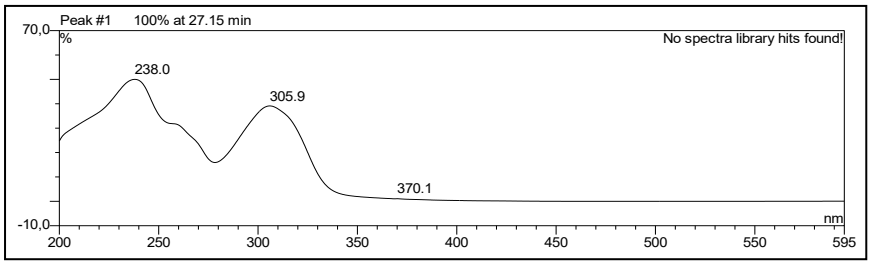

Figure S31. HPLC chromatogram (A) and UV spectrum (B) of compound **5**.

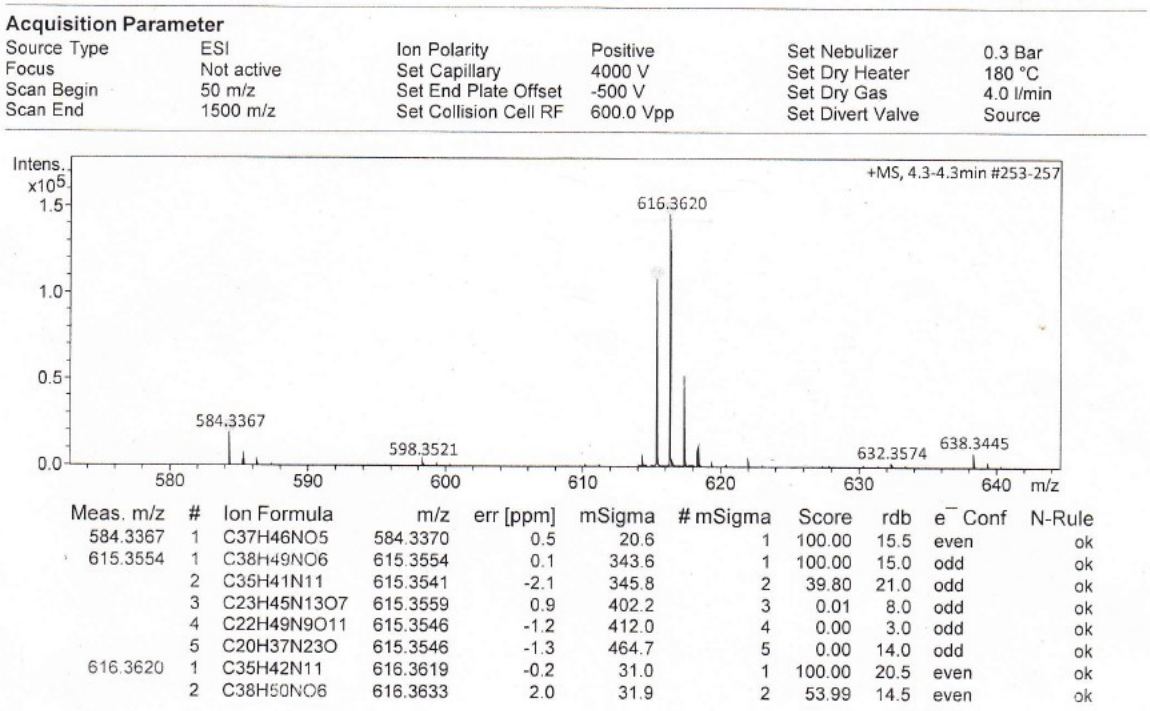

Meas. m/z	#	Ion Formula	m/z	err [ppm]	mSigma	# mSigma	Score	rdb	e⁻ Conf	N-Rule
584.3367	1	C37H46NO5	584.3370	0.5	20.6	1	100.00	15.5	even	ok
615.3554	1	C38H49NO6	615.3554	0.1	343.6	1	100.00	15.0	odd	ok
	2	C35H41N11	615.3541	-2.1	345.8	2	39.80	21.0	odd	ok
	3	C23H45N13O7	615.3559	0.9	402.2	3	0.01	8.0	odd	ok
	4	C22H49N9O11	615.3546	-1.2	412.0	4	0.00	3.0	odd	ok
	5	C20H37N23O	615.3546	-1.3	464.7	5	0.00	14.0	odd	ok
616.3620	1	C35H42N11	616.3619	-0.2	31.0	1	100.00	20.5	even	ok
	2	C38H50NO6	616.3633	2.0	31.9	2	53.99	14.5	even	ok

Figure S32. HRESIMS spectrum of compound **5**.

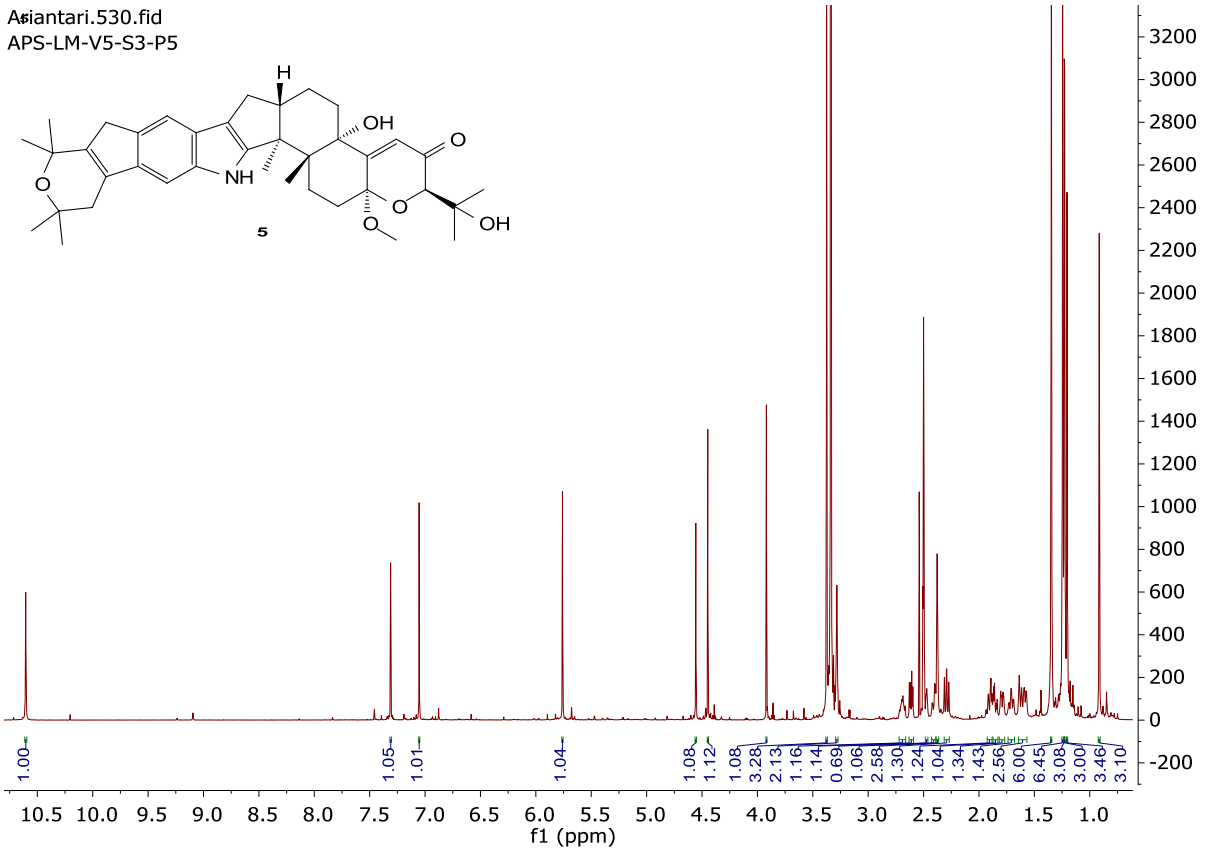

Figure S33. ^{1}H NMR (600 MHz, DMSO-d_6) spectrum of compound **5**.

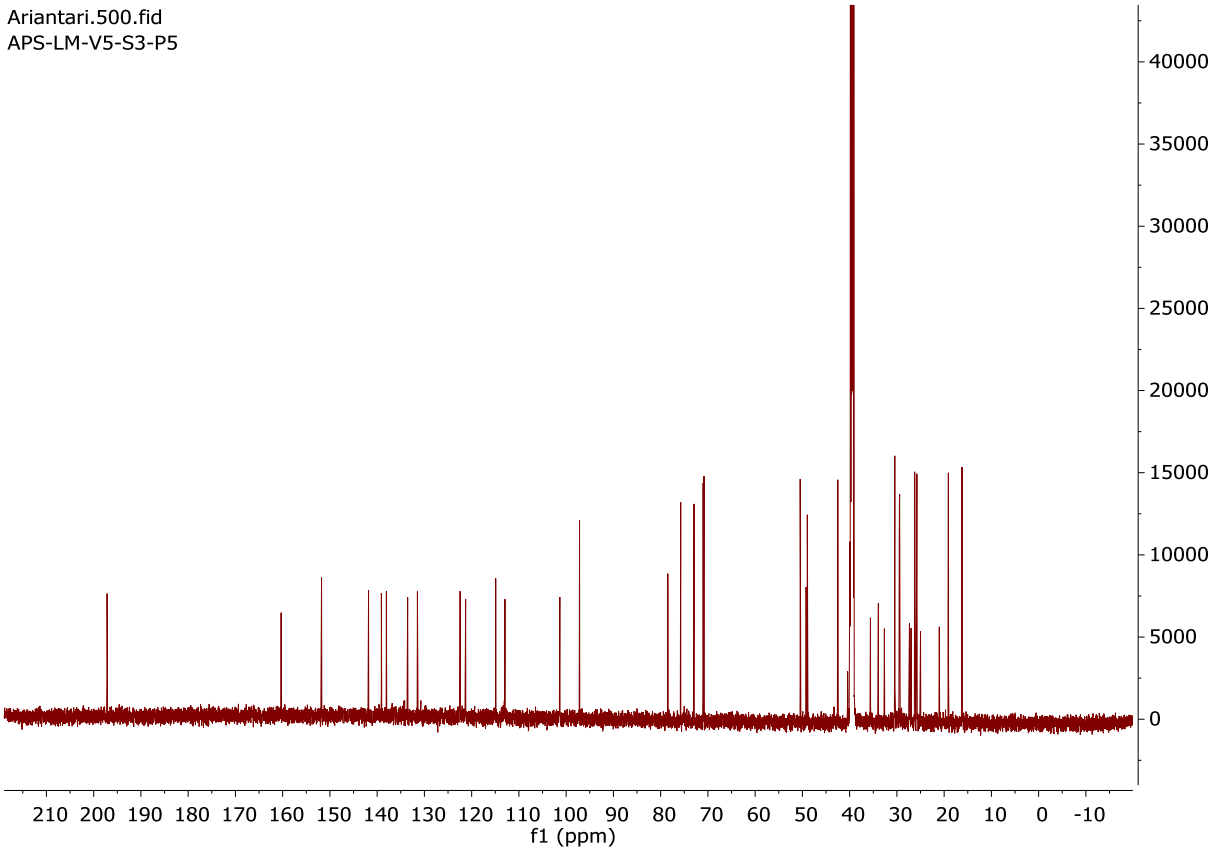

Figure S34. ^{13}C NMR (150 MHz, DMSO-d_6) spectrum of compound **5**.

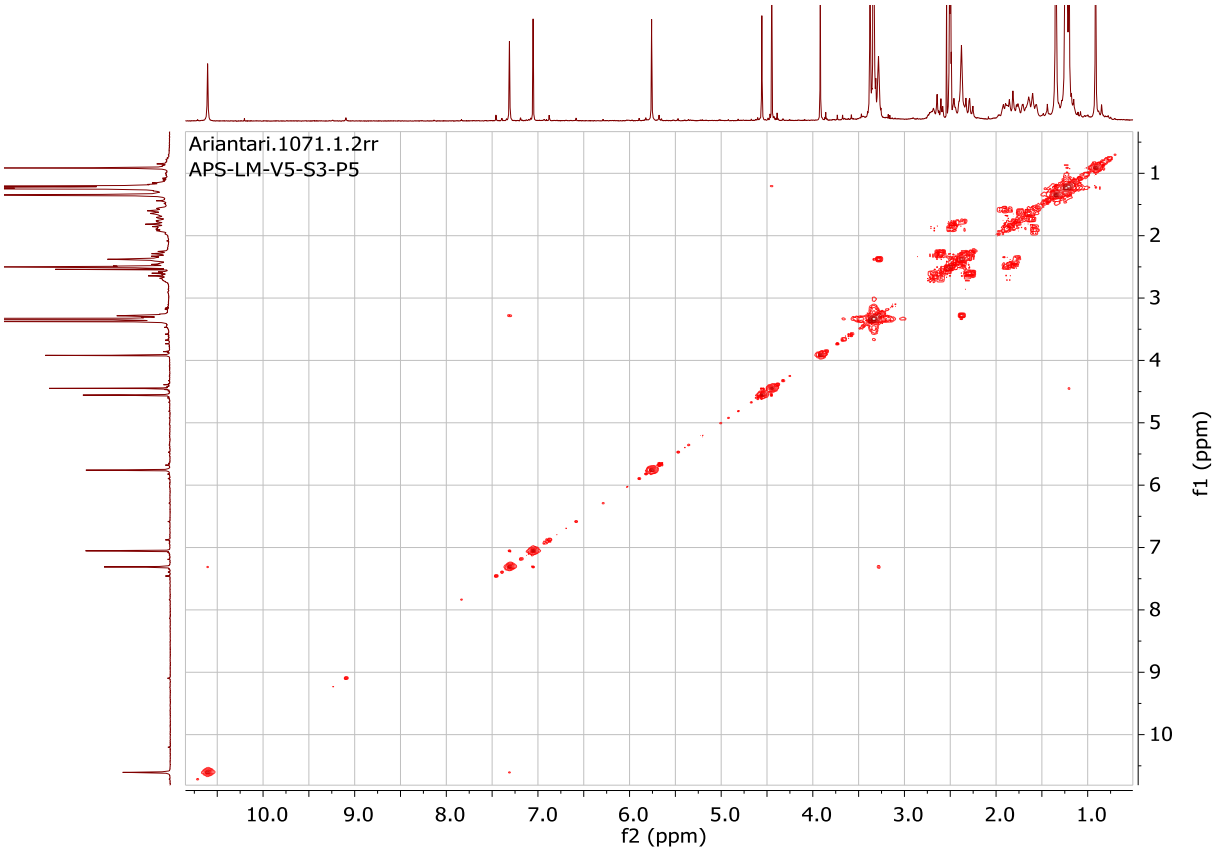

Figure S35. ^{1}H-^{1}H COSY (300 MHz, DMSO-d_6) spectrum of compound **5**.

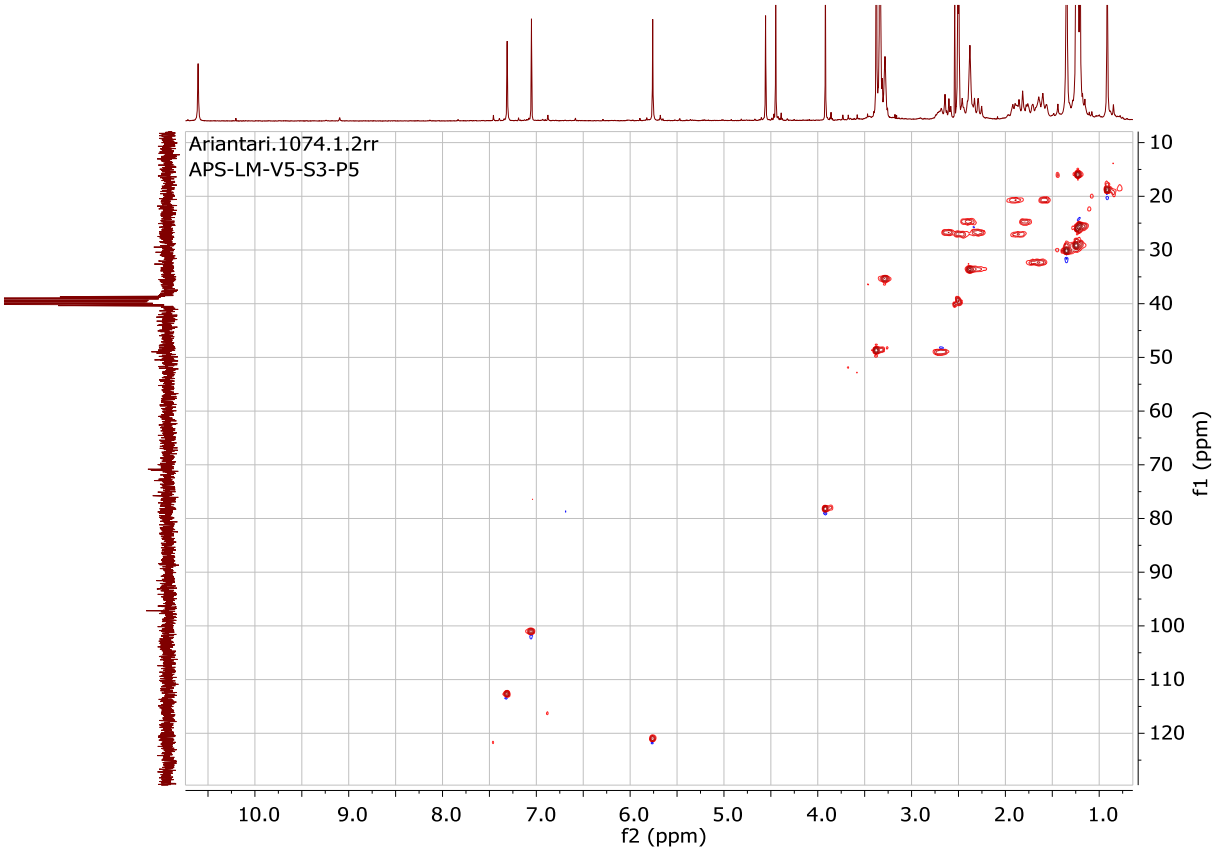

Figure S36. HSQC (300 and 75 MHz, DMSO-d_6) spectrum of compound **5**.

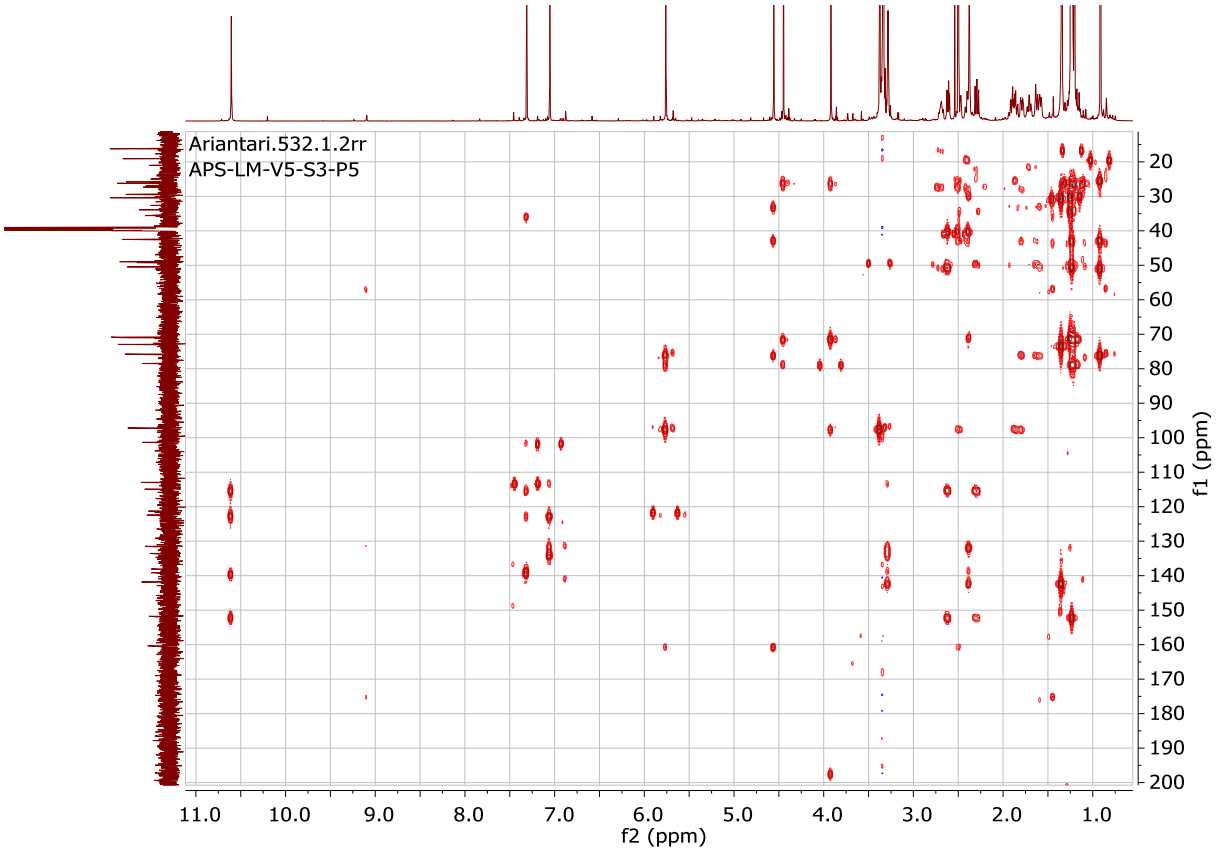

Figure S37. HMBC (600 and 150 MHz, DMSO-d_6) spectrum of compound **5**.

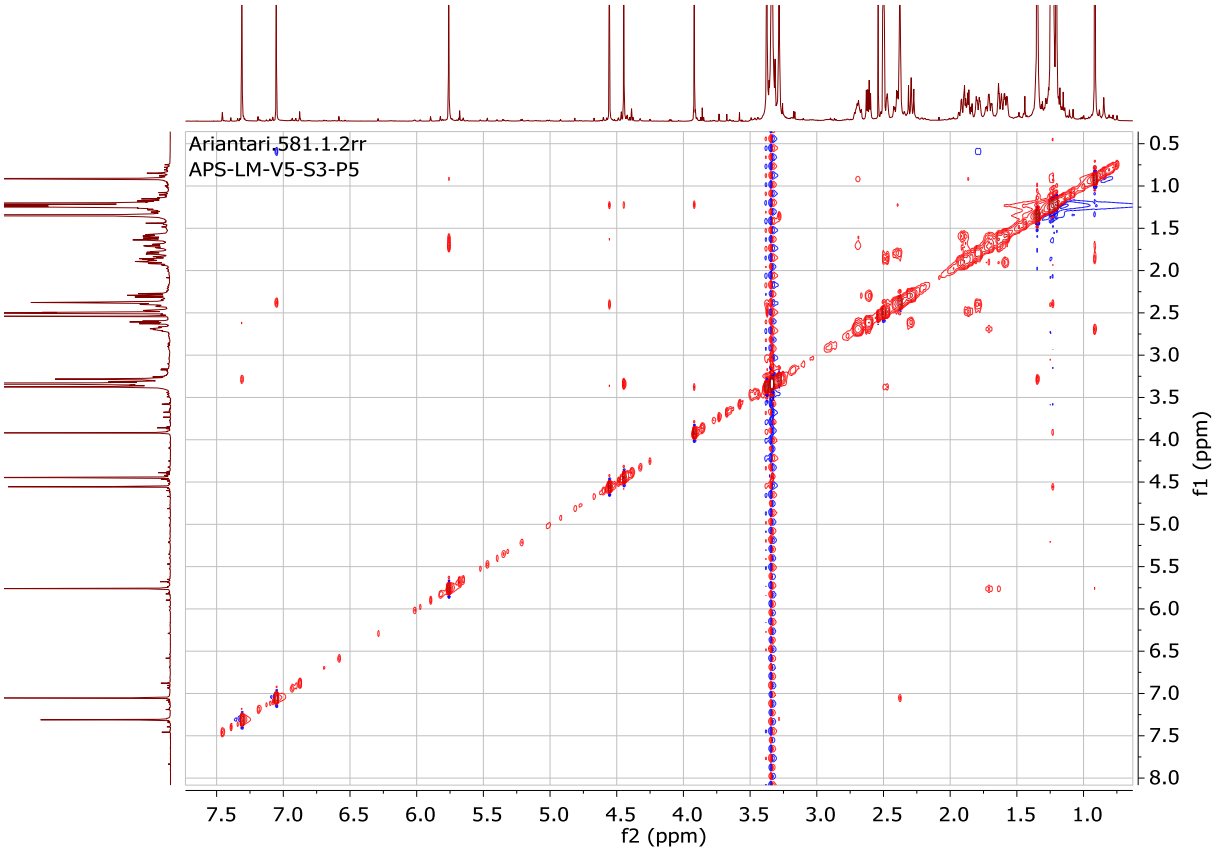

Figure S38. NOESY (600 MHz, DMSO-d_6) spectrum of compound **5**.

(A)

(B)

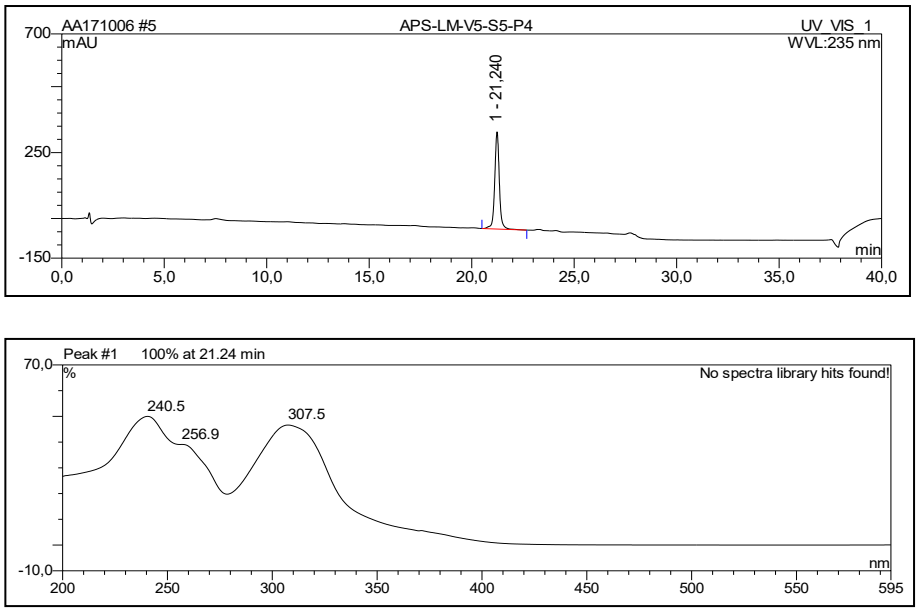

Figure S39. HPLC chromatogram (A) and UV spectrum (B) of compound **6**.

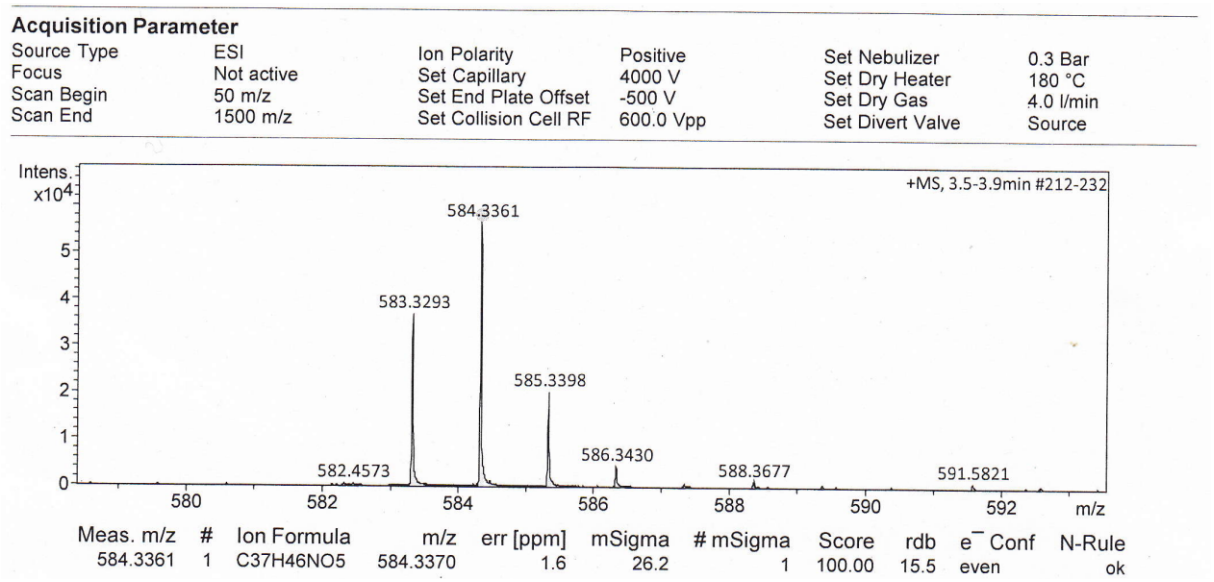

Figure S40. HRESIMS spectrum of compound **6**.

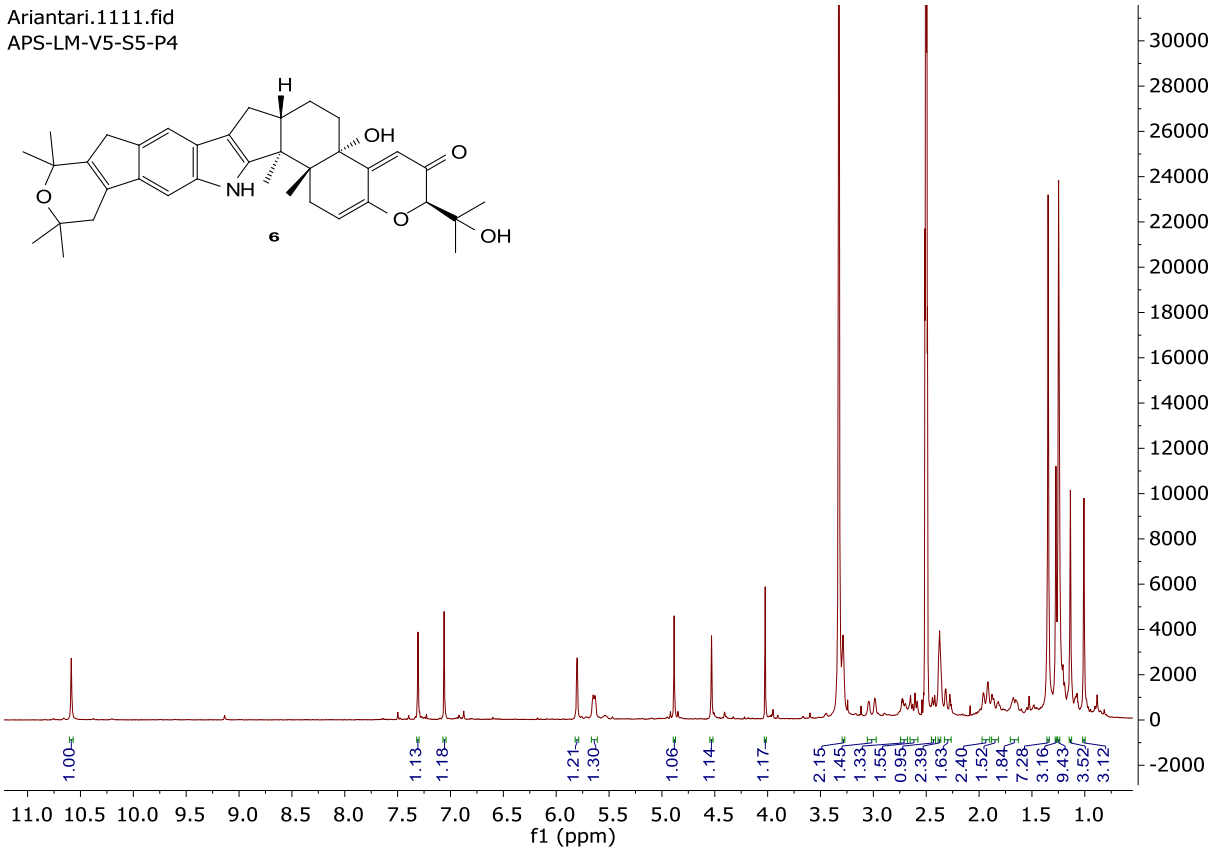

Figure S41. ^{1}H NMR (300 MHz, DMSO-d_6) spectrum of compound **6**.

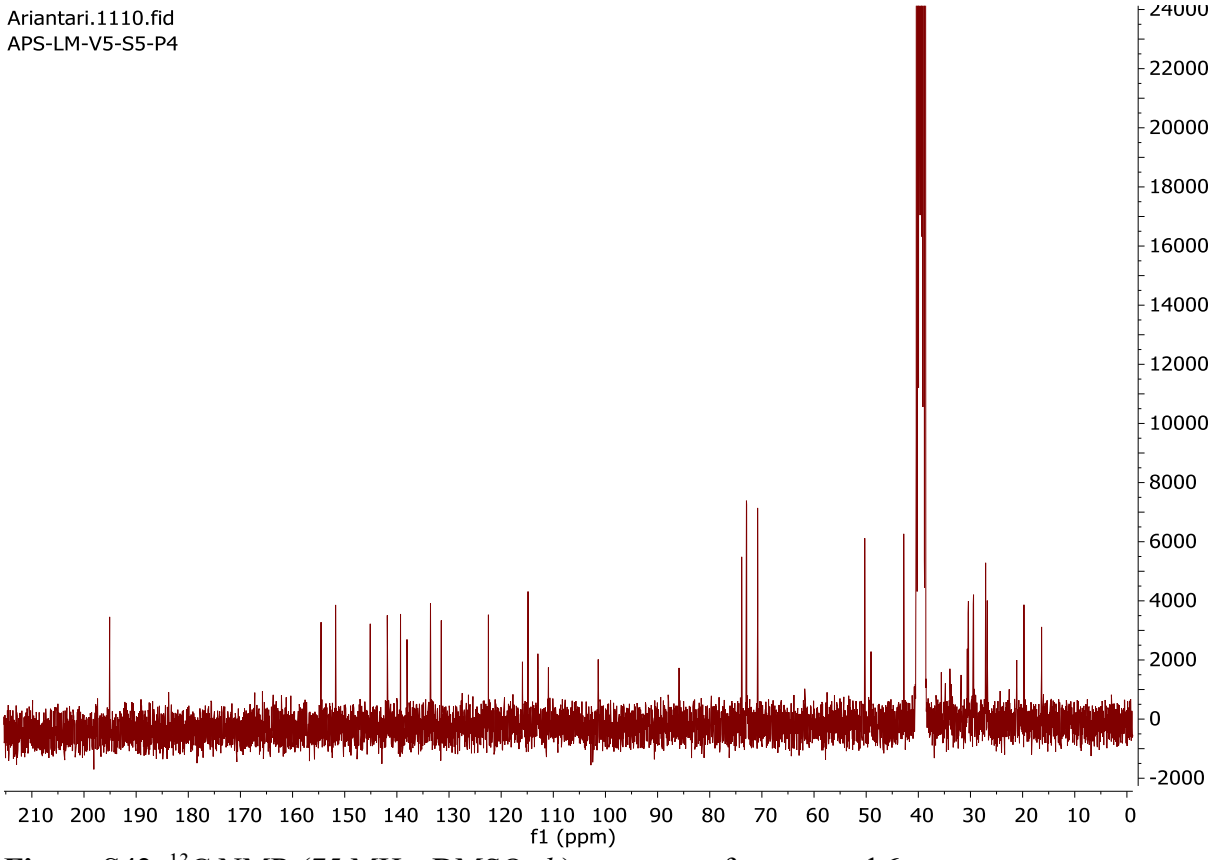

Figure S42. ^{13}C NMR (75 MHz, DMSO-d_6) spectrum of compound **6**.

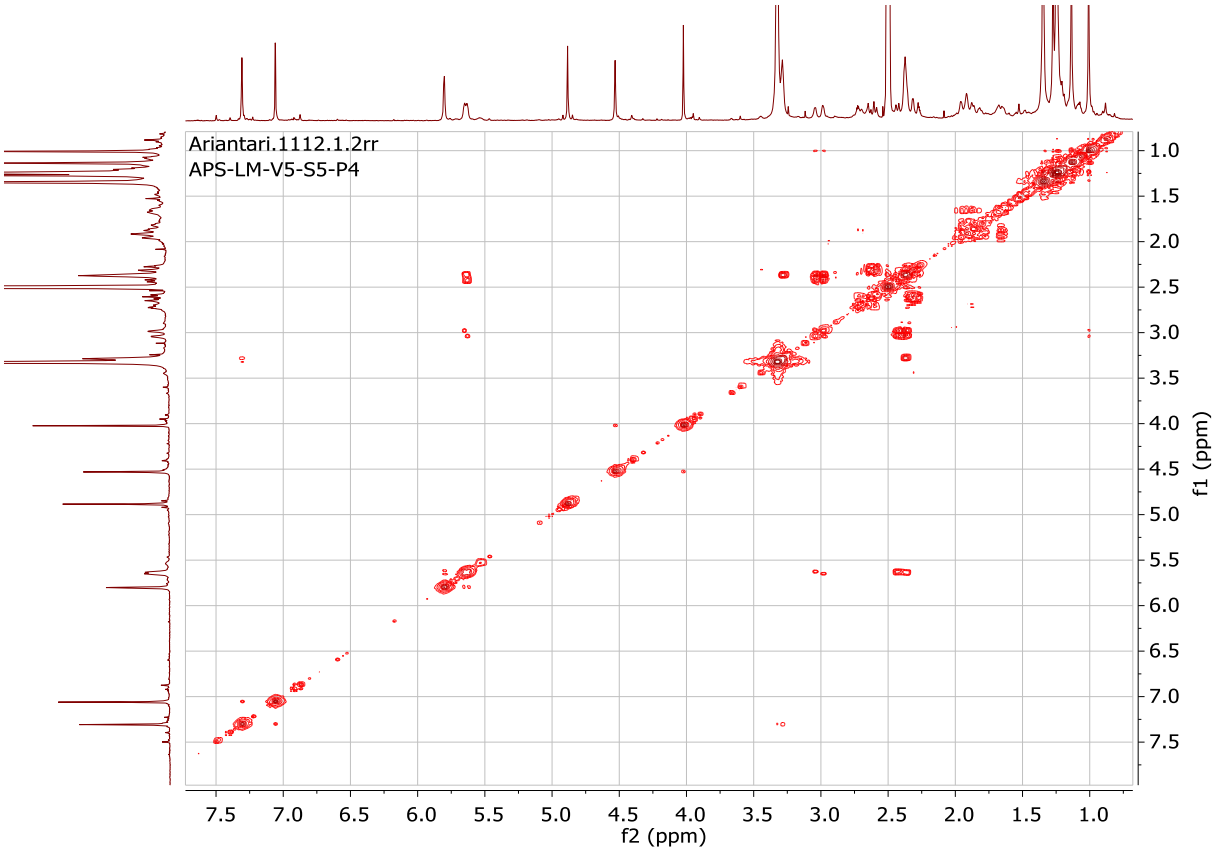

Figure S43. ^{1}H-^{1}H COSY (300 MHz, DMSO-d_6) spectrum of compound **6**.

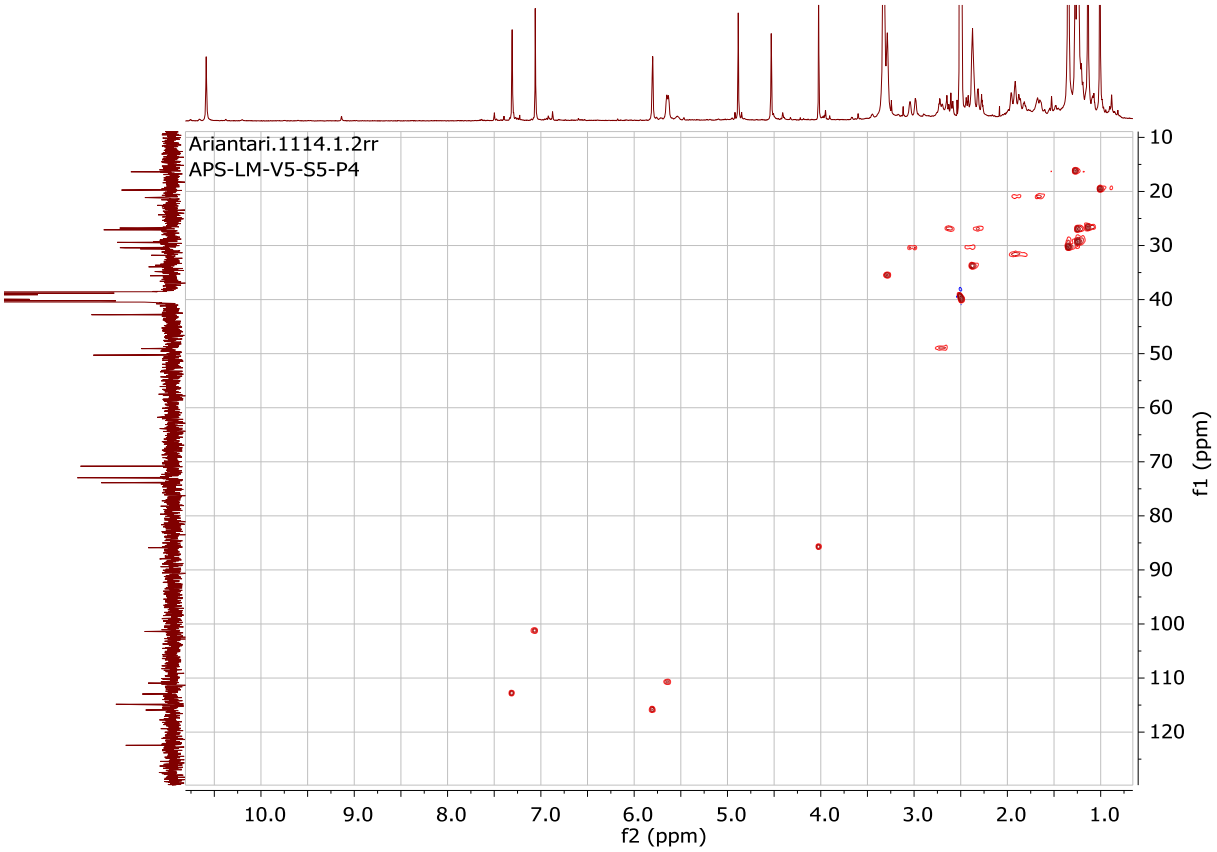

Figure S44. HSQC (300 and 75 MHz, DMSO-d_6) spectrum of compound **6**.

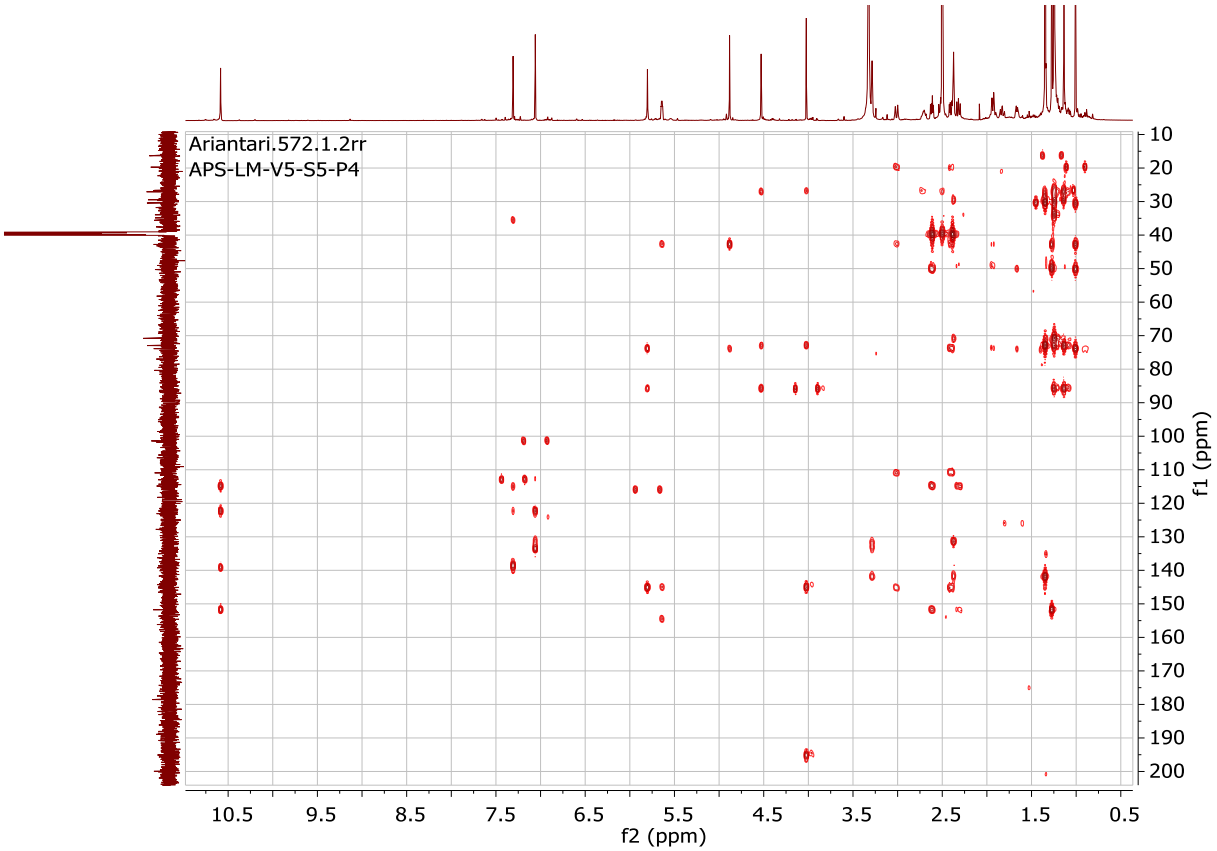

Figure S45. HMBC (600 and 150 MHz, DMSO-d_6) spectrum of compound **6**.

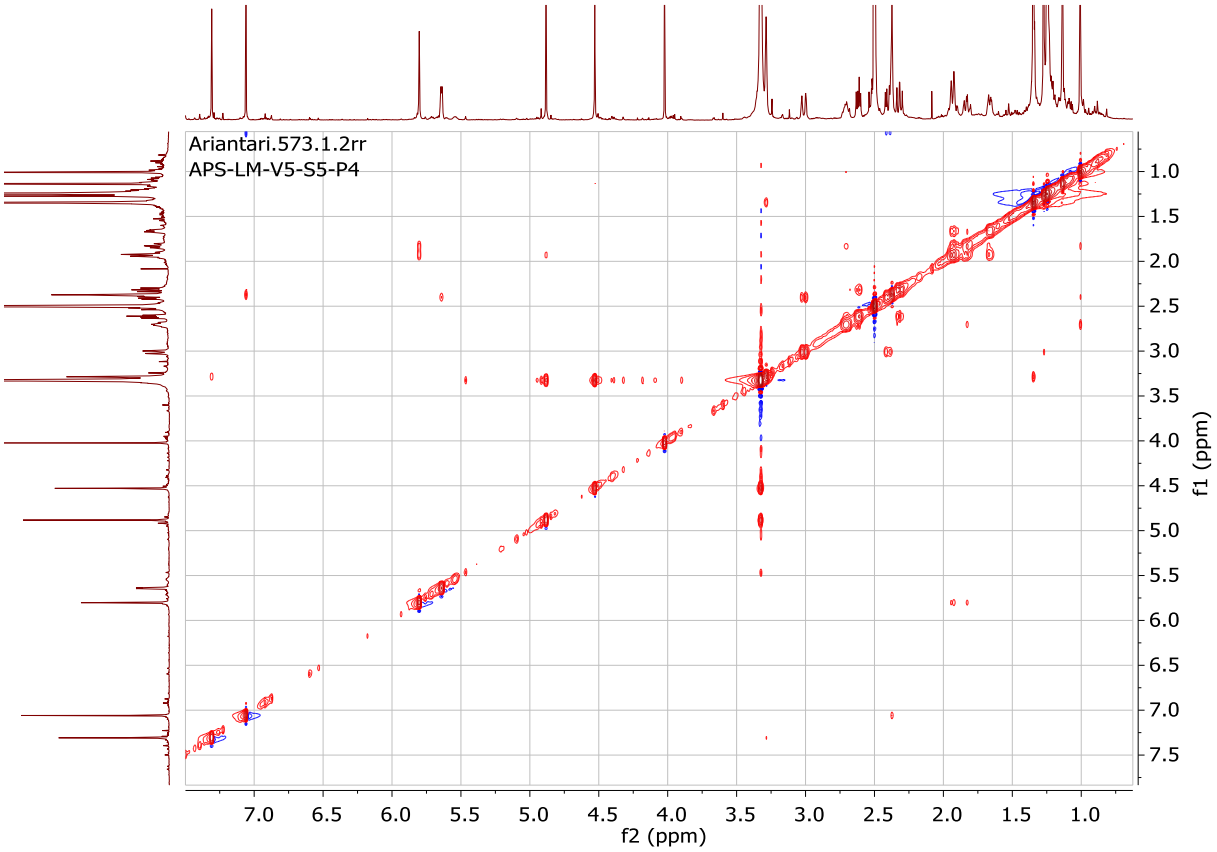

Figure S46. NOESY (600 MHz, DMSO-d_6) spectrum of compound **6**.

(A)

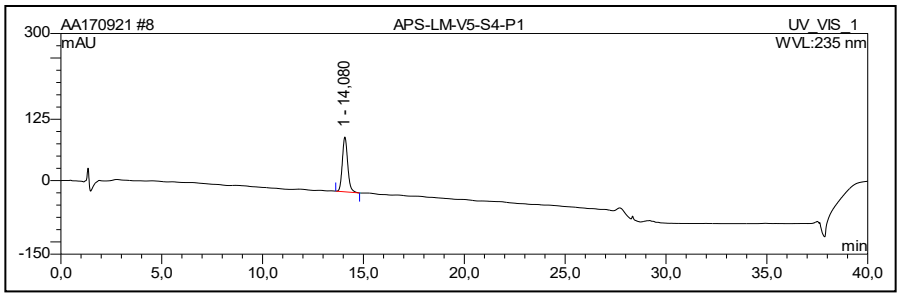

(B)

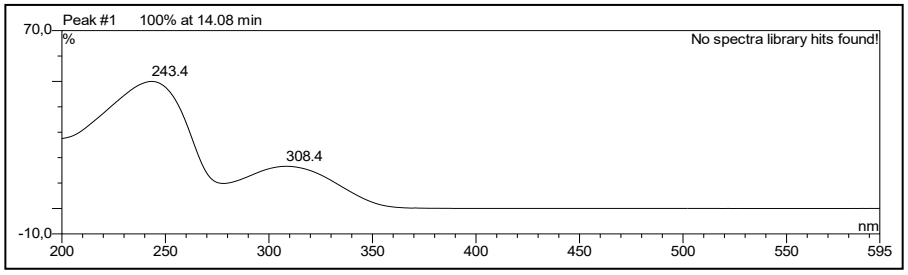

Figure S47. HPLC chromatogram (A) and UV spectrum (B) of compound **7**.

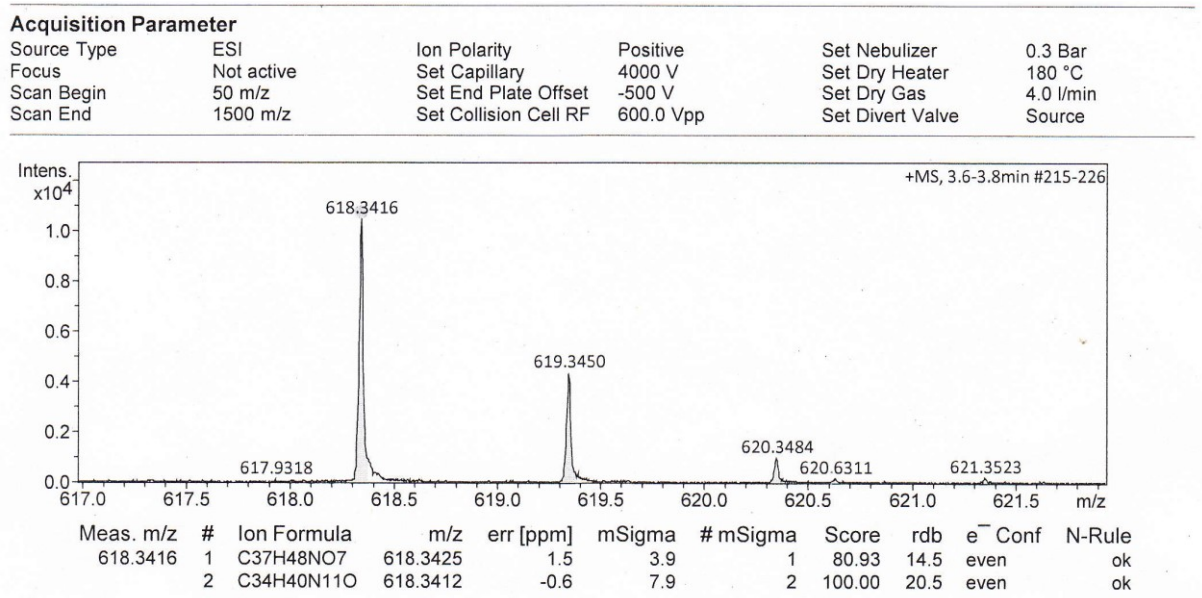

Figure S48. HRESIMS spectrum of compound **7**.

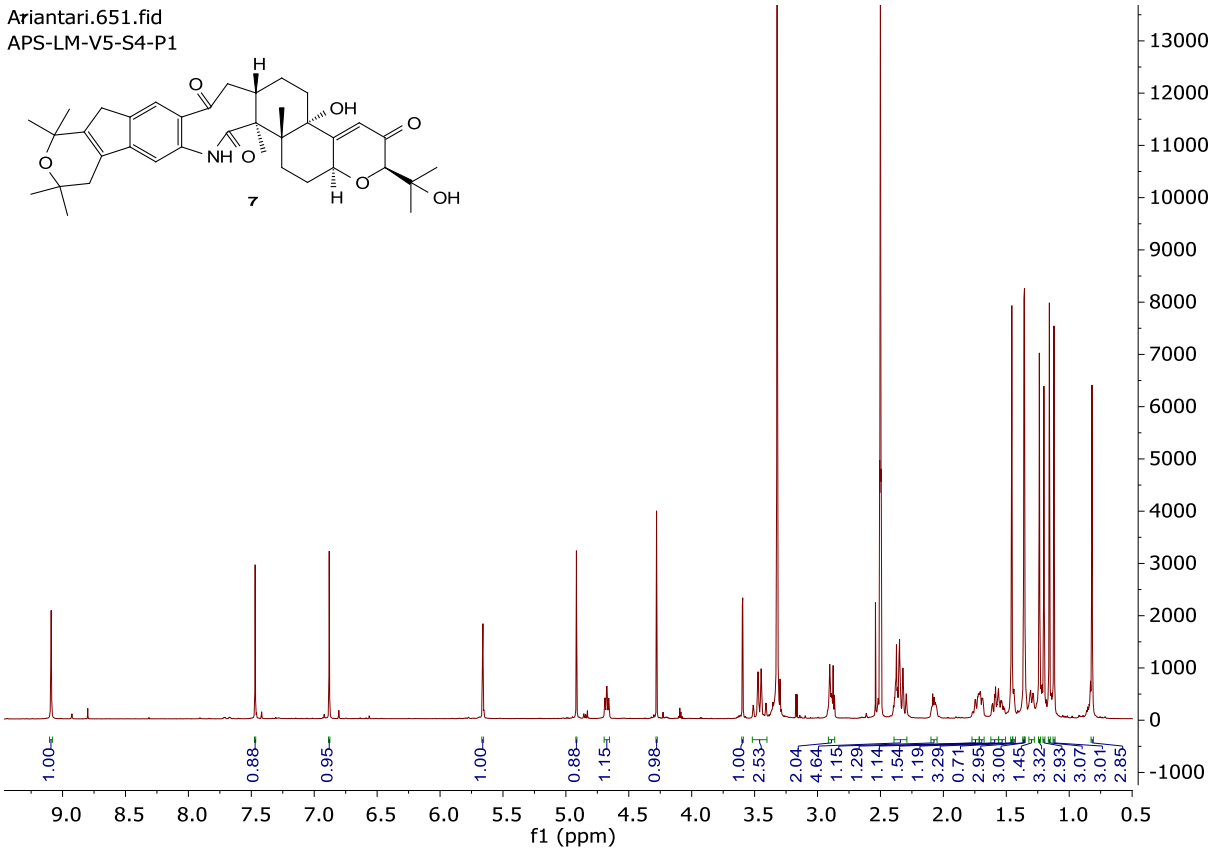

Figure S49. ^{1}H NMR (600 MHz, DMSO-d_6) spectrum of compound **7**.

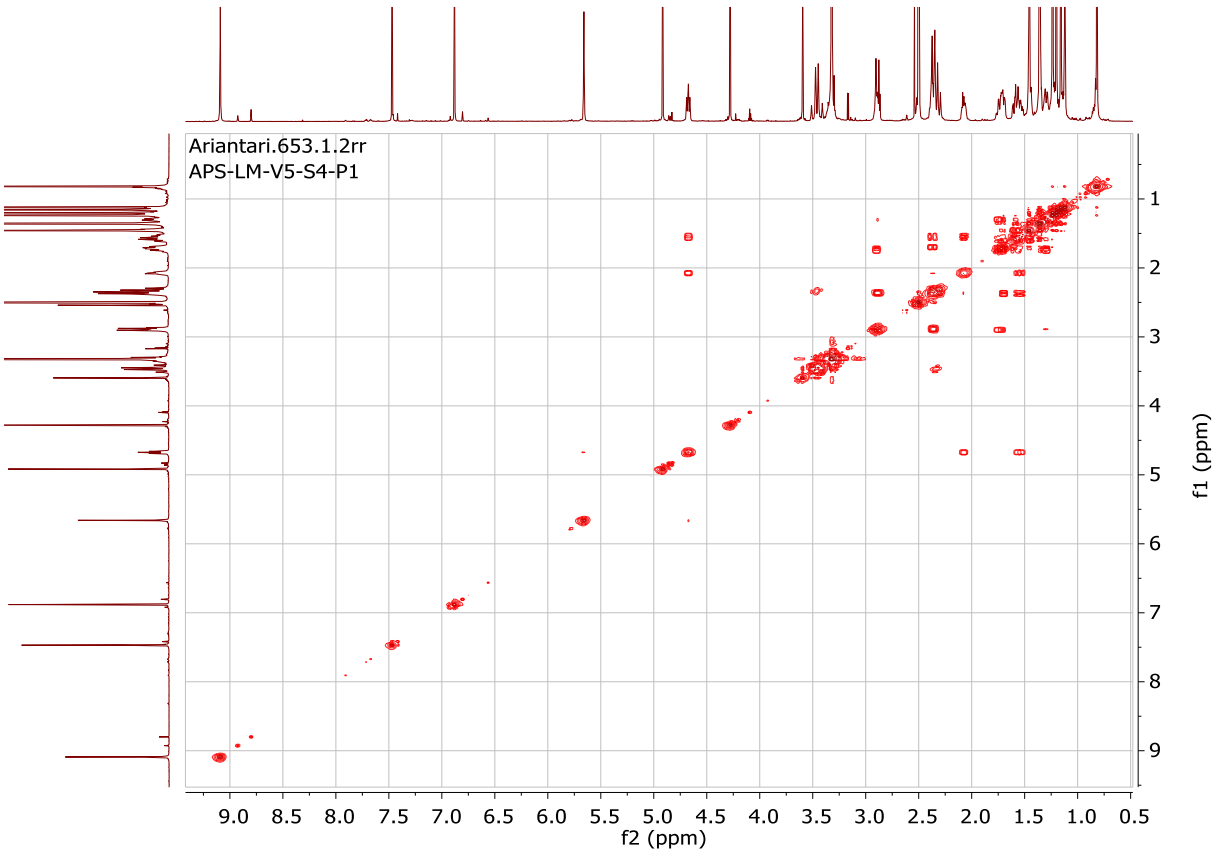

Figure S50. ^{1}H-^{1}H COSY (600 MHz, DMSO-d_6) spectrum of compound **7**.

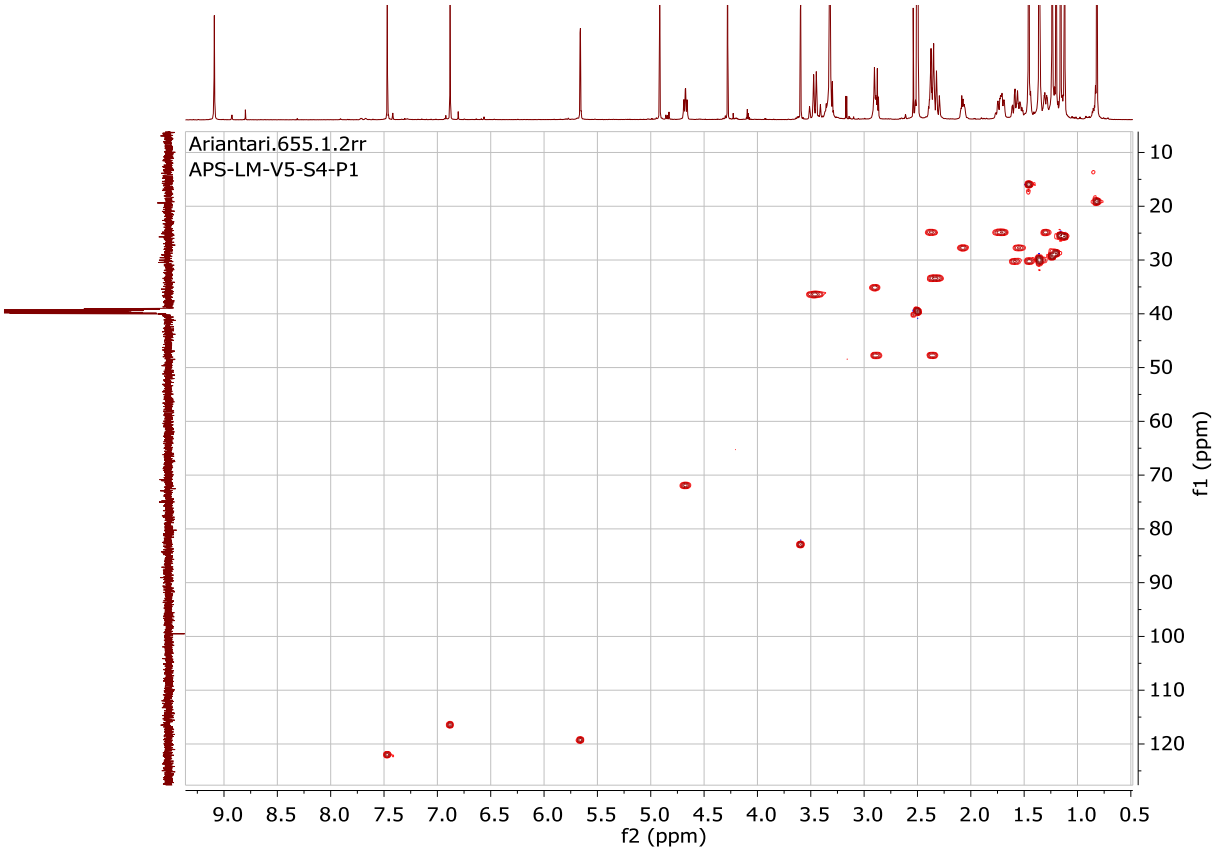

Figure S51. HSQC (600 and 150 MHz, DMSO-d_6) spectrum of compound **7**.

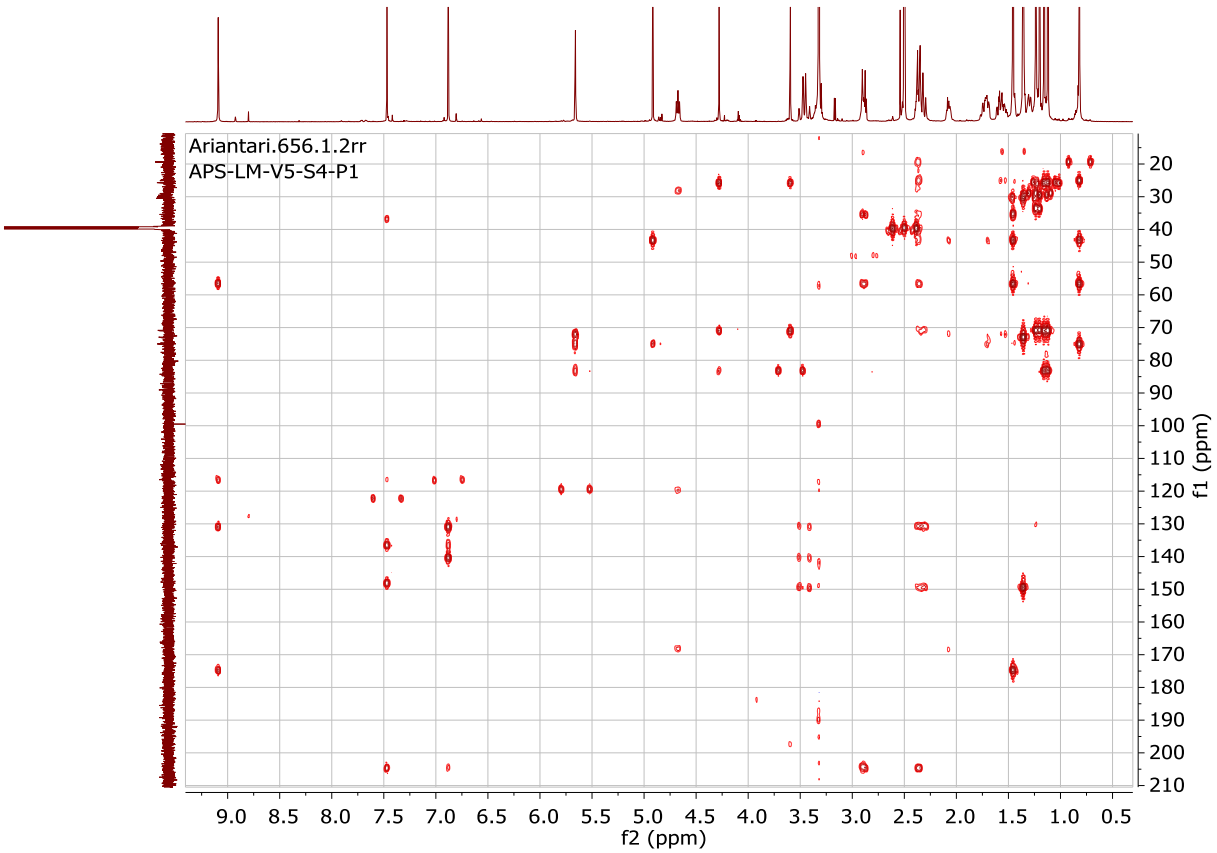

Figure S52. HMBC (600 and 150 MHz, DMSO-d_6) spectrum of compound **7**.

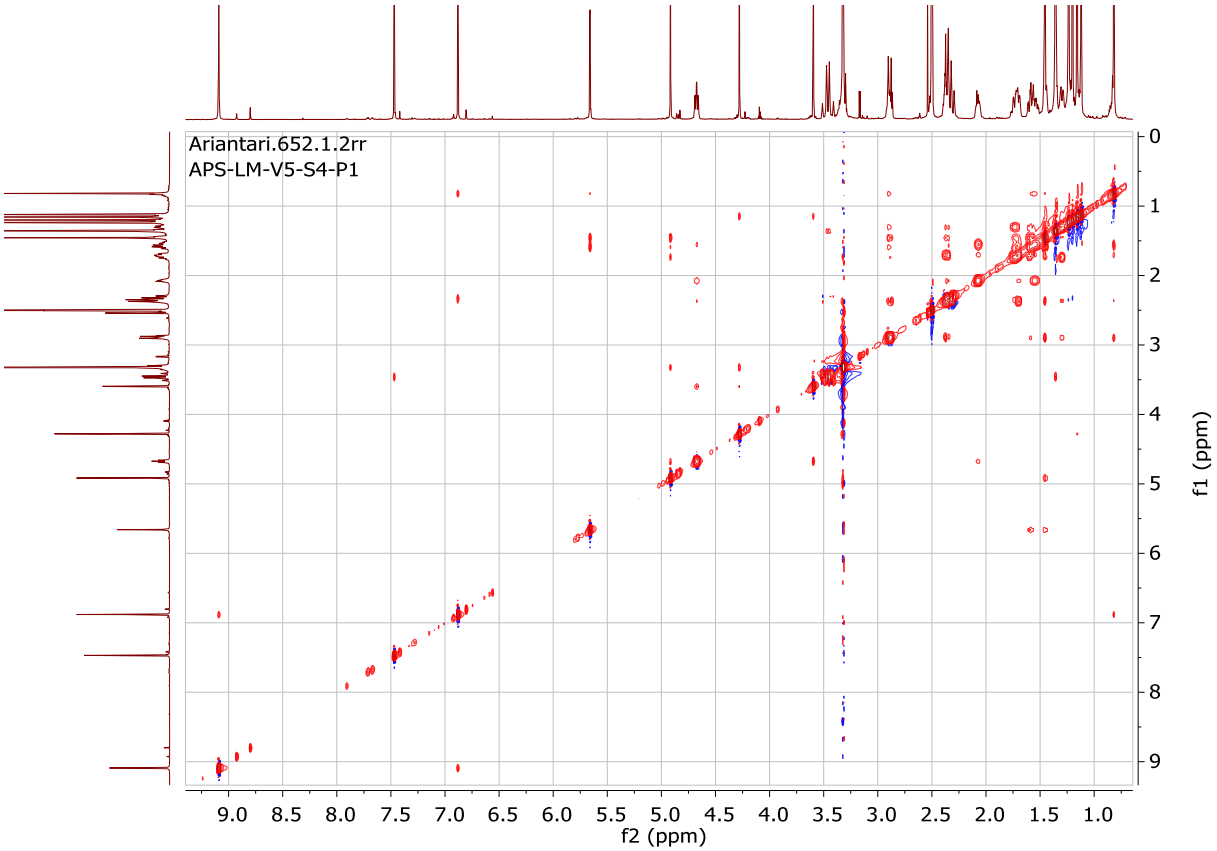

Figure S53. NOESY (600 MHz, DMSO-d_6) spectrum of compound **7**.

(A)

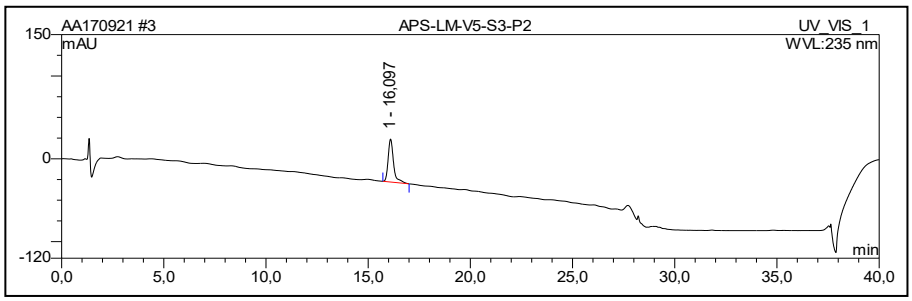

(B)

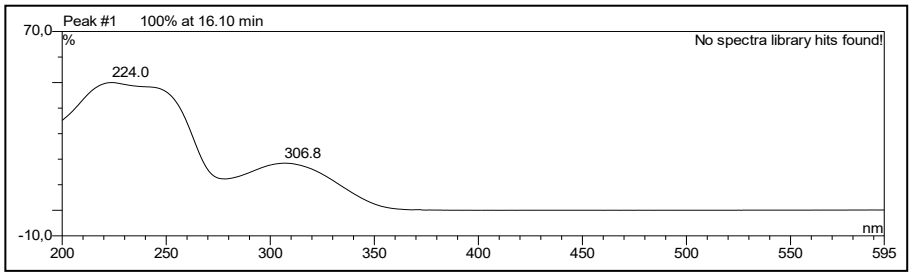

Figure S54. HPLC chromatogram (A) and UV spectrum (B) of compound **8**.

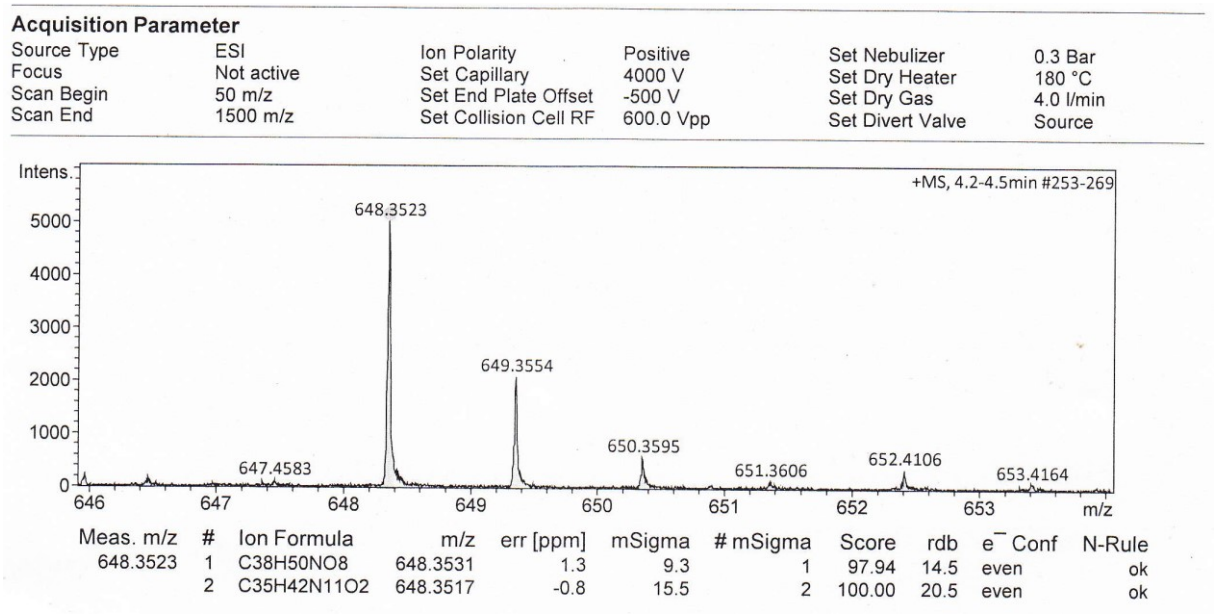

Figure S55. HRESIMS spectrum of compound **8**.

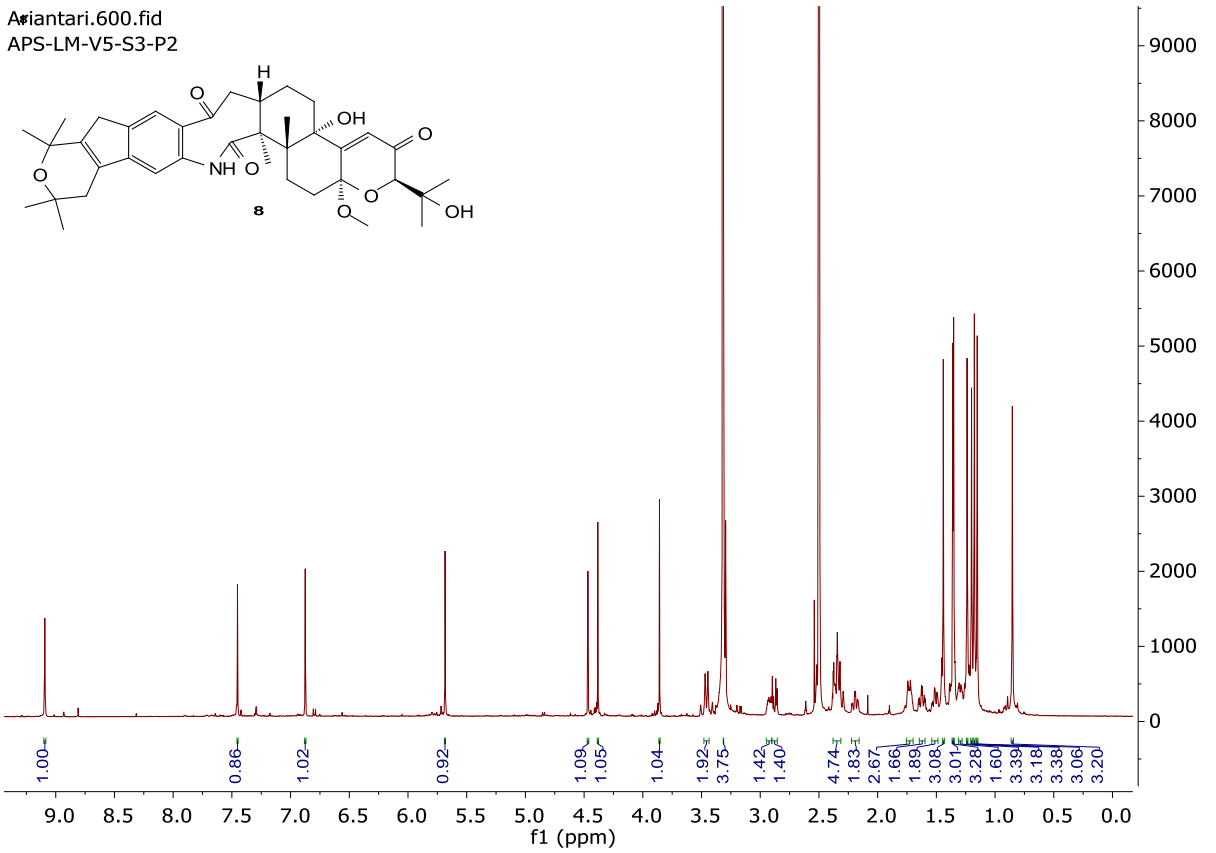

Figure S56. ^{1}H NMR (600 MHz, DMSO-d_6) spectrum of compound **8**.

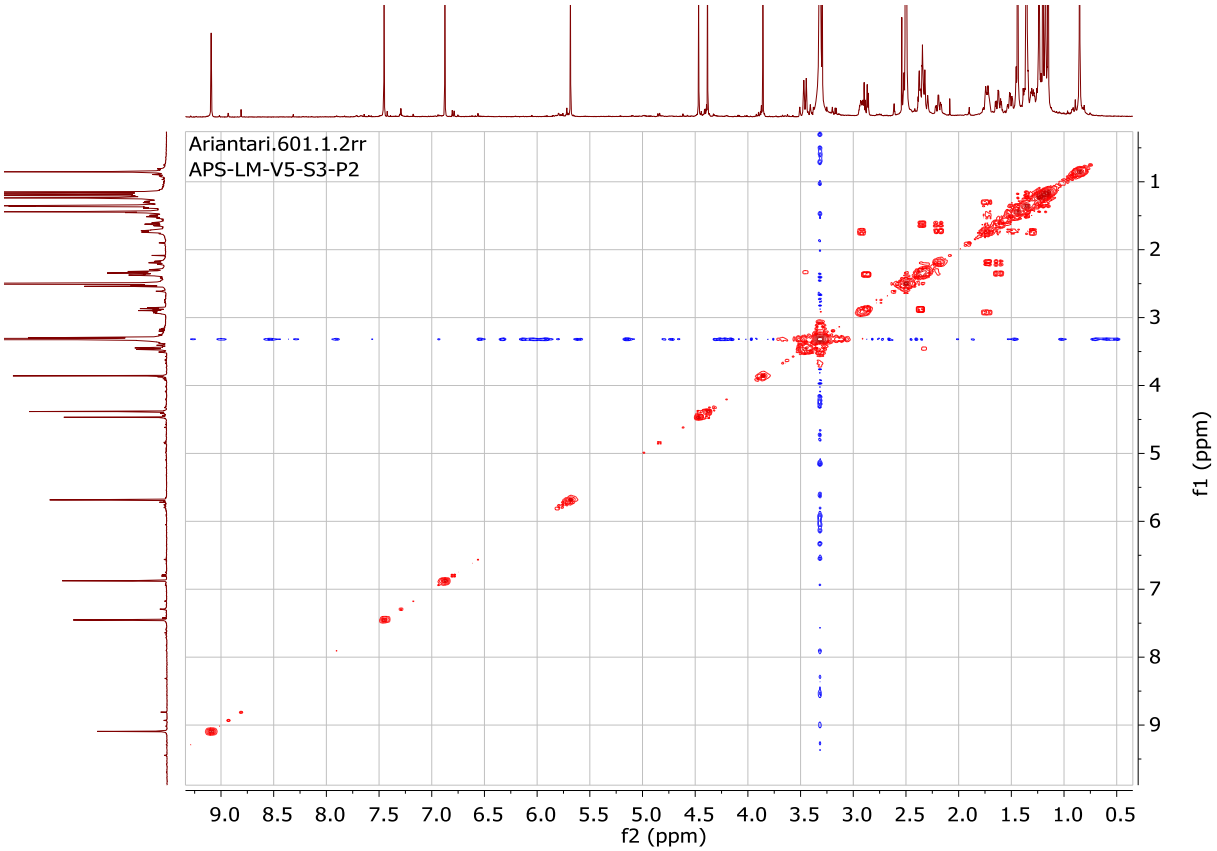

Figure S57. ^{1}H-^{1}H COSY (600 MHz, DMSO-d_6) spectrum of compound **8**.

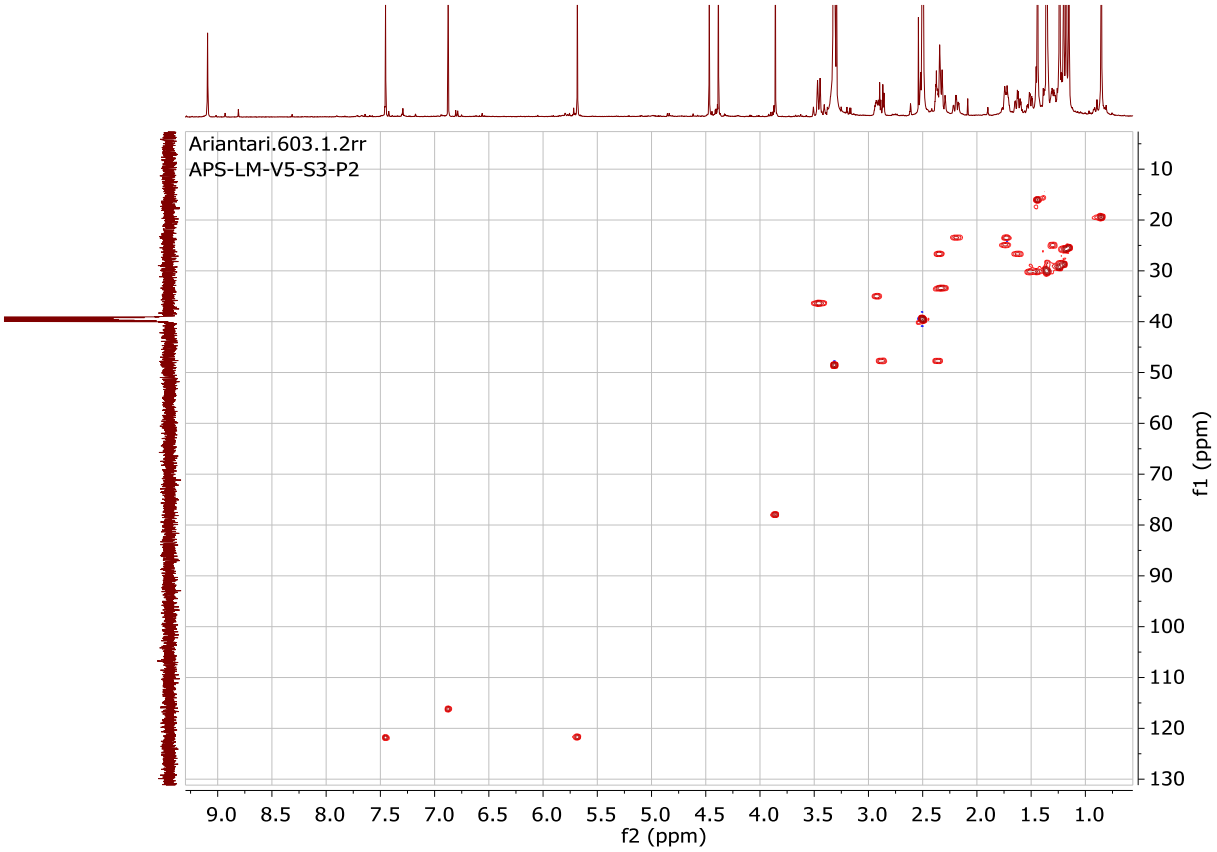

Figure S58. HSQC (600 and 150 MHz, DMSO-d_6) spectrum of compound **8**.

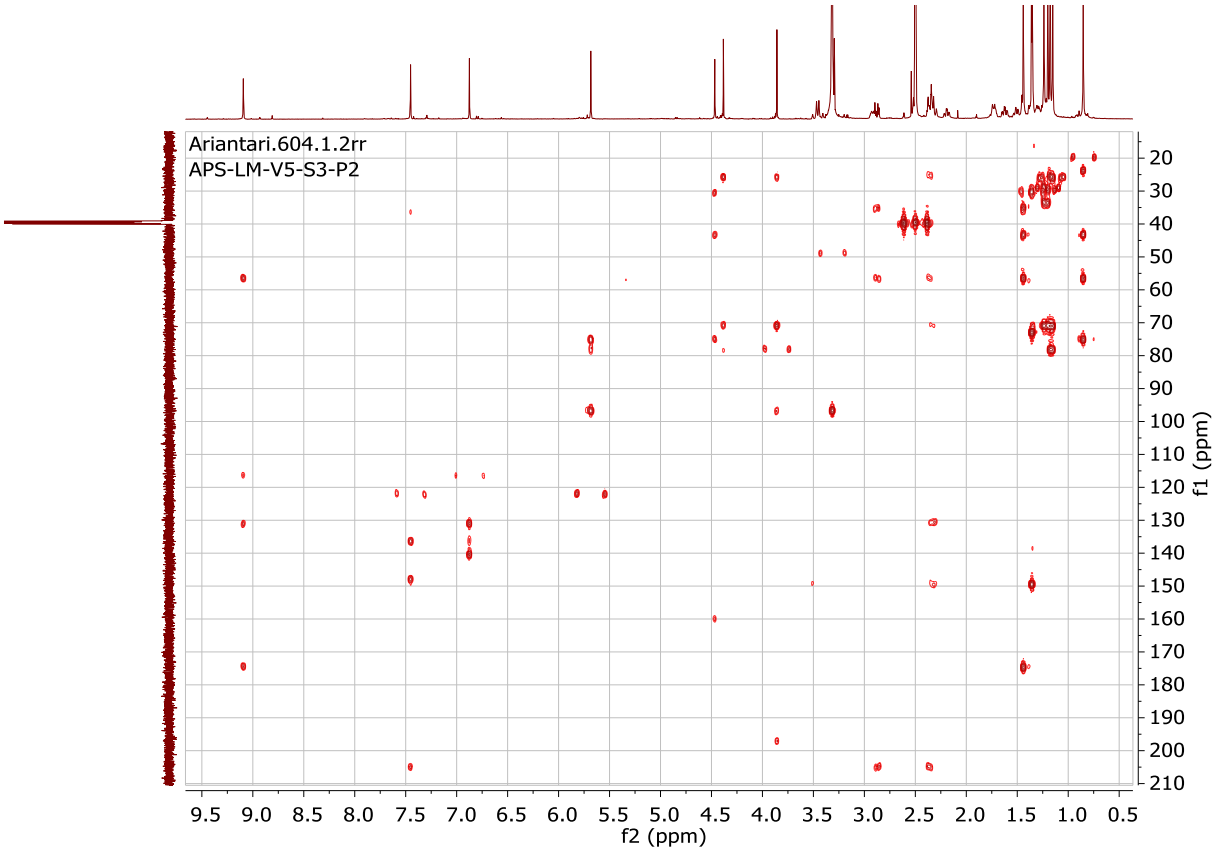

Figure S59. HMBC (600 and 150 MHz, DMSO-d_6) spectrum of compound **8**.

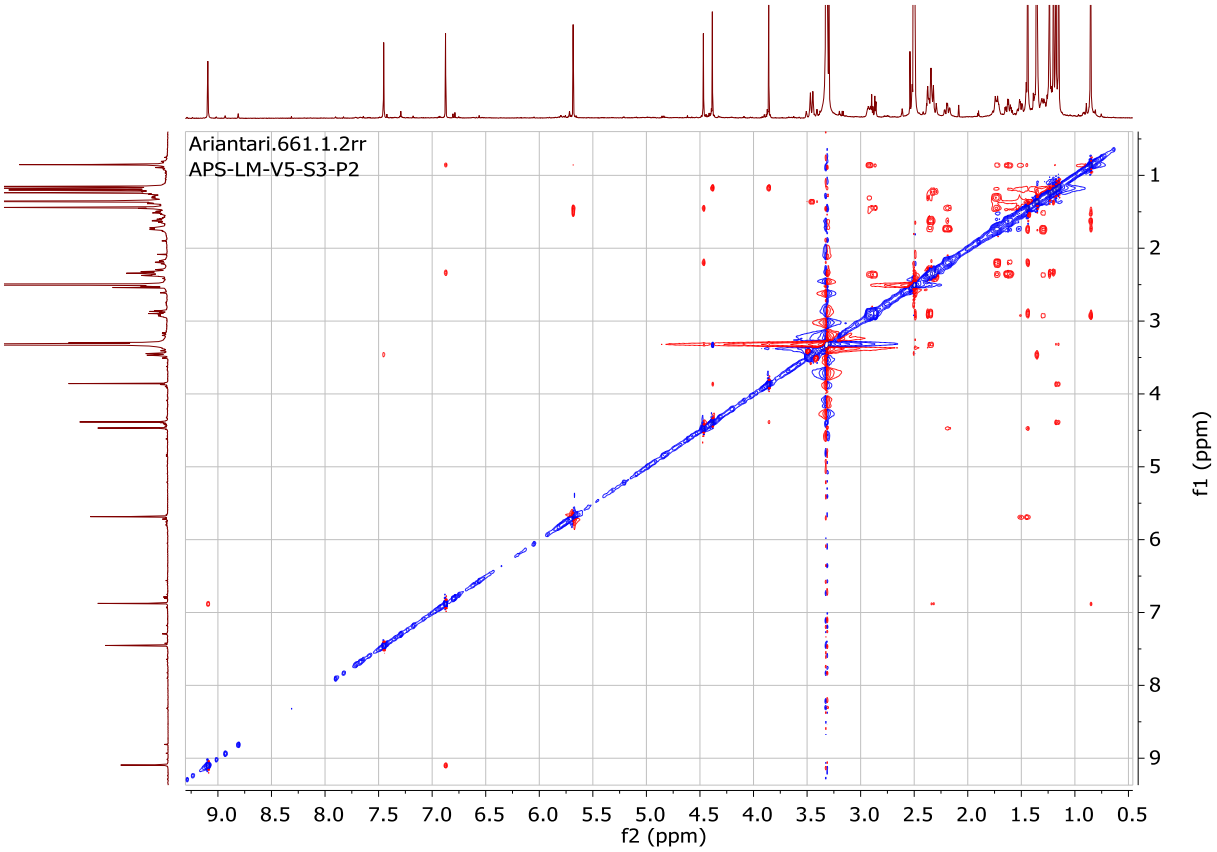

Figure S60. NOESY (600 MHz, DMSO-d_6) spectrum of compound **8**.

(A)

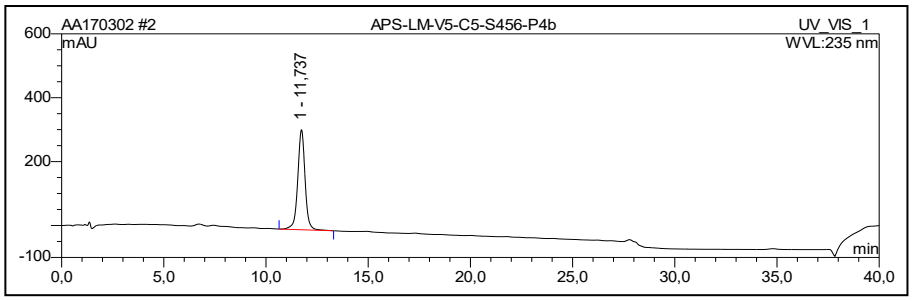

(B)

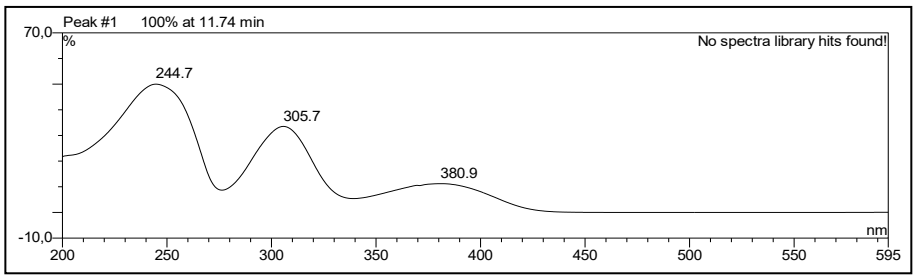

Figure S61. HPLC chromatogram (A) and UV spectrum (B) of compound **9**.

Acquisition Parameter

Source Type	ESI	Ion Polarity	Positive	Set Nebulizer	0.3 Bar
Focus	Not active	Set Capillary	4000 V	Set Dry Heater	180 °C
Scan Begin	50 m/z	Set End Plate Offset	-500 V	Set Dry Gas	4.0 l/min
Scan End	1500 m/z	Set Collision Cell RF	600.0 Vpp	Set Divert Valve	Source

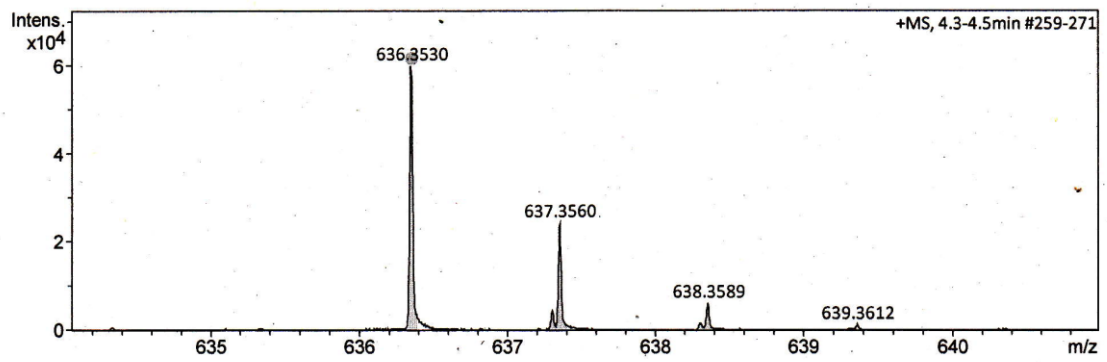

Meas. m/z	#	Ion Formula	m/z	err [ppm]	mSigma	# mSigma	Score	rdb	e⁻ Conf	N-Rule
636.3530	1	C37H50NO8	636.3531	0.2	3.9	1	100.00	13.5	even	ok
	2	C34H42N11O2	636.3517	-1.9	9.7	2	51.52	19.5	even	ok

Figure S62. HRESIMS spectrum of compound **9**.

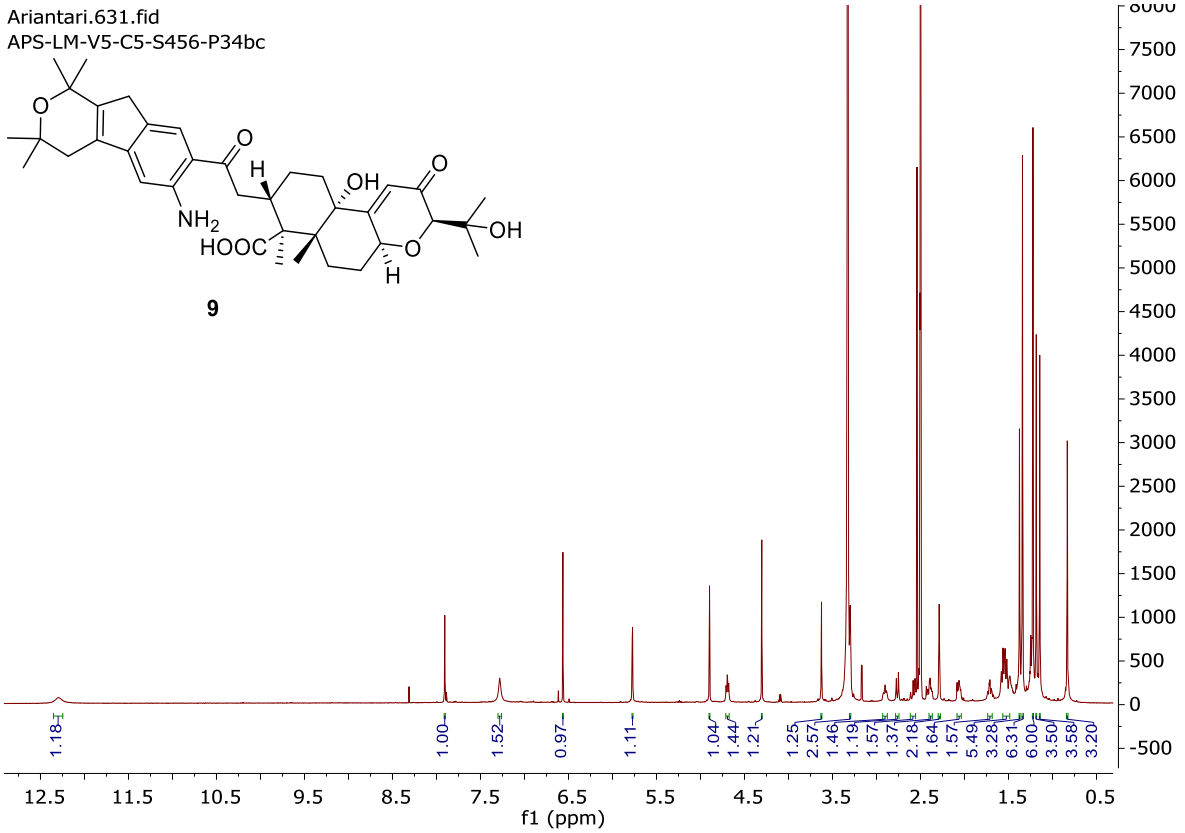

Figure S63. ^{1}H NMR (600 MHz, DMSO-d_6) spectrum of compound **9**.

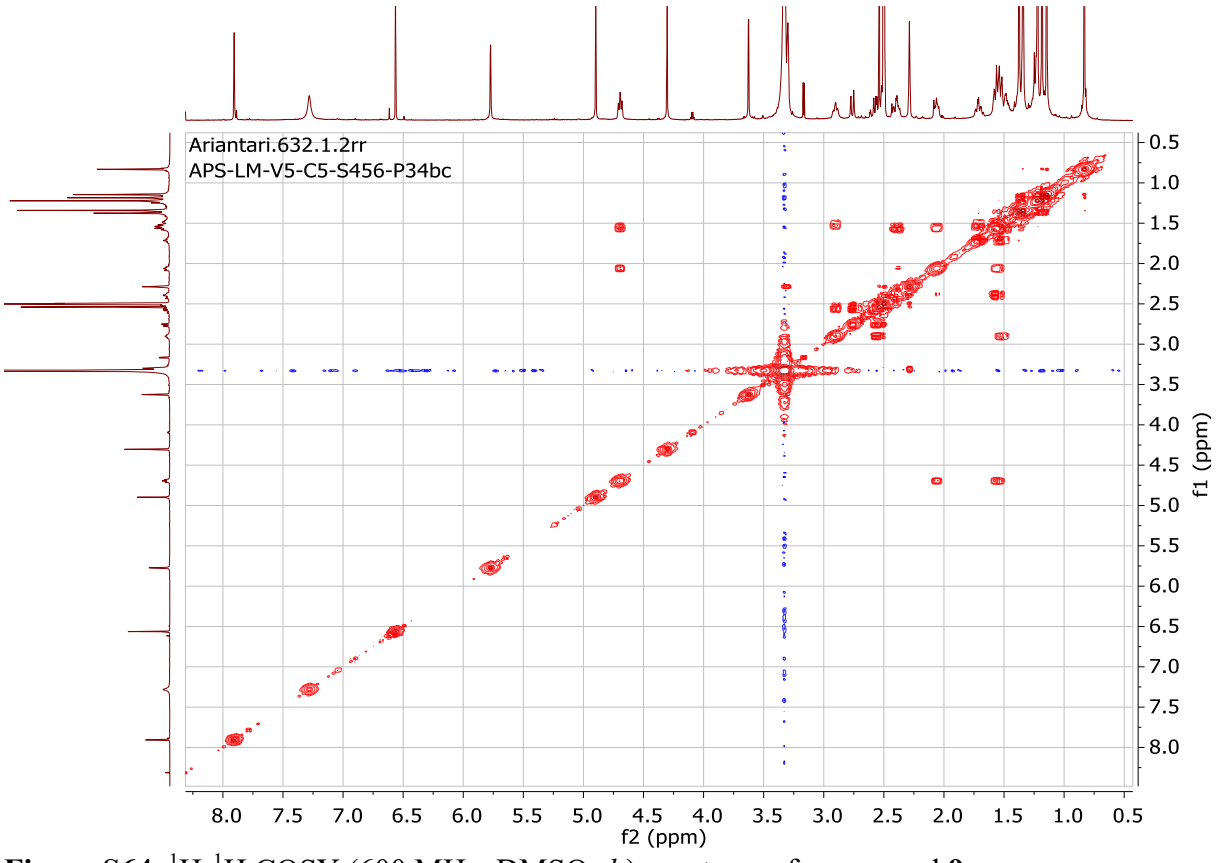

Figure S64. ^{1}H-^{1}H COSY (600 MHz, DMSO-d_6) spectrum of compound **9**.

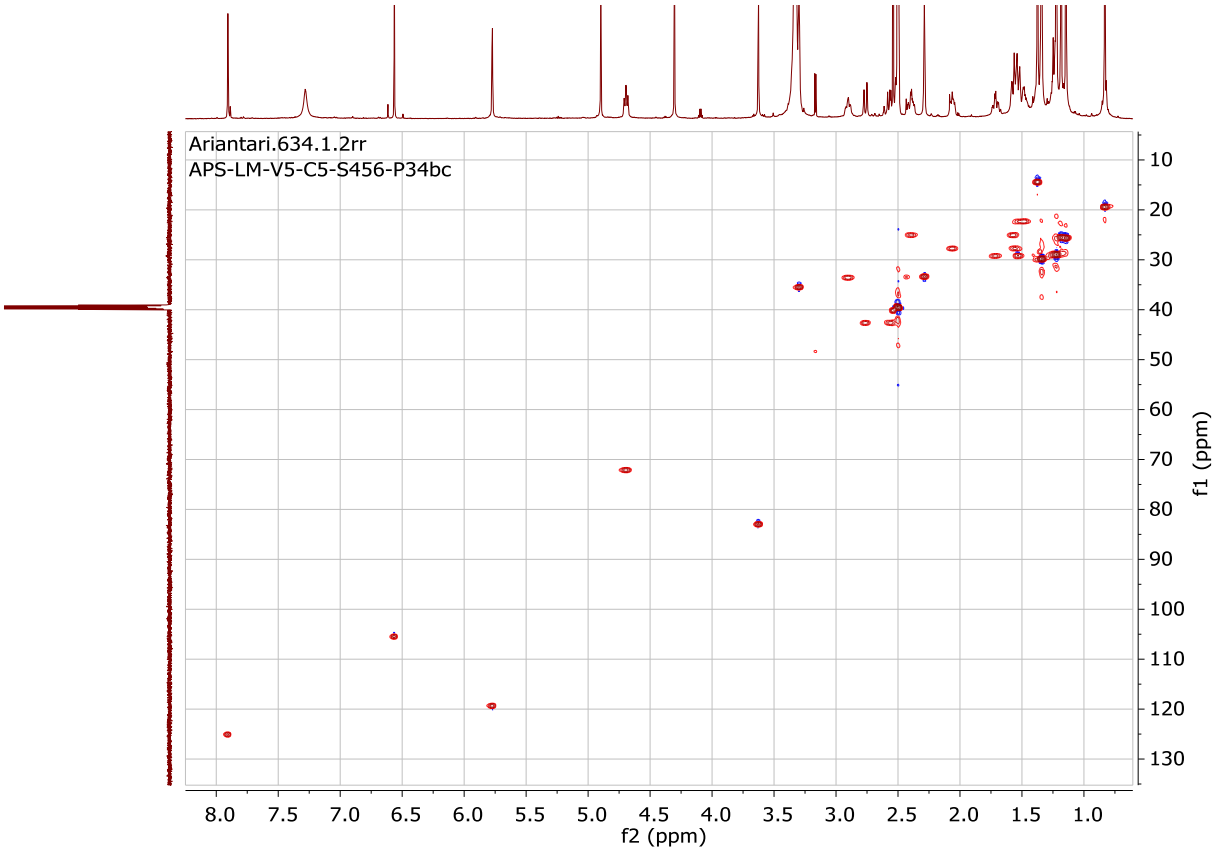

Figure S65. HSQC (600 and 150 MHz, DMSO-d_6) spectrum of compound **9**.

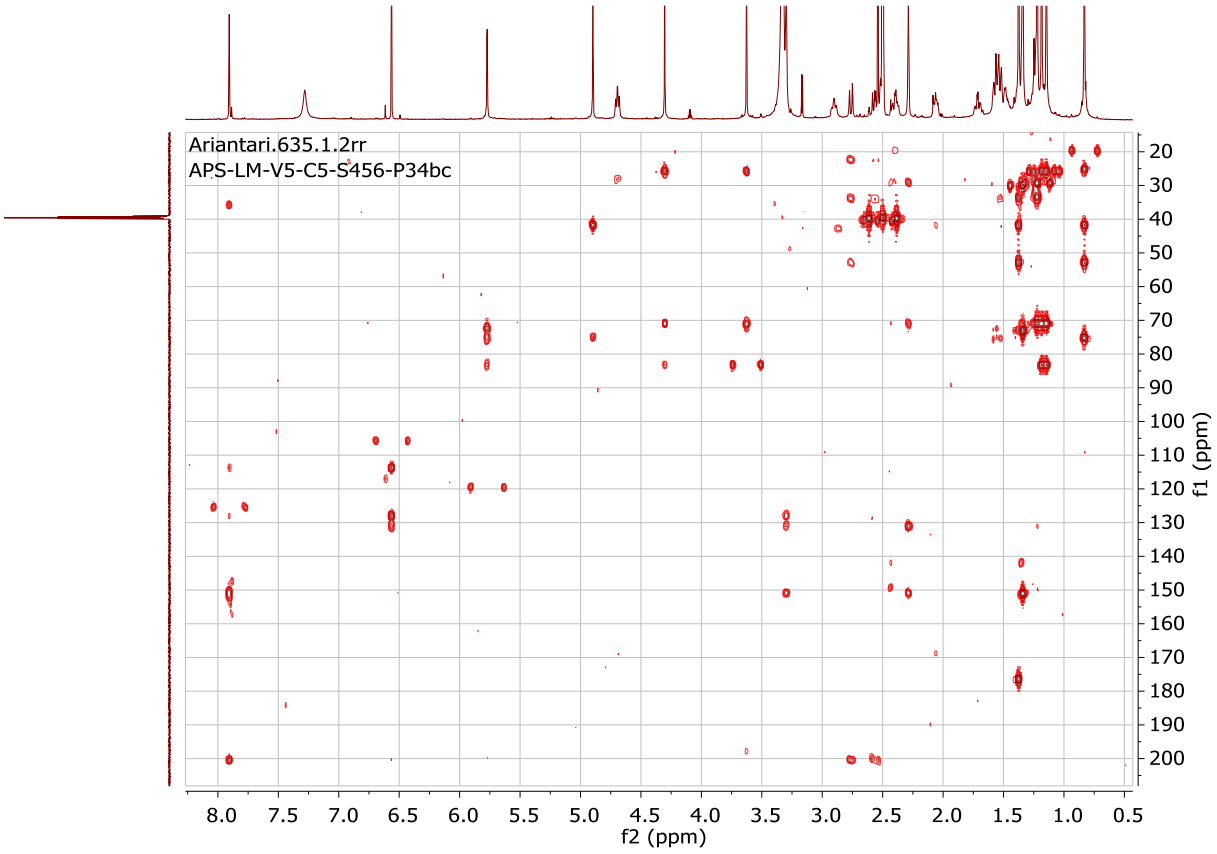

Figure S66. HMBC (600 and 150 MHz, DMSO-d_6) spectrum of compound **9**.

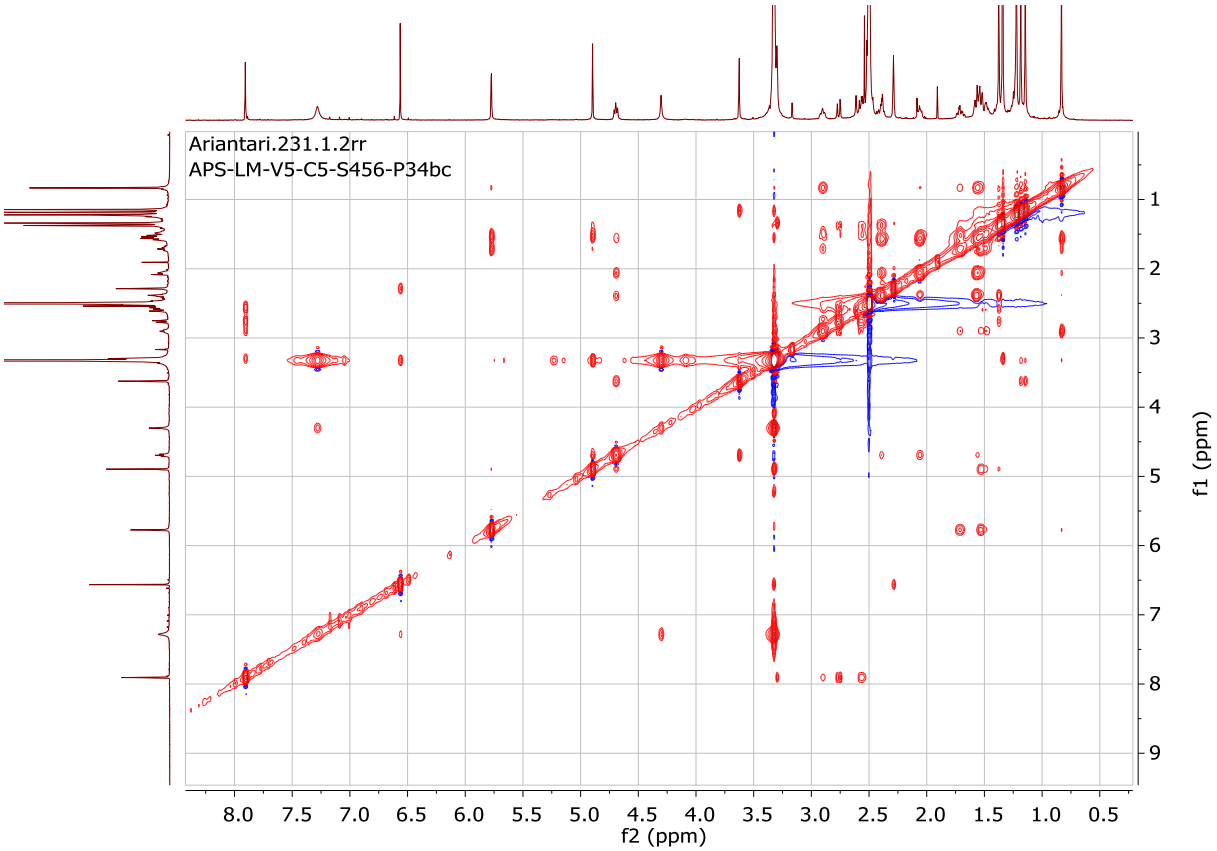

Figure S67. NOESY (600 MHz, DMSO-d_6) spectrum of compound **9**.

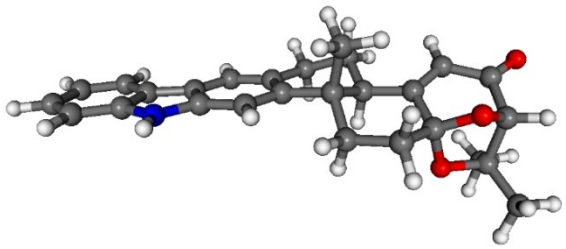

Figure S68. Structure of the single low-energy CAM-B3LYP/TZVP PCM/MeCN conformer (99.7%) of (5*S*,8*R*,10*S*,14*R*)-**1**.

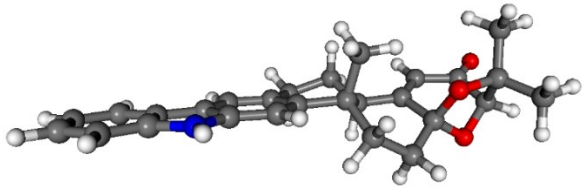

Figure S69. Structure of the single CAM-B3LYP/TZVP PCM/MeCN conformer of (5*S*,8*S*,10*R*,14*R*)-**1**.

Table S70. Comparison of the computed ^{13}C NMR data of (5*S*,8*R*,10*S*,14*R*)-**1** and (5*S*,8*S*,10*R*,14*R*)-**1** [calculated at the mPW1PW91/6-311+G(2d,p) level for the mPW1PW91/6-311+G(2d,p) conformers] with the experimental data. Corrected mean absolute error (CMAE) values were computed for all carbon atoms. For better comparison Δδ values ≥ 2.5 are highlighted with yellow and ≥ 5 with red.

Numbering	Exp	(5*S*,8*R*,10*S*,14*R*)	$\Delta\delta_{(5S,8R,10S,14R)}$	(5*S*,8*S*,10*R*,14*R*)	$\Delta\delta_{(5S,8S,10R,14R)}$
C-2	139.79	138.06	1.73	138.01	1.78
C-3	107.79	106.06	1.73	106.91	0.88
C-4	147.60	143.97	3.63	148.80	1.20
C-5	35.88	43.19	7.31	40.27	4.39
C-6	34.49	35.99	1.50	35.35	0.86
C-7	27.73	31.28	3.55	28.71	0.98
C-8	103.88	103.95	0.07	104.37	0.49
C-10	88.05	87.21	0.84	88.55	0.50
C-11	197.52	193.74	3.78	195.40	2.12
C-12	120.35	121.64	1.29	121.36	1.01
C-13	171.02	171.00	0.02	174.97	3.95
C-14	43.25	47.76	4.51	44.15	0.90
C-15	19.85	21.33	1.48	20.57	0.72
C-16	29.45	31.66	2.21	31.07	1.62
C-17	125.64	127.12	1.48	126.41	0.77
C-18	119.69	121.68	1.99	121.08	1.39
C-19	122.18	122.68	0.50	122.34	0.16
C-20	123.06	123.41	0.35	124.17	1.11
C-21	120.19	120.75	0.56	120.75	0.56
C-22	119.10	119.50	0.40	119.29	0.19
C-23	125.79	125.94	0.15	125.86	0.07
C-24	110.74	108.44	2.30	108.20	2.54
C-25	140.11	139.06	1.05	139.02	1.09
C-26	30.81	22.97	7.84	29.70	1.11
C-27	78.66	82.84	4.18	81.14	2.48
C-28	22.75	21.44	1.31	22.10	0.65
C-29	28.65	27.49	1.16	27.53	1.12
CMAE			2.11		1.28

Table S71. Comparison of the computed ^{13}C NMR data of (5*S*,8*R*,10*S*,14*R*)-**1** and (5*S*,8*S*,10*R*,14*R*)-**1** [calculated at the mPW1PW91/6-311+G(2d,p) SMD/$CHCl_3$ level for the mPW1PW91/6-311+G(2d,p) conformers] with the experimental data. Corrected mean absolute error (CMAE) values were computed for all carbon atoms. For better comparison Δδ values ≥ 2.5 are highlighted with yellow and ≥ 5 with red.

Numbering	Exp	(5*S*,8*R*,10*S*,14*R*)	$\Delta\delta_{(5S,8R,10S,14R)}$	(5*S*,8*S*,10*R*,14*R*)	$\Delta\delta_{(5S,8S,10R,14R)}$
C-2	139.79	136.31	3.48	136.19	3.60
C-3	107.79	105.63	2.16	106.60	1.19
C-4	147.60	143.18	4.42	147.67	0.07
C-5	35.88	43.74	7.86	40.57	4.69
C-6	34.49	35.57	1.08	35.32	0.83
C-7	27.73	31.52	3.79	28.76	1.03
C-8	103.88	102.84	1.04	103.26	0.62
C-10	88.05	86.26	1.79	87.66	0.39
C-11	197.52	193.47	4.05	195.02	2.50
C-12	120.35	119.64	0.71	119.39	0.96
C-13	171.02	171.95	0.93	175.98	4.96
C-14	43.25	48.20	4.95	44.47	1.22
C-15	19.85	21.42	1.57	20.65	0.80
C-16	29.45	31.52	2.07	30.93	1.48
C-17	125.64	126.36	0.72	125.68	0.04
C-18	119.69	119.73	0.04	119.13	0.56
C-19	122.18	120.00	2.18	119.70	2.48
C-20	123.06	121.27	1.79	121.97	1.09
C-21	120.19	119.17	1.02	119.20	0.99
C-22	119.10	117.22	1.88	117.06	2.04
C-23	125.79	124.17	1.62	124.13	1.66
C-24	110.74	107.99	2.75	107.82	2.92
C-25	140.11	137.51	2.60	137.48	2.63
C-26	30.81	22.94	7.87	29.52	1.29
C-27	78.66	82.43	3.77	80.64	1.98
C-28	22.75	21.21	1.54	21.85	0.90
C-29	28.65	27.38	1.27	27.45	1.20
CMAE			2.55		1.63

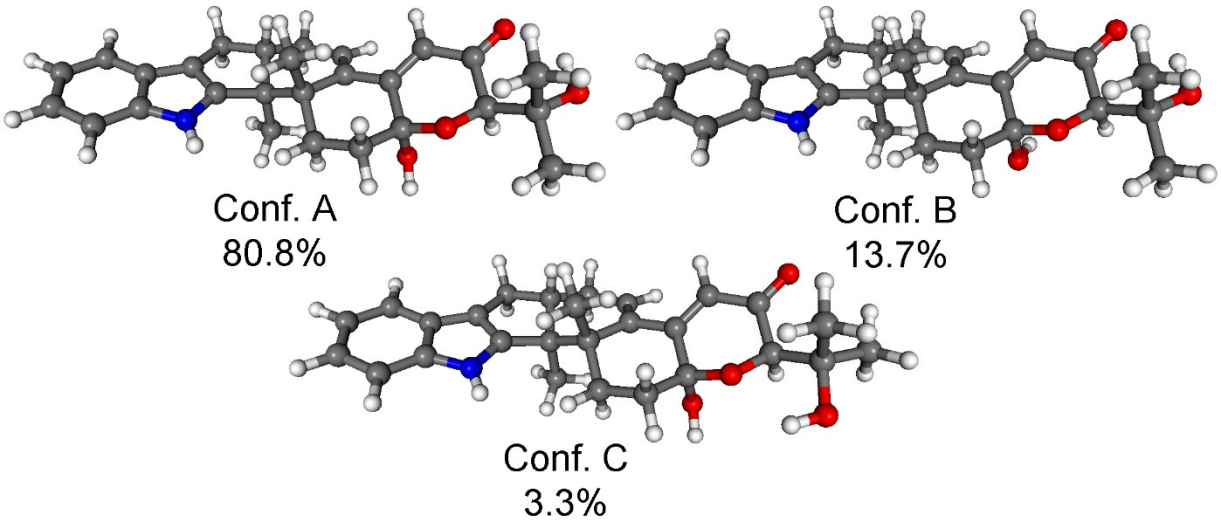

Figure S72. Structure and population of the low-energy CAM-B3LYP/TZVP PCM/MeCN conformers (≥ 1%) of (3*S*,4*S*,7*S*,9*R*,16*S*)-**3**.

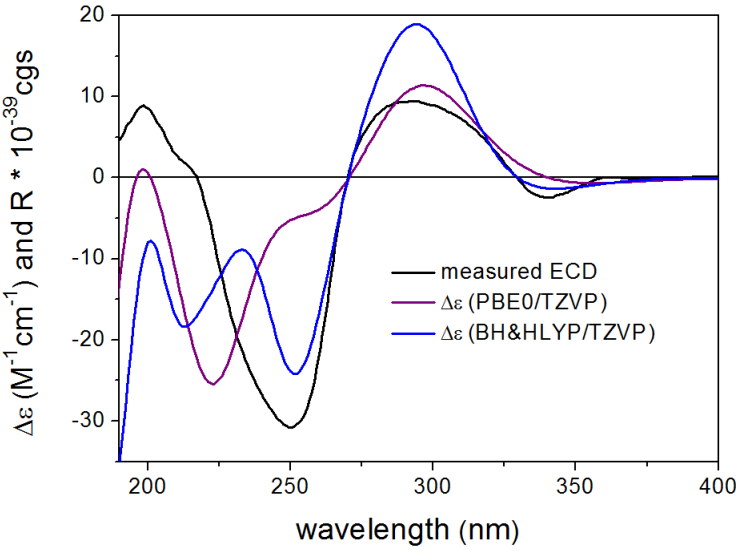

Figure S73. Experimental ECD spectrum of **7** in MeCN compared with the Boltzmann-averaged PBE0/TZVP PCM/MeCN and the BH&HLYP/TZVP PCM/MeCN ECD spectra of (3*S*,4*R*,7*S*,9*R*,13*S*,16*S*)-**7** computed for the low-energy (≥ 1%) CAM-B3LYP/TZVP PCM/MeCN conformers. Bars represent the rotational strength values of conformer A.

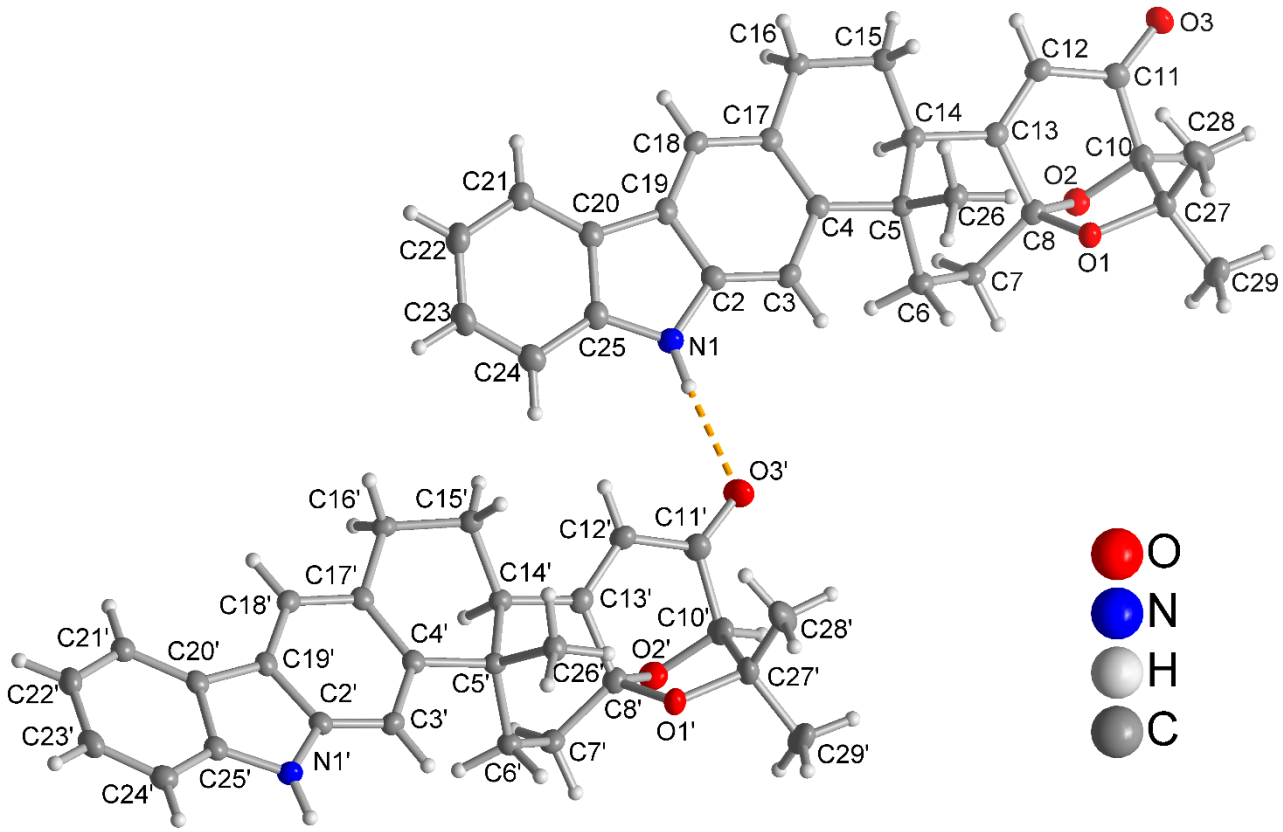

Figure S74. Molecular structures of the two independent molecules in the asymmetric unit of **1**, showing their intermolecular interaction through an N1–H1···O3' bond as dashed orange lines. Hydrogen bond details (Å, °): N1–H1 0.88(2), H1···O3' 2.18(2), N1···O3' 3.057(2), N1–H1···O3' 172(2); not shown N1'–H1' 0.87(2), H1'···O3^{i} 2.23(2), N1'···O3^{i} 3.090(2), N1'–H1'···O3^{i} 170(2); symmetry transformation i = x, y, z-1.

Table S75. Crystal data for compound **1**.

Data set	Cu_TOK_Proksch_AA102_2_0m_a
CCDC number	1862565
Empirical formula	$C_{27}H_{27}NO_3$
M [g mol^{-1}]	413.49
Crystal size [mm^3]	0.3 x 0.3 x 0.3
Temperature [K]	140
θ range [°] (completeness)	3.7 – 65.7 (0.99)
h; k; l range	±13 ; ±8 ; ±28
Crystal system	Monoclinic
Space group	$P2_1$
a [Å]	11.8611(5)
b [Å]	7.1874(3)
c [Å]	24.2244(10)
β [°]	94.496(1)
V [Å^3]	2058.79(15)
Z	4
D_{calc} [g cm^{-3}]	1.334
μ (Cu Kα)[mm^{-1}]	0.69
F(000)	880
Max./min. transmission	0.772/ 0.864
Reflections collected	26702
Independent reflect. (R_{int})	7034
Data/restraints/parameters	7034/ 1/ 572
Max./min. Δρ [e Å^{-3}] [a]	0.17/ -0.14
R_1/wR_2 [I>2σ(I)]	0.028/ 0.075
Goodness-of-fit on F^2	1.03
Flack parameter [b]	-0.01(7)

[a] Largest difference peak and hole, [b] Absolute structure parameter.

Table S76. Fractional atomic coordinates and isotropic or equivalent isotropic displacement parameters ($Å^2$) for compound **1**.

	x	y	z	U_{iso}*/U_{eq}
O1	0.01172 (10)	0.52536 (18)	0.84088 (5)	0.0212 (3)
O2	0.05671 (10)	0.28180 (18)	0.89714 (5)	0.0235 (3)
O3	0.14205 (11)	0.5885 (2)	1.00498 (5)	0.0293 (3)
N1	0.36876 (13)	0.4473 (2)	0.57614 (6)	0.0243 (3)
H1	0.305 (2)	0.447 (4)	0.5551 (9)	0.037*
C2	0.38243 (14)	0.4808 (3)	0.63254 (7)	0.0205 (4)
C3	0.30175 (14)	0.4841 (3)	0.67120 (7)	0.0206 (4)
H3	0.223634	0.474706	0.659469	0.025*
C4	0.33648 (14)	0.5016 (2)	0.72747 (7)	0.0180 (4)
C5	0.24540 (14)	0.5062 (3)	0.76923 (7)	0.0179 (4)
C6	0.14953 (14)	0.3625 (3)	0.75297 (7)	0.0217 (4)
H6A	0.086741	0.428490	0.731912	0.026*
H6B	0.179312	0.268786	0.727931	0.026*
C7	0.10155 (14)	0.2601 (3)	0.80181 (7)	0.0219 (4)
H7A	0.024928	0.213289	0.789988	0.026*
H7B	0.150024	0.151331	0.811986	0.026*
C8	0.09489 (14)	0.3822 (3)	0.85181 (7)	0.0201 (4)
C10	0.02837 (15)	0.4301 (3)	0.93321 (7)	0.0236 (4)
H10	-0.018983	0.384146	0.962761	0.028*
C11	0.13557 (15)	0.5230 (3)	0.95797 (7)	0.0229 (4)
C12	0.22731 (15)	0.5328 (3)	0.92115 (7)	0.0229 (4)
H12	0.298187	0.585331	0.933785	0.027*
C13	0.21052 (14)	0.4671 (2)	0.86948 (7)	0.0188 (4)
C14	0.29863 (13)	0.4569 (3)	0.82798 (7)	0.0179 (3)
H14	0.321942	0.323376	0.826471	0.021*
C15	0.40592 (14)	0.5668 (3)	0.84483 (7)	0.0197 (4)
H15A	0.435146	0.529938	0.882657	0.024*
H15B	0.387961	0.701289	0.845350	0.024*
C16	0.49650 (14)	0.5315 (3)	0.80463 (7)	0.0191 (4)
H16A	0.553313	0.632448	0.808912	0.023*
H16B	0.535468	0.413340	0.814993	0.023*
C17	0.45269 (14)	0.5206 (2)	0.74440 (7)	0.0174 (3)
C18	0.53153 (14)	0.5216 (2)	0.70479 (7)	0.0182 (4)

H18	0.609546	0.534923	0.716271	0.022*
C19	0.49832 (14)	0.5034 (2)	0.64875 (7)	0.0185 (4)
C20	0.55752 (14)	0.4870 (3)	0.59868 (7)	0.0198 (4)
C21	0.67136 (15)	0.4948 (3)	0.58723 (7)	0.0227 (4)
H21	0.728442	0.521751	0.615829	0.027*
C22	0.69957 (15)	0.4627 (3)	0.53366 (7)	0.0279 (4)
H22	0.776231	0.472202	0.525214	0.033*
C23	0.61596 (16)	0.4162 (3)	0.49176 (7)	0.0287 (4)
H23	0.637419	0.390496	0.455565	0.034*
C24	0.50318 (17)	0.4070 (3)	0.50193 (8)	0.0259 (4)
H24	0.447056	0.374046	0.473480	0.031*
C25	0.47429 (14)	0.4477 (3)	0.55532 (7)	0.0213 (4)
C26	0.19661 (14)	0.7056 (3)	0.76850 (7)	0.0208 (4)
H26A	0.137010	0.713266	0.794237	0.031*
H26B	0.164899	0.735931	0.731013	0.031*
H26C	0.256969	0.793954	0.779804	0.031*
C27	-0.04025 (15)	0.5619 (3)	0.89229 (7)	0.0245 (4)
C28	-0.03063 (19)	0.7674 (3)	0.90579 (8)	0.0342 (5)
H28A	-0.062755	0.791537	0.941157	0.051*
H28B	-0.072085	0.839439	0.876444	0.051*
H28C	0.049177	0.804177	0.908507	0.051*
C29	-0.16262 (15)	0.4977 (4)	0.88487 (8)	0.0341 (5)
H29A	-0.199180	0.519363	0.919202	0.051*
H29B	-0.165032	0.364672	0.876016	0.051*
H29C	-0.202539	0.567749	0.854609	0.051*
O1'	0.01754 (10)	0.48928 (19)	0.33598 (5)	0.0225 (3)
O2'	0.06470 (10)	0.23197 (19)	0.38549 (5)	0.0261 (3)
O3'	0.14797 (11)	0.4909 (2)	0.50334 (5)	0.0350 (4)
N1'	0.37079 (12)	0.6233 (2)	0.07457 (6)	0.0216 (3)
H1'	0.3062 (19)	0.628 (4)	0.0547 (9)	0.032*
C2'	0.38481 (14)	0.5764 (3)	0.13030 (7)	0.0189 (4)
C3'	0.30568 (14)	0.5579 (3)	0.16919 (7)	0.0197 (4)
H3'	0.227188	0.565343	0.158108	0.024*
C4'	0.34213 (14)	0.5282 (2)	0.22488 (7)	0.0178 (4)
C5'	0.25174 (14)	0.5137 (3)	0.26665 (7)	0.0176 (4)
C6'	0.15716 (14)	0.3738 (3)	0.24526 (7)	0.0208 (4)

H6C	0.092790	0.445518	0.227623	0.025*
H6D	0.187042	0.294584	0.216317	0.025*
C7'	0.11261 (14)	0.2464 (3)	0.28994 (7)	0.0215 (4)
H7C	0.037435	0.197266	0.276504	0.026*
H7D	0.164502	0.139361	0.296455	0.026*
C8'	0.10293 (14)	0.3484 (3)	0.34352 (7)	0.0202 (4)
C10'	0.03457 (15)	0.3673 (3)	0.42553 (7)	0.0275 (4)
H10'	-0.013979	0.311017	0.453047	0.033*
C11'	0.14120 (15)	0.4518 (3)	0.45396 (7)	0.0254 (4)
C12'	0.23212 (14)	0.4849 (3)	0.41762 (7)	0.0221 (4)
H12'	0.300816	0.541794	0.431606	0.026*
C13'	0.21706 (14)	0.4340 (2)	0.36448 (7)	0.0190 (4)
C14'	0.30526 (13)	0.4405 (3)	0.32296 (6)	0.0176 (3)
H14'	0.326932	0.308296	0.316449	0.021*
C15'	0.41434 (14)	0.5409 (3)	0.34247 (7)	0.0197 (4)
H15C	0.442326	0.494097	0.379473	0.024*
H15D	0.399512	0.675854	0.345634	0.024*
C16'	0.50390 (14)	0.5085 (3)	0.30144 (7)	0.0183 (4)
H16C	0.565118	0.601088	0.308578	0.022*
H16D	0.537269	0.383480	0.308087	0.022*
C17'	0.45901 (14)	0.5223 (2)	0.24134 (7)	0.0173 (3)
C18'	0.53671 (14)	0.5304 (2)	0.20126 (7)	0.0183 (4)
H18'	0.615171	0.520075	0.212122	0.022*
C19'	0.50145 (14)	0.5533 (2)	0.14556 (7)	0.0177 (4)
C20'	0.55933 (14)	0.5762 (3)	0.09538 (7)	0.0187 (4)
C21'	0.67179 (15)	0.5571 (3)	0.08281 (7)	0.0225 (4)
H21'	0.728362	0.518927	0.110419	0.027*
C22'	0.69938 (15)	0.5948 (3)	0.02934 (7)	0.0259 (4)
H22'	0.775158	0.579727	0.020022	0.031*
C23'	0.61652 (16)	0.6549 (3)	-0.01089 (7)	0.0262 (4)
H23'	0.637717	0.684509	-0.046869	0.031*
C24'	0.50433 (17)	0.6724 (3)	0.00030 (8)	0.0236 (4)
H24'	0.448700	0.714852	-0.027167	0.028*
C25'	0.47583 (14)	0.6254 (3)	0.05331 (7)	0.0202 (4)
C26'	0.20182 (15)	0.7100 (3)	0.27381 (7)	0.0209 (4)
H26D	0.138611	0.702601	0.297464	0.031*

H26E	0.174787	0.759735	0.237492	0.031*
H26F	0.260386	0.792255	0.291031	0.031*
C27'	-0.03258 (15)	0.5134 (3)	0.38839 (7)	0.0275 (4)
C28'	-0.01789 (19)	0.7154 (4)	0.40664 (9)	0.0383 (5)
H28D	-0.048418	0.731978	0.442752	0.057*
H28E	-0.058466	0.796656	0.379343	0.057*
H28F	0.062675	0.747361	0.409561	0.057*
C29'	-0.15653 (16)	0.4597 (4)	0.38012 (8)	0.0407 (6)
H29D	-0.193339	0.484527	0.414198	0.061*
H29E	-0.162835	0.326948	0.371135	0.061*
H29F	-0.193419	0.532822	0.349705	0.061*

Table S77. Atomic displacement parameters (Å^2) for compound **1**.

	U^{11}	U^{22}	U^{33}	U^{12}	U^{13}	U^{23}
O1	0.0185 (6)	0.0286 (7)	0.0169 (6)	0.0021 (5)	0.0030 (5)	0.0004 (5)
O2	0.0239 (6)	0.0255 (7)	0.0217 (6)	-0.0038 (5)	0.0052 (5)	0.0025 (5)
O3	0.0288 (7)	0.0435 (9)	0.0157 (6)	0.0004 (6)	0.0017 (5)	-0.0022 (6)
N1	0.0205 (7)	0.0356 (9)	0.0169 (7)	-0.0001 (7)	0.0008 (6)	0.0008 (7)
C2	0.0224 (8)	0.0211 (9)	0.0178 (8)	0.0008 (8)	0.0014 (6)	-0.0004 (7)
C3	0.0160 (8)	0.0260 (10)	0.0197 (8)	0.0010 (7)	0.0001 (6)	0.0012 (7)
C4	0.0185 (8)	0.0167 (8)	0.0187 (8)	0.0005 (7)	0.0019 (6)	0.0012 (7)
C5	0.0161 (8)	0.0211 (9)	0.0163 (8)	-0.0011 (7)	0.0001 (6)	-0.0014 (7)
C6	0.0207 (8)	0.0249 (9)	0.0196 (8)	-0.0031 (7)	0.0013 (7)	-0.0033 (8)
C7	0.0194 (8)	0.0228 (9)	0.0234 (9)	-0.0054 (7)	0.0012 (7)	-0.0029 (7)
C8	0.0183 (8)	0.0232 (9)	0.0190 (8)	-0.0011 (7)	0.0026 (6)	0.0033 (7)
C10	0.0221 (8)	0.0314 (10)	0.0180 (8)	-0.0004 (8)	0.0053 (7)	0.0015 (8)
C11	0.0240 (9)	0.0279 (10)	0.0165 (8)	0.0023 (7)	-0.0002 (7)	0.0036 (7)
C12	0.0178 (8)	0.0309 (10)	0.0199 (8)	-0.0023 (7)	0.0005 (7)	0.0000 (8)
C13	0.0188 (8)	0.0184 (9)	0.0191 (8)	0.0007 (7)	0.0011 (6)	0.0024 (7)
C14	0.0176 (8)	0.0186 (8)	0.0174 (8)	-0.0005 (7)	0.0009 (6)	0.0004 (7)
C15	0.0189 (8)	0.0237 (10)	0.0163 (8)	-0.0016 (7)	0.0007 (6)	-0.0002 (7)
C16	0.0163 (8)	0.0213 (9)	0.0193 (8)	-0.0014 (7)	-0.0006 (6)	0.0007 (7)
C17	0.0195 (8)	0.0149 (8)	0.0177 (8)	0.0007 (7)	0.0012 (6)	0.0014 (7)
C18	0.0163 (8)	0.0168 (9)	0.0211 (8)	0.0007 (7)	-0.0004 (6)	0.0012 (7)
C19	0.0200 (8)	0.0158 (9)	0.0200 (8)	0.0020 (7)	0.0043 (6)	0.0024 (7)
C20	0.0230 (8)	0.0168 (8)	0.0199 (8)	0.0009 (7)	0.0035 (7)	0.0021 (7)

C21	0.0222 (8)	0.0225 (9)	0.0239 (9)	0.0010 (7)	0.0044 (7)	0.0023 (8)
C22	0.0251 (9)	0.0325 (11)	0.0272 (9)	0.0012 (8)	0.0093 (7)	0.0024 (9)
C23	0.0319 (9)	0.0337 (11)	0.0217 (8)	0.0029 (9)	0.0095 (7)	0.0008 (8)
C24	0.0292 (9)	0.0292 (10)	0.0195 (8)	0.0009 (8)	0.0029 (6)	0.0014 (8)
C25	0.0226 (8)	0.0213 (9)	0.0204 (8)	0.0021 (7)	0.0043 (6)	0.0033 (7)
C26	0.0198 (8)	0.0216 (9)	0.0214 (8)	0.0005 (7)	0.0029 (6)	0.0012 (7)
C27	0.0211 (9)	0.0360 (11)	0.0166 (8)	0.0034 (8)	0.0036 (7)	-0.0022 (8)
C28	0.0406 (11)	0.0373 (12)	0.0237 (9)	0.0118 (10)	-0.0034 (8)	-0.0054 (9)
C29	0.0214 (9)	0.0590 (15)	0.0221 (9)	0.0012 (10)	0.0040 (7)	-0.0007 (9)
O1’	0.0183 (6)	0.0308 (7)	0.0187 (6)	0.0035 (5)	0.0038 (4)	0.0000 (5)
O2’	0.0254 (6)	0.0296 (7)	0.0237 (6)	-0.0062 (6)	0.0045 (5)	0.0036 (6)
O3’	0.0300 (7)	0.0589 (10)	0.0161 (6)	-0.0051 (7)	0.0027 (5)	-0.0008 (6)
N1’	0.0184 (7)	0.0300 (9)	0.0161 (7)	-0.0003 (6)	-0.0004 (5)	0.0006 (6)
C2’	0.0202 (8)	0.0193 (9)	0.0172 (8)	-0.0007 (7)	0.0012 (6)	-0.0023 (7)
C3’	0.0161 (8)	0.0227 (9)	0.0198 (8)	0.0015 (7)	-0.0006 (6)	-0.0007 (7)
C4’	0.0191 (8)	0.0160 (8)	0.0185 (8)	0.0001 (7)	0.0022 (6)	-0.0014 (7)
C5’	0.0166 (8)	0.0191 (9)	0.0166 (8)	0.0001 (7)	-0.0004 (6)	-0.0016 (7)
C6’	0.0195 (8)	0.0248 (9)	0.0179 (8)	-0.0012 (7)	0.0004 (6)	-0.0023 (7)
C7’	0.0185 (8)	0.0222 (9)	0.0237 (9)	-0.0035 (7)	0.0012 (6)	-0.0022 (7)
C8’	0.0191 (8)	0.0224 (9)	0.0196 (8)	-0.0010 (7)	0.0034 (6)	0.0032 (7)
C10’	0.0235 (9)	0.0405 (11)	0.0194 (8)	-0.0057 (9)	0.0065 (7)	0.0008 (8)
C11’	0.0242 (9)	0.0332 (11)	0.0187 (8)	0.0008 (8)	0.0012 (7)	0.0030 (8)
C12’	0.0187 (8)	0.0282 (10)	0.0191 (8)	-0.0013 (8)	-0.0002 (6)	0.0021 (8)

C13’	0.0184 (8)	0.0178 (8)	0.0207 (8)	0.0020 (7)	0.0016 (6)	0.0035 (7)
C14’	0.0177 (8)	0.0186 (8)	0.0165 (8)	0.0007 (7)	0.0006 (6)	0.0004 (7)
C15’	0.0188 (8)	0.0234 (9)	0.0169 (8)	-0.0018 (7)	0.0008 (6)	-0.0005 (7)
C16’	0.0167 (8)	0.0197 (9)	0.0180 (8)	-0.0016 (7)	-0.0019 (6)	0.0001 (7)
C17’	0.0200 (8)	0.0146 (8)	0.0175 (8)	0.0001 (7)	0.0019 (6)	-0.0004 (7)
C18’	0.0170 (8)	0.0171 (9)	0.0206 (8)	0.0013 (7)	0.0002 (6)	-0.0009 (7)
C19’	0.0196 (8)	0.0156 (9)	0.0181 (8)	0.0003 (7)	0.0030 (6)	-0.0011 (7)
C20’	0.0217 (8)	0.0163 (8)	0.0184 (8)	-0.0007 (7)	0.0030 (6)	-0.0027 (7)
C21’	0.0211 (8)	0.0247 (10)	0.0218 (8)	-0.0004 (7)	0.0019 (7)	-0.0040 (8)
C22’	0.0228 (9)	0.0317 (11)	0.0242 (9)	-0.0033 (8)	0.0077 (7)	-0.0049 (8)
C23’	0.0307 (9)	0.0292 (10)	0.0196 (8)	-0.0051 (8)	0.0073 (7)	-0.0029 (8)
C24’	0.0267 (8)	0.0251 (9)	0.0189 (8)	-0.0026 (8)	0.0006 (6)	-0.0006 (7)
C25’	0.0215 (8)	0.0198 (9)	0.0195 (8)	-0.0008 (7)	0.0027 (6)	-0.0033 (7)
C26’	0.0208 (8)	0.0210 (9)	0.0212 (8)	0.0015 (7)	0.0037 (6)	0.0009 (7)
C27’	0.0210 (9)	0.0436 (12)	0.0184 (8)	0.0033 (8)	0.0047 (7)	-0.0039 (8)
C28’	0.0383 (11)	0.0467 (14)	0.0293 (10)	0.0143 (10)	-0.0004 (8)	-0.0121 (10)
C29’	0.0203 (9)	0.0778 (18)	0.0246 (9)	-0.0026 (11)	0.0058 (7)	-0.0023 (11)

Table S78. Geometric parameters (Å, º) for compound **1**.

O1—C8	1.436 (2)	O1'—C8'	1.434 (2)
O1—C27	1.456 (2)	O1'—C27'	1.454 (2)
O2—C8	1.418 (2)	O2'—C8'	1.419 (2)
O2—C10	1.435 (2)	O2'—C10'	1.439 (2)
O3—C11	1.229 (2)	O3'—C11'	1.225 (2)
N1—C2	1.384 (2)	N1'—C25'	1.385 (2)
N1—C25	1.386 (2)	N1'—C2'	1.389 (2)
N1—H1	0.88 (2)	N1'—H1'	0.87 (2)
C2—C3	1.391 (2)	C2'—C3'	1.387 (2)
C2—C19	1.409 (2)	C2'—C19'	1.414 (2)
C3—C4	1.398 (2)	C3'—C4'	1.400 (2)
C3—H3	0.9500	C3'—H3'	0.9500
C4—C17	1.414 (2)	C4'—C17'	1.413 (2)
C4—C5	1.537 (2)	C4'—C5'	1.534 (2)
C5—C26	1.545 (2)	C5'—C26'	1.545 (2)
C5—C14	1.552 (2)	C5'—C14'	1.551 (2)
C5—C6	1.563 (2)	C5'—C6'	1.564 (2)
C6—C7	1.540 (2)	C6'—C7'	1.542 (2)
C6—H6A	0.9900	C6'—H6C	0.9900
C6—H6B	0.9900	C6'—H6D	0.9900
C7—C8	1.503 (2)	C7'—C8'	1.503 (2)
C7—H7A	0.9900	C7'—H7C	0.9900
C7—H7B	0.9900	C7'—H7D	0.9900
C8—C13	1.531 (2)	C8'—C13'	1.537 (2)
C10—C11	1.518 (3)	C10'—C11'	1.518 (3)
C10—C27	1.555 (3)	C10'—C27'	1.560 (3)
C10—H10	1.0000	C10'—H10'	1.0000
C11—C12	1.462 (2)	C11'—C12'	1.464 (2)
C12—C13	1.338 (2)	C12'—C13'	1.337 (2)
C12—H12	0.9500	C12'—H12'	0.9500
C13—C14	1.508 (2)	C13'—C14'	1.508 (2)
C14—C15	1.526 (2)	C14'—C15'	1.524 (2)
C14—H14	1.0000	C14'—H14'	1.0000
C15—C16	1.527 (2)	C15'—C16'	1.528 (2)
C15—H15A	0.9900	C15'—H15C	0.9900

C15—H15B	0.9900	C15’—H15D	0.9900
C16—C17	1.512 (2)	C16’—C17’	1.514 (2)
C16—H16A	0.9900	C16’—H16C	0.9900
C16—H16B	0.9900	C16’—H16D	0.9900
C17—C18	1.391 (2)	C17’—C18’	1.391 (2)
C18—C19	1.390 (2)	C18’—C19’	1.391 (2)
C18—H18	0.9500	C18’—H18’	0.9500
C19—C20	1.453 (2)	C19’—C20’	1.452 (2)
C20—C21	1.401 (2)	C20’—C21’	1.398 (2)
C20—C25	1.412 (2)	C20’—C25’	1.409 (2)
C21—C22	1.385 (2)	C21’—C22’	1.387 (2)
C21—H21	0.9500	C21’—H21’	0.9500
C22—C23	1.403 (3)	C22’—C23’	1.397 (3)
C22—H22	0.9500	C22’—H22’	0.9500
C23—C24	1.381 (3)	C23’—C24’	1.384 (3)
C23—H23	0.9500	C23’—H23’	0.9500
C24—C25	1.395 (3)	C24’—C25’	1.395 (3)
C24—H24	0.9500	C24’—H24’	0.9500
C26—H26A	0.9800	C26’—H26D	0.9800
C26—H26B	0.9800	C26’—H26E	0.9800
C26—H26C	0.9800	C26’—H26F	0.9800
C27—C28	1.515 (3)	C27’—C29’	1.518 (3)
C27—C29	1.520 (3)	C27’—C28’	1.523 (3)
C28—H28A	0.9800	C28’—H28D	0.9800
C28—H28B	0.9800	C28’—H28E	0.9800
C28—H28C	0.9800	C28’—H28F	0.9800
C29—H29A	0.9800	C29’—H29D	0.9800
C29—H29B	0.9800	C29’—H29E	0.9800
C29—H29C	0.9800	C29’—H29F	0.9800
C8—O1—C27	107.61 (13)	C8’—O1’—C27’	107.84 (13)
C8—O2—C10	101.43 (13)	C8’—O2’—C10’	101.21 (14)
C2—N1—C25	108.64 (14)	C25’—N1’—C2’	108.75 (14)
C2—N1—H1	126.8 (15)	C25’—N1’—H1’	124.8 (14)
C25—N1—H1	123.5 (14)	C2’—N1’—H1’	125.4 (14)
N1—C2—C3	129.36 (16)	C3’—C2’—N1’	130.36 (16)

N1—C2—C19	109.36 (15)	C3'—C2'—C19'	120.77 (15)
C3—C2—C19	121.20 (15)	N1'—C2'—C19'	108.84 (14)
C2—C3—C4	119.50 (15)	C2'—C3'—C4'	119.64 (15)
C2—C3—H3	120.3	C2'—C3'—H3'	120.2
C4—C3—H3	120.3	C4'—C3'—H3'	120.2
C3—C4—C17	119.83 (15)	C3'—C4'—C17'	119.91 (15)
C3—C4—C5	118.36 (15)	C3'—C4'—C5'	117.82 (15)
C17—C4—C5	121.78 (15)	C17'—C4'—C5'	122.18 (15)
C4—C5—C26	107.12 (14)	C4'—C5'—C26'	107.81 (14)
C4—C5—C14	110.01 (13)	C4'—C5'—C14'	110.13 (13)
C26—C5—C14	110.32 (14)	C26'—C5'—C14'	110.19 (14)
C4—C5—C6	110.77 (14)	C4'—C5'—C6'	110.19 (13)
C26—C5—C6	110.20 (13)	C26'—C5'—C6'	110.67 (14)
C14—C5—C6	108.41 (14)	C14'—C5'—C6'	107.87 (14)
C7—C6—C5	115.31 (14)	C7'—C6'—C5'	115.17 (13)
C7—C6—H6A	108.4	C7'—C6'—H6C	108.5
C5—C6—H6A	108.4	C5'—C6'—H6C	108.5
C7—C6—H6B	108.4	C7'—C6'—H6D	108.5
C5—C6—H6B	108.4	C5'—C6'—H6D	108.5
H6A—C6—H6B	107.5	H6C—C6'—H6D	107.5
C8—C7—C6	112.70 (15)	C8'—C7'—C6'	111.70 (15)
C8—C7—H7A	109.1	C8'—C7'—H7C	109.3
C6—C7—H7A	109.1	C6'—C7'—H7C	109.3
C8—C7—H7B	109.1	C8'—C7'—H7D	109.3
C6—C7—H7B	109.1	C6'—C7'—H7D	109.3
H7A—C7—H7B	107.8	H7C—C7'—H7D	107.9
O2—C8—O1	104.54 (13)	O2'—C8'—O1'	104.21 (13)
O2—C8—C7	111.56 (15)	O2'—C8'—C7'	112.41 (15)
O1—C8—C7	110.41 (14)	O1'—C8'—C7'	109.62 (14)
O2—C8—C13	108.65 (13)	O2'—C8'—C13'	108.80 (13)
O1—C8—C13	110.67 (15)	O1'—C8'—C13'	110.77 (14)
C7—C8—C13	110.84 (14)	C7'—C8'—C13'	110.85 (14)
O2—C10—C11	109.80 (14)	O2'—C10'—C11'	109.51 (15)
O2—C10—C27	101.57 (13)	O2'—C10'—C27'	102.06 (14)
C11—C10—C27	111.36 (16)	C11'—C10'—C27'	111.23 (17)

O2—C10—H10	111.2	O2'—C10'—H10'	111.2
C11—C10—H10	111.2	C11'—C10'—H10'	111.2
C27—C10—H10	111.2	C27'—C10'—H10'	111.2
O3—C11—C12	123.47 (17)	O3'—C11'—C12'	123.68 (17)
O3—C11—C10	121.63 (16)	O3'—C11'—C10'	121.54 (16)
C12—C11—C10	114.87 (15)	C12'—C11'—C10'	114.77 (15)
C13—C12—C11	119.37 (16)	C13'—C12'—C11'	119.03 (16)
C13—C12—H12	120.3	C13'—C12'—H12'	120.5
C11—C12—H12	120.3	C11'—C12'—H12'	120.5
C12—C13—C14	125.51 (15)	C12'—C13'—C14'	125.93 (16)
C12—C13—C8	117.82 (15)	C12'—C13'—C8'	118.40 (15)
C14—C13—C8	116.52 (14)	C14'—C13'—C8'	115.54 (14)
C13—C14—C15	113.79 (14)	C13'—C14'—C15'	115.10 (14)
C13—C14—C5	110.29 (13)	C13'—C14'—C5'	109.85 (13)
C15—C14—C5	113.45 (14)	C15'—C14'—C5'	113.03 (14)
C13—C14—H14	106.2	C13'—C14'—H14'	106.0
C15—C14—H14	106.2	C15'—C14'—H14'	106.0
C5—C14—H14	106.2	C5'—C14'—H14'	106.0
C14—C15—C16	110.91 (14)	C14'—C15'—C16'	110.04 (14)
C14—C15—H15A	109.5	C14'—C15'—H15C	109.7
C16—C15—H15A	109.5	C16'—C15'—H15C	109.7
C14—C15—H15B	109.5	C14'—C15'—H15D	109.7
C16—C15—H15B	109.5	C16'—C15'—H15D	109.7
H15A—C15—H15B	108.0	H15C—C15'—H15D	108.2
C17—C16—C15	114.74 (14)	C17'—C16'—	113.92 (14)

		C15’	
C17—C16—H16A	108.6	C17’—C16’—H16C	108.8
C15—C16—H16A	108.6	C15’—C16’—H16C	108.8
C17—C16—H16B	108.6	C17’—C16’—H16D	108.8
C15—C16—H16B	108.6	C15’—C16’—H16D	108.8
H16A—C16—H16B	107.6	H16C—C16’—H16D	107.7
C18—C17—C4	119.55 (15)	C18’—C17’—C4’	119.39 (15)
C18—C17—C16	117.81 (15)	C18’—C17’—C16’	118.14 (15)
C4—C17—C16	122.58 (15)	C4’—C17’—C16’	122.47 (14)
C19—C18—C17	121.25 (15)	C19’—C18’—C17’	121.11 (15)
C19—C18—H18	119.4	C19’—C18’—H18’	119.4
C17—C18—H18	119.4	C17’—C18’—H18’	119.4
C18—C19—C2	118.61 (15)	C18’—C19’—C2’	118.77 (15)
C18—C19—C20	134.78 (16)	C18’—C19’—C20’	134.43 (16)
C2—C19—C20	106.42 (15)	C2’—C19’—C20’	106.56 (14)
C21—C20—C25	119.28 (16)	C21’—C20’—C25’	119.71 (16)
C21—C20—C19	134.31 (16)	C21’—C20’—C19’	133.87 (16)
C25—C20—C19	106.35 (14)	C25’—C20’—C19’	106.41 (15)
C22—C21—C20	119.11 (17)	C22’—C21’—C20’	118.88 (17)
C22—C21—H21	120.4	C22’—C21’—H21’	120.6
C20—C21—H21	120.4	C20’—C21’—H21’	120.6
C21—C22—C23	120.59 (17)	C21’—C22’—C23’	120.48 (16)
C21—C22—H22	119.7	C21’—C22’—H22’	119.8

C23—C22—H22	119.7	C23'—C22'—H22'	119.8
C24—C23—C22	121.47 (17)	C24'—C23'—C22'	121.72 (17)
C24—C23—H23	119.3	C24'—C23'—H23'	119.1
C22—C23—H23	119.3	C22'—C23'—H23'	119.1
C23—C24—C25	117.87 (18)	C23'—C24'—C25'	117.67 (18)
C23—C24—H24	121.1	C23'—C24'—H24'	121.2
C25—C24—H24	121.1	C25'—C24'—H24'	121.2
N1—C25—C24	129.17 (17)	N1'—C25'—C24'	129.42 (17)
N1—C25—C20	109.18 (15)	N1'—C25'—C20'	109.27 (15)
C24—C25—C20	121.55 (16)	C24'—C25'—C20'	121.28 (16)
C5—C26—H26A	109.5	C5'—C26'—H26D	109.5
C5—C26—H26B	109.5	C5'—C26'—H26E	109.5
H26A—C26—H26B	109.5	H26D—C26'—H26E	109.5
C5—C26—H26C	109.5	C5'—C26'—H26F	109.5
H26A—C26—H26C	109.5	H26D—C26'—H26F	109.5
H26B—C26—H26C	109.5	H26E—C26'—H26F	109.5
O1—C27—C28	109.32 (16)	O1'—C27'—C29'	108.21 (15)
O1—C27—C29	107.95 (14)	O1'—C27'—C28'	108.78 (17)
C28—C27—C29	112.12 (18)	C29'—C27'—C28'	111.62 (18)
O1—C27—C10	101.52 (13)	O1'—C27'—C10'	101.42 (14)
C28—C27—C10	115.46 (16)	C29'—C27'—C10'	110.49 (18)
C29—C27—C10	109.73 (17)	C28'—C27'—C10'	115.61 (16)
C27—C28—H28A	109.5	C27'—C28'—H28D	109.5
C27—C28—H28B	109.5	C27'—C28'—H28E	109.5

H28A—C28—H28B	109.5	H28D—C28'—H28E	109.5
C27—C28—H28C	109.5	C27'—C28'—H28F	109.5
H28A—C28—H28C	109.5	H28D—C28'—H28F	109.5
H28B—C28—H28C	109.5	H28E—C28'—H28F	109.5
C27—C29—H29A	109.5	C27'—C29'—H29D	109.5
C27—C29—H29B	109.5	C27'—C29'—H29E	109.5
H29A—C29—H29B	109.5	H29D—C29'—H29E	109.5
C27—C29—H29C	109.5	C27'—C29'—H29F	109.5
H29A—C29—H29C	109.5	H29D—C29'—H29F	109.5
H29B—C29—H29C	109.5	H29E—C29'—H29F	109.5

Table S79. Hydrogen-bond geometry (Å, º) for compound **1**.

D—H···A	D—H	H···A	D···A	D—H···A
N1′—H1′···O3^{i}	0.87 (2)	2.23 (2)	3.090 (2)	170 (2)
N1—H1···O3′	0.88 (2)	2.18 (2)	3.057 (2)	172 (2)
C28′—H28D···O3′^{ii}	0.98	2.61	3.404 (2)	138

Symmetry codes: (i) x, y, z-1; (ii) -x, y+1/2, -z+1.

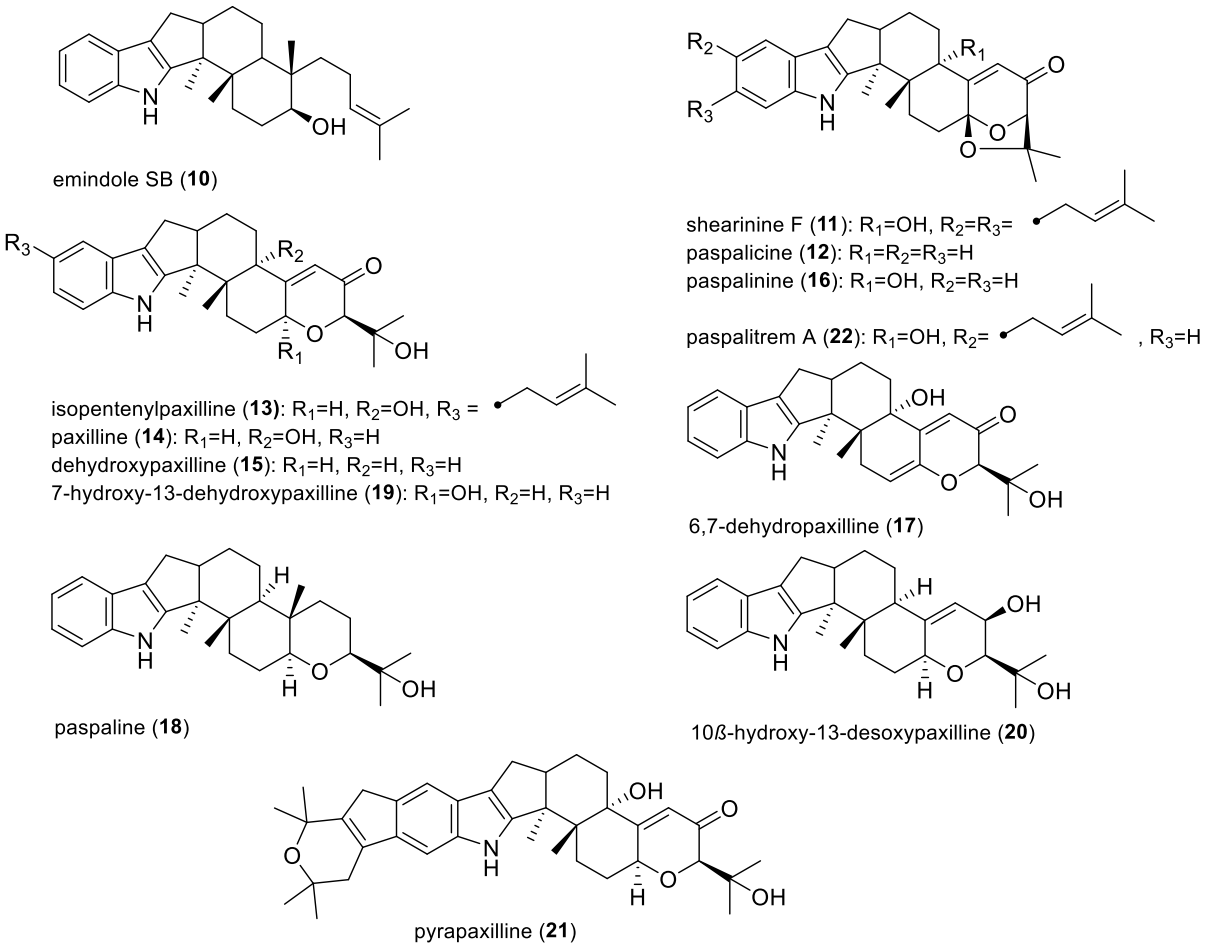

Figure S80. Structures of known compounds isolated from *Penicillium* sp.

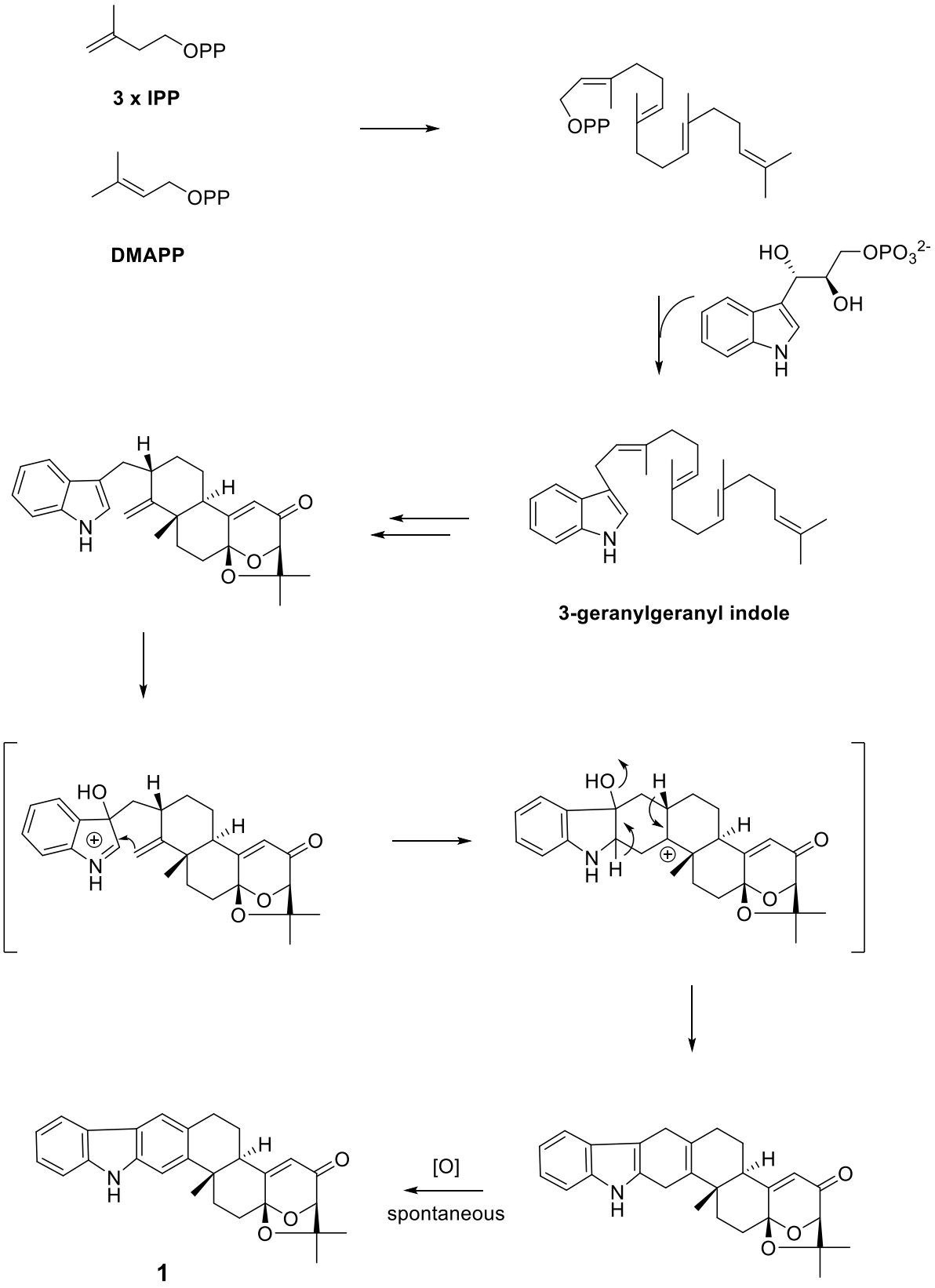

Figure S81. Proposed biosynthesis of the compound **1**.

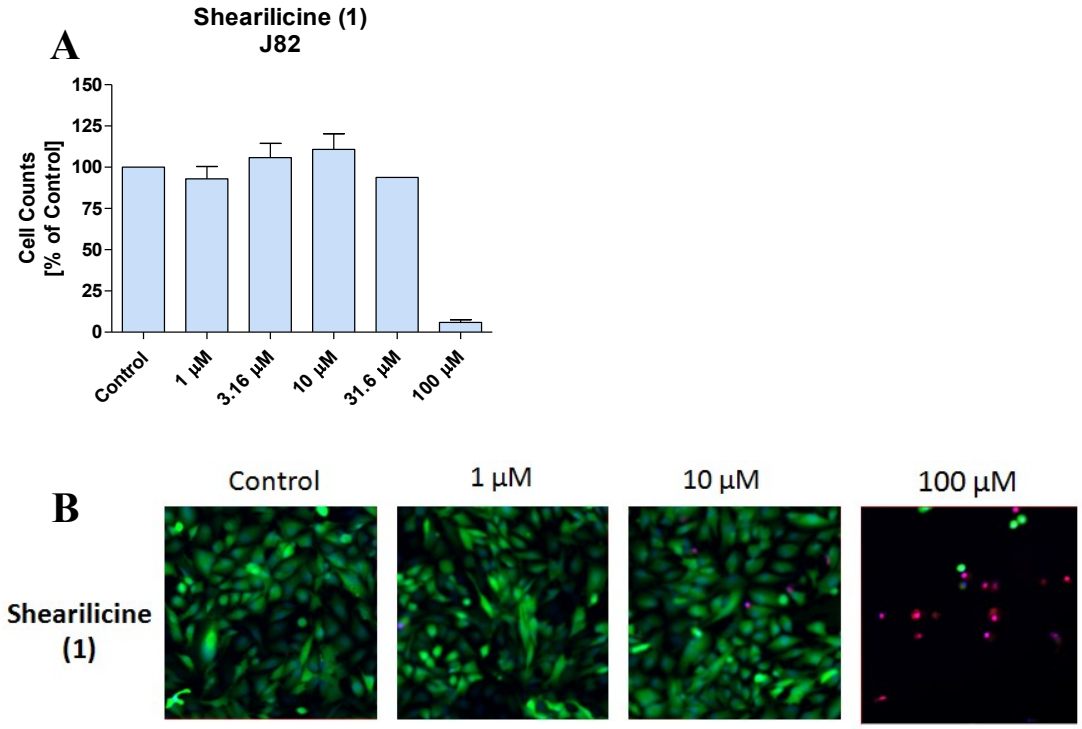

Figure S82. Cell viability assay of **1** in urothelial bladder cancer cell line J82.

(A) Percentage of control cell counts of J82 after 72 h treatment with **1** using High Content Analysis-based fluorescent live/dead assay. (B) Staining of live (calcein-AM, green) and dead (PI, red) J82 cells after 72 h treatment with different concentrations of **1**. Data shown in A are mean +/- SEM from 2 independent experiments each with 3 replicates.

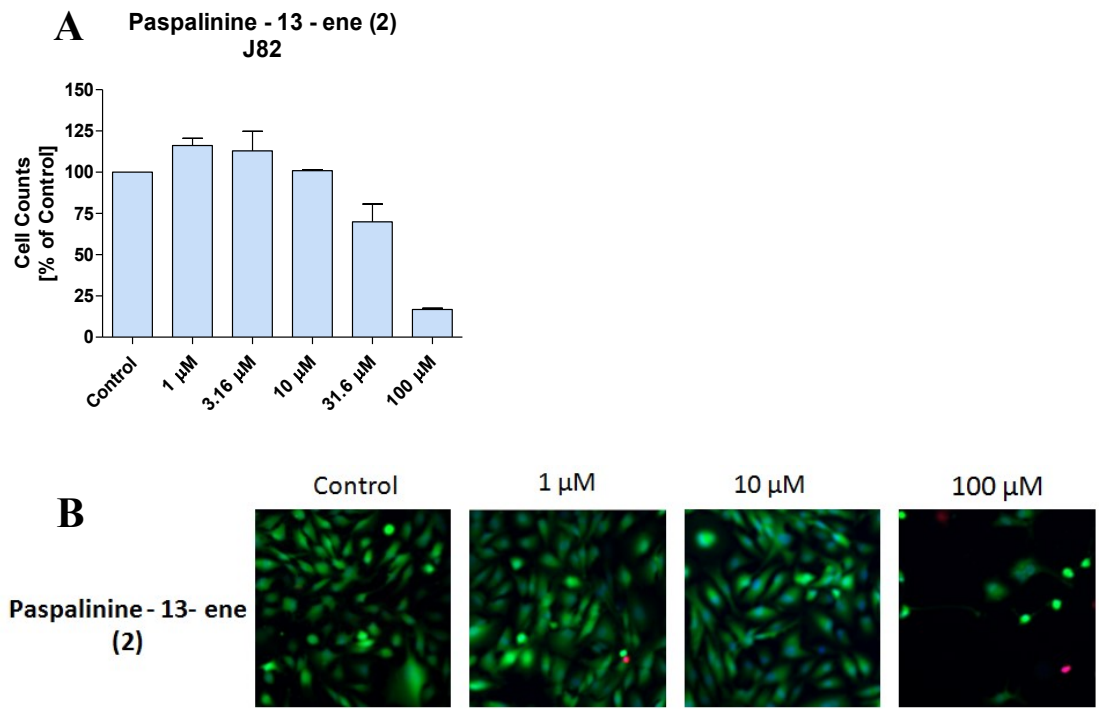

Figure S83. Cell viability assay of **2** in urothelial bladder cancer cell line J82.

(A) Percentage of control cell counts of J82 after 72 h treatment with **2** using High Content Analysis-based fluorescent live/dead assay. (B) Staining of live (calcein-AM, green) and dead (PI, red) J82 cells after 72 h treatment with different concentrations of **2**. Data shown in A are mean +/- SEM from 2 independent experiments each with 3 replicates.

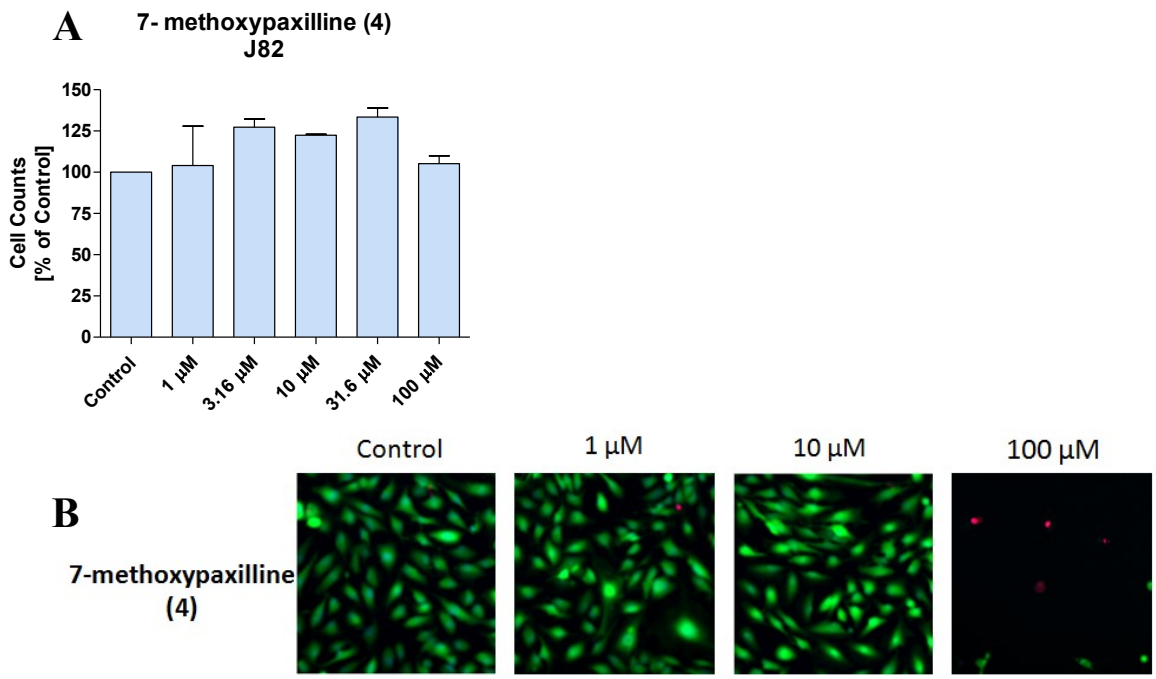

Figure S84. Cell viability assay of **4** in urothelial bladder cancer cell line J82.

(A) Percentage of control cell counts of J82 after 72 h treatment with **4** using High Content Analysis-based fluorescent live/dead assay. (B) Staining of live (calcein-AM, green) and dead (PI, red) J82 cells after 72 h treatment with different concentrations of **4**. Data shown in A and B are mean +/- SEM from 2 independent experiments each with 3 replicates.

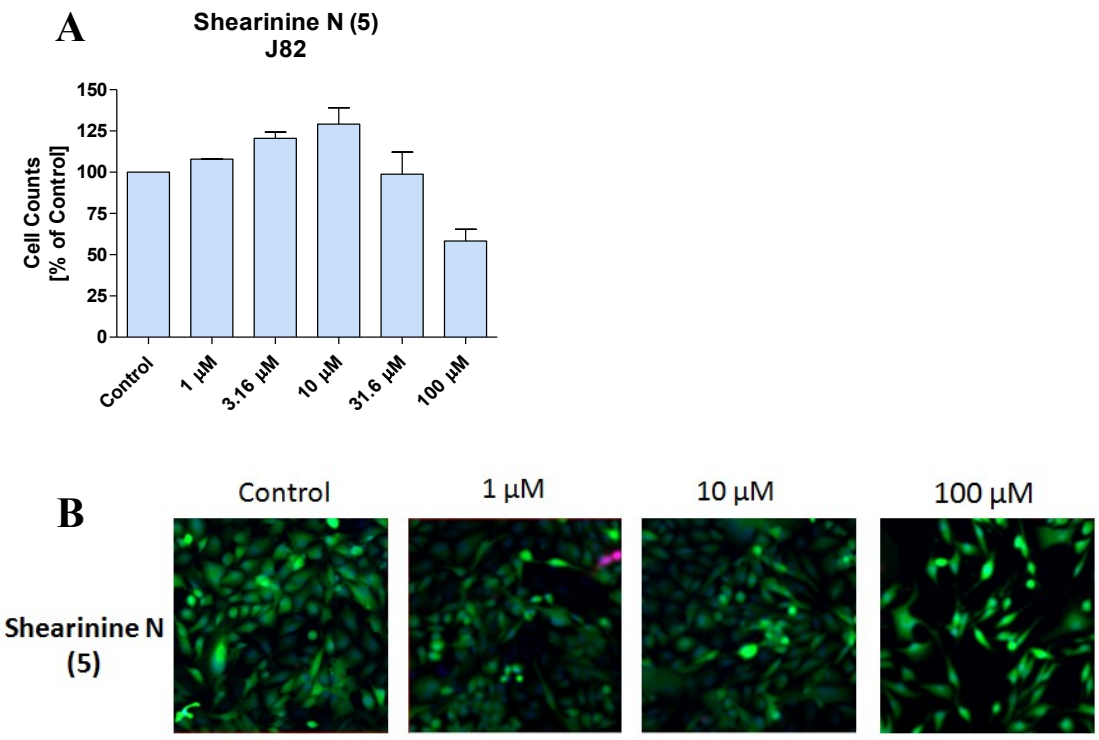

Figure S85. Cell viability assay of **5** in urothelial bladder cancer cell line J82.

(A) Percentage of control cell counts of J82 after 72 h treatment with **5** using High Content Analysis-based fluorescent live/dead assay. (B) Staining of live (calcein-AM, green) and dead (PI, red) J82 cells after 72 h treatment with different concentrations of **5**. Data shown in A are mean +/- SEM from 2 independent experiments each with 3 replicates.

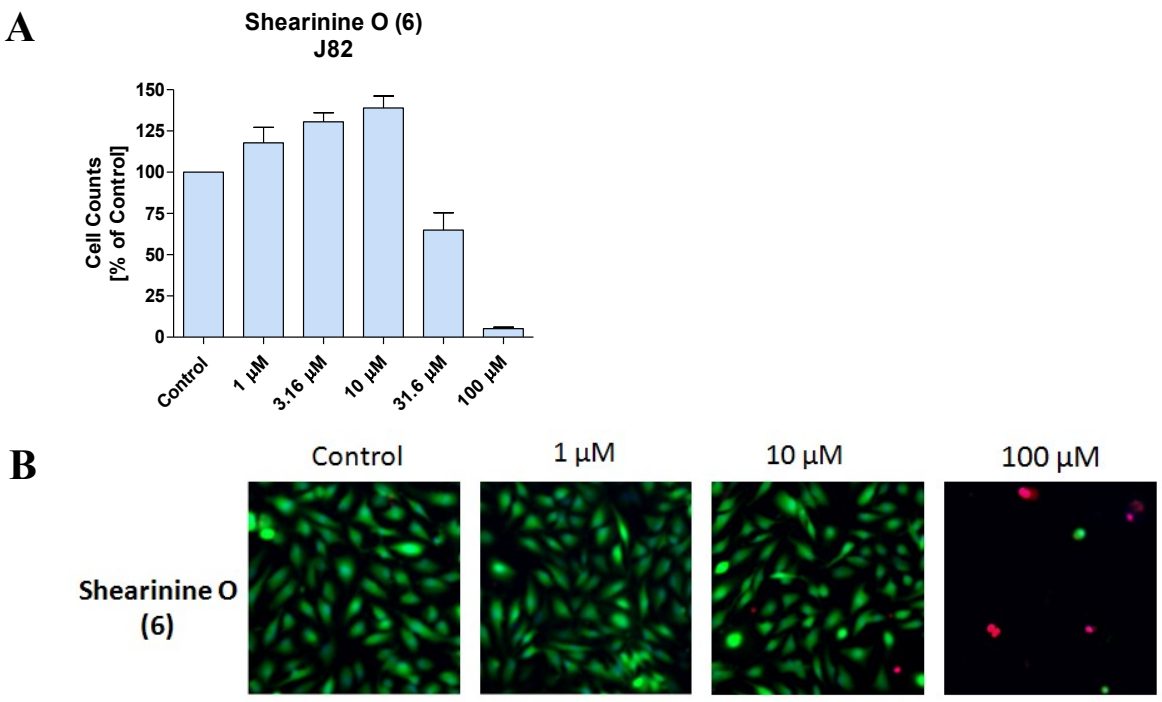

Figure S86. Cell viability assay of **6** in urothelial bladder cancer cell line J82. Percentage of control cell counts of J82 after 72 h treatment with **6** using High Content Analysis-based fluorescent live/dead assay. Staining of live (calcein-AM, green) and dead (PI, red) J82 cells after 72 h treatment with different concentrations of **6**. Data shown in A are mean +/- SEM from 2 independent experiments each with 3 replicates.

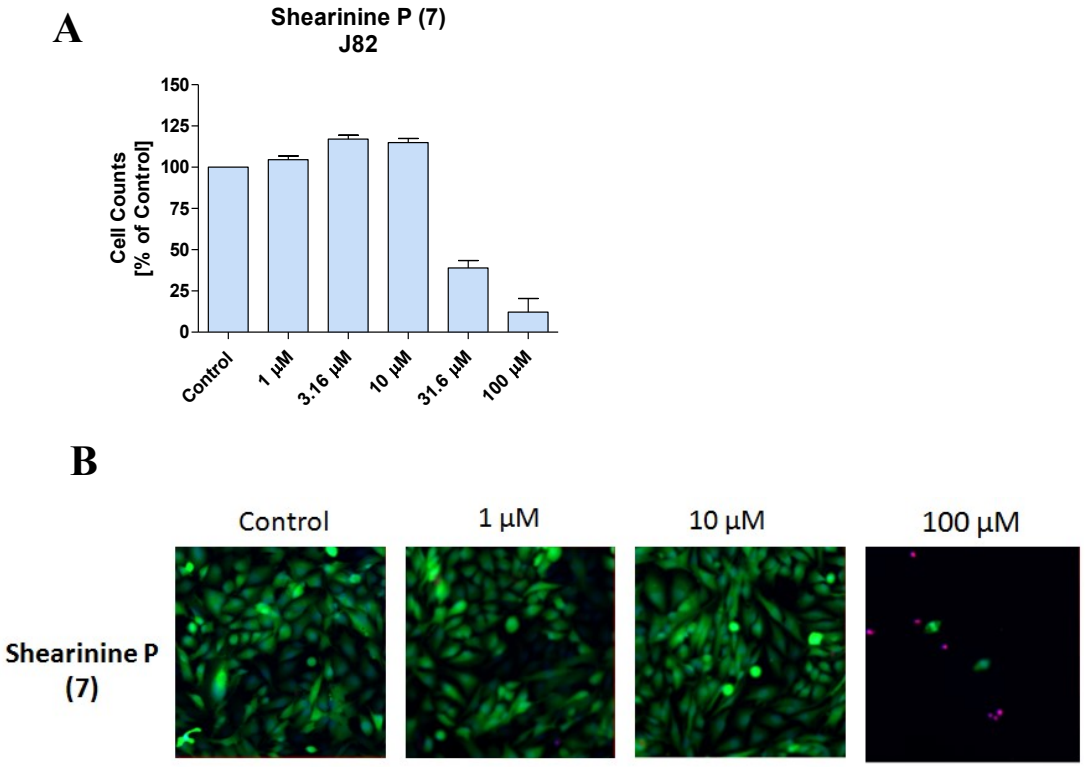

Figure S87. Cell viability assay of **7** in urothelial bladder cancer cell line J82. Percentage of control cell counts of J82 after 72 h treatment with **7** using High Content Analysis-based fluorescent live/dead assay. Staining of live (calcein-AM, green) and dead (PI, red) J82 cells after 72 h treatment with different concentrations of **7**. Data shown in A are mean +/- SEM from 2 independent experiments each with 3 replicates.

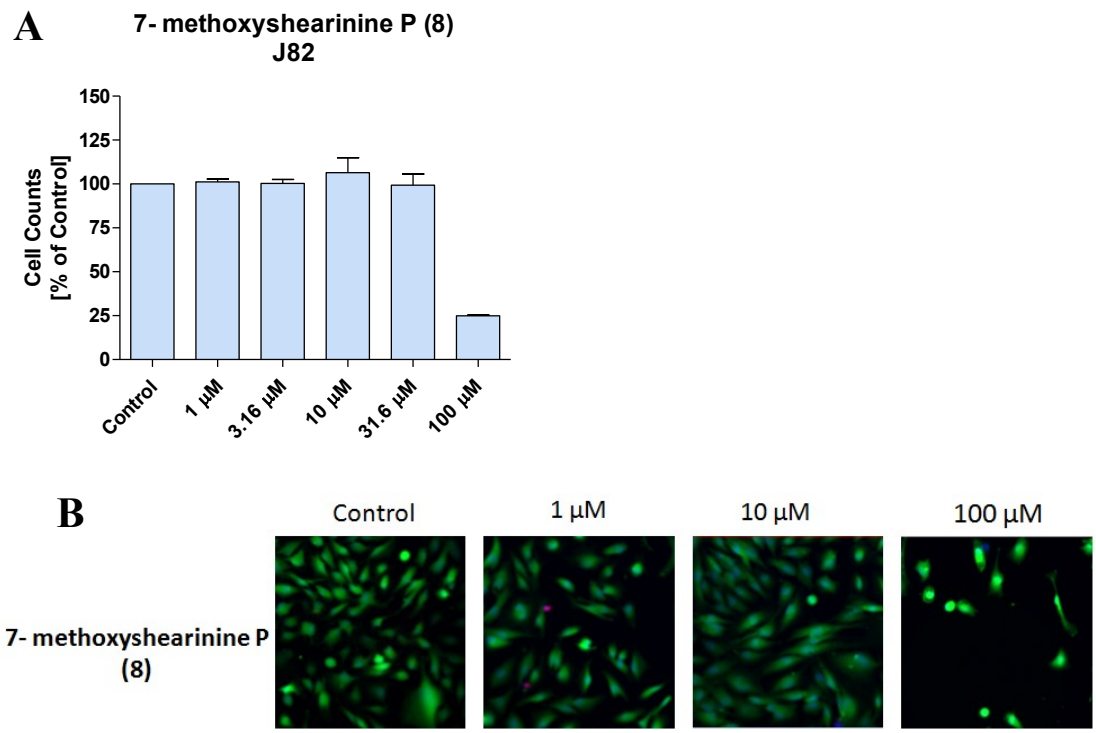

Figure S88. Cell viability assay of **8** in urothelial bladder cancer cell line J82.

(A) Percentage of control cell counts of J82 after 72 h treatment with **8** using High Content Analysis-based fluorescent live/dead assay. (B) Staining of live (calcein-AM, green) and dead (PI, red) J82 cells after 72 h treatment with different concentrations of **8**. Data shown in A are mean +/- SEM from 2 independent experiments each with 3 replicates.

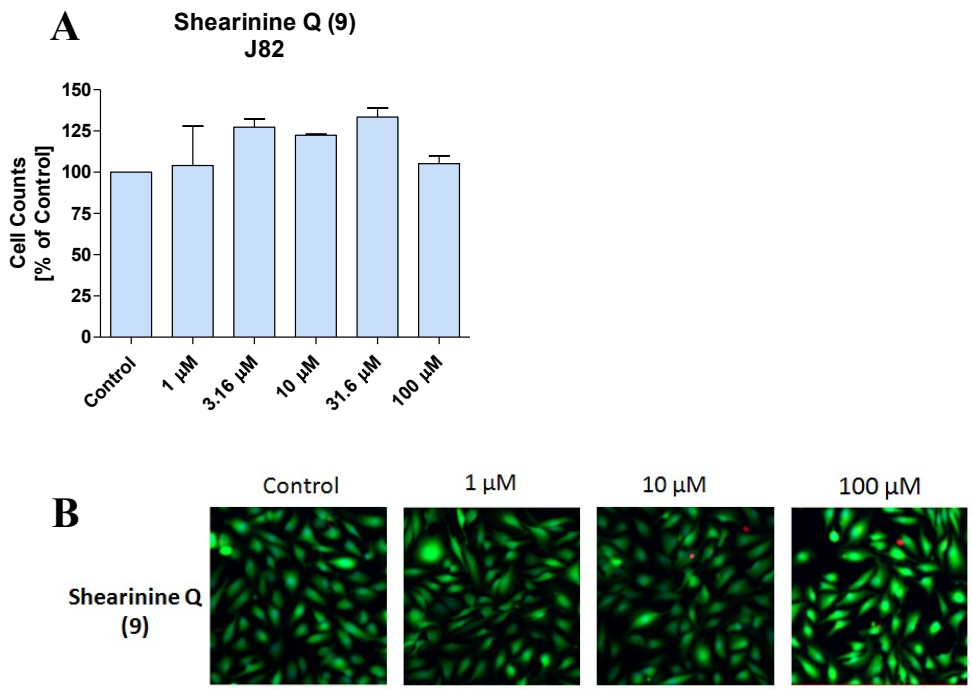

Figure S89. Cell viability assay of **9** in urothelial bladder cancer cell line J82.

(A) Percentage of control cell counts of J82 after 72 h treatment with **9** using High Content Analysis-based fluorescent live/dead assay. (B) Staining of live (calcein-AM, green) and dead (PI, red) J82 cells after 72 h treatment with different concentrations of **9**. Data shown in A are mean +/- SEM from 2 independent experiments each with 3 replicates.

Chapter 3

Publication 2

Expanding the chemical diversity of an endophytic fungus *Bulgaria inquinans*, an ascomycete associated with mistletoe, through an OSMAC approach

Published in : "RSC Advances"

Impact factor : 3.049

Research contribution: first authorship, contributed to 60% of this publication. The first author conducted most of the laboratory experiments including the application of OSMAC protocol, isolation and structure elucidation of secondary metabolites, Mosher's reaction, as well as preparation of the manuscript.

RSC Advances

PAPER

View Article Online
View Journal | View Issue

Cite this: *RSC Adv.*, 2019, **9**, 25119

Expanding the chemical diversity of an endophytic fungus *Bulgaria inquinans*, an ascomycete associated with mistletoe, through an OSMAC approach†

Ni P. Ariantari, [ab] Georgios Daletos, ‡[a] Attila Mándi, [c] Tibor Kurtán, [c] Werner E. G. Müller, [d] Wenhan Lin, [e] Elena Ancheeva *[a] and Peter Proksch*[a]

An endophytic fungus *Bulgaria inquinans* (isolate MSp3-1), isolated from mistletoe (*Viscum album*), was subjected to fermentation on solid Czapek medium. Chromatographic workup of the crude EtOAc extract yielded five new natural products (**1–5**). Subsequent application of the "One Strain, MAny Compounds" (OSMAC) strategy on this strain by the addition of a mixture of salts ($MgSO_4$, $NaNO_3$ and NaCl) to solid Czapek medium induced the accumulation of nine additional new secondary metabolites (**6–13**, **16**), with most of them (**8**, **10–12**) not detectable in cultures lacking the salt mixture. The structures of the new compounds were established on the basis of the 1D/2D NMR and HRESIMS data. The TDDFT-ECD method was applied to determine the absolute configurations of the new compounds **1**, **4** and **6** as well as of the previously reported bulgarialactone B (**14**), for which the absolute configuration was unknown so far. The modified Mosher's method was performed to assign the absolute configurations of **12** and **13**. TDDFT-ECD analysis also allowed determining the absolute configuration of (+)-epicocconone, which had an enantiomeric absolute configuration in the tricyclic moiety compared to that of bulgarialactone B (**14**). All the isolated metabolites were evaluated for their cytotoxic activity. Compound **2** was found to possess strong cytotoxic activity against the murine lymphoma cell line L5178Y with an IC_{50} value of 1.8 μM, while the remaining metabolites were shown to be inactive.

Received 16th May 2019
Accepted 11th July 2019

DOI: 10.1039/c9ra03678d

rsc.li/rsc-advances

Introduction

Fungi are well-known producers of novel drug leads, as exemplified by the fascinating discovery of beta-lactam antibiotics, cyclosporin A, caspofungin, lovastatin and fingolimod.[1–3] In particular, endophytic fungi, which live asymptomatically within plant tissues, have been recognized for their capability to produce therapeutically interesting natural products.[4] Remarkable examples include the antimycotic natural products cryptocandin[5] and cryptocin,[6] the insecticidal compound nodulisporic acid A,[7] the mitochondrial toxin phomoxanthone A[8,9] as well as the immunosuppressant diterpene pyrones subglutinols A and B,[10] among others. Interestingly, isolation of the important anticancer agents, paclitaxel from *Taxomyces andreanae*, an endophyte of *Taxus brevifolia*,[11] and camptothecin produced by *Entrophospora infrequens*, a fungus associated with *Nothapodytes foetida*,[12] as well as the identification of lycopodine-type alkaloids recently detected in an UV-irradiated strain of *Paraboeremia*, a fungal endophyte of *Lycopodium serratum* var. *longipetiolatum*,[13] highlights the special importance of endophytes as a reservoir of metabolites previously known only from the host plant.[14,15]

[a]*Institute of Pharmaceutical Biology and Biotechnology, Heinrich Heine University Düsseldorf, Universitätsstrasse 1, 40225 Düsseldorf, Germany. E-mail: Elena.Ancheeva@uni-duesseldorf.de; proksch@uni-duesseldorf.de; Fax: +49 211 81 11923; Tel: +49 211 81 14175; +49 211 81 14163*

[b]*Department of Pharmacy, Faculty of Mathematic and Natural Sciences, Udayana University, 80361 Bali, Indonesia*

[c]*Department of Organic Chemistry, University of Debrecen, P.O.B. 400, 4002 Debrecen, Hungary*

[d]*Institute for Physiological Chemistry, University Medical Center of the Johannes Gutenberg University Mainz, Duesbergweg 6, 55128 Mainz, Germany*

[e]*State Key Laboratory of Natural and Biomimetic Drugs, Peking University, 100191 Beijing, China*

† Electronic supplementary information (ESI) available: HPLC chromatograms, UV, HRESIMS, NMR spectra of **1–13**, **16**, structure and population of the low-energy conformers of (*S*)-**1**, classification of the 22 low-energy conformers of (8*R*,9*S*)-**4**, experimental ECD spectrum of **6** compared with the Boltzmann-weighted PBE0/TZVP PCM/MeCN ECD spectrum of (*R*)-**6**, and classification of the 26 low-energy conformers of (3*S*,11*S*,23*S*)-**14** into conformer groups. See DOI: 10.1039/c9ra03678d

‡ Present address: G. Daletos, Department of Chemical Engineering, Massachusetts Institute of Technology, 25 Ames Street, Cambridge, Massachusetts 02139, United States.

Gene clusters involved in the biosynthesis of fungal secondary metabolites often remain silent under standard laboratory culture conditions, leading to a frequent rediscovery of known metabolites.[16,17] To overcome this problem, several strategies for enhancing the biosynthetic potential of fungi can be applied. One of them is the OSMAC (One Strain, MAny Compounds) approach,[18] a powerful experimental method used to enhance the chemical diversity of microorganisms using the selective modification of the fermentation parameters, such as the media type and composition, the physical parameters (pH value, temperature, aeration conditions), the addition of enzyme inducers/inhibitors and chemical elicitors.[16–19] Even a difference in water quality in preparing the culture media, such as exchanging tap water for distilled water, was reported to influence the pattern of the main metabolites of *Paraphaeosphaeria quadriseptata*, due to the presence of traces of metal ions (Cu^{2+}, Cd^{2+} and Cr^{3+}) in tap water.[20] Successful application of the OSMAC approach on the fungal endophyte, *Dothideomycete* sp. CRI7 by changing the medium type (PDB *vs.* Czapek malt medium) as well as by using different nutrient sources (potato for PDB medium and malt extract for Czapek malt medium) resulted in distinct secondary metabolite production of this fungus.[21,22] Interestingly, a series of studies have reported the isolation of halogenated natural products from fungal cultures grown on media to which different halide salts had been added, thus highlighting the fungal capability to utilize different halogen sources when present in the media.[23–26] In addition, supplementing media with trace elements, *e.g.* the addition of $CuCl_2$ to cultures of *Pestalotiopsis* sp. Z233 or the addition of $ZnSO_4$ to cultures of *Aspergillus clavatus*, induced the production of new sesquiterpenes possessing tyrosinase inhibitory activity,[27] and the production of a new metabolite, clavatustide C,[28] respectively.

As part of our ongoing studies aimed at influencing the biosynthetic capacity of endophytic fungi utilizing the OSMAC approach, we investigated the metabolic profiles of *Bulgaria inquinans* (isolate MSp3-1), an ascomycete fungus isolated from sprouts of common mistletoe (*Viscum album*). Previous chemical investigations of this fungus resulted in the isolation of azaphilone pigments, namely bulgarialactones A–D,[29,30] of which bulgarialactones A and B exhibited antimicrobial, cytotoxic and nematocidal activities.[29] Moreover, quinones containing a benzofluoranthenequinone nucleus, bulgarhodin and bulgarein[31] as well as cytotoxic anthraquinone dimers, bulgareones A and B,[32] were isolated from this fungus.

In the present study, we report the isolation and structure elucidation of 14 new natural products, including five new natural products (**1–5**) derived from *B. inquinans* cultured on solid Czapek medium and nine new compounds (**6–13**, **16**) isolated from this fungus when grown on solid Czapek medium with the addition of a salt mixture ($MgSO_4$, $NaNO_3$ and NaCl). Furthermore, determination of the absolute configurations of the new compounds and of the known derivative, bulgarialactone B (**14**), is described herein. The cytotoxicity assay results of the isolated natural products are briefly discussed.

Results and discussion

Chemical investigation of *B. inquinans* grown on solid Czapek medium resulted in the isolation of five new natural products, namely butyrolactones (**1–3**, **5**) and a new metabolite bearing a diol moiety (**4**) together with known compounds, such as the azaphilone pigment bulgarialactone B (**14**)[29] as well as phenylbutyrolactone IIa (**15**)[33,34] and xenofuranone B (**17**)[35] (Fig. 1). After this fermentation, we studied the chemical profiles of the fungus when grown in the presence of different salts that had been added to solid Czapek medium. *B. inquinans* was cultured on solid Czapek medium following the addition of either NaCl, NaBr, NaI, $NaNO_3$, or $(NH_4)_2SO_4$ (3.5 g of each) or following the addition of salt mixtures: (a) $MgSO_4 \cdot 7H_2O$, $NaNO_3$ and NaCl (2.5 g each), (b) $FeSO_4 \cdot 7H_2O$, $NaNO_3$ and NaCl (2.5 g each) or (c) $ZnSO_4 \cdot 7H_2O$, $NaNO_3$ and NaCl (2.5 g each), as described in the Experimental section. *B. inquinans* failed to grow on media containing either $(NH_4)_2SO_4$, or mixtures (b) and (c). No changes in the chromatographic profiles were observed following the addition of either NaCl, NaBr, NaI or $NaNO_3$ to solid Czapek medium when compared to chromatograms of the fungus grown on the medium without salts. However, the presence of a mixture of $MgSO_4$, $NaNO_3$ and NaCl in the medium resulted in a significant change in the metabolite profile of *B. inquinans*, as indicated by HPLC-DAD analysis (Fig. S1, ESI†). Chromatographic workup of this fungal extract led to the isolation of nine new secondary metabolites (**6–13**, **16**), including a butyrolactone derivative **6**, two unusual 1,3-oxazine containing natural products (**7** and **8**), five new α-pyrones (**9–13**) and (−)-(*S*)-flavipesin B (**16**), together with the known compound bulgarialactone D (**18**)[30] (Fig. 1). Compounds **9**, **13** and **18** were subsequently also detected (albeit in minor amounts) in HPLC chromatograms of the fungus following cultivation on solid Czapek medium without the addition of salts. The OSMAC approach nevertheless enhanced their production, enabling isolation and structural characterization of these compounds. Moreover, the accumulation of compounds **8** and **10–12** was only induced in the presence of the salt mixture, whereas these latter compounds were not detected in fungal cultures lacking salts.

Compound **1** was obtained as a yellow solid. Its UV spectrum displayed a maximum absorption at 288 nm, which was characteristic for butyrolactone-type metabolites.[36] The HRESIMS spectrum exhibited a prominent pseudomolecular ion peak at *m*/*z* 253.0600 $[M + H]^+$, attributed to the molecular formula $C_{12}H_{10}O_5$, indicating 8 degrees of unsaturation. The ^{1}H NMR data of **1** (Table 1) revealed signals of one methyl at δ_H 1.74 (H_3-12) and five aromatic protons resonating at δ_H 7.74 (H-7/H-11), 7.41 (H-8/H-10) and 7.34 (H-9), implying the presence of a mono-substituted benzene ring. Moreover, the ^{13}C NMR data of **1** (Table 1) displayed signals of a carbonyl carbon at δ_C 170.3 (C-2), two sp^2 carbons at δ_C 140.6 (C-3) and 131.2 (C-4), and one oxygenated sp^3 carbon at δ_C 85.2 (C-5), attributed to a conjugated five-membered lactone ring. The HMBC correlations observed from H-7/H-11 to C-4 and from H_3-12 to C-4, C-5 and C-1′ (Fig. 2) provided the connections of the aromatic ring and of the methyl group to the butyrolactone ring as well as the attachment of the carboxylic acid group to C-5.

In order to elucidate the absolute configuration of **1**, the TDDFT-ECD protocol was performed on the arbitrarily chosen (*S*) stereoisomer. B3LYP/6-31+G(d,p) and CAM-B3LYP/TZVP PCM/MeCN reoptimization of the initial 13 MMF conformers resulted in three

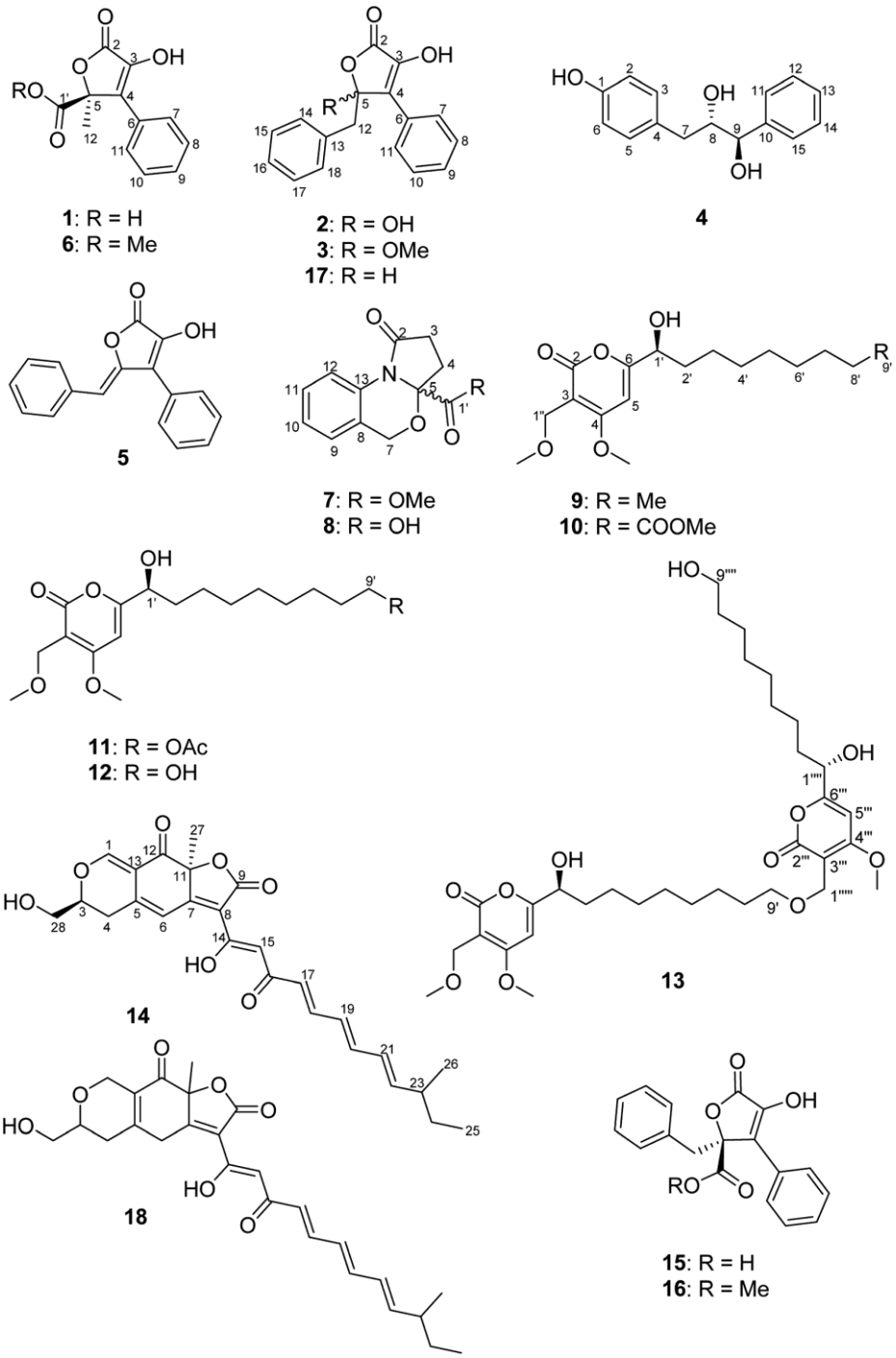

Fig. 1 Structures of compounds 1–18 isolated from *B. inquinans*.

and eight low-energy conformers over a 1% Boltzmann-population, respectively. ECD spectra computed at various levels for both sets of conformers effectively reproduced the experimental ECD spectrum of **1** (Fig. 3), allowing the elucidation of the absolute configuration as (*S*). Accordingly, the structure of **1** was established as a new natural product, for which the name bulgariline A is proposed (Fig. 1).

Table 1 ^{1}H and ^{13}C NMR data (MeOH-d_4)[a] for compounds **1–3** and **5–6**

	1		**2**		**3**		**5**		**6**	
Position	δ_C, type	δ_H (J in Hz)	δ_C, type	δ_H (J in Hz)	δ_C, type	δ_H (J in Hz)	δ_C, type	δ_H (J in Hz)	δ_C, type	δ_H (J in Hz)
2	170.3, C		168.9, C		168.1, C		166.6, C		169.9, C	
3	140.6, C		141.4, C		143.0, C		141.4, C		140.8, C	
4	131.2, C		127.3, C		123.9, C		126.5, C		130.6, C	
5	85.2, C		107.4, C		110.4, C		148.1, C		84.9, C	
6	131.4, C		132.3, C		131.8, C		130.5, C		131.2, C	
7/11	128.7, CH	7.74, br d (7.5)	129.4, CH	8.00, br d (7.5)	128.8, CH	7.94, br d (7.4)	130.4, CH	7.57, br d (7.5)	128.6, CH	7.66, br d (7.3)
8/10	129.6, CH	7.41, br t (7.5)	129.5, CH	7.46, br t (7.5)	129.8, CH	7.48, br d (7.4)	129.8, CH	7.51, br t (7.5)	129.8, CH	7.42, br t (7.3)
9	129.7, CH	7.34, tt (7.5, 1.2)	129.4, CH	7.37, tt (7.5, 1.6)	129.8, CH	7.39, tt (7.4, 1.1)	128.9, CH	7.45, tt (7.5, 1.3)	129.8, CH	7.35, tt (7.3, 1.2)
12	22.1, CH_3	1.76, s	44.9, CH_2	3.39, d (13.8); 3.34, d (13.8)	44.6, CH_2	3.37, d (13.8); 3.34, d (13.8)	109.6, CH	5.97, s	22.2, CH_3	1.79, s
13			135.7, C		135.2, C		135.3, C			
14/18			131.4, CH	6.85, br d (6.9)	131.5, CH	6.85, br d (6.9)	130.9, CH	7.68, br d (7.4)		
15/17			128.8, CH	7.10, br t (6.9)	128.8, CH	7.10, br t (6.9)	129.6, CH	7.35, br t (7.4)		
16			127.9, CH	7.12, tt (6.9, 1.6)	128.0, CH	7.12, tt (6.9, 1.5)	128.8, CH	7.25, tt (7.4, 1.1)		
5-OMe					50.9, CH_3	3.24, s				
1′	172.4, C								171.4, C	
1′-OMe									53.9, CH_3	3.76, s

[a] Recorded at 600 MHz (^{1}H) and 150 MHz (^{13}C).

The molecular formulae of **2** and **3** were assigned as $C_{17}H_{14}O_4$ and $C_{18}H_{16}O_4$, respectively, based on their prominent pseudomolecular ion peaks in the HRESIMS spectra. The ^{1}H and ^{13}C NMR data of **2** (Table 1) were almost identical to those of phenylbutyrolactone IIa (**15**), except for the replacement of the carboxylic acid functionality with a hydroxyl group, as indicated by the absence of a carbonyl signal in the ^{13}C NMR spectrum, as well as a 28 amu difference in the molecular weight of **2** compared with that of phenylbutyrolactone IIa (**15**). The NMR data of **3** (Table 1) were in good agreement with those of **2**, apart from the presence of a methoxy signal at δ_H 3.24 (δ_C 50.9). Accordingly, a methoxy substituent was assigned to C-5 instead of a hydroxyl group as in **2**, based on the evident HMBC correlation from 5-OMe to C-5. Thus, **2** and **3** were elucidated as new butyrolactone derivatives and were named as bulgarilines B and C, respectively. The zero value of their specific rotations indicated that **2** and **3** were obtained as racemic mixtures.

The molecular formula of **4** was determined as $C_{15}H_{16}O_3$ based on its HRESIMS data, implying 8 degrees of unsaturation. Investigation of its ^{1}H NMR data (Table 2) revealed typical signals of phenyl and *p*-hydroxy phenyl moieties in the structure

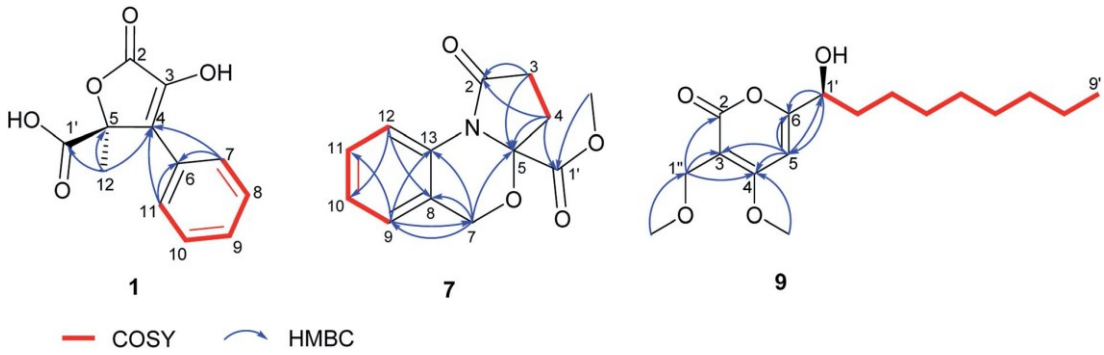

Fig. 2 COSY and selected HMBC correlations of **1**, **7** and **9**.

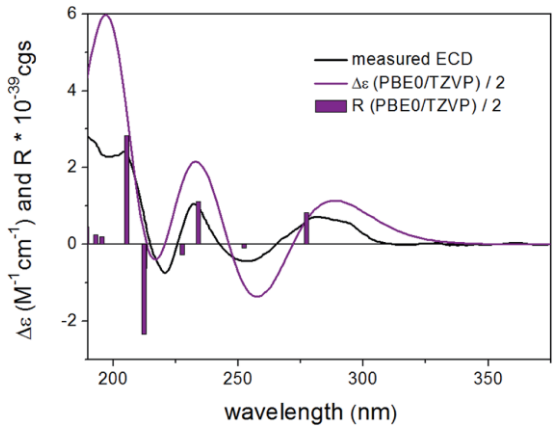

Fig. 3 Experimental ECD spectrum (black) of **1** in MeCN compared with the Boltzmann-weighted PBE0/TZVP PCM/MeCN ECD spectrum (purple) of (*S*)-**1** computed for the eight low-energy CAM-B3LYP/TZVP PCM/MeCN conformers. The bars represent the rotational strength of the lowest-energy conformer.

of **4**. In addition, consecutive COSY correlations were observed between a set of methylene protons resonating at δ_H 2.51/2.84 (H_2-7) and two *O*-methine protons at δ_H 3.87 and 4.53 (H-8 and H-9), which permitted the assignment of a 1,2-propanediol moiety. The HMBC correlations from H_2-7 to C-3, C-4, C-5, C-8 and C-9 and in turn from H-9 to C-10, C-11 and C-15 established the connectivity of the partial structures. The relative configuration of **4** was deduced to be *erythro*, based on the large coupling constant value between the two vicinal methines at positions 8 and 9 (5.8 Hz), while a smaller value ($J = 2.5$ Hz) is suggested for *threo*, as previously reported for related vicinal diols.[37,38] Hence, the structure of **4** was elucidated and the trivial name bulgariol is suggested for this compound.

DFT reoptimization of the initial 41 MMFF conformers of (8*R*,9*S*)-**4** resulted in 15 and 22 low-energy conformers over a 1% Boltzmann-population. Despite the flexibility of the molecule and the substantially different ECD spectra of the individual low-energy conformers, the Boltzmann-averaged ECD spectra computed at various levels for both sets of conformers gave moderate to good mirror-image agreement with the experimental ECD spectrum (Fig. 4). Furthermore, the sign of the highest-wavelength ECD transition was the same for all the conformers over a 1.2% Boltzmann-population, allowing elucidation of the absolute configuration as (8*S*,9*R*).

Compound **5** had the molecular formula $C_{17}H_{12}O_3$, requiring 12 degrees of unsaturation. The ^{1}H and ^{13}C NMR data of **5** (Table 1) were similar to those of **2** and **3**. However, an additional olefinic signal appeared at δ_H 5.97 (H-12), which provided HMBC correlations to C-4, C-5, C-13, C-14/C-18, along with a long-range correlation to C-2. Thus, the position of the double bond was deduced at $\Delta^{5(12)}$, contributing to one additional degree of unsaturation of **5** compared to **2** and **3**. The geometry of the exocyclic double bond C-5/C-12 in **5** was determined based on the NOESY spectrum. The NOE correlations observed between H-12 with H-7/H-11 implied the close proximity of H-12 to the aromatic ring, thus confirming the *Z* configuration of the double bond.[39,40] Compound **5**, (5*Z*)-3-hydroxy-4-phenyl-5-(phenylmethylene)-2(5*H*)-furanone, was reported previously only as a synthetic product.[41] In the present study, we report **5** for the first time as a natural product and provide its complete NMR data (Table 1).

The molecular ion of **6** was 14 amu larger than that of **1**, as indicated by the HRESIMS spectrum, corresponding to the molecular formula $C_{13}H_{12}O_5$. The ^{1}H and ^{13}C NMR data of **6** (Table 1) were in perfect agreement with those of **1**, except for the additional methoxy group signal at δ_H 3.76/δ_C 53.9, which showed the respective HMBC correlation to C-1′, hinting at a substitution of the carboxylic acid group with a carbomethoxy attached to C-5 in the structure of **6**. Finally, **6** was elucidated as a methyl ester of bulgariline A to which the trivial name bulgariline D is given.

Table 2 ^{1}H and ^{13}C NMR data (MeOH-d_4) for compound **4**

	4[a]	
Position	δ_C, type	δ_H (J in Hz)
1	156.6, C	
2/6	115.9, CH	6.68, br d (8.5)
3/5	131.4, CH	7.02, br d (8.5)
4	131.6, C	
7	38.9, CH_2	2.51, dd (14.2, 9.2)
		2.84, dd (14.2, 3.1)
8	77.8, CH	3.87, ddd (9.2, 5.8, 3.1)
9	78.2, CH	4.53, d (5.8)
10	143.5, C	
11/15	128.4, CH	7.41, br d (7.0)
12/14	129.0, CH	7.33, br t (7.0)
13	128.3, CH	7.26, tt (7.0, 1.5)

[a] Recorded at 600 MHz (^{1}H) and 150 MHz (^{13}C).

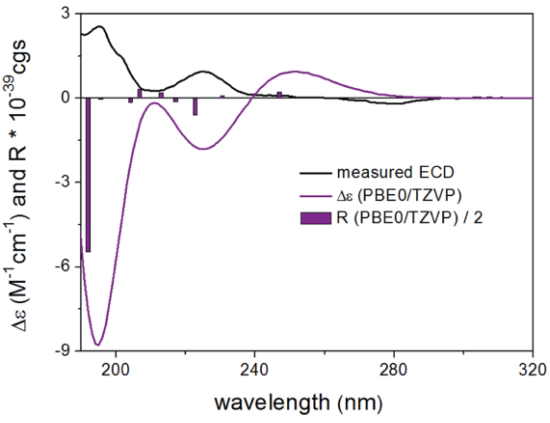

Fig. 4 Experimental ECD spectrum (black) of **4** in MeCN compared with the Boltzmann-weighted PBE0/TZVP PCM/MeCN ECD spectrum (purple) of (8*R*,9*S*)-**4** computed for the 22 low-energy CAM-B3LYP/TZVP PCM/MeCN conformers. The bars represent the rotational strength of the lowest-energy conformer.

The absolute configuration of **6** was concluded to be the same as that of **1** on the basis of biogenetic considerations, similar positive values of their specific rotation, $[\alpha]_D^{20}$ +16 for **1** and $[\alpha]_D^{25}$ +26 for **6**, as well as the identical ECD spectra of **1** and **6**. Furthermore, TDDFT-ECD calculations performed on the arbitrarily chosen (*R*) enantiomer gave mirror-image agreement (Fig. S106, ESI†), verifying the (*S*) absolute configuration of **6**. It is interesting to compare the ECD spectra of **1** and **6** with those of the related compounds chaetobutenolide C, WF-3681 and WF-3681 methyl ester described by some of us in 2017 and where the carboxylic acid/ester group is attached through two carbons to the central unit.[36] The positive transition at *ca.* 260–280 nm, which is stronger in two recent cases, and the negative one around 220 nm, belonging to the homochiral derivatives, becomes more complex in **1** and **6**, but they are still in accordance with the two characteristic bands. Moreover, **6** was proven to be a true natural product, by incubating 1.0 mg of **1** in 1.0 mL MeOH containing 0.1% formic acid at room temperature for 1 week, which did not result in methylation, as indicated by HPLC analysis.

Nitrogen-containing metabolites (**7** and **8**) were obtained as yellow solids. The HRESIMS spectra exhibited prominent pseudomolecular ion peaks at *m*/*z* 248.0919 $[M + H]^+$ and *m*/*z* 234.0760 $[M + H]^+$, consistent with the molecular formula $C_{13}H_{13}NO_4$ and $C_{12}H_{11}NO_4$, respectively, both corresponding to 8 degrees of unsaturation. Inspection of the ^{1}H NMR spectrum of **7** (Table 3) revealed the resonances of four aromatic protons, three sets of methylenes and one methoxy group. The COSY correlations of the aromatic protons from H-9 until H-12 suggested a 1,2-disubstituted aromatic ring for **7**, as corroborated by HMBC correlations from H-9 to C-11 and C-13 as well as from H-12 to C-8 and C-10. The last spin system observed in the COSY spectrum between δ_H 2.60/2.67 (H_2-3) and 2.30/2.54 (H_2-4) afforded HMBC correlations from H_2-3 to C-2 and C-5 and from H_2-4 to C-5 and C-1′, respectively. Additionally, the HMBC correlation from 1′-OMe to C-1′ established the substructure of an oxoproline residue bearing a 5-carbomethoxy group (Fig. 2). Further HMBC correlations from the methylene at δ_H 4.96/5.10 (H_2-7) to C-5, C-8, C-9 and C-13 established the linkage between these two substructures, which accounted for the last degree of unsaturation in **7**. The ^{1}H and ^{13}C NMR data of **8** were in a good agreement with those of **7**, apart from the absence of an OMe signal, which is in accordance with the 14 amu difference in the molecular weight of **8** compared to **7**, thus indicating a carboxylic acid group attached at C-5, instead of a carbomethoxy function. Accordingly, **7** and **8** possess unusual heterocyclic structures containing a 1,3-oxazine nucleus, which rarely occurs in natural products. A few examples of natural 1,3-oxazines include the antimycobacterial oxazinin A, isolated from the *Eurotiomycetes* strain 110162,[42] as well as salinazinones A and B from the bacterial strain *Streptomyces* sp. KMF-004.[43] The latter two compounds have been also reported from the marine-derived bacterium *Streptomyces spinoverrucosus* as spinoxazines A and B.[44] However, compared to the aforementioned natural products, the structures of **7** and **8** lack a keto function in the 1,3-oxazine core, which is mostly attributed to synthetic compounds.[45,46] The trivial names bulgarixines A (**7**) and B (**8**) were assigned to these compounds. Considering the possibility that **7** might arise as an artifact of its non-methoxylated analogue (**8**) during the isolation process, an experiment was carried out by incubating 0.5 mg of **8** in 0.5 mL MeOH containing 0.1% formic acid for 1 week at room temperature. HPLC analysis showed that no methylated product was present in the chromatogram, thus indicating that **7** is a natural product. The baseline ECD curves of both **7** and **8** indicated that both of them were isolated as a racemate.

Compound **9** was afforded as a brown solid. Its molecular formula was determined as $C_{17}H_{28}O_5$ on the basis of its HRESIMS spectrum, requiring 4 degrees of unsaturation. Its UV

Table 3 ^{1}H and ^{13}C NMR data (MeOH-d_4) for compounds **7** and **8**

	7[a]		**8**[a]	
Position	δ_C, type	δ_H (*J* in Hz)	δ_C, type[b]	δ_H (*J* in Hz)
2	174.3, C		174.3, C	
3	30.6, CH_2	2.60, ddd (17.2, 10.1, 2.3) 2.67, dt (17.2, 9.6)	30.5, CH_2	2.59, ddd (17.2, 10.1, 2.2) 2.70, dt (17.2, 9.7)
4	31.4, CH_2	2.30, dt (13.5, 10.1) 2.54, ddd (13.5, 9.6, 2.3)	31.3, CH_2	2.28, dt (13.5, 10.1) 2.54, ddd (13.5, 9.7, 2.2)
5	92.6, C		92.6, C	
7	66.1, CH_2	4.96, d (15.8); 5.10, d (15.8)	65.7, CH_2	4.93, d (15.7) 5.19, d (15.7)
8	124.4, C		124.6, C	
9	125.5, CH	7.10, br d (8.0)	125.2, CH	7.10, br d (8.0)
10	125.9, CH	7.14, td (8.0, 1.2)	125.3, CH	7.13, td (8.0, 1.2)
11	128.5, CH	7.27, br t (8.0)	128.0, CH	7.26, br t (8.0)
12	120.4, CH	8.27, br d (8.0)	120.3, CH	8.29, br d (8.0)
13	134.0, C		133.8, C	
1′	171.4, C		172.6, C	
1′-OMe	53.7, CH_3	3.73, s		

[a] Recorded at 600 MHz (^{1}H) and 150 MHz (^{13}C). [b] Chemical shifts extracted from HSQC and HMBC spectra.

spectrum displayed a maximum absorption at around 299 nm, suggesting a pyrone nucleus.[47,48] Detailed analysis of the ^{1}H and ^{13}C NMR data of **9** (Table 4) indicated signals of an isolated olefinic proton at δ_H 6.65 (H-5), an oxygenated methine at δ_H 4.40 (H-1′) and an isolated methylene at δ_H 4.31 (H_2-1″), in addition to seven aliphatic methylenes observed at δ_H 1.31–1.82 (H_2-2′–H_2-8′), two methoxy groups at δ_H 4.00 and 3.32, one methyl group at δ_H 0.90 (H_3-9′), along with signals for a carbonyl at δ_C 166.7 (C-2) and sp^2 carbons at δ_C 101.8 (C-3), 171.7 (C-4) and 171.4 (C-5). COSY correlations observed from H-1′ to H_3-9′ allowed the assignment of a 1-nonanol side-chain (Fig. 2). The HMBC correlations from H-5 to C-3, C-4 and C-6, as well as from H_2-1″ to C-2, C-3 and C-4, confirmed the presence of a conjugated α-pyrone nucleus in the structure of **9**. Additionally, the position of two methoxy groups (4-OMe and 1″-OMe) as substituents of the α-pyrone ring was deduced based on their respective HMBC correlations. Finally, the presence of HMBC correlations from H-5 to C-1′ and in turn from H-1′ to C-5 and C-6, indicated the connection of the 1-nonanol side-chain with the α-pyrone nucleus at C-6 (Fig. 2). The structure of **9** is closely related to dothideopyrone B, which was isolated from the endophyte *Dothideomycete* sp. LRUB20,[49] and with dothideopyrone F, a recently reported α-pyrone from the endolichenic fungus *Dothideomycetes* sp. EL003334.[47] However, **9** features two extra methylene protons in the saturated aliphatic chain in comparison with dothideopyrone B,[49] and an additional OMe at C-1″ in comparison with dothideopyrone F.[47] Therefore, compound **9** was elucidated as a new α-pyrone derivative, for which the trivial name bulgariapyrone A is suggested.

Compounds **10–12** exhibited similar UV spectra as **9**, indicative of pyrone derivatives (see ESI†). Their molecular formulae were determined as $C_{18}H_{28}O_7$, $C_{19}H_{30}O_7$ and $C_{17}H_{28}O_6$, respectively, as indicated by their HRESIMS spectra. The ^{1}H and ^{13}C NMR data of **10–12** (Table 4) were similar to those of **9** and indicated that **10–12** retained the same α-pyrone core structure as **9**, differing from the latter only in the nature of their aliphatic side-chains. The molecular weight of **10** was 44 amu larger than that of **9**, which together with an additional methoxy signal at δ_H 3.65/δ_C 51.9 and an additional carbonyl resonating at δ_C 176.0 (C-9′), implied that the aliphatic chain of **10** is terminated by a carbomethoxy group instead of a methyl group. This deduction was corroborated by the observed HMBC correlation from H_2-7′/H_2-8′ to C-9′, in addition to a further degree of unsaturation of **10** in comparison with **9**. The ^{1}H NMR data of **11** (Table 4) displayed an additional oxygenated methylene at δ_H 4.05 (H_2-9′) and a signal of a downfield shifted methyl group at δ_H 2.02 (H_3-12′), which along with the observed HMBC correlations from H_2-9′ to C-7′, C-8′ and C-11′, as well as from H_3-12′ to C-11, hinted at the presence of an acetoxy group at the terminus of the aliphatic side-chain in **11**. The molecular weight

Table 4 ^{1}H and ^{13}C NMR data (MeOH-d_4) for compounds **9–13**

	9[a]		**10**[a]		**11**[a]		**12**[a]		**13**[b,d]	
Position	δ_C, type[c]	δ_H (J in Hz)	δ_C, type	δ_H (J in Hz)	δ_C, type[c]	δ_H (J in Hz)	δ_C, type	δ_H (J in Hz)	δ_C, type	δ_H (J in Hz)
2	166.7, C		166.8, C		166.7, C		166.8, C		166.7, C	
3	101.8, C		101.8, C		101.8, C		101.8, C		101.9, C	
4	171.7, C		171.7, C		171.7, C		171.7, C		171.7, C	
5	94.4, CH	6.65, s	94.4, CH	6.65, s	94.4, CH	6.65, s	94.4, CH	6.65, s	94.5, CH	6.65, br s
6	171.4, C		171.3, C		171.3, C		171.3, C		171.3, C	
1′	71.5, CH	4.40, dd (7.9, 4.5)	71.5, CH	4.40, m	71.5, CH	4.40, dd (7.9, 4.5)	71.5, CH	4.40, dd (8.0, 4.5)	71.5, CH	4.40, br dd (7.9, 4.4)
2′	36.3, CH_2	1.68, m; 1.82, m	36.2, CH_2	1.68, m; 1.83, m	36.2, CH_2	1.69, m; 1.82, m	36.2, CH_2	1.68, m; 1.82, m	36.3, CH_2	1.68, m; 1.82, m
3′	26.2, CH_2	1.42, m	26.1, CH_2	1.43, m	26.1, CH_2	1.44, m	26.1, CH_2	1.44, m	26.1, CH_2	1.44, m; 1.41 m
4′	30.4,[e] CH_2	1.27–1.37, ov[f]	30.2,[e] CH_2	1.31–1.38, ov	30.2,[e] CH_2	1.31–1.39, ov	30.4,[e] CH_2	1.31–1.39, ov	30.4,[e] CH_2	1.30–1.37, ov
5′	30.5,[e] CH_2	1.27–1.37, ov	30.1,[e] CH_2	1.31–1.38, ov	30.3,[e] CH_2	1.31–1.39, ov	30.5,[e] CH_2	1.31–1.39, ov	30.5,[e] CH_2	1.30–1.37, ov
6′	30.6,[e] CH_2	1.27–1.37, ov	30.2,[e] CH_2	1.31–1.38, ov	30.4,[e] CH_2	1.31–1.39, ov	30.6,[e] CH_2	1.31–1.39, ov	30.6,[e] CH_2	1.30–1.37, ov
7′	33.0, CH_2	1.27–1.37, ov	26.0, CH_2	1.61, p (7.4)	27.0, CH_2	1.36, ov	26.9, CH_2	1.34, ov	27.1, CH_2	1.34, ov
8′	23.7, CH_2	1.31, ov	34.8, CH_2	2.31, t (7.4)	29.7, CH_2	1.62, p (6.7)	33.6, CH_2	1.52, p (6.7)	30.6, CH_2	1.54, m
9′	14.4, CH_3	0.90, t (7.0)	176.0, C		65.7, CH_2	4.05, t (6.7)	63.0, CH_2	3.53, t (6.7)	71.6, CH_2	3.46, t (6.6)
11′					173.1, C					
12′					20.8, CH_3	2.02, s				
1″	64.1, CH_2	4.31, s	64.1, CH_2	4.30, s	64.1, CH_2	4.31, s	64.1, CH_2	4.30, s	64.1, CH_2	4.30, s
4-OMe	57.7, CH_3	4.00, s	57.7, CH_3	4.00, s	57.7, CH_3	4.00, s	57.7, CH_3	4.00, s	57.7, CH_3	4.00, s
9′-OMe			51.9, CH_3	3.65, s						
1″-OMe	58.3, CH_3	3.32, s	58.3, CH_3	3.32, s	58.3, CH_3	3.32, s	58.3, CH_3	3.32, s	58.3, CH_3	3.32, s

[a] Recorded at 600 MHz (^{1}H) and 150 MHz (^{13}C). [b] Recorded at 600 MHz (^{1}H) and 125 MHz (^{13}C). [c] Chemical shifts extracted from the HSQC and HMBC spectra. [d] Signals for another monomeric unit are identical, except for δ_C 166.8 (C, C-2‴), 102.3 (C, C-3‴), 171.5 (C, C-4‴), 94.4 (CH, C-5‴), 171.1 (C, C-6‴), 26.9 (CH_2, C-7‴′), as well as signals at δ_C 33.6 (CH_2, C-8‴′)/δ_H 1.52 (2H, m, H-8‴′), δ_C 63.0 (CH_2, C-9‴′)/δ_H 3.53 (2H, t, J = 6.7 Hz, H-9‴′) and δ_C 62.3 (CH_2, C-1‴′)/δ_H 4.34 (2H, s, H-1‴′). [e] Signals can be interchangeable. [f] ov stands for overlapped signals.

of compound **12** was 16 amu larger than that of **9**. Moreover, the ^{1}H NMR data of **12** (Table 4) displayed an extra oxygenated methylene (δ_H 3.53) split into a triplet, which revealed a COSY correlation to δ_H 1.52 (H-8′), suggesting the presence of a hydroxyl group at C-9′. Accordingly, compounds **10–12** were established as new α-pyrone analogues, for which the trivial names bulgariapyrones B–D are proposed.

In order to assign the absolute configurations of **9–12**, the modified Mosher's reaction was carried out, and **12** was chosen as a model compound for this reaction. Both primary and secondary alcohol groups in **12** were converted to either (*S*)- or (*R*)-MTPA esters. Based on the calculated values of $\Delta\delta_{(S)-(R)}$ of MTPA esters, the absolute configuration at C-1′ was established as (*S*), which is in agreement with the literature data of previously described α-pyrone derivatives related to **12** (Fig. 5).[47] Similar specific optical rotation values of **9–11** suggested that these α-pyrones share the same (*S*) absolute configuration at C-1′.

The molecular formula of **13** was determined as $C_{33}H_{52}O_{11}$, based on the prominent pseudomolecular ion peak at *m*/*z* 625.3587 $[M + H]^+$ in the HRESIMS spectrum, corresponding to 8 degrees of unsaturation. Analysis of the molecular formula and of the 1D/2D NMR data of **13** (Table 4, ESI†) suggested it contained two substructures similar to bulgariapyrone D (**12**). However, the NMR data of **13** revealed additional signals of an isolated methylene at δ_H 4.34/δ_C 62.3 (H_2-1′′′′′) and one set of methylene as a triplet at δ_H 3.46/δ_C 71.6 (H_2-9′), suggesting an asymmetry of the molecule. The HMBC correlations observed from H_2-1′′′′′ to C-2′′′, C-3′′′, C-4′′′ and C-9′, and in turn from H_2-9′ to C-7′, C-8′ and C-1′′′′′, together with the NOESY correlation H_2-9′/H_2-1′′′′′ allowed connecting these two monomeric units *via* an ether bridge between C-1′′′′′ and C-9′, suggesting that **13** could be formed through a condensation reaction between two molecules of **12**. Thus, the planar structure of **13** was elucidated as shown and the name bulgariapyrone E is proposed. Notably, only two related naturally occurring symmetrical α-pyrone dimers have been reported so far, multiforisin D, previously isolated from *Gelasinospora multiforis*,[50] and dothideopyrone D, a metabolite from the endophytic fungus *Dothideomycete* sp. LRUB20,[49] which emphasize the rare nature of these dimeric compounds. Moreover, compound **13** seems to be a product of a "head to tail" condensation, where the side chain of one monomeric unit is connected through an ether bond to the C-1′′′′′ of the α-pyrone nucleus of the other monomeric unit, which creates an asymmetry in the structure of **13** and makes it structurally different from known symmetrical C2-type bis-pyrone dimers. As the condensation of primary alcohols might take place under acidic conditions, an experiment was carried out by incubating 0.2 mg of **12** in 0.2 mL MeOH containing different concentrations of formic acid (0.1%, 1%, 5% and 10%), at room temperature for 1 week, followed by HPLC analysis. The HPLC chromatograms showed no formation of compound **13**, which indicated that **13** is a true natural product, and not an artifact arising during the isolation procedure.

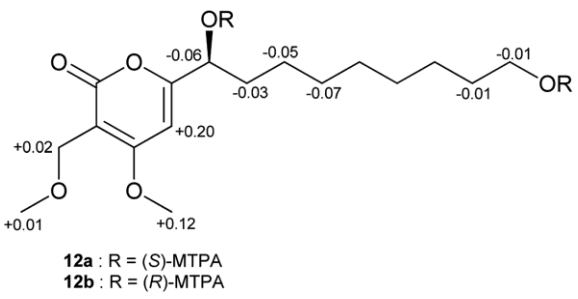

Fig. 5 $\Delta\delta_{(S)-(R)}$ values in ppm for the MTPA esters of **12**.

Following the same Mosher's reaction protocol for compound **13** as for **12**, the (*S*)- or (*R*)-MTPA ester products were obtained (see the Experimental section). The MALDI-MS spectra of the reaction products indicated that all the primary and secondary alcohol groups in **13** reacted with the reagent (*m*/*z* 1295 $[M + Na]^+$). Thus, the absolute configuration of **13** was unequivocally assigned as (*S*) for both stereocenters at C-1′ and C-1′′′′, which is in accordance with biosynthetic considerations and the reported configuration of the structurally related homodimer dothideopyrone D.[49]

Compound **14** was obtained as a dark red solid. Its molecular formula was determined as $C_{26}H_{28}O_7$, on the basis of a prominent pseudomolecular ion peak at *m*/*z* 453.1910 $[M + H]^+$ in the HRESIMS spectrum, requiring 13 degrees of unsaturation. Detailed analysis of the 1D and 2D NMR spectra showed that **14** is a known compound, bulgarialactone B,[29] first isolated from the same fungus more than two decades ago. However, in this first paper, the absolute configuration was not determined for bulgarialactone B and the relative configuration was elucidated on the basis of the weak NOESY correlation between H-3 and H_3-27. Further reports on bulgarialactone B focused on the Hsp90 inhibitory activity and were not engaged in the elucidation of the absolute configuration.[30,51] The SciFinder database indicates the absolute configuration for the closely related compound epicocconone, which lacks a chirality centre in the unsaturated side-chain and exhibits potent fluorescent properties, but the original paper[52] reported only the relative configuration of the two chirality centres as elucidated by the comparison of the HF/6-31G(d,p) optimized low-energy geometries of the high-temperature molecular dynamics trajectories with the experimental NMR data. Subsequent papers did not address the elucidation of the absolute configuration of epicocconone.

Bulgarialactone B (**14**) had positive Cotton effects (CEs) at 437 and 269 nm and negative ones at 315 and 232 nm. In order to determine the absolute configuration of bulgarialactone B, the solution TDDFT-ECD method was applied on the arbitrarily chosen (3*S*,11*S*,23*R*) and (3*S*,11*S*,23*S*) stereoisomers.[53,54] Although the core part was expected to govern mostly the ECD spectrum, the C-23 chirality centre located in the allylic position of the conjugated π system of the side-chain was also supposed to have at least a minor contribution, which would have allowed distinguishing the C-23 epimers. A MMFF (Merck Molecular Force Field) conformational search of the two epimers resulted in 549 and 541 conformer clusters in a 21 kJ mol^{-1} energy window, respectively, indicating high conformational flexibility.

These geometries were reoptimized at the CAM-B3LYP/TZVP PCM/MeCN level. Despite the large number of low-energy conformers, the Boltzmann-averaged ECD spectra of both epimers computed at four different levels (B3LYP/TZVP, BH&HLYP/TZVP, CAM-B3LYP/TZVP and PBE0/TZVP, all with PCM for MeCN) gave consistently moderate to good agreement with the experimental ECD spectrum (Fig. 6 and 7). Interestingly, the difference between the computed ECD spectra of the epimers was rather small, which suggested that the influence of C-23 on the overall ECD is marginal. Accordingly, the absolute configuration of the core part could be elucidated as (3*S*,11*S*), while the C-23 chirality centre remained unassigned. By analyzing the individual ECD spectra of the low-energy computed conformers, it turned out that the features of the ECD spectra were influenced by the helicity of the dihydropyrane ring and the orientation of the conjugating side-chain, the latter of which was also described by Syzgantseva *et al.* to influence the UV characteristics.[55]

The experimental ECD spectra of **14** and that of (+)-epicocconone reported by Bell and Karuso[52] have a mirror image relationship, suggesting that (+)-epicocconone showing an intense negative CE above 400 nm has an (3*R*,11*R*) absolute configuration in *Epicoccum nigrum*,[52] which is an example of the chiral switching of the tricyclic skeleton.[56] It is also clear that the absolute configuration presented in the SciFinder database for epicocconone[57] is incorrect and it should specify only the relative configuration.

The planar structure of compound **16** was shown to be identical to the previously described flavipesin B, isolated from the fungal endophyte *Aspergillus flavipes* AIL8,[58] which has been previously reported as a synthetic compound.[59,60] In a recent study, it was isolated from an engineered strain of *A. nidulans*.[61] However, **16** possesses an opposite sign of the specific optical rotation, $[\alpha]_D^{25}$ −72 (MeOH), compared to that of the reported value for flavipesin B: $[\alpha]_D^{25}$ +133 (acetone).[58] Therefore, in this study, we assigned **16** as (−)-(*S*)-flavipesin B.

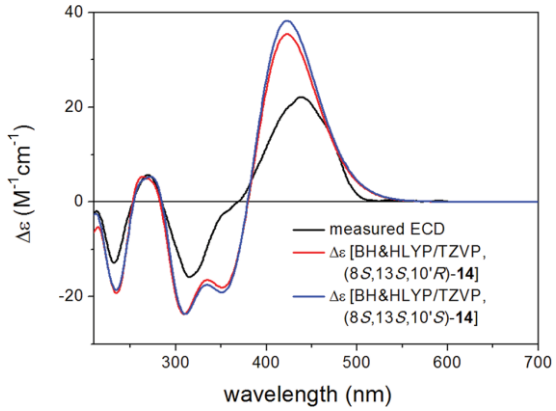

Fig. 6 Experimental ECD spectrum of **14** in MeCN compared with the Boltzmann-weighted BH&HLYP/TZVP PCM/MeCN spectra of (3*S*,11*S*,23*R*)-**14** and (3*S*,11*S*,23*S*)-**14** computed for the low-energy (≥1%) CAM-B3LYP/TZVP PCM/MeCN conformers (26 and 26 conformers, respectively).

The structures of the remaining known compounds isolated from *B. inquinans* were established as phenylbutyrolactone IIa (**15**),[33,34,59] xenofuranone B (**17**)[35,67] and bulgarialactone D (**18**),[30] based on their spectroscopic data as well as on a comparison with the literature.

All the isolated compounds were evaluated for cytotoxicity towards the murine lymphoma cell line L5178Y. However, only **2** exhibited pronounced activity against the L5178Y cell line, with an IC_{50} value of 1.8 μM, which was stronger than that of the positive control kahalalide F (IC_{50} 4.3 μM). The presence of a hydroxy group attached to C-5 in the 2-furanone ring in the structure of **2** was apparently important for its cytotoxic activity as no activity was found for compounds **3**, phenylbutyrolactone IIa (**15**), **16** and xenofuranone B (**17**). Furthermore, a closely related derivative, 4-*O*-demethylisobutyrolactone II, which bears an additional hydroxy group on both aromatic rings at the positions 9 and 16 (tyrosine-derived residues) compared to **2**, was shown to be inactive against the L5178Y cell line,[62] thus suggesting that the phenyl substituents were required for its cytotoxicity. The remaining compounds showed no significant cytotoxic properties. Interestingly, related α-pyrones were previously reported to be nontoxic or exhibited only moderate cytotoxicity against several cancer cell lines.[49] A number of α-pyrone analogues, however, revealed promising biological activities as antibacterial agents,[63] HIV-1 protease inhibitors,[64] tyrosinase inhibitors[65] or inhibitors of nitric oxide production,[47] making these metabolites attractive scaffolds for synthetic chemical studies. In our study, bulgarialactone B (**1**) revealed no cytotoxicity against the tested L5178Y cell line, albeit in a previous study it was reported to possess antitumor activity against an ascitic ovarian carcinoma xenograft.[30]

Butyrolactone analogues similar to the derivatives isolated in this study were previously described from *Aspergillus* species,[58,62,66–68] Here we report *B. inquinans* as a source of this type of metabolites for the first time. Moreover, the results obtained upon application of the OSMAC approach employing a mixture of salts ($MgSO_4$, $NaNO_3$ and NaCl) highlighted the usefulness of this strategy not only for diversifying secondary metabolites produced by this strain, but also to afford rare natural product scaffolds, as exemplified by the isolation of 1,3-oxazine derivatives (**7** and **8**) and of an unusual α-pyrone dimer **13**. Another set of OSMAC experiments was performed to investigate which salt mainly contributes to the changes in the metabolic profile of *B. inquinans*, by adding separately $MgSO_4 \cdot 7H_2O$ (2.5 and 3.5 g), and a mixture of $NaNO_3$ and NaCl (2.5 g each) to Czapek medium with and without $MgSO_4$. The fungus failed to grow in the presence of the mixture of $NaNO_3$ and NaCl, when $MgSO_4$ was completely excluded from Czapek medium, suggesting that Mg^{2+} ions are apparently critical for fungal growth. However, the addition of $MgSO_4$ alone did not result in any changes in the HPLC chromatogram in comparison with the chromatogram of the fungus grown on solid Czapek medium, suggesting that the fungus was only metabolically affected by adding the mixture of these three salts simultaneously. Interestingly, OSMAC studies with the marine-derived fungus, *Ascotricha* sp. ZJ-M-5, involving $MgCl_2$ in Czapek Dox broth medium, previously reported that Mg^{2+} ions

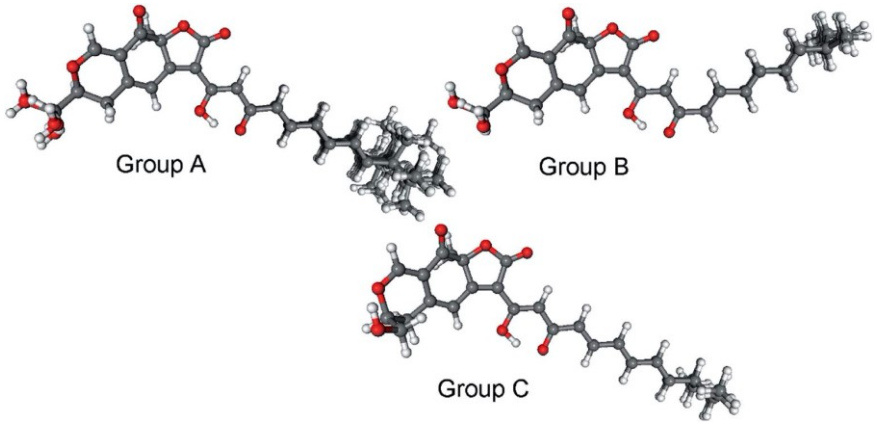

Fig. 7 Classification of the 26 low-energy (≥1%) CAM-B3LYP/TZVP PCM/MeCN conformers of (3*S*,11*S*,23*R*)-**14** into conformer groups. Group A (70.3%) contains conformers A, B, C, D, E, F, H, I, J, L, M, N, Q, R, S, T, U, V, W, Y, Z; group B (5.6%) contains conformers G, K, X; group C (3.2%) contains conformers O and P.

influenced the secondary metabolites profile of this fungus.[69] With respect to the findings in this study, the compounds obtained from the OSMAC experiments in the presence of Mg^{2+} were mostly methoxylated derivatives. Thus, it may be speculated that Mg^{2+} ions under certain conditions might trigger *O*-alkylation reactions.

Experimental section

General procedures

A Jasco P-2000 polarimeter was used to measure the optical rotations. ^{1}H (600 and 300 MHz), ^{13}C (150, 125 and 75 MHz) and 2D NMR spectra were recorded on Bruker AVANCE DMX 600, 500 and 300 NMR spectrometers. The chemical shifts (δ) were referenced to the residual solvent peaks at δ_H 3.31 (MeOH-d_4) ppm for ^{1}H or δ_C 49.0 (MeOH-d_4) ppm for ^{13}C. Mass spectra (ESI) were measured with a Finnigan LCQ Deca mass spectrometer. HRESIMS spectra were recorded with an UHR-QTOF maXis 4G (Bruker Daltonics) mass spectrometer. HPLC analysis was performed with a Dionex UltiMate 3000 with an UltiMate 3000 pump coupled to a photodiode array detector (DAD 3000 RS). Detection wavelengths were set at 235, 254, 280 and 340 nm. The column was prefilled with Eurospher 100–10 C_{18}, 125 × 4 mm (Knauer, Germany). The following gradient was used for routine analysis (MeOH: 0.1% HCOOH in H_2O): 0 min (10% MeOH); 5 min (10% MeOH); 35 min (100% MeOH); 45 min (100% MeOH). Semipreparative HPLC was performed with a Merck Hitachi Chromaster HPLC system (UV detector 5410; pump 5110; column Eurospher 100–10 C_{18}, 300 × 8 mm, Knauer, Germany; flow rate 5 mL min^{-1}). Column chromatography was performed using Silica 60 M (0.040–0.063 mm; Macherey-Nagel, Germany), Silica gel 90 C_{18}-reversed phase and Sephadex LH-20. TLC plates pre-coated with silica gel 60 F_{254} (Macherey-Nagel, Germany) were used for analysis, detection was under UV 254 and 366 nm. ECD spectra were recorded on a JASCO J-810 spectropolarimeter.

Fungal material and fermentation

The fungus *Bulgaria inquinans* (isolate MSp3-1) was isolated from a healthy sprout of mistletoe (*Viscum album*),[70] collected in January 2017 at Jülich, Germany. Fungal identification was carried out according to a standard molecular biology protocol,[70] followed by a BlastN search in the NCBI database. The sequence was submitted to the GenBank (accession no. MK246763). The fungal strain is kept in one of the author's laboratory (P. P.).

The fungus was cultivated on solid Czapek medium, which was prepared by autoclaving 200 mL of liquid Czapek medium with the addition of 5.0 g of bacto agar in a 1 L Erlenmeyer flask. The composition of liquid Czapek medium was 10.0 g dextrose, 20.0 g mannitol, 20.0 g maltose, 3.0 g yeast extract, 1.0 g corn steep liquor, 0.5 g tryptophan, 0.5 g $K_2HPO_4 \cdot 3H_2O$, 0.3 g $MgSO_4 \cdot 7H_2O$ and 1 L of distilled water (pH value of the medium adjusted between 7.2–7.8). The fermentation was performed in 15 flasks at room temperature, under static conditions for 27 days.

OSMAC experiments were carried out by growing the fungus on solid Czapek medium containing either 3.5 g NaCl, 3.5 g NaBr, 3.5 g NaI, 3.5 g $NaNO_3$, 3.5 g $(NH_4)_2SO_4$ or mixtures of (a) $MgSO_4 \cdot 7H_2O$, $NaNO_3$ and NaCl (2.5 g of each), (b) $FeSO_4 \cdot 7H_2O$, $NaNO_3$ and NaCl (2.5 g of each), or (c) $ZnSO_4 \cdot 7H_2O$, $NaNO_3$ and NaCl (2.5 g of each), added to each 1 L flask followed by extraction when the flasks were completely overgrown by the fungus. Based on the chromatographic profiles obtained from these experiments, a large-scale fermentation of *B. inquinans* was carried out by adding a mixture of $MgSO_4 \cdot 7H_2O$, $NaNO_3$ and NaCl (2.5 g of each) to solid Czapek medium. The fungus was grown under static conditions for 33 days followed by extraction.

Extraction and isolation

The fungal culture grown on solid Czapek medium was extracted with 500 mL EtOAc added to each flask followed by

concentration *in vacuo* to afford the crude extract (5.1 g). The extract was then loaded on silica gel 60 (VLC) and eluted successively with *n*-hexane–EtOAc followed by CH_2Cl_2–MeOH to obtain 13 fractions (V1–V13). Fractions V3, V4 and V5 eluted with *n*-hexane–EtOAc (6 : 4), (4 : 6) and (2 : 8), respectively, were subjected to further separation based on their HPLC chromatograms. Fraction V5 (1.7 g) was separated over Sephadex LH-20 and eluted with MeOH to afford nine subfractions (V5.1–V5.9). Purification of the V5.3 subfraction (65.9 mg) was achieved by semipreparative HPLC using ACN–H_2O (from 65% to 100% ACN, 20 min), to yield bulgarialactone B (**14**, 27.0 mg). Fraction V4 (507.9 mg) was submitted to Sephadex LH-20, employing CH_2Cl_2–MeOH (1 : 1) as the mobile phase to obtain 12 subfractions (V4.1–V4.12). Semipreparative HPLC was used to purify the subfraction V4.10 (270.0 mg), using MeOH-0.1% HCOOH in H_2O (from 30% to 100% MeOH, 25 min), to afford the new compounds **1** (20.0 mg) and **4** (2.2 mg) along with phenylbutyrolactone IIa (**15**, 124.0 mg). In a similar manner, the separation of fraction V3 (150 mg) on Sephadex LH-20 resulted in 10 subfractions (V3.1–V3.10). Purification by semipreparative HPLC of the V3.6 subfraction (26.0 mg), employing MeOH-0.1% HCOOH in H_2O as the eluent (from 65% to 100% MeOH, 20 min), yielded the new natural products **2** (2.8 mg), **3** (1.5 mg) and **5** (1.9 mg) together with xenofuranone B (**17**, 1.2 mg).

The fungal culture obtained from the large-scale fermentation on the Czapek medium with the salt mixture was extracted with 500 mL EtOAc added to each flask. Following the previously described procedure, the crude extract (7.7 g) obtained after removal of the solvent was chromatographed on Silica gel 60 (VLC) to afford 13 fractions (MV1–MV13). Fractions MV3, MV4, MV6 and MV9 eluted with *n*-hexane–EtOAc (6 : 4), (4 : 6), 100% EtOAc and DCM–MeOH (1 : 9), respectively, were selected for further isolation work-up, guided by their HPLC results. The separation of fraction MV9 (1.5 g) was carried out on a Silica gel 90 C_{18}-reversed phase column by a step gradient elution employing mixtures of H_2O–MeOH to yield 10 subfractions (MV9.1–MV9.10). The MV9.7 subfraction (95.1 mg) was submitted to Sephadex LH-20 using CH_2Cl_2–MeOH (1 : 1) as the eluent to yield seven subfractions (MV9.7.1–MV9.7.7). Purification of the MV9.7.2 subfraction (24.5 mg) was achieved by semipreparative HPLC using MeOH-0.1% HCOOH in H_2O (from 65% to 100% MeOH, 20 min) to afford **13** (9.3 mg). The new compound **12** (30.4 mg) was afforded by the purification of MV9.7.5 (64.7 mg) with semipreparative HPLC using MeOH-0.1% HCOOH in H_2O (from 40% to 100% MeOH, 20 min). The new compound **8** (1.5 mg) was obtained by the separation of the MV9.1 subfraction (40.0 mg) on Sephadex LH-20, and final purification was achieved by semipreparative HPLC using MeOH-0.1% HCOOH in H_2O (from 25% to 100% MeOH, 20 min). Fraction MV6 (452.5 mg) was applied on Sephadex LH-20 employing MeOH as the eluent to yield nine subfractions (MV6.1–MV6.9). Purification of the MV6.6 subfraction (21.0 mg) was carried out by semipreparative HPLC using ACN–H_2O (from 60% to 100% ACN, 25 min) to afford bulgarialactone D (**18**, 4.0 mg). The new compounds **9** (2.6 mg), **10** (9.1 mg) and **11** (2.6 mg) were obtained from purification of MV6.3 subfraction (59.3 mg) by semipreparative HPLC using MeOH-0.1% HCOOH in H_2O (from 55% to 100% MeOH, 20 min). Furthermore, fraction MV4 (622.4 mg) was chromatographed on Sephadex LH-20, eluting with CH_2Cl_2–MeOH (1 : 1), to give eight subfractions (MV4.1–MV4.8). The MV4.6 subfraction (54.4 mg) was then purified by semipreparative HPLC using MeOH-0.1% HCOOH in H_2O (from 40% to 100% MeOH, 25 min), which yielded **3** (14.6 mg) and **6** (3.2 mg) along with **16** (6.5 mg). Application of the latter procedure for the purification of fraction MV3 (164.9 mg) by semipreparative HPLC following separation on Sephadex LH-20 yielded compounds **5** (2.8 mg) and **7** (2.0 mg). The total amounts of **3** and **5**, both from the fungal culture grown on solid Czapek medium and from the OSMAC experiment, were 16.1 and 4.7 mg, respectively.

Bulgariline A (**1**): yellow solid; $[\alpha]_D^{20}$ +16 (*c* 0.20, MeOH); UV (MeOH, PDA): λ_{max} 288, 218 nm; ECD (MeCN, λ [nm] ($\Delta\varepsilon$), *c* 0.529 mM): 294sh (+0.56), 282 (+0.71), 254 (−0.44), 232 (+1.05), 221 (−0.74), 205sh (+2.42); ^{1}H and ^{13}C NMR data, see Table 1; HRESIMS *m*/*z* 235.0600 $[M + H]^+$ (calcd for $C_{12}H_{11}O_5$, 235.0601).

Bulgariline B (**2**): yellow solid; $[\alpha]_D^{20}$ 0 (*c* 0.20, MeOH); UV (MeOH, PDA): λ_{max} 291, 204 nm; ^{1}H and ^{13}C NMR data, see Table 1; HRESIMS *m*/*z* 283.0962 $[M + H]^+$ (calcd for $C_{17}H_{15}O_4$, 283.0965).

Bulgariline C (**3**): yellow solid; $[\alpha]_D^{20}$ 0 (*c* 0.20, MeOH); UV (MeOH, PDA): λ_{max} 293, 201 nm; ^{1}H and ^{13}C NMR data, see Table 1; HRESIMS *m*/*z* 297.1123 $[M + H]^+$ (calcd for $C_{18}H_{17}O_4$, 297.1121).

Bulgariol (**4**): yellow, solid; $[\alpha]_D^{20}$ −25 (*c* 0.20, MeOH); UV (MeOH, PDA): λ_{max} 277 nm; ECD (MeCN, λ [nm] ($\Delta\varepsilon$), *c* 0.409 mM): 280 (−0.19), 245sh (+0.10), 225 (+0.95), 201sh (+1.52), 195 (+2.55); ^{1}H and ^{13}C NMR data, see Table 2; HRESIMS *m*/*z* 267.0989 $[M + Na]^+$ (calcd for $C_{15}H_{16}NaO_3$, 267.0992).

(5*Z*)-3-Hydroxy-4-phenyl-5-(phenylmethylene)-2(5*H*)-furanone (**5**): yellow solid; UV (MeOH, PDA): λ_{max} 336, 263, 245 nm; ^{1}H and ^{13}C NMR data, see Table 1; HRESIMS *m*/*z* 265.0861 $[M + H]^+$ (calcd for $C_{17}H_{13}O_3$, 265.0859).

Bulgariline D (**6**): yellow solid; $[\alpha]_D^{25}$ +26 (*c* 0.20, MeOH); UV (MeOH, PDA): λ_{max} 287, 217 nm; ECD (MeCN, λ [nm] ($\Delta\varepsilon$), *c* 0.201 mM): 296sh (+2.70), 281 (+3.94), 253sh (−0.95), 249 (−1.18), 231 (+2.99), 221 (−3.22), 218sh (−2.90), 204sh (+7.03); ^{1}H and ^{13}C NMR data, see Table 1; HRESIMS *m*/*z* 249.0757 $[M + H]^+$ (calcd for $C_{13}H_{13}O_5$, 249.0757).

Bulgarixine A (**7**): yellow solid; $[\alpha]_D^{25}$ 0 (*c* 0.11, MeOH); UV (MeOH, PDA): λ_{max} 243, 206 nm; ^{1}H and ^{13}C NMR data, see Table 3; HRESIMS *m*/*z* 248.0919 $[M + H]^+$ (calcd for $C_{13}H_{14}NO_4$, 248.0917).

Bulgarixine B (**8**): yellow solid; $[\alpha]_D^{25}$ 0 (*c* 0.20, MeOH); UV (MeOH, PDA): λ_{max} 244, 206 nm; ^{1}H and ^{13}C NMR data, see Table 3; HRESIMS *m*/*z* 234.0760 $[M + H]^+$ (calcd for $C_{12}H_{12}NO_4$, 234.0761).

Bulgariapyrone A (**9**): brown solid; $[\alpha]_D^{25}$ −48 (*c* 0.20, MeOH); UV (MeOH, PDA): λ_{max} 300, 206 nm; ^{1}H and ^{13}C NMR data, see Table 4; HRESIMS *m*/*z* 313.2013 $[M + H]^+$ (calcd for $C_{17}H_{29}O_5$, 313.2010).

Bulgariapyrone B (**10**): brown solid; $[\alpha]_D^{25}$ −72 (*c* 0.40, MeOH); UV (MeOH, PDA): λ_{max} 299, 211 nm; ^{1}H and ^{13}C NMR data, see Table 4; HRESIMS *m*/*z* 357.1919 $[M + H]^+$ (calcd for $C_{18}H_{29}O_7$, 357.1908).

Bulgariapyrone C (**11**): brown solid; $[\alpha]_D^{25}$ −70 (*c* 0.20, MeOH); UV (MeOH, PDA): λ_{max} 300, 206 nm; ^{1}H and ^{13}C NMR data, see Table 4; HRESIMS *m*/*z* 371.2070 $[M + H]^+$ (calcd for $C_{19}H_{31}O_7$, 371.2064).

Bulgariapyrone D (**12**): brown solid; $[\alpha]_D^{25}$ −90 (*c* 0.20, MeOH); UV (MeOH, PDA): λ_{max} 298, 212 nm; ^{1}H and ^{13}C NMR data, see Table 4; HRESIMS *m*/*z* 329.1960 $[M + H]^+$ (calcd for $C_{17}H_{29}O_6$, 329.1959).

Bulgariapyrone E (**13**): brown solid; $[\alpha]_D^{25}$ −32 (*c* 0.20, MeOH); UV (MeOH, PDA): λ_{max} 299, 208 nm; ^{1}H and ^{13}C NMR data, see Table 4; HRESIMS *m*/*z* 625.3587 $[M + H]^+$ (calcd for $C_{33}H_{53}O_{11}$, 625.3582).

Bulgarialactone B (**14**): dark red solid; $[\alpha]_D^{20}$ +344 (*c* 0.10, $CHCl_3$); UV (MeOH, PDA): λ_{max} 441, 322 nm; ECD (MeCN, λ [nm] ($\Delta\varepsilon$), *c* 0.147 mM): 470sh (+14.51), 437 (+22.20), 417sh (+18.22), 352sh (−2.59), 323sh (−14.77), 315 (−15.84), 269 (+5.71), 232 (−12.87); HRESIMS *m*/*z* 453.1910 $[M + H]^+$ (calcd for $C_{26}H_{29}O_7$, 453.1908).

(−)-(*S*)-Flavipesin B (**16**): yellow solid; $[\alpha]_D^{25}$ −72 (*c* 0.20, MeOH); UV (MeOH, PDA): λ_{max} 290, 204 nm; ^{1}H and ^{13}C NMR data, see ESI;† HRESIMS *m*/*z* 325.1073 $[M + H]^+$ (calcd for $C_{19}H_{17}O_5$, 325.1071).

Mosher ester analysis of 12 and 13

Both (*S*)- and (*R*)-MTPA esters of **12** were prepared in NMR tubes by the addition of either (*R*)-MTPA-Cl (10 μL, 53.44 μmol) or (*S*)-MTPA-Cl (10 μL, 53.44 μmol) to a solution of **12** (1.0 mg, 3.05 μmol) and pyridine-d_5 (10 μL, 130.75 μmol) in 100 μL $CDCl_3$, according to a protocol described earlier.[71] Each reaction mixture was maintained for 3 h at room temperature, and 500 μL $CDCl_3$ was added afterwards. In a similar manner, (*S*)- and (*R*)-MTPA esters of **13** were prepared. Ester products were confirmed by LC-ESIMS at *m*/*z* 761 $[M + H]^+$ for **12** and by MALDI-MS at *m*/*z* 1295 $[M + Na]^+$ for **13**.

(*S*)-MTPA ester of **12** (**12a**): ^{1}H NMR ($CDCl_3$, 600 MHz) δ_H 6.19 (1H, s, H-5), 5.63 (1H, dd, J = 7.5, 5.3 Hz, H-1′), 4.30 (1H, m, Hb-9′), 4.29 (2H, s, H_2-1″), 4.26 (1H, m, Ha-9′), 3.80 (3H, s, 4-OMe), 3.52 (3H, s, OMe), 3.48 (3H, s, OMe), 3.36 (3H, s, 1″-OMe), 1.88 (2H, m, H_2-2′), 1.64 (2H, p, J = 6.8 Hz, H_2-8′), 1.19 (2H, m, H_2-3′), 1.25 (2H, m, H_2-7′), 1.13–1.25 (6H, m, H_2-4′–H_2-6′).

(*R*)-MTPA ester of **12** (**12b**): ^{1}H NMR ($CDCl_3$, 600 MHz) δ_H 5.99 (1H, s, H-5), 5.69 (1H, dd, J = 7.3, 5.0 Hz, H-1′), 4.31 (1H, m, Hb-9′), 4.27 (2H, s, H_2-1″), 4.27 (1H, m, Ha-9′), 3.68 (3H, s, 4-OMe), 3.54 (3H, s, OMe), 3.52 (3H, s, OMe), 3.35 (3H, s, 1″-OMe), 1.91 (2H, m, H_2-2′), 1.65 (2H, p, J = 6.8 Hz, H_2-8′), 1.26 (2H, m, H_2-3′) 1.25 (2H, m, H_2-7′) 1.17–1.30 (6H, m, H_2-4′–H_2-6′).

(*S*)-MTPA ester of **13** (**13a**): ^{1}H NMR ($CDCl_3$, 600 MHz) δ_H 6.20 (1H, s, H-5/H-5‴), 6.18 (1H, s, H-5‴/H-5), 5.63 (2H, m, H-1′, H-1⁗), 4.31 (2H, s, H_2-1⁗), 4.31 (1H, m, Hb-9⁗) 4.30 (2H, s, H_2-1″), 4.27 (1H, m, Ha-9⁗) 3.82 (3H, s, 4-OMe/4‴-OMe), 3.80 (3H, s, 4‴-OMe/4-OMe), 3.53 (3H, s, OMe), 3.49 (6H, s, OMe), 3.47 (2H, t, J = 6.8 Hz, H_2-9′), 3.37 (3H, s, 1″-OMe), 1.90 (4H, m, H_2-2′, H_2-2⁗), 1.65 (2H, p, J = 6.7 Hz, H_2-8′/H_2-8⁗), 1.54 (2H, p, J = 6.7 Hz, H_2-8⁗/H_2-8′), 1.27 (4H, m, H_2-7′, H_2-7⁗), 1.21 (4H, m, H_2-3′, H_2-3⁗), 1.16–1.25 (12H, m, H_2-4′–H_2-6′, H_2-4⁗–H_2-6⁗).

(*R*)-MTPA ester of **13** (**13b**): ^{1}H NMR ($CDCl_3$, 600 MHz) δ_H 5.99 (2H, s, H-5, H-5‴), 5.68 (2H, m, H-1′, H-1⁗), 4.31 (1H, m, Hb-9⁗), 4.30 (2H, s, H_2-1″), 4.27 (1H, m, Ha-9⁗), 4.28 (2H, s, H_2-1⁗), 3.68 (3H, s, 4-OMe/4‴-OMe), 3.67 (3H, s, 4‴-OMe/4-OMe), 3.54 (6H, s, OMe), 3.53 (3H, s, OMe), 3.45 (2H, t, J = 6.8 Hz, H_2-9′), 3.36 (3H, s, 1″-OMe), 1.91 (4H, m, H_2-2′, H_2-2⁗), 1.66 (2H, p, J = 6.7 Hz, H_2-8′/H_2-8⁗), 1.54 (2H, p, J = 6.7 Hz, H_2-8⁗/H_2-8′), 1.29 (4H, m, H_2-3′, H_2-3⁗), 1.27 (4H, m, H_2-7′, H_2-7⁗), 1.16–1.25 (12H, m, H_2-4′–H_2-6′, H_2-4⁗–H_2-6⁗).

Cytotoxicity assay

Cytotoxicity was assayed against the murine lymphoma cell line L5178Y, using the MTT method.[62] Kahalalide F was used as a positive control and a medium containing 0.1% DMSO was included as a negative control.

Computational section

Mixed torsional/low-mode conformational searches were carried out by using the Macromodel 10.8.011 software[72] with the Merck Molecular Morce Field (MMFF) with an implicit solvent model for $CHCl_3$ applying a 21 kJ mol^{-1} energy window. Geometry optimizations [B3LYP/6-31+G(d,p) *in vacuo* and CAM-B3LYP/TZVP[73] with the PCM solvent model for MeCN] and TDDFT [B3LYP/TZVP, BH&HLYP/TZVP, CAM-B3LYP/TZVP and PBE0/TZVP with the same or no solvent model as in the preceding optimization step] calculations were performed with Gaussian 09.[74] The ECD spectra were generated as the sum of the Gaussians with 3000 and 4200 cm^{-1} half-height widths using dipole-velocity-computed rotational strength values.[75] Boltzmann distributions were estimated from the B3LYP and the CAM-B3LYP energies. The MOLEKEL software package was used for visualization of the results.[76]

Conflicts of interest

There are no conflicts to declare.

Acknowledgements

N. P. A. wishes to thank DAAD Program Biodiversity and Health for the doctoral scholarship. P. P. wants to thank the Manchot Foundation for support. We further want to thank Dr Margareta Proksch for help during mistletoe collection. The research of the Hungarian authors was supported by the EU and cofinanced by the European Regional Development Fund under the project GINOP-2.3.2-15-2016-00008. We also thank the National Research, Development and Innovation Office (NKFI K120181 and PD121020). The Governmental Information-Technology Development Agency (KIFÜ) is acknowledged for CPU time.

Notes and references

1 A. L. Demain, *J. Ind. Microbiol. Biotechnol.*, 2014, **41**, 185–201.
2 C. R. Strader, C. J. Pearce and N. H. Oberlies, *J. Nat. Prod.*, 2011, **74**, 900–907.

3 G. M. Cragg and D. J. Newman, *Biochim. Biophys. Acta*, 2013, **1830**, 3670–3695.
4 G. A. Strobel, *Crit. Rev. Biotechnol.*, 2002, **22**, 315–333.
5 G. A. Strobel, R. V. Miller, C. Martinez-Miller, M. M. Condron, D. B. Teplow and W. Hess, *Microbiology*, 1999, **145**, 1919–1926.
6 J. Li, G. Strobel, J. Harper, E. Lobkovsky and J. Clardy, *Org. Lett.*, 2000, **2**, 767–770.
7 J. G. Ondeyka, G. L. Helms, O. D. Hensens, M. A. Goetz, D. L. Zink, A. Tsipouras, W. L. Shoop, L. Slayton, A. W. Dombrowski, J. D. Polishook, D. A. Ostlind, N. N. Tsou, R. G. Ball and S. B. Singh, *J. Am. Chem. Soc.*, 1997, **119**, 8809–8816.
8 D. Rönsberg, A. Debbab, A. Mándi, V. Vasylyeva, P. Böhler, B. Stork, L. Engelke, A. Hamacher, R. Sawadogo, M. Diederich, V. Wray, W. Lin, M. U. Kassack, C. Janiak, S. Scheu, S. Wesselborg, T. Kurtán, A. H. Aly and P. Proksch, *J. Org. Chem.*, 2013, **78**, 12409–12425.
9 P. Böhler, F. Stuhldreier, R. Anand, A. K. Kondadi, D. Schlütermann, N. Berleth, J. Deitersen, N. Wallot-Hieke, W. Wu, M. Frank, H. Niemann, E. Wesbuer, A. Barbian, T. Luyten, J. B. Parys, S. Weidtkamp-Peters, A. Borchardt, A. S. Reichert, A. Peña-Blanco, A. J. García-Sáez, S. Itskanov, A. M. van der Bliek, P. Proksch, S. Wesselborg and B. Stork, *Cell Death Dis.*, 2018, **9**, 286.
10 J. C. Lee, E. Lobkovsky, N. B. Pliam, G. Strobel and J. Clardy, *J. Org. Chem.*, 1995, **60**, 7076–7077.
11 A. Stierle, G. Strobel and D. Stierle, *Science*, 1993, **260**, 214–216.
12 S. C. Puri, V. Verma, T. Amna, G. N. Qazi and M. Spiteller, *J. Nat. Prod.*, 2005, **68**, 1717–1719.
13 K. Ishiuchi, D. Hirose, T. Suzuki, W. Nakayama, W.-P. Jiang, O. Monthakantirat, J.-B. Wu, S. Kitanaka and T. Makino, *J. Nat. Prod.*, 2018, **81**, 1143–1147.
14 A. H. Aly, A. Debbab and P. Proksch, *Appl. Microbiol. Biotechnol.*, 2011, **90**, 1829–1845.
15 A. H. Aly, A. Debbab and P. Proksch, *Pharmazie*, 2013, **68**, 499–505.
16 K. Scherlach and C. Hertweck, *Org. Biomol. Chem.*, 2009, **7**, 1753–1760.
17 G. Daletos, W. Ebrahim, E. Ancheeva, M. El-Neketi, W. Lin and P. Proksch, in *Chemical Biology of Natural Products; Microbial Co-culture and OSMAC Approach as Strategies to Induce Cryptic Fungal Biogenetic Gene Clusters*, ed. P. Grothaus, G. M. Cragg and D. J. Newman, CRC Press, Boca Raton, FL, USA, 2017, pp. 233–284.
18 H. B. Bode, B. Bethe, R. Höfs and A. Zeeck, *ChemBioChem*, 2002, **3**, 619–627.
19 S. Kusari, C. Hertweck and M. Spiteller, *Chem. Biol.*, 2012, **19**, 792–798.
20 P. A. Paranagama, E. M. K. Wijeratne and A. A. L. Gunatilaka, *J. Nat. Prod.*, 2007, **70**, 1939–1945.
21 S. P. D. Senadeera, S. Wiyakrutta, C. Mahidol, S. Ruchirawat and P. Kittakoop, *Org. Biomol. Chem.*, 2012, **10**, 7220–7226.
22 R. T. Hewage, T. Aree, C. Mahidol, S. Ruchirawat and P. Kittakoop, *Phytochemistry*, 2014, **108**, 87–94.
23 L. Hammerschmidt, A. H. Aly, M. Abdel-Aziz, W. E. G. Müller, W. Lin, G. Daletos and P. Proksch, *Bioorg. Med. Chem.*, 2015, **23**, 712–719.
24 H. Wang, H. Dai, C. Heering, C. Janiak, W. Lin, R. S. Orfali, W. E. G. Müller, Z. Liu and P. Proksch, *RSC Adv.*, 2016, **6**, 81685–81693.
25 H. Yamazaki, H. Rotinsulu, R. Narita, R. Takahashi and M. Namikoshi, *J. Nat. Prod.*, 2015, **78**, 2319–2321.
26 S. Sureram, C. Kesornpun, C. Mahidol, S. Ruchirawat and P. Kittakoop, *RSC Adv.*, 2013, **3**, 1781–1788.
27 B. Wu, X. Wu, M. Sun and M. Li, *Mar. Drugs*, 2013, **11**, 2713–2721.
28 P. Ye, L. Shen, W. Jiang, Y. Ye, C.-T. A. Chen, X. Wu, K. Wang and B. Wu, *Mar. Drugs*, 2014, **12**, 3203–3217.
29 M. Stadler, H. Anke, K. Dekermendjian, R. Reiss, O. Sterner and R. Witt, *Nat. Prod. Lett.*, 1995, **7**, 7–14.
30 L. Musso, S. Dallavalle, L. Merlini, A. Bava, G. Nasini, S. Penco, G. Giannini, C. Giommarelli, A. De Cesare, V. Zuco, L. Vesci, C. Pisano, F. Dal Piaz, N. De Tommasi and F. Zunino, *Bioorg. Med. Chem.*, 2010, **18**, 6031–6043.
31 R. L. Edwards and H. J. Lockett, *J. Chem. Soc., Perkin Trans. 1*, 1976, 2149–2155.
32 N. Li, J. Xu, X. Li and P. Zhang, *Fitoterapia*, 2013, **84**, 85–88.
33 J. W. van Dijk, C.-J. Guo and C. C. C. Wang, *Org. Lett.*, 2016, **18**, 6236–6239.
34 E. Hühner, K. Öqvist and S.-M. Li, *Org. Lett.*, 2019, **21**, 498–502.
35 A. O. Brachmann, S. Forst, G. M. Furgani, A. Fodor and H. B. Bode, *J. Nat. Prod.*, 2006, **69**, 1830–1832.
36 E. Ancheeva, L. Küppers, S. H. Akone, W. Ebrahim, Z. Liu, A. Mándi, T. Kurtán, W. Lin, R. Orfali, N. Rehberg, R. Kalscheuer, G. Daletos and P. Proksch, *Eur. J. Org. Chem.*, 2017, **2017**, 3256–3264.
37 N. Tabata, T. Sunazuka, H. Tomoda, T. Nagamitsu, Y. Iwai and S. Omura, *J. Antibiot.*, 1993, **46**, 762–769.
38 Z. Lin, L. Marett, R. W. Hughen, M. Flores, I. Forteza, M. A. Ammon, G. P. Concepcion, S. Espino, B. M. Olivera, G. Rosenberg, M. G. Haygood, A. R. Light and E. W. Schmidt, *Bioorg. Med. Chem. Lett.*, 2013, **23**, 4867–4869.
39 A. N. Pearce, E. W. Chia, M. V. Berridge, E. W. Maas, M. J. Page, V. L. Webb, J. L. Harper and B. R. Copp, *J. Nat. Prod.*, 2007, **70**, 111–113.
40 J. Sikorska, S. Parker-Nance, M. T. Davies-Coleman, O. B. Vining, A. E. Sikora and K. L. McPhail, *J. Nat. Prod.*, 2012, **75**, 1824–1827.
41 Scifinder®, Chemical Abstracts Service, Columbus, OH, 2019, RN 73764-04-2 (accessed March 23, 2019).
42 Z. Lin, M. Koch, M. H. Abdel Aziz, R. Galindo-Murillo, M. D. Tianero, T. E. Cheatham, L. R. Barrows, C. A. Reilly and E. W. Schmidt, *Org. Lett.*, 2014, **16**, 4774–4777.
43 M. C. Kim, J. H. Lee, B. Shin, L. Subedi, J. W. Cha, J.-S. Park, D.-C. Oh, S. Y. Kim and H. C. Kwon, *Org. Lett.*, 2015, **17**, 5024–5027.
44 P. Fu, S. La and J. B. MacMillan, *J. Nat. Prod.*, 2015, **79**, 455–462.

45 A. N. Cayley, K. A. Gallagher, C. Menard-Moyon, J. P. Schmidt, L. J. Diorazio and R. J. Taylor, *Synthesis*, 2008, **2008**, 3846–3856.
46 Y. Zhou, Y. Zhai, X. Ji, G. Liu, E. Feng, D. Ye, L. Zhao, H. Jiang and H. Liu, *Adv. Synth. Catal.*, 2010, **352**, 373–378.
47 G. S. Kim, W. Ko, J. W. Kim, M.-H. Jeong, S.-K. Ko, J.-S. Hur, H. Oh, J.-H. Jang and J. S. Ahn, *J. Nat. Prod.*, 2018, **81**, 1084–1088.
48 D. R. McMullin, T. K. Nsiama and J. D. Miller, *J. Nat. Prod.*, 2014, 77, 206–212.
49 P. Chomcheon, S. Wiyakrutta, N. Sriubolmas, N. Ngamrojanavanich, C. Mahidol, S. Ruchirawat and P. Kittakoop, *Phytochemistry*, 2009, **70**, 121–127.
50 H. Fujimoto, Y. Satoh, M. Nakayama, T. Takayama and M. Yamazaki, *Chem. Pharm. Bull.*, 1995, **43**, 547–552.
51 Y. I. Oh, N. A. Kim, Y. H. Kim, T. H. Lee and Y. S. Lee, *Saengyak Hakhoechi*, 2013, **44**, 209–219.
52 P. J. L. Bell and P. Karuso, *J. Am. Chem. Soc.*, 2003, **125**, 9304–9305.
53 S. Superchi, P. Scafato, M. Gorecki and G. Pescitelli, *Curr. Med. Chem.*, 2018, **25**, 287–320.
54 A. Mandi, I. W. Mudianta, T. Kurtan and M. J. Garson, *J. Nat. Prod.*, 2015, **78**, 2051–2056.
55 O. A. Syzgantseva, V. Tognetti, L. Joubert, A. Boulangé, P. A. Peixoto, S. Leleu and X. Franck, *J. Phys. Chem. A*, 2012, **116**, 8634–8643.
56 W. Ebrahim, A. H. Aly, A. Mándi, F. Totzke, M. H. Kubbutat, V. Wray, W. H. Lin, H. Dai, P. Proksch, T. Kurtán and A. Debbab, *Eur. J. Org. Chem.*, 2012, **2012**, 3476–3484.
57 Scifinder®, Chemical Abstracts Service, Columbus, OH, 2019, RN 371163-96-1 (accessed March 23, 2019).
58 Z.-Q. Bai, X. Lin, Y. Wang, J. Wang, X. Zhou, B. Yang, J. Liu, X. Yang, Y. Wang and Y. Liu, *Fitoterapia*, 2014, **95**, 194–202.
59 H. Morishima, K. Fujita, M. Nakano, S. Atsumi, M. Ookubo, M. Kitagawa, H. Matsumoto, A. Okuyama and T. Okabe, Japanese Kokai Tokkyo Koho JP, 1994, 6100445.
60 K. Nitta, N. Fujita, T. Yoshimura, K. Arai and Y. Yamamoto, *Chem. Pharm. Bull.*, 1983, **31**, 1528–1533.
61 J. W. van Dijk and C. C. C. Wang, *Org. Lett.*, 2018, **20**, 5082–5085.
62 H. Chen, G. Daletos, M. S. Abdel-Aziz, D. Thomy, H. Dai, H. Brötz-Oesterhelt, W. Lin and P. Proksch, *Phytochem. Lett.*, 2015, **12**, 35–41.
63 M. P. Singh, F. Kong, J. E. Janso, D. A. Arias, P. A. Suarez, V. S. Bernan, P. J. Petersen, W. J. Weiss, G. Carter and M. Greenstein, *J. Antibiot.*, 2003, **56**, 1033–1044.
64 C.-L. Sun, R.-F. Pang, H. Zhang and M. Yang, *Bioorg. Med. Chem. Lett.*, 2005, **15**, 3257–3262.
65 D. Zhang, X. Li, J.-S. Kang, H.-D. Choi and B.-W. Son, *Bull. Korean Chem. Soc.*, 2007, **28**, 887–888.
66 R. R. Parvatkar, C. D'Souza, A. Tripathi and C. G. Naik, *Phytochemistry*, 2009, **70**, 128–132.
67 K. Zhou, L. Zhu, X. Wang, T. Zhang, Y. Wang, W. Dong, B. Ji, H. Yang, G. Du, Q. Hu and M. Zhou, *Chem. Nat. Compd.*, 2016, **52**, 591–594.
68 X. Pang, J.-Y. Zhao, X.-M. Fang, T. Zhang, D.-W. Zhang, H.-Y. Liu, J. Su, S. Cen and L.-Y. Yu, *J. Nat. Prod.*, 2017, **80**, 2595–2601.
69 W.-J. Wang, D.-Y. Li, Y.-C. Li, H.-M. Hua, E.-L. Ma and Z.-L. Li, *J. Nat. Prod.*, 2014, 77, 1367–1371.
70 J. Kjer, A. Debbab, A. H. Aly and P. Proksch, *Nat. Protoc.*, 2010, **5**, 479.
71 T. R. Hoye, C. S. Jeffrey and F. Shao, *Nat. Protoc.*, 2007, **2**, 2451.
72 Macromodel, Schrödinger, LLC, 2015, http://www.schrodinger.com/MacroModel.
73 T. Yanai, D. P. Tew and N. C. Handy, *Chem. Phys. Lett.*, 2004, **393**, 51–57.
74 M. J. Frisch, G. W. Trucks, H. B. Schlegel, G. E. Scuseria, M. A. Robb, J. R. Cheeseman, G. Scalmani, V. Barone, B. Mennucci, G. A. Petersson, H. Nakatsuji, M. Caricato, X. Li, H. P. Hratchian, A. F. Izmaylov, J. Bloino, G. Zheng, J. L. Sonnenberg, M. Hada, M. Ehara, K. Toyota, R. Fukuda, J. Hasegawa, M. Ishida, T. Nakajima, Y. Honda, O. Kitao, H. Nakai, T. Vreven, J. A. Montgomery Jr., J. E. Peralta, F. Ogliaro, M. Bearpark, J. J. Heyd, E. Brothers, K. N. Kudin, V. N. Staroverov, R. Kobayashi, J. Normand, K. Raghavachari, A. Rendell, J. C. Burant, S. S. Iyengar, J. Tomasi, M. Cossi, N. Rega, J. M. Millam, M. Klene, J. E. Knox, J. B. Cross, V. Bakken, C. Adamo, J. Jaramillo, R. Gomperts, R. E. Stratmann, O. Yazyev, A. J. Austin, R. Cammi, C. Pomelli, J. W. Ochterski, R. L. Martin, K. Morokuma, V. G. Zakrzewski, G. A. Voth, P. Salvador, J. J. Dannenberg, S. Dapprich, A. D. Daniels, Ö. Farkas, J. B. Foresman, J. V. Ortiz, J. Cioslowski, D. J. Fox, *Gaussian 09, Revision E.01*, Gaussian, Inc., Wallingford, CT, 2013.
75 P. J. Stephens and N. Harada, *Chirality*, 2010, **22**, 229–233.
76 U. Varetto, *MOLEKEL, v. 5.4*, Swiss National Supercomputing Centre, Manno, Switzerland, 2009.

Supporting Information

Expanding the chemical diversity of an endophytic fungus *Bulgaria inquinans*, an ascomycete associated with mistletoe, through an OSMAC approach

Ni P. Ariantari,[ab] Georgios Daletos,[a] Attila Mándi,[c] Tibor Kurtán,[c] Werner E. G. Müller,[d] Wenhan Lin,[e] Elena Ancheeva,*[a] Peter Proksch*[a]

[a]Institute of Pharmaceutical Biology and Biotechnology, Heinrich Heine University Düsseldorf, Universitätsstrasse 1, 40225 Düsseldorf, Germany

[b]Department of Pharmacy, Faculty of Mathematic and Natural Sciences, Udayana University, 80361 Bali, Indonesia

[c]Department of Organic Chemistry, University of Debrecen, P.O.B. 400, 4002 Debrecen, Hungary

[d]Institute of Physiological Chemistry, Universitätsmedizin der Johannes Gutenberg-Universität Mainz, Duesbergweg 6, 55128 Mainz, Germany

[e]State Key Laboratory of Natural and Biomimetic Drugs, Peking University, 100191 Beijing, China

*Corresponding author

Table of Contents

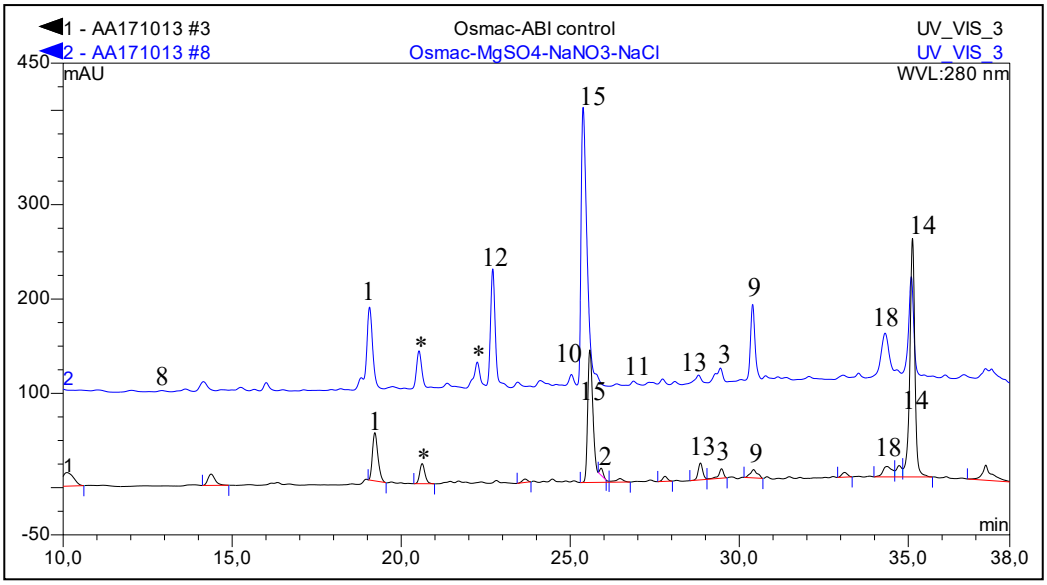

Figure S1. HPLC chromatograms of EtOAc extract of *B. inquinans* (isolate MSp3-1) cultured on solid Czapek medium (black) compared to the OSMAC culture on solid Czapek medium with addition of a mixture of $MgSO_4$, $NaNO_3$ and NaCl (blue) under UV detection at 280 nm. *: unidentified peaks

Compounds **4**, **5**, **6**, **7**, **16** and xenofuranone B (**17**) were not detected neither in the HPLC analysis of the crude extract of *B. inquinans* (isolate MSp3-1) cultured on solid Czapek medium, nor in the HPLC analysis of the crude extract of the fungal culture with addition of a mixture of $MgSO_4$, $NaNO_3$ and NaCl, perhaps due to their low amount and/or low UV absorption. However, compounds **6**, **7** and **16** were only obtained from chromatographic workup on OSMAC extract, while compound **4** and xenofuranone B (**17**) were only afforded from extract of fungal culture without salt mixture. Compound **5** was isolated from both extracts.

(A)

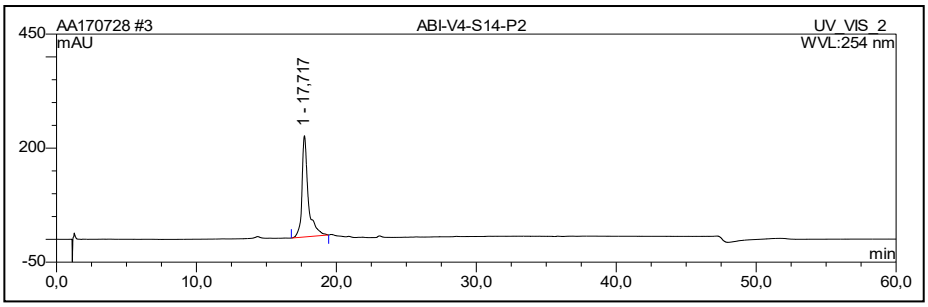

(B)

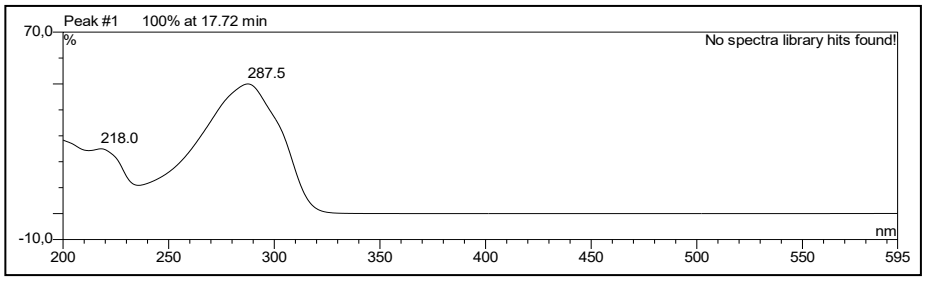

Figure S2. HPLC chromatogram (A) and UV spectrum (B) of compound **1**.

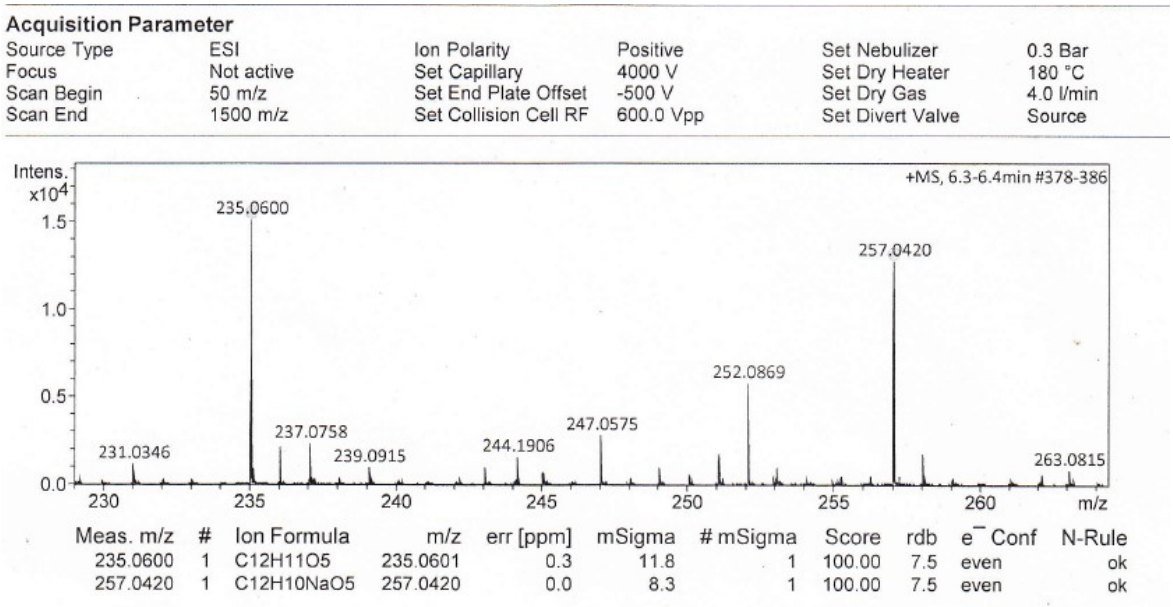

Figure S3. HRESIMS spectrum of compound **1**.

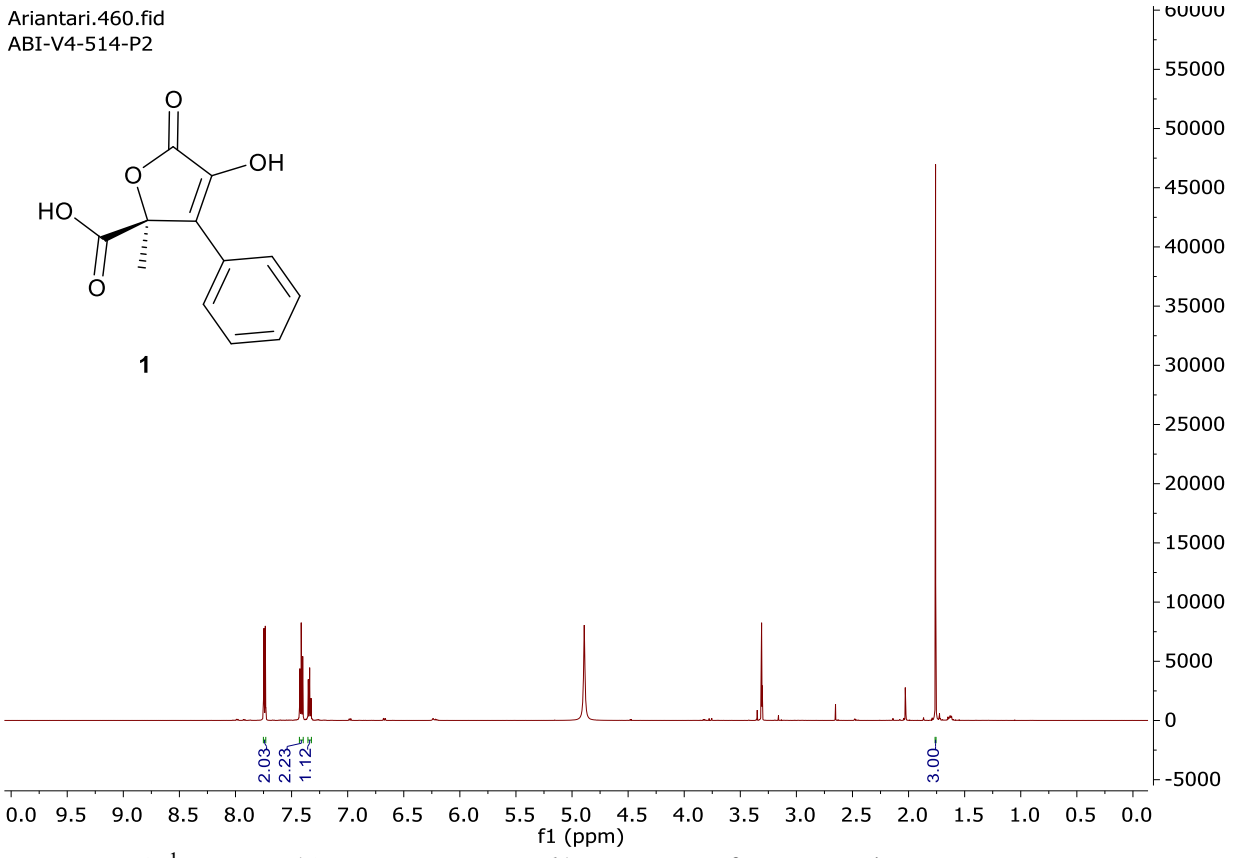

Figure S4. ^{1}H NMR (600 MHz, MeOH-d_4) spectrum of compound **1**.

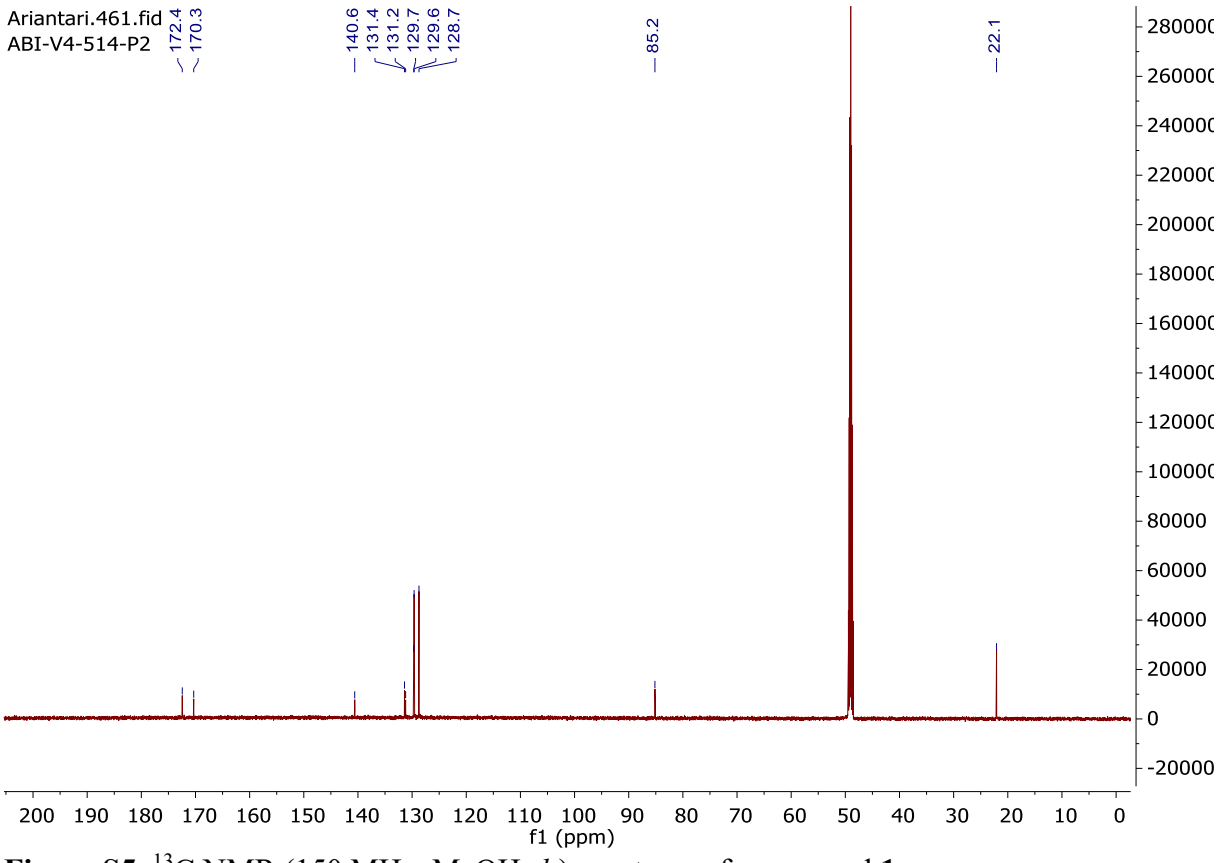

Figure S5. ^{13}C NMR (150 MHz, MeOH-d_4) spectrum of compound **1**.

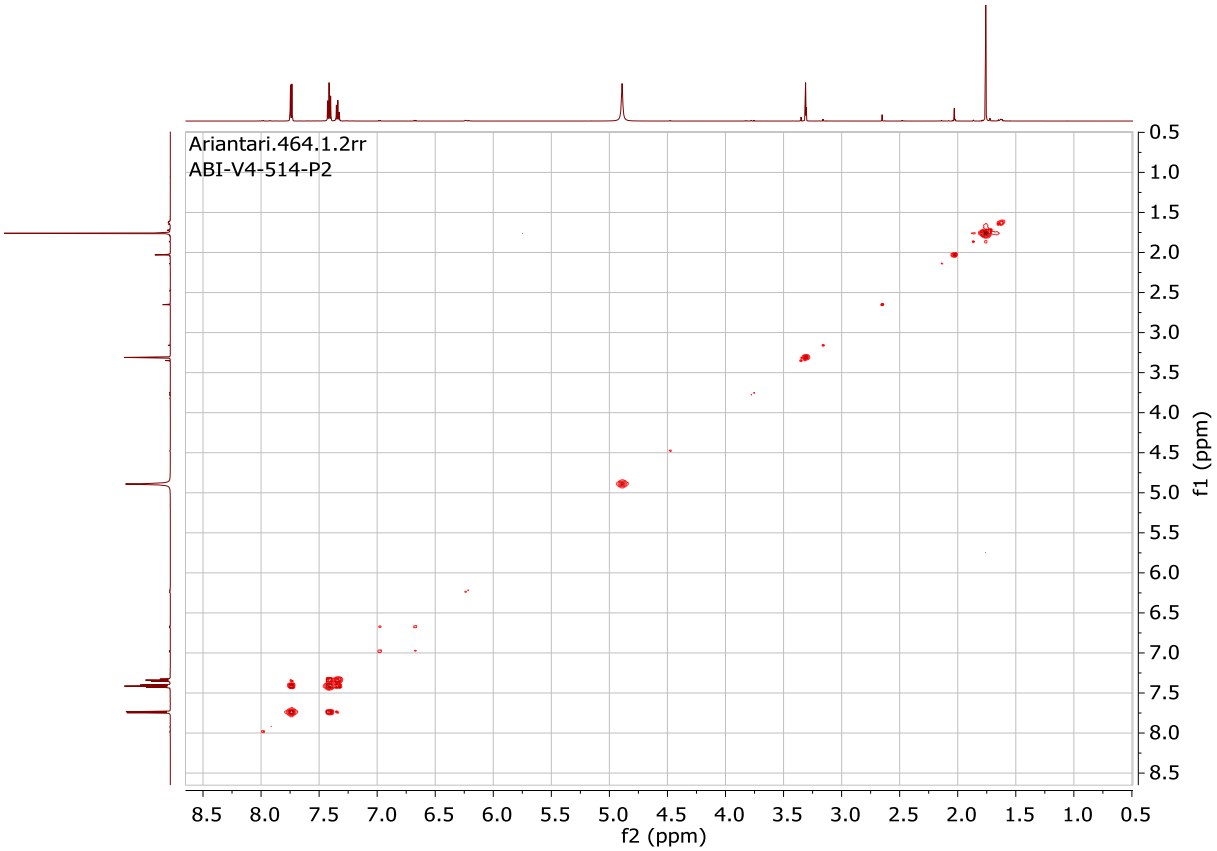

Figure S6. ^{1}H-^{1}H COSY (600 MHz, MeOH-d_4) spectrum of compound **1**.

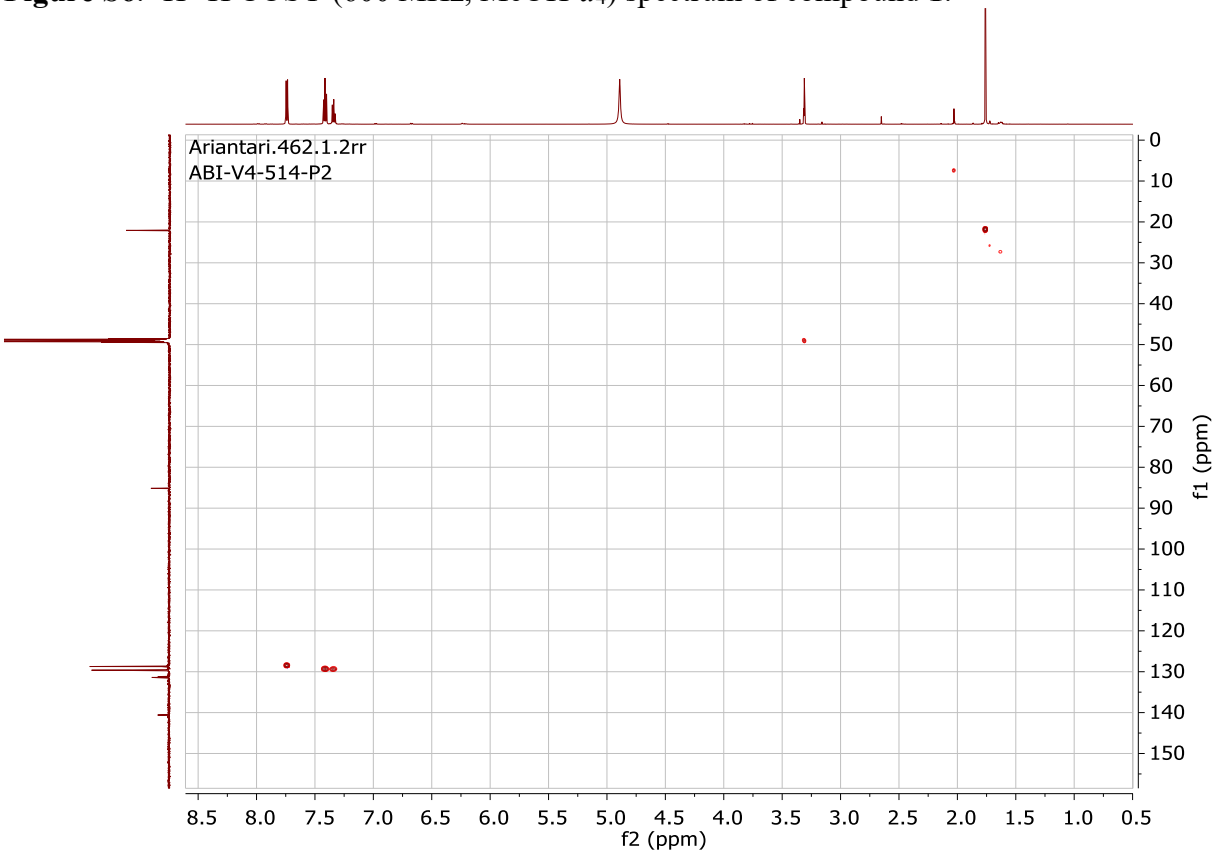

Figure S7. HSQC (600 and 150 MHz, MeOH-d_4) spectrum of compound **1**.

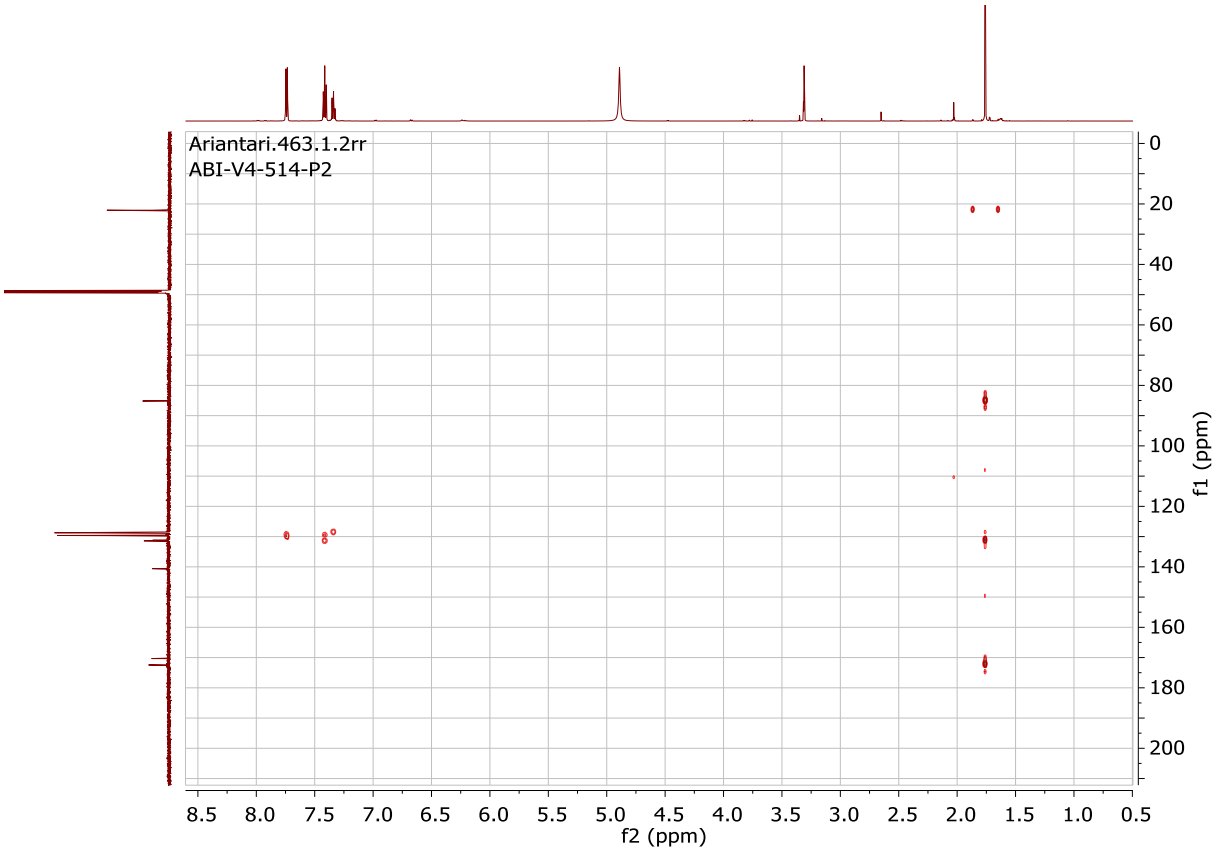

Figure S8. HMBC (600 and 150 MHz, MeOH-d_4) spectrum of compound **1**.

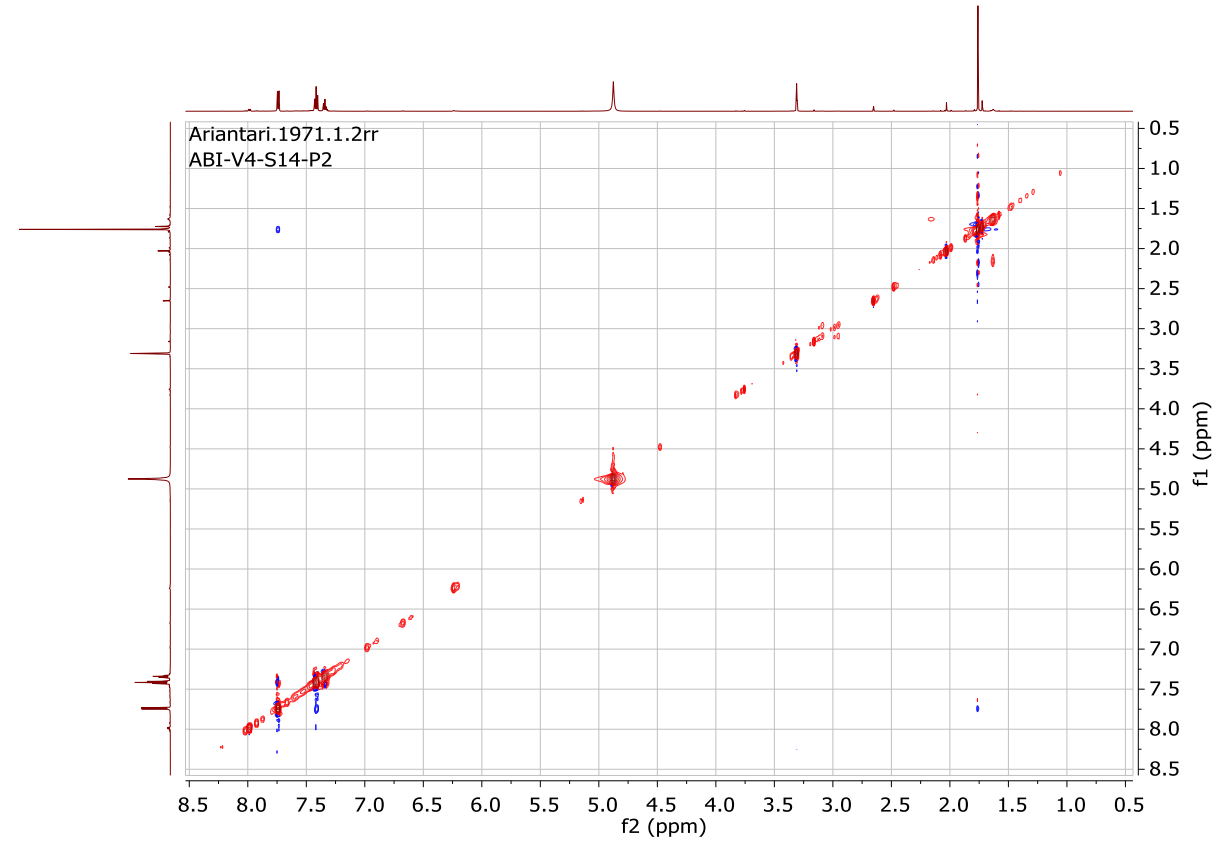

Figure S9. NOESY (600 MHz, MeOH-d_4) spectrum of compound **1**.

(A)

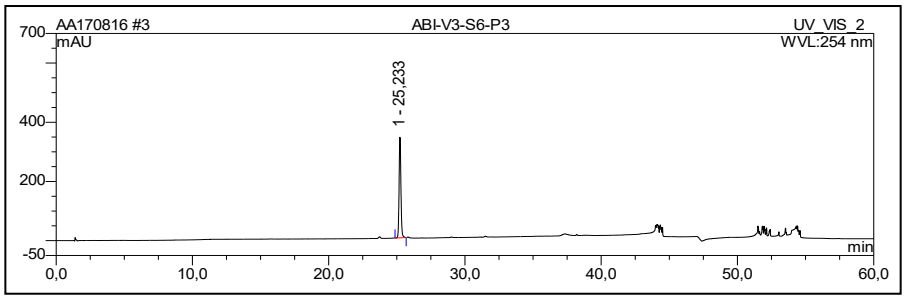

(B)

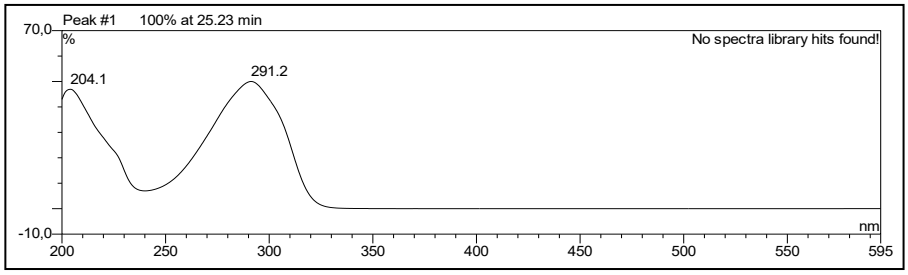

Figure S10. HPLC chromatogram (A) and UV spectrum (B) of compound **2**.

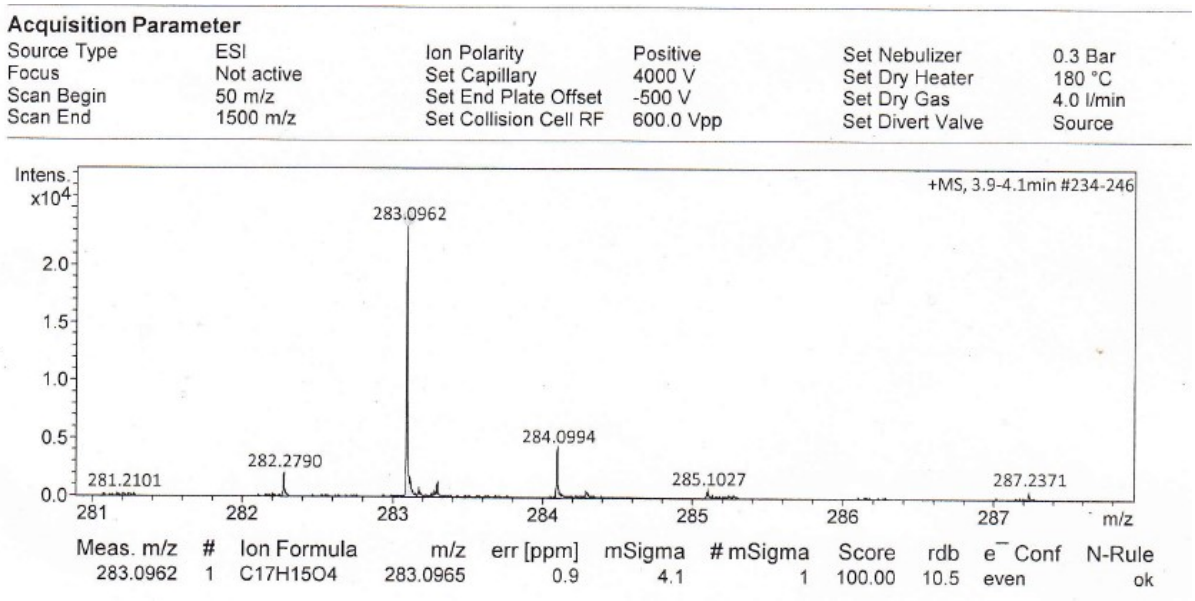

Figure S11. HRESIMS spectrum of compound **2**.

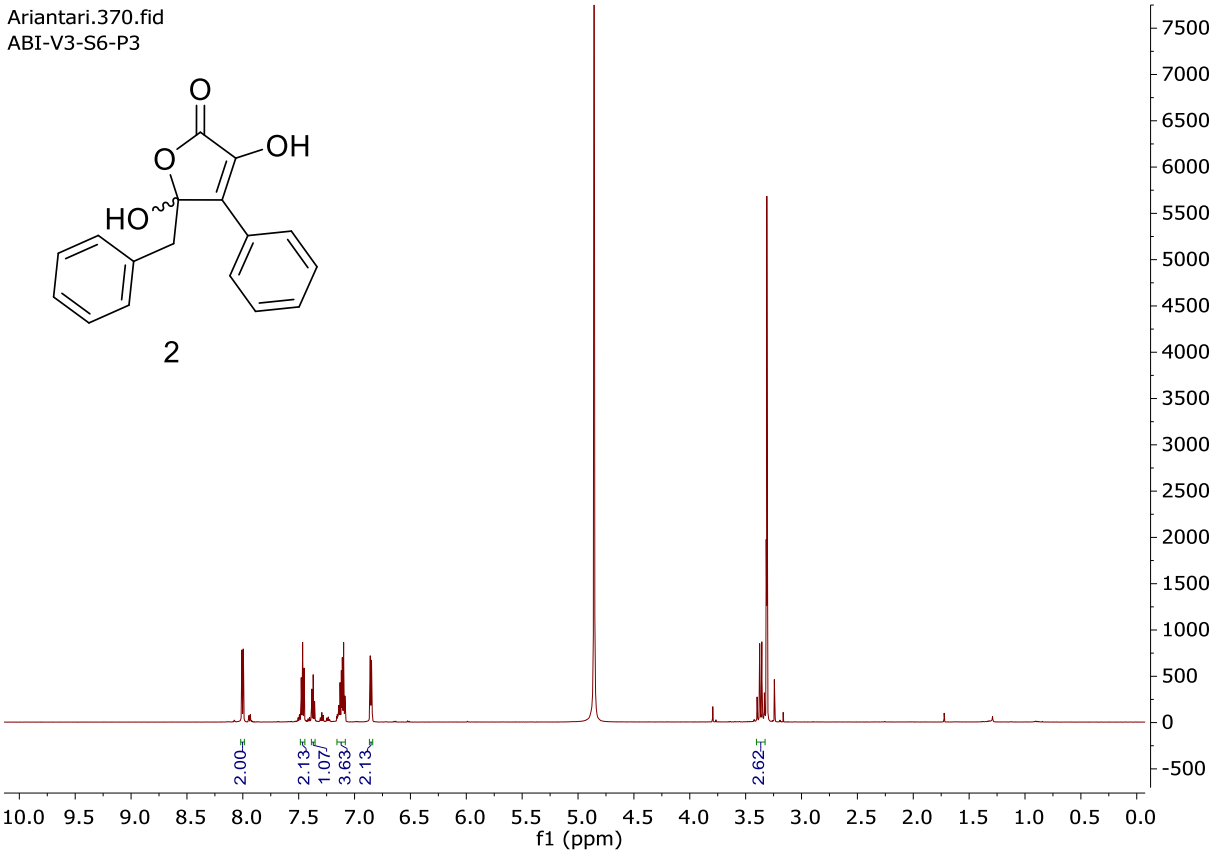

Figure S12. [1]H NMR (600 MHz, MeOH-d_4) spectrum of compound **2**.

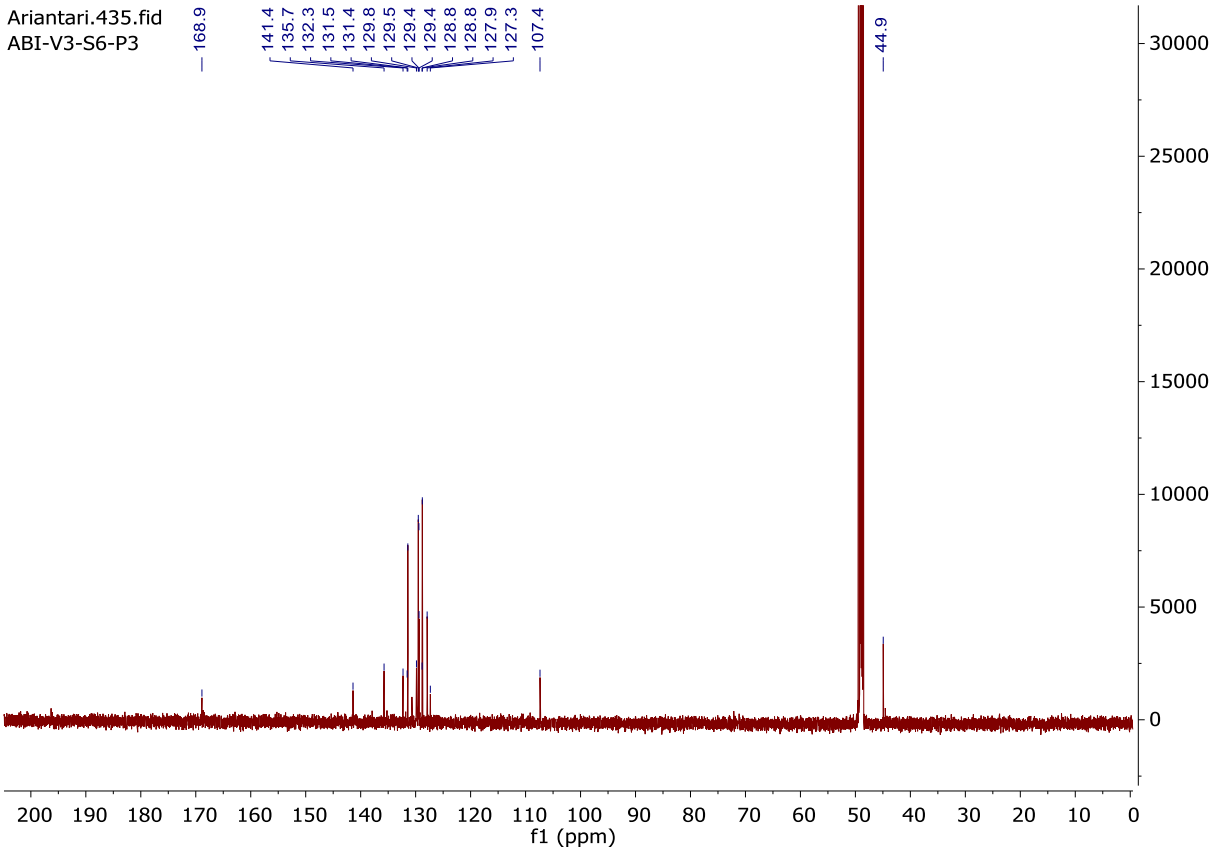

Figure S13. [13]C NMR (150 MHz, MeOH-d_4) spectrum of compound **2**.

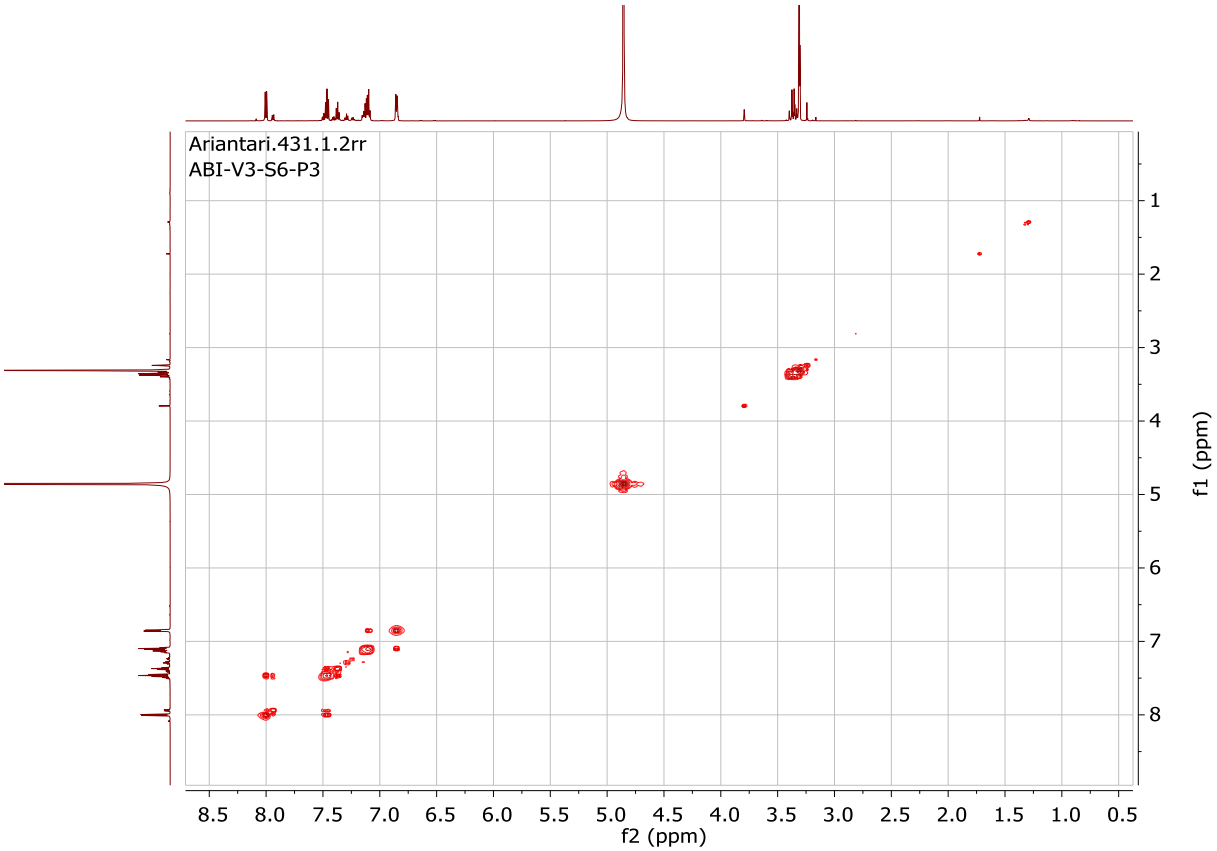

Figure S14. ^{1}H-^{1}H COSY (600 MHz, MeOH-d_4) spectrum of compound **2**.

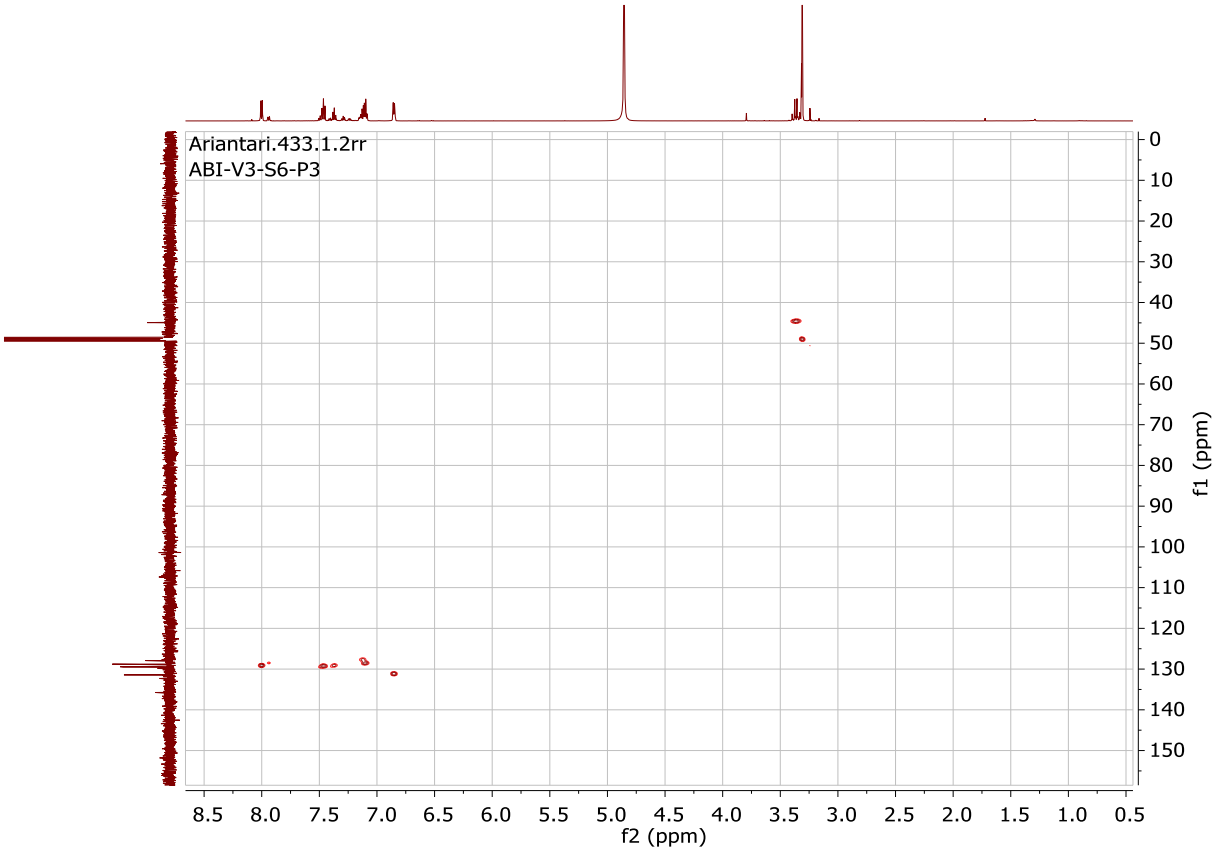

Figure S15. HSQC (600 and 150 MHz, MeOH-d_4) spectrum of compound **2**.

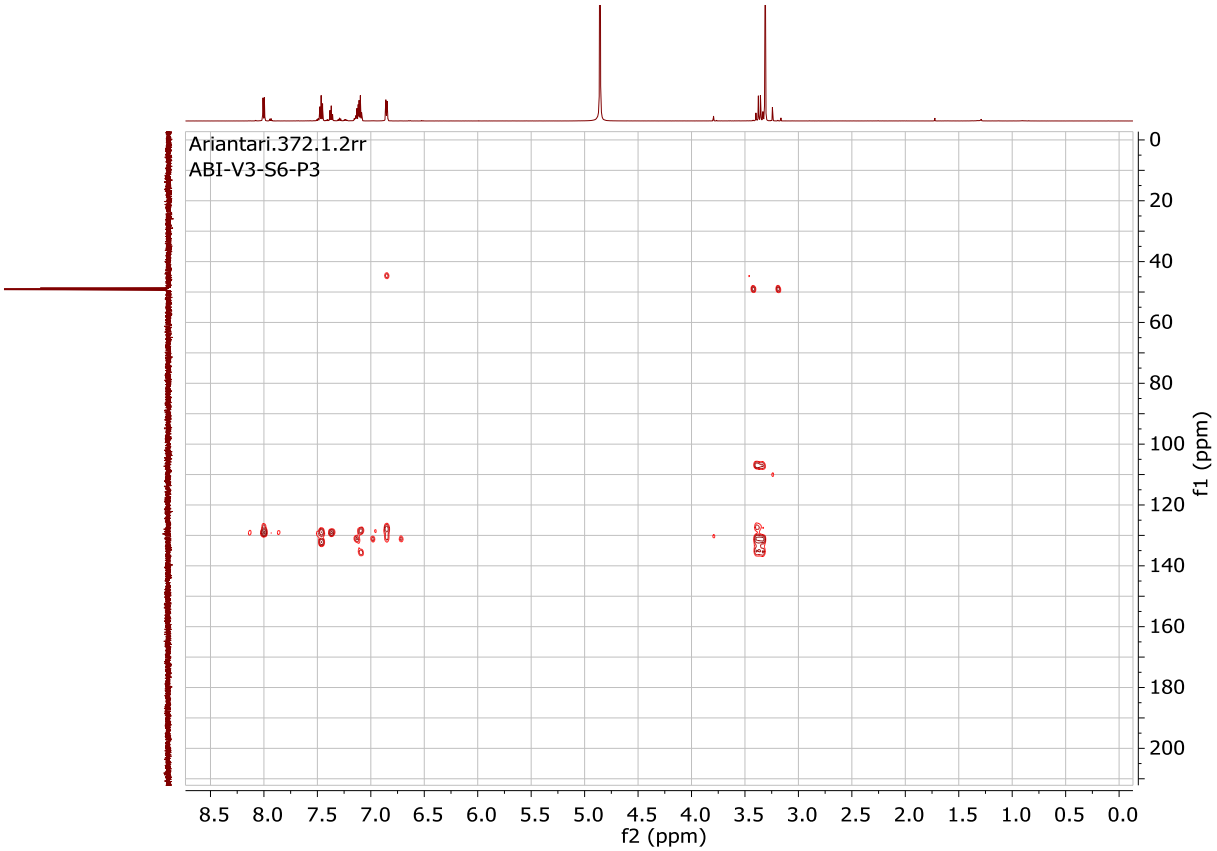

Figure S16. HMBC (600 and 150 MHz, MeOH-d_4) spectrum of compound **2**.

(A)

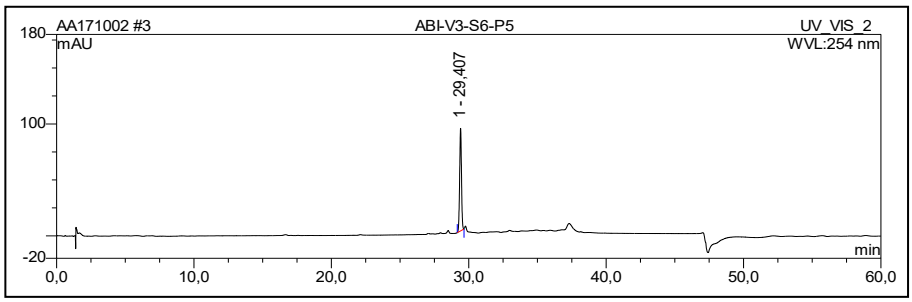

(B)

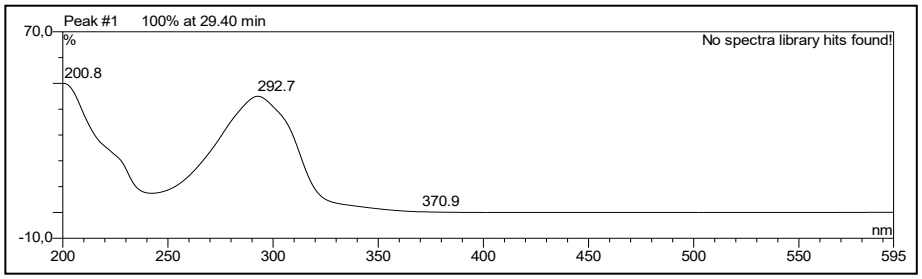

Figure S17. HPLC chromatogram (A) and UV spectrum (B) of compound **3**.

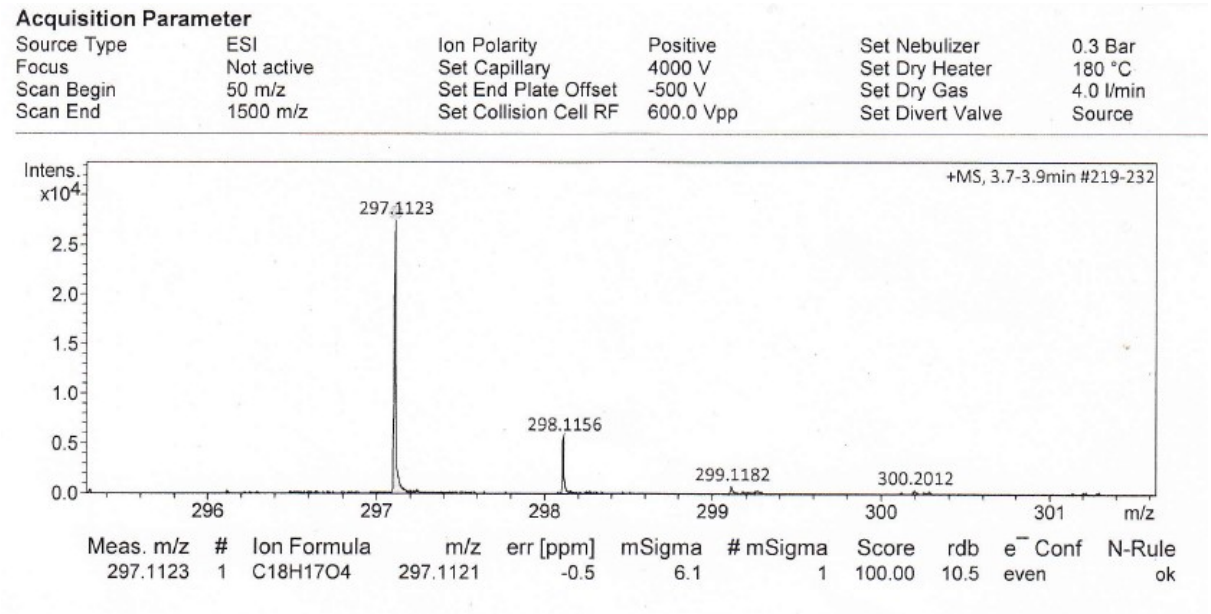

Figure S18. HRESIMS spectrum of compound **3**.

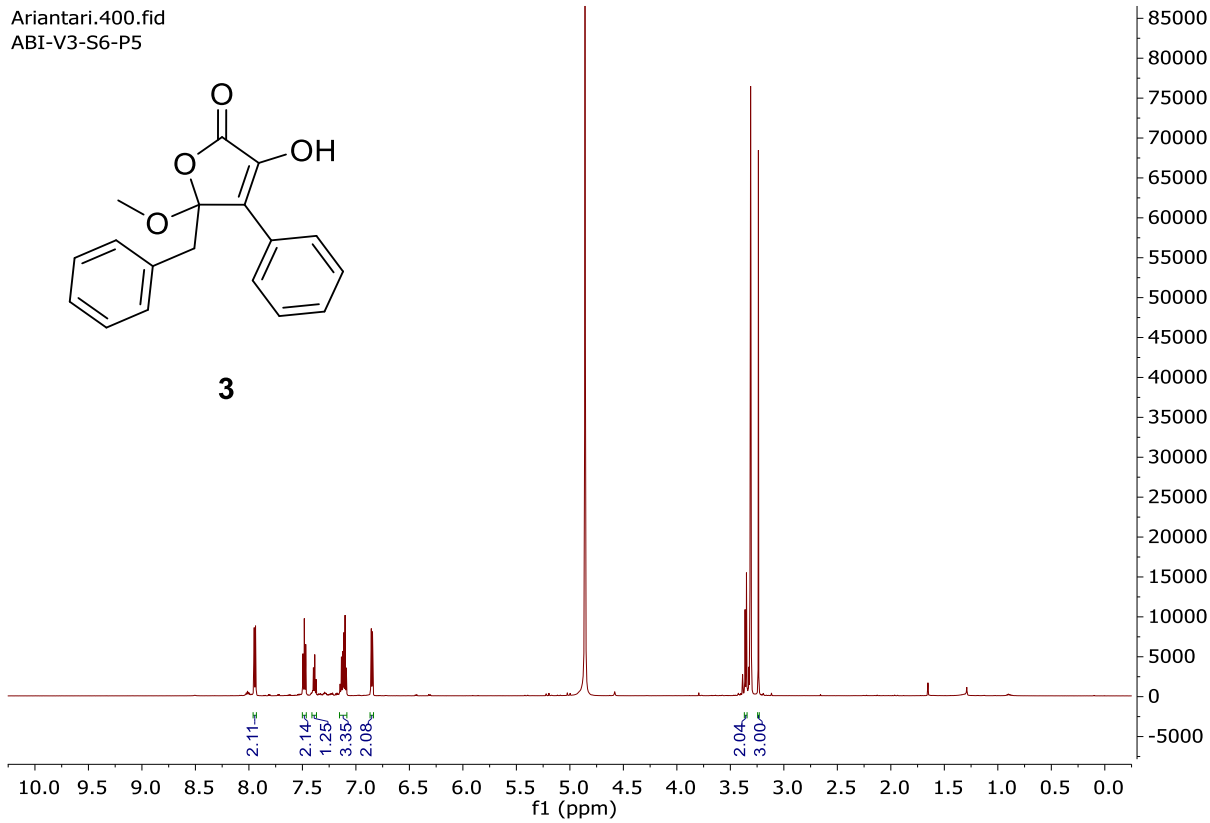

Figure S19. ^{1}H NMR (600 MHz, MeOH-d_4) spectrum of compound **3**.

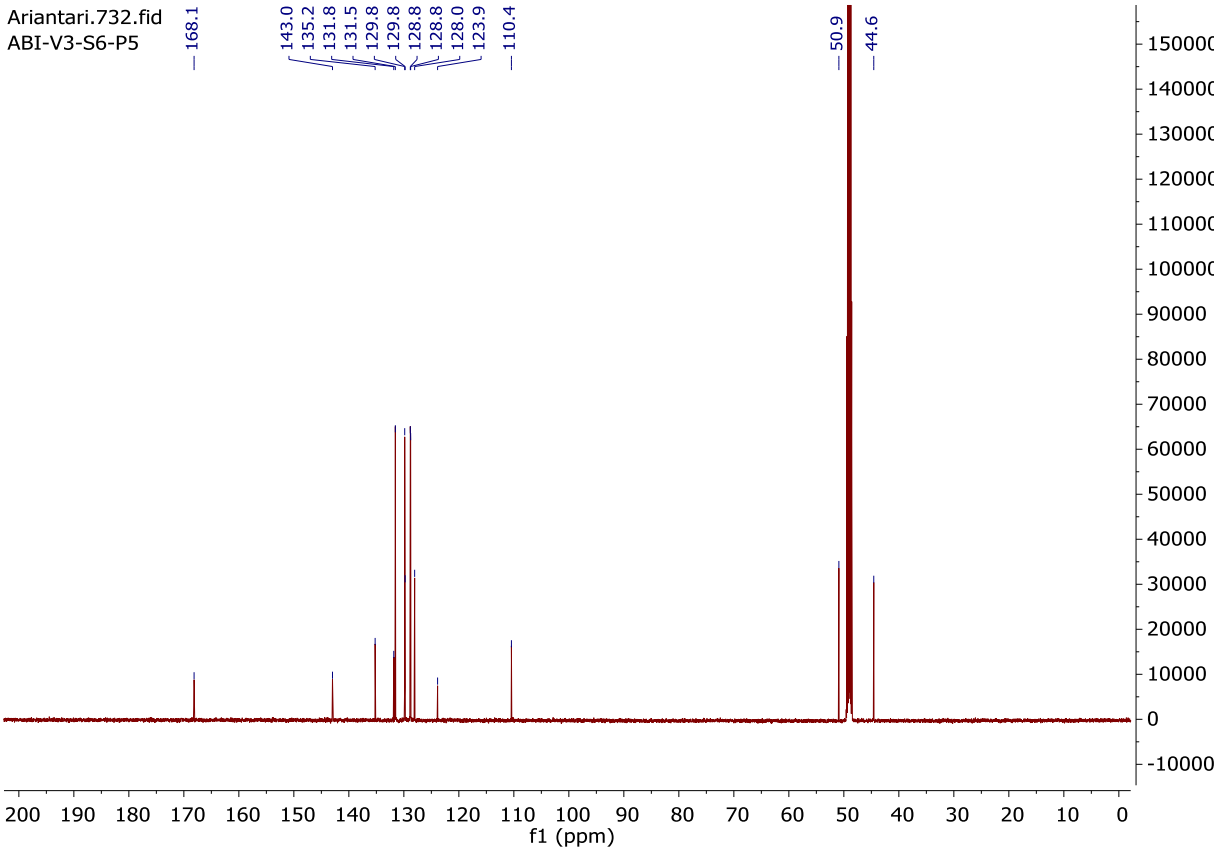

Figure S20. ^{13}C NMR (150 MHz, MeOH-d_4) spectrum of compound **3**.

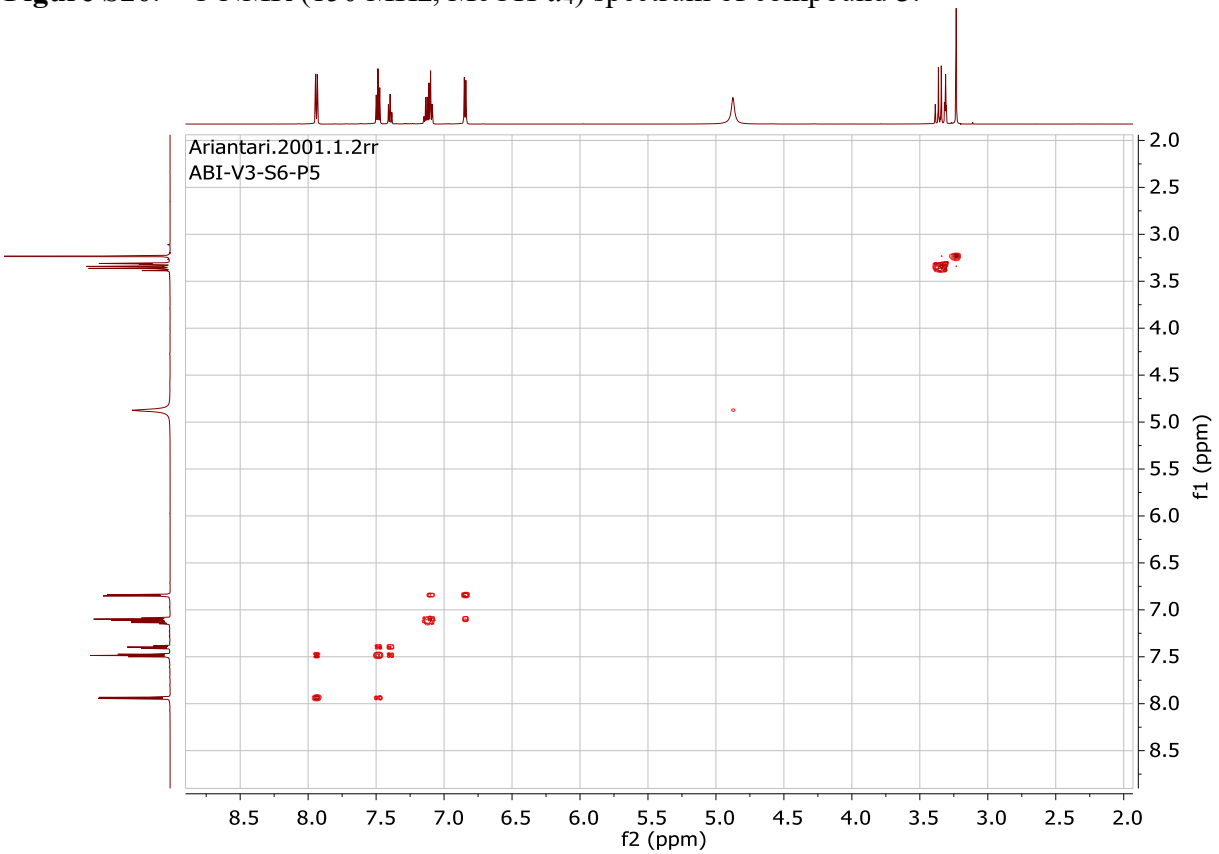

Figure S21. ^{1}H-^{1}H COSY (600 MHz, MeOH-d_4) spectrum of compound **3**.

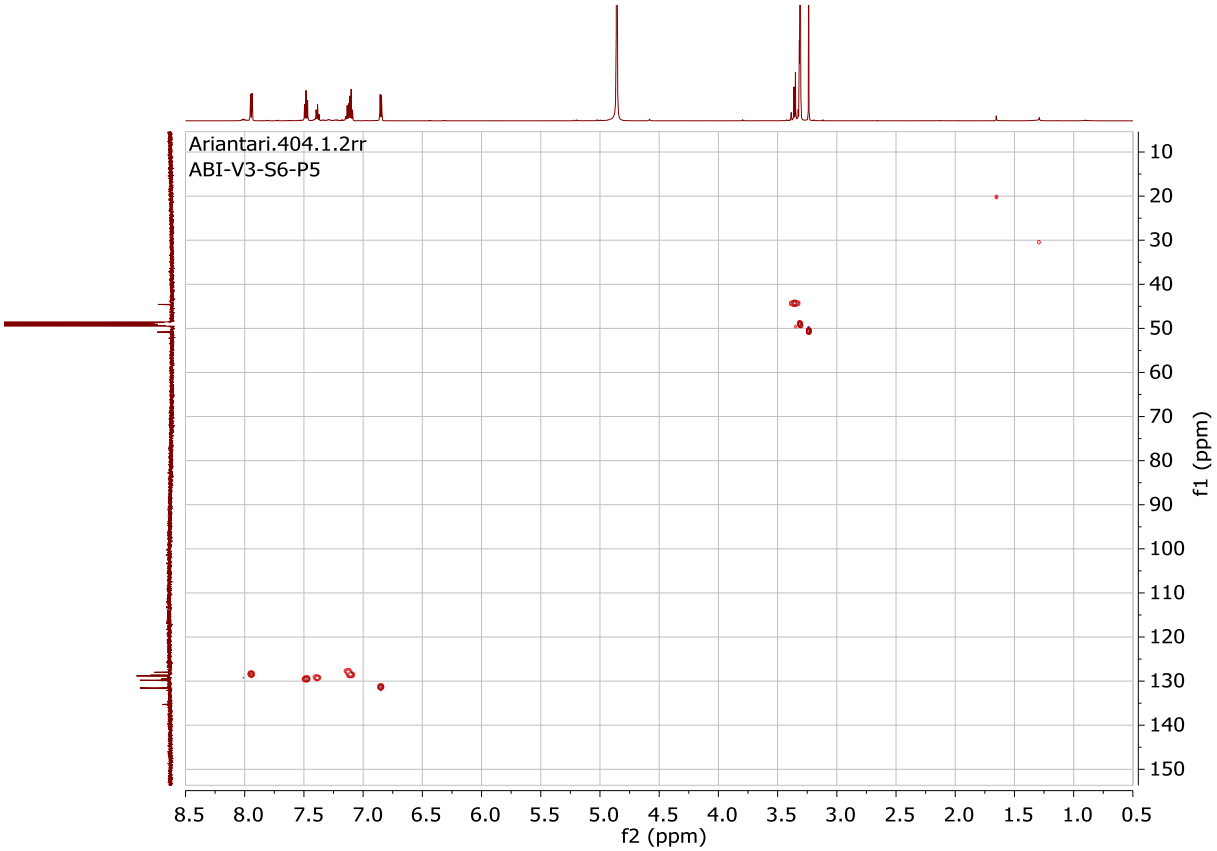

Figure S22. HSQC (600 and 150 MHz, MeOH-d_4) spectrum of compound **3**.

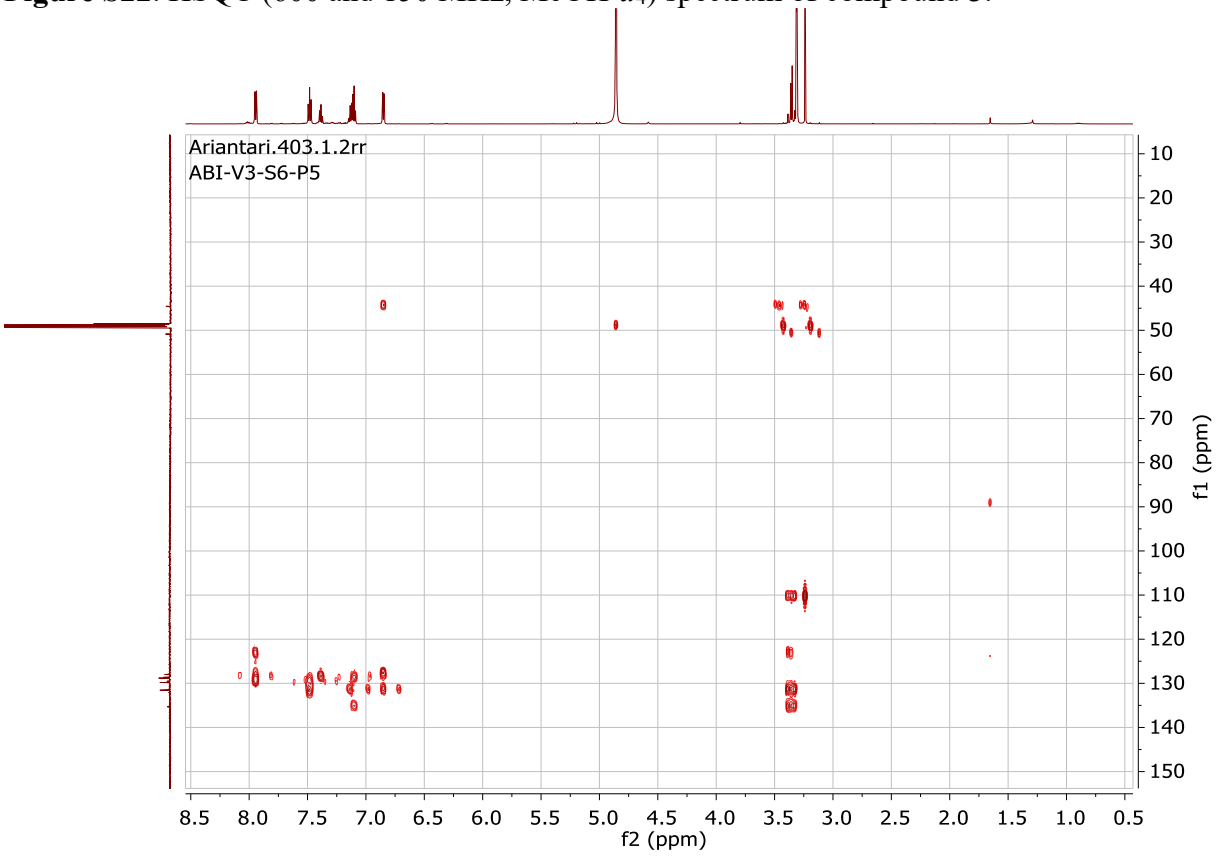

Figure S23. HMBC (600 and 150 MHz, MeOH-d_4) spectrum of compound **3**.

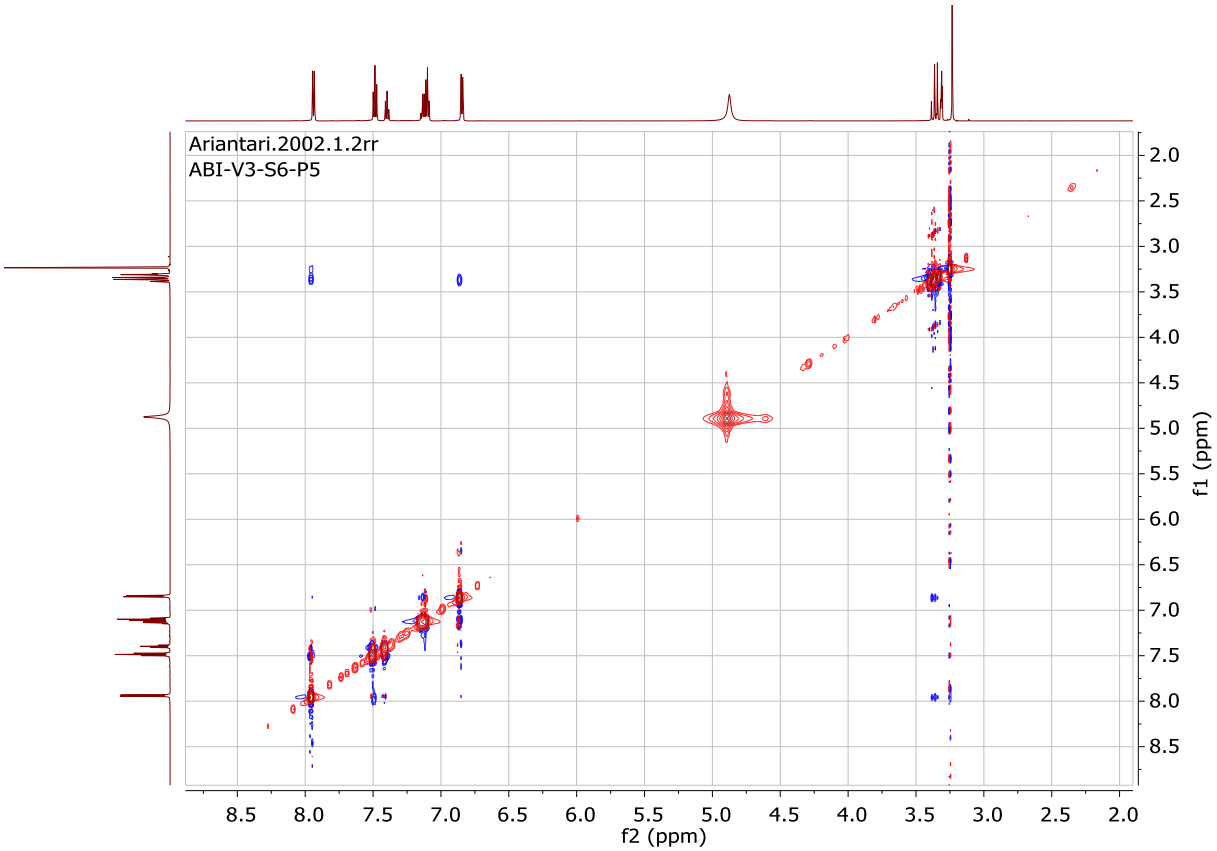

Figure S24. NOESY (600 MHz, MeOH-d_4) spectrum of compound **3**.

(A)

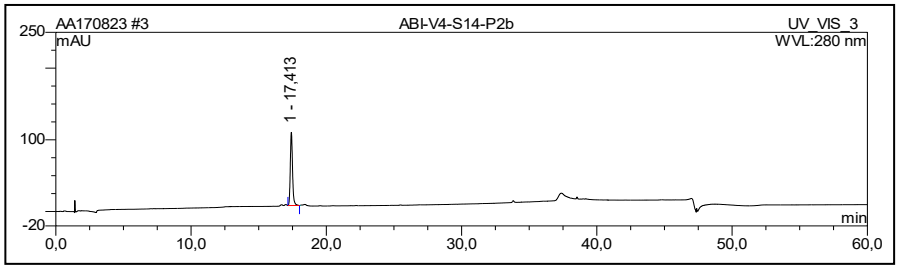

(B)

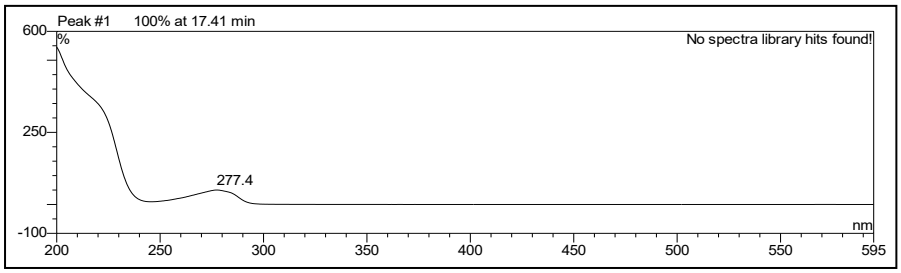

Figure S25. HPLC chromatogram (A) and UV spectrum (B) of compound **4**.

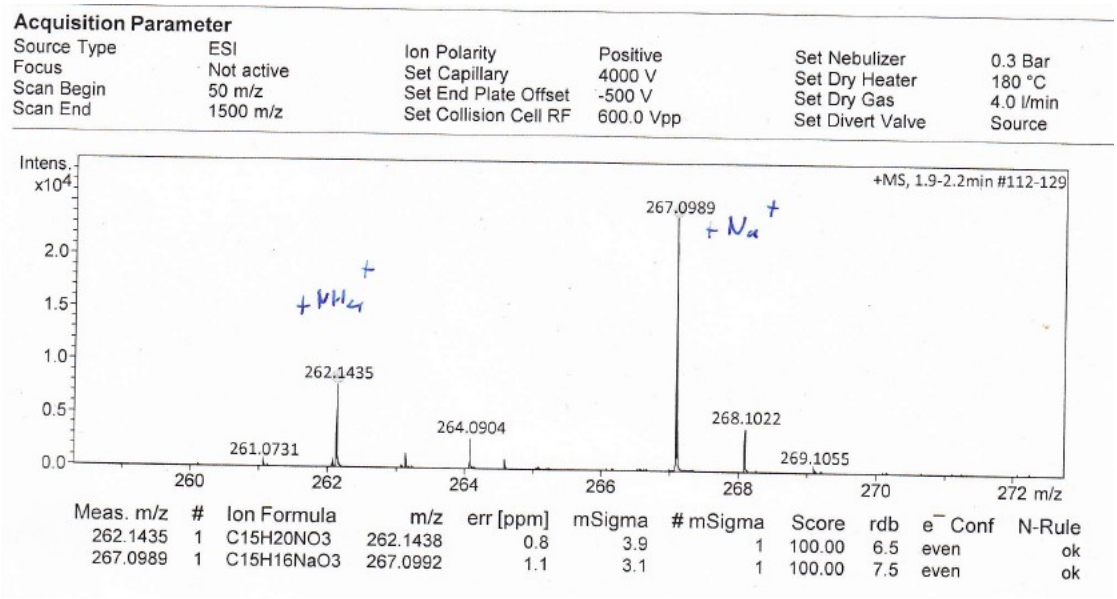

Figure S26. HRESIMS spectrum of compound **4**.

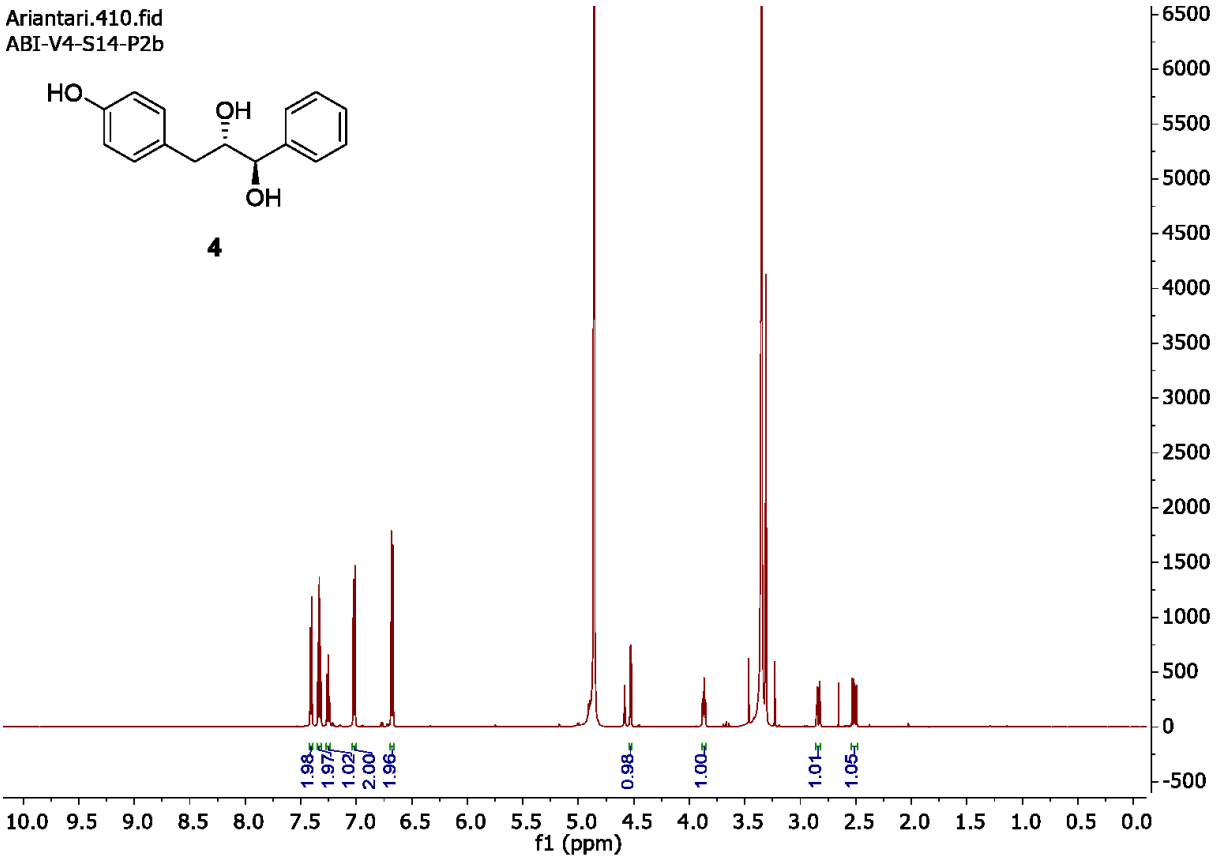

Figure S27. ^{1}H NMR (600 MHz, MeOH-d_4) spectrum of compound **4**.

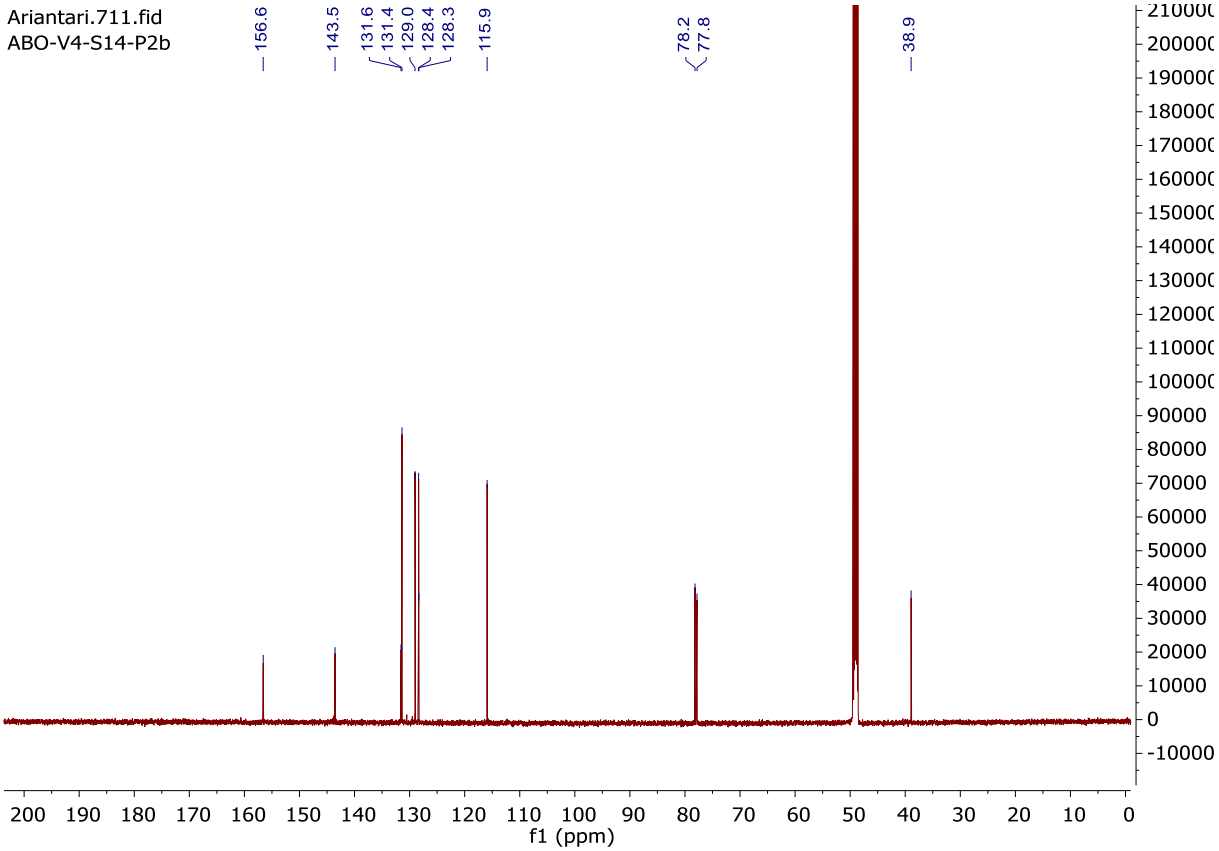

Figure S28. ^{13}C NMR (150 MHz, MeOH-d_4) spectrum of compound **4**.

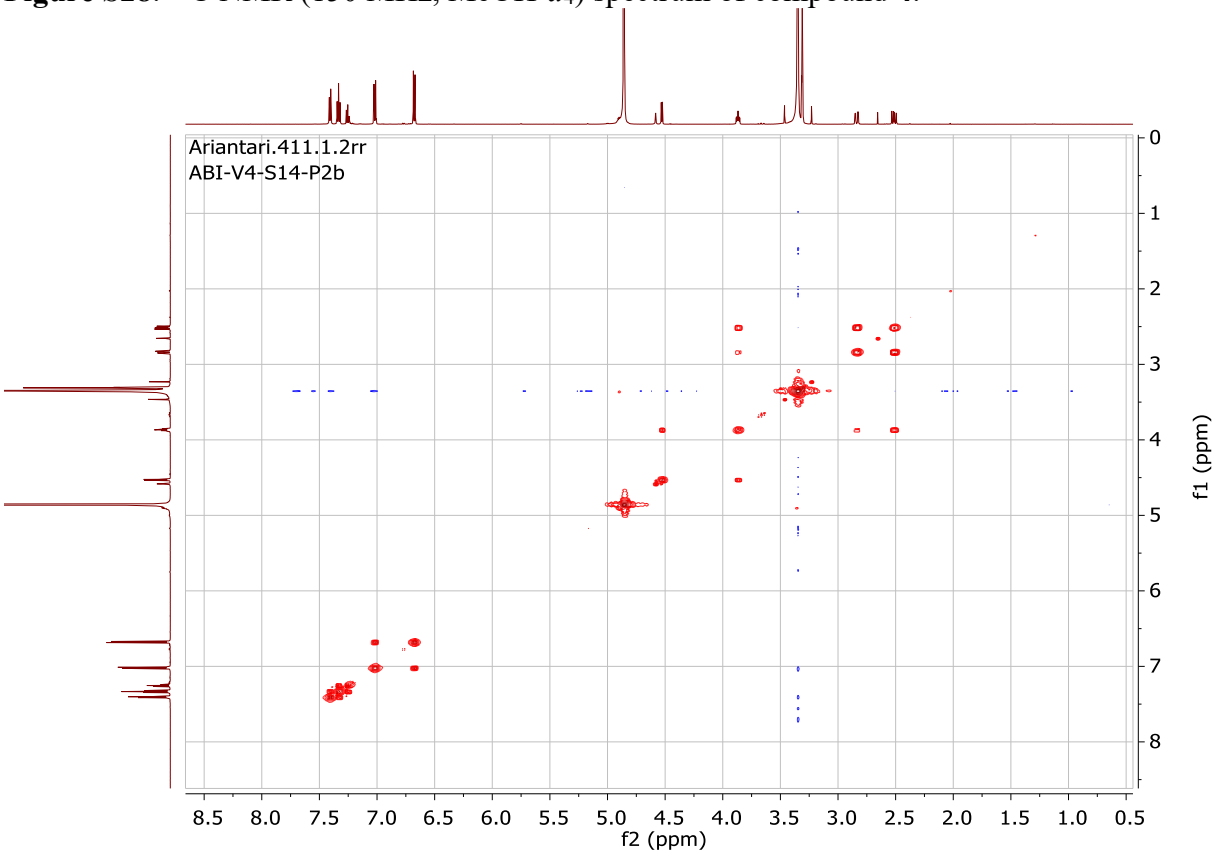

Figure S29. ^{1}H-^{1}H COSY (600 MHz, MeOH-d_4) spectrum of compound **4**.

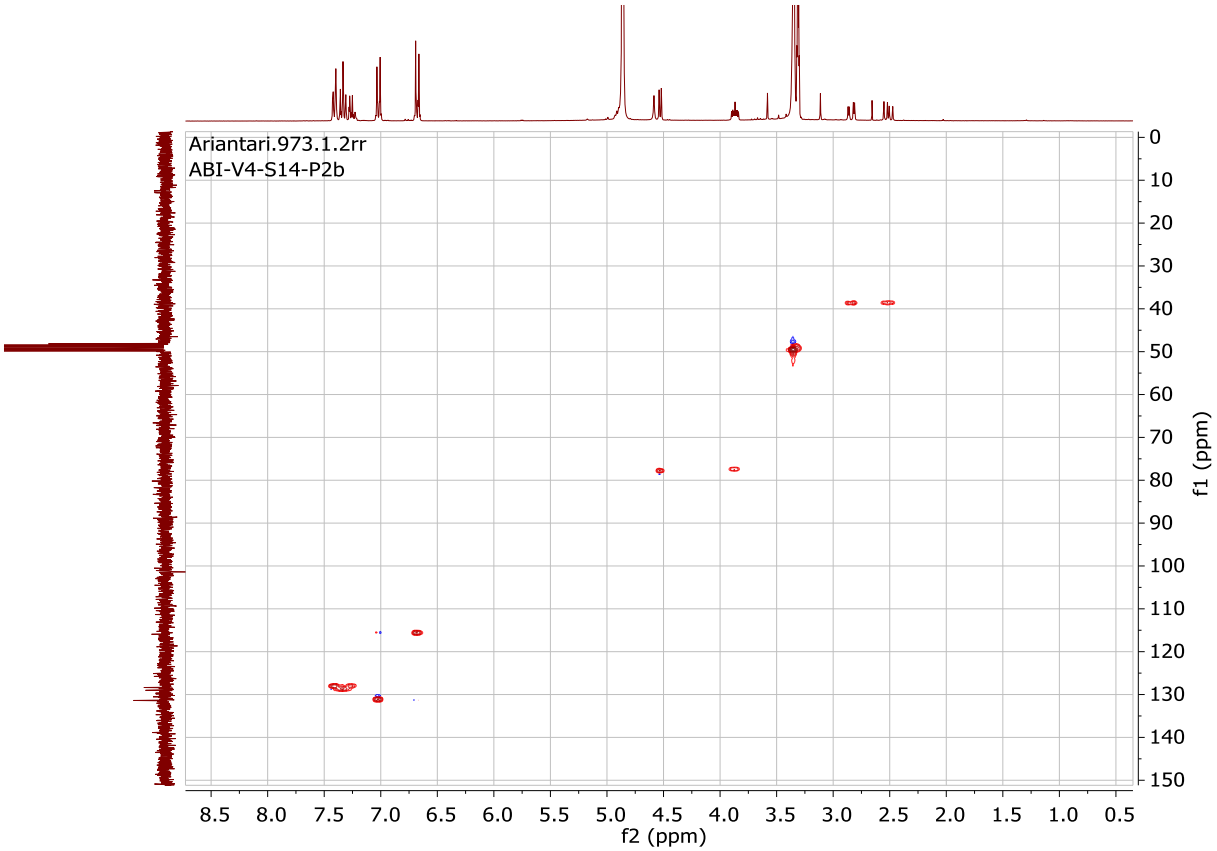

Figure S30. HSQC (300 and 75 MHz, MeOH-d_4) spectrum of compound **4**.

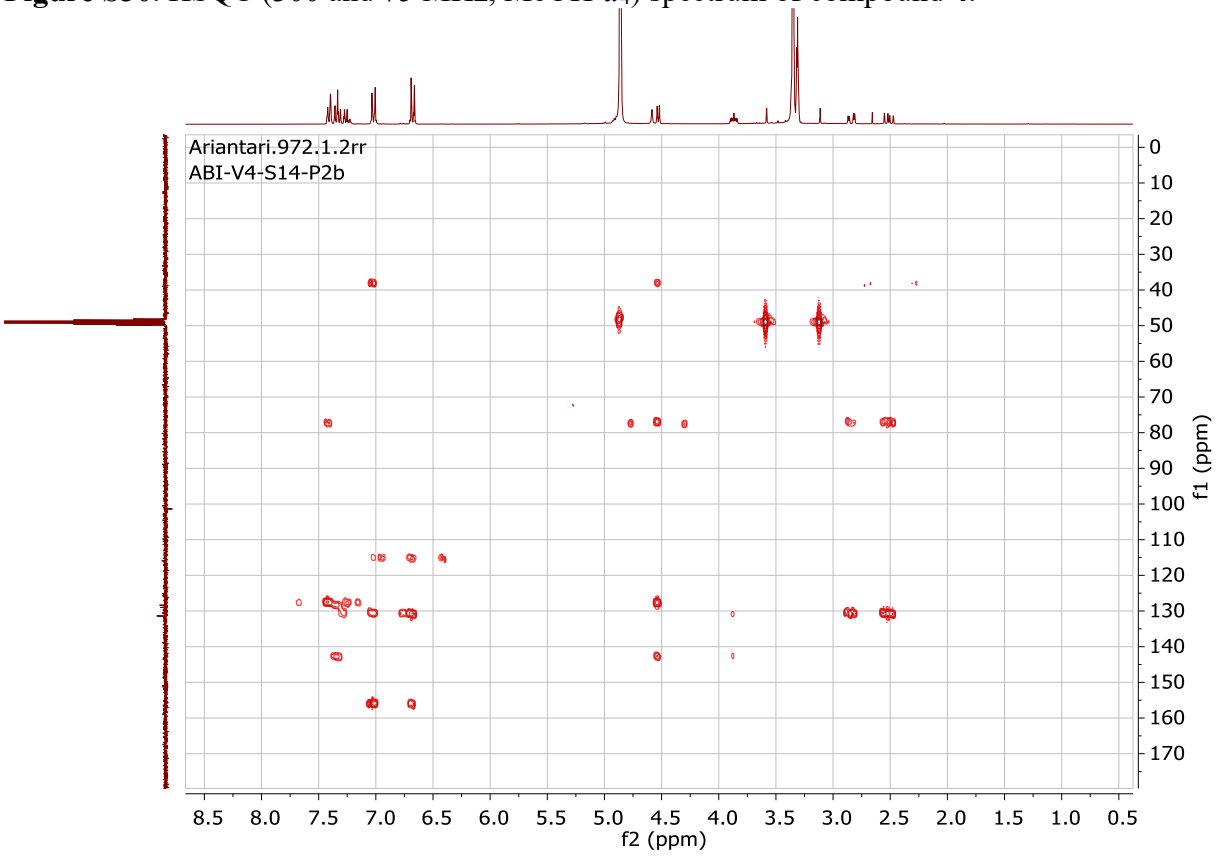

Figure S31. HMBC (300 and 75 MHz, MeOH-d_4) spectrum of compound **4**.

(A)

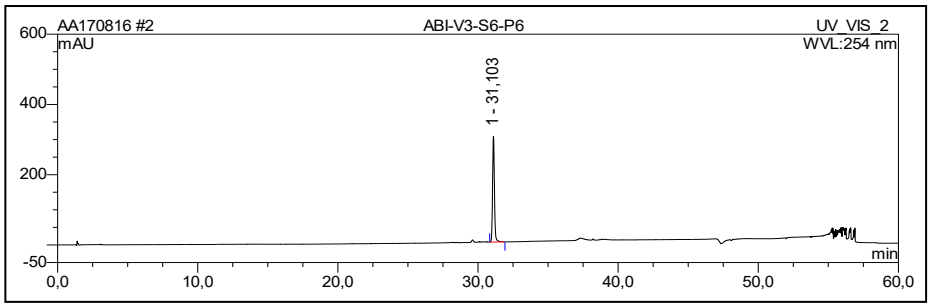

(B)

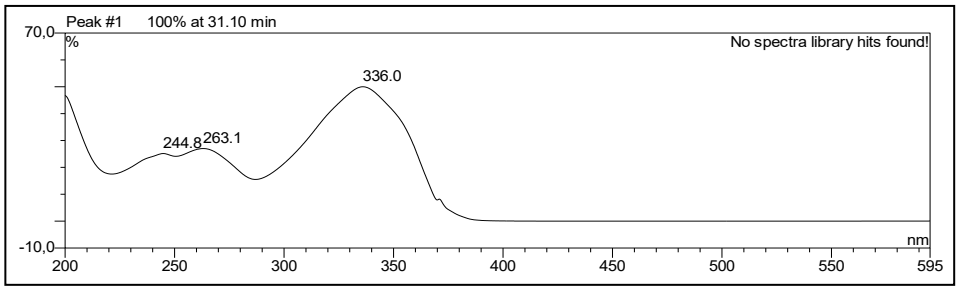

Figure S32. HPLC chromatogram (A) and UV spectrum (B) of compound **5**.

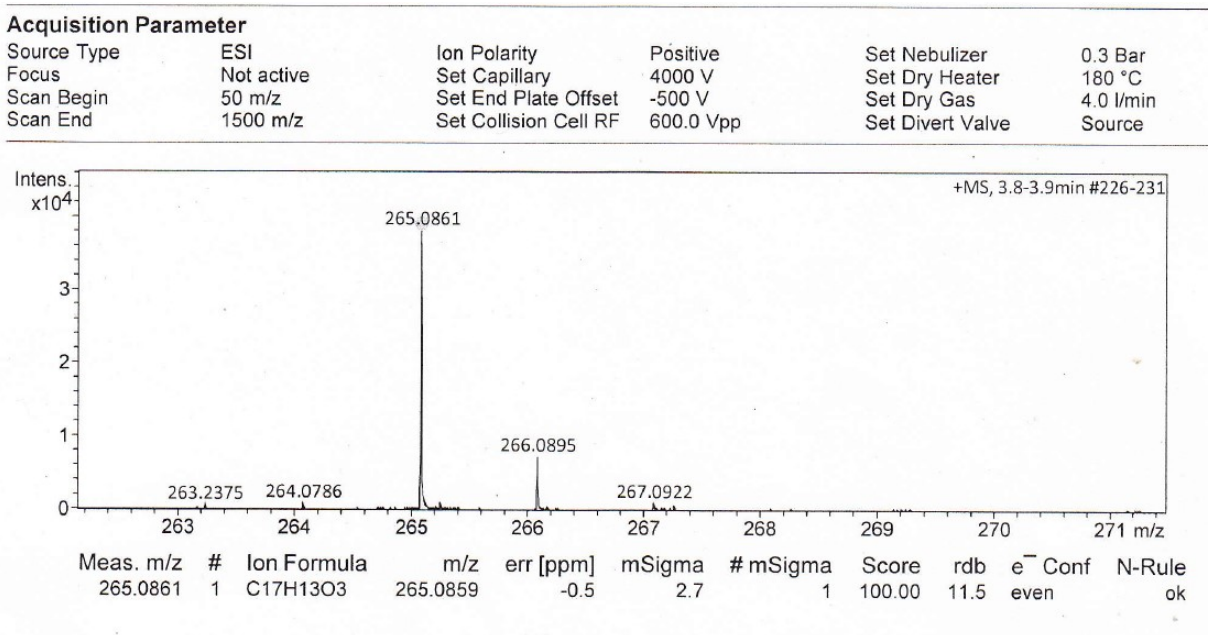

Figure S33. HRESIMS spectrum of compound **5**.

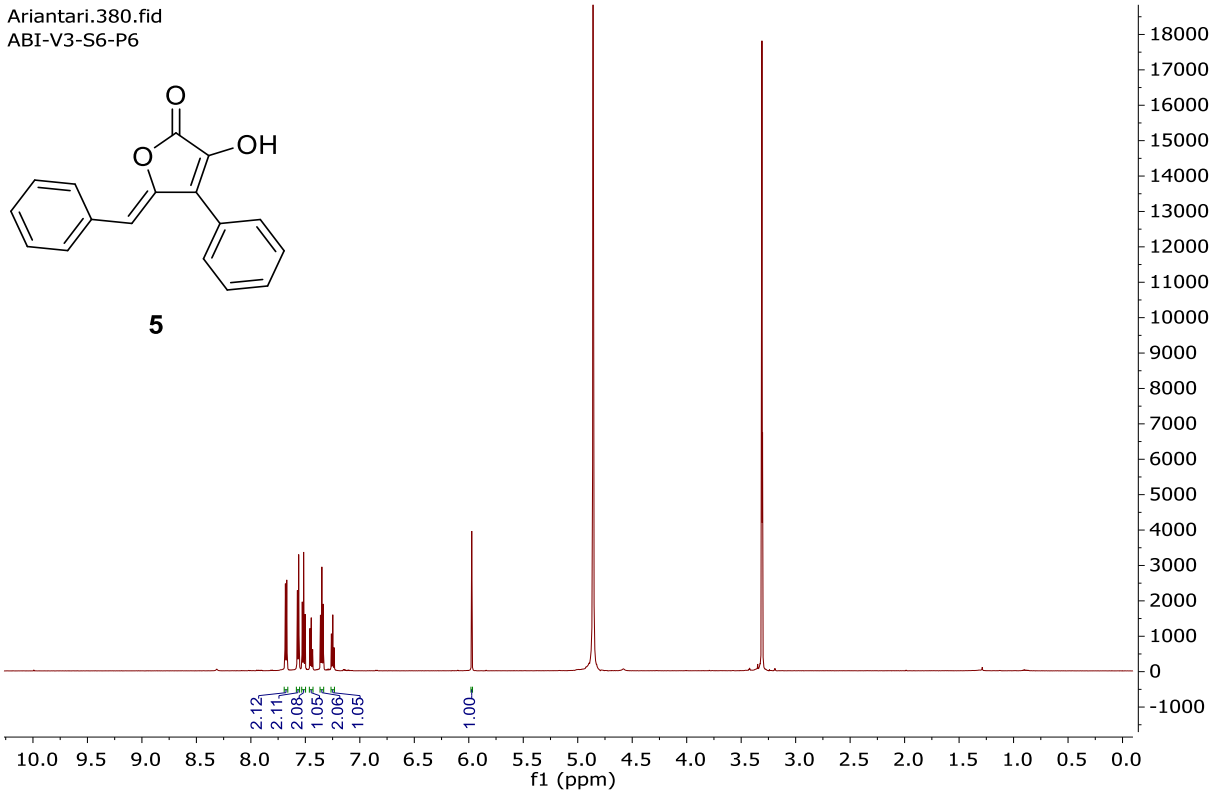

Figure S34. [1]H NMR (600 MHz, MeOH-d_4) spectrum of compound **5**.

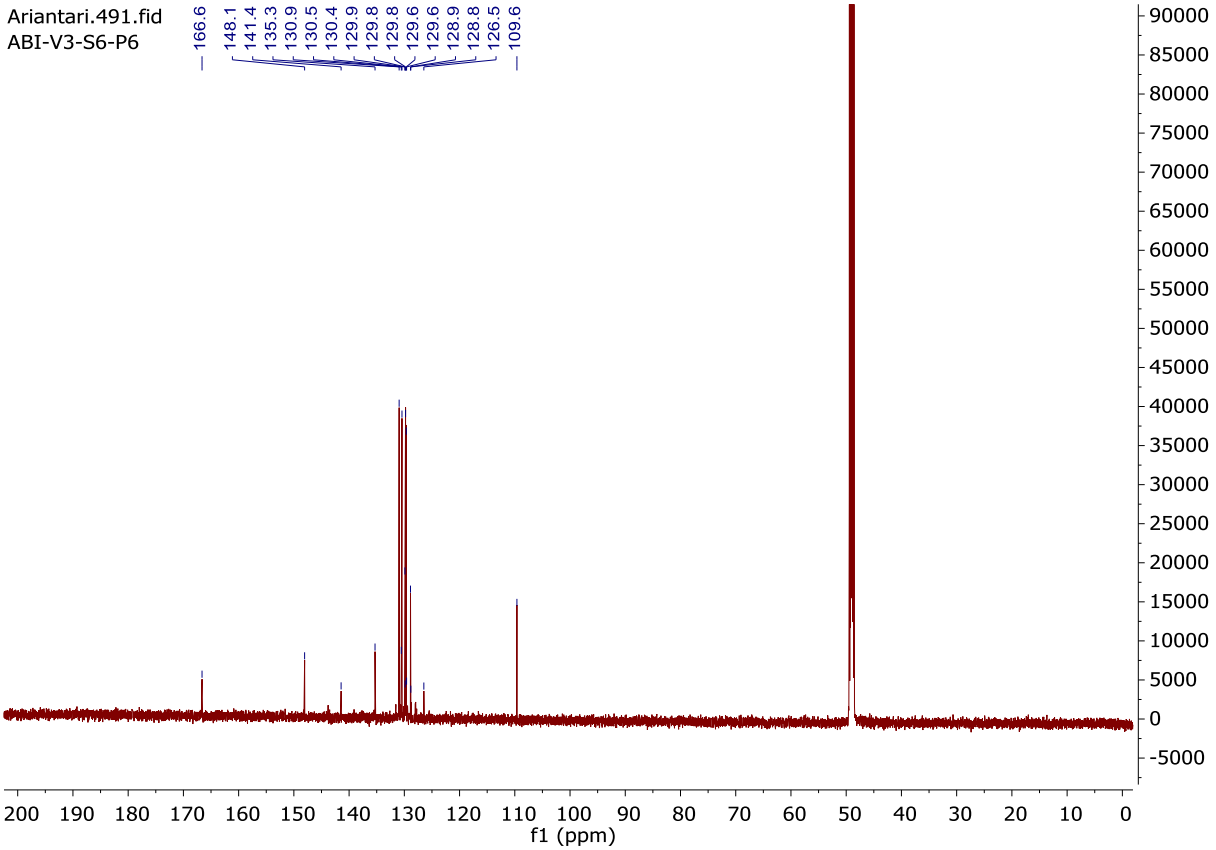

Figure S35. [13]C NMR (150 MHz, MeOH-d_4) spectrum of compound **5.**

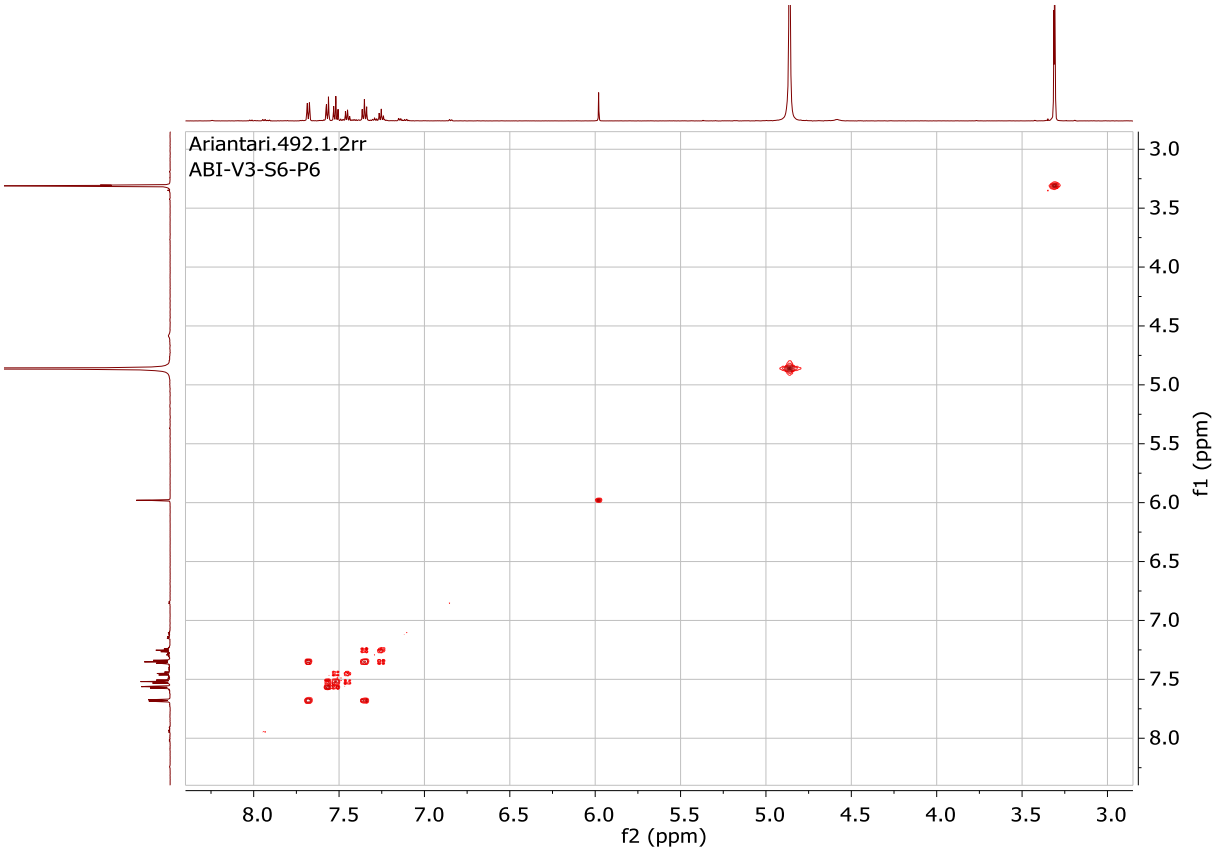

Figure S36. ^{1}H-^{1}H COSY (600 MHz, MeOH-d_4) spectrum of compound **5**.

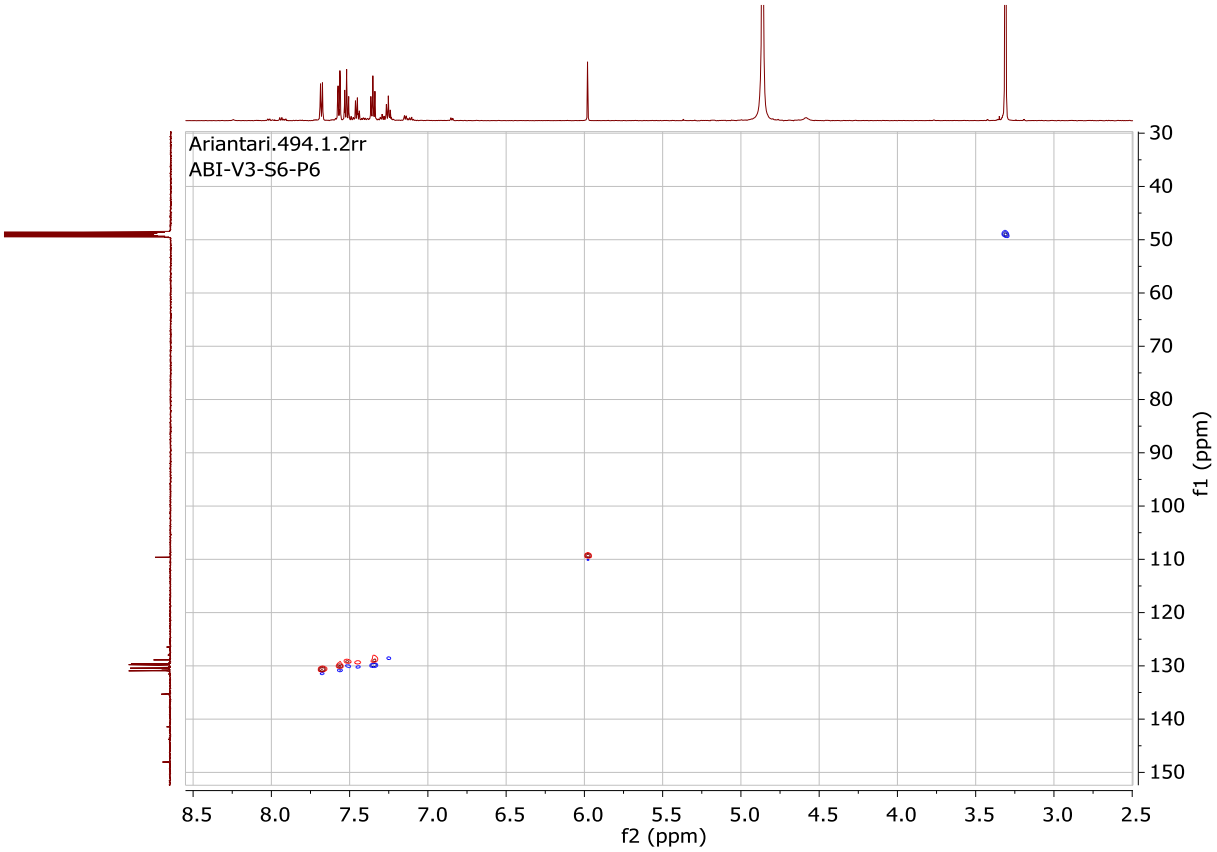

Figure S37. HSQC (600 and 150 MHz, MeOH-d_4) spectrum of compound **5**.

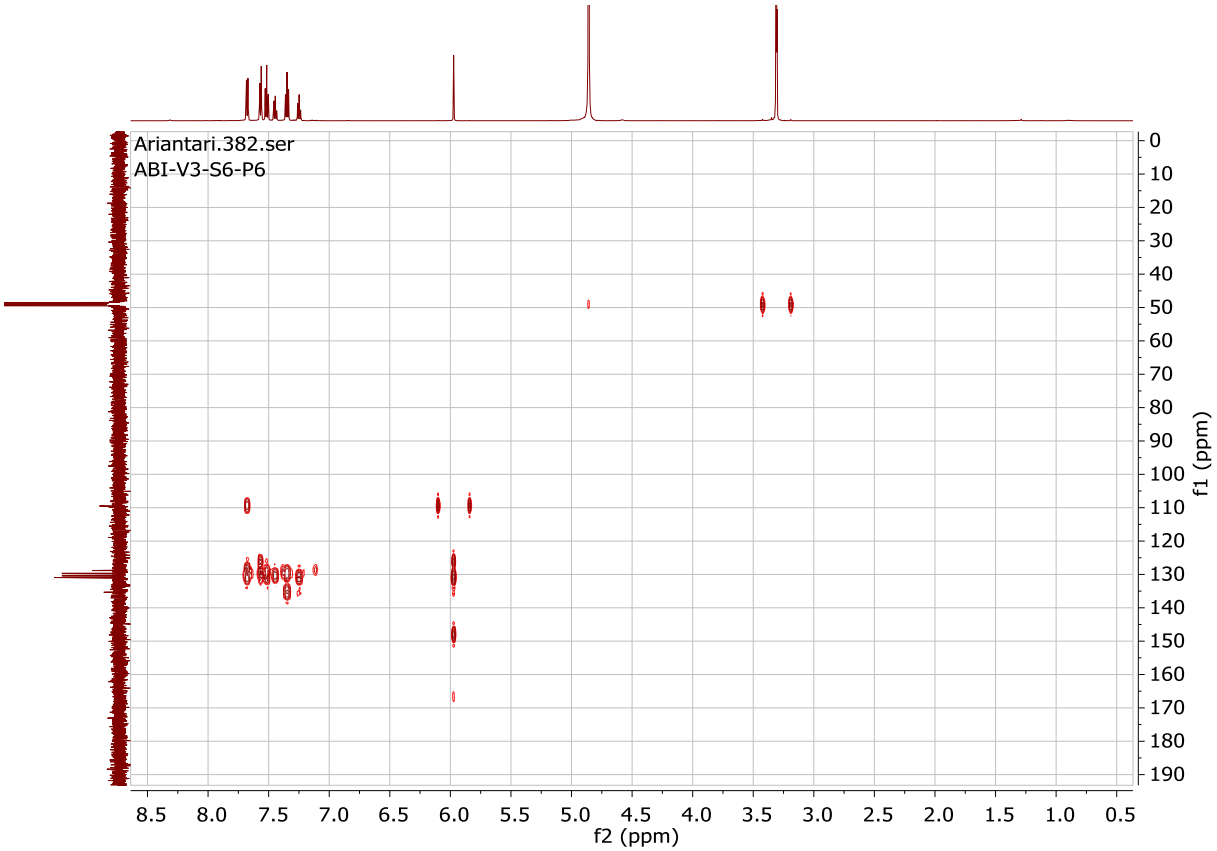

Figure S38. HMBC (600 and 150 MHz, MeOH-d_4) spectrum of compound **5**.

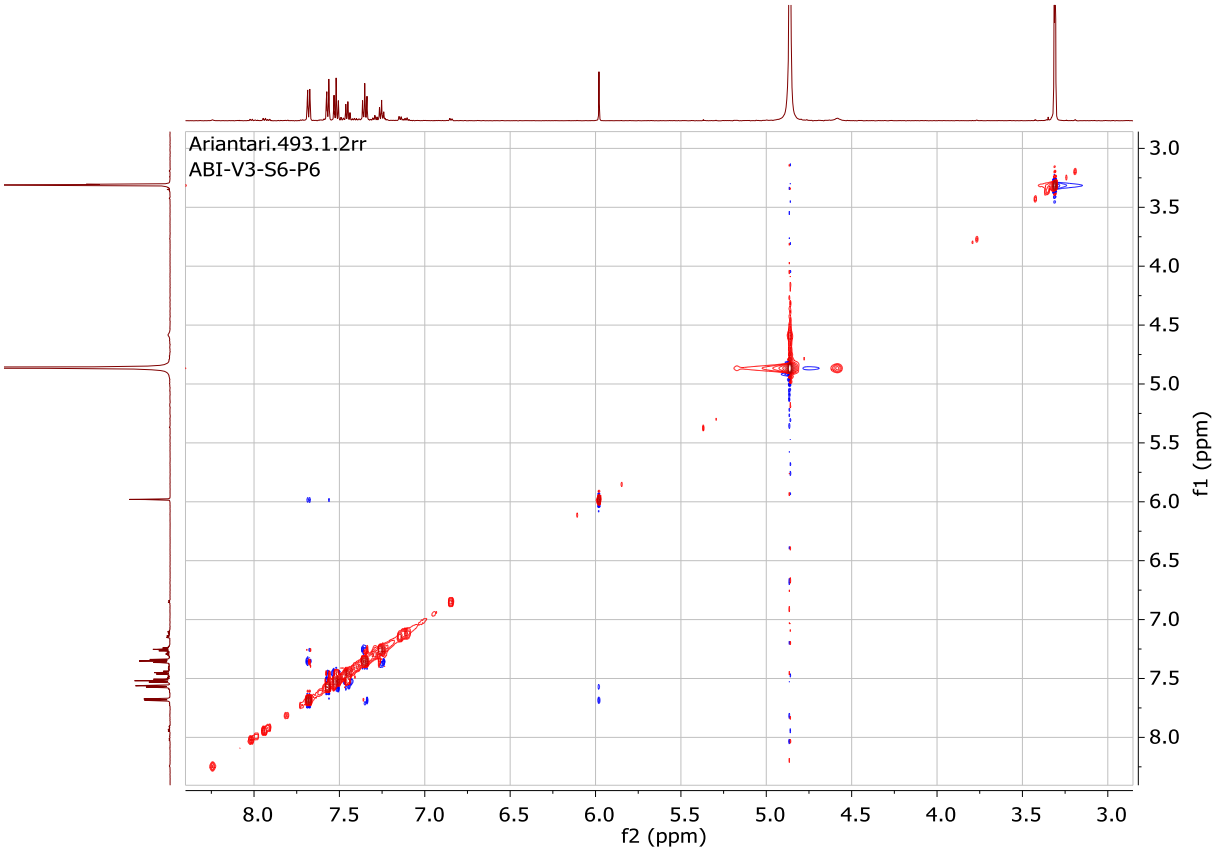

Figure S39. NOESY (600 MHz, MeOH-d_4) spectrum of compound **5**.

(A)

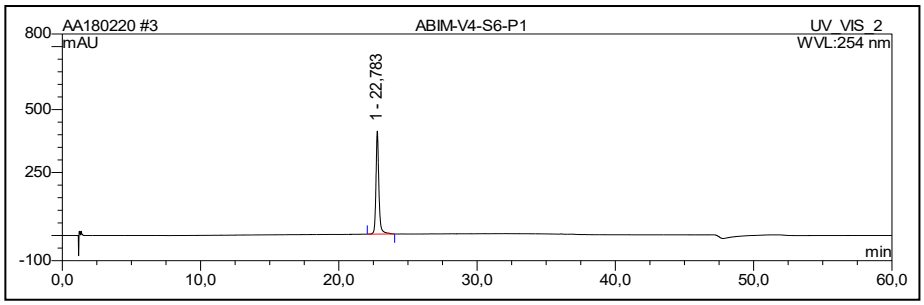

(B)

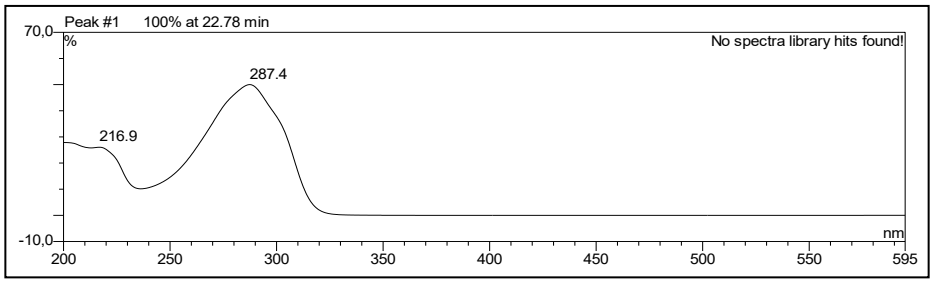

Figure S40. HPLC chromatogram (A) and UV spectrum (B) of compound **6**.

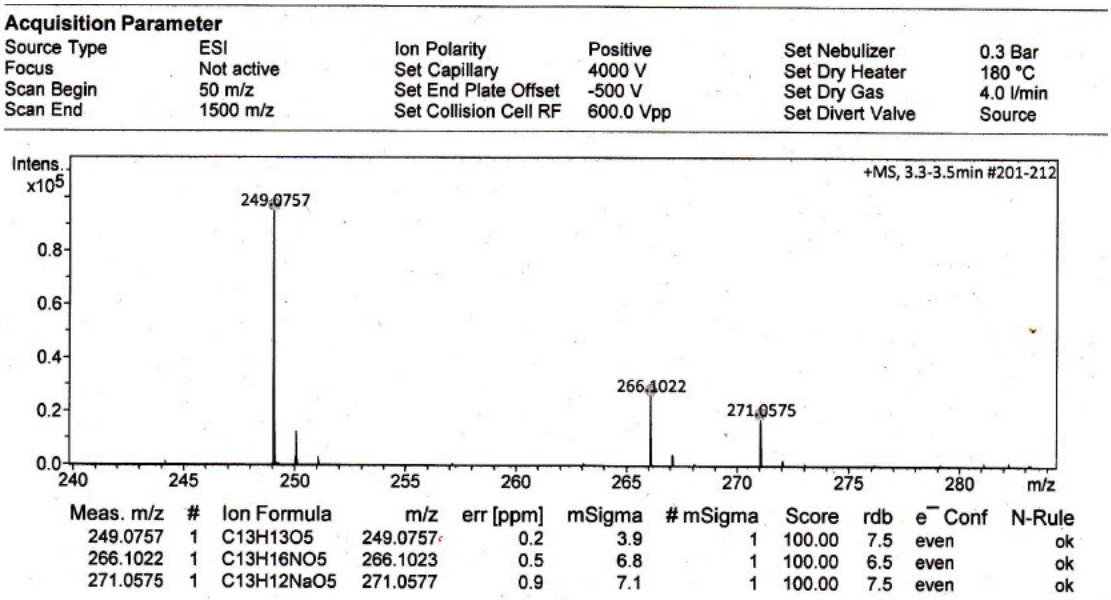

Figure S41. HRESIMS spectrum of compound **6**.

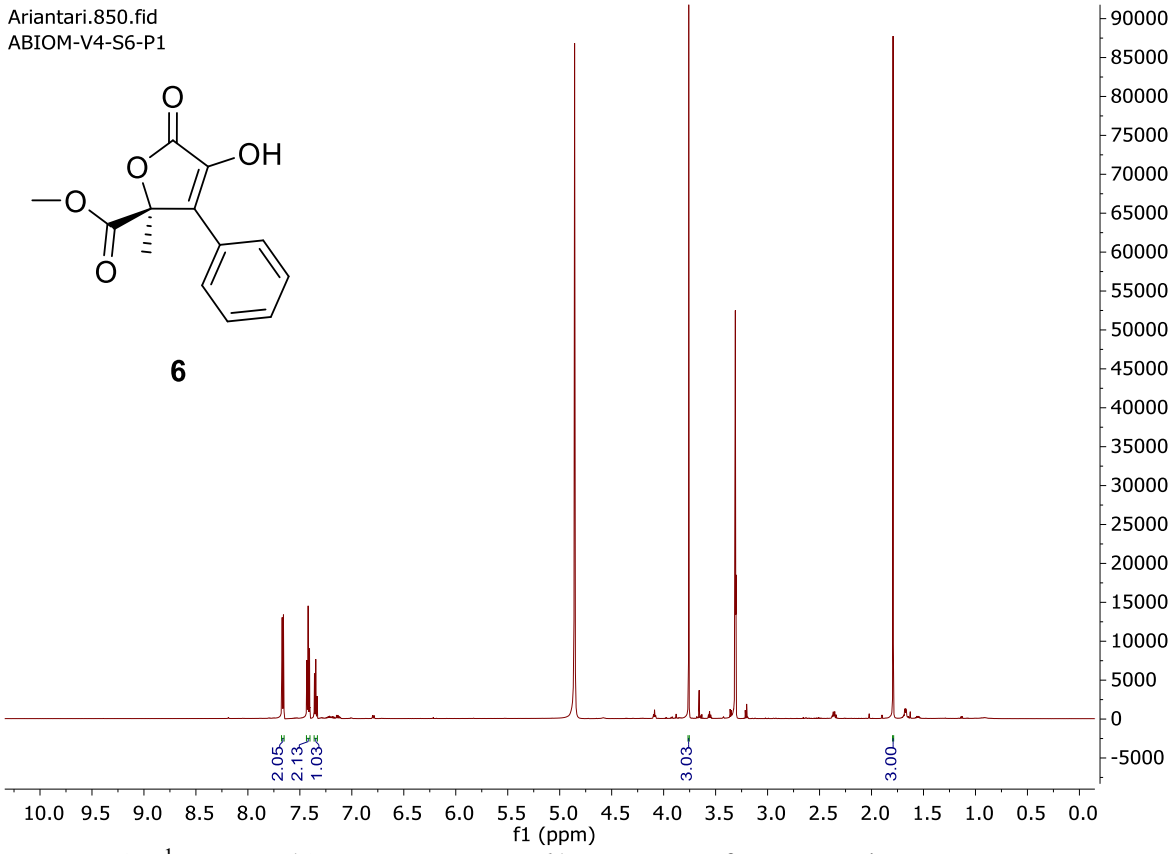

Figure S42. [1]H NMR (600 MHz, MeOH-d_4) spectrum of compound **6**.

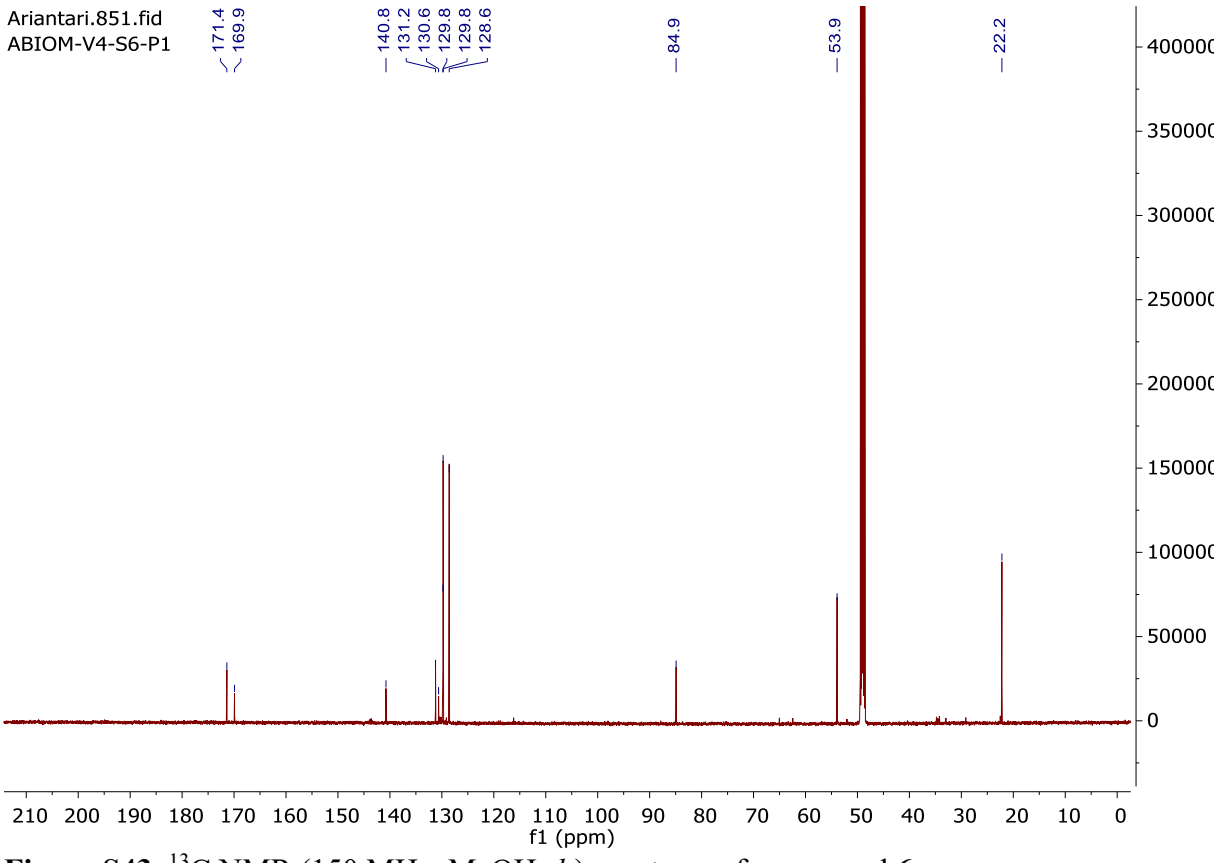

Figure S43. [13]C NMR (150 MHz, MeOH-d_4) spectrum of compound **6**.

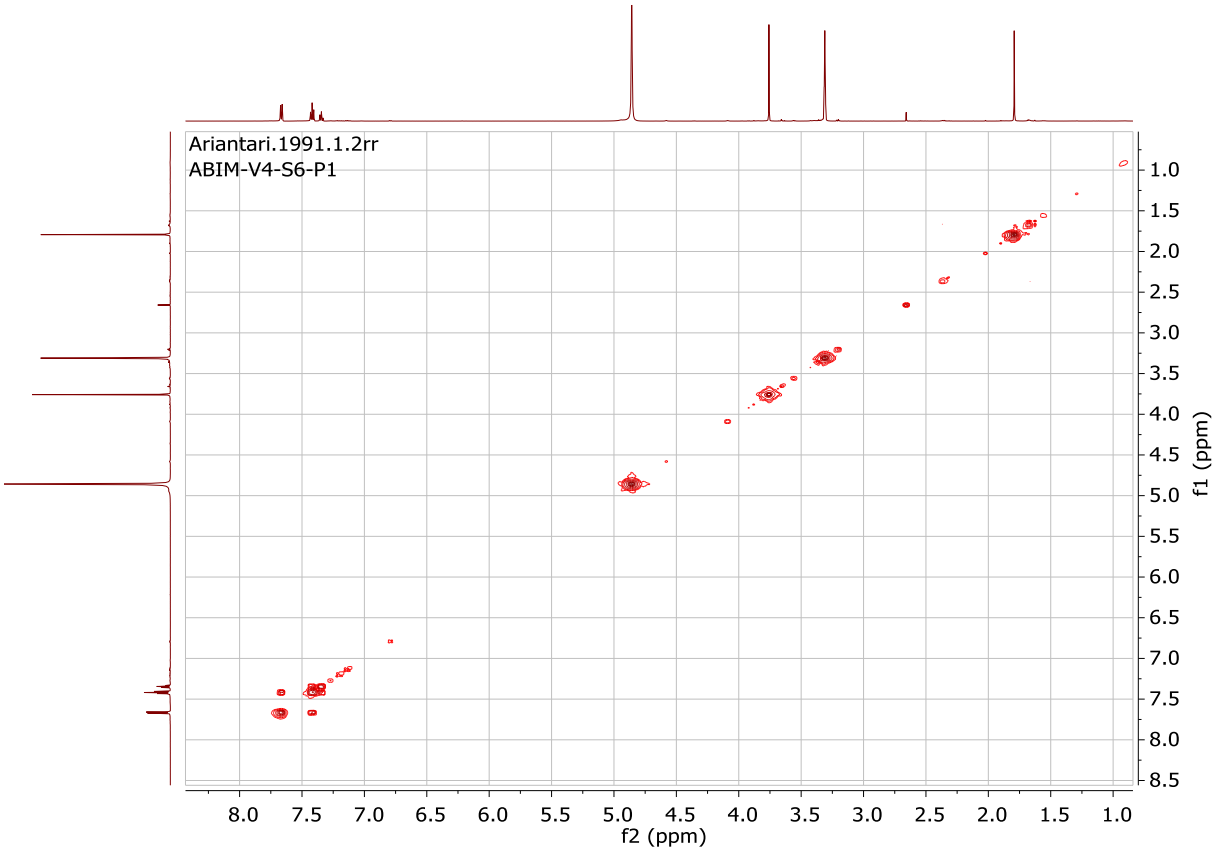

Figure S44. ^{1}H-^{1}H COSY (600 MHz, MeOH-d_4) spectrum of compound **6**.

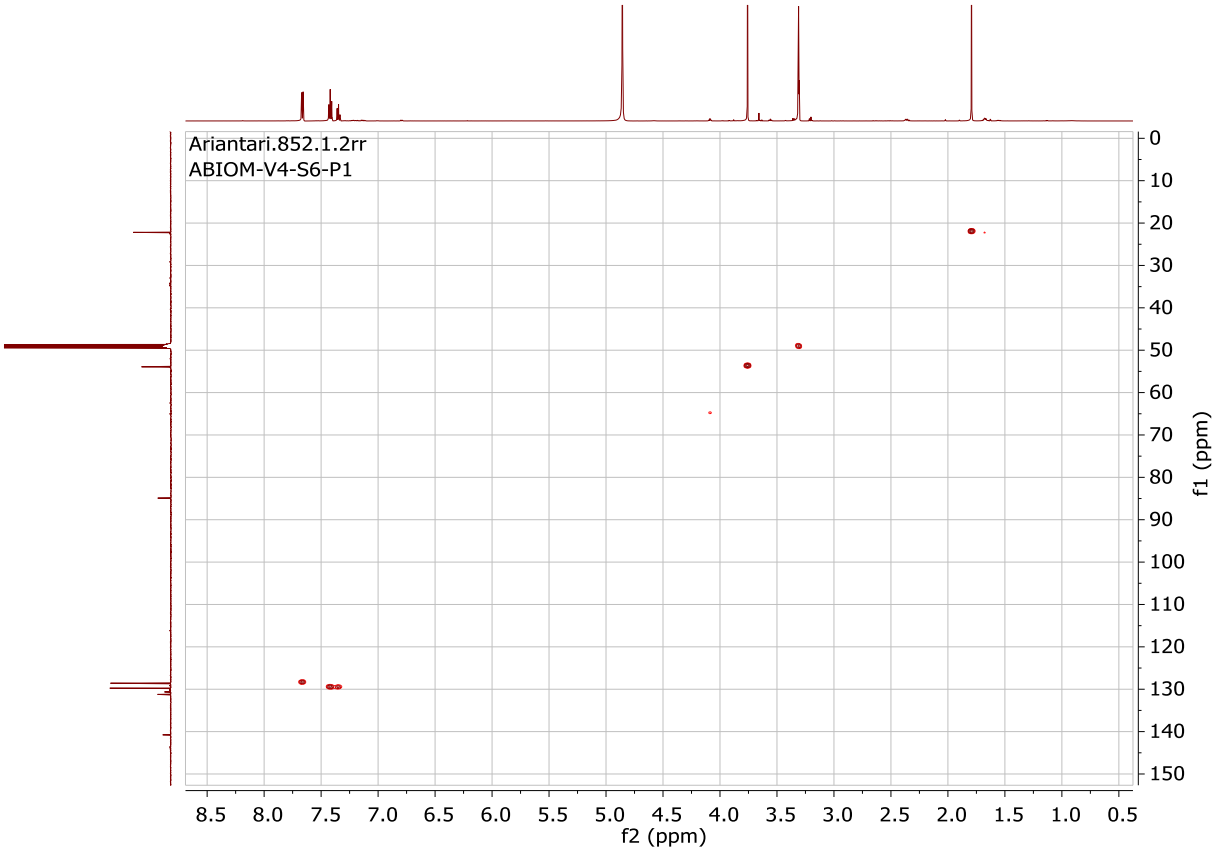

Figure S45. HSQC (600 and 150 MHz, MeOH-d_4) spectrum of compound **6**.

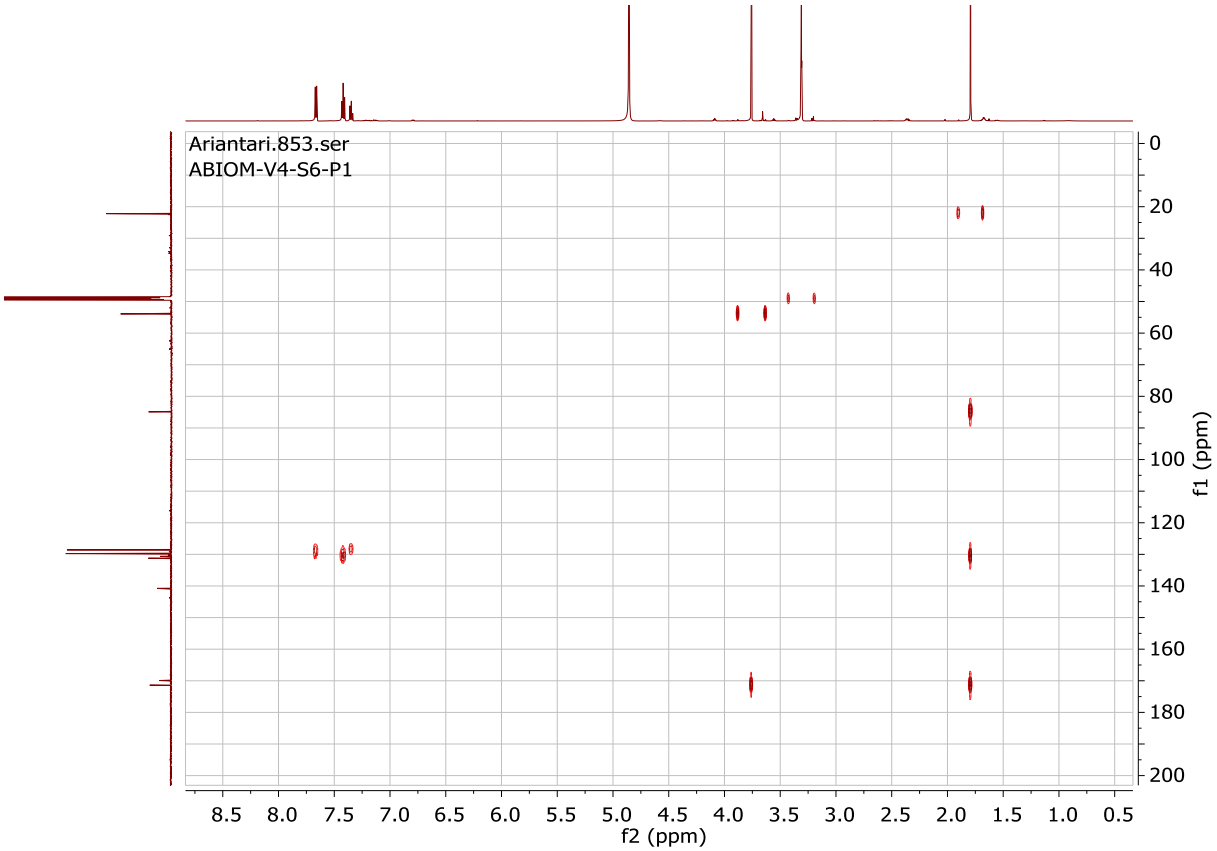

Figure S46. HMBC (600 and 150 MHz, MeOH-d_4) spectrum of compound **6**.

(A)

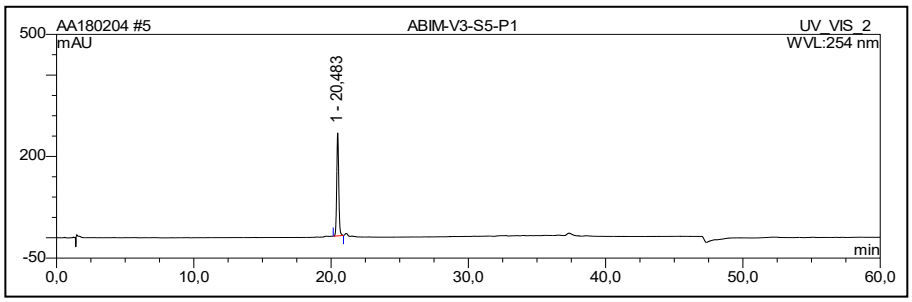

(B)

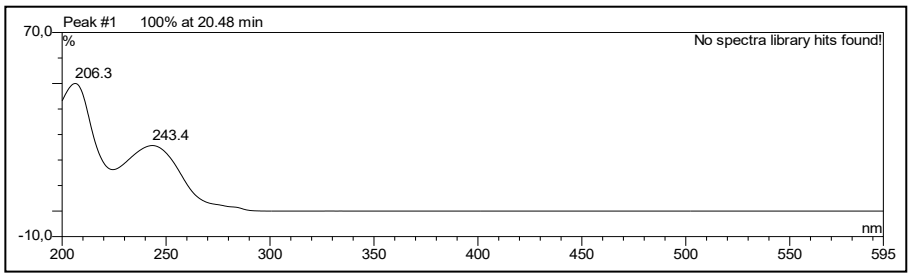

Figure S47. HPLC chromatogram (A) and UV spectrum (B) of compound **7**.

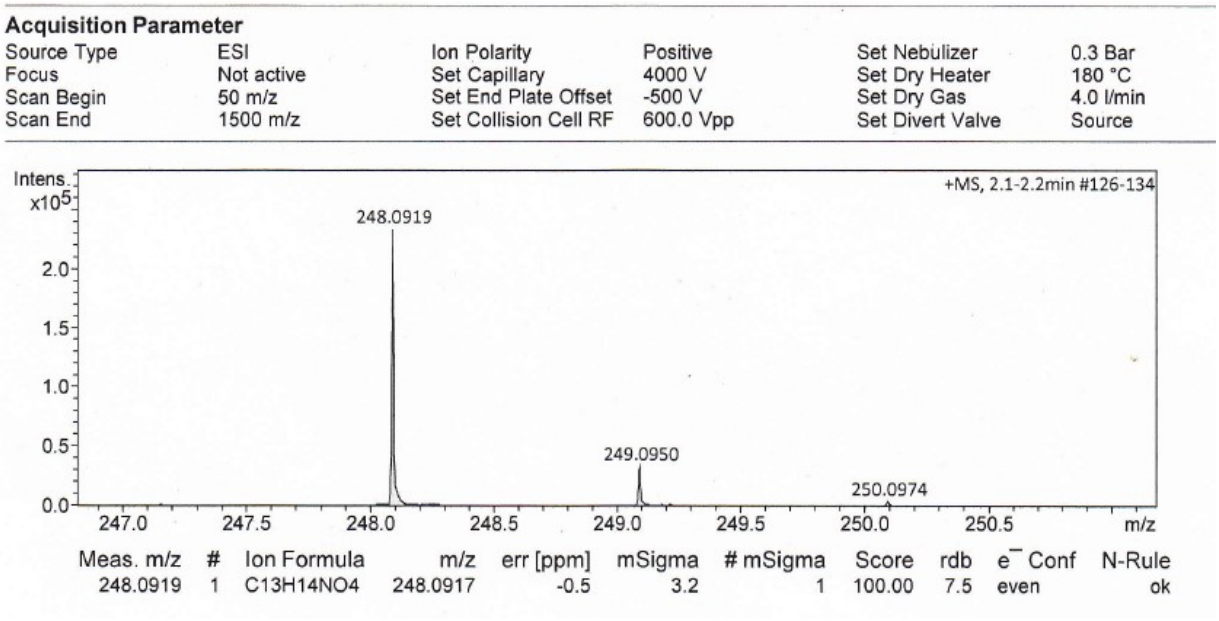

Figure S48. HRESIMS spectrum of compound **7**.

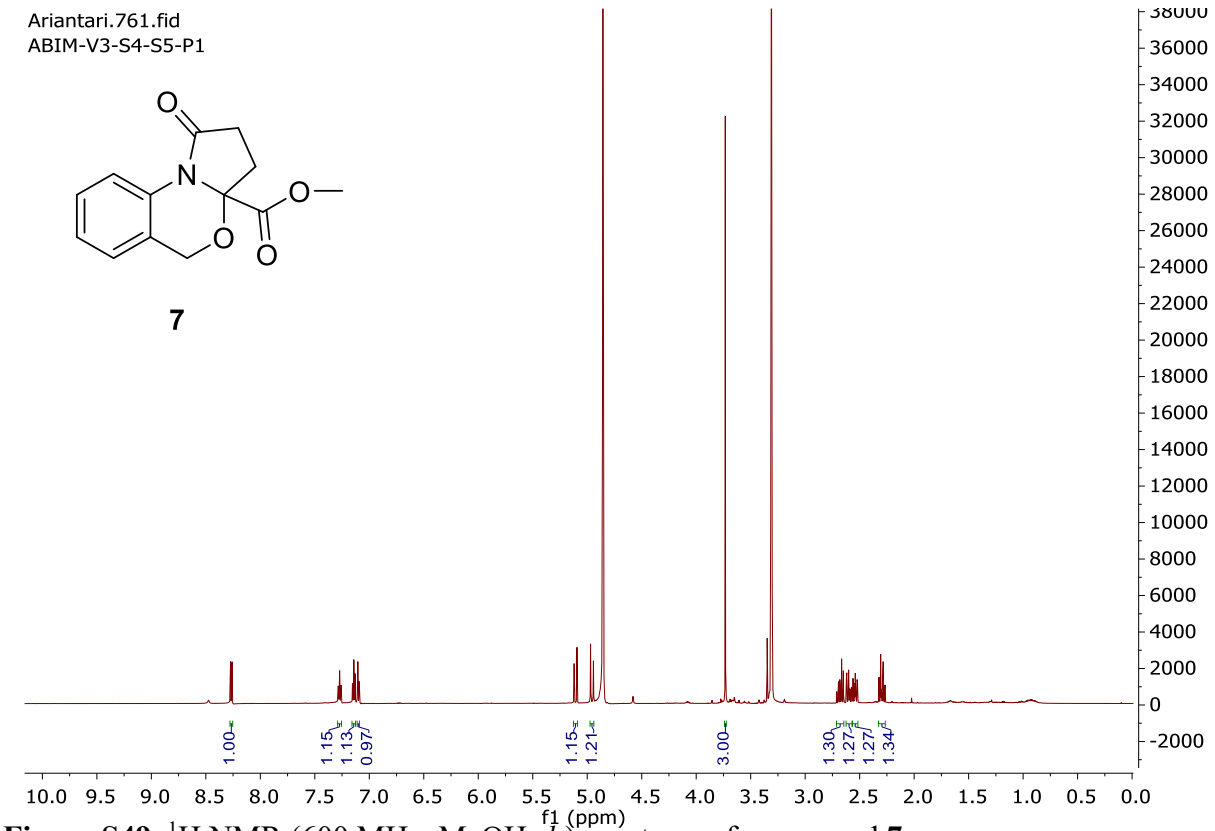

Figure S49. ^{1}H NMR (600 MHz, MeOH-d_4) spectrum of compound **7**.

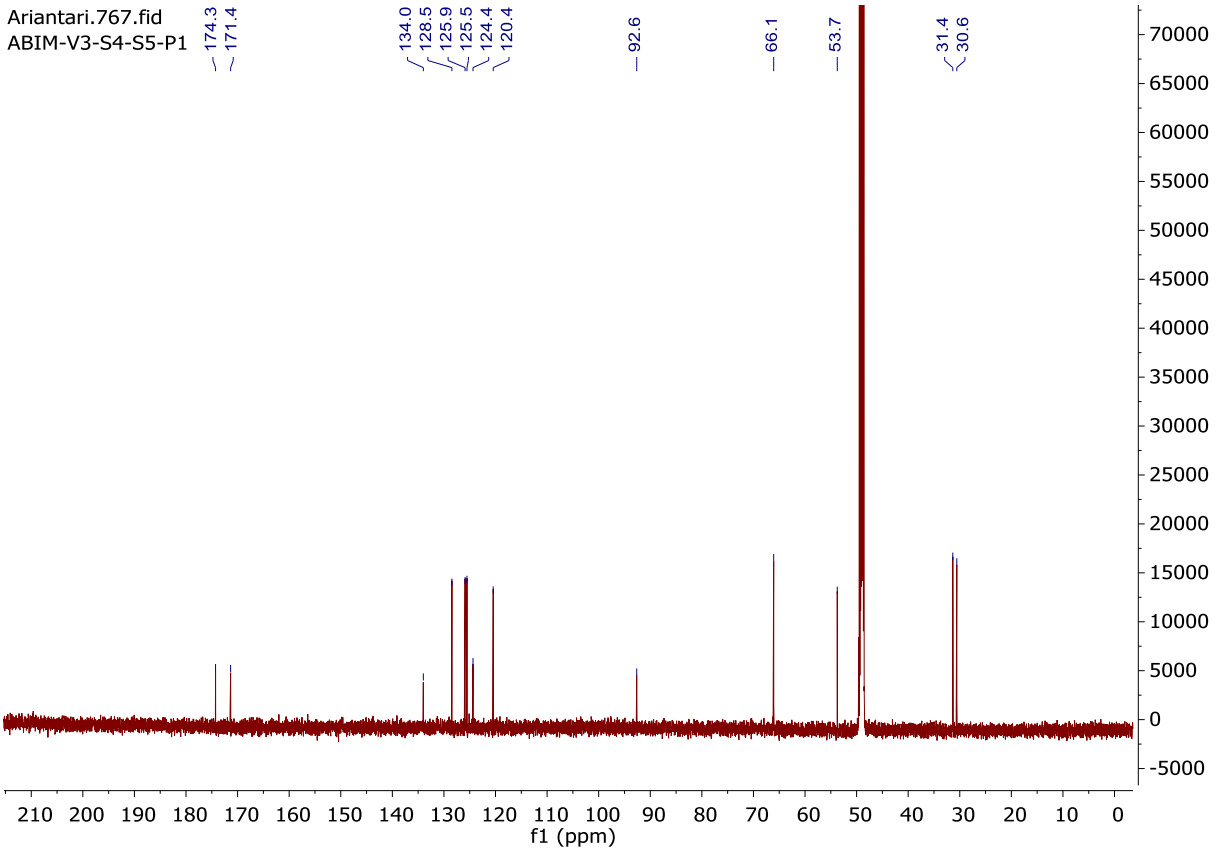

Figure S50. ^{13}C NMR (150 MHz, MeOH-d_4) spectrum of compound **7**.

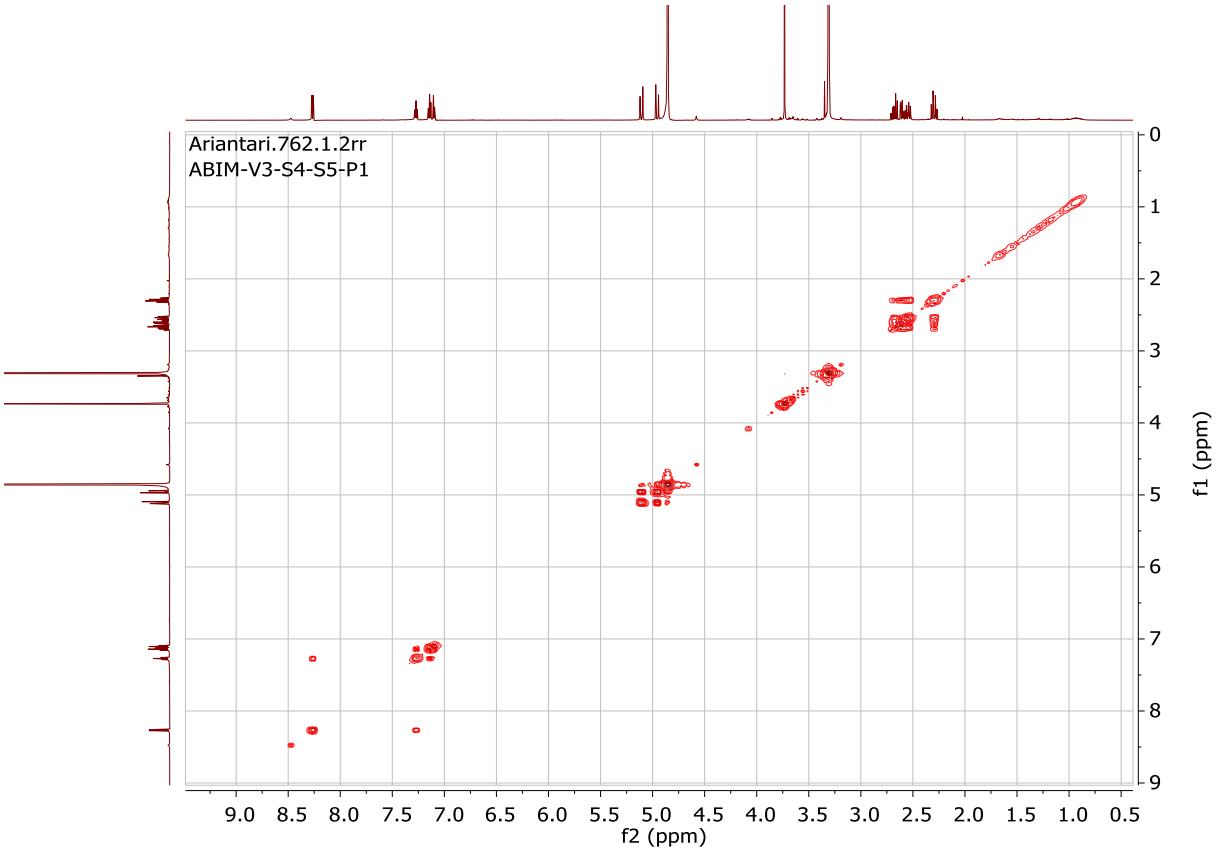

Figure S51. ^{1}H-^{1}H COSY (600 MHz, MeOH-d_4) spectrum of compound **7**.

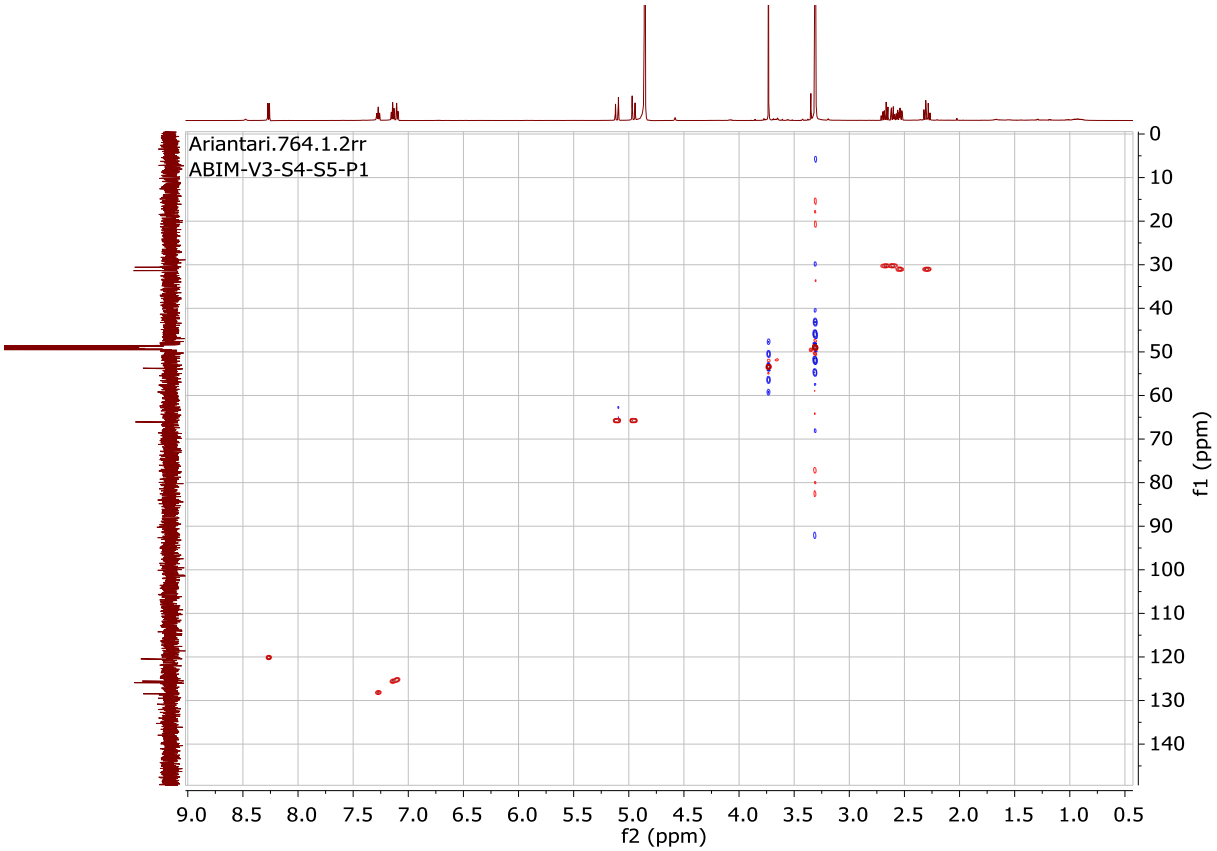

Figure S52. HSQC (600 and 150 MHz, MeOH-d_4) spectrum of compound **7**.

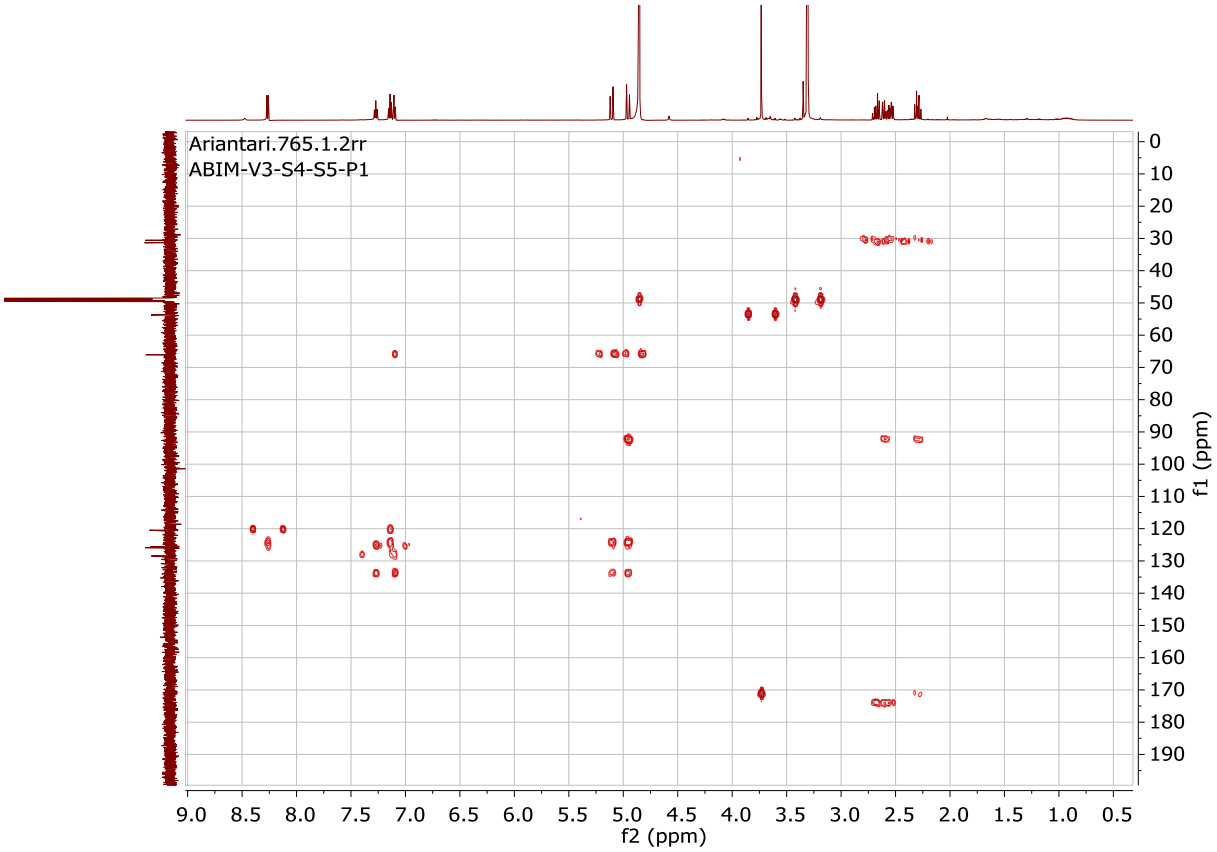

Figure S53. HMBC (600 and 150 MHz, MeOH-d_4) spectrum of compound **7**.

(A)

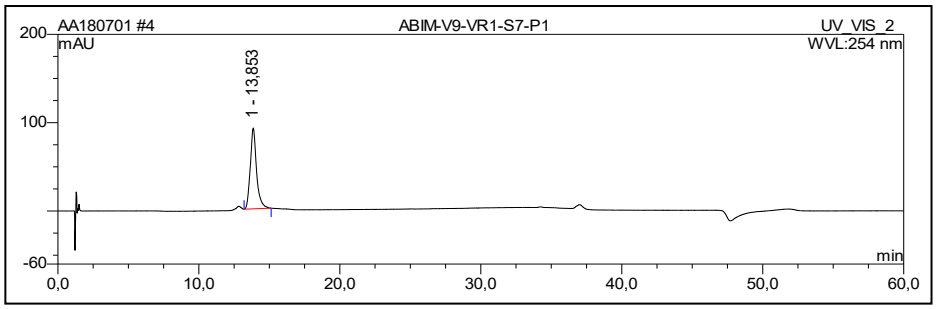

(B)

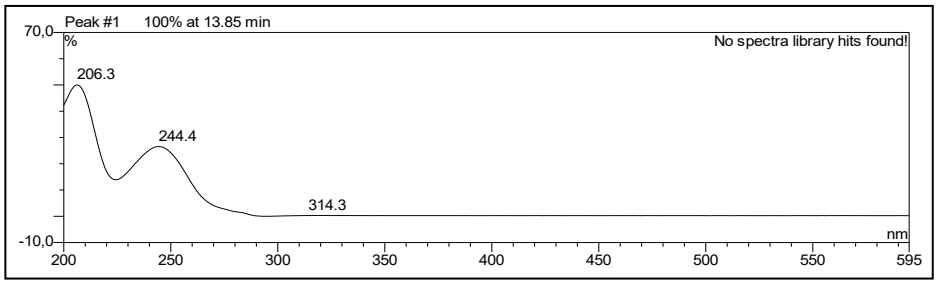

Figure S54. HPLC chromatogram (A) and UV spectrum (B) of compound **8**.

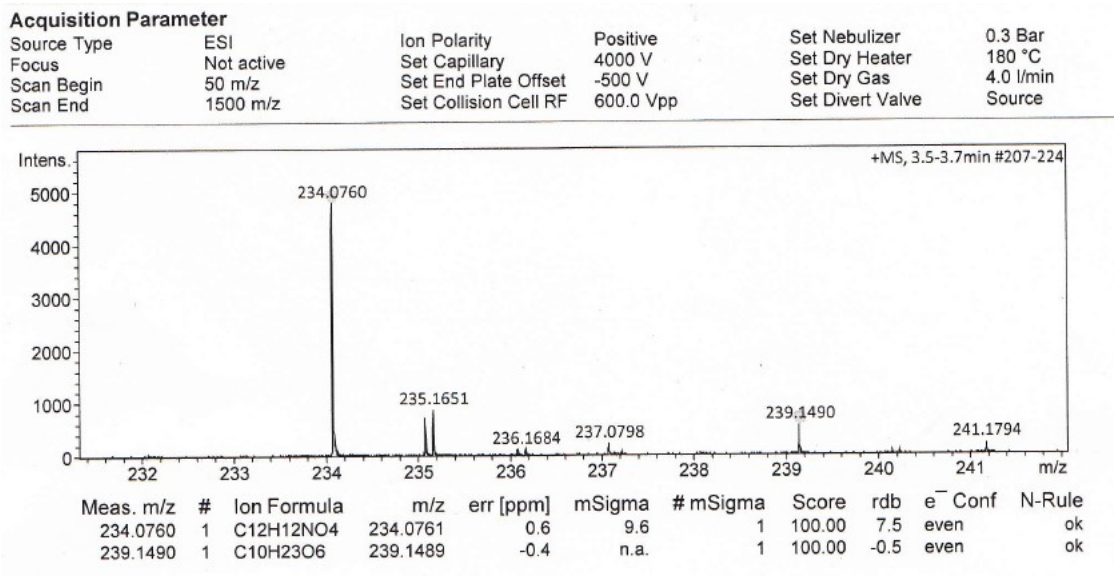

Figure S55. HRESIMS spectrum of compound **8**.

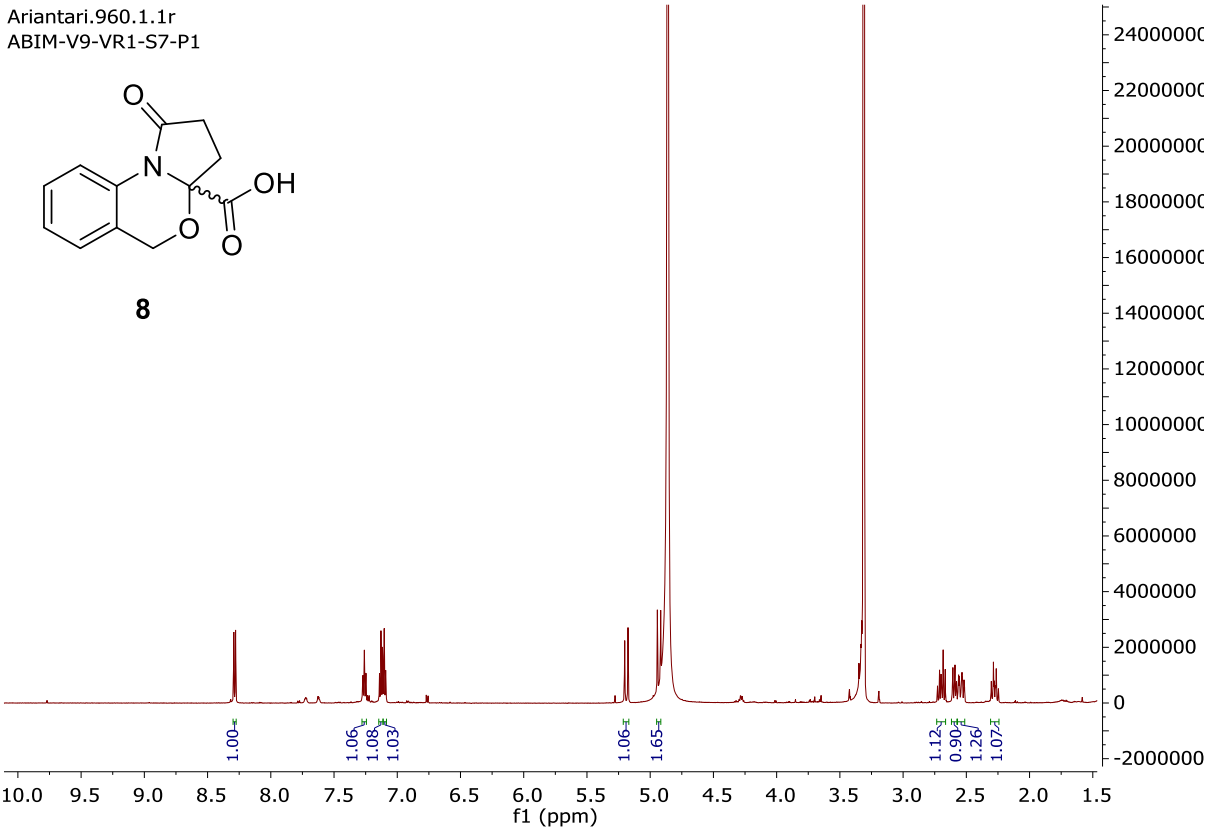

Figure S56. ^{1}H NMR (600 MHz, MeOH-d_4) spectrum of compound **8**.

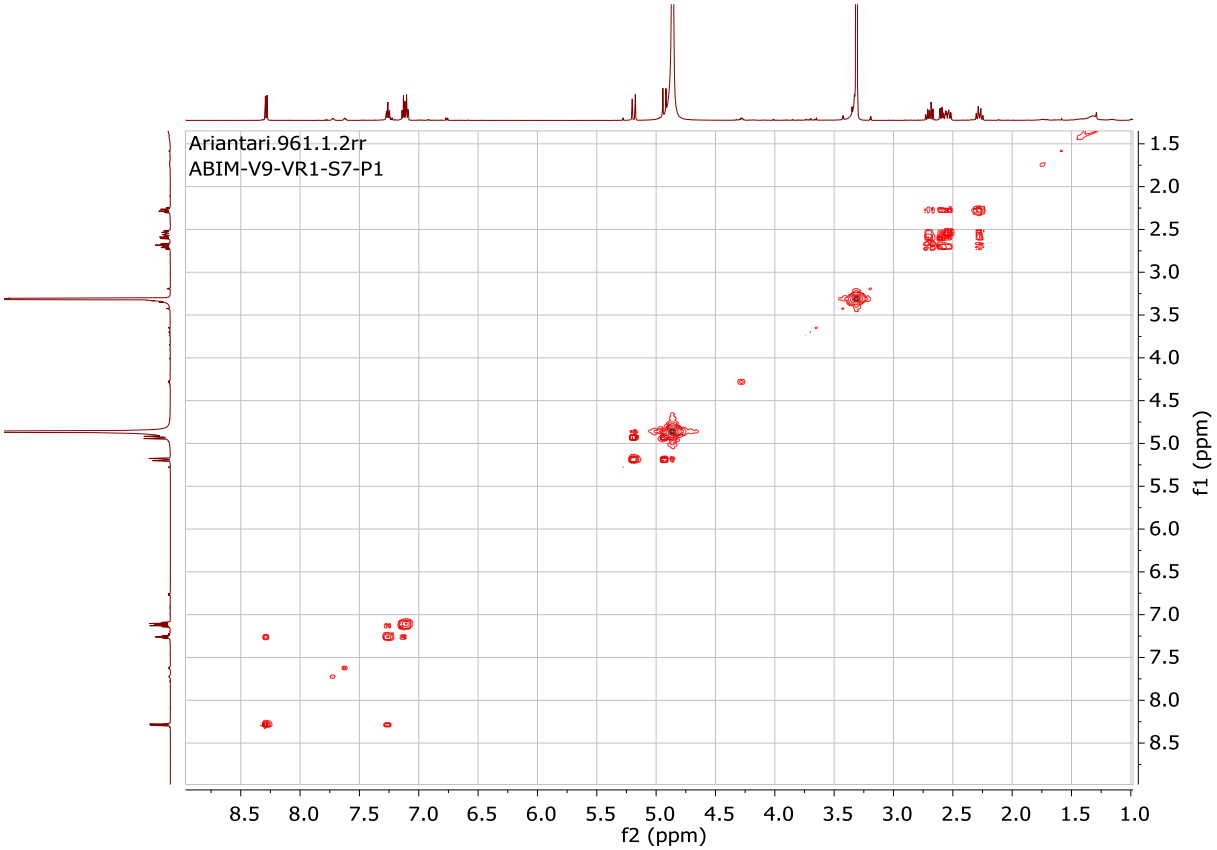

Figure S57. ^{1}H-^{1}H COSY (600 MHz, MeOH-d_4) spectrum of compound **8**.

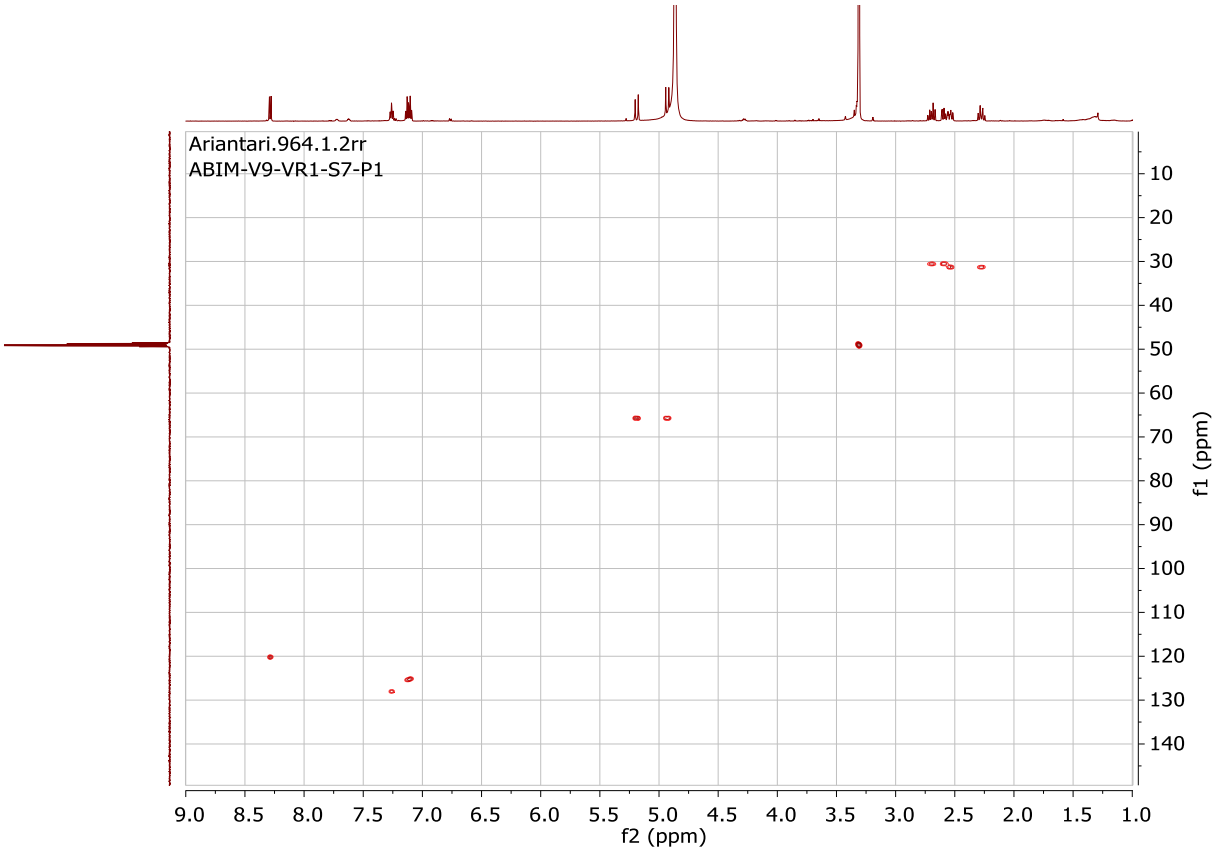

Figure S58. HSQC (600 and 150 MHz, MeOH-d_4) spectrum of compound **8**.

Figure S59. HMBC (600 and 150 MHz, MeOH-d_4) spectrum of compound **8**.

(A)

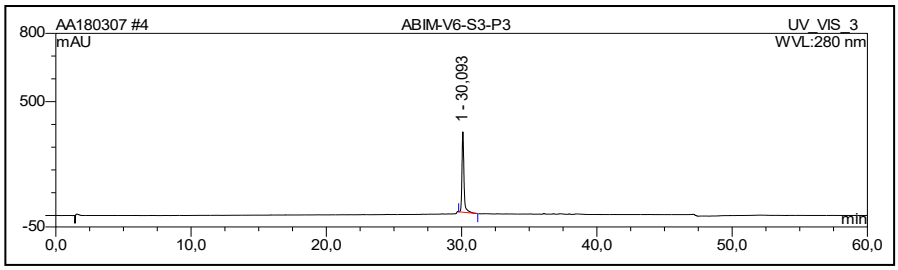

(B)

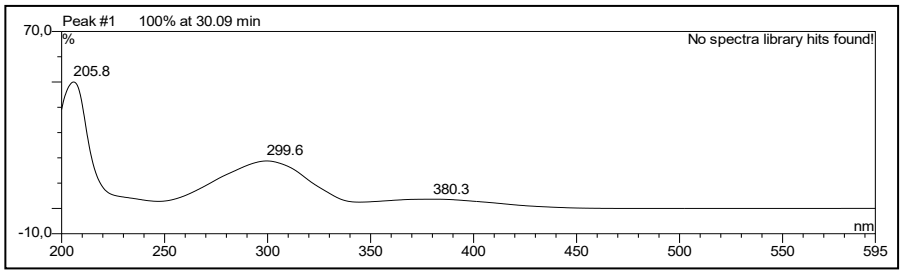

Figure S60. HPLC chromatogram (A) and UV spectrum (B) of compound **9**.

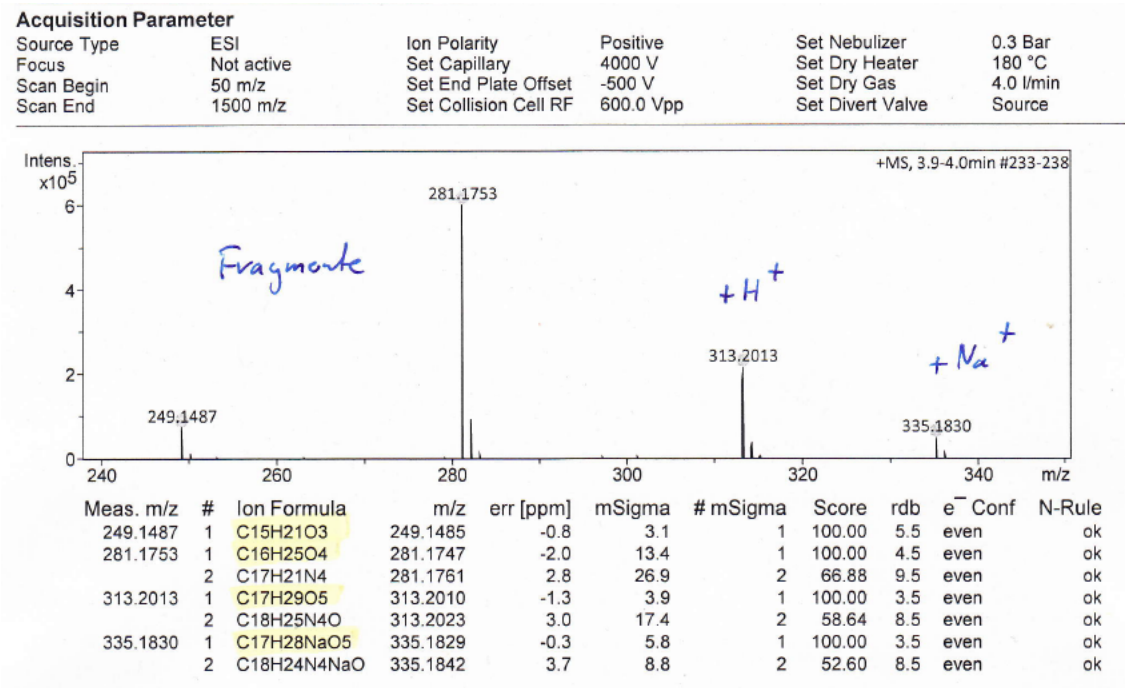

Figure S61. HRESIMS spectrum of compound **9**.

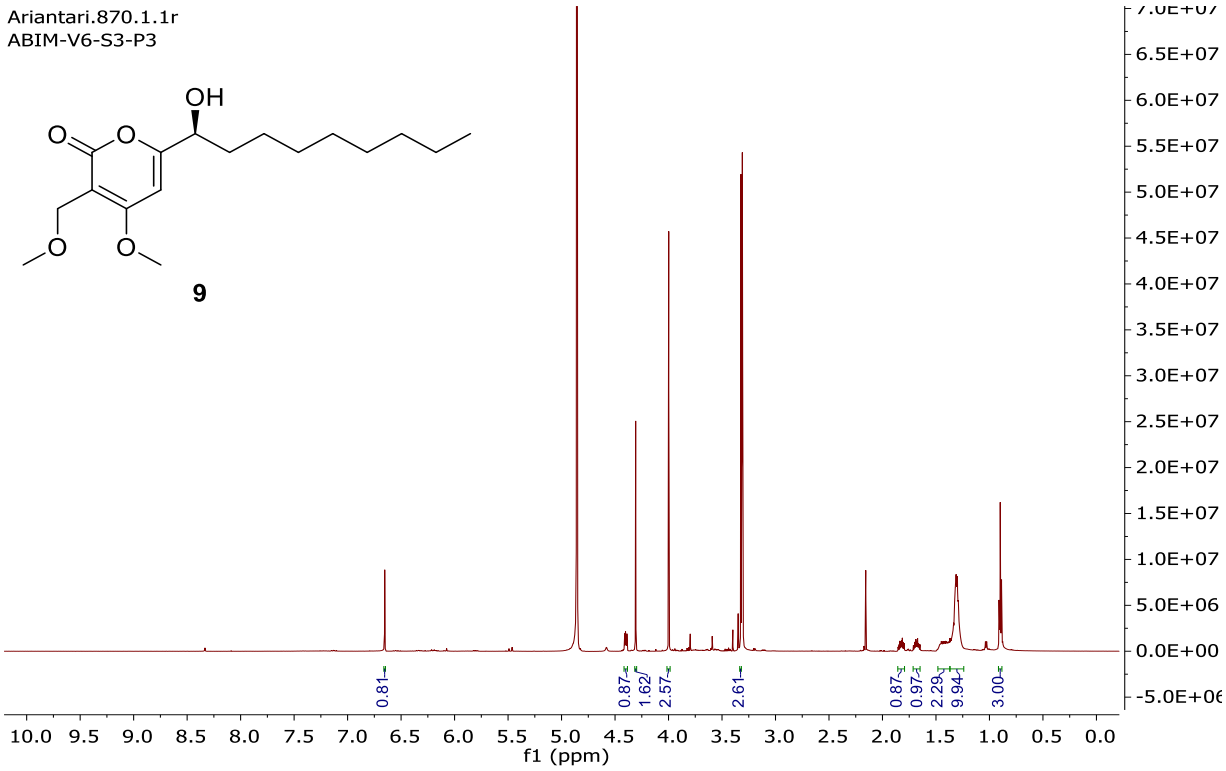

Figure S62. ^{1}H NMR (600 MHz, MeOH-d_4) spectrum of compound **9**.

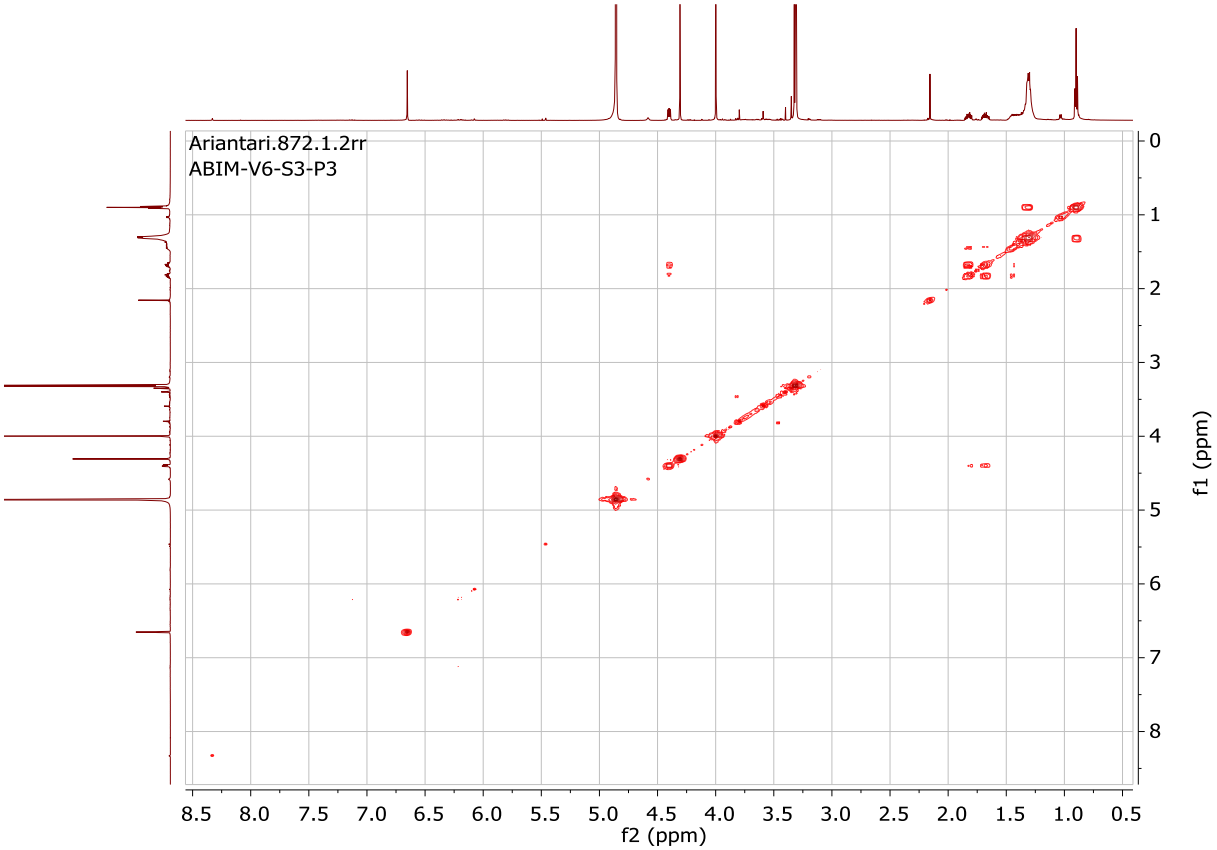

Figure S63. ^{1}H-^{1}H COSY (600 MHz, MeOH-d_4) spectrum of compound **9**.

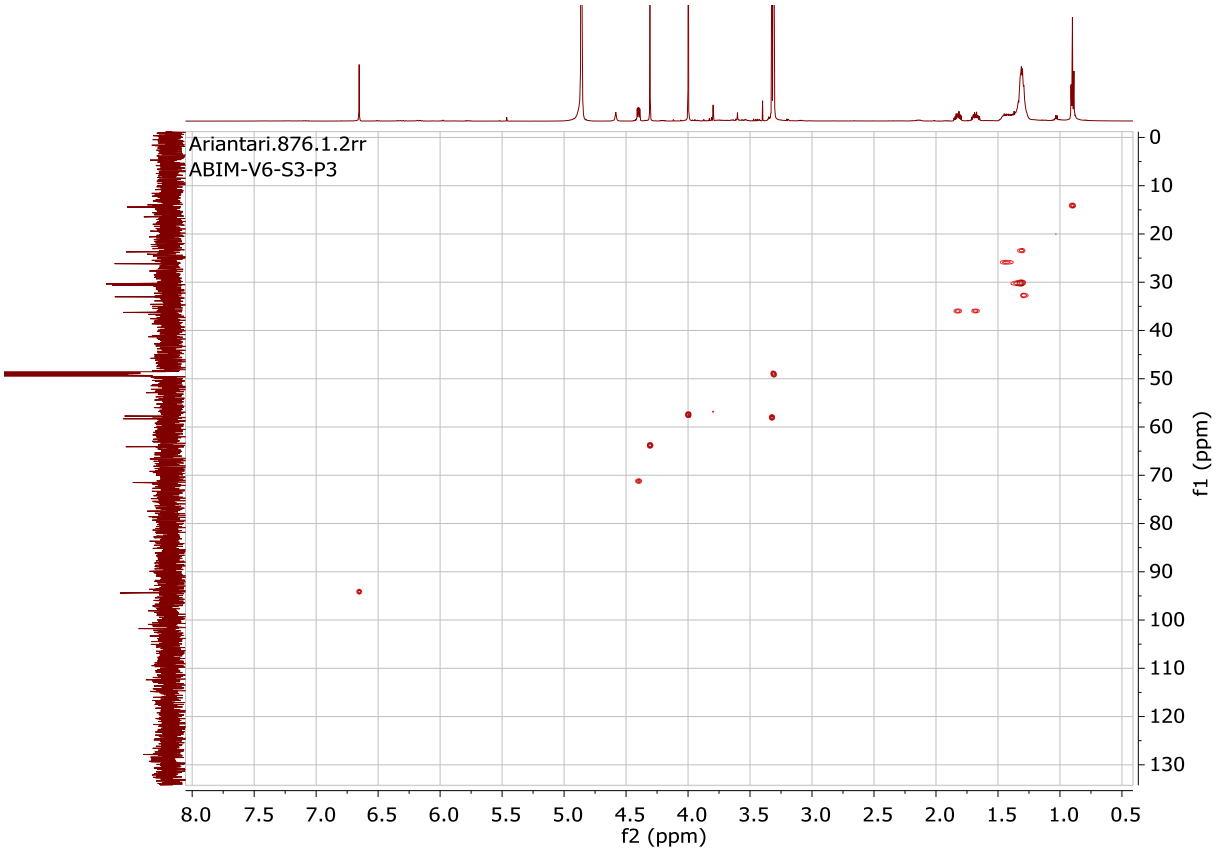

Figure S64. HSQC (600 and 150 MHz, MeOH-d_4) spectrum of compound **9**.

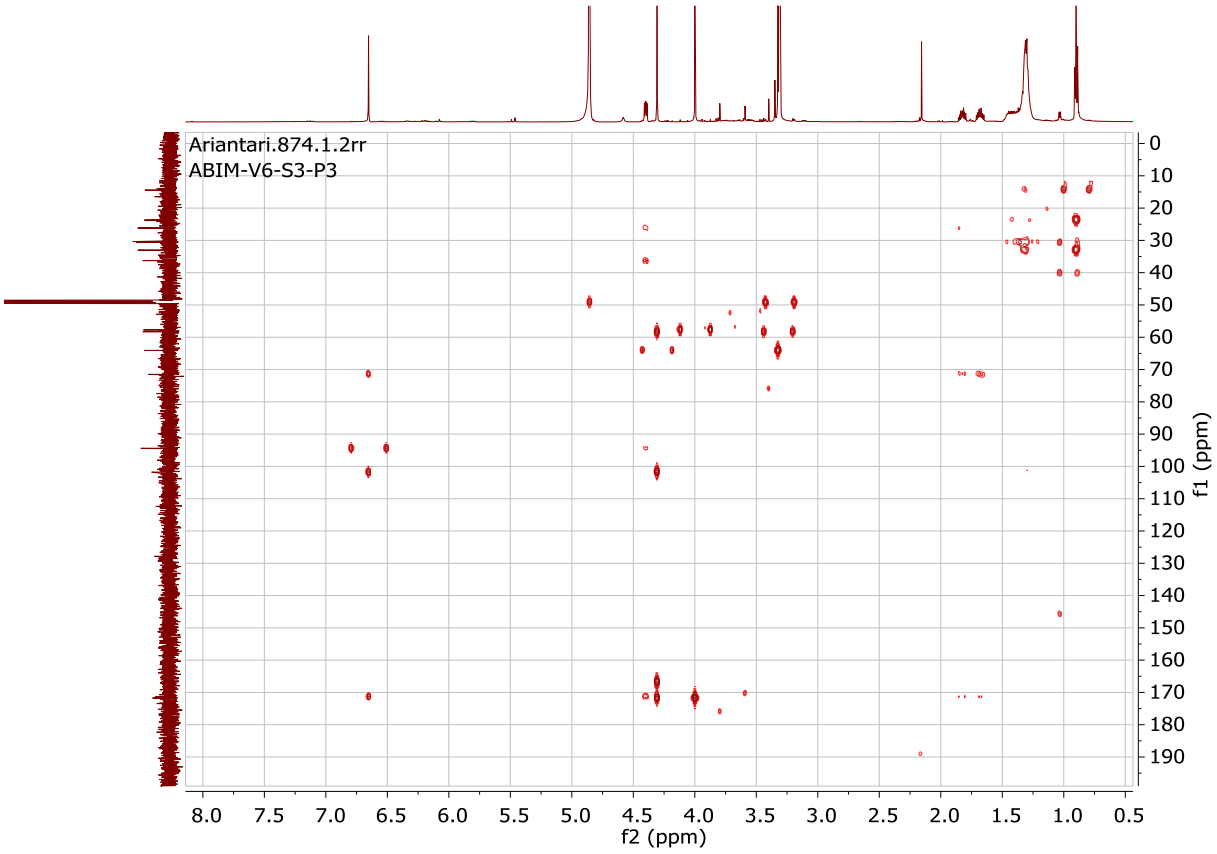

Figure S65. HMBC (600 and 150 MHz, MeOH-d_4) spectrum of compound **9**.

(A)

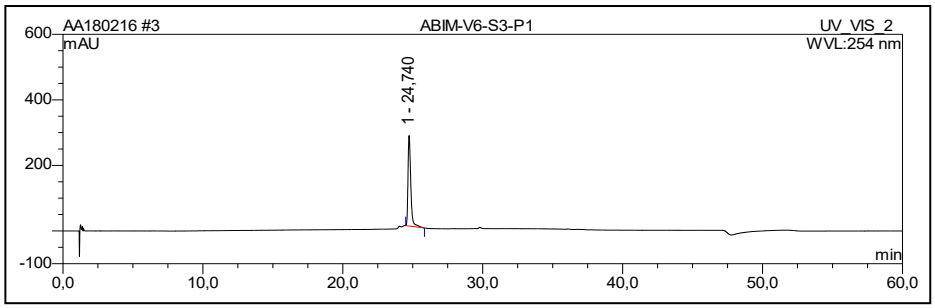

(B)

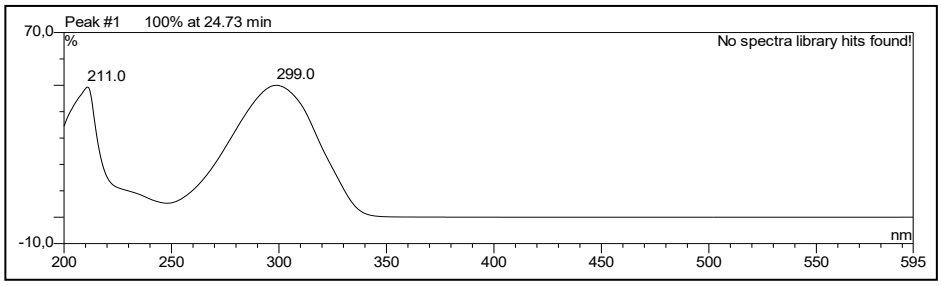

Figure S66. HPLC chromatogram (A) and UV spectrum (B) of compound **10**.

Acquisition Parameter

Source Type	ESI	Ion Polarity	Positive	Set Nebulizer	0.3 Bar
Focus	Not active	Set Capillary	4000 V	Set Dry Heater	180 °C
Scan Begin	50 m/z	Set End Plate Offset	-500 V	Set Dry Gas	4.0 l/min
Scan End	1500 m/z	Set Collision Cell RF	600.0 Vpp	Set Divert Valve	Source

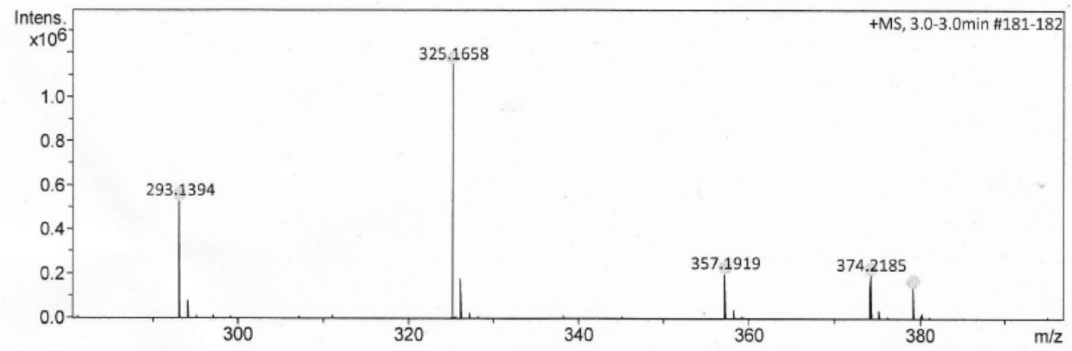

Meas. m/z	#	Ion Formula	m/z	err [ppm]	mSigma	# mSigma	Score	rdb	e⁻ Conf	N-Rule
293.1394	1	C16H21O5	293.1384	-3.6	13.4	1	89.06	6.5	even	ok
	2	C17H17N4O	293.1397	1.0	26.3	2	100.00	11.5	even	ok
325.1658	1	C17H25O6	325.1646	-3.7	18.5	1	78.77	5.5	even	ok
	2	C18H21N4O2	325.1659	0.4	31.6	2	100.00	10.5	even	ok
357.1919	1	C18H29O7	357.1908	-3.2	0.7	1	76.93	4.5	even	ok
	2	C19H25N4O3	357.1921	0.5	14.1	2	100.00	9.5	even	ok
374.2185	1	C18H32NO7	374.2173	-3.1	8.1	1	78.34	3.5	even	ok
	2	C19H28N5O3	374.2187	0.5	21.5	2	100.00	8.5	even	ok
379.1739	1	C18H28NaO7	379.1727	-3.1	2.4	1	76.65	4.5	even	ok
	2	C19H24N4NaO3	379.1741	0.4	16.1	2	100.00	9.5	even	ok

Figure S67. HRESIMS spectrum of compound **10**.

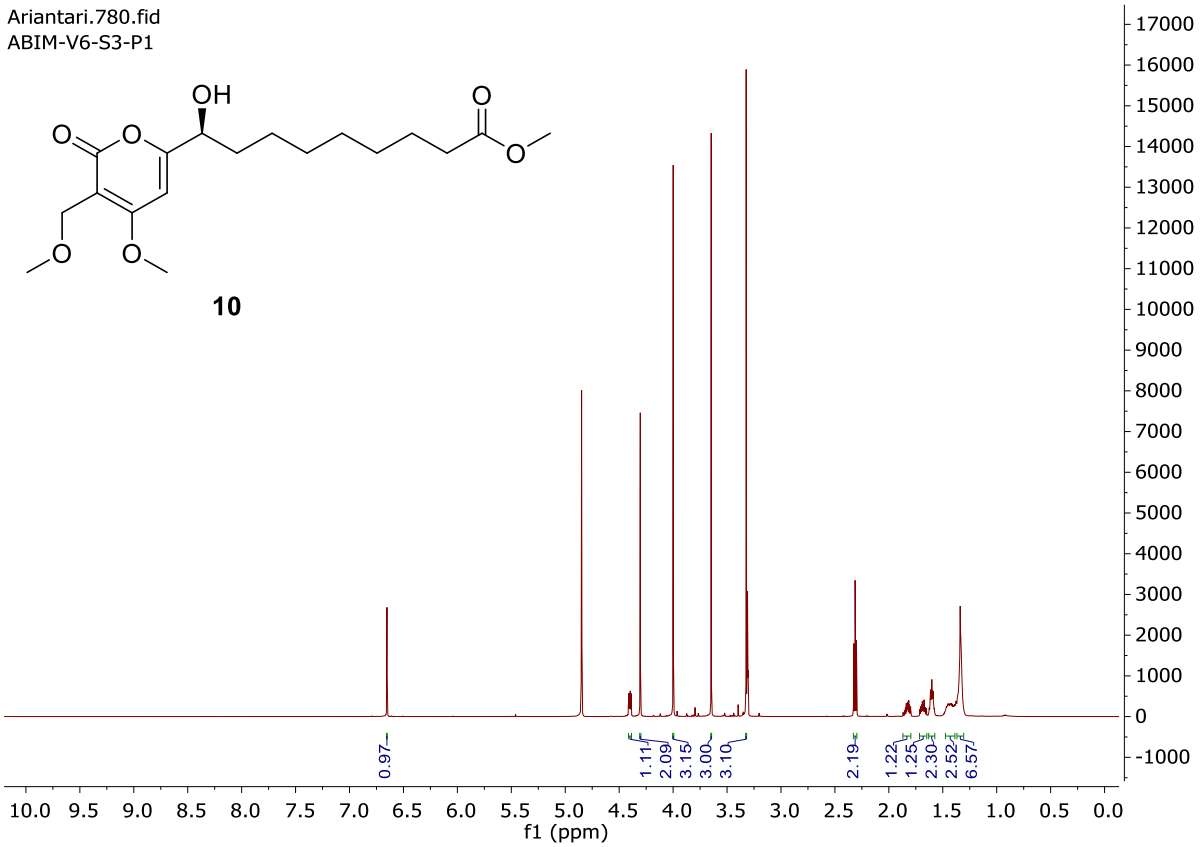

Figure S68. [1]H NMR (600 MHz, MeOH-d_4) spectrum of compound **10**.

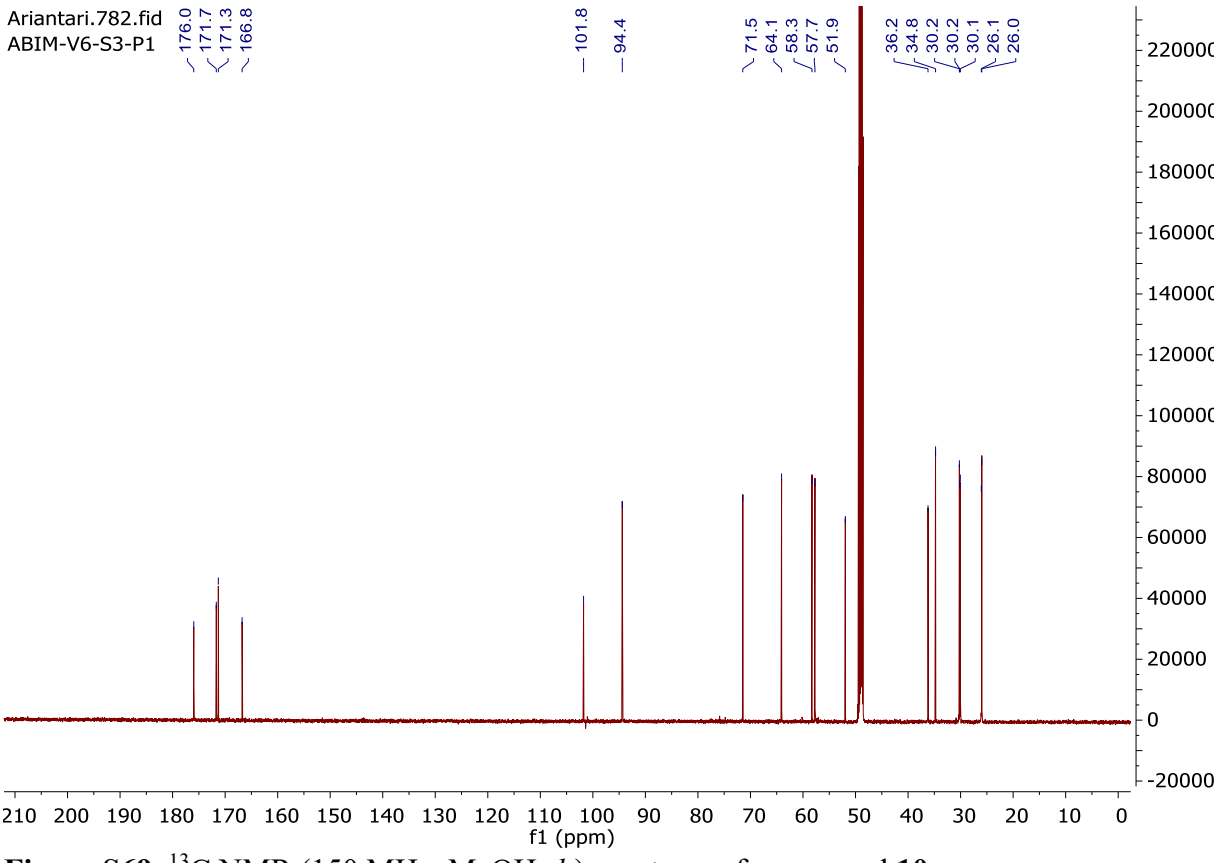

Figure S69. [13]C NMR (150 MHz, MeOH-d_4) spectrum of compound **10**.

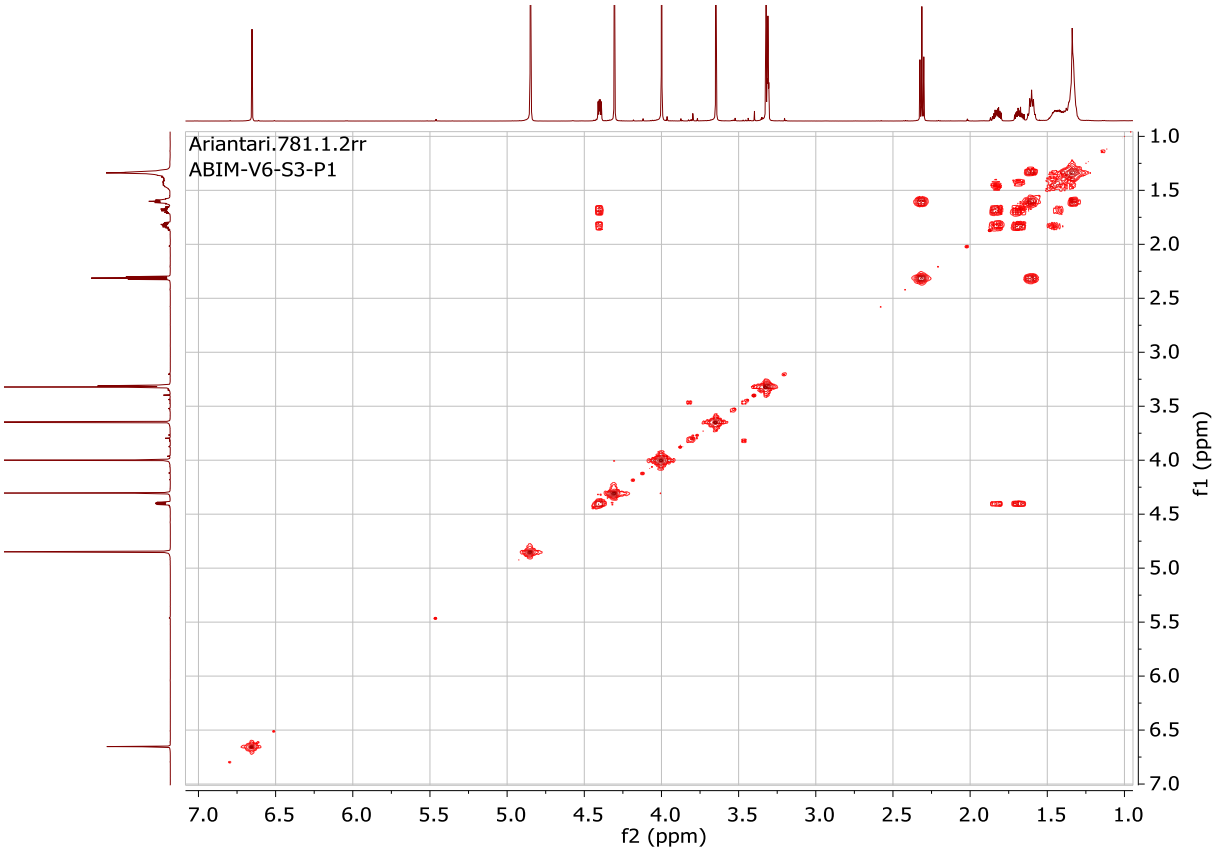

Figure S70. ^{1}H-^{1}H COSY (600 MHz, MeOH-d_4) spectrum of compound **10**.

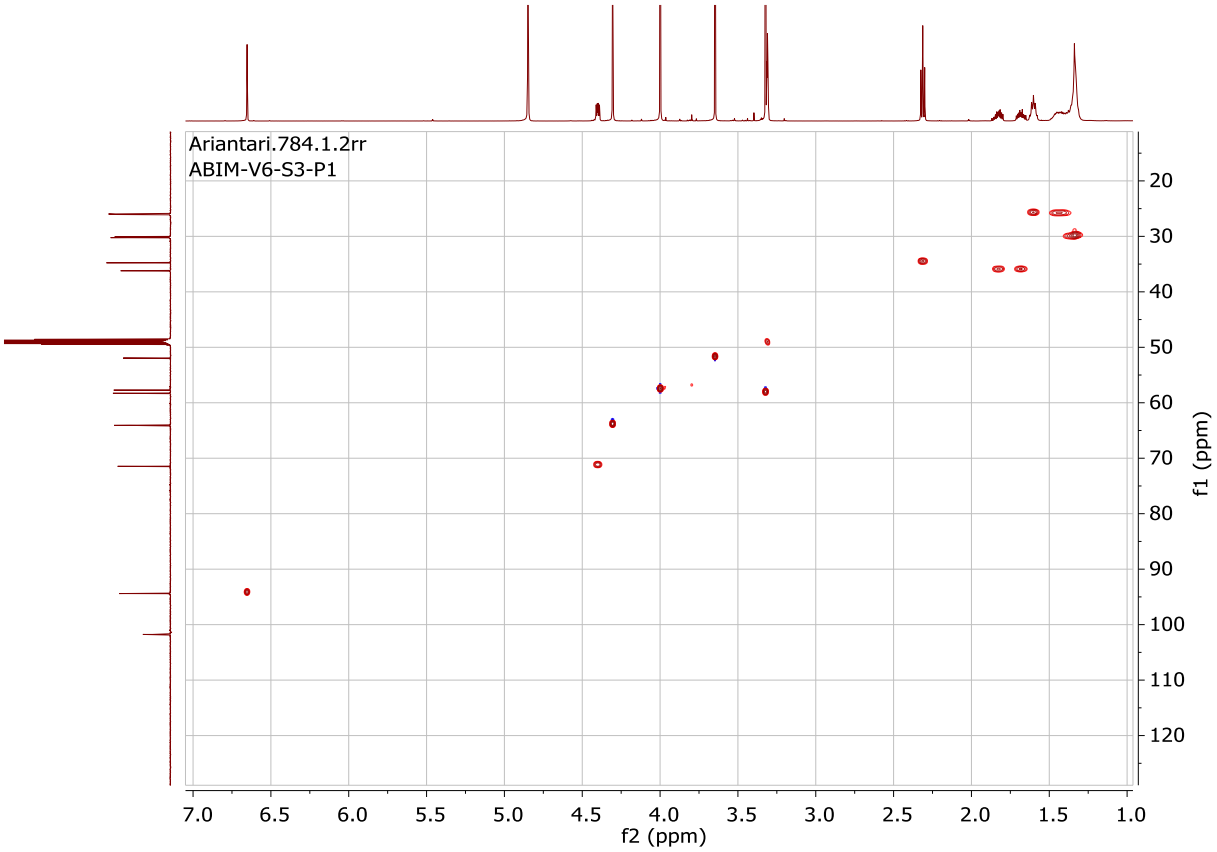

Figure S71. HSQC (600 and 150 MHz, MeOH-d_4) spectrum of compound **10**.

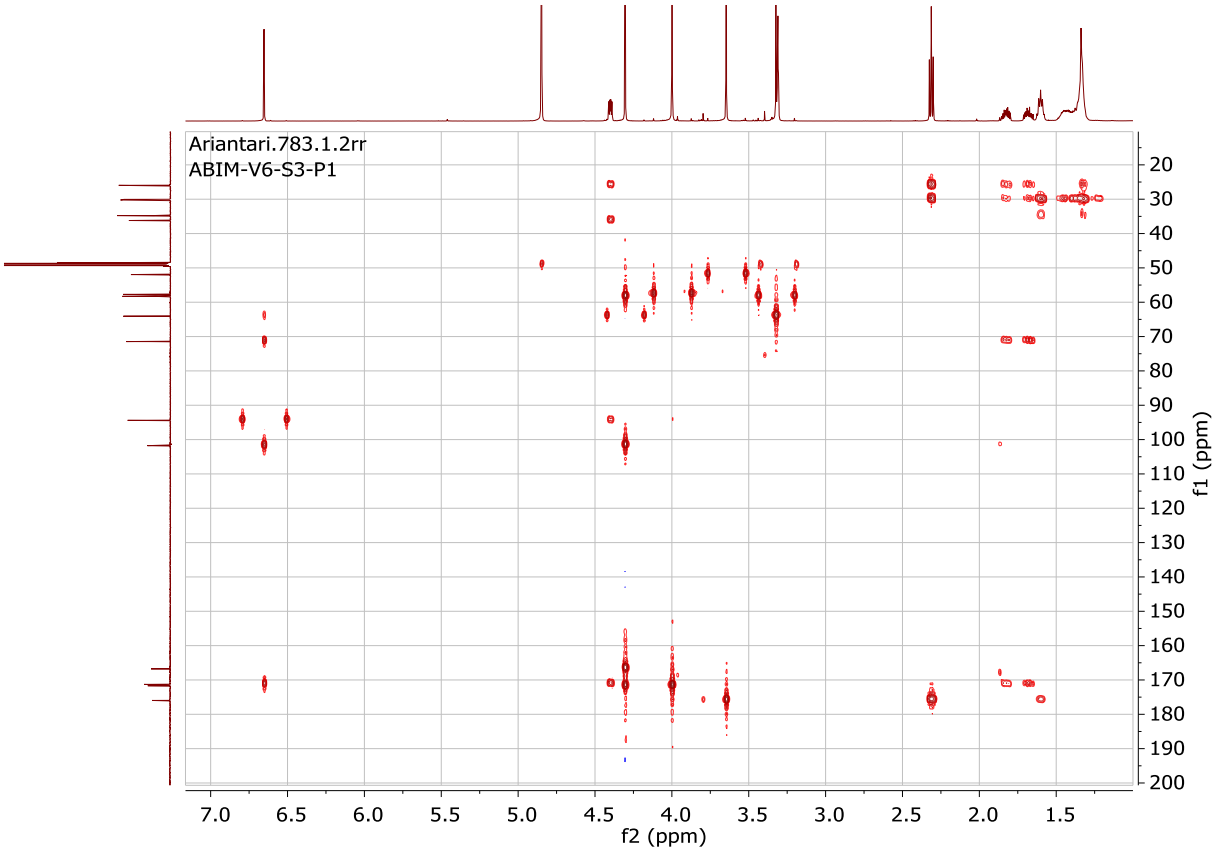

Figure S72. HMBC (600 and 150 MHz, MeOH-d_4) spectrum of compound **10**.

(A)

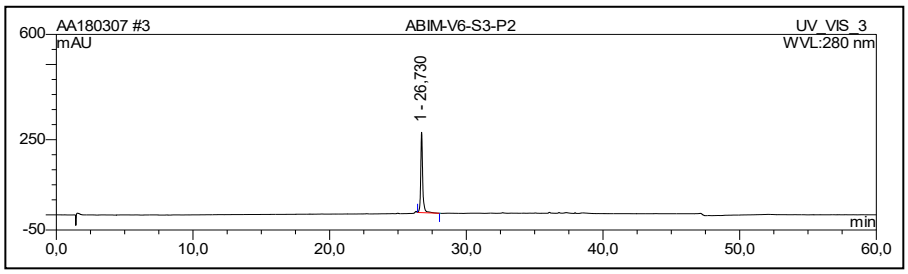

(B)

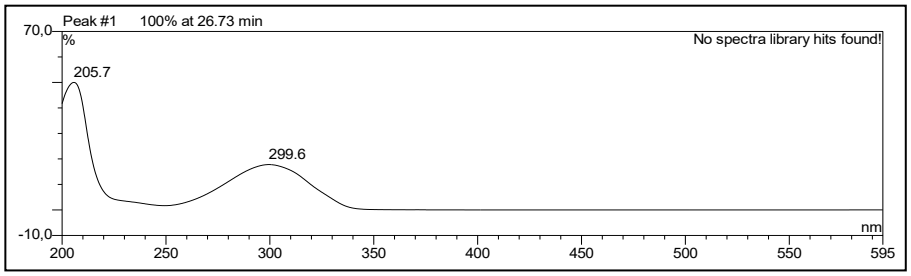

Figure S73. HPLC chromatogram (A) and UV spectrum (B) of compound **11**.

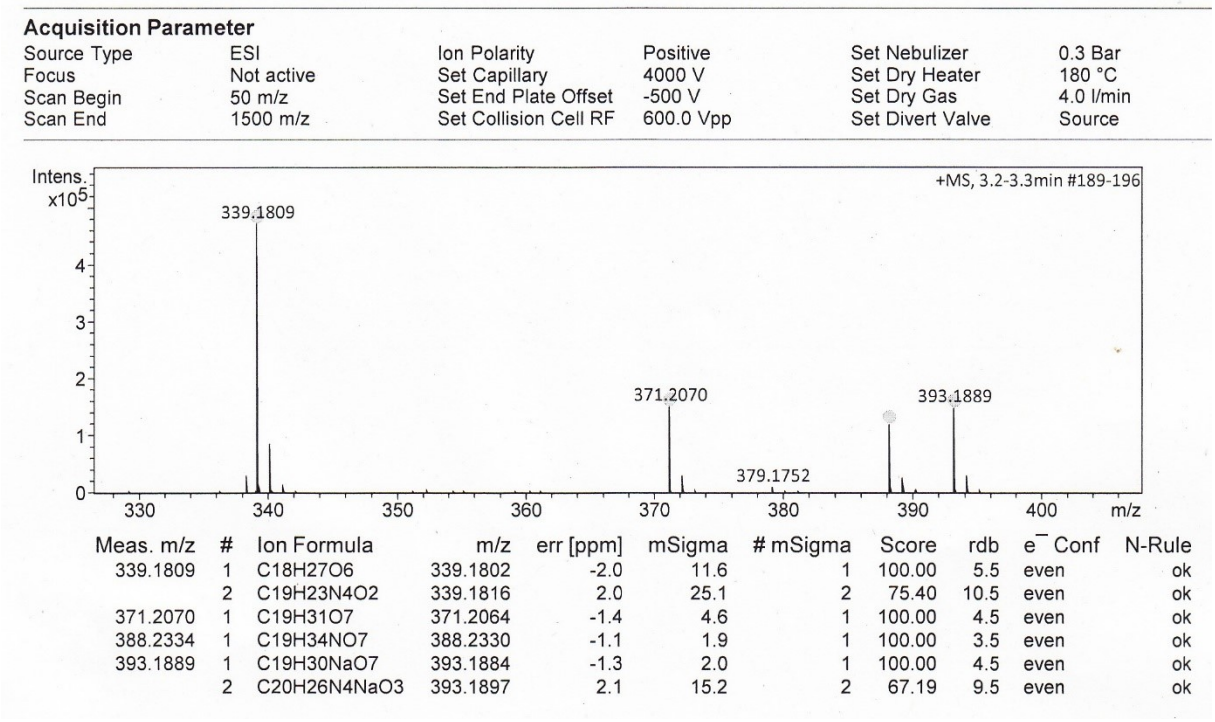

Meas. m/z	#	Ion Formula	m/z	err [ppm]	mSigma	# mSigma	Score	rdb	e⁻ Conf	N-Rule
339.1809	1	C18H27O6	339.1802	-2.0	11.6	1	100.00	5.5	even	ok
	2	C19H23N4O2	339.1816	2.0	25.1	2	75.40	10.5	even	ok
371.2070	1	C19H31O7	371.2064	-1.4	4.6	1	100.00	4.5	even	ok
388.2334	1	C19H34NO7	388.2330	-1.1	1.9	1	100.00	3.5	even	ok
393.1889	1	C19H30NaO7	393.1884	-1.3	2.0	1	100.00	4.5	even	ok
	2	C20H26N4NaO3	393.1897	2.1	15.2	2	67.19	9.5	even	ok

Figure S74. HRESIMS spectrum of compound **11**.

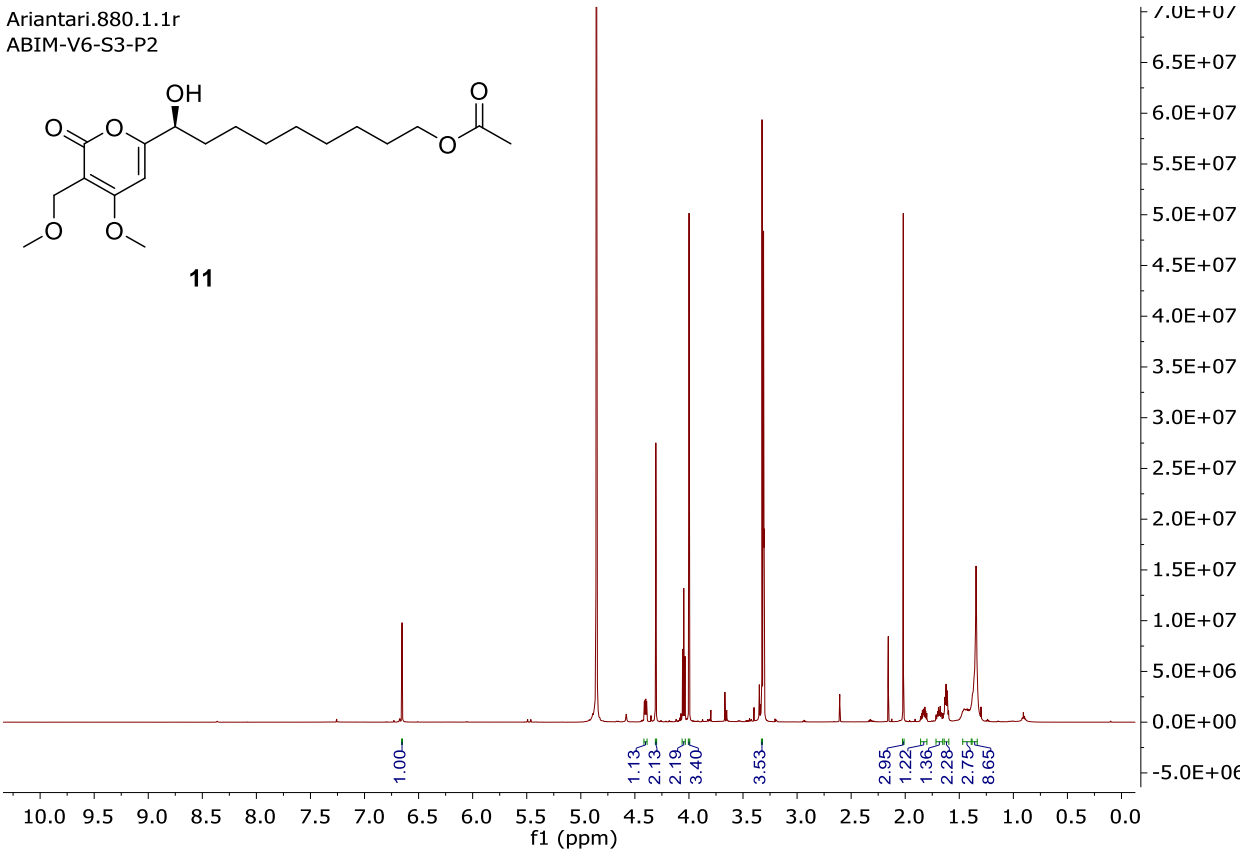

Figure S75. ^{1}H NMR (600 MHz, MeOH-d_4) spectrum of compound **11**.

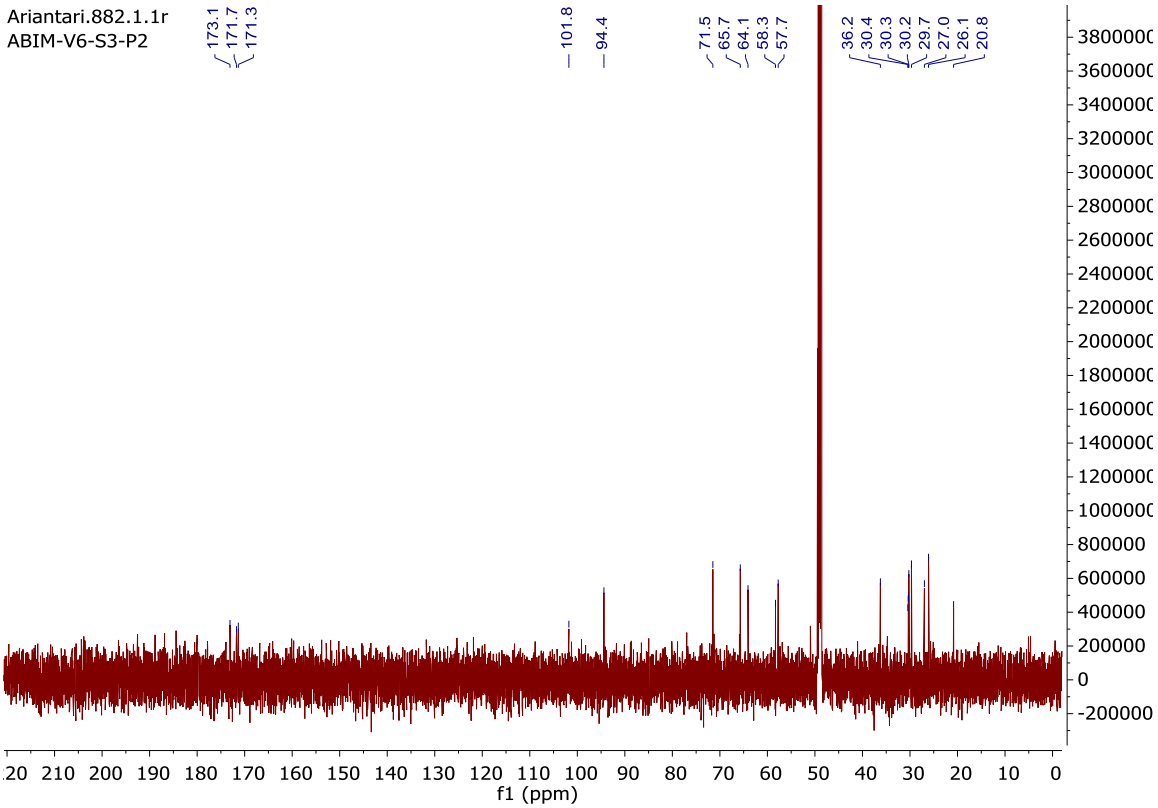

Figure S76. ^{13}C NMR (150 MHz, MeOH-d_4) spectrum of compound **11**.
Note: δ_C 166.7 was hidden in the baseline, but could be extracted from the HMBC spectrum.

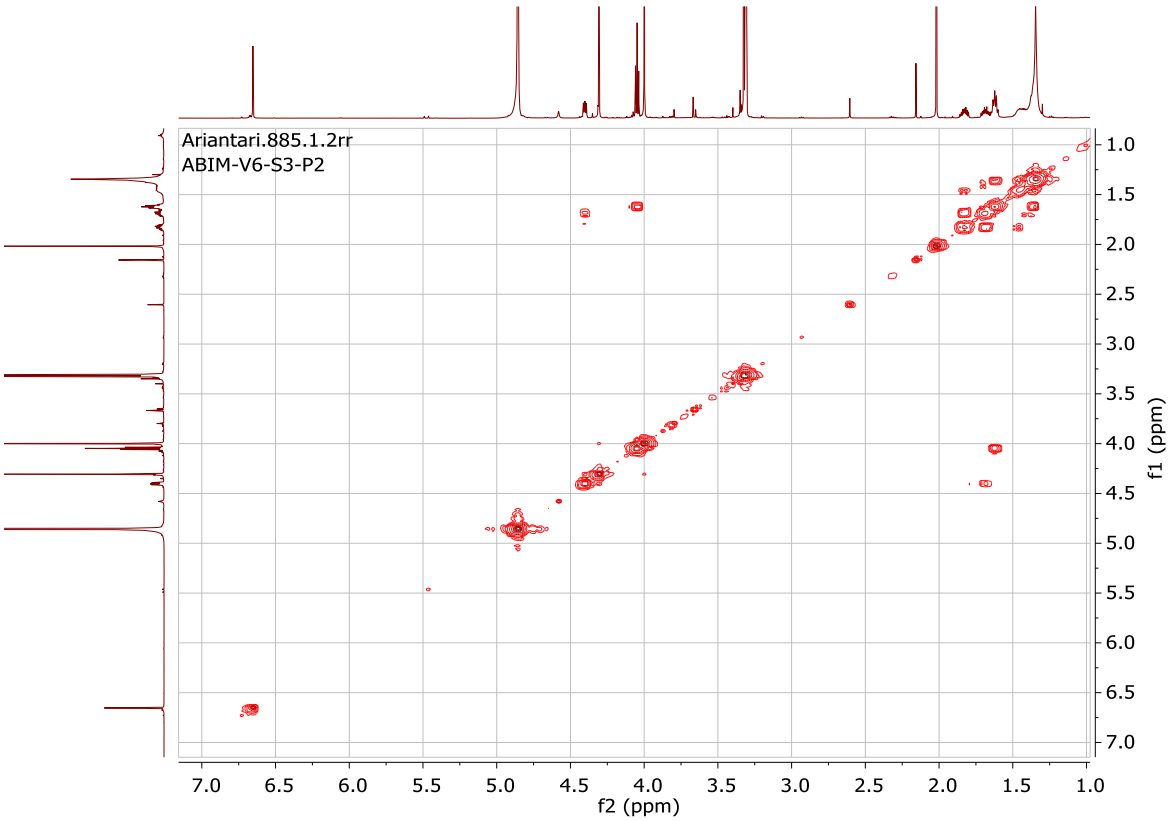

Figure S77. ^{1}H-^{1}H COSY (600 MHz, MeOH-d_4) spectrum of compound **11**.

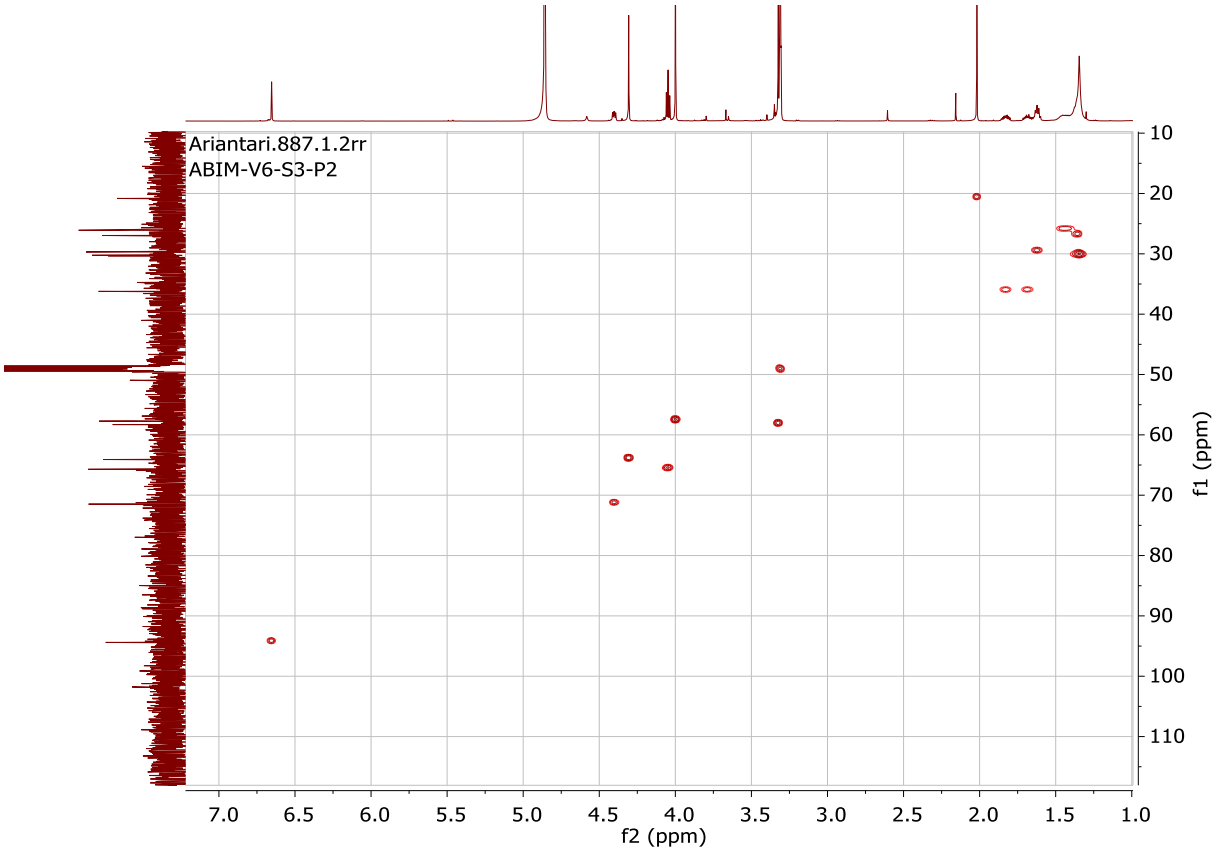

Figure S78. HSQC (600 and 150 MHz, MeOH-d_4) spectrum of compound **11**.

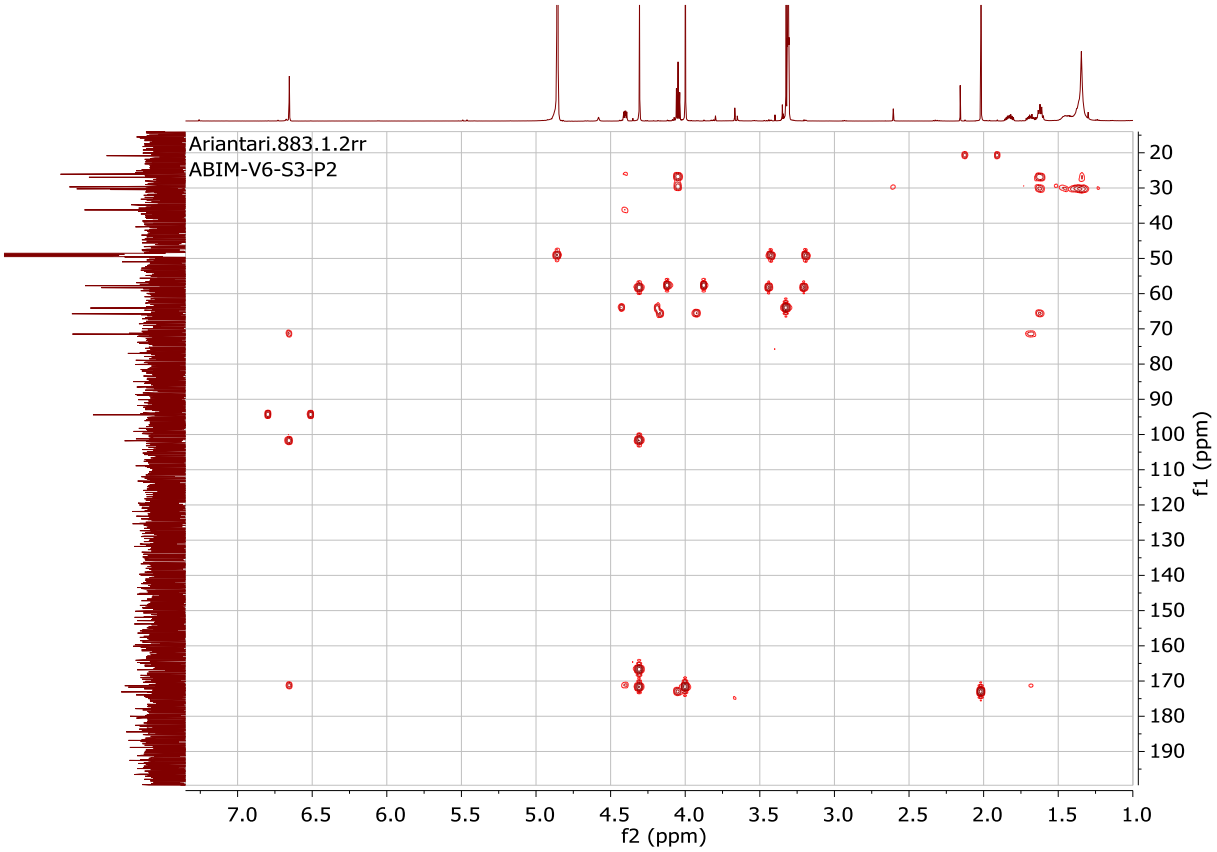

Figure S79. HMBC (600 and 150 MHz, MeOH-d_4) spectrum of compound **11**.

(A)

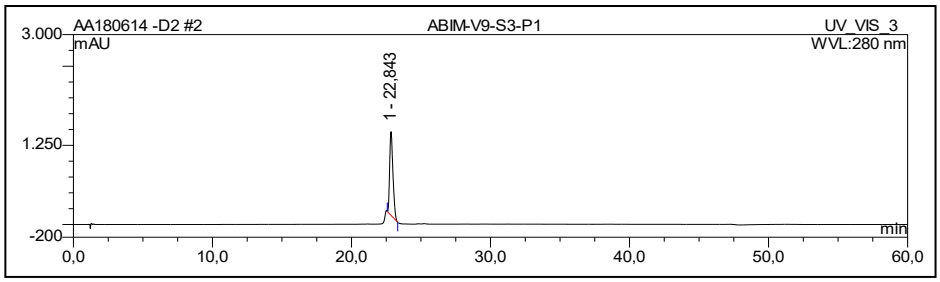

(B)

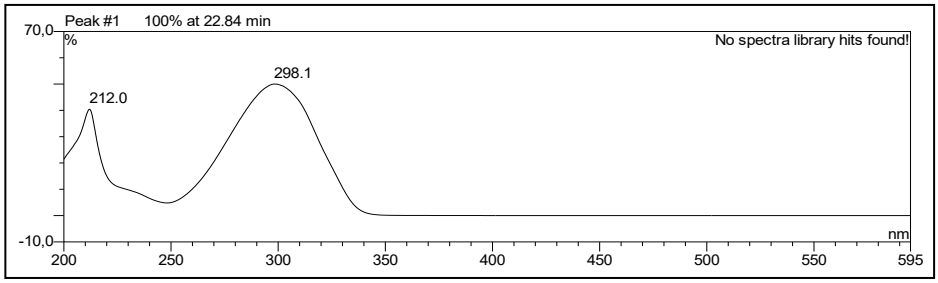

Figure S80. HPLC chromatogram (A) and UV spectrum (B) of compound **12**.

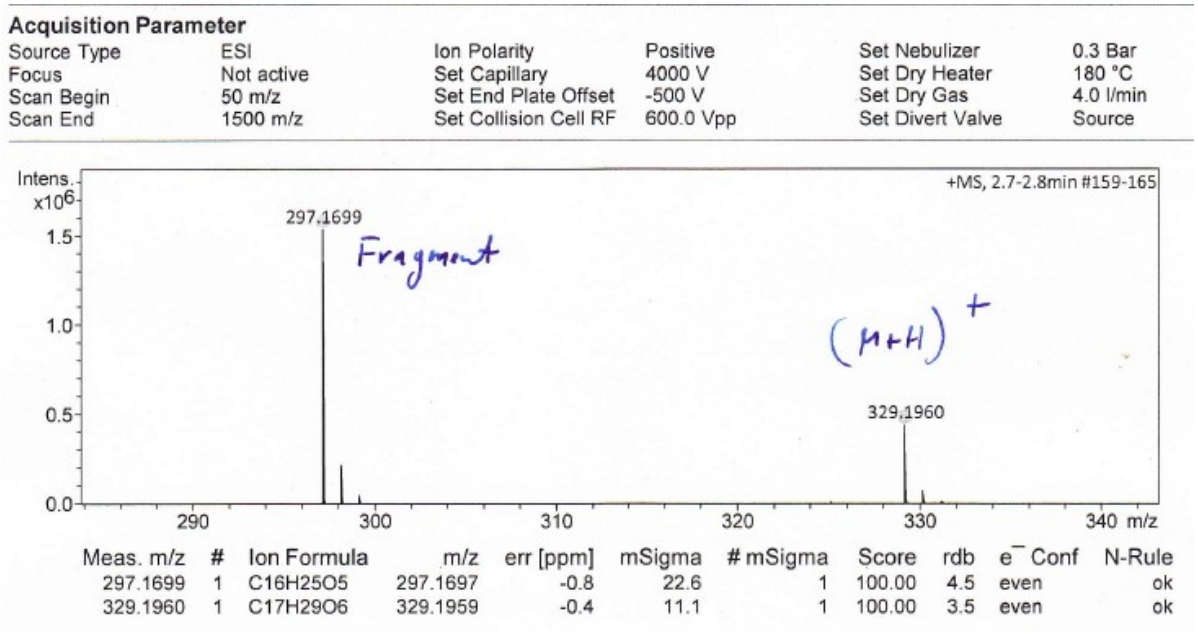

Figure S81. HRESIMS spectrum of compound **12**.

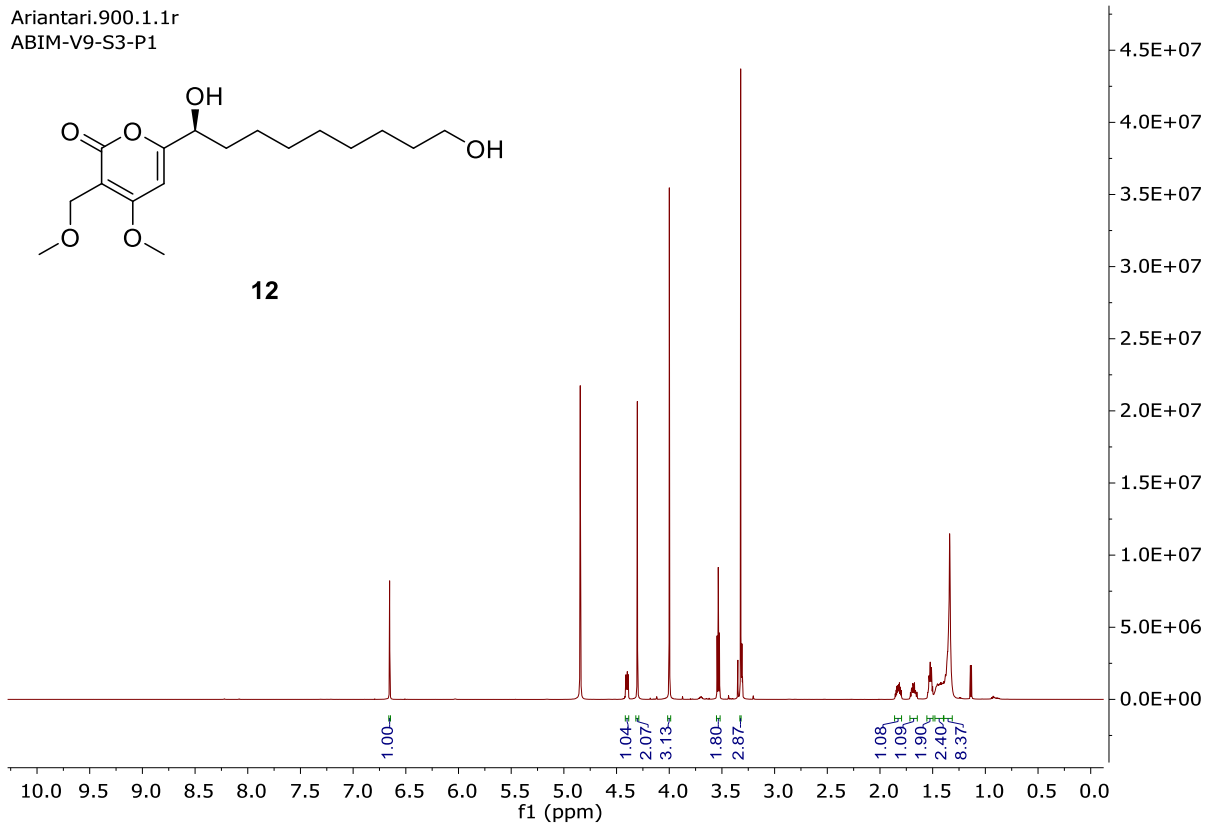

Figure S82. ^{1}H NMR (600 MHz, MeOH-d_4) spectrum of compound **12**.

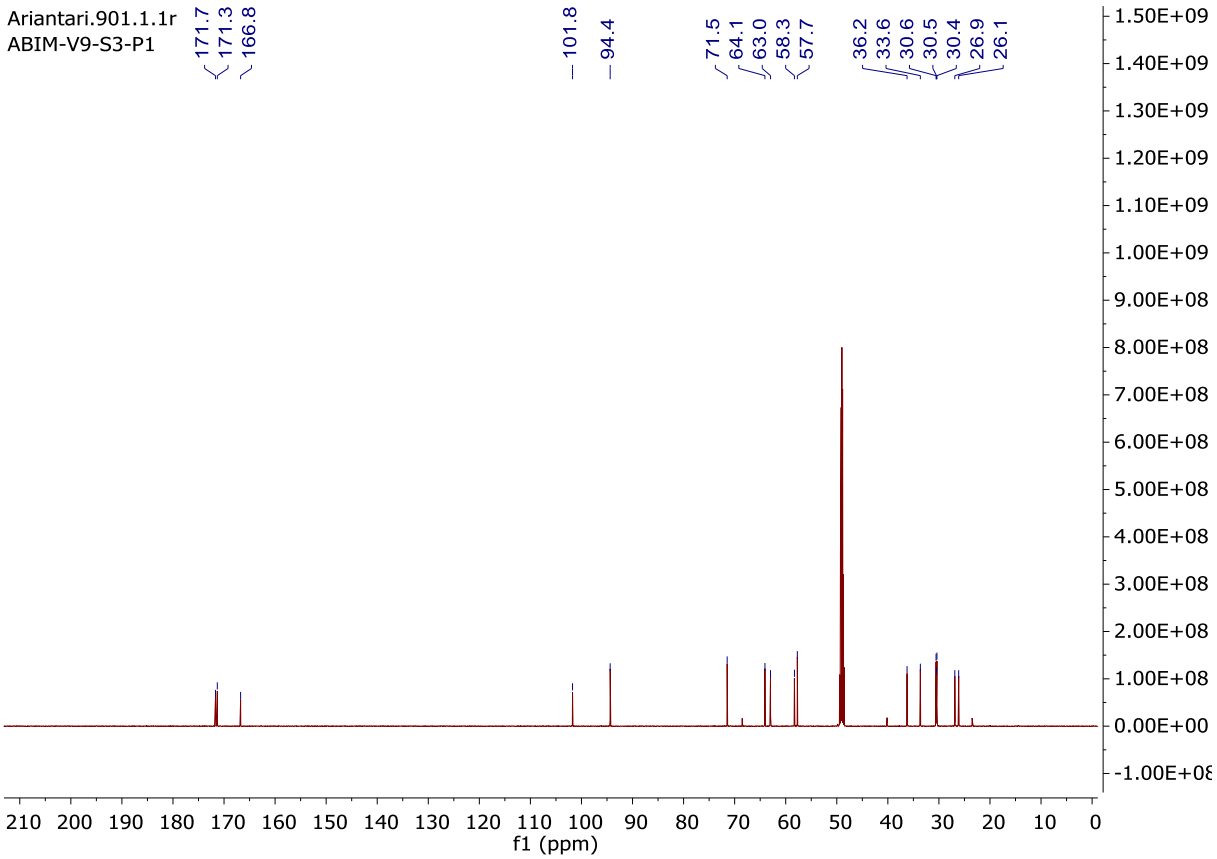

Figure S83. ^{13}C NMR (150 MHz, MeOH-d_4) spectrum of compound **12**.

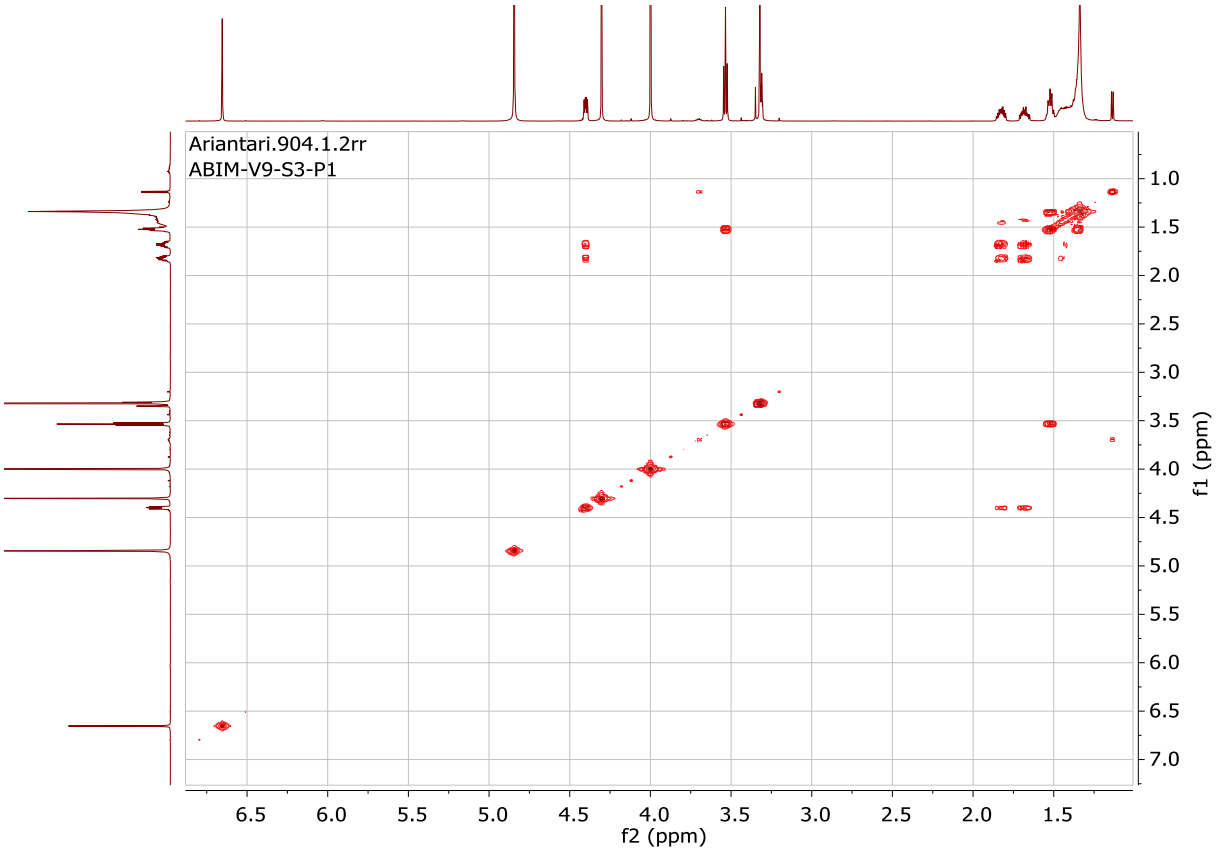

Figure S84. ^{1}H-^{1}H COSY (600 MHz, MeOH-d_4) spectrum of compound **12**.

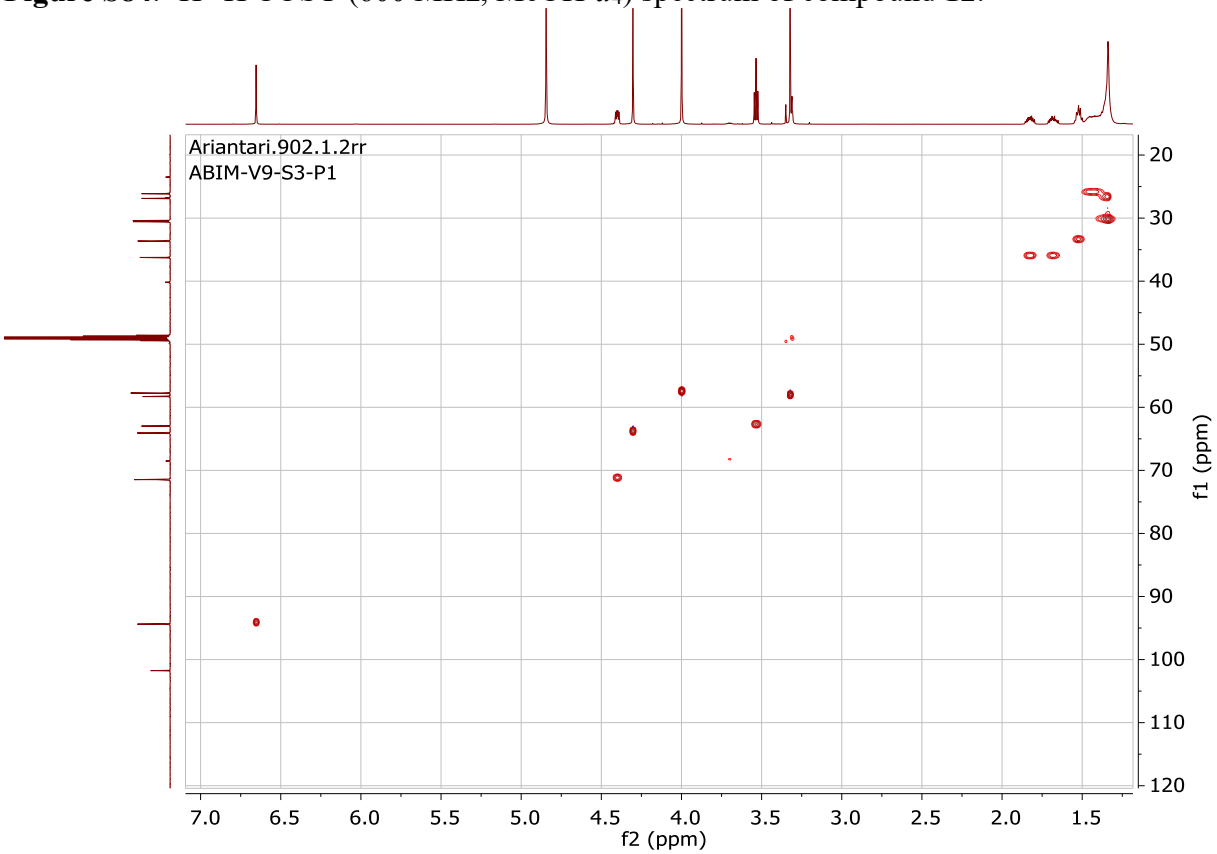

Figure S85. HSQC (600 and 150 MHz, MeOH-d_4) spectrum of compound **12**.

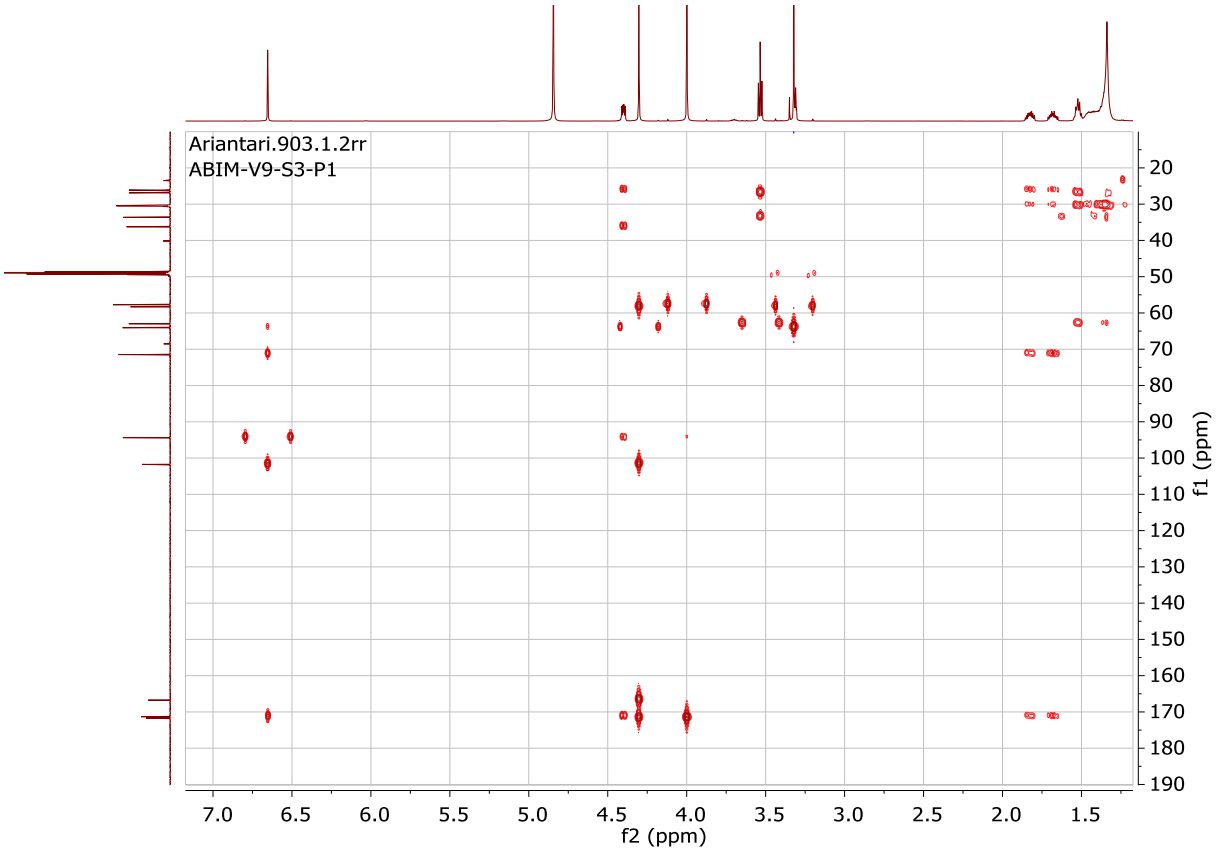

Figure S86. HMBC (600 and 150 MHz, MeOH-d_4) spectrum of compound **12**.

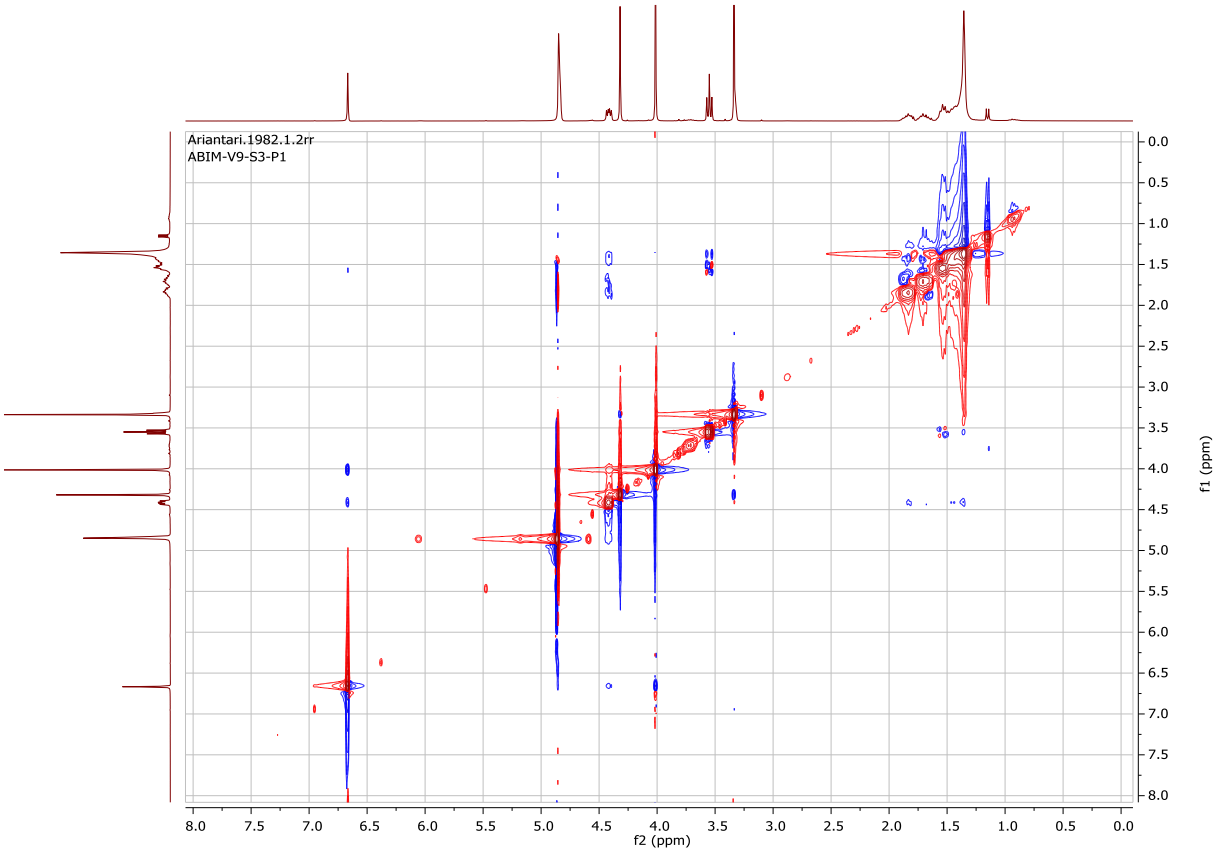

Figure S87. NOESY (300 MHz, MeOH-d_4) spectrum of compound **12**.

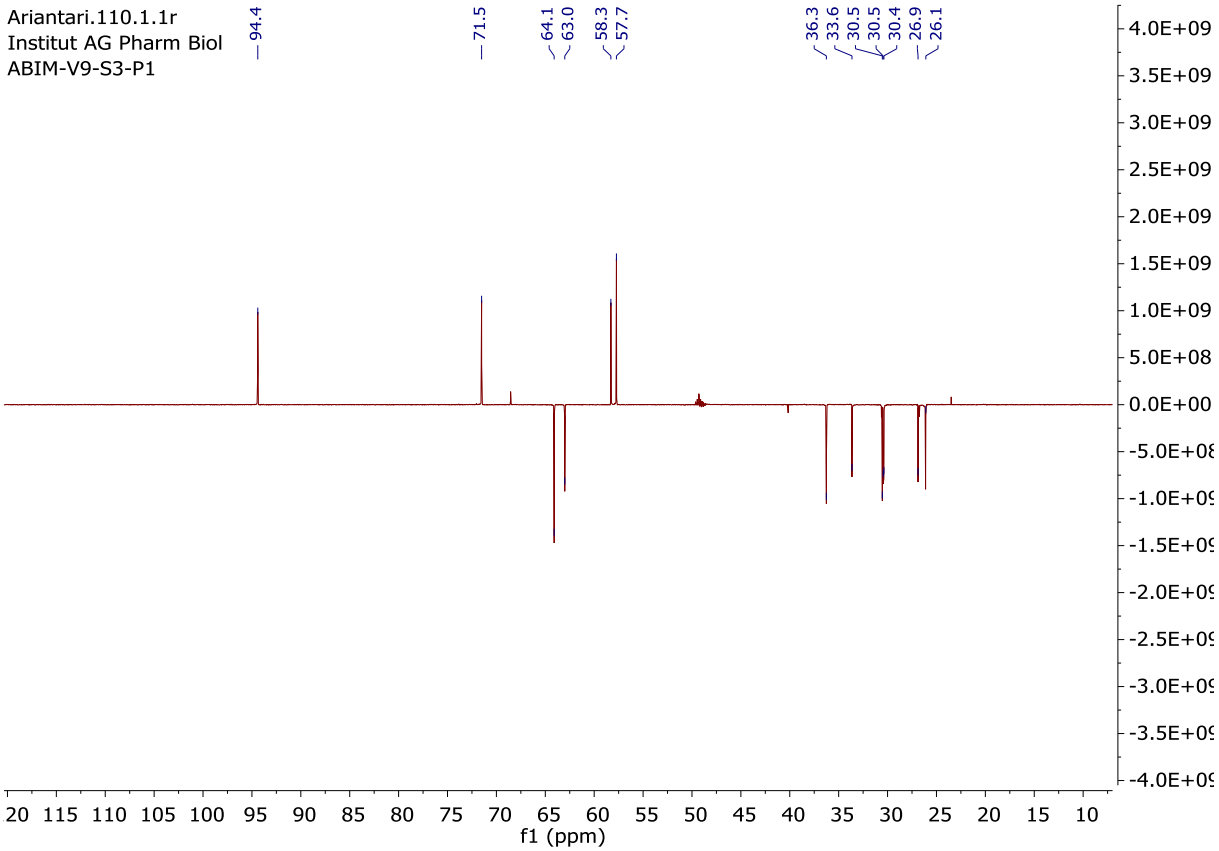

Figure S88. DEPT 135 (125 MHz, MeOH-d_4) spectrum of compound **12**.

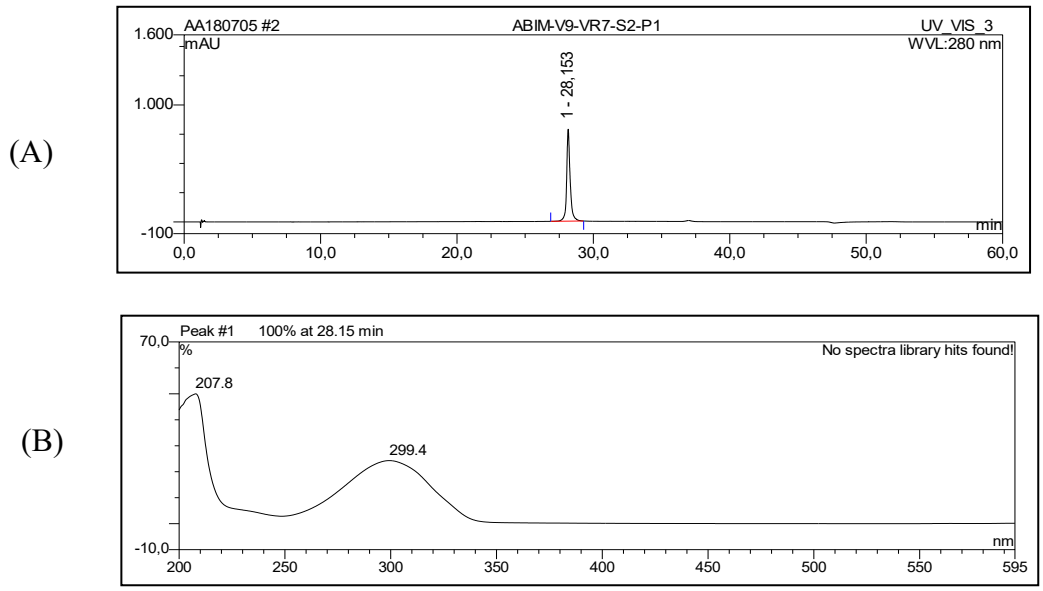

Figure S89. HPLC chromatogram (A) and UV spectrum (B) of compound **13**.

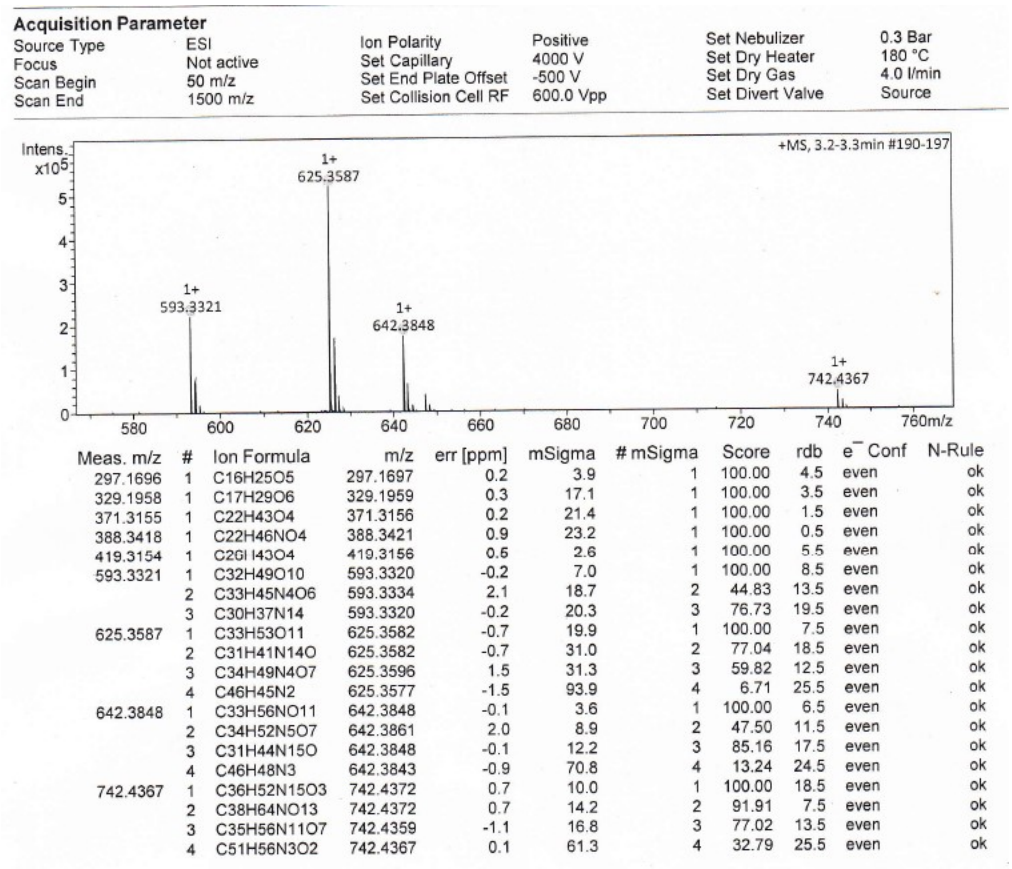

Meas. m/z	#	Ion Formula	m/z	err [ppm]	mSigma	# mSigma	Score	rdb	e⁻ Conf	N-Rule
297.1696	1	C16H25O5	297.1697	0.2	3.9	1	100.00	4.5	even	ok
329.1958	1	C17H29O6	329.1959	0.3	17.1	1	100.00	3.5	even	ok
371.3155	1	C22H43O4	371.3156	0.2	21.4	1	100.00	1.5	even	ok
388.3418	1	C22H46NO4	388.3421	0.9	23.2	1	100.00	0.5	even	ok
419.3154	1	C2GI I43O4	419.3156	0.6	2.6	1	100.00	5.5	even	ok
593.3321	1	C32H49O10	593.3320	-0.2	7.0	1	100.00	8.5	even	ok
	2	C33H45N4O6	593.3334	2.1	18.7	2	44.83	13.5	even	ok
	3	C30H37N14	593.3320	-0.2	20.3	3	76.73	19.5	even	ok
625.3587	1	C33H53O11	625.3582	-0.7	19.9	1	100.00	7.5	even	ok
	2	C31H41N14O	625.3582	-0.7	31.0	2	77.04	18.5	even	ok
	3	C34H49N4O7	625.3596	1.5	31.3	3	59.82	12.5	even	ok
	4	C46H45N2	625.3577	-1.5	93.9	4	6.71	25.5	even	ok
642.3848	1	C33H56NO11	642.3848	-0.1	3.6	1	100.00	6.5	even	ok
	2	C34H52N5O7	642.3861	2.0	8.9	2	47.50	11.5	even	ok
	3	C31H44N15O	642.3848	-0.1	12.2	3	85.16	17.5	even	ok
	4	C46H48N3	642.3843	-0.9	70.8	4	13.24	24.5	even	ok
742.4367	1	C36H52N15O3	742.4372	0.7	10.0	1	100.00	18.5	even	ok
	2	C38H64NO13	742.4372	0.7	14.2	2	91.91	7.5	even	ok
	3	C35H56N11O7	742.4359	-1.1	16.8	3	77.02	13.5	even	ok
	4	C51H56N3O2	742.4367	0.1	61.3	4	32.79	25.5	even	ok

Figure S90. HRESIMS spectrum of compound **13**.

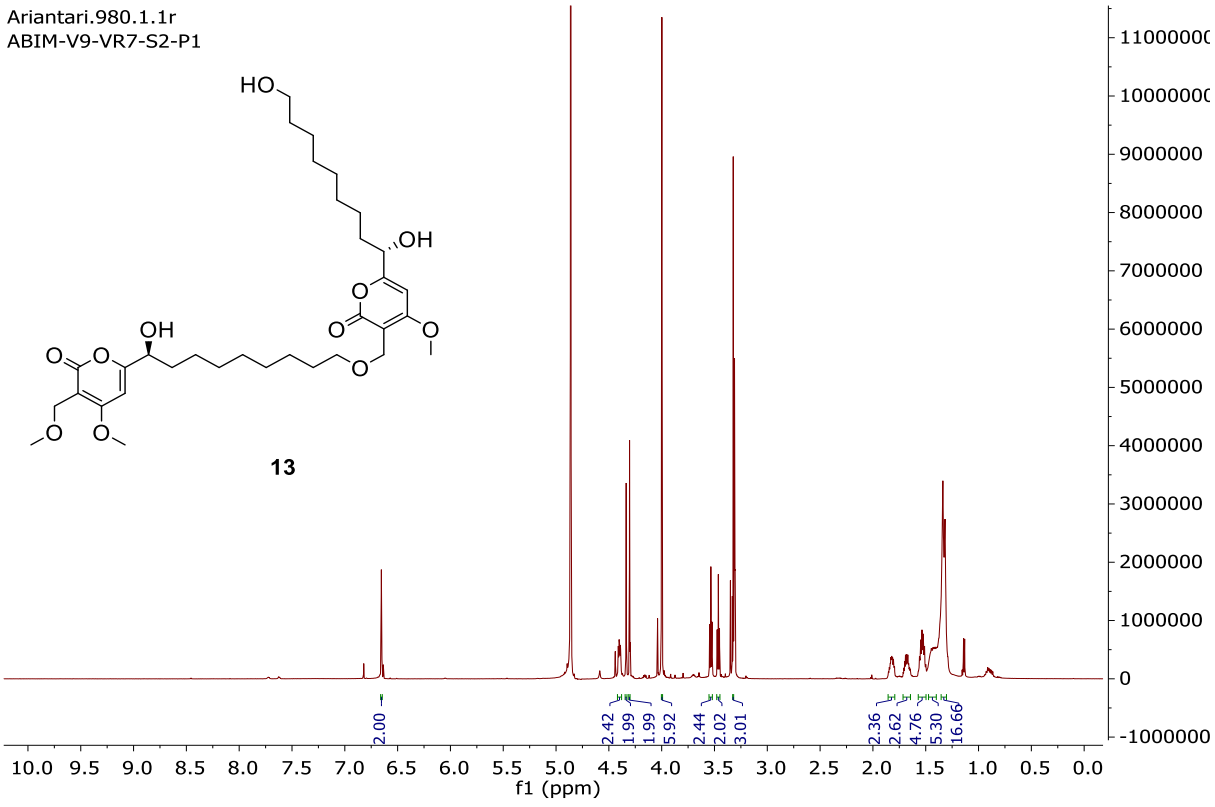

Figure S91. ^{1}H NMR (600 MHz, MeOH-d_4) spectrum of compound **13**.

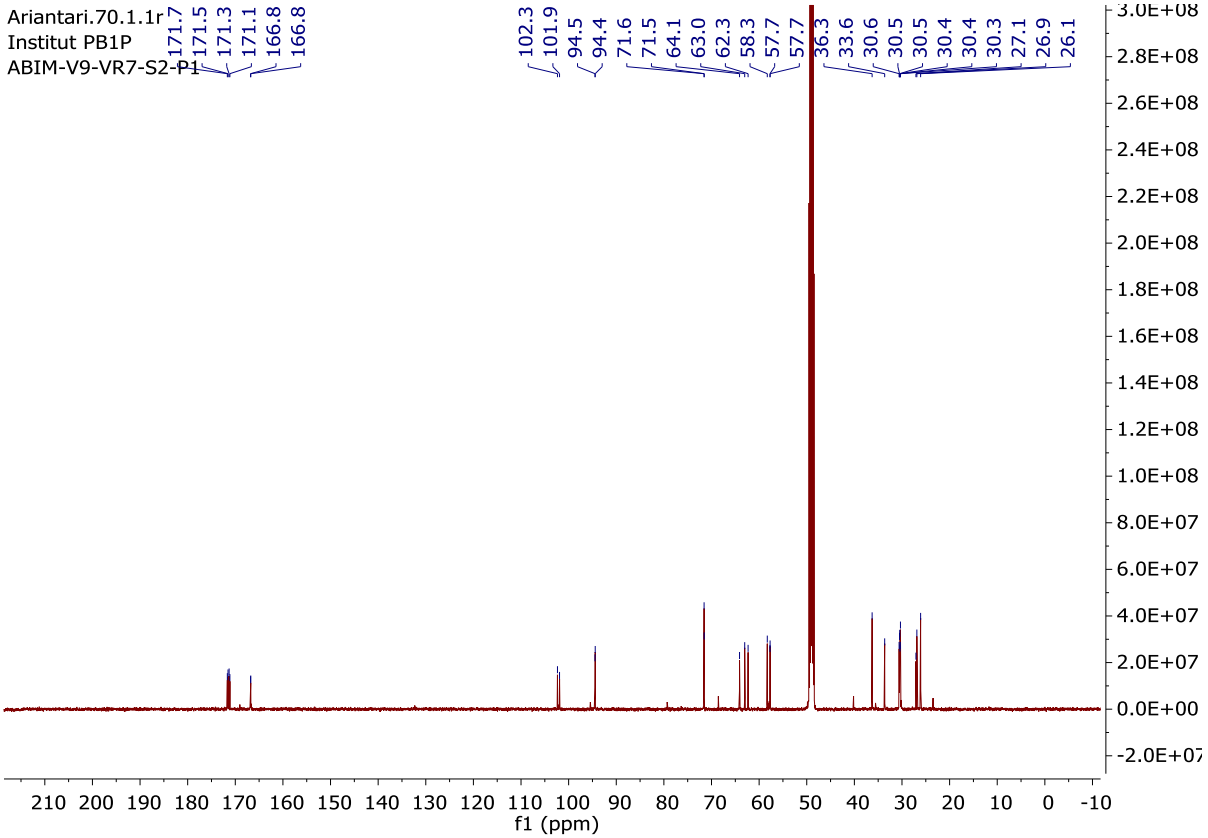

Figure S92. ^{13}C NMR (125 MHz, MeOH-d_4) spectrum of compound **13**.

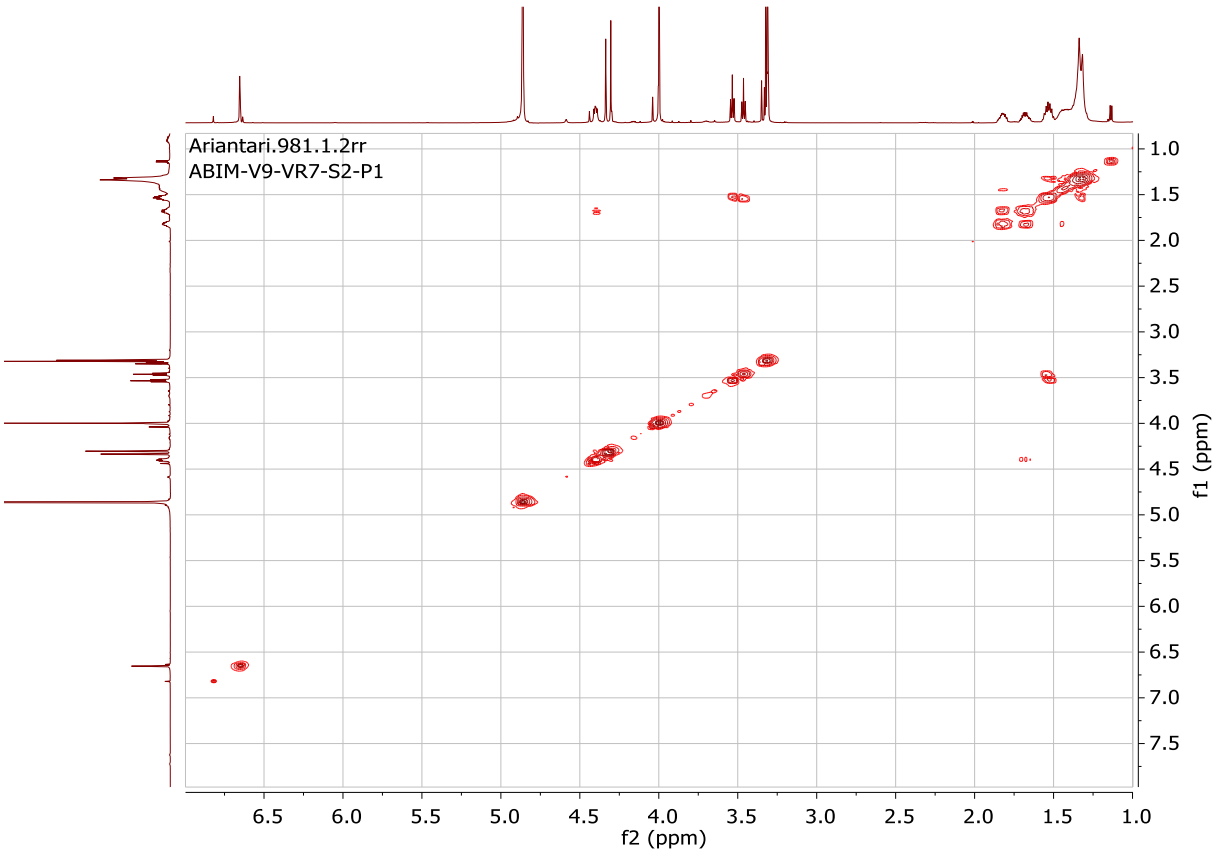

Figure S93. ^{1}H-^{1}H COSY (600 MHz, MeOH-d_4) spectrum of compound **13**.

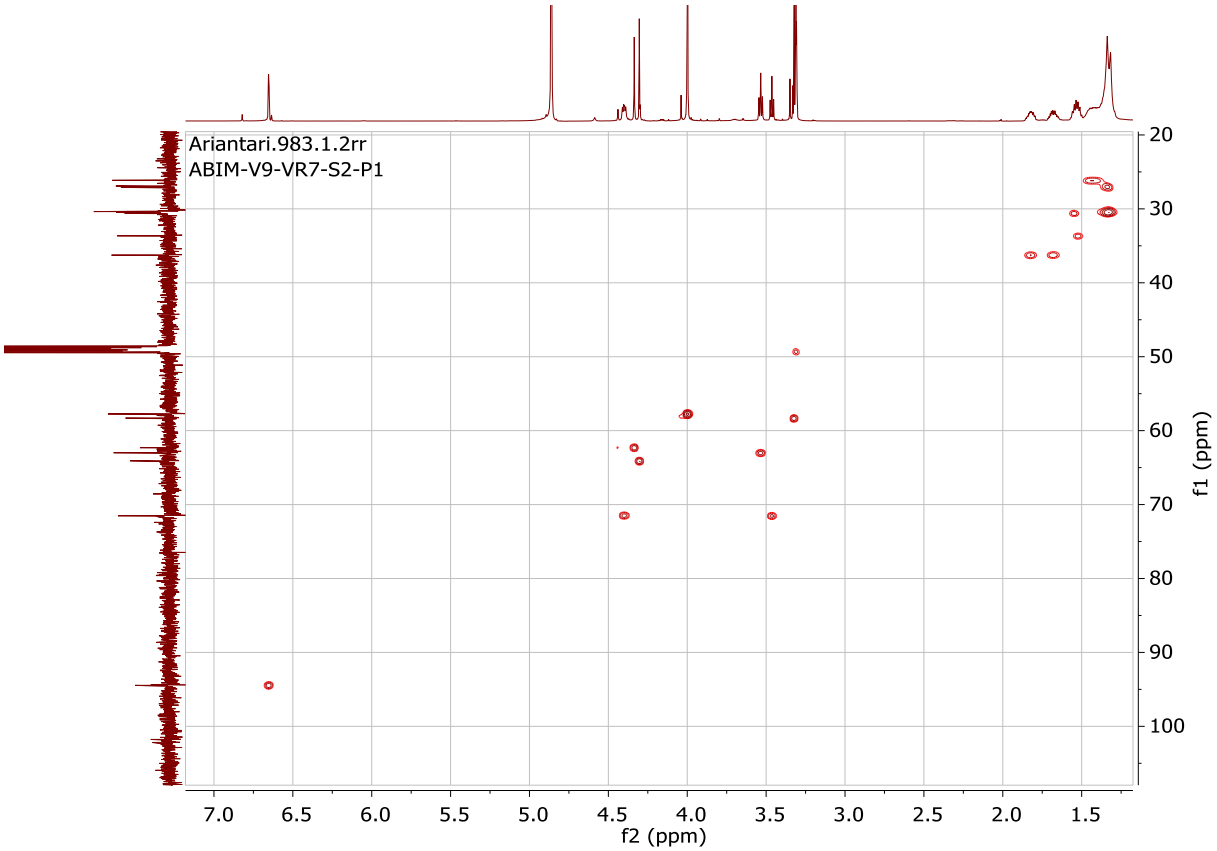

Figure S94. HSQC (600 and 150 MHz, MeOH-d_4) spectrum of compound **13**.

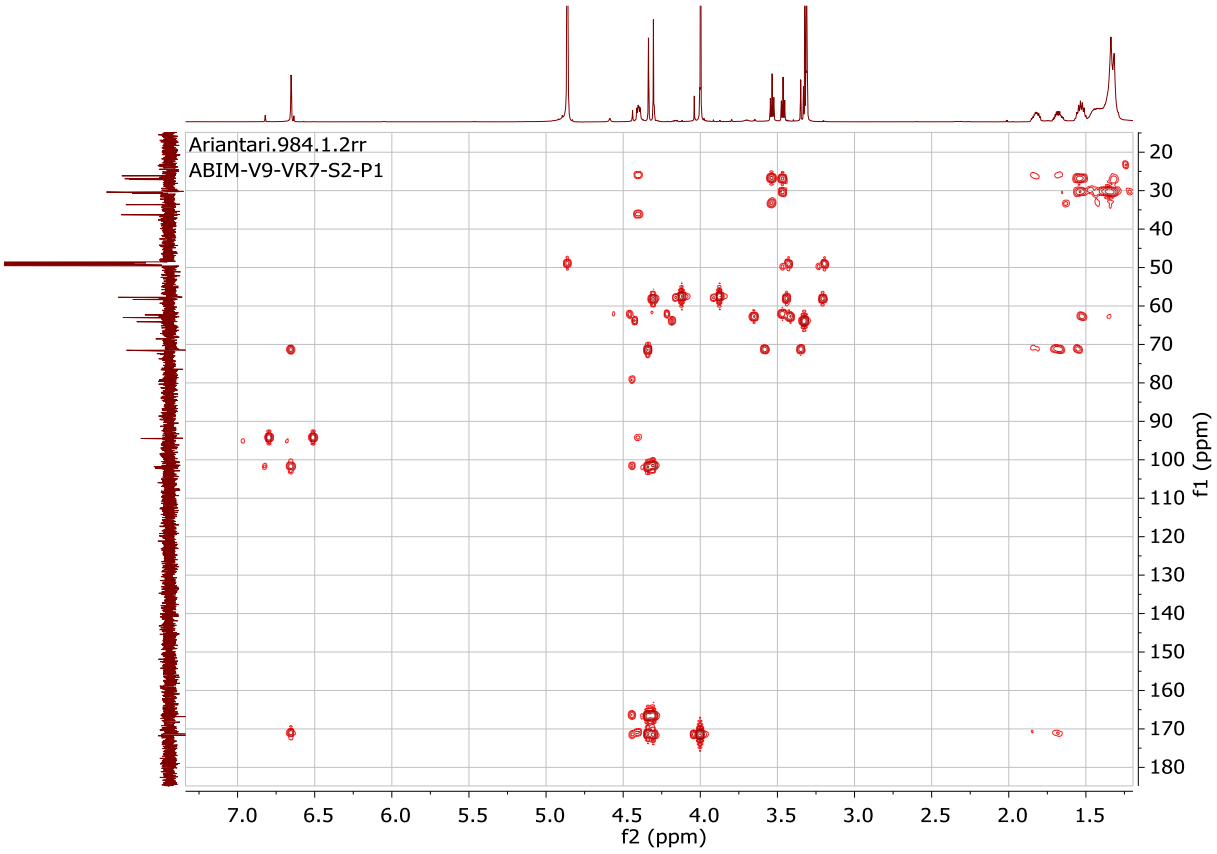

Figure S95. HMBC (600 and 150 MHz, MeOH-d_4) spectrum of compound **13**.

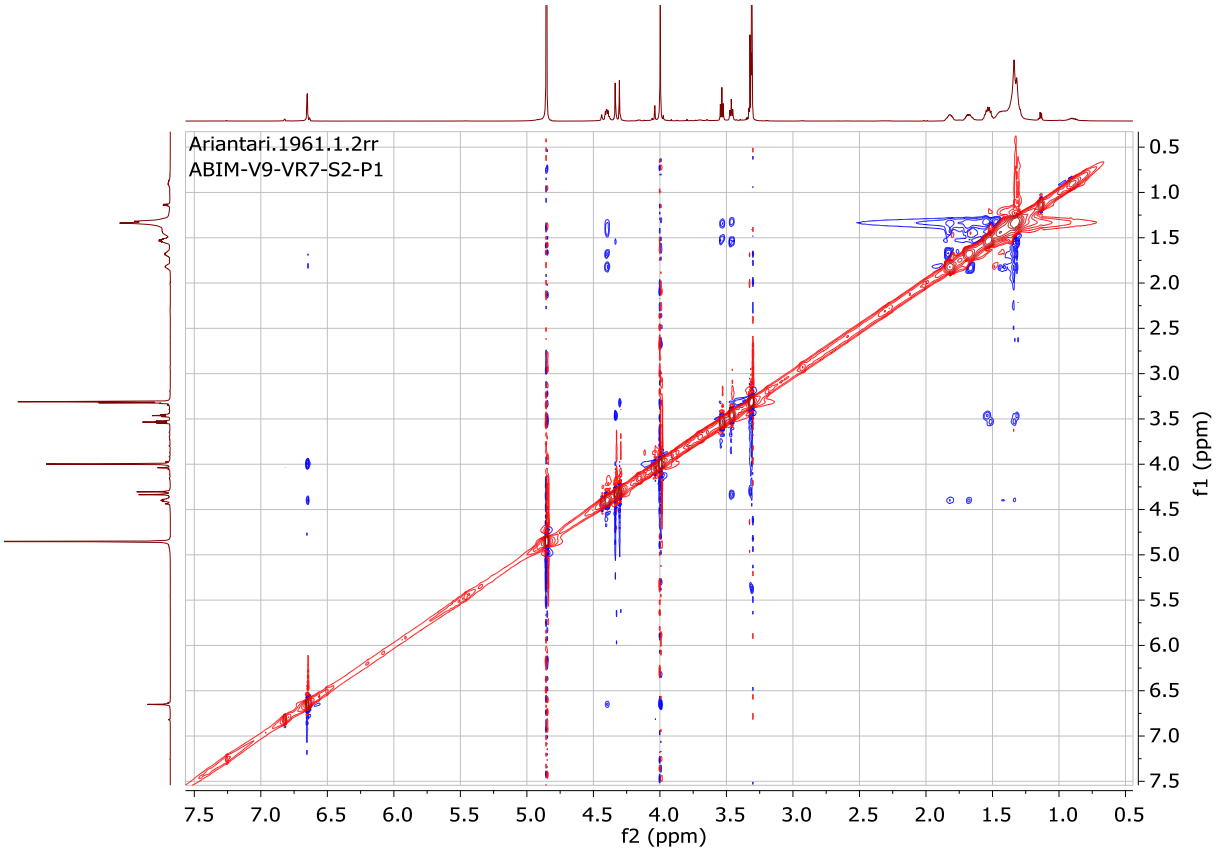

Figure S96. NOESY (600 MHz, MeOH-d_4) spectrum of compound **13**.

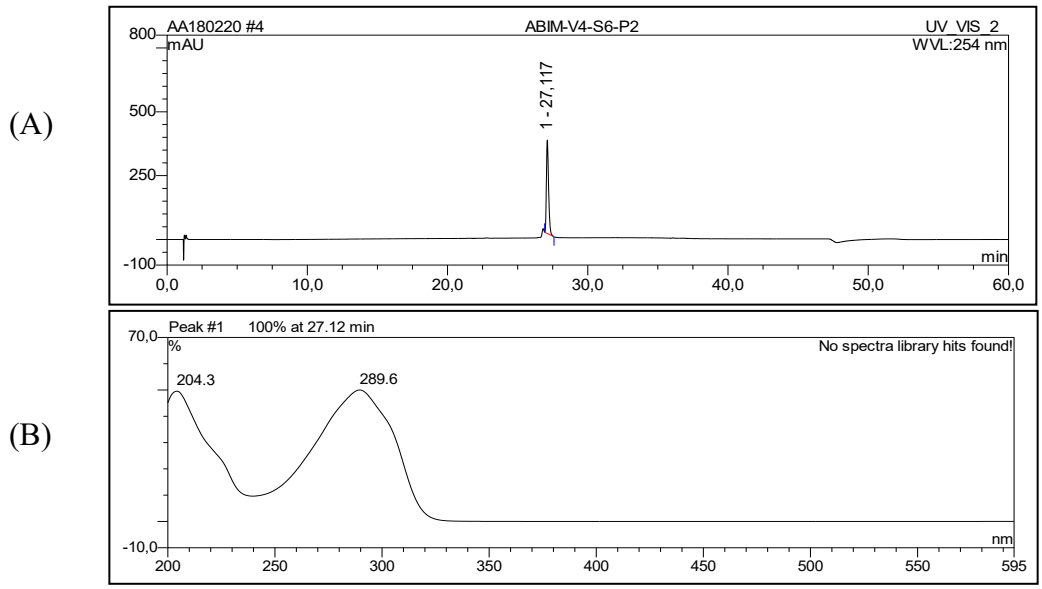

Figure S97. HPLC chromatogram (A) and UV spectrum (B) of compound **16**.

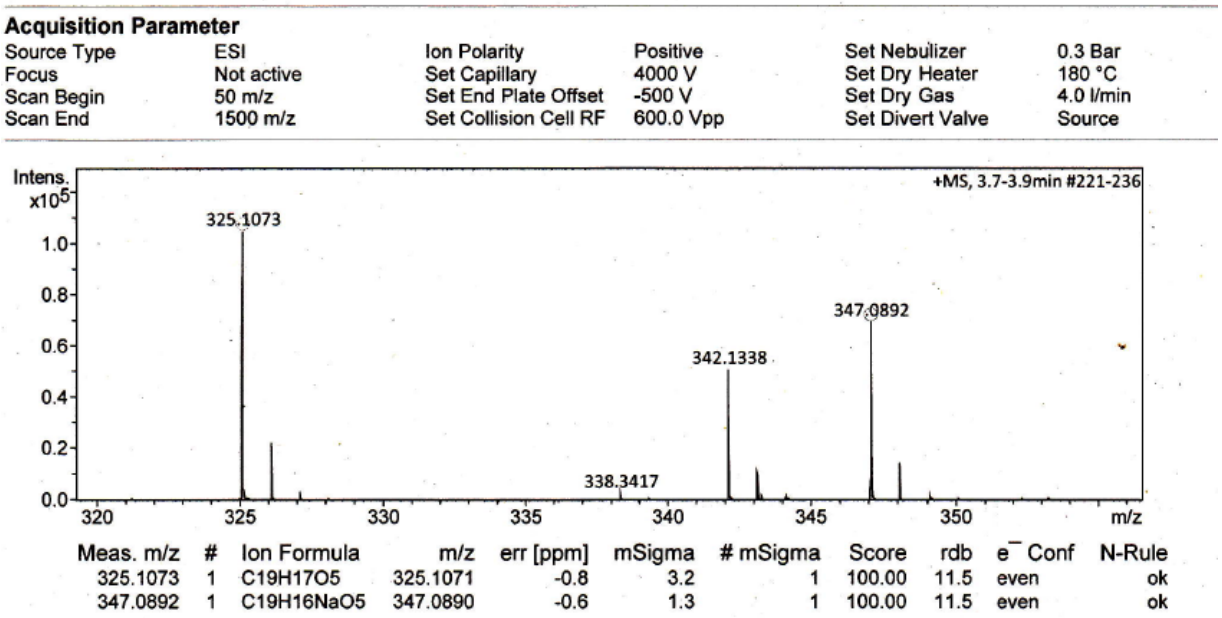

Figure S98. HRESIMS spectrum of compound **16**.

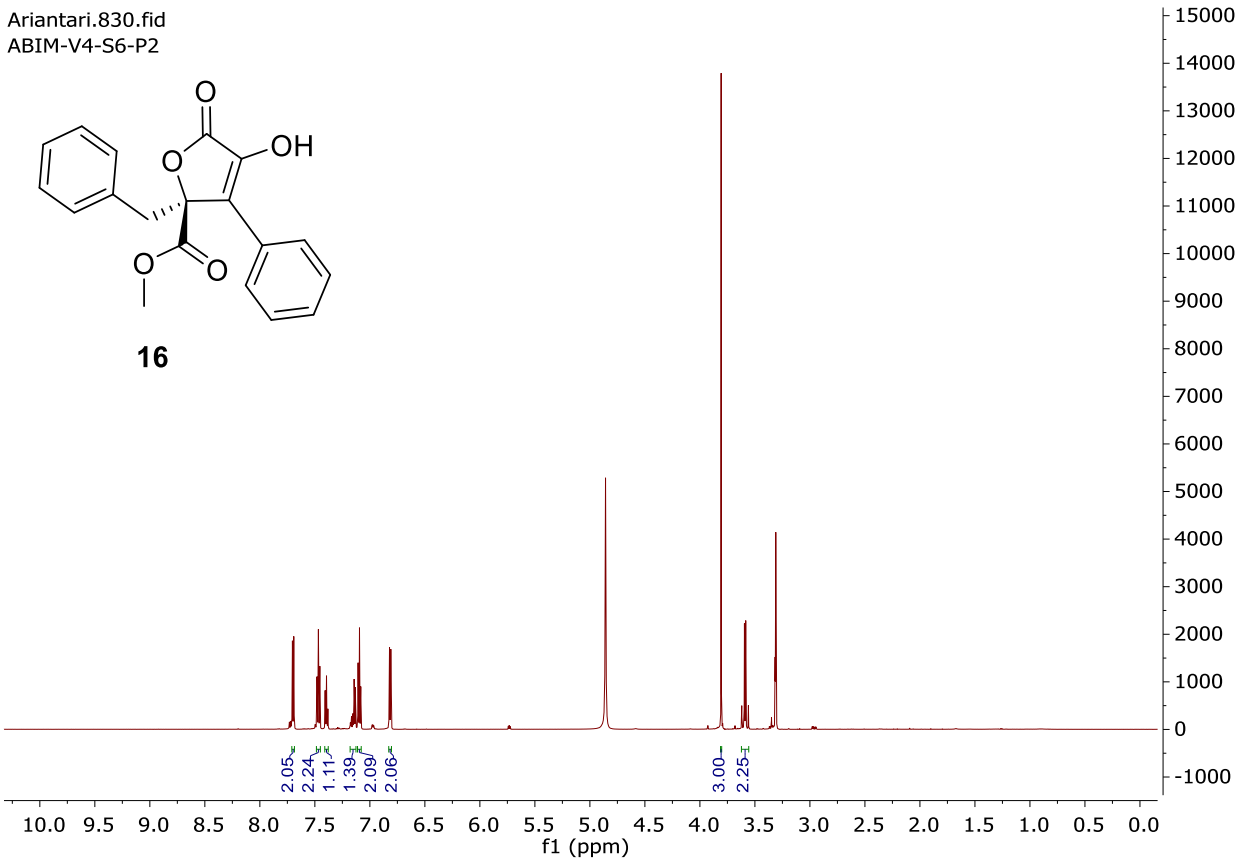

Figure S99. ^{1}H NMR (600 MHz, MeOH-d_4) spectrum of compound **16**.

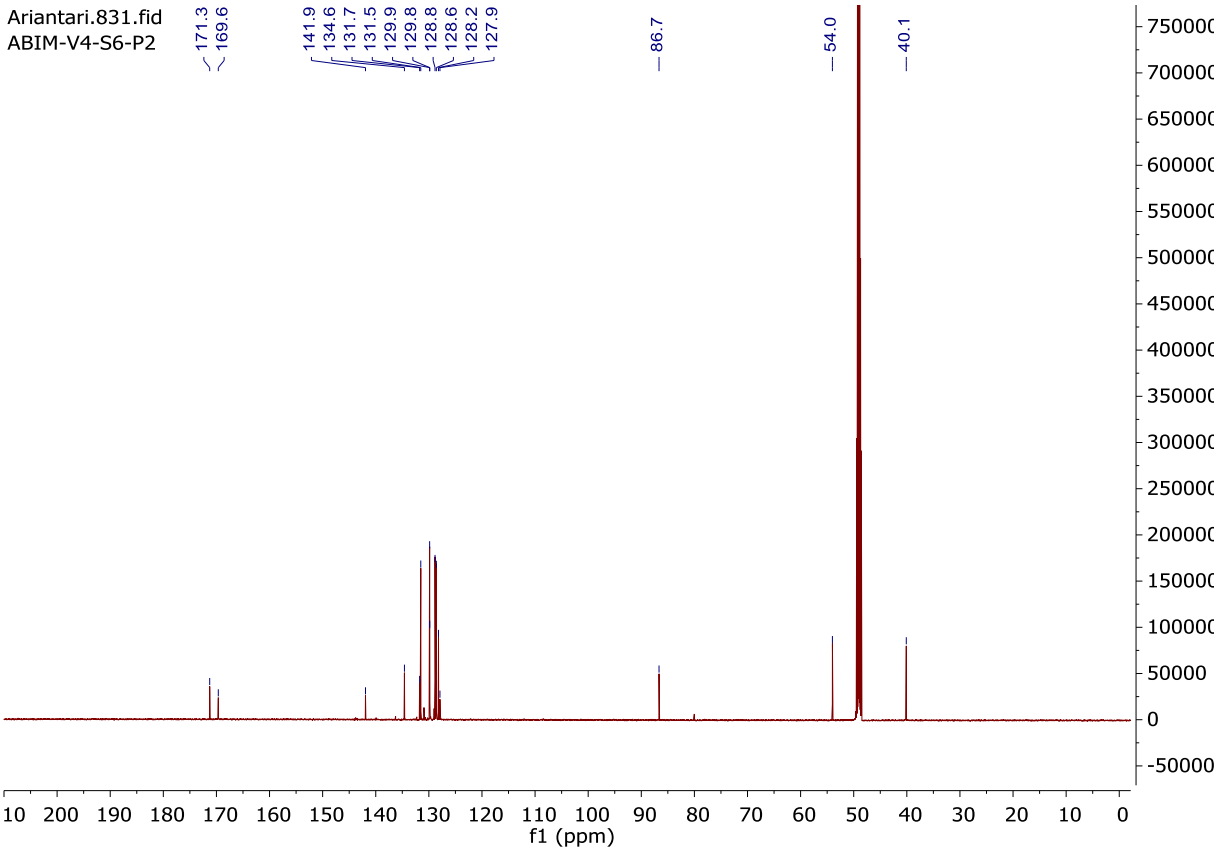

Figure S100. ^{13}C NMR (150 MHz, MeOH-d_4) spectrum of compound **16**.

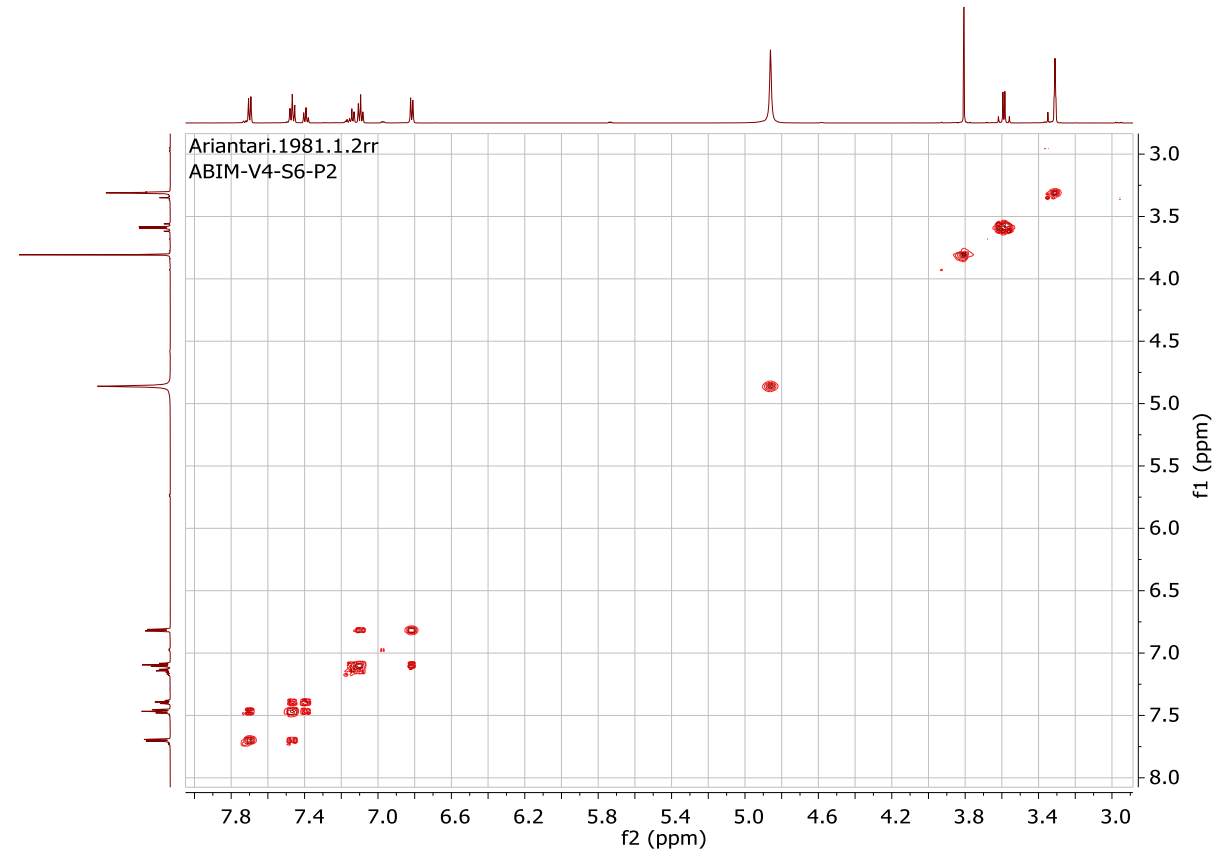

Figure S101. ^{1}H-^{1}H COSY (600 MHz, MeOH-d_4) spectrum of compound **16**.

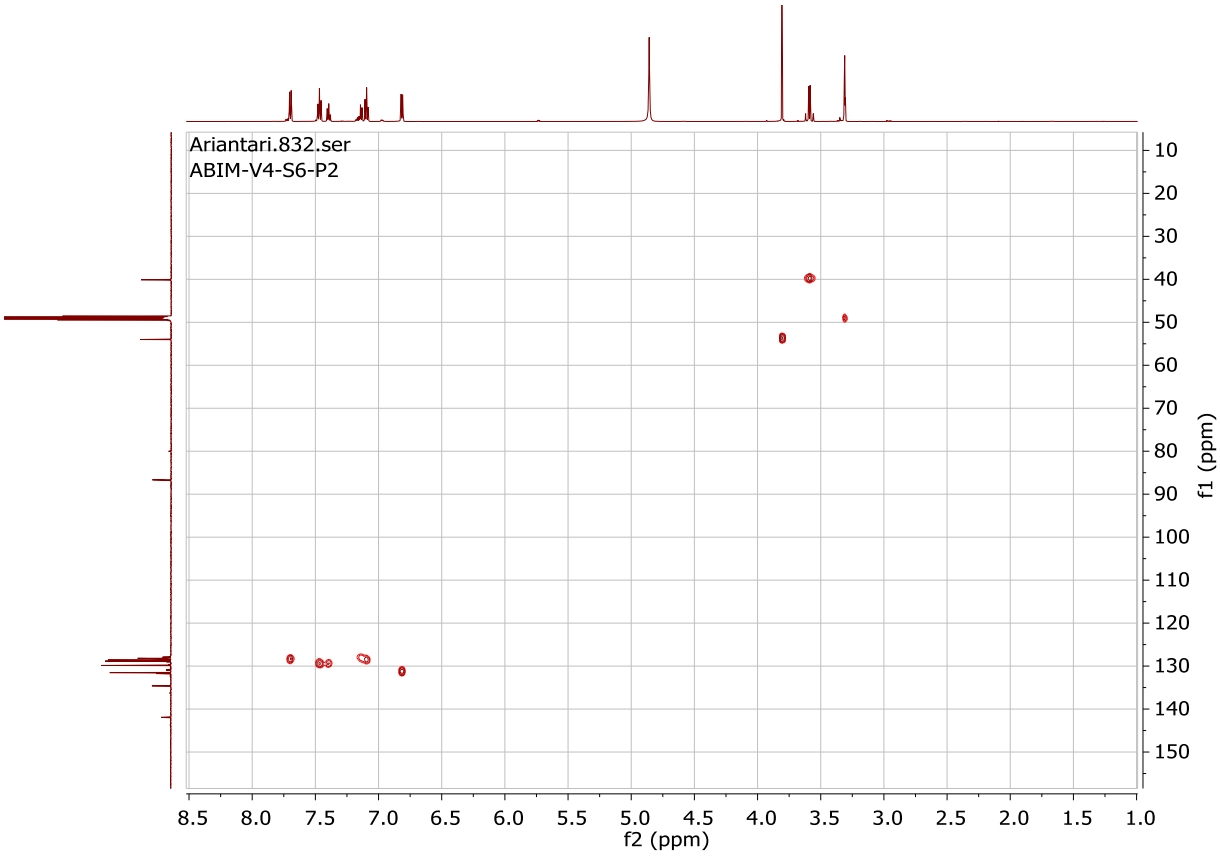

Figure S102. HSQC (600 and 150 MHz, MeOH-d_4) spectrum of compound **16**.

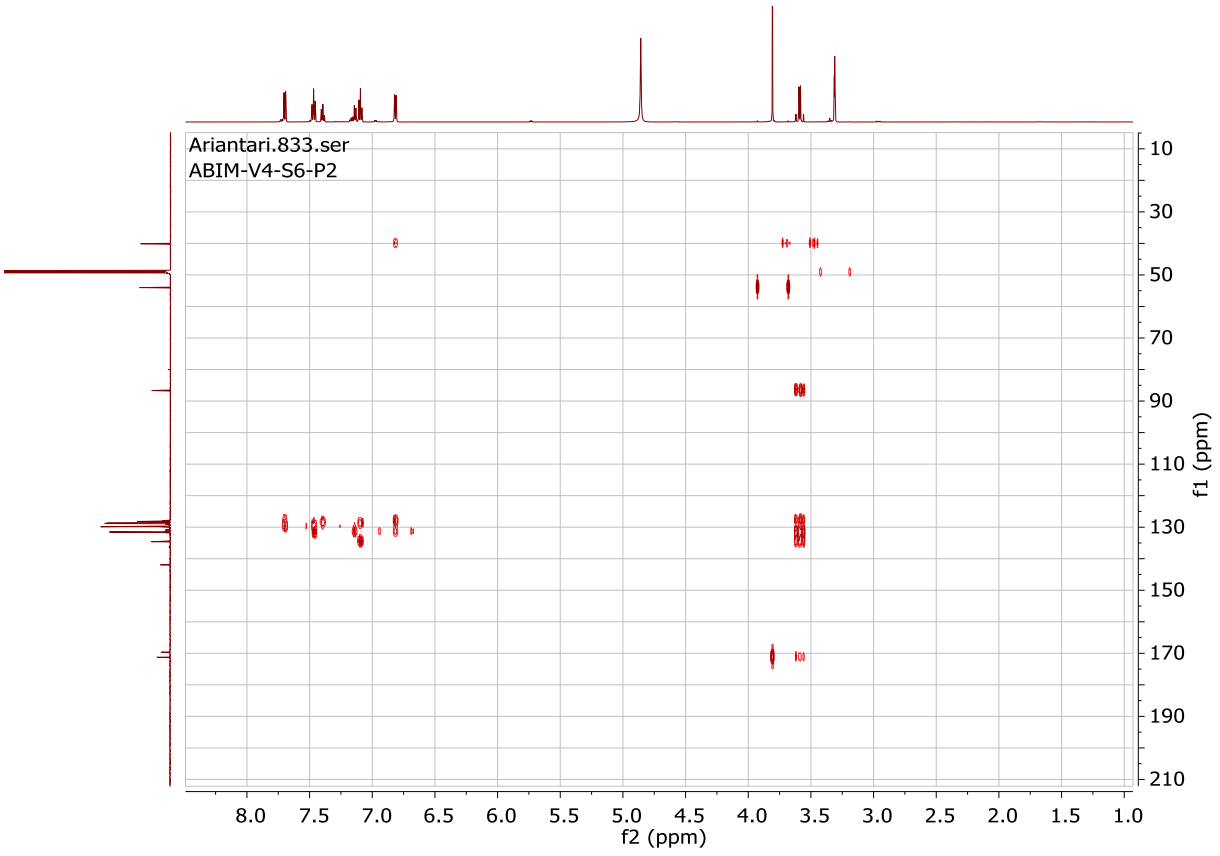

Figure S103. HMBC (600 and 150 MHz, MeOH-d_4) spectrum of compound **16**.

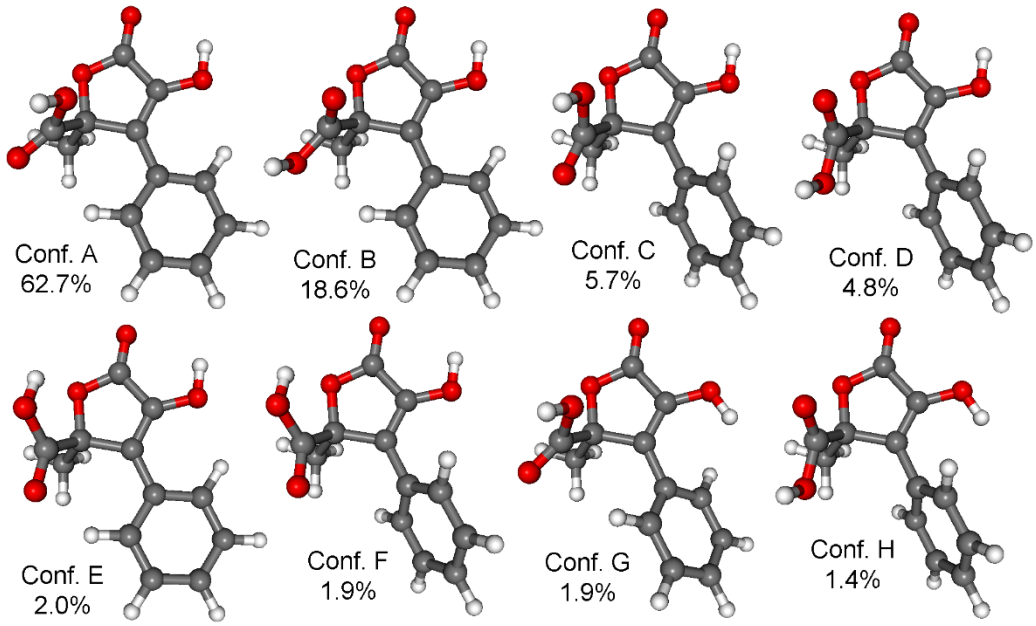

Figure S104. Structure and population of the low-energy CAM-B3LYP/TZVP PCM/MeCN conformers (≥ 1%) of (*S*)-**1**.

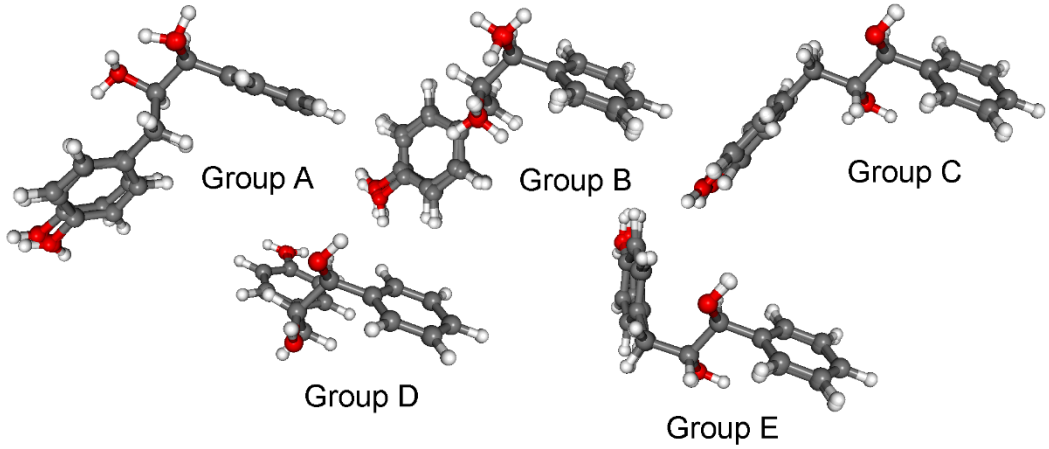

Figure S105. Classification of the twenty-two low-energy (≥ 1%) CAM-B3LYP/TZVP PCM/MeCN conformers of (8*R*,9*S*)-**4**. Group A (44.9%) contains conformers A, B, E, F; group B (27.5%) contains conformers C, D, G, H, K, L, Q, R; group C (10.1%) contains conformers I, J, M, N; group D (3.2%) contains conformers O, P; group E (4.4%) contains conformers S, T, U and V.

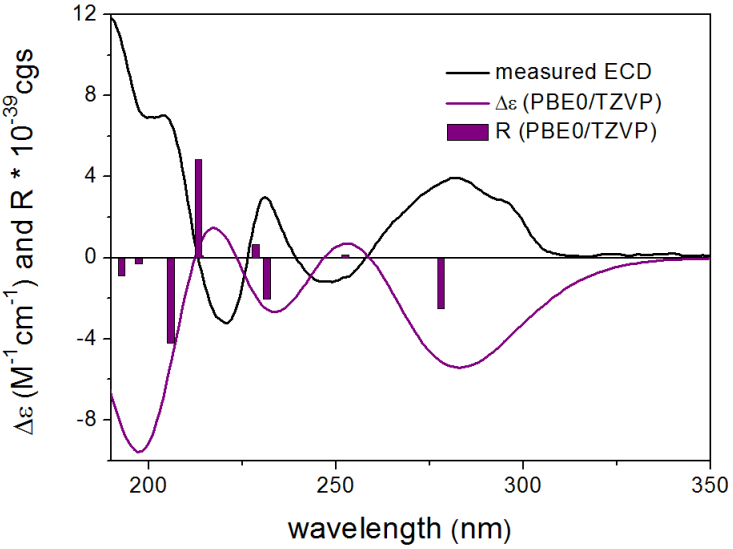

Figure S106. Experimental ECD spectrum (black) of **6** in MeCN compared with the Boltzmann-weighted PBE0/TZVP PCM/MeCN ECD spectrum (purple) of (*R*)-**6** computed for the 6 low-energy CAM-B3LYP/TZVP PCM/MeCN conformers. The bars represent the rotational strength of the lowest-energy conformer.

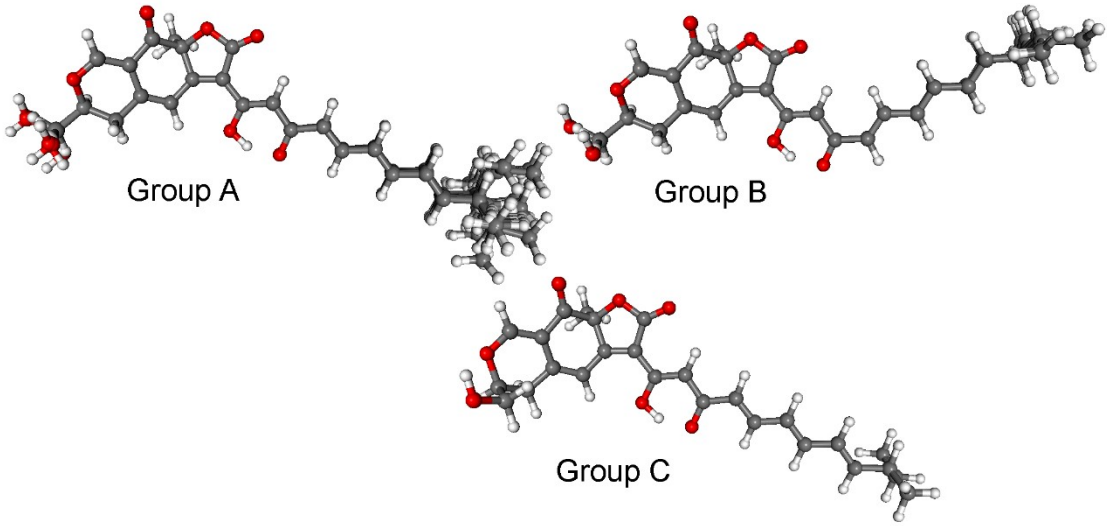

Figure S107. Classification of the twenty-six low-energy (≥ 1%) CAM-B3LYP/TZVP PCM/MeCN conformers of (3*S*,11*S*,23*S*)-**14** into conformer groups. Group A (72.5%) contains conformers A, B, C, D, E, F, G, I, J, K, M, N, O, Q, R, S, T, U, V, W, Y, Z; group B (5.0%) contains conformers H, L, X; group C (1.6%) contains conformer P.

Chapter 4

Publication 3

Didymellanosine, a new decahydrofluorene analogue, and ascolactone C from *Didymella* sp. IEA-3B.1 an endophyte of *Terminalia catappa*

Submitted to : "RSC Advances"

Impact factor : 3.049

Research contribution: first authorship, contributed to 60% of this manuscript. The first author conducted most of the laboratory experiments including the application of OSMAC approach, isolation and structure elucidation of secondary metabolites, as well as preparation of the manuscript.

Didymellanosine, A New Decahydrofluorene Analogue, and Ascolactone C from *Didymella* sp. IEA-3B.1 an Endophyte of *Terminalia catappa*

Ni P. Ariantari,[a,b] Elena Ancheeva,[a] Marian Frank,[a] Fabian Stuhldreier,[c] Dieter Meier,[a] Yvonne Gröner,[a] Irene Reimche,[d] Nicole Teusch,[d] Sebastian Wesselborg,[c] Werner E. G. Müller,[e] Rainer Kalscheuer,[a] Zhen Liu,[a,] * Peter Proksch[a,] *

[a]Institute of Pharmaceutical Biology and Biotechnology, Heinrich Heine University Düsseldorf, Universitätsstrasse 1, 40225 Düsseldorf, Germany

[b]Department of Pharmacy, Faculty of Mathematics and Natural Sciences, Udayana University, 80361 Bali, Indonesia

[c]Institute of Molecular Medicine I, Medical Faculty, Heinrich Heine University Düsseldorf, Universitätsstrasse 1, 40225 Düsseldorf, Germany.

[d]Department of Biomedical Sciences, Institute of Health Research and Education, University of Osnabrück, Germany

[e]Institute for Physiological Chemistry, University Medical Center of the Johannes Gutenberg University Mainz Duesbergweg 6, 55128 Mainz, Germany

*corresponding authors

Abstract

Didymellanosine (**1**), the first analogue of the decahydrofluorene-class of natural products bearing a 13-membered macrocyclic alkaloid conjugated with adenosine, and a new benzolactone derivative, ascolactone C (**4**) along with eight known compounds (**2**, **3**, **5**−**10**), were isolated from a solid rice fermentation of the endophytic fungus *Didymella* sp. IEA-3B.1 derived from the host plant *Terminalia catappa*. In addition, ascochitamine (**11**) was obtained when $(NH_4)_2SO_4$ was added to rice medium and is reported here for the first time as a natural product. The structures of the new compounds were established through extensive analysis of one- and two-dimensional NMR data as well as HRESIMS data. Didymellanosine (**1**) displayed strong to moderate activity against the murine lymphoma cell line L5178Y, Burkitt's lymphoma B cells (Ramos) and adult lymphoblastic leukemia T cells (Jurkat J16), with IC_{50} values of 2.2, 7.6, and 11.0 μM, respectively. Moreover, when subjected to a NFκB inhibition assay, didymellanosine (**1**) and phomapyrrolidone A (**2**) efficiently blocked NFκB activation. In an antimicrobial assay, ascomylactam C (**3**) was the most active compound when tested against a panel of Gram-positive bacteria including drug-resistant strains with MICs of 3.1−6.3 μM, while **1** revealed weaker activity. Interestingly, both compounds were also found active against Gram-negative *Acinetobacter baumannii* with MICs of 3.1 μM, in the presence of a sublethal concentration (0.1 μM) of colistin.

Keywords: endophytic fungus, *Didymella* sp., cytotoxicity, NFκB inhibition, antibacterial activity.

Introduction

Endophytic fungi are microorganisms which reside in inner tissues of host plants, that represent a notable reservoir for a wide array of biologically active molecules.[1, 2] These metabolites provide natural product pharmacophores which are of importance for the discovery of molecules for pharmaceutical and agricultural purposes.[1, 3] A few examples of bioactive natural products derived from fungal endophytes include the insecticidal compound nodulisporic acid A,[4] and a number of potent anti-HIV compounds such as altertoxins I−III and V.[5] Moreover, the isolation of remarkable anticancer agents from endophytes, especially those that were originally obtained from host plants, such as paclitaxel,[6] podophyllotoxin,[7] and camptothecin[8] point to their potential as alternative sources of pharmaceutically valuable metabolites.

In our search for bioactive metabolites from endophytes, we investigated *Didymella* sp. IEA-3B.1, a fungus isolated from leaves of *Terminalia catappa* (Combretaceae) from Bali, Indonesia. Species of the genus *Didymella* have been identified as teleomorphs of numerous important plant pathogens formerly only known from their corresponding anamorphs. Examples within the family Didymellaceae include several environmentally relevant species of *Ascochyta*,[9, 10] and *Phoma*.[11, 12] Literature survey of the genus *Didymella* revealed the occurrence of the phytotoxin pinolidoxin,[10] tricycloalternarene derivatives,[13] and desmethyldichlorodiaportintone, a dichloroisocoumarin that showed significant inhibition of NO production.[14] Another recent study on this genus afforded five compounds of the decahydrofluorene-class, including cytotoxic ascomylactams A−C, along with phomapyrrolidones A and C.[15] In the present study, we describe the isolation and structure elucidation of two newly discovered metabolites (**1** and **4**) from a solid rice fermentation of *Didymella* sp. IEA-3B.1, and of ascochitamine (**11**) obtained from a fungal fermentation on solid rice medium following addition of $(NH_4)_2SO_4$, as well as the results of cytotoxicity, NFκB inhibition and antimicrobial assays conducted

with the isolated compounds.

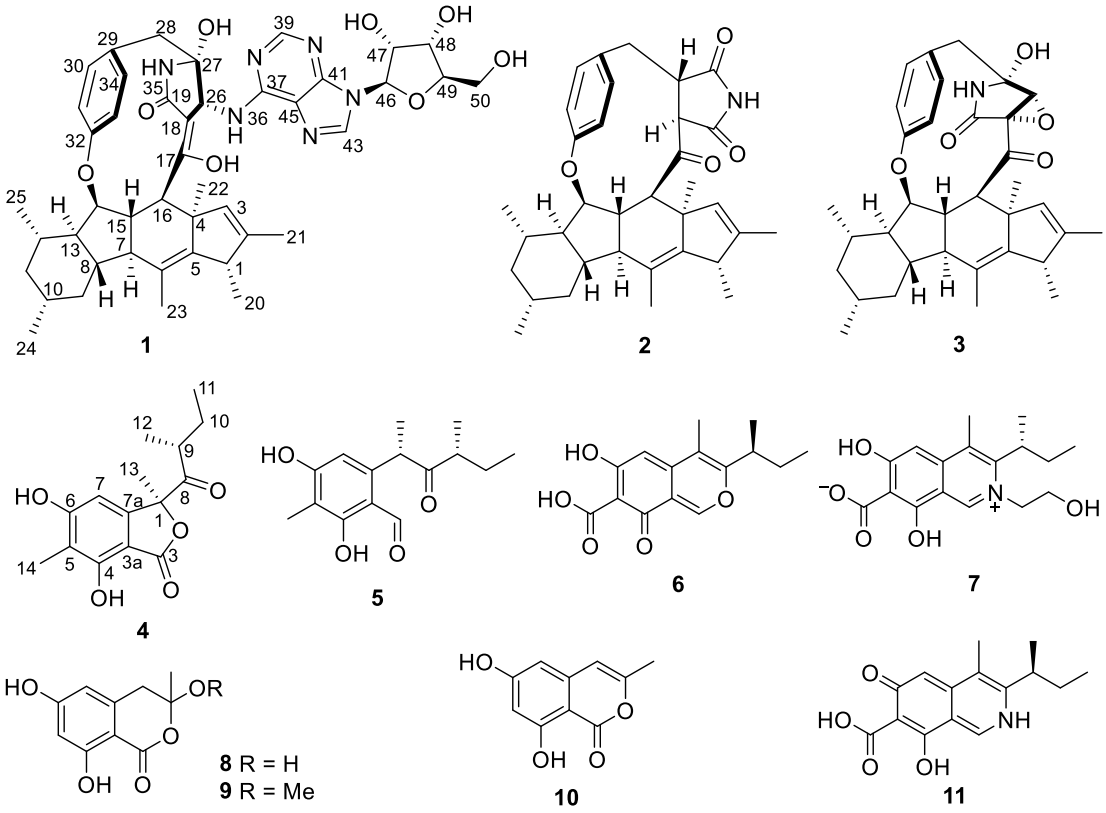

Figure 1. Compounds isolated from *Didymella* sp. IEA-3B.1.

Results and discussion

Chromatographic workup of the EtOAc extract of the fungal endophyte *Didymella* sp. cultured on solid rice medium, yielded two new natural products, didymellanosine (**1**) and ascolactone C (**4**), together with eight known compounds, phomapyrrolidone A (**2**),[15, 16] ascomylactam C (**3**),[15] (9*S*,11*R*)-(+)-ascosalitoxin (**5**),[17] ascochitine (**6**),[18, 19] fusarimine (**7**),[20] 3,6,8-trihydroxy-3-methyl-3,4-dihydroisocoumarin (**8**),[21] 3-methoxy-6,8-dihydroxy-3-methyl-3,4-dihydro-isocoumarin (**9**),[21] and 6,8-dihydroxy-3-methyl-isocoumarin (**10**),[22] (Fig. 1). The known compounds were identified by comparison of their NMR and MS data, as well as their specific optical rotations with data reported in the literature.

Didymellanosine (**1**) was isolated as a white, amorphous solid. The molecular formula of **1** was established as $C_{44}H_{54}N_6O_8$ from the HRESIMS data, accounting for

twenty-one degrees of unsaturation. The planar structure of **1** was deduced by detailed analysis of 1D and 2D NMR spectra, as well as by comparison of its NMR data to those of reported structurally related alkaloids.[15, 16, 23] The ^{1}H and ^{13}C NMR spectra of **1** (Table 1) aided by HSQC revealed signals of six methyl groups, four methylenes and twenty-one methines, including six aromatic methines at δ_H 8.47 (H-43), 8.20 (H-39), 7.10 (H-30 and H-34), 6.97 (H-33) and 6.71 (H-31), as well as thirteen quaternary carbons (eleven sp^2 and two sp^3). The consecutive COSY correlations (Fig. 2) observed from H-7 through H-16, and between H-1/H-20, H-7/H-15, H-8/H-13, H-10/Me-24, and H-14/Me-25, together with the HMBC correlations from Me-20 to C-1, C-2 and C-5, from Me-21 to C-1, C-2 and C-3, from Me-22 to C-3, C-4, C-5, and C-16, and from Me-23 to C-5, C-6 and C-7, indicated the presence of a 5/6/5/6 tetracyclic system with six methyl groups at C-1, C-2, C-4, C-6, C-10 and C-12. The COSY correlations between H-30/H-31, H-33/H-34 along with the HMBC correlations from H-30 and H-34 to C-32, and from H-31 and H-33 to C-29 confirmed the presence of a *para*-substituted benzene ring in **1**. Moreover, the NH signal resonating at δ_H 7.70 (H-35) showed HMBC correlations to C-18, C-26, C-27 and to a carbonyl C-19, while H-26 showed HMBC correlations to C-18, C-19, and C-27, suggesting the presence of a γ-lactam ring, which was further connected to the benzene ring through a methylene group, as evident from the HMBC correlations from H_2-28 to C-26, C-27, C-29 and C-30, and from 27-OH to C-27 and C-28. Additional HMBC correlations from H-15 to C-32, from H-16 and H-26 to C-17, and from 17-OH (δ_H 11.44) to C-16, C-17, and C-18 indicated an ether bridge between C-15 and C-32 and the linkage of lactam ring and tetracyclic core through C-17. Thus, a macrocyclic decahydrofluorene skeleton similar to **3** was established for **1**. The attachment of an additional adenosine moiety at C-26 was deduced by the spin systems from H-46 to H_2-50 and between H-26 and NH-36, the HMBC correlations from H-46 to C-41 and C-43, from H-43 to C-41 and C-45, from H-39 to C-37 and C-41, from NH-

36 to C-37 and C-45, and from H-26 to C-37, along with the molecular formula of **1**. Thus, the planar structure of **1** was elucidated as shown (Fig. 2). Compound **1** shares a similar partial structure with embellicine B,[23] and ascomylactam A,[15] except for the presence of an adenosine unit in **1** instead of hydroxy or methoxy groups in the former compounds.

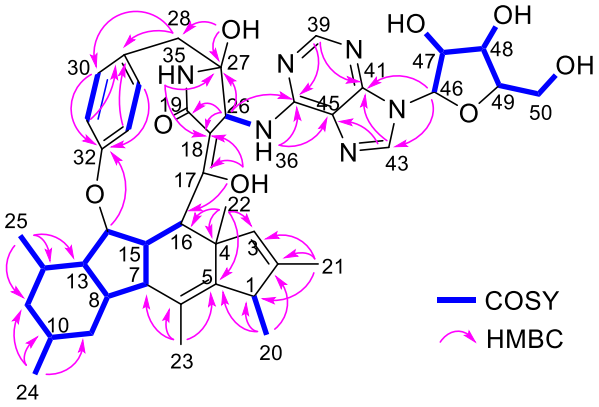

Figure 2. COSY and key HMBC correlations of compound **1**.

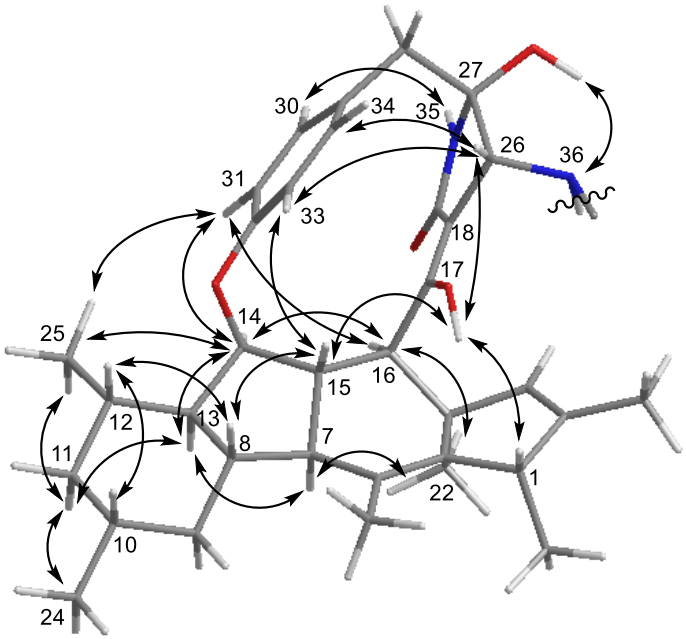

Figure 3. Key NOE correlations of compound **1**.

The relative configuration of **1** was deduced through analysis of the NOESY spectrum of **1** and by comparison with those of ascomylactams A and C (**3**),[15] (Fig. 3). The NOE correlations between H-16/H-14, H-14/H-13, H-13/H-7, H-7/Me-22, Me-22/H-16, H-16/H-31, H-31/Me-25, Me-25/H-14, H-14/H-31, Me-25/H-11b, H-11b/H-

13 and H-11b/Me-24 suggested these protons to be on the same side of the molecule, whereas NOEs observed for H-1/OH-17, OH-17/H-15, H-15/H-8, H-8/H-12, H-12/H-10, OH-17/H-26, H-26/H-33, and H-33/H-15 indicated them to be on the opposite side. In addition, the NOE correlations between H-26/H-34, H-26/H-33, H-33/H-15, and between NH-35/H-30, H-31/H-14, H-31/Me-25, OH-27/NH-36 indicated restricted rotation of the benzene ring and its parallel orientation to the γ-lactam ring, the same as reported for ascomylactams A and C (**3**).[15] Moreover, the relative configuration of the adenosine moiety was elucidated by the NOE correlations between H-46/H-49, H-46/OH-47, and H-49/OH-48, as well as by comparison of the chemical shifts and coupling constants with literature data.[24, 25] Thus, the structure of compound **1** was determined as shown, representing the first example within decahydrofluorene-type alkaloids bearing a 13-membered macrocyclic skeleton conjugated with an adenosine moiety.

Table 1. ^{1}H and ^{13}C NMR data for compound **1**.[a]

NO.	δ_C, type	δ_H (*J* in Hz)	NO.	δ_C, type	δ_H (*J* in Hz)
1	43.5, CH	2.68, q (7.1)	27	85.7, C	
2	138.0, C		28	46.0, CH_2	2.94, d (12.5); 2.88, d (12.5)
3	131.3, CH	4.44, s	29	128.9, C	
4	52.6, C		30	130.6, CH	7.10, d (8.4)
5	144.7, C		31	119.4, CH	6.97, dd (8.4, 2.2)
6	125.5, C		32	157.3, C	
7	46.9, CH	1.95, t (12.0)	33	122.0, CH	6.71, dd (8.4, 2.2)
8	42.7, CH	1.54, m	34	129.9, CH	7.11, d (8.4)
9	39.6, CH_2	2.08, d (12.2); 0.72, m	35		7.70, s
10	31.8, CH	1.52, m	36		7.46, d (5.1)
11	44.7, CH_2	1.74, m; 0.68, m	37	152.2, C	
12	30.9, CH	1.79, m	39	150.8, CH	8.20, s
13	56.3, CH	1.16, m	41	147.8, C	
14	87.0, CH	4.52, dd (8.1, 5.2)	43	140.4, CH	8.47, s
15	52.3, CH	1.97, m	45	119.8, C	
16	46.2, CH	3.49, d (7.2)	46	87.9, CH	5.89, d (5.2)
17	163.6, C		47	73.7, CH	4.48, q (5.4)
18	106.6, C		48	70.0, CH	4.13, q (4.6)
19	169.6, C		49	85.3, CH	3.94, q (3.9)
20	18.4, CH_3	0.80, d (7.1)	50	61.1, CH_2	3.68, ddd (12.0, 4.7, 4.2); 3.52, ddd (12.0, 6.3, 3.8)
21	12.3, CH_3	0.40, s	17-OH		11.44, s
22	27.6, CH_3	0.95, s	27-OH		6.62, s
23	15.3, CH_3	1.73, s	47-OH		5.47, d (6.0)
24	22.4, CH_3	0.92, d (6.5)	48-OH		5.18, d (5.1)

25	19.9, CH_3	1.07, d (6.1)	50-OH	5.16, t (5.5)
26	55.5, CH	4.11, d (5.1)		

[a] Recorded at 600 MHz (^{1}H) and 125 MHz (^{13}C) in DMSO-d_6.

Ascolactone C (**4**), was obtained as a white, amorphous solid. Its HRESIMS spectrum exhibited a prominent pseudomolecular ion peak at *m/z* 279.1226 $[M+H]^+$, which was attributed to the molecular formula $C_{15}H_{18}O_5$, corresponding to 7 degrees of unsaturation. Inspection of the ^{1}H NMR data of **4** (Table 2) revealed resonances of one aromatic singlet, four methyl groups, one set of methylene protons and one methine. The aromatic proton which appeared at δ_H 6.58 (H-7), exhibited HMBC correlations to C-3a, C-5 and C-6, while the aromatic methyl singlet at δ_H 2.09 (Me-14) showed HMBC correlations to C-4, C-5 and C-6, suggesting the presence of a penta-substituted benzene ring bearing a methyl substituent at the *meta*-position (Fig. 4). The COSY correlations between Me-11/H_2-10/H-9/Me-12, along with the HMBC correlations from H-9, H_2-10 and Me-12 to a ketone carbonyl at δ_C 210.8 (C-8), allowed the establishment of 2-methyl-1-oxobutyl moiety. The HMBC correlations from Me-13 (δ_H 1.67) to C-1, C-7a, and C-8, and from H-7 to C-1, confirmed the connection of 2-methyl-1-oxobutyl moiety to the aromatic ring through C-1. Moreover, the weak HMBC correlation detected from H-7 and to the carbonyl C-3, together with the chemical shift of C-1 (δ_C 90.7) and the remaining one degree of unsaturation, indicated the presence of a γ-lactone fused to the benzene ring, thus forming the benzolactone skeleton. In addition, two hydroxy groups were deduced at C-4 and C-6 of the benzene ring based on the chemical shifts of C-4 and C-6 and the molecular formula of **4**. Accordingly, the planar structure of **4** was established as shown (Fig. 4). Compound **4** is structurally related to ascolactones A and B, except for the replacement of the carboxy group at C-5 by a methyl group in **4**.[19] The absolute configuration of the latter two compounds was determined by TDDFT-ECD calculations and chemical reactions. The absolute configuration of **4** was concluded to be the same as that of ascolactone B (1*S*,9*R*) on the basis of a good agreement of the ^{1}H

NMR data with regard to resonances of the side chain (δ_H 0.49, 1.06 for Me-11,12 in ascolactone A compared to δ_H 0.85, 0.78 for Me-11,12 in ascolactone B), as well as based on similar negative values of their specific optical rotations.[19]

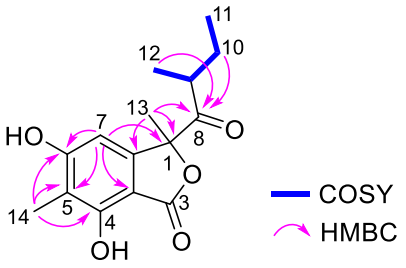

Figure 4. COSY and key HMBC correlations of compound **4**.

Table 2. ^{1}H and ^{13}C NMR data for compound **4**.[a]

position	δ_C, type[b]	δ_H (J in Hz)
1	90.7, C	
3	160.7, C	
3a	102.8, C	
4	156.2, C	
5	112.7, C	
6	163.7, C	
7	101.3, CH	6.58, s
7a	149.0, C	
8	210.8, C	
9	42.2, CH	2.83, m
10	26.6, CH_2	1.71, ddd (14.0, 7.4, 6.7)
		1.36, ddd (14.0, 7.4, 6.7)
11	11.7, CH_3	0.87, t (7.4)
12	16.7, CH_3	0.79, d (6.8)
13	23.4, CH_3	1.67, s
14	7.7, CH_3	2.09, s

[a] Recorded at 600 MHz (^{1}H) and 150 MHz (^{13}C). [b] Data were extracted from HSQC and HMBC.

In an attempt to influence the metabolite pattern of the fungus *Didymella* sp. IEA-3B.1, the strain was subjected to further fermentation in presence of 3.5 g $(NH_4)_2SO_4$ that had been added to solid rice medium. HPLC analysis of the extracts resulting from fungal fermentation on rice with and without addition of $(NH_4)_2SO_4$, revealed distinct differences of the metabolite profiles between these two cultures (Fig. S1). The production of the main fungal metabolite during fermentation on solid rice medium, ascochitine (**6**), an azaphilone contributing to the green color of this culture, dramatically decreased when $(NH_4)_2SO_4$ was added to rice medium, thus resulting in a white coloration of the fungal culture in the presence of $(NH_4)_2SO_4$ (Fig. S2). Similarly,

isocoumarins (**8**−**10**) and decahydrofluorene analogues (**1**−**3**) were significantly down-regulated in the salt containing culture. In contrast, compound **11** (Fig. 1) was only detected in the presence of $(NH_4)_2SO_4$. The ^{1}H NMR data of **11** were similar to those of ascochitine (**6**) and fusarimine (**7**), two azaphilone derivatives co-isolated in this study. Detailed investigation of HRESIMS and 2D NMR data of **11** identified it as the previously reported synthetic compound, ascochitamine, which was prepared by adding NH_3 or NH_4OH to ascochitine (**6**).[26] The formation of nitrogen containing azaphilones through substitution of the pyrane oxygen by nitrogen derived from endogenous ammonia or exogenous amino acids during fungal fermentation is well known.[27, 28] The different pH values and nitrogen sources [$(NH_4)_2SO_4$, $NaNO_3$ and peptone], in the culture medium of *Monascus anka* have been shown to affect the composition and color of *Monascus* pigments as well.[29] Therefore, the accumulation of ascochitamine (**11**) in this study is presumably due to the fungal response to the presence of ammonium present in the culture medium containing $(NH_4)_2SO_4$. This result also provided further evidence of the effects of media composition (*e.g.* addition of salts) on the profile of azaphilone pigments, as we reported recently for bulgarialactone D isolated from a mistletoe-associated fungus, *Bulgaria inquinans*, cultured on solid Czapek medium containing different salt mixtures ($MgSO_4$, $NaNO_3$ and NaCl).[30]

All isolated compounds were investigated for their cytotoxicity towards the murine lymphoma cell line L5178Y. Compound **1** showed pronounced activity with an IC_{50} value of 2.2 μM, even more active than that of the positive control, kahalalide F (IC_{50} 4.3 μM), while the remaining compounds were inactive. Furthermore, **1** was assayed for cytotoxicity against two human cancer cell lines, Burkitt's lymphoma B cells (Ramos) and the adult lymphoblastic leukemia T cells (Jurkat J16). After 24 h of treatment, compound **1** displayed moderate cytotoxicity against Ramos and Jurkat J16 cells, with IC_{50} values of 7.6 and 11.0 μM, respectively. When the treatment was extended to 72 h,

1 gave stronger inhibitory effect with IC_{50} values of 3.3 and 4.4 μM towards each cell line.

Furthermore, we evaluated the impact of compounds **1**–**3** on NFκB inhibitory activity. For NFκB inhibition studies, **1**–**3** were tested in the triple-negative breast cancer (TNBC) cell line NFκB-MDA-MB-231. Based on the NFκB-dependent luciferase activity and the calculated half-maximal inhibitory concentration (IC_{50}), NFκB inhibition was induced by compound **1** (15.5 ± 1.1 μM), as well as **2** and **3** both at a similar concentration range with 54.1 ± 5.4 μM and 45.04 ± 11.6 μM, respectively (Table 3 and Fig. S23). To exclude that cytotoxicity decreased NFκB activation, cell viability was determined in parallel. Compound **1** was about 3-times more potent in the NFκB inhibition assay compared to its cytotoxicity (45.4 ± 8.1 μM) and also **2** was at least two times more potent in the NFκB assays than in the cytotoxicity assay (> 100 μM). Cytotoxicity of **3** (47.5 ± 8.5 μM) on the other hand was comparable to its NFκB inhibitory capacity and therefore, reduction in NFκB activity may be caused by cytotoxicity. Whereas antitumor activity of compound **3** may not depend on NFkB blockade, compounds **1** and **2** efficiently blocked NFκB activation.

Table 3. IC_{50} values (in μM)[a] of compounds **1**–**3** obtained by NFκB inhibition and cell viability assay.

	NFκB inhibition	Cell viability
1	15.5 ± 1.1	45.4 ± 8.1
2	54.1 ± 5.4	> 100
3	45.0 ± 11.6	47.5 ± 8.5

[a] Average IC_{50} of at least four individual experiments ± standard deviation.

Moreover, all isolated compounds were subjected to an antibacterial screening. Compound **3** was the most active substance against drug-susceptible and drug-resistant strains of the Gram-positive bacteria *Staphylococcus aureus*, *Enterococcus faecalis* and *Enterococcus faecium*, with MIC values ranging from 3.1 to 6.3 μM (Table 4). Compound **1** likewise inhibited the growth of the latter bacteria with MICs ranging from

6.3 to 12.5 μM, whereas much weaker activity was observed for **2** compared to the two aforementioned analogues. Intriguingly, **1** and **3** were also found to be active against the Gram-negative bacterium *Acinetobacter baumannii*, with comparable MIC values of 3.1 μM, both tested in the presence of a sublethal concentration of colistin (0.1 μM). Compounds with activity against *A. baumannii* are of substantial interest, as the increasing emergence of multidrug-resistant strains has led to serious clinical challenges due to the limited number of effective antimicrobial drugs.[31, 32] Combination therapy of colistin with other antibacterial agents is currently considered as a promising alternative for the treatment of *A. baumannii* infections.[33, 34] All compounds were inactive against the Gram-positive bacterium *Mycobacterium tuberculosis* when tested up to 100 μM. On the basis of the antimicrobial activity of these alkaloids, the presence of a γ-lactam substructure as present in **1** and **3** seems to be preferable for the activity rather than a succinimide moiety as in **2**. As a lower potency towards Gram-positive bacteria was observed for **1** in comparison to **3**, it is suggested that the adenosine conjugate in **1** might attenuate its antimicrobial activity with regard to particular strains, while it had no effect on the tested Gram-negative bacterium.

Table 4. Antibacterial activity (MIC in μM) of compounds **1**–**3** and **6**.

	M. tuberculosis	*S. aureus*		*E. faecalis*		*E. faecium*		*A. baumannii*
	H37Rv	ATCC 29213[a]	ATCC 700699[b]	ATCC 29212[a]	ATCC 51299[c]	ATCC 35667[a]	ATCC 700221[d]	BAA 1605[e]
1	>100	6.3	6.3	6.3	12.5	12.5	6.3	3.1
2	>100	25	12.5	100	50	25	12.5	12.5
3	>100	3.1	3.1	6.3	3.1	6.3	3.1	3.1
6	>100	50	50	>100	>100	50	>100	>100

[a] Drug-susceptible strain. [b] Methicillin-resistant strain of *S. aureus* (MRSA). [c] Vancomycin-resistant strain of *E. faecalis*. [d] Vancomycin-resistant strain of *E. faecium*. [e] Tested in the presence of a sublethal concentration (0.1 μM) of colistin.

Of note, biosynthetically related fungal alkaloids belonging to the decahydrofluorene-class, such as GKK1032s,[35, 36] pyrrocidines,[37-40] hirsutellones,[41, 42], trichobamide A,[43] and penicipyrrodiether A,[44] were found in previous studies to exhibit antibacterial activity against Gram-positive bacteria including drug-resistant strains,[36-

[38, 44] and against *Mycobacterium tuberculosis*.[41, 42] These compounds furthermore exhibited antifungal activity,[37] were active as inhibitors of prolyl oligopeptidase,[39] and were shown to be cytotoxic against numerous cancer cell lines.[35, 40, 43] The complex molecular architecture, consisting of a tricyclic polyketide fused to a 12 or 13-membered macroether ring which contains a *γ*-lactam or a succinimide moiety, combined with their intriguing bioactivities, have triggered tremendous efforts in synthetic and biosynthetic studies as well.[45-47] However, decahydrofluorenes featuring a tetracyclic core as encountered in compound **1** are rarely reported. To date, only embellicines A and B, possessing cytostatic, cytotoxic and NFκB inhibitory activities, from a fungal endophyte *Embellisia eureka*,[23] antitubercular phomapyrrolidones A−C from an endophytic *Phoma* sp. NRRL 46751,[16] and cytotoxic ascomylactams A−C from a mangrove associated fungus *Didymella* sp. CYSK-4,[15] stand as examples. Thus, in light of the bioactivity results reported for didymellanosine (**1**) in this study and its new chemical feature bearing an adenosine unit attached to a pyrrolidinone, further studies on the pharmacological properties of this metabolite seem promising.

Experimental section

General procedures

HPLC analysis was carried out with a Dionex UltiMate 3000 system coupled with an UltiMate 3000 pump linked to a photodiode array detector (DAD 3000 RS). Detection wavelengths were set at 235, 254, 280, and 340 nm. The column was prefilled with Eurospher 100-10 C_{18}, 125 × 4 mm (Knauer, Germany). The routine HPLC analysis was performed with the following gradient (MeOH: 0.1% HCOOH in H_2O): 0 min (10% MeOH); 5 min (10% MeOH); 35 min (100 % MeOH); 45 min (100% MeOH). Semipreparative HPLC was conducted with a Merck Hitachi Chromaster HPLC system (UV detector 5410; pump 5110; column Eurospher 100-10 C_{18}, 300 × 8 mm, Knauer; flow rate at 5 mL/min). Silica gel 60 M (Macherey-Nagel) was used for vacuum liquid

chromatography (VLC) and Sephadex LH-20 for column chromatography. TLC plates pre-coated with silica gel 60 F_{254} (Macherey-Nagel) were used for routine analysis. One- and two-dimensional NMR spectra were recorded on Bruker AVANCE DMX 600 or 500 NMR spectrometers. ESIMS and HRESIMS data were acquired by a Finnigan LCQ Deca mass spectrometer and an UHR-QTOF maXis 4G (Bruker Daltonics) mass spectrometer, respectively. Optical rotations were measured on a Jasco P-2000 polarimeter.

Fungal isolation, identification and cultivation

The fungus, *Didymella* sp. IEA-3B.1, was isolated from healthy leaves of *Terminalia catappa* (Combretaceae), collected in April 2018, in Jimbaran in the south of Bali, Indonesia. The fungal culture was identified by a standard molecular biology protocol, through DNA amplification and sequencing of the ITS region as described before.[48] The sequence data have been submitted to the GenBank with accession No. MN227696.1. The voucher strain was deposited in the Institute of Pharmaceutical Biology and Biotechnology, Düsseldorf, Germany. The fungus was cultured on twenty 1 L Erlenmeyer flasks, each flask containing 100 g rice in 100 mL distilled water followed by autoclaving. Another set of fungal fermentation was carried out on five 1 L Erlenmeyer flasks by adding 3.5 g $(NH_4)_2SO_4$ to 100 g rice in 100 mL distilled water to each flask, followed by autoclaving. The fungal culture was maintained under static conditions at room temperature until the rice medium was completely covered by the fungus (30 days).

Extraction and isolation

The fungal culture grown on solid rice medium was extracted twice, each with 500 mL EtOAc added to each flask. The EtOAc extract was concentrated *in vacuo* and the obtained crude extract (32.9 g) was subjected to liquid-liquid partitioning between *n*-hexane and 90% aqueous MeOH. The 90% aqueous MeOH extract (5.0 g) was

chromatographed on silica gel 60 (VLC) by a step gradient elution with *n*-hexane-EtOAc followed by CH_2Cl_2-MeOH to afford 13 fractions (V1−V13). Based on HPLC chromatograms, fractions V3, V4, V5, V9, and V10 eluted with *n*-hexane-EtOAc (6:4), (4:6), (2:8), and CH_2Cl_2-MeOH (9:1), (7:3), respectively, were subjected to further separation. Fraction V3 (315.7 mg) was applied to a Sephadex LH-20 column and eluted with CH_2Cl_2-MeOH (1:1) to obtain 4 subfractions. Purification of subfraction V3.2 (164.6 mg) was carried out with semipreparative HPLC employing MeOH-H_2O as mobile phase (from 85% to 100% MeOH) to afford **2** (45.6 mg). Meanwhile, compounds **4** (1.8 mg), **5** (5.8 mg) and **10** (2.1 mg) were obtained after purification of subfraction V3.3 (34.3 mg) by semipreparative HPLC with gradient elution of MeOH-H_2O (from 50% to 100% MeOH). Separation of fraction V4 (200.3 mg) on Sephadex LH-20 using CH_2Cl_2-MeOH (1:1) as eluent, followed by purification using semipreparative HPLC eluted with MeOH-0.1% HCOOH in H_2O (from 85% to 100% MeOH), yielded **3** (3.4 mg). In a similar manner, fraction V5 (625.5 mg) was submitted to a Sephadex LH-20 column, to give **6** (263.0 mg) along with 5 subfractions. Subfraction V5.6 (37.8 mg) was purified by semipreparative HPLC, employing MeOH-0.1% HCOOH in H_2O (from 30% to 70% MeOH) as mobile phase, to yield **8** (11.6 mg) and **9** (2.2 mg). Furthermore, compound **7** (30.0 mg) was obtained by separation of fraction V9 (272.8 mg) on a Sephadex LH-20 column employing CH_2Cl_2-MeOH (1:1) as eluent. Compound **1** (20.8 mg) was afforded through separation of fraction V10 (308.6 mg) over a Sephadex LH-20 column, eluted with CH_2Cl_2-MeOH (1:1), followed by purification using semipreparative HPLC with MeOH-H_2O (from 85% to 100% MeOH). Following the same procedure, the fungal culture by supplementing rice medium with $(NH_4)_2SO_4$ was extracted with EtOAc, taken to dryness, and followed by liquid-liquid partition between *n*-hexane and 90% aqueous MeOH. The resulting MeOH fraction (340.2 mg) was rinsed with various solvents which yielded the pure compound **11** (3.0 mg).

Didymellanosine (**1**): white amorphous solid; $[\alpha]_D^{25}$ −28 (*c* 0.15, MeOH); UV (MeOH): λ_{max} 207 and 260 nm; 1D and 2D NMR data, see Table 1; HRESIMS *m*/*z* 795.4072 $[M+H]^+$ (calcd for $C_{44}H_{55}N_6O_8$, 795.4076).

Ascolactone C (**4**): white amorphous solid; $[\alpha]_D^{25}$ −98 (*c* 0.20, MeOH); UV (MeOH): λ_{max} 215, 228, and 264 nm; 1D and 2D NMR data, see Table 2; HRESIMS *m*/*z* 279.1226 $[M+H]^+$ (calcd for $C_{15}H_{19}O_5$, 279.1227).

Ascochitamine (**11**): yellowish brown amorphous solid; $[\alpha]_D^{25}$ −48 (*c* 0.10, DMSO); UV (MeOH): λ_{max} 264 and 357 nm; 1D and 2D NMR data, see Table S1 in the Supporting Information; HRESIMS *m*/*z* 276.1229 $[M+H]^+$ (calcd for $C_{15}H_{18}NO_4$, 276.1230).

Cytotoxicity assay

Cytotoxicity was tested against the murine lymphoma cell line L5178Y using the MTT method, and kahalalide F was included as positive control.[30] Meanwhile, cytotoxicity against the human cell lines Ramos (Burkitt's lymphoma B cells) and Jurkat J16 (adult lymphoblastic leukemia T cells) was determined by the resazurin reduction assay. In brief, cells were incubated with the indicated compounds in 96-well plates for 24 or 72 h, respectively. Subsequently, resazurin was added to a final concentration of 40 μM. After 3 h of incubation fluorescence of resorufin (excitation: 535 nm, emission: 590 nm) was measured via a microplate spectrophotometer. The reduction of resazurin to resorufin is proportional to aerobic respiration and therefore can be used as an indicator for cell viability.[49] Staurosporine (2.5 μM) was employed for Ramos and Jurkat J16 cells. Culture medium containing 0.1% DMSO was used as a negative control for the assay.

Cell culture for MDA-MB-231 cells and materials

Culture medium and supplements were purchased from Gibco™ (Fisher Scientific, Schwerte, Germany). Consumable materials such as 96-well and 384-well plates were

purchased by Sarstedt (Nümbrecht, Germany) or Greiner bio-one (Frickenhausen, Germany). Cells were grown and incubated in a humidified 5 % CO_2 atmosphere at constant 37°C. The metastatic breast cancer cell line, MDA-MB -231, was obtained from the European Collection of Authenticated Cell Cultures (ECACC, Salisbury, UK). Subculture in 175 cm^2 flasks was done in RPMI 1640 medium (Cat# 21875-034) supplemented with 15 % (*v*/*v*) FCS and 1 % (*v*/*v*) penicillin-streptomycin (pen-strep) (10,000 U/mL). The monoclonal NFκB-MDA-MB-231 cell line contains a NFκB response element to control the luciferase reporter gene. For the procedure of cell line generation see the publication of Sperlich et al. (2017).[50] Subculture was performed in high glucose DMEM (Cat#41966-029) supplemented with 10 % (*v*/*v*) FCS, 1 % (*v*/*v*) pen-strep (10,000 U/mL) and 400 μg/mL hygromycin B (Life Technologies, Darmstadt, Germany, Cat# 10687010) for selection. Hunger medium for the NFκB inhibition assay was composed of high glucose DMEM medium supplemented with 1 % (*v*/*v*) FCS, 1 % (*v*/*v*) penicillin-streptomycin (10,000 U/mL). Cell detachment occurred by trypsinization in 0.25 % trypsin-EDTA and cell counting was performed at 1:1 (*v*/*v*) dilution in Erythrosin B (BioCat, Heidelberg, Germany; #L13002) using the LUNA II automated cell counter (BioCat). The compounds used for NFκB inhibition and cell viability assay, namely didymellanosine (**1**), phomapyrrolidone A (**2**) and ascomylactam C (**3**), were dissolved in dimethylsulfoxide (DMSO) to a final concentration of 10 mM and diluted in cell culture medium for further use.

Cytotoxicity against MDA-MB-231 cells.

Cytotoxicity against triple-negative breast cancer was determined on the cell line MDA-MB-231. Using the CyBio® Well vario pipetting robot (Analytik Jena, Jena, Germany; #OL3381-24-730), 18 μL of the cell suspension (2.8×10^5 cells/mL) were seeded on a 384-well plate (Greiner; #781074) and incubated for 24 hours. For treatment in quadruples, 2 μL of the medium + 1 % DMSO (negative control) or the tenfold

concentrated substance was applied to reach a final volume of 20 μL per well. The final concentration for compounds ranged in two-fold dilution steps from 100 μM to 0.78 μM in 8 points. Compound stimulation endured for 2 hours and final cell lysis and measurement was done as prescribed in the manufacturer's instruction of the CellTiter-Glo® Luminescent Cell Viability Assay (Promega, Mannheim, Germany; #G7570). In short, it was applied the equal volume of CellTiter-Glo® and luminescence was measured using the Spark® microplate reader (TECAN, Männedorf, Switzerland).

NFκB inhibition assay

For testing the compound **1**–**3** concerning the NFκB activity, 4×10^4 NFκB-MDA-MB-231 cells were seeded in total 100 μL medium per well on a 96-well plate (Greiner, Cat# 655098). The next day, medium was exchanged and cells pre-incubated for 20 minutes without (negative control) or with diluted substance in total 100 μL hunger medium (DMEM + 1 % FCS + 1 % pen-strep + 1 % DMSO). The final concentration of the compounds ranged a two-fold serial dilution from 100 μM downwards to 0.78 μM in 8 points. To activate NFκB signaling, cells were subsequently stimulated for 2 hours with 1 μg/mL lipopolysaccharide (Sigma-Aldrich, Taufkirchen, Germany; #L2630). Last, cell lysis and measurement was done according to the manufacturer's instruction of the Nano-Glo Luciferase Assay System (Promega; # N1110). In short, it was applied the equal volume of 1:50 (v/v) diluted Nano-Glo reagent and luminescence was measured using the Spark® microplate reader (TECAN).

Statistical analysis

Data of NFκB inhibition assay and cell viability assay against MDA-MB-231 were analyzed using GraphPad Prism (GraphPad Software, San Diego, USA; Version 8.1.2) and represent at least four individual experiments which were depicted as mean ± SEM. For calculation of the half-maximal inhibitory concentration (IC_{50}) in NFκB inhibition assay and cell viability assay, substance concentration [M] was transformed as common

logarithm to obtain log(M). IC_{50} values were determined by nonlinear regression analysis based on dose-response inhibition calculation without curve fitting.

Antimicrobial activity

The tested bacteria included *Staphylococcus aureus* (ATCC 29213 and 700699), *Enterococcus faecium* (ATCC 35667 and 700221), *Enterococcus faecalis* (ATCC 29212 and 51299), *Acinetobacter baumannii* (ATCC BAA1605), and *Mycobacterium tuberculosis* (H37Rv). Except for *M. tuberculosis*, antimicrobial activity was evaluated utilizing the microdilution method in accordance with the CLSI guidelines.[51] Activity against *M. tuberculosis* was assessed employing the resazurin dye reduction method as described previously.[52] Moxifloxacin was used as positive control for all tested Gram-positive and Gram-negative bacteria except for *Mycobacterium tuberculosis*, where rifampicin was used as positive control.

Acknowledgements

N.P.A. wishes to thank DAAD Program Biodiversity and Health for the doctoral scholarship. This work was supported by the Deutsche Forschungsgemeinschaft (DFG, German Research Foundation) – project number 270650915 / GRK 2158 (to P.P., S.W. and R.K.). P.P. also wants to thank the Manchot Foundation for support.

References and notes

1. A. H. Aly, A. Debbab, J. Kjer and P. Proksch, *Fungal Divers.*, 2010, **41**, 1−16.
2. G. Strobel, *J. Fungi*, 2018, **4**, 57.
3. H. Gao, G. Li and H.-X. Lou, *Molecules*, 2018, **23**, 646.
4. J. G. Ondeyka, G. L. Helms, O. D. Hensens, M. A. Goetz, D. L. Zink, A. Tsipouras, W. L. Shoop, L. Slayton, A. W. Dombrowski, J. D. Polishook, D. A. Ostlind, N. N. Tsou, R. G. Ball and S. B. Singh, *J. Am. Chem. Soc.*, 1997, **119**, 8809−8816.
5. B. P. Bashyal, B. P. Wellensiek, R. Ramakrishnan, S. H. Faeth, N. Ahmad and A. A. L. Gunatilaka, *Bioorg. Med. Chem*., 2014, **22**, 6112−6116.
6. A. Stierle, G. Strobel and D. Stierle, *Science*, 1993, **260**, 214−216.
7. S. C. Puri, A. Nazir, R. Chawla, R. Arora, S. Riyaz-ul-Hasan, T. Amna, B. Ahmed, V. Verma, S. Singh, R. Sagar, A. Sharma, R. Kumar, R. K. Sharma and G. N. Qazi, *J. Biotechnol.*, 2006, **122**, 494−510.
8. S. Kusari, S. Zühlke and M. Spiteller, *J. Nat. Prod.*, 2009, **72**, 2−7.
9. M. I. Chilvers, J. D. Rogers, F. M. Dugan, J. E. Stewart, W. Chen and T. L. Peever, *Mycol. Res.*, 2009, **113**, 391−400.

10. A. Cimmino, A. Andolfi, S. Fondevilla, M. A. Abouzeid, D. Rubiales and A. Evidente, *J. Agric. Food Chem.*, 2012, **60**, 5273−5278.
11. M. M. Aveskamp, J. de Gruyter, J. H. C. Woudenberg, G. J. M. Verkley and P. W. Crous, *Stud. Mycol.*, 2010, **65**, 1−60.
12. Q. Chen, J. R. Jiang, G. Z. Zhang, L. Cai and P. W. Crous, *Stud. Mycol.*, 2015, **82**, 137−217.
13. C. Li, Z. Hu, Q. Liu, X. Wu and S. Cao, *Tetrahedron Lett.*, 2018, **59**, 3381−3383.
14. Y. Chen, Z. Liu, H. Liu, Y. Pan, J. Li, L. Liu and Z. She, *Mar. Drugs*, 2018, **16**, 54.
15. Y. Chen, Z. Liu, Y. Huang, L. Liu, J. He, L. Wang, J. Yuan and Z. She, *J. Nat. Prod.*, 2019, **82**, 1752−1758.
16. E. M. K. Wijeratne, H. He, S. G. Franzblau, A. M. Hoffman and A. A. L. Gunatilaka, *J. Nat. Prod.*, 2013, **76**, 1860−1865.
17. M. Leyte-Lugo, M. González-Andrade, M. d. C. González, A. E. Glenn, C. M. Cerda-Garcia-Rojas and R. Mata, *J. Nat. Prod.*, 2012, **75**, 1571−1577.
18. L. Colombo, C. Gennari, G. S. Ricca, C. Scolastico and F. Aragozzini, *J. Chem. Soc., Perkin Trans. 1*, 1980, 675−676.
19. S. F. Seibert, E. Eguereva, A. Krick, S. Kehraus, E. Voloshina, G. Raabe, J. Fleischhauer, E. Leistner, M. Wiese, H. Prinz, K. Alexandrov, P. Janning, H. Waldmann and G. M. König, *Org. Biomol. Chem.*, 2006, **4**, 2233−2240.
20. S.-X. Yang, J. Xiao, H. Laatsch, J. J. Holstein, B. Dittrich, Q. Zhang and J.-M. Gao, *Tetrahedron Lett.*, 2012, **53**, 6372−6375.
21. K. Kameda, H. Aoki, H. Tanaka and M. Namiki, *Agr. Biol. Chem.*, 1973, **37**, 2137−2146.
22. D. S. Zinad, K. A. Shaaban, M. A. Abdalla, M. T. Islam, A. Schüffler and H. Laatsch, *Nat. Prod. Commun.*, 2011, **6**, 45−48.
23. W. Ebrahim, A. H. Aly, V. Wray, A. Mándi, M.-H. Teiten, F. Gaascht, B. Orlikova, M. U. Kassack, W. Lin, M. Diederich, T. Kurtán, A. Debbab and P. Proksch, *J. Med. Chem.*, 2013, **56**, 2991−2999.
24. H. Rosemeyer, G. Toth and F. Seela, *Nucleos. Nucleot.*, 1989, **8**, 587−597.
25. P. Ciuffreda, S. Casati and A. Manzocchi, *Magn. Reson. Chem.*, 2007, **45**, 781−784.
26. H. Mishima, M. Kurabayashhi, H. Oku and I. Iwai, *Annu. Rep. Sankyo Res. Laboratories*, 1970, **22**, 67−79.
27. T. F. Lin, K. Yakushijin, G. H. Büchi and A. L. Demain, *J. Ind. Microbiol.*, 1992, **9**, 173−179.
28. X. Wang, J. G. S. Filho, A. R. Hoover, J. B. King, T. K. Ellis, D. R. Powell and R. H. Cichewicz, *J. Nat. Prod.*, 2010, **73**, 942−948.
29. K. Shi, D. Song, G. Chen, M. Pistolozzi, Z. Wu and L. Quan, *J. Biosci. Bioeng.*, 2015, **120**, 145−154.
30. N. P. Ariantari, G. Daletos, A. Mándi, T. Kurtán, W. E. G. Müller, W. Lin, E. Ancheeva and P. Proksch, *RSC Adv.*, 2019, **9**, 25119−25132.
31. J. Li, C. R. Rayner, R. L. Nation, R. J. Owen, D. Spelman, K. E. Tan and L. Liolios, *Antimicrob. Agents Chemother.*, 2006, **50**, 2946−2950.
32. L.-C. Kuo, C.-C. Lai, C.-H. Liao, C.-K. Hsu, Y.-L. Chang, C.-Y. Chang and P.-R. Hsueh, *Clin. Microbiol. Infect.*, 2007, **13**, 196−198.
33. S. Biswas, J.-M. Brunel, J.-C. Dubus, M. Reynaud-Gaubert and J.-M. Rolain, *Expert Rev. Anti Infect. Ther.*, 2012, **10**, 917−934.
34. A. M. Peri, Y. Doi, B. A. Potoski, P. N. A. Harris, D. L. Paterson and E. Righi, *Diagn. Microbiol. Infect. Dis.*, 2019, **94**, 413−425.
35. F. Koizumi, *Jpn. Kokat Tokkyo Koho Japanese Patent P2001-247574A*, 2001.
36. X. Qi, X. Li, J. Zhao, N. He, Y. Li, T. Zhang, S. Wang, L. Yu and Y. Xie, *J. Antibiot.*, 2019, **72**, 237−240.
37. H. He, H. Y. Yang, R. Bigelis, E. H. Solum, M. Greenstein and G. T. Carter, *Tetrahedron Lett.*, 2002, **43**, 1633−1636.

38. T. M. Casella, V. Eparvier, H. Mandavid, A. Bendelac, G. Odonne, L. Dayan, C. Duplais, L. S. Espindola and D. Stien, *Phytochemistry*, 2013, **96**, 370−377.
39. Y. Shiono, A. Kosukegawa, T. Koseki, T. Murayama, E. Kwon, S. Uesugi and K.-i. Kimura, *Phytochem. Lett.*, 2012, **5**, 91−95.
40. S. Uesugi, N. Fujisawa, J. Yoshida, M. Watanabe, S. Dan, T. Yamori, Y. Shiono and K.-i. Kimura, *J. Antibiot.*, 2016, **69**, 133−140.
41. M. Isaka, N. Rugseree, P. Maithip, P. Kongsaeree, S. Prabpai and Y. Thebtaranonth, *Tetrahedron*, 2005, **61**, 5577−5583.
42. M. Isaka, W. Prathumpai, P. Wongsa and M. Tanticharoen, *Org. Lett.*, 2006, **8**, 2815−2817.
43. S. Chen, H. Shen, P. Zhang, H. Cheng, X. Dai and L. Liu, *Chem. Commun.*, 2019, **55**, 1438−1441.
44. T. Song, M. Chen, Z.-W. Ge, W. Chai, X.-C. Li, Z. Zhang and X.-Y. Lian, *J. Org. Chem.*, 2018, **83**, 13395−13401.
45. H. Oikawa, *J. Org. Chem.*, 2003, **68**, 3552−3557.
46. H. Uchiro, R. Kato, Y. Arai, M. Hasegawa and Y. Kobayakawa, *Org. Lett.*, 2011, **13**, 6268−6271.
47. A. Ear, S. Amand, F. Blanchard, A. Blond, L. Dubost, D. Buisson and B. Nay, *Org. Biomol. Chem.*, 2015, **13**, 3662−3666.
48. J. Kjer, A. Debbab, A. H. Aly and P. Proksch, *Nat. Protoc.*, 2010, **5**, 479−490.
49. J. O'Brien, I. Wilson, T. Orton and F. Pognan, *Eur. J. Biochem.*, 2000, **267**, 5421−5426.
50. J. Sperlich, R. Kerr and N. Teusch, *Mar. Drugs*, 2017, **15**, 262.
51. CLSI, *Methods for Dilution Antimicrobial Susceptibility Tests for Bacteria That Grow Aerobically*, Approved Standard Ninth ed. CLSI document M07-A9, Clinical and Laboratory Standards Institute, Wayne, PA, 2012.
52. N. Rehberg, E. Omeje, S. S. Ebada, L. van Geelen, Z. Liu, P. Sureechatchayan, M. U. Kassack, T. R. Ioerger, P. Proksch and R. Kalscheuer, *Antimicrob. Agents Chemother.*, 2019, **63**, e00136−19.

Supporting Information

Didymellanosine, a new decahydrofluorene analogue, and ascolactone C from *Didymella* sp. IEA-3B.1 an endophyte of *Terminalia catappa*

Ni P. Ariantari,[a,b] Elena Ancheeva,[a] Marian Frank,[a] Fabian Stuhldreier,[c] Dieter Meier,[a] Yvonne Gröner,[a] Irene Reimche,[d] Nicole Teusch,[d] Sebastian Wesselborg,[c] Werner E. G. Müller,[e] Rainer Kalscheuer,[a] Zhen Liu,[a,] * Peter Proksch[a,] *

[a]Institute of Pharmaceutical Biology and Biotechnology, Heinrich Heine University Düsseldorf, Universitätsstrasse 1, 40225 Düsseldorf, Germany

[b]Department of Pharmacy, Faculty of Mathematics and Natural Sciences, Udayana University, 80361 Bali, Indonesia

[c]Institute of Molecular Medicine I, Medical Faculty, Heinrich Heine University Düsseldorf, Universitätsstrasse 1, 40225 Düsseldorf, Germany.

[d]Department of Biomedical Sciences, Institute of Health Research and Education, University of Osnabrück, Germany

[e]Institute for Physiological Chemistry, University Medical Center of the Johannes Gutenberg University Mainz Duesbergweg 6, 55128 Mainz, Germany

[*]corresponding authors

Table of Contents

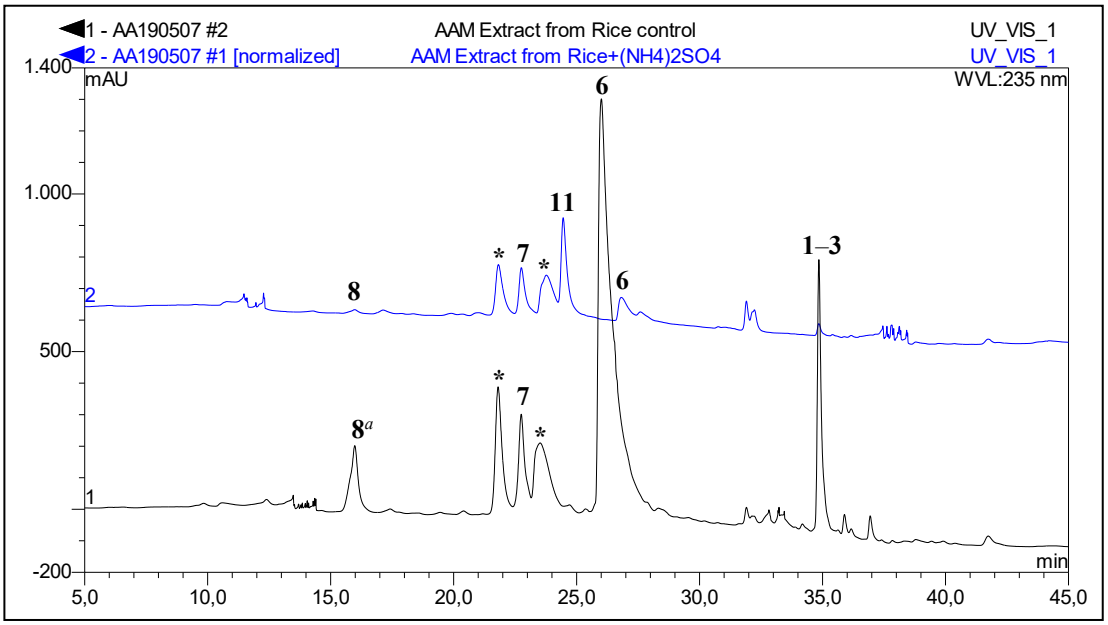

Figure S1. HPLC chromatograms of EtOAc extract of *Didymella* sp. IEA-3B.1 cultured on rice medium (black) compared to the OSMAC culture on rice medium with addition of 3.5 g $(NH_4)_2SO_4$ (blue) under UV detection at 235 nm.
[a] number refers to compound's number. * unidentified peaks

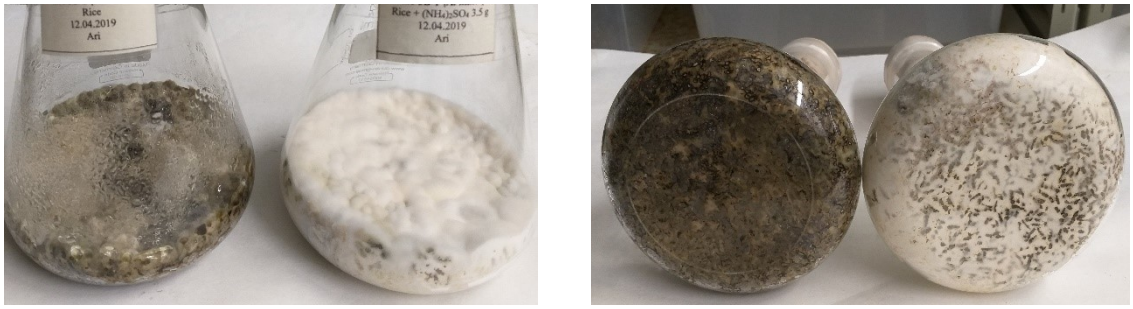

Figure S2. An endophytic *Didymella* sp. IEA-3B.1 cultured on rice medium (A) and on rice medium with addition of 3.5 g $(NH_4)_2SO_4$ (B).

(A)

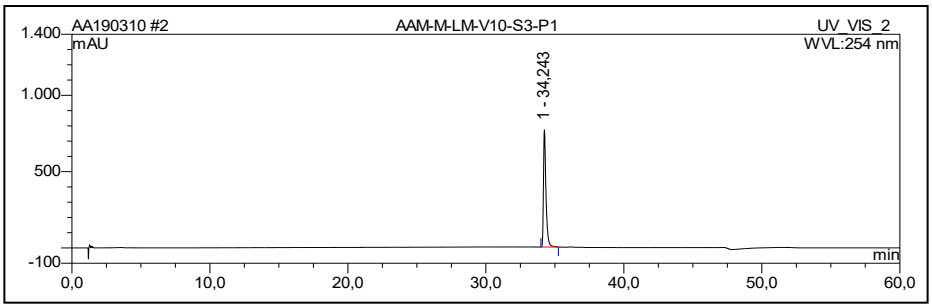

(B)

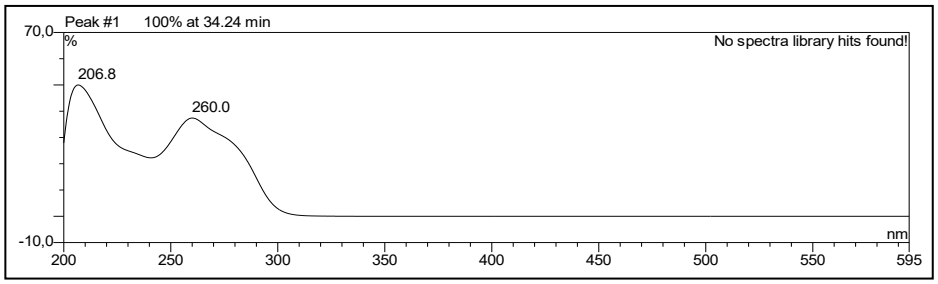

Figure S3. HPLC chromatogram (A) and UV spectrum (B) of compound **1**.

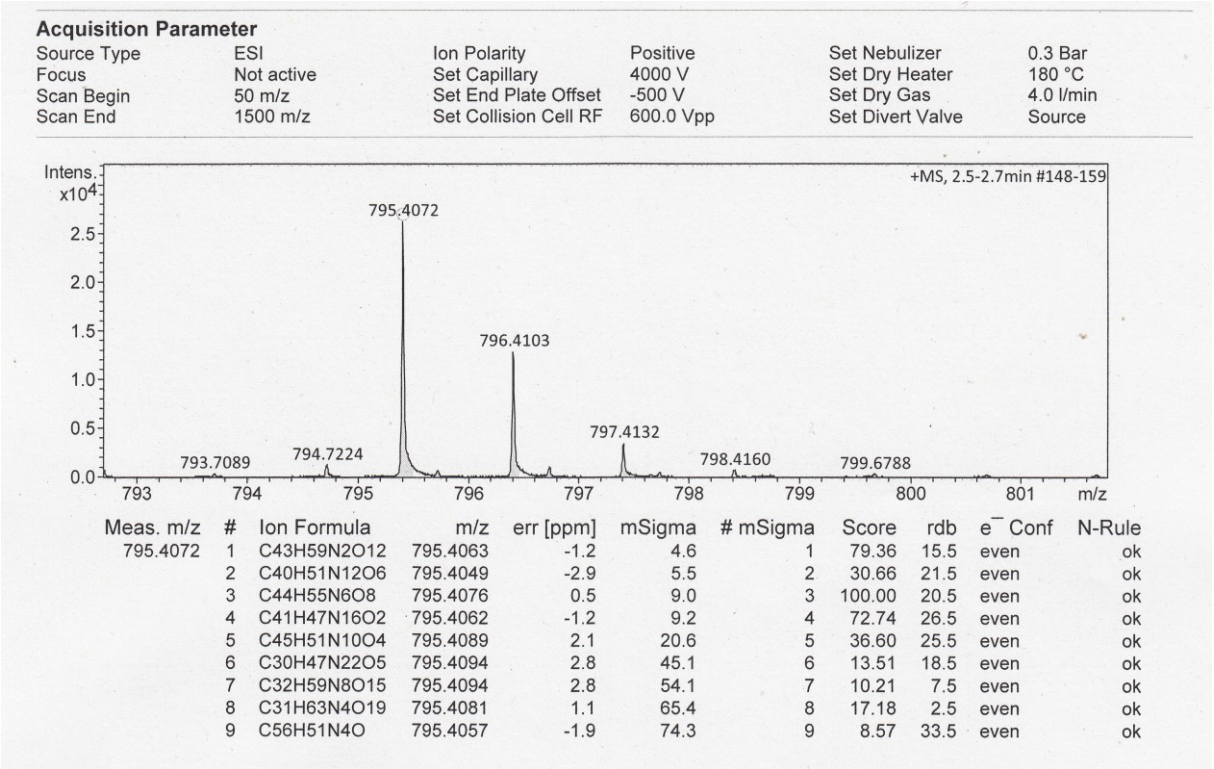

Meas. m/z	#	Ion Formula	m/z	err [ppm]	mSigma	# mSigma	Score	rdb	e⁻ Conf	N-Rule
795.4072	1	C43H59N2O12	795.4063	-1.2	4.6	1	79.36	15.5	even	ok
	2	C40H51N12O6	795.4049	-2.9	5.5	2	30.66	21.5	even	ok
	3	C44H55N6O8	795.4076	0.5	9.0	3	100.00	20.5	even	ok
	4	C41H47N16O2	795.4062	-1.2	9.2	4	72.74	26.5	even	ok
	5	C45H51N10O4	795.4089	2.1	20.6	5	36.60	25.5	even	ok
	6	C30H47N22O5	795.4094	2.8	45.1	6	13.51	18.5	even	ok
	7	C32H59N8O15	795.4094	2.8	54.1	7	10.21	7.5	even	ok
	8	C31H63N4O19	795.4081	1.1	65.4	8	17.18	2.5	even	ok
	9	C56H51N4O	795.4057	-1.9	74.3	9	8.57	33.5	even	ok

Figure S4. HRESIMS spectrum of compound **1**.

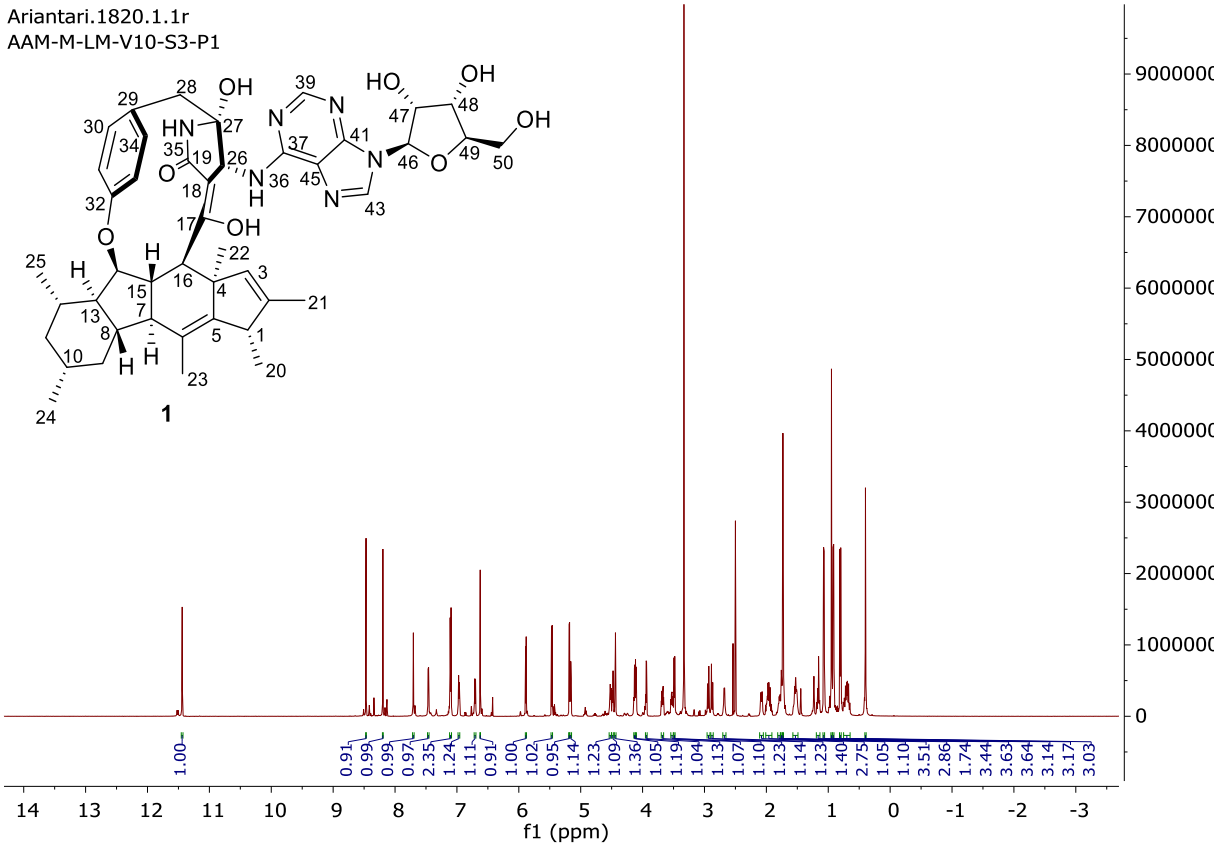

Figure S5. ^{1}H NMR (600 MHz, DMSO-d_6) spectrum of compound **1**.

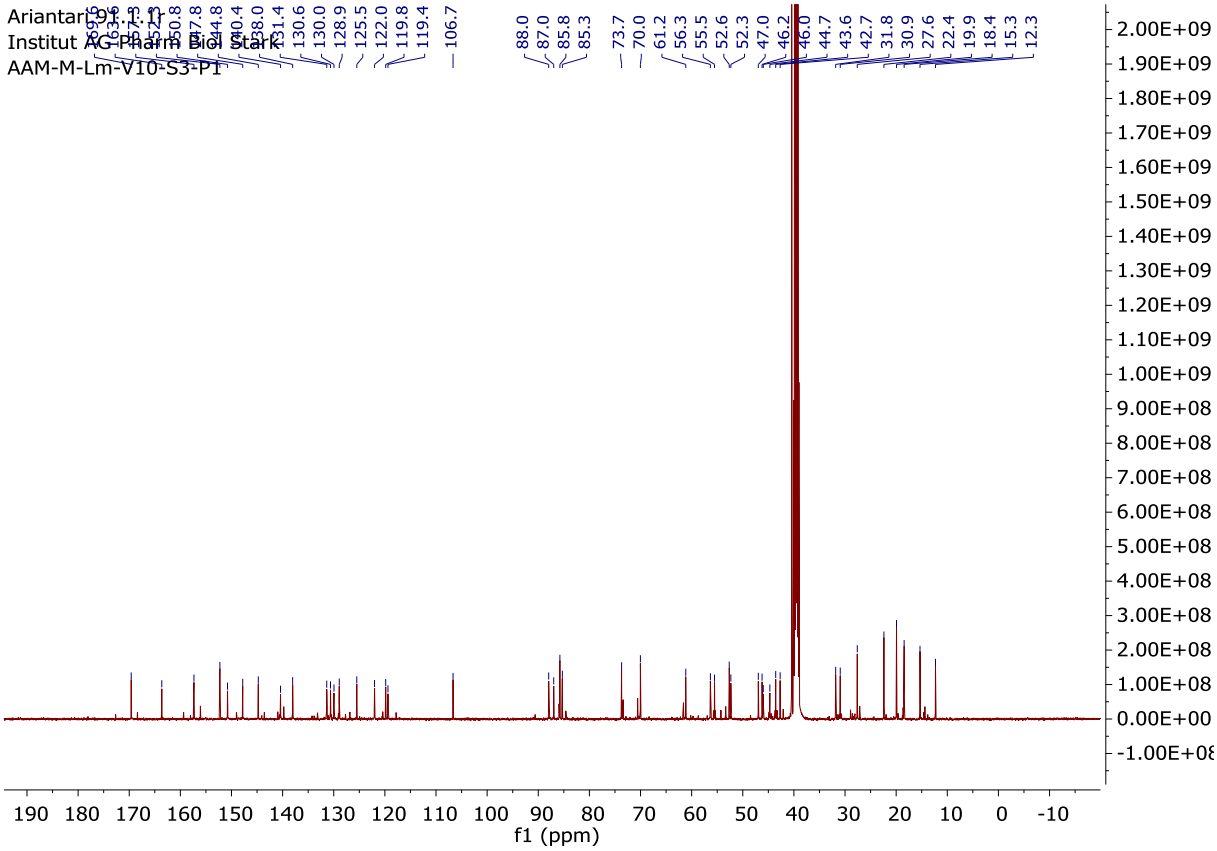

Figure S6. ^{13}C NMR (125 MHz, DMSO-d_6) spectrum of compound **1**.

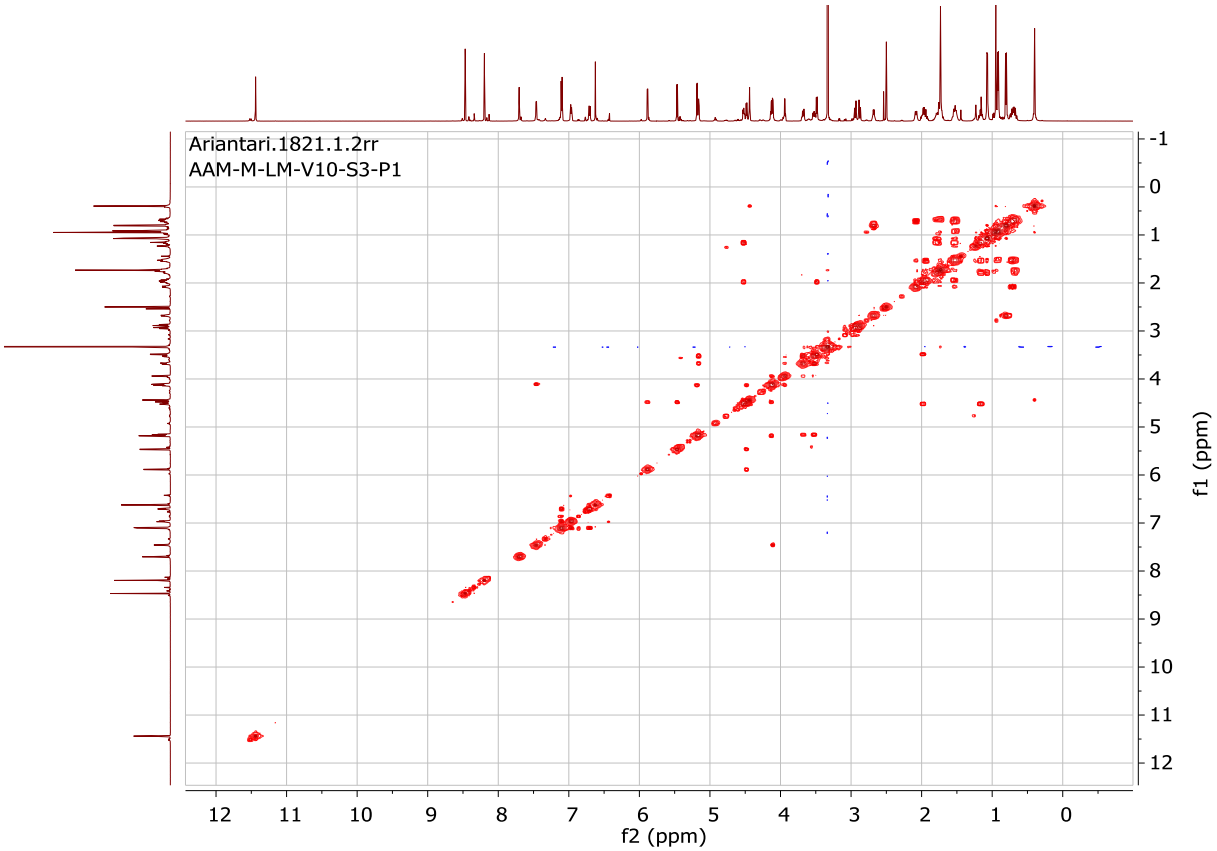

Figure S7. ^{1}H-^{1}H COSY (600 MHz, DMSO-d_6) spectrum of compound **1**.

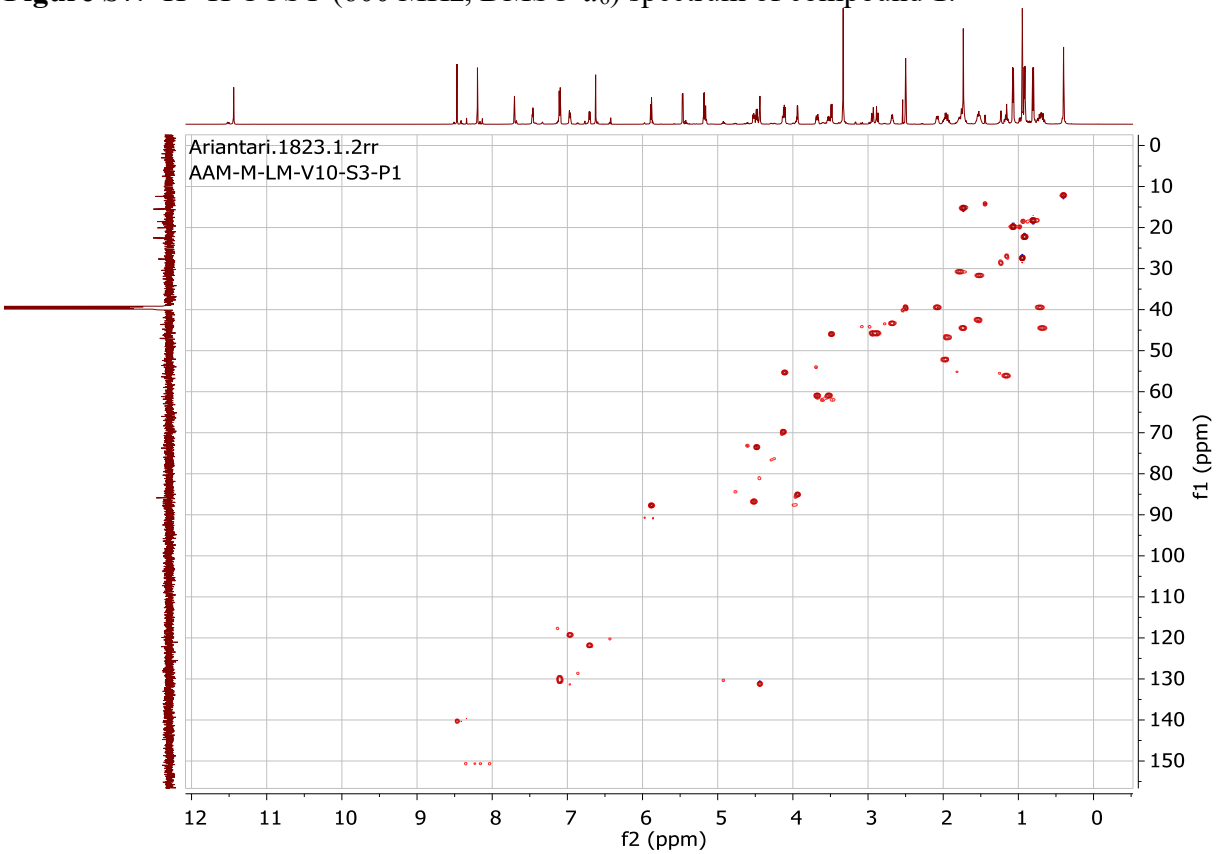

Figure S8. HSQC (600 and 150 MHz, DMSO-d_6) spectrum of compound **1**.

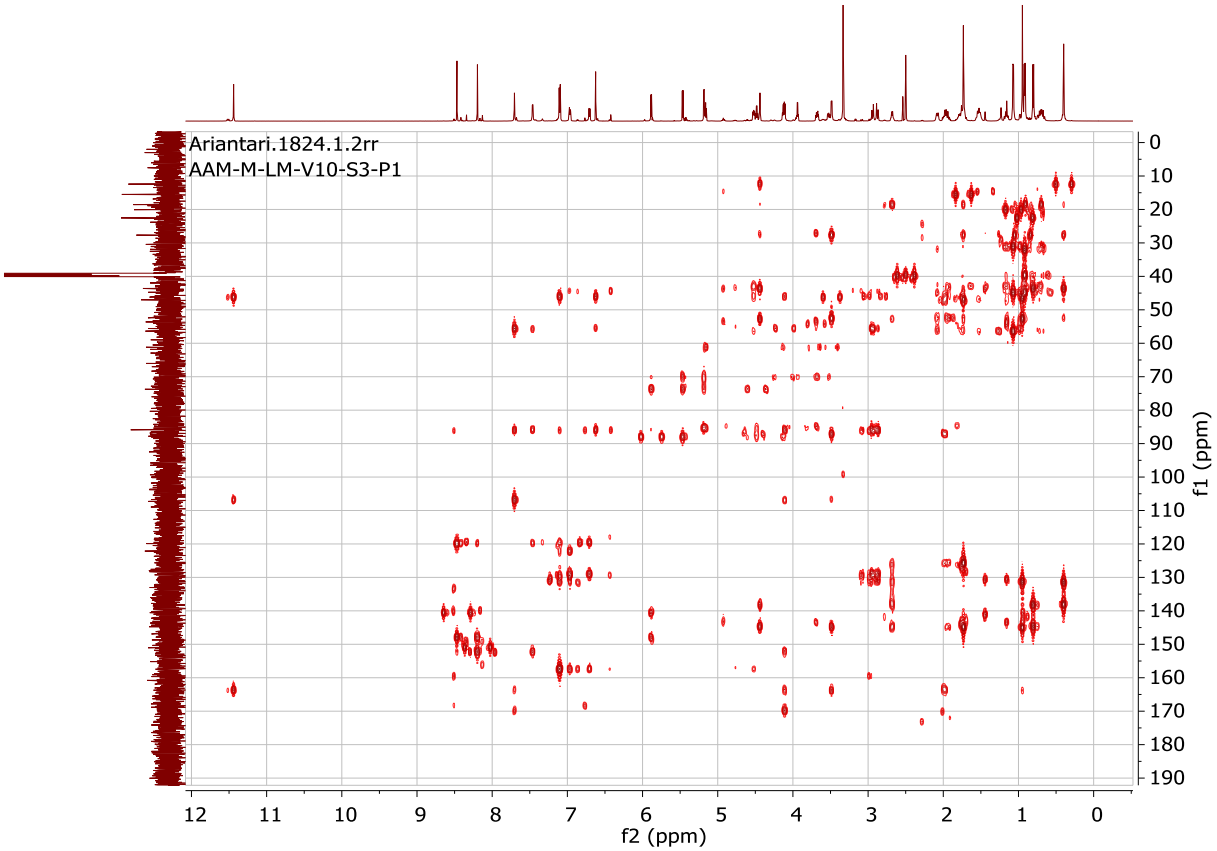

Figure S9. HMBC (600 and 150 MHz, DMSO-d_6) spectrum of compound **1**.

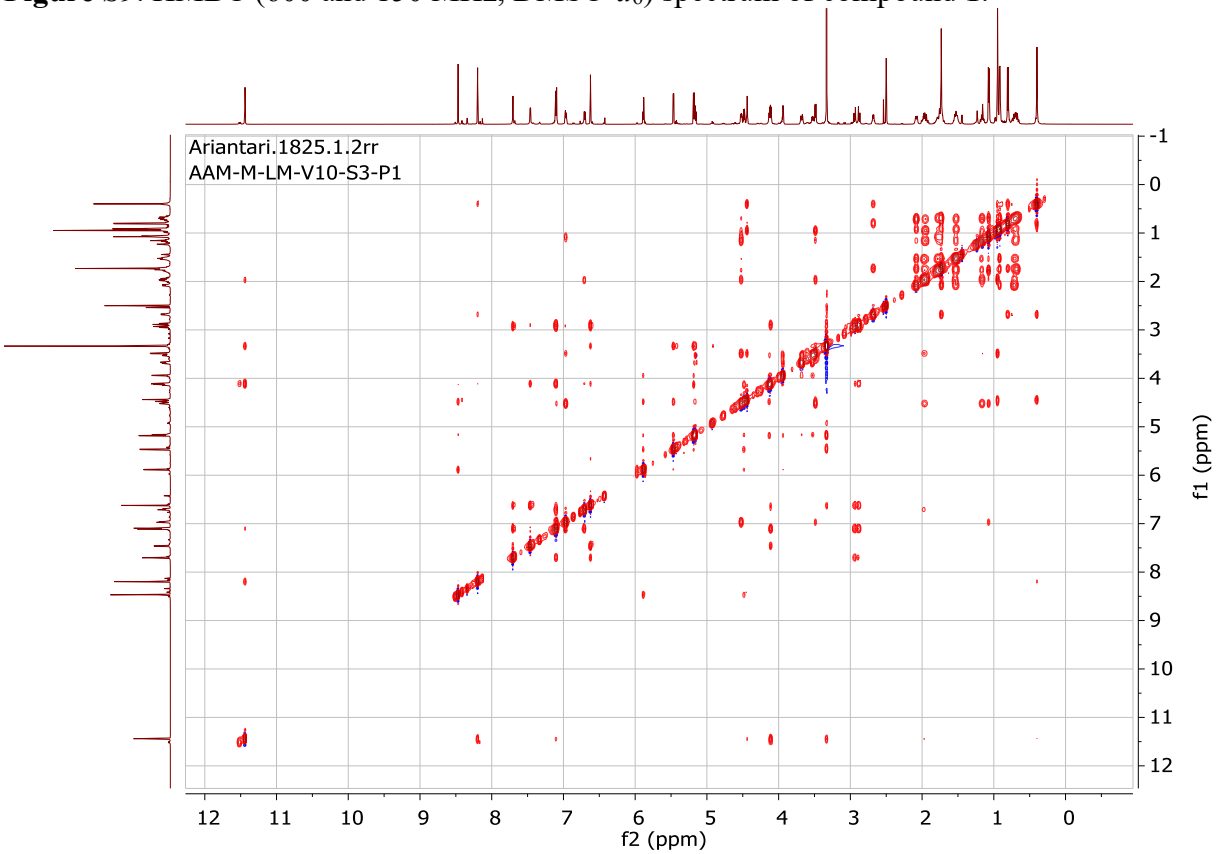

Figure S10. NOESY (600 MHz, DMSO-d_6) spectrum of compound **1**.

(A)

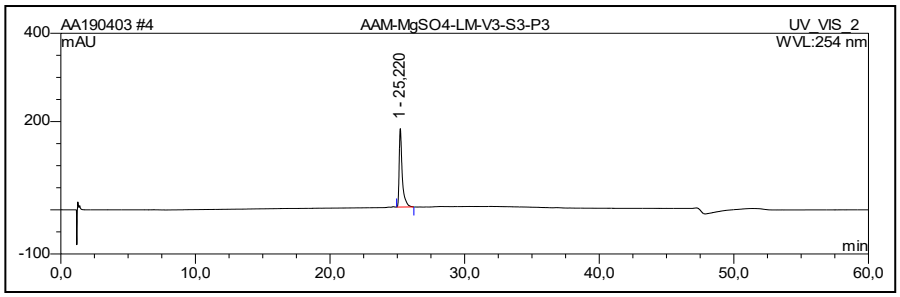

(B)

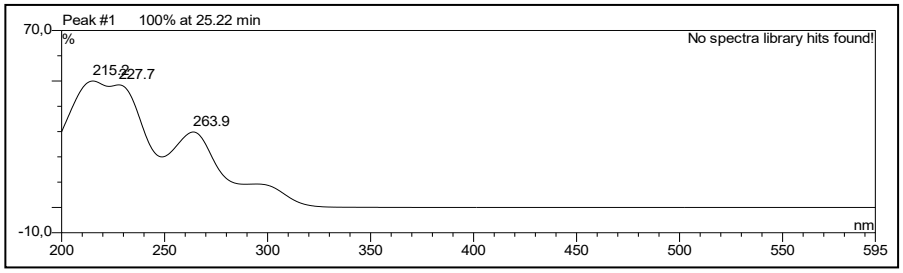

Figure S11. HPLC chromatogram (A) and UV spectrum (B) of compound **4**.

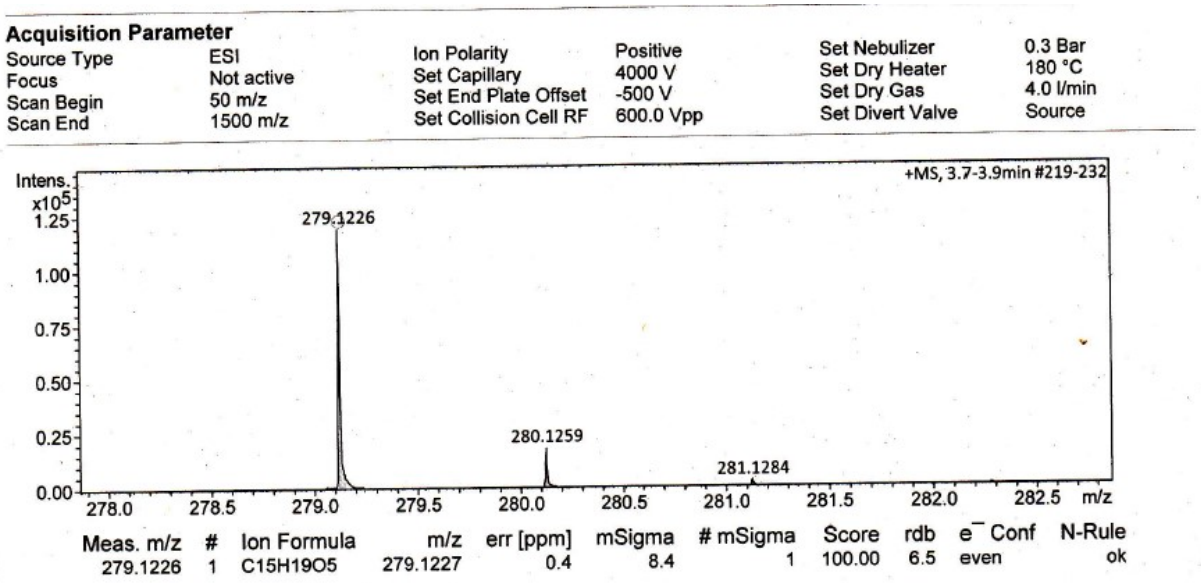

Figure S12. HRESIMS spectrum of compound **4**.

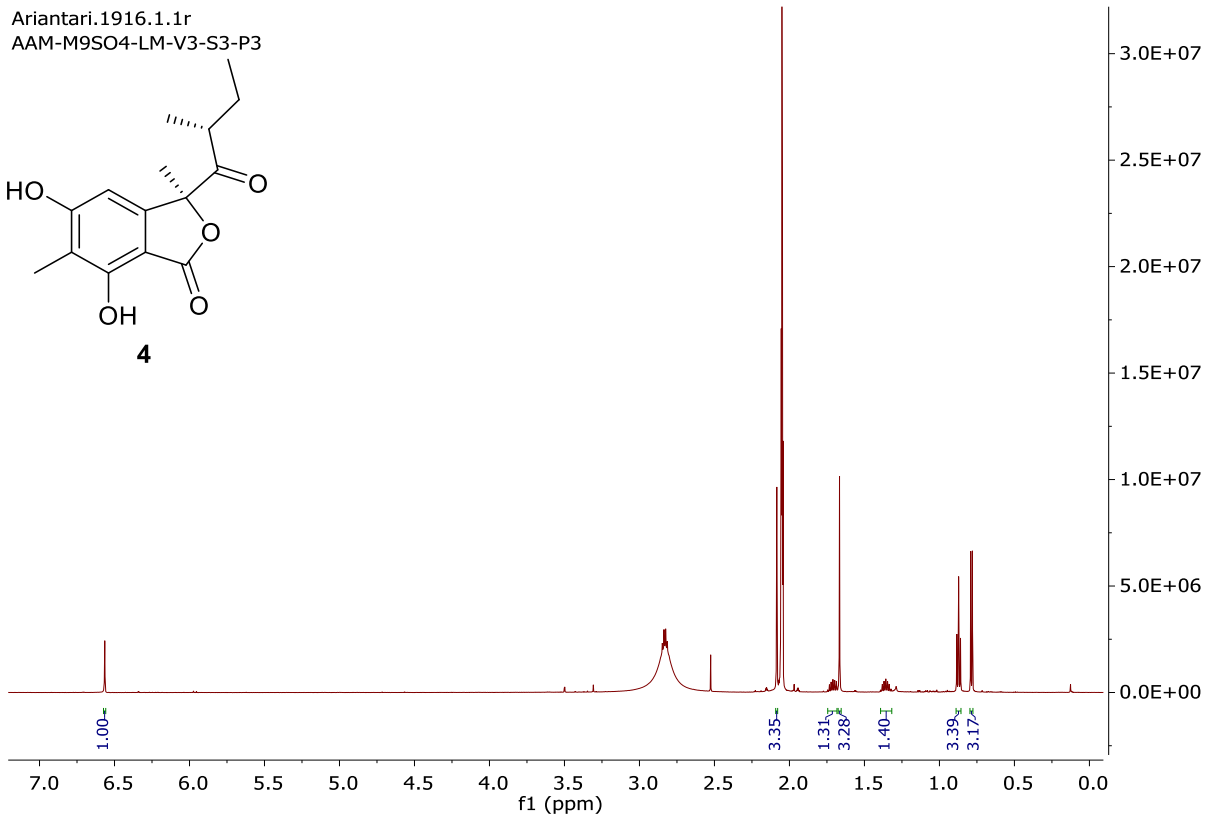

Figure S13. ^{1}H NMR (600 MHz, $(CD_3)_2CO$) spectrum of compound **4**.

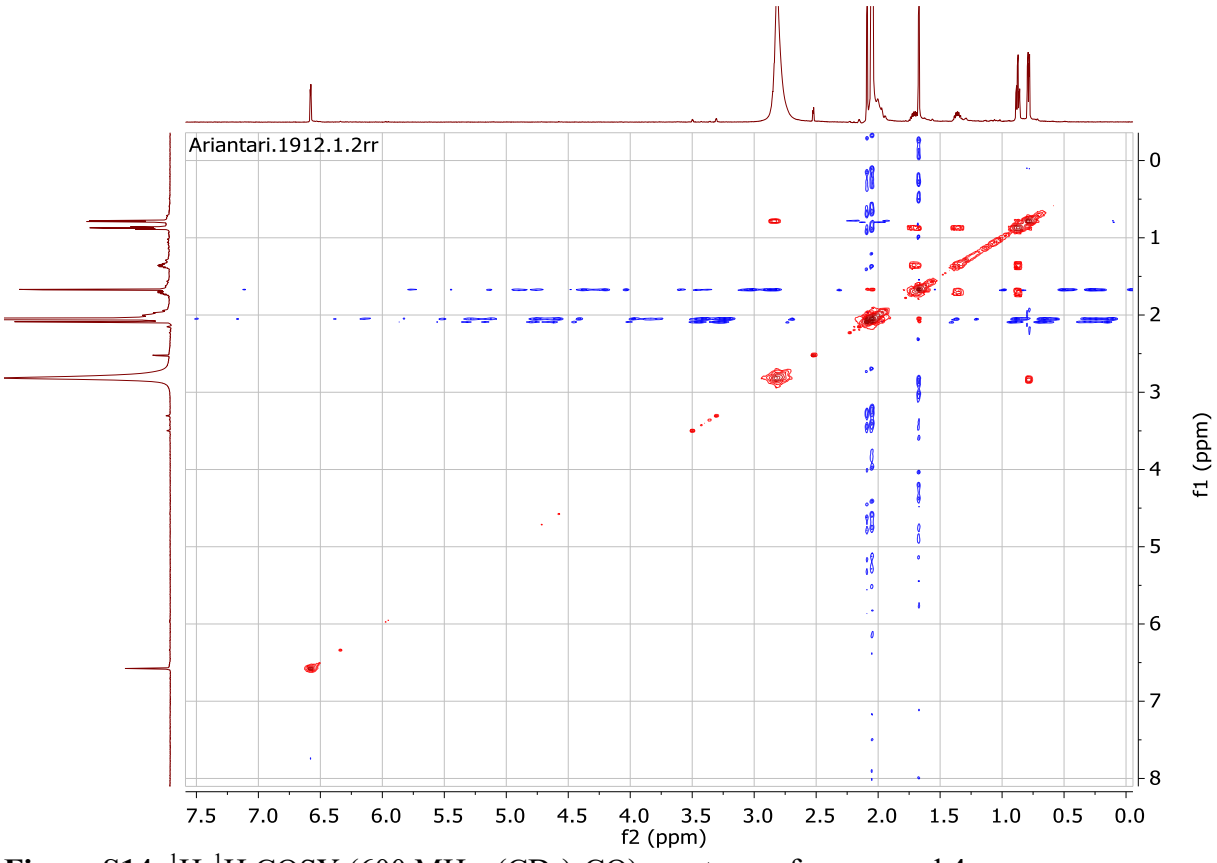

Figure S14. ^{1}H-^{1}H COSY (600 MHz, $(CD_3)_2CO$) spectrum of compound **4**.

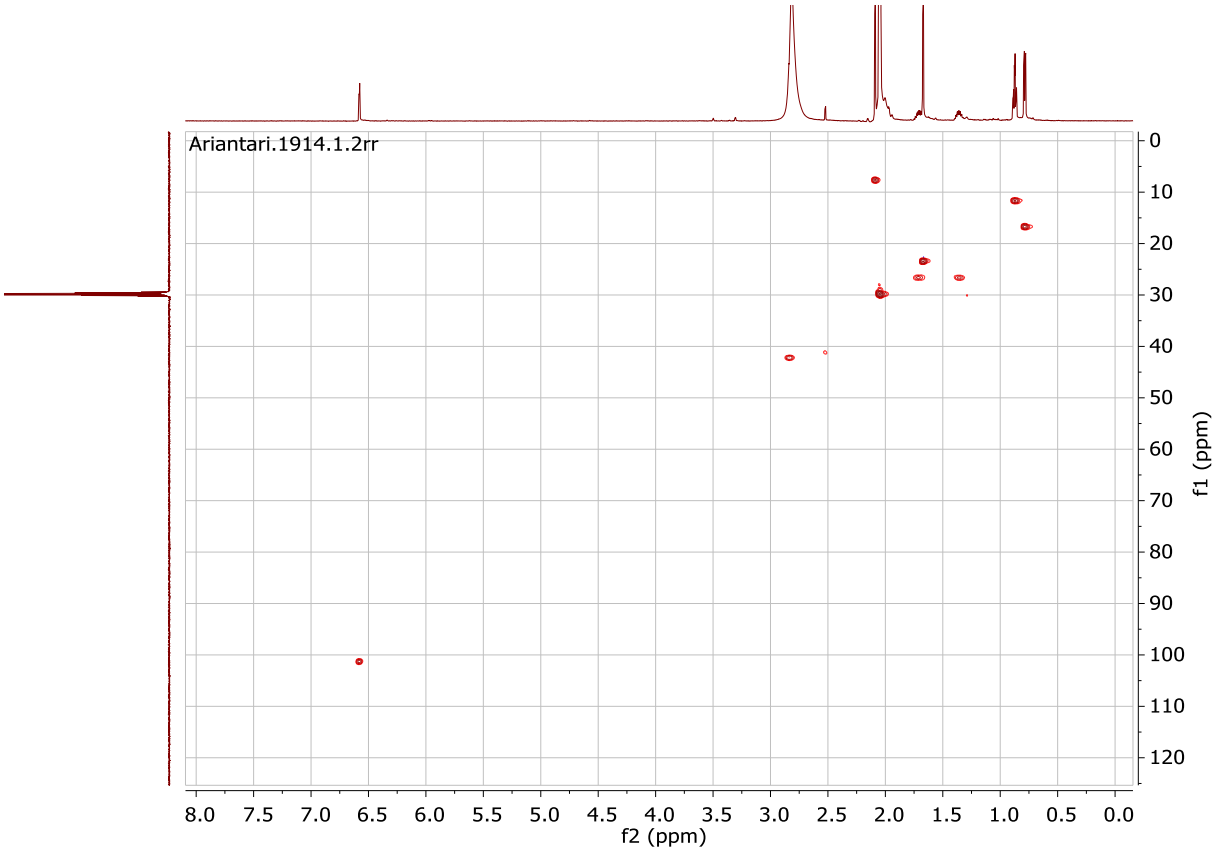

Figure S15. HSQC (600 and 150 MHz, $(CD_3)_2CO$) spectrum of compound **4**.

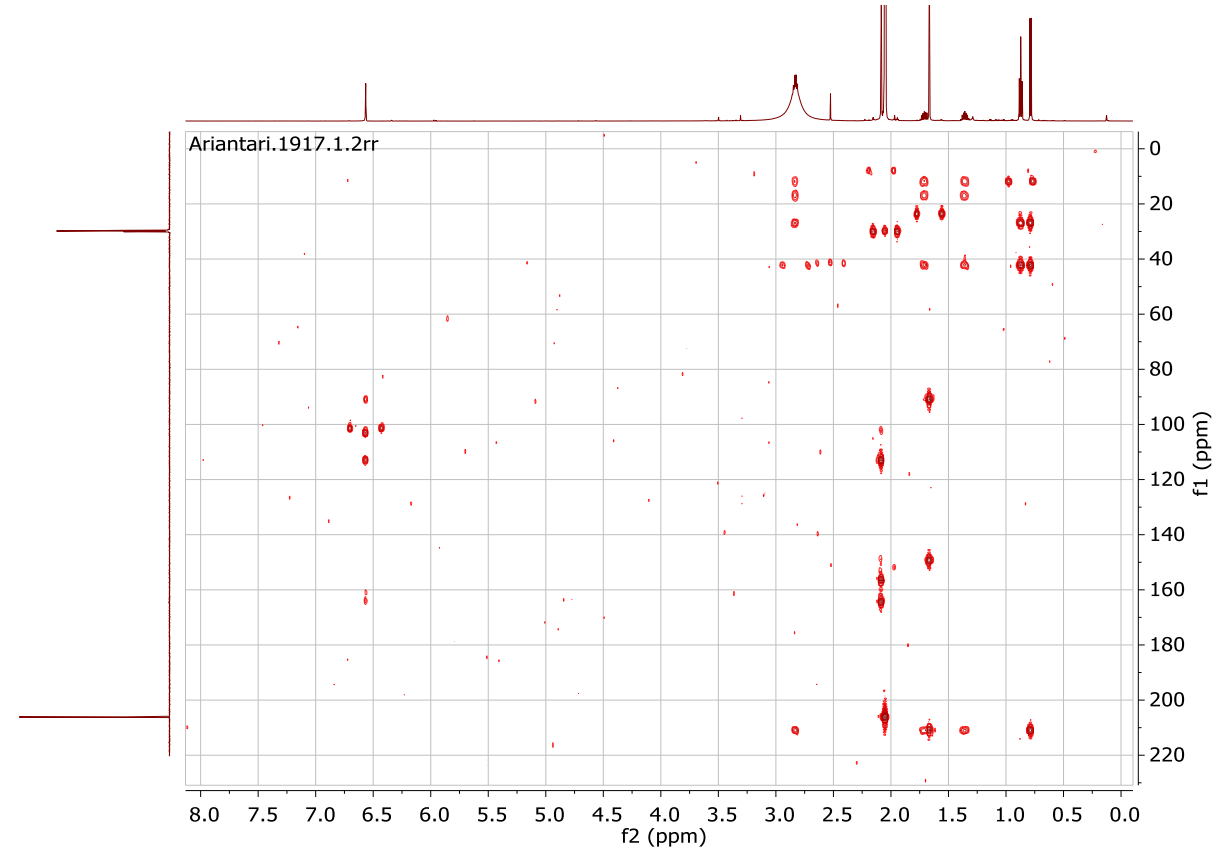

Figure S16. HMBC (600 and 150 MHz, $(CD_3)_2CO$) spectrum of compound **4**.

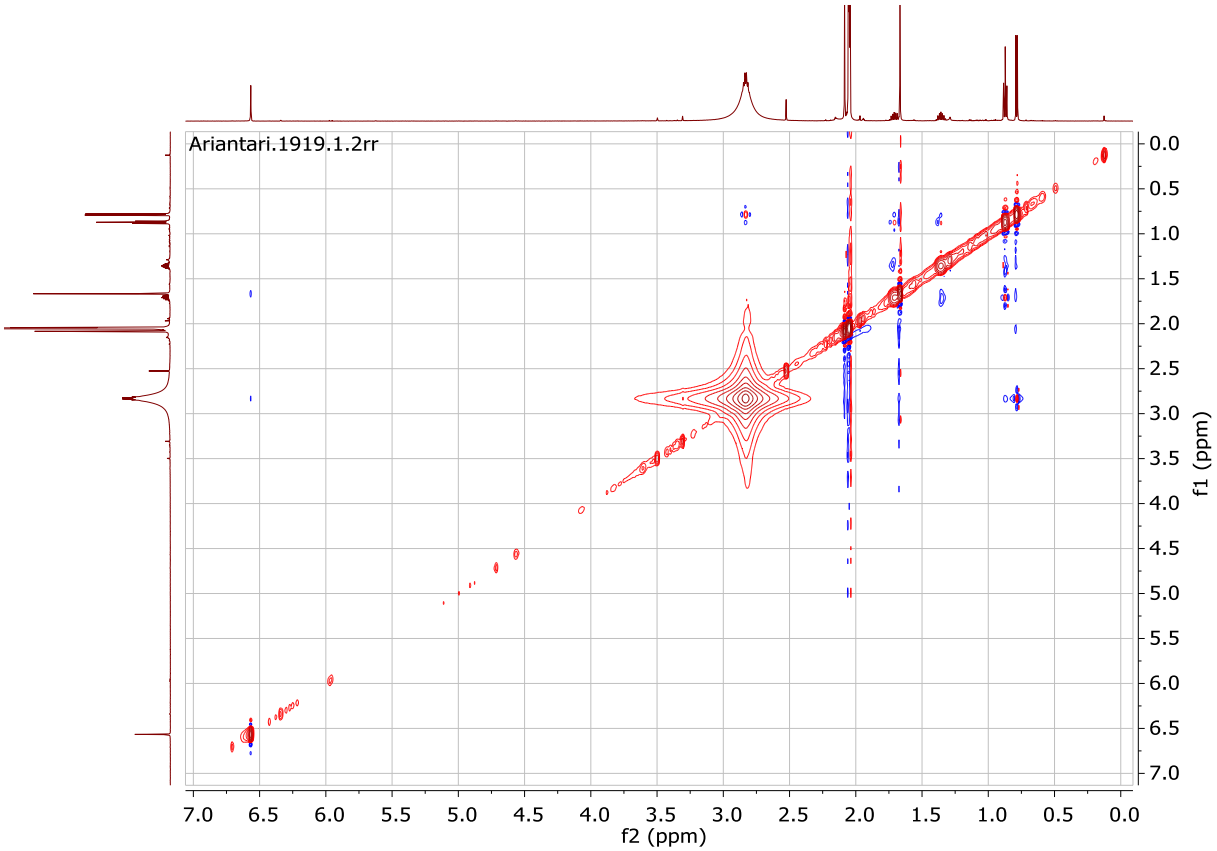

Figure S17. NOESY (600 MHz, $(CD_3)_2CO$) spectrum of compound **4**.

(A)

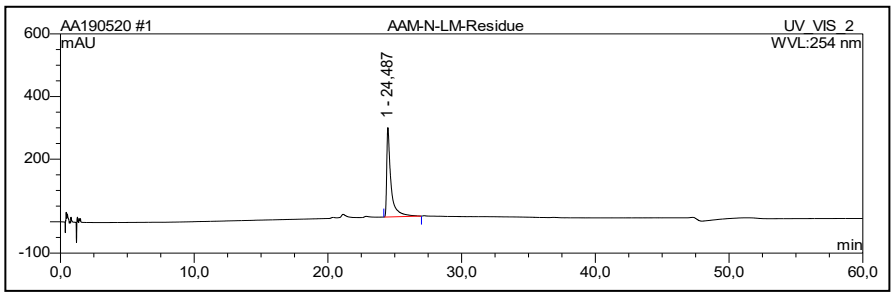

(B)

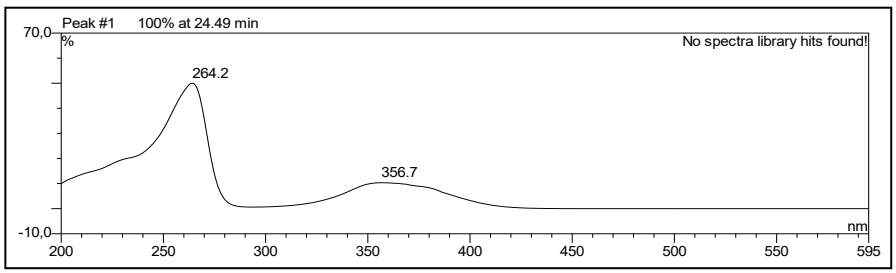

Figure S18. HPLC chromatogram (A) and UV spectrum (B) of compound **11**.

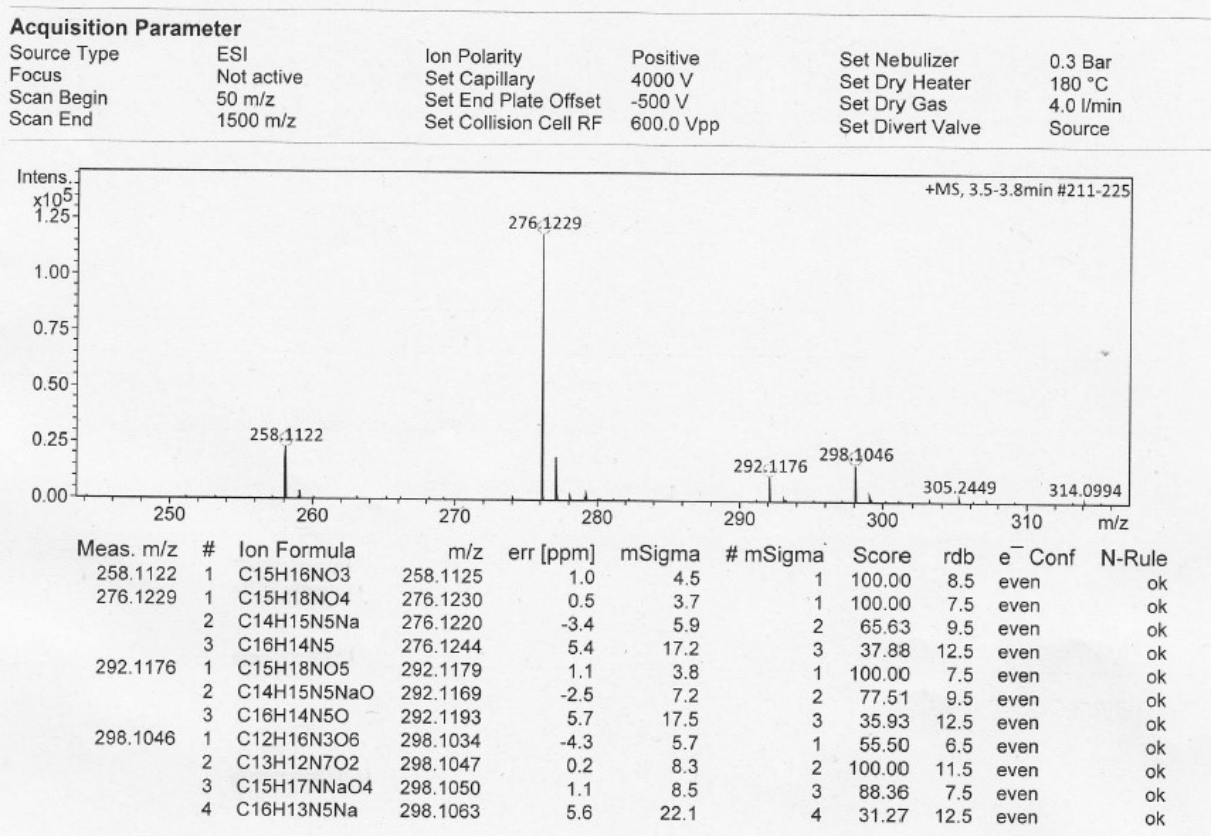

Meas. m/z	#	Ion Formula	m/z	err [ppm]	mSigma	# mSigma	Score	rdb	e⁻ Conf	N-Rule
258.1122	1	C15H16NO3	258.1125	1.0	4.5	1	100.00	8.5	even	ok
276.1229	1	C15H18NO4	276.1230	0.5	3.7	1	100.00	7.5	even	ok
	2	C14H15N5Na	276.1220	-3.4	5.9	2	65.63	9.5	even	ok
	3	C16H14N5	276.1244	5.4	17.2	3	37.88	12.5	even	ok
292.1176	1	C15H18NO5	292.1179	1.1	3.8	1	100.00	7.5	even	ok
	2	C14H15N5NaO	292.1169	-2.5	7.2	2	77.51	9.5	even	ok
	3	C16H14N5O	292.1193	5.7	17.5	3	35.93	12.5	even	ok
298.1046	1	C12H16N3O6	298.1034	-4.3	5.7	1	55.50	6.5	even	ok
	2	C13H12N7O2	298.1047	0.2	8.3	2	100.00	11.5	even	ok
	3	C15H17NNaO4	298.1050	1.1	8.5	3	88.36	7.5	even	ok
	4	C16H13N5Na	298.1063	5.6	22.1	4	31.27	12.5	even	ok

Figure S19. HRESIMS spectrum of compound **11**.

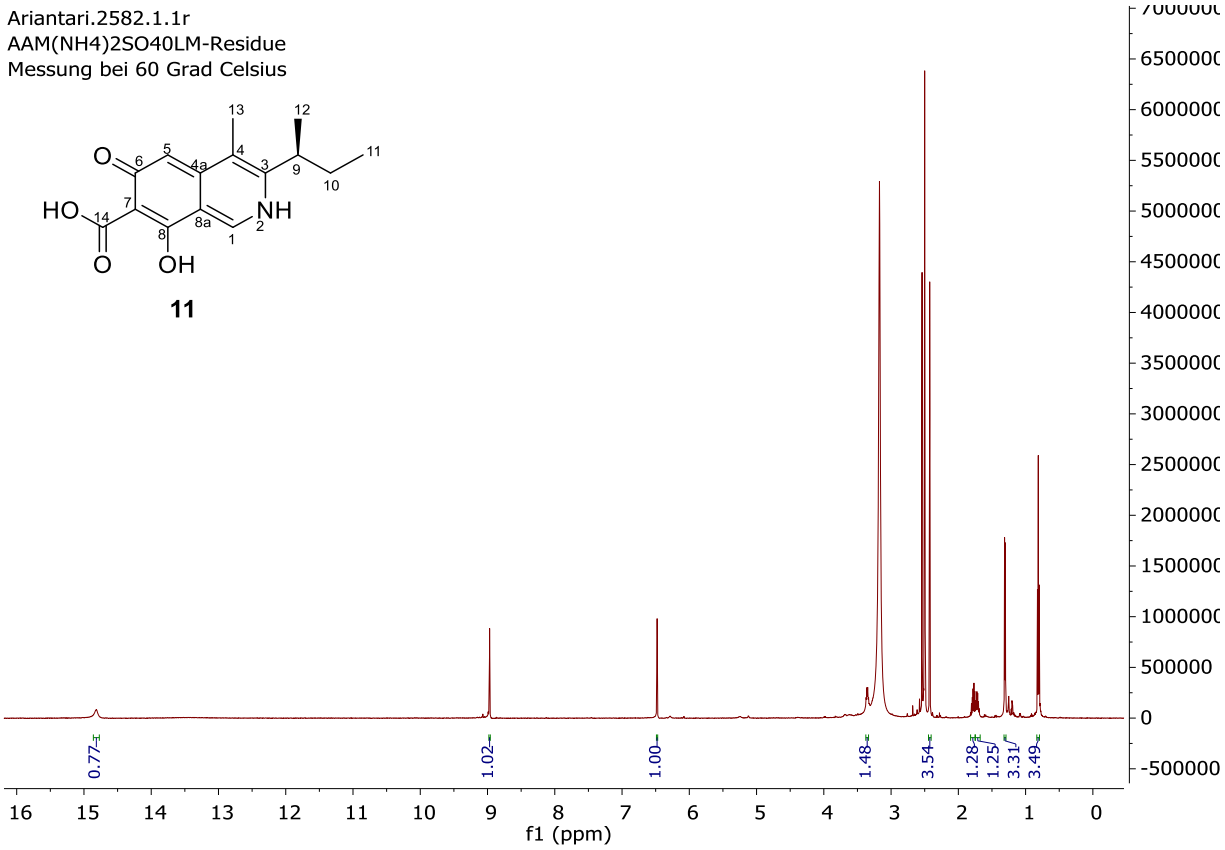

Figure S20. ^{1}H NMR (600 MHz, DMSO-d_6) spectrum of compound **11**.

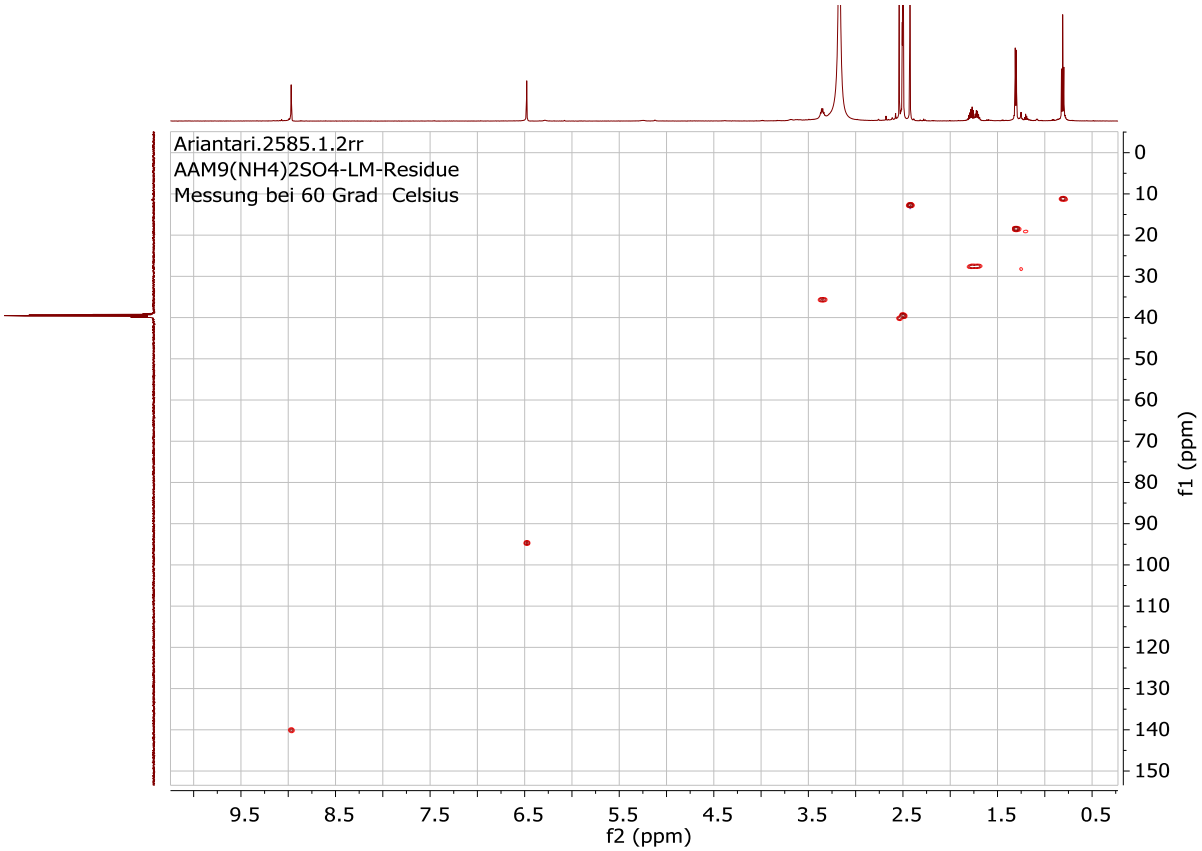

Figure S21. HSQC (600 and 150 MHz, DMSO-d_6) spectrum of compound **11**.

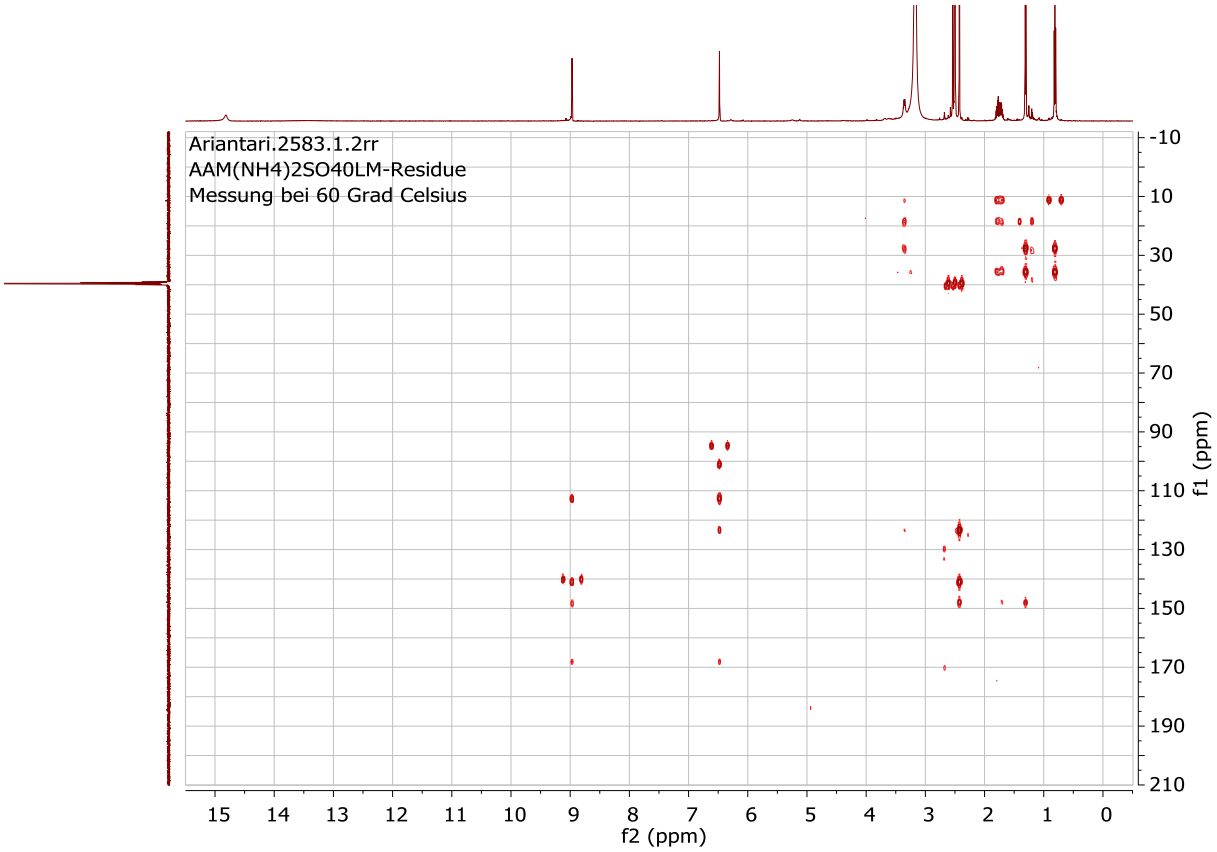

Figure S22. HMBC (600 and 150 MHz, DMSO-d_6) spectrum of compound **11**.

Tabel S1. ^{1}H and ^{13}C NMR data[a] (DMSO-d_6) for compound **11**

position	δ_C, type[b]	δ_H (J in Hz)
1	140.1, CH	8.97, s
3	148.0, C	
4	123.4, C	
4a	141.0, C	
5	94.7, CH	6.48, s
6	nd[c]	
7	101.0, C	
8	168.1, C	
8a	112.8, C	
9	35.6, CH	3.35, m
10	27.6, CH_2	1.78, dt (14.0, 7.0)
		1.71, dt (14.0, 7.3)
11	11.2, CH_3	0.81, t (7.3)
12	18.5, CH_3	1.31, d (7.0)
13	12.8, CH_3	2.43, s
14	nd	

[a] Recorded at 600 MHz (^{1}H) and 150 MHz (^{13}C) at 60°C.
[b] Chemical shifts were extracted from HSQC and HMBC.
[c] not detected

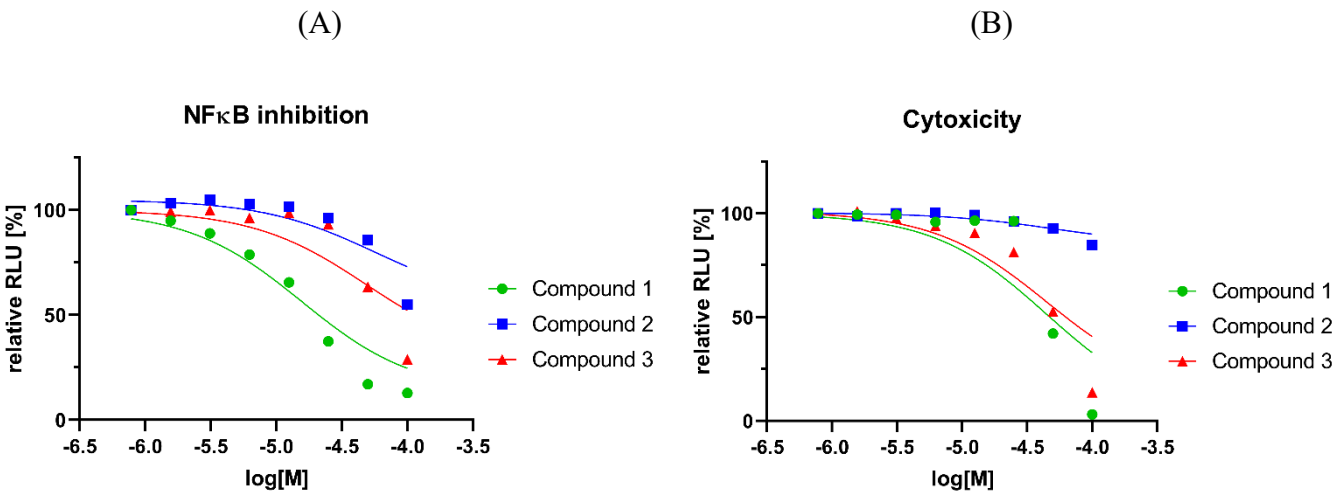

Figure S23. NFκB inhibitory and cytotoxic potential of compound **1**–**3**.

(A) Quantification of NFκB dependent luciferase activity was performed by NFκB inhibition assay. In short, NFκB-MDA-MB-231 cells were treated with two-fold serial diluted compound in the range of 100 μM to 0.78 μM in 8 points. (B) Cytotoxicity was determined by cell viability assay. In brief, MDA-MB-231 cells were treated with two-fold serial diluted compound in the range of 100 μM to 0.78 μM in 8 points. For normalization of relative light units (RLU) the highest RLU in each individual experiment was set as 100 %. Each data point represents the mean of at least four independent experiments. Nonlinear regression without curve fitting was applied for data illustration using GraphPad Prism (GraphPad Software, San Diego, USA; Version 8.1.2).

Chapter 5

Discussion

5.1. Endophytic *Penicillium* sp. produces cytotoxic indole diterpenoids

5.1.1. Indole diterpenoids and biosynthesis

Indole diterpenoids are known for some species of the genera *Acremonium*, *Aspergillus*, *Epichlöe*, *Claviceps* and *Penicillium* (Saikia *et al*., 2008). Given by the fact that many producing strains perform an endophytic lifestyle, the synthesis of indole diterpenoids may confer an ecological benefit to their relationship with the host plants (Saikia *et al*., 2008; Reddy *et al*., 2019). The tremorgenic syndrome in mammals and toxicity against insects are two impacts commonly associated with these compounds as a result of the modulation of ion channels (Uhlig *et al*., 2009). The former effect is of great economic concern due to potential losses in the livestock industry (Reddy *et al*., 2019), while the latter renders them beneficial for insecticidal and antiparasitic applications, as exemplified by nodulisporic acid A (Ondeyka *et al*., 1997).

As described in Chapter 2 (Publication 1), the study of the fungal endophyte *Penicillium* sp. yielded 22 structurally diverse indole diterpenoids, which can be divided into two main classes of indole diterpenes, the paxilline-like compounds and non-paxilline indole diterpenes, with emindole SB as the sole example for the latter. The majority of paxilline-like structures shares a tetracyclic diterpene skeleton that is fused to an indole moiety. This leads to the formation of a 6/5/5/6/6/6 hexacyclic ring system, which further includes the janthitremane and paspalinine structural motif. In janthitremane-type compounds, two additional isoprene units are attached to the indole unit, which is then followed by oxidative cyclization to install a bicyclic system. Further modification results in the formation of more complex structures, such as of eight-membered ring skeletons, as exemplified by the shearinine derivatives. Meanwhile, paspalinine-type compounds bear an additional dioxolane formed via oxidation and acetalization at position 7 (Saikia *et al*., 2008).

In view of their core skeleton, members of janthitremane indole diterpenes further show different levels of oxidation at ring H that construct either paxilline or paspalinine-type of janthitremanes (Liu *et al*., 2016). Both types of janthitremanes were produced by the studied *Penicillium* sp. and shearinine F was the only representative paspalinine-type of janthitremane obtained from this strain. So far, such a case has only been reported from *Eupenicillium shearii* (Belofsky *et al*., 1995).

Following the characterization of gene clusters involved in the biosynthesis of paxilline (*pax* cluster) in *Penicillium paxilli* (Scott *et al*., 2013; Liu *et al*., 2014) and shearinines (*jan* cluster) in *Penicillium janthinellum* (Nicholson *et al*., 2015), 3-geranylgeranyl indole was suggested to be the common precursor to all observed indole diterpenes. The subsequent epoxidation, oxidation, cyclization and prenylation reactions result in one of the most structurally diverse classes of indole diterpenoids observed from fungi thus far (Scott *et al*., 2013; Nicholson *et al*., 2015). By deletion and gene expression analysis, a set of seven genes was identified to be required for paxilline production, namely *pax*G, *pax*A, *pax*M, *pax*B, *pax*C, *pax*P and *pax*Q (Scott *et al*., 2013). Homologues of these genes were discovered in a shearinine-producing strain of *P. janthinellum (*Nicholson *et al*., 2015). Moreover, according to studies performed by Liu *et al*. (2016), it was suggested that the *pax* cluster (*pax*D) might be responsible for the diprenylation of paxilline core containing jantithremanes and the *jan* cluster (*jan*D) for paspalinine core bearing shearinines. The latter then require the function of *jan*O for oxidative cyclization forming the *A/B* rings. Thus, the isolation of a series of new naturally occurring congeners (**2**–**9**) further expands the evidence supporting the putative biosynthetic pathway for this class of metabolites (Figure 5.1.1.1.). Additional methylation, dehydration, oxidation and hydrolysis reactions lead to the diversity of indole diterpene structures encountered in this study (Chapter 2 Publication 1).

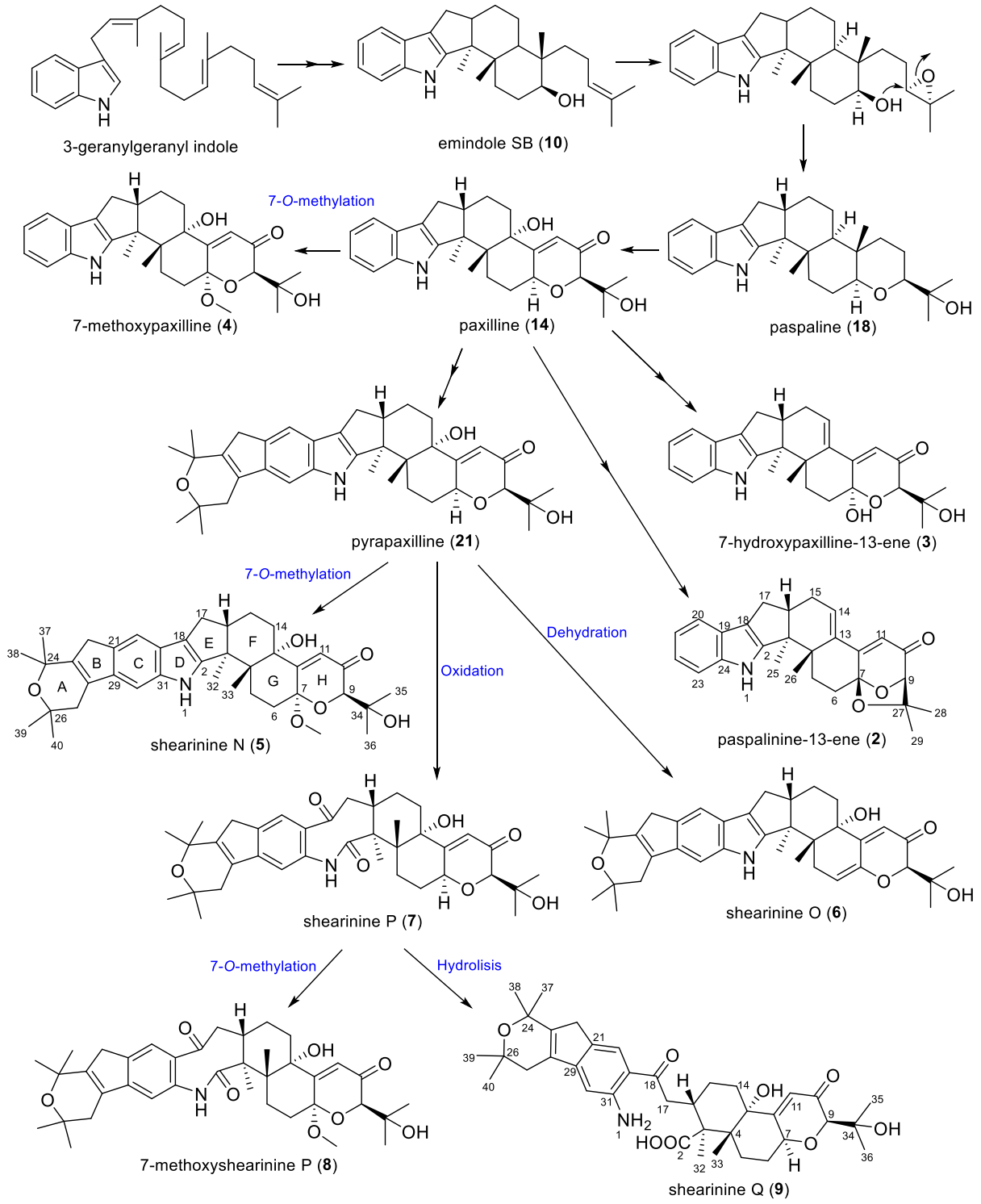

Figure 5.1.1.1. The putative biosynthetic pathway leading to diverse structures of the isolated indole diterpenes **2**–**9** from *Penicillium* sp.
Numbers refer to the compound's number in Chapter 2 Publication 1.

Among other newly discovered indole diterpenes, shearilicine features a new type of scaffold with 6/5/6/6/6/6/5 ring system bearing a unique carbazole motif. Such a motif has rarely been reported from fungi and is limited to the heterocyclic system of tubingensins A and

B from *Aspergillus tubingensis* (TePaske *et al*., 1989; TePaske *et al*., 1989) and aflavazole from *Aspergillus flavus* (TePaske *et al*., 1990).

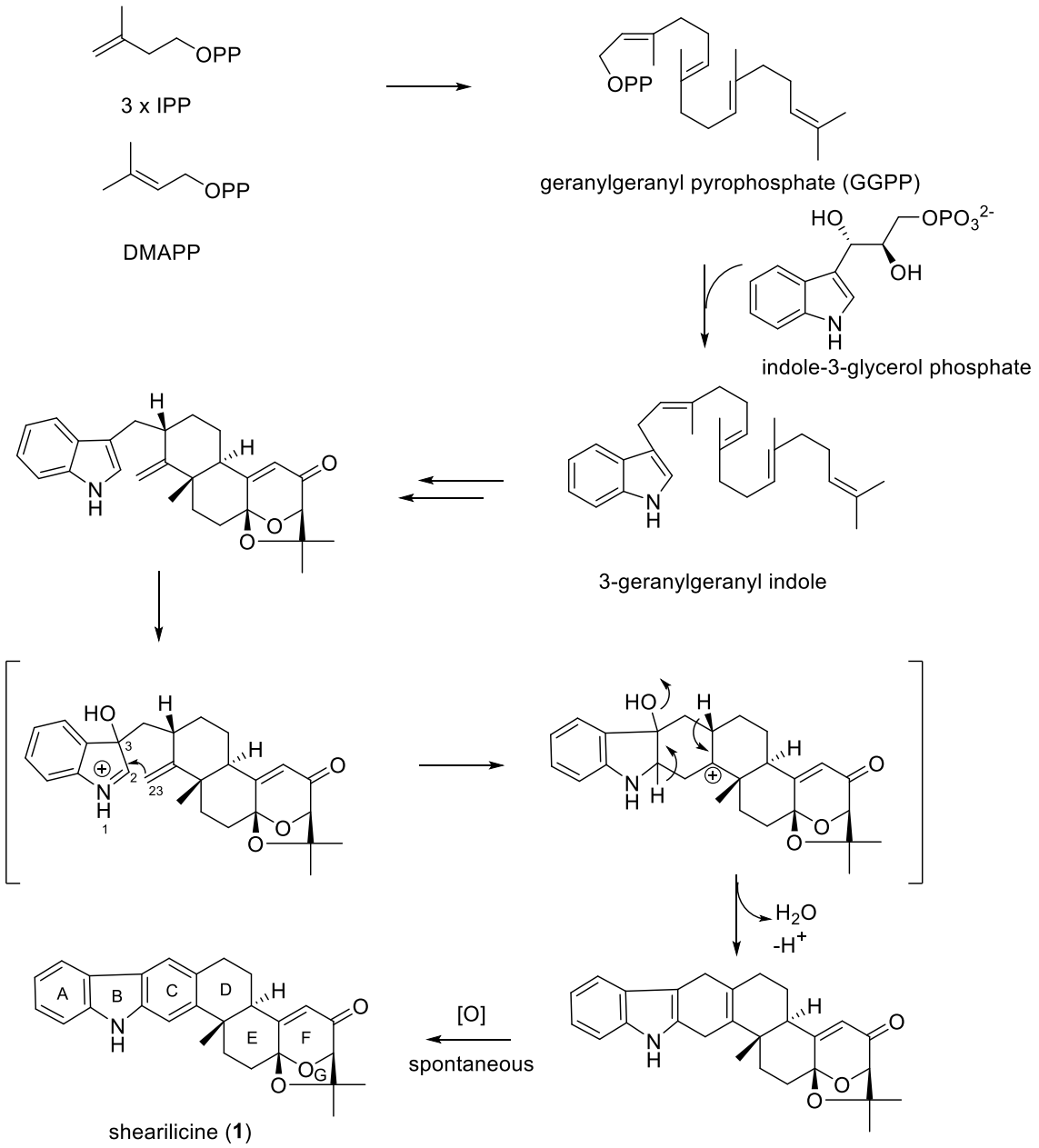

Figure 5.1.1.2. Plausible biosynthetic pathway of shearilicine (**1**) isolated from *Penicillium* sp.
The number refers to the compound's number in Chapter 2 Publication 1.

A similar scaffold such as the one present in tubingensin A was later found in xiamycins A and B, unusual indole sesquiterpenes from the endophytic bacterium *Streptomyces* sp. (Ding *et al*., 2010; Ding *et al*., 2011). Shearilicine is most likely biosynthesized from the same 3-geranylgeranyl indole precursor as other indole diterpenoids. However, it would involve a

different mechanism for ring formation, which might be related to the novel cyclization mechanism discovered for the bacterial compound xiamycin A (Li *et al*., 2012; Li *et al*., 2014). The indole moiety was proposed to undergo a flavoprotein-catalyzed hydroxylation forming an indole C-3-hydroxyiminium species. The neighboring C-23 olefinic function further attacked the resulting C-2 carbanion equivalent. Following the cyclization reaction, sequential steps of dehydration, proton loss and spontaneous oxidative aromatization take place leading to the formation of the carbazole unit, as in the case of xiamycin A (Figure 5.1.1.2.).

5.1.2. The clues from structure-activity relationship

Structurally related indole diterpenoids have been reported for their cytotoxicity against numerous human cell lines, such as glioblastoma U251 (Abdullaev *et al*., 2010), human breast cancer MCF-7 and MDA-MB-231 (Sallam *et al*., 2013), human leukemia HL-60 and human lung adenocarcinoma A549 cells (Gao *et al*., 2016). Several derivatives afforded from this study also displayed significant cytotoxicity towards the tested murine L5178Y and human ovarian cancer A2780 cells. Analysis of their structures suggests a number of structural features implicated in affecting their cytotoxic activity, thereby providing further insight into their structure-activity relationship (Chapter 2 Publication 1).

The presence of a carbazole unit in the structure of shearilicine seems to be essential for its potent cytotoxic activity with IC_{50} values of 3.6 and 8.7 μM, towards L5178Y and A2780 cells, respectively, while no activity was observed for paspalicine. In line with our findings, related carbazole-containing metabolites, tubingensins A and B, were previously determined to be cytotoxic against HeLa cells (TePaske *et al*., 1989; TePaske *et al*., 1989). More recently, a series of synthetic carbazole derivatives demonstrated impressive activity against a panel of cancer cells (Padmaja *et al*., 2016), thus highlighting the importance of this feature for antiproliferative activity.

In paspalinine-type derivatives, the double bond at $\Delta^{13(14)}$ enhances the cytotoxicity [paspalinine-13-ene *vs* paspalicine], while it has only a minor influence on the activity of

paxilline-type derivatives [7-hydroxypaxilline-13-ene *vs* 7-hydroxy-13-dehydroxypaxilline]. These two latter compounds showed pronounced activity only against L5178Y cells.

The cleavage of the keto-amide ring in the janthitremane skeleton, weakens or removes the activity as shown by the comparison of shearinines Q and P. The presence of a methoxy group instead of a proton at position 7 in this type of indole diterpenes, attenuates the cytotoxicity as observed in the activity of pyrapaxilline and shearinine P compared to their corresponding methoxylated derivatives. However, in paxilline-type structures, a methoxy function at this position seems to contribute to the activity of 7-methoxypaxilline, as paxilline was found inactive. Similarly, an additional *A/B* ring system promotes the cytotoxic activity of pyrapaxilline when compared to its biosynthetic intermediate, paxilline. A double bond introduced at $\Delta^{6(7)}$ slightly increases the activity as shown in shearinine O *vs* pyrapaxilline. Moreover, replacement of the keto function at position 10 in paxilline with 10*β*-OH, together with the loss of 13-OH as seen in the structure of 10*β*-hydroxy-13-desoxypaxilline might contribute to the cytotoxicity of the latter compound against A2780 cells (albeit weak activity). This result is in accordance with the proposed structure-activity relationship in a previous study based on its cytotoxic activity towards A-549 and HL-60 cells (Gao *et al*., 2016).

Two structurally less complex indole diterpene progenitors, emindole SB and paspaline, displayed significant cytotoxic activity towards the tested A2780 cells with IC_{50} values of 8.2 and 5.3 μM, respectively (Chapter 2 Publication 1). In a previous study, both compounds revealed good antiproliferative and anti-migratory activities against MCF-7 and MDA-MB-231 cells (Sallam *et al*., 2013). The mechanism of their anticancer actions was attributed to the suppression of total *β*-catenin levels in the latter cell target (Sallam *et al*., 2013). Recently, paspaline was found potently cytotoxic against HeLa cells and strongly inhibited mitotic kinesin Eg5 (Nagumo *et al*., 2017). Pharmacophore modeling demonstrated that both compounds retain the simplest pharmacophoric features required for their biological activity. Moreover, the lack

of BK channel inhibition and tremorgenicity of these compounds make them intriguing scaffolds for further pharmacological investigation (Sallam *et al*., 2013).

Furthermore, the new congeners were investigated against human urothelial bladder cancer J82 cells as well (Chapter 2 Publication 1). Most of them tested generally less cytotoxic compared to their activity against L5178Y and A2780 cells, with IC_{50} values between 30 and 100 μM. When evaluated against non-cancerous cells HEK-293, shearilicine, shearinine O, emindole SB and paspaline possessed a relatively high selectivity index (SI) values (SI 3.3–8.1), comparable to that of the reference drug, cisplatin (SI 5.2). Taken together, the findings in this study support further studies on the anticancer potential of these derivatives. In contrast to the cytotoxic activity of the isolated indole diterpenes, none of them showed significant antibacterial activity towards the tested Gram-positive and Gram-negative strains.

5.2. OSMAC, a powerful approach to release fungal chemical diversity

As part of our effort in the search for anticancer and antibacterial compounds from endophytic fungi, the OSMAC approach was utilized to diversify natural products produced by the studied strains of *Bulgaria inquinans* and *Didymella* sp. OSMAC protocols have been extensively adapted to explore the biosynthetic potential of promising endophyte strains for the past two decades and have resulted in the discovery of a significant number of interesting natural products (Daletos *et al*., 2017).

In Chapter 3 (Publication 2), fermentation of the fungal endophyte *Bulgaria inquinans* on solid Czapek medium produced mostly butyrolactone derivatives, one metabolite bearing a diol moiety, bulgariol and the main azaphilone pigment bulgarialactone B. The OSMAC strategy was applied to this strain by supplementing the solid Czapek medium with different types of salts and mixtures of salts. Interestingly, cultivation of the fungus in the presence of a mixture of salts ($MgSO_4$, $NaNO_3$ and NaCl) in the culture medium, resulted in a significant change in fungal metabolite pattern as indicated by the HPLC chromatograms (Figure 5.2.1.).

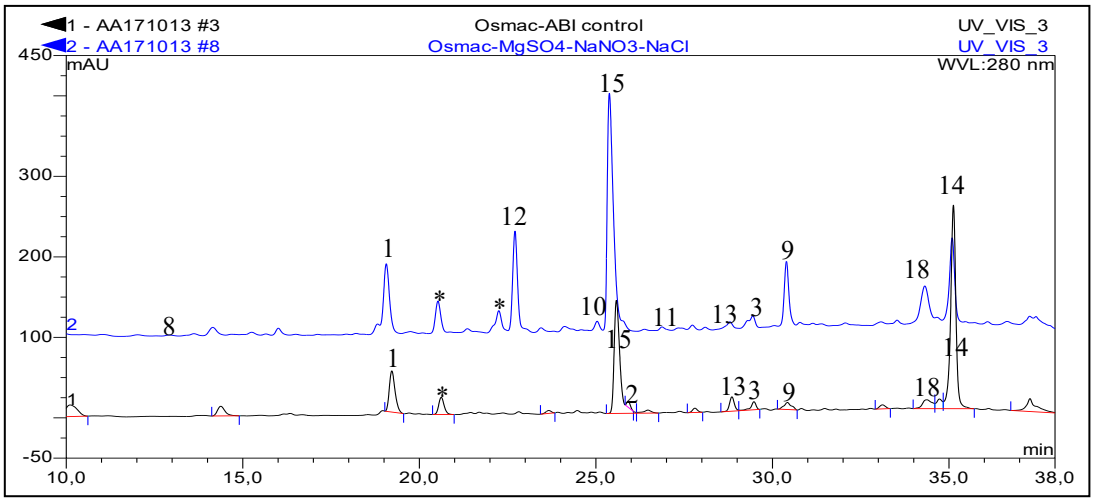

Figure 5.2.1. HPLC chromatograms of EtOAc extract of *B. inquinans* cultured on solid Czapek medium (black) compared to the OSMAC culture on solid Czapek medium with addition of a mixture of $MgSO_4$, $NaNO_3$ and NaCl (blue).
Numbers refer to the compound's number in Chapter 3 Publication 2.

The addition of a salt mixture ($MgSO_4$, $NaNO_3$ and NaCl) to the culture medium enhanced the production of the α-pyrone type of compounds bulgariapyrone A and its dimeric analogue bulgariapyrone E, as well as the azaphilone bulgarialactone D. The compounds were previously detected only in low amounts in cultures lacking the salt mixture, preventing their isolation and identification. Notably, other new metabolites, such as the unusual 1,3-oxazine containing natural product bulgarixine B and the α-pyrone derivatives bulgariapyrones B–D, were undetected in cultures lacking the salt mixture, indicating that those were induced by the presence of the salt mixture in the culture medium. Further chromatographic workup yielded bulgarixine A and the two butyrolactones bulgariline D and (–)-(*S*)-flavipesin B. These three latter compounds were not clearly distinguished in the total extract chromatogram, due to their low amounts. Considering the possibility that these might arise during the isolation process involving MeOH, their corresponding non-methylated analogues were kept in MeOH solution containing 0.1% formic acid for 1 week. No methylated products were observed following the HPLC analysis, indicating that these are naturally occurring products rather than isolation artifacts.

During further OSMAC experiments (Chapter 3 Publication 2), the fungus was unable to grow in the presence of a mixture of $NaNO_3$ and NaCl, when $MgSO_4$ was completely removed from the solid Czapek medium. This suggests the essential role of Mg^{2+} ions to support the fungal growth under such fermentation condition, although its metabolite profile was unaffected upon addition of solely $MgSO_4$ to the culture medium. Hence, the fungus seems to be metabolically affected only by the combination of MgSO4, $NaNO_3$ and NaCl present in the culture medium.

The presence of NaCl contributes to the increasing medium salinity, which is known to affect microbial growth and biochemical reactions. In some cases, fungi were capable of utilizing halide salts in the culture medium apparently as a result of activation of the biosynthetic pathway to restore osmotic balance (Pan *et al*., 2019). However, no halogenated natural products were discovered during this study. On the other hand, inorganic nitrate can serve as an alternative nitrogen source for many species of fungi, in the absence of favored nitrogen sources, such as ammonium or glutamine, by a mechanism called nitrogen metabolite repression. Fungi are able to respond to changes in the type and concentration of nitrogen sources as well (Tudzynski, 2014). The influence of $NaNO_3$ on the production of metabolites by *B. inquinans* could not be clarified in this study, although two nitrogen-containing metabolites, bulgarixines A and B, were obtained following the presence of a salt mixture ($MgSO_4$, $NaNO_3$ and NaCl) in OSMAC cultures. Apart from this, a previous OSMAC study employing $MgCl_2$ in the culture medium revealed that Mg^{2+} ions can alter metabolites production of the marine fungus *Ascotricha* sp. (Wang *et al*., 2014). Many metal ions, including Mg^{2+}, Ca^{2+}, Mn^{2+}, Fe^{2+}, Co^{2+}, Ni^{+}, Cu^{2+}, Zn^{2+} and Mo^{+}, are known to be important for microbial growth and metabolism (Mou *et al*., 2013; Fill *et al*., 2016). For instance, the presence of certain amounts of Ca^{2+}, Cu^{2+} and Al^{3+} ions (separately or a combination) in the liquid culture of endophytic *Berkleasmium* sp. Dzf12 enhanced the fungal growth and production of secondary metabolites, palmarumycins C_{12} and C_{13} (Mou *et al*., 2013). Further evidence is shown by the

findings in the present study. Metal ions can possibly interact with microbes in three mechanisms, such as triggering reactions in the microbial cells, conserving energy during dissimilation process and assimilation reactions (Pan *et al*., 2019).

In a recent study, a planar structure identical to that of (–)-(*S*)-flavipesin B called phenylbutyrolactone II was isolated as a product of an engineered strain of *Aspergillus nidulans* bearing hybrid NRPS-like enzyme and methyltransferase (van Dijk and Wang, 2018). This biosynthetic pathway engineering showed that a methyltransferase was involved in methylation of the carboxylic acid side chain of phenylbutyrolactone IIa yielding phenylbutyrolactone II. When the heterocyclic core of the precursor molecule slightly changed, no methylated product was synthesized, underlining the specificity of this enzyme. Using the same mutant strain, further addition of a prenyltransferase did not result in any observed prenylated products, since this enzyme requires the presence of OH group on the phenyl side chain of the precursor, which are not present in phenylbutyrolactone IIa.

Considering these findings, we speculate that Mg^{2+} ions might contribute to the influencing effects on the metabolite profile of *B. inquinans* in this study, under fermentation conditions with $NaNO_3$ and NaCl present in the medium. The presence of Mg^{2+} ions or a combined effect of these three salts might trigger methylation of the particular type of butyrolactone structures, as a result of activation of the corresponding biosynthetic gene cluster. This may extend to the putative biosynthesis of other types of metabolites such as 1,3-oxazine and α-pyrones. However, this hypothesis needs to be validated experimentally.

Natural products afforded in this study (Chapter 3 Publication 2) were evaluated for cytotoxicity against L5178Y cells. Among them, only bulgariline B showed excellent activity with an IC_{50} value of 1.8 μM, indicating the presence of OH group attached to C-5 of the 2-furanone core to be essential for the activity. None of these metabolites showed activity in the antibacterial screening.

Further application of the OSMAC strategy on the endophytic fungus *Didymella* sp., by supplementing rice medium with $(NH_4)_2SO_4$, resulted in an obvious change of the metabolite pattern of the fungus. The addition of this salt remarkably decreased the production of the main azaphilone pigment ascochitine and led to a white coloration of fungal culture containing salt (Chapter 4 Publication 3, Figures S1 and S2 in the Supporting Information). Instead, a nitrogen-containing azaphilone related to ascochitine, called ascochitamine, was only detectable when $(NH_4)_2SO_4$ was present in the rice medium. The fungus was presumably able to facilitate substitution of the pyrane oxygen with nitrogen when exposed to ammonium during cultivation. This process is well documented for other azaphilones (Lin *et al*., 1992; Wang *et al*., 2010; Gao *et al*., 2013).

5.3. Bioactivities of the decahydrofluorene-class of natural products

A group of pathogens so-called ESKAPE, comprises both Gram-positive and Gram-negative bacteria, such as *Enterococcus faecium*, *Staphylococcus aureus*, *Klebsiella pneumoniae*, *Acinetobacter baumannii*, *Pseudomonas aeruginosa* and *Enterobacter* spp., is the main cause of nosocomial infections. These bacteria can lead to life-threatening hospital-acquired infections, particularly to vulnerable hospitalized and immunocompromised individuals (Pendleton *et al*., 2013). The emergence of resistant strains of these bacteria to the currently available antimicrobial options, limits the number of effective antibiotics and poses a great challenge to the clinical practice. ESKAPE pathogens develop antimicrobial resistance through several mechanisms, including drug inactivation (*e.g*. production of *β*-lactamases), mutations of drug binding sites, decreased intracellular drug accumulation by reduction of outer the membrane protein porin and increase of efflux pump expression, as well as biofilm formation (Chambers, 1997; Santajit and Indrawattana, 2016). The mounting threat of antimicrobial resistance certainly leads to the urgent need for new antimicrobial agents, in addition to the appropriate antibiotic stewardship. Among Gram-positive bacteria, the

methicillin-resistant *Staphylococcus aureus* (MRSA) and vancomycin-resistant *Enterococcus faecium* were particularly documented in the WHO high priority list of resistant bacterial strains in 2017, that urged for development of new antibiotics for tackling antimicrobial resistance (Tacconelli *et al*., 2018)

In Chapter 4 (Publication 3), a new decahydrofluorene analogue, didymellanosine, along with the known phomapyrrolidone A and ascomylactam C, were afforded following chemical investigation of an endophytic *Didymella* sp. cultured on rice medium. Didymellanosine represents the first analogue of this class of metabolites conjugated with adenosine. It features a tetracyclic decahydrofluorene skeleton, which is encountered only in a few fungal metabolites, such as embellicines A and B (Ebrahim *et al*., 2013), phomapyrrolidones A–C (Wijeratne *et al*., 2013) and ascomylactams A–C (Chen *et al*., 2019). In the antibacterial screening against Gram-positive bacteria, including MRSA, vancomycin-resistant strains of *Enterococcus faecalis* and *Enterococcus faecium*, the known ascomylactam C showed the most significant inhibition. Didymellanosine was less active than ascomylactam C, while phomapyrrolidone A showed much weaker activity than the two aforementioned compounds. Interestingly, these compounds displayed comparable or even stronger inhibition against the tested drug-resistant strains than those against drug-susceptible Gram-positive bacteria. This suggests the compounds might exert their antibacterial action through a different mechanism than those known for the β-lactam, methicillin and the glycopeptide antibiotic, vancomycin. Similarly, a related alkaloid containing a tricyclic decahydrofluorene backbone namely GKK1032C was found in a recent study particularly active against MRSA (Qi *et al*., 2019).

When further tested against a drug-susceptible strain of Gram-negative *Acinetobacter baumannii* in the presence of a sublethal concentration (0.1 μM) of colistin, both didymellanosine and ascomylactam C revealed pronounced activity with MIC values of 3.1 μM. However, they tested inactive in the absence of colistin (Chapter 4 Publication 3). Colistin

is a polycationic peptide, which was banned from clinical use in the past due to the neurotoxicity and nephrotoxicity adverse effects. Nevertheless, in the mid-1990s clinicians re-introduced it to treat infections caused by drug-resistant Gram-negative bacteria, in the paucity of new effective antimicrobials. Currently, colistin is considered as "last line" therapeutic option to confront these pathogens. Colistin interacts with negatively charged phosphate groups of lipopolysaccharide (LPS) and disrupts the outer membrane of Gram-negative bacterial cells (Ezadi *et al*., 2019). As the toxicity of colistin is known to be dose-dependent and in view of its main mode-of-action by affecting outer membrane permeability of bacteria, the combination therapy of colistin with other antimicrobials is of considerable interest, as this allows for a dose reduction of colistin. A recent study revealed the synergistic effect of the combination therapy of colistin at sub-inhibitory concentration with other existing antibiotics that act intracellularly (Armengol *et al*., 2019). Therefore, while unable to kill *A. baumannii* themselves, the activity of didymellanosine and ascomylactam C is presumably favored by the mechanism of colistin-induced membrane disturbance, enabling the penetration of these compounds into bacterial cells and increasing their antibacterial activity (Chapter 4 Publication 3).

Taking into account the antimicrobial activity of the isolated decahydrofluorenes (Chapter 4 Publication 3), the presence of γ-lactam substructure is suggested to be important for the activity. The adenosine conjugate present in the structure of didymellanosine weakens its activity against Gram-positive, while it has no effect on the activity against the tested *A. baumannii*. Further studies on the antibacterial action of this class of metabolites, particularly against drug-resistant strains of Gram-positive bacteria and Gram-negative *A. baumannii* seem to be promising.

In addition, the cytotoxicity of the isolated decahydrofluorenes was estimated against L5178Y cells. In this assay, didymellanosine exhibited good activity (IC_{50} 2.2 μM), while phomapyrrolidone A and ascomylactam C were found inactive. When tested further towards human cancer cells, Burkitt's lymphoma B cells (Ramos) and adult lymphoblastic leukemia T

cells (Jurkat J16), didymellanosine showed moderate cytotoxicity with IC_{50} values of 7.6 and 11.0 μM, respectively (Chapter 4 Publication 3).

In the NFκB inhibition assay, the isolated decahydrofluorenes were tested in the triple-negative breast cancer (TNBC) cells NFκB-MDA-MB-231. In parallel, cell viability was determined to exclude the decreased NFκB activation due to cytotoxicity. While displaying only weak cytotoxic activity against MDA-MB-231 cells (IC_{50} 45.4 μM), didymellanosine significantly inhibited NFκB activation in the corresponding NFκB-MDA-MB-231 cells with an IC_{50} value of 15.5 μM. The related known decahydrofluorene, phomapyrrolidone A revealed weaker NFκB inhibition with an IC_{50} value of 54.1 μM, but its NFκB inhibitory activity was two times more potent than its cytotoxicity (> 100 μM). On the other hand, the NFκB inhibitory capacity of ascomylactam C was found comparable to its cytotoxicity, indicating the reduction in NFκB activity may be a consequence of the cytotoxicity. Thus, among the tested decahydrofluorenes, didymellanosine and phomapyrrolidone A efficiently inhibited NFκB activation (Chapter 4 Publication 3). NFκB signaling is known to be implicated in the inflammation process and carcinogenesis, therefore considered as a potential target for the prevention and treatment of cancers (Naugler and Karin, 2008).

References for chapters 1 and 5

Abdullaev, I. F., Rudkouskaya, A., Mongin, A. A. and Kuo Y.-H. (2010). Calcium-activated potassium channels BK and IK1 are functionally expressed in human gliomas but do not regulate cell proliferation. *PloS One*, **5**(8), e12304.

Alberts, A.W., Chen, J., Kuron, G., Hunt, V., Huff, J., Hoffman, C., Rothrock, J., Lopez, M., Joshua, H., Harris, E., Patchett, A., Monaghan, R., Currie, S., Stapley, E., Albers-Schonberg, G., Hensens, O., Hirshfield, J., Hoogsteen, K., Liesch, J. and Springer, J. (1980). Mevinolin: a highly potent competitive inhibitor of hydroxymethylglutaryl-coenzyme A reductase and a cholesterol-lowering agent. *Proceedings of the National Academy of Sciences*, **77**(7), 3957–3961.

Aly, A. H., Debbab, A., Kjer, J. and Proksch, P. (2010). Fungal endophytes from higher plants: a prolific source of phytochemicals and other bioactive natural products. *Fungal Diversity*, **41**(1), 1–16.

Aly, A. H., Debbab, A. and Proksch, P. (2011). Fungal endophytes: unique plant inhabitants with great promises. *Applied Microbiology and Biotechnology*, **90**(6), 1829–1845.

Amedei, A. and D'Elios, M. M. (2012). New therapeutic approaches by using microorganism-derived compounds. *Current Medicinal Chemistry*, **19**(22), 3822–3840.

Ancheeva, E., Küppers, L., Akone, S. H., Ebrahim, W., Liu, Z., Mandi, A., Kurtan, T., Lin, W., Orfali, R., Rehberg, N., Kalscheuer, R., Daletos, D. and Proksch, P. (2017). Expanding the metabolic profile of the fungus *Chaetomium* sp. through co-culture with autoclaved *Pseudomonas aeruginosa*. *European Journal of Organic Chemistry*, **2017**(22), 3256–3264.

Ancheeva, E., Mandi, A., Kiraly, S. B., Kurtan, T., Hartmann, R., Akone, S. H., Weber, H., Daletos, D. and Proksch, P. (2018). Chaetolines A and B, pyrano [3,2-*f*] isoquinoline alkaloids from cultivation of *Chaetomium* sp. in the presence of autoclaved *Pseudomonas aeruginosa*. *Journal of Natural Products*, **81**(11), 2392–2398.

Armengol, E., Domenech, O., Fusté, E., Pérez-Guillén, I., Borrell, J. H., Sierra, J. M. and Vinas, M. (2019). Efficacy of combinations of colistin with other antimicrobials involves membrane fluidity and efflux machinery. *Infection and Drug Resistance***, 12**, 2031–2038.

Asai, T., Yamamoto, T., Shirata, N., Taniguchi, T., Monde, K., Fujii, I., Gomi, K. and Oshima, Y. (2013). Structurally diverse chaetophenol productions induced by chemically mediated epigenetic manipulation of fungal gene expression. *Organic Letters,* **15**(13), 3346–3349.

Belofsky, G. N., Gloer, J. B., Wicklow, D. T. and Dowd, P. F. (1995). Antiinsectan alkaloids: shearinines A–C and a new paxilline derivative from the ascostromata of *Eupenicillium shearii*. *Tetrahedron*, **51**(14), 3959–3968.

Bentley, R. (2009). Different roads to discovery; prontosil (hence sulfa drugs) and penicillin (hence *β*-lactams). *Journal of Industrial Microbiology and Biotechnology*, **36**(6), 775–786.

Benz, F., Knüsel, F., Nüesch, J., Treichler, H., Voser, W., Nyfeler, R. and Keller-Schierlein, W. (1974). Echinocandin B, ein neuartiges polypeptid-antibioticum aus *Aspergillus nidulans* var. echinulatus: Isolierung und bausteine. *Helvetica Chimica Acta*, **57**(8), 2459–2477.

Berdy, J. (2005). Bioactive microbial metabolites. *The Journal of Antibiotics*, **58**(1), 1–26

Bertrand, S., Bohni, N., Schnee, S., Schumpp, O., Gindro, K. and Wolfender, J. -L. (2014). Metabolite induction via microorganism co-culture: a potential way to enhance chemical diversity for drug discovery. *Biotechnology Advances*, **32**(6), 1180–1204.

Bode, H. B., Bethe, B., Höfs, R. and Zeeck, A. (2002). Big effects from small changes: possible ways to explore nature's chemical diversity. *ChemBioChem,* **3**(7), 619–627.

Brakhage, A. A. (2013). Regulation of fungal secondary metabolism. *Nature Reviews Microbiology***, 11**(1), 21–32.

Brakhage, A. A. and Schroeckh, V. (2011). Fungal secondary metabolites–strategies to activate silent gene clusters. *Fungal Genetics and Biology*, **48**(1), 15–22.

Brown, A. G., Smale, T. C., King, T. J., Hasenkamp, R. and Thompson, R. H. (1976). Crystal and molecular structure of compactin, a new antifungal metabolite from *Penicillium brevicompactum*. *Journal of The Chemical Society, Perkin Transactions 1*, **1**(11), 1165–1170.

Butler, M. S. (2004). The role of natural product chemistry in drug discovery. *Journal of Natural Products*, **67**(12), 2141–2153.

Chambers, H. F. (1997). Methicillin resistance in staphylococci: molecular and biochemical basis and clinical implications. *Clinical Microbiology Reviews*, **10**(4), 781–791.

Chandra, S. (2012). Endophytic fungi: novel sources of anticancer lead molecules. *Applied Microbiology and Biotechnology*, **95**(1), 47–59.

Chatterji, U., Bobardt, M. D., Stanfield, R., Ptak, R. G., Pallansch, L. A., Ward, P. A., Jones, M. J., Stoddart, C. A., Scalfaro, P., Dumont, J. -M., Besseghir, K., Rosenwirth, B. and Gallay, P. A. (2005). Naturally occurring capsid substitutions render HIV-1 cyclophilin A independent in human cells and TRIM-cyclophilin-resistant in Owl monkey cells. *Journal of Biological Chemistry*, **280**(48), 40293–40300.

Chen, S. C. -A., Slavin, M. A. and Sorrell, T. C. (2011). Echinocandin antifungal drugs in fungal infections. *Drugs*, **71**(1), 11–41.

Chen, Y., Liu, Z., Huang, Y., Liu, L., He, J., Wang, L., Yuan, J. and She, Z. (2019). Ascomylactams A–C, cytotoxic 12- or 13-membered-ring macrocyclic alkaloids isolated from the mangrove endophytic fungus *Didymella* sp. CYSK-4, and structure revisions of phomapyrrolidones A and C. *Journal of Natural Products*, **82**(7), 1752–1758.

Clardy, J. and Walsh, C. (2004). Lessons from natural molecules. *Nature*, **432**(7019), 829–837.

Cragg, G. M., Grothaus, P. G. and Newman, D. J. (2014). New horizons for old drugs and drug leads. *Journal of Natural Products*, **77**(3), 703–723.

Cragg, G. M. and Newman, D. J. (2013). Natural products: a continuing source of novel drug leads. *Biochimica et Biophysica Acta*, **1830**(6), 3670–3695.

Daletos, G., Ebrahim, W., Ancheeva, E., El-Neketi, M., Lin, W. and Proksch, P. (2017). in *Chemical Biology of Natural Products; Microbial co-culture and OSMAC approach as strategies to induce cryptic fungal biogenetic gene clusters*. Grothaus P. G., Cragg, G. M. and Newman, D. J. Eds., CRC Press: Boca Raton, FL, USA, 233–284.

de la Torre, B. G. and Albericio, F. (2019). The pharmaceutical industry in 2018. An analysis of FDA drug approvals from the perspective of molecules. *Molecules*, **24**(4), 1–12.

Deepika, V., Murali, T. S. and Satyamoorthy, K. (2016). Modulation of genetic clusters for synthesis of bioactive molecules in fungal endophytes: a review. *Microbiological Research*, **182**, 125–140.

Demain, A. L. (2014). Importance of microbial natural products and the need to revitalize their discovery. *Journal of Industrial Microbiology and Biotechnology*, **41**(2), 185–201.

Dias, D. A., Urban, S. and Roessner, U. (2012). A historical overview of natural products in drug discovery. *Metabolites*, **2**(2), 303–336.

Ding, L., Maier, A., Fiebig, H. -H., Lin, W. -H. and Hertweck, C. (2011). A family of multicyclic indolosesquiterpenes from a bacterial endophyte. *Organic and Biomolecular Chemistry*, **9**(11), 4029–4031.

Ding, L., Münch, J., Goerls, H., Maier, A., Fiebig, H. -H., Lin, W. -H. and Hertweck, C. (2010). Xiamycin, a pentacyclic indolosesquiterpene with selective anti-HIV activity from a bacterial mangrove endophyte. *Bioorganic and Medicinal Chemistry Letters*, **20**(22), 6685–6687.

Ebrahim, W., Aly, A. H., Wray, V., Mándi, A., Teiten, M. -H., Gaascht, F., Orlikova, B., Kassack, M. U., Lin, W., Diederich, M., Kurtán, T., Debbab, A. and Proksch, P. (2013). Embellicines A and B: absolute configuration and NF-κB transcriptional inhibitory activity. *Journal of Medicinal Chemistry*, **56**(7), 2991–2999.

Eckstein, J. W. and Fung, J. (2003). A new class of cyclosporin analogues for the treatment of asthma. *Expert Opinion on Investigational Drugs*, **12**(4), 647–653.

Elander, R. P. (2003). Industrial production of *β*-lactam antibiotics. *Applied Microbiology and Biotechnology*, **61**(5-6), 385–392.

Eyberger, A. L., Dondapati, R. and Porter, J. R. (2006). Endophyte fungal isolates from *Podophyllum peltatum* produce podophyllotoxin. *Journal of Natural Products*, **69**(8), 1121–1124.

Ezadi, F., Ardebili, A. and Mirnejad, R. (2019). Antimicrobial susceptibility testing for polymyxins: challenges, issues, and recommendations. *Journal of Clinical Microbiology*, **57**(4), e01390–18.

Fill, T. P., Pallini, H. F., Amaral, L. S., da Silva, J. V., Bidóia, D. L., Peron, F., Garcia, F. P., Nakamura, C. V. and Rodrigues-Filho, E. (2016). Copper and manganese cations alter secondary metabolism in the fungus *Penicillium brasilianum*. *Journal of The Brazilian Chemical Society*, **27**(8), 1444–1451.

Friedhoff, L. T., Cullen, E. I., Geoghagen, N. S. M. and Buxbaum, J. D. (2001). Treatment with controlled-release lovastatin decreases serum concentrations of human *β*-amyloid (A*β*) peptide. *International Journal of Neuropsychopharmacology*, **4**(2), 127–130.

Gao, J. -M., Yang, S. -X. and Qin, J. -C. (2013). Azaphilones: chemistry and biology. *Chemical Reviews*, **113**(7), 4755–4811.

Gao, S. -S., Li, X. -M., Williams, K., Proksch, P., Ji, N. -Y. and Wang, B. -G. (2016). Rhizovarins A–F, indole-diterpenes from the mangrove-derived endophytic fungus *Mucor irregularis* QEN-189. *Journal of Natural Products*, **79**(8), 2066–2074.

Grabowski, K., Baringhaus, K. -H. and Schneider, G. (2008). Scaffold diversity of natural products: inspiration for combinatorial library design. *Natural Product Reports*, **25**(5), 892–904.

Gunatilaka, A. A. L. (2006). Natural products from plant-associated microorganisms: distribution, structural diversity, bioactivity, and implications of their occurrence. *Journal of Natural Products*, **69**(3), 509–526.

Harvey, A. L., Edrada-Ebel, R. and Quinn, R. J. (2015). The re-emergence of natural products for drug discovery in the genomics era. *Nature Reviews Drug Discovery*, **14**(2), 111–129.

Hashimoto, S. (2009). Micafungin: a sulfated echinocandin. *The Journal of Antibiotics*, **62**(1), 27–35.

Hindler, K., Cleeland, C. S., Rivera, E. and Collard, C. D. (2006). The role of statins in cancer therapy. *The Oncologist*, **11**(3), 306–315.

Iwamoto, T., Fujie, A., Sakamoto, K., Tsurumi, Y., Shigematsu, N., Yamashita, M., Hashimoto, S., Okuhara, M. and Kohsaka, M. (1994). WF11899A, B and C, novel antifungal lipopeptides. *The Journal of Antibiotics*, **47**(10), 1084–1091.

Jia, M., Chen. L., Xin, H. -L., Zheng, C. -J., Rahman, K., Han, T. and Qin, L. -P. (2016). A friendly relationship between endophytic fungi and medicinal plants: a systematic review. *Frontiers in Microbiology*, **7**, 906.

Jørgensen, K. A., Koefoed-Nielsen, P. B. and Karamperis, N. (2003). Calcineurin phosphatase activity and immunosuppression. A review on the role of calcineurin phosphatase activity and the immunosuppressive effect of cyclosporin A and tacrolimus. *Scandinavian Journal of Immunology*, **57**(2), 93–98.

Kellenberger, E., Hofmann, A. and Quinn, R. J. (2011). Similar interactions of natural products with biosynthetic enzymes and therapeutic targets could explain why nature produces such a large proportion of existing drugs. *Natural Product Reports*, **28**(9), 1483–1492.

Klockgether-Radke, A. P. (2002). FW Sertürner and the discovery of morphine. 200 years of pain therapy with opioids. *Anästhesiol Intensivmed Notfallmed Schmerzther*, **37**, 244–249.

Knight, V., Sanglier, J. -J., DiTullio, D., Braccili, S., Bonner, P., Waters, J., Hughes, D. and Zhang, L. (2003). Diversifying microbial natural products for drug discovery. *Applied Microbiology and Biotechnology*, **62**(5–6), 446–458.

Kumar, A., Patil. D., Rajamohanan, P. R. and Ahmad, A. (2013). Isolation, purification and characterization of vinblastine and vincristine from endophytic fungus *Fusarium oxysporum* isolated from *Catharanthus roseus*. *PloS One*, **8**(9), e71805.

Kusari, S., Hertweck, C. and Spiteller, M. (2012). Chemical ecology of endophytic fungi: origins of secondary metabolites. *Chemistry and Biology*, **19**(7), 792–798.

Kusari, S. and Spiteller, M. (2011). Are we ready for industrial production of bioactive plant secondary metabolites utilizing endophytes? *Natural Product Reports*, **28**(7), 1203–1207.

Kusari, S., Zühlke, S. and Spiteller, M. (2009). An endophytic fungus from *Camptotheca acuminata* that produces camptothecin and analogues. *Journal of Natural Products*, **72**(1), 2–7.

Lachance, H., Wetzel, S., Kumar, K. and Waldmann, H. (2012). Charting, navigating, and populating natural product chemical space for drug discovery. *Journal of Medicinal Chemistry*, **55**(13), 5989–6001.

Lam, K. S. (2007). New aspects of natural products in drug discovery. *Trends in Microbiology*, **15**(6), 279–289.

Lazarova, T. and Weng, Z. (2003). Cyclosporin A analogues: recent advances, *Expert Opinion on Therapeutic Patents*, **13**(9), 1327–1332

Li, G., Kusari, S., Golz, C., Laatsch, H., Strohmann, C. and Spiteller, M. (2017). Epigenetic modulation of endophytic *Eupenicillium* sp. LG41 by a histone deacetylase inhibitor for production of decalin-containing compounds. *Journal of Natural Products*, **80**(4), 983–988.

Li, H., Sun, Y., Zhang, Q., Zhu, Y., Li, S. -M., Li, A. and Zhang, C. (2014). Elucidating the cyclization cascades in xiamycin biosynthesis by substrate synthesis and enzyme characterizations. *Organic Letters*, **17**(2), 306–309.

Li, H., Zhang, Q., Li, S., Zhu, Y., Zhang, G., Zhang, H., Tian, X., Zhang, S., Ju, J. and Zhang, C. (2012). Identification and characterization of xiamycin A and oxiamycin gene cluster reveals an oxidative cyclization strategy tailoring indolosesquiterpene biosynthesis. *Journal of The American Chemical Society*, **134**(21), 8996–9005.

Li, J. Y., Strobel, G., Harper, J., Lobkovsky, E. and Clardy, J. (2000). Cryptocin, a potent tetramic acid antimycotic from the endophytic fungus *Cryptosporiopsis cf. quercina*. *Organic Letters*, **2**(6), 767–770.

Lin, T. F., Yakushijin, K., Büchi, G. H. and Demain, A. L. (1992). Formation of water-soluble Monascus red pigments by biological and semi-synthetic processes. *Journal of Industrial Microbiology*, **9**(3-4), 173–179.

Liu, C., Minami, A., Dairi, T., Gomi, K., Scott, B. and Oikawa, H. (2016). Biosynthesis of shearinine: diversification of a tandem prenyl moiety of fungal indole diterpenes. *Organic Letters*, **18**(19), 5026–5029.

Liu, C., Noike, M., Minami, A., Oikawa, H. and Dairi, T. (2014). Functional analysis of a prenyltransferase gene (*pax*D) in the paxilline biosynthetic gene cluster. *Applied Microbiology and Biotechnology*, **98**(1), 199–206.

Lobanovska, M. and Pilla, G. (2017). Penicillin's discovery and antibiotic resistance: lessons for the future? *The Yale Journal of Biology and Medicine*, **90**(1), 135–145.

Meinke, P. T., Smith, M. M. and Shoop, W. L. (2002). Nodulisporic acid: its chemistry and biology. *Current Topics in Medicinal Chemistry*, **2**(7), 655–674.

Meng, L. -H., Li, X. -M., Liu, Y., Xu, G. -M. and Wang, B. -G. (2017). Antimicrobial alkaloids produced by the mangrove endophyte *Penicillium brocae* MA-231 using the OSMAC approach. *RSC Advances*, **7**(87), 55026–55033.

Meng, L. -H., Li, X. -M., Lv, C. -T., Huang, C. -G. and Wang, B. -G. (2014). Brocazines A–F, cytotoxic bisthiodiketopiperazine derivatives from *Penicillium brocae* MA-231, an endophytic fungus derived from the marine mangrove plant *Avicennia marina*. *Journal of Natural Products*, **77**(8), 1921–1927.

Mou, Y., Luo, H., Mao, Z., Shan, T., Sun, W., Zhou, K. and Zhou, L. (2013). Enhancement of palmarumycins C_{12} and C_{13} production in liquid culture of endophytic fungus *Berkleasmium* sp. Dzf12 after treatments with metal ions. *International Journal of Molecular Sciences*, **14**(1), 979–998.

Moussa, M., Ebrahim, W., Bonus, M., Gohlke, H., Mandi, A., Kurtan, T., Hartmann, R., Kalscheuer, R., Lin, W., Liu, Z. and Proksch, P. (2019). Co-culture of the fungus *Fusarium tricinctum* with *Streptomyces lividans* induces production of cryptic naphthoquinone dimers. *RSC Advances*, **9**(3), 1491–1500.

Nagumo, Y., Motoyama, T., Hayashi, T., Hirota, H., Aono, H., Kawatani, M., Osada, H. and Usui, T. (2017). Structure-activity relationships of terpendole E and its natural derivatives. *ChemistrySelect*, **2**(4), 1533–1536.

Nakagawa, M., Sakamoto, N., Enomoto, N., Tanabe, Y., Kanazawa, N., Koyama, T., Kurosaki, M., Maekawa, S., Yamashiro, T., Chen, C. -H., Itsui, Y., Kakinuma, S. and Watanabe, M. (2004). Specific inhibition of hepatitis C virus replication by cyclosporin A. *Biochemical and Biophysical Research Communications*, **313**(1), 42–47.

Naugler, W. E. and Karin, M. (2008). NF-κB and cancer–identifying targets and mechanisms. *Current Opinion in Genetics and Development*, **18**(1), 19–26.

Newman, D. J. and Cragg, G. M. (2016). Natural products as sources of new drugs from 1981 to 2014. *Journal of Natural Products*, **79**(3), 629–661.

Newman, D. J., Cragg, G. M. and Snader, K. M. (2000). The influence of natural products upon drug discovery. *Natural Product Reports*, **17**(3), 215–234.

Nicholson, M. J., Eaton, C. J., Stärkel, C., Tapper, B. A., Cox, M. P. and Scott, B. (2015). Molecular cloning and functional analysis of gene clusters for the biosynthesis of indole-diterpenes in *Penicillium crustosum* and *P. janthinellum*. *Toxins*, **7**(8), 2701–2722.

Nielsen, K. F. and Larsen, T. O. (2015). The importance of mass spectrometric dereplication in fungal secondary metabolite analysis. *Frontiers in Microbiology*, **6**, 71.

Odds, F. C., Brown, A. J. P. and Gow, N. A. R. (2003). Antifungal agents: mechanisms of action. *Trends in Microbiology*, **11**(6), 272–279.

Ola, A. R. B., Thomy, D., Lai, D., Brötz-Oesterhelt, H. and Proksch, P. (2013). Inducing secondary metabolite production by the endophytic fungus *Fusarium tricinctum* through coculture with *Bacillus subtilis*. *Journal of Natural Products*, **76**(11), 2094–2099.

Ondeyka, J. G., Helms, G. L., Hensens, O. D., Goetz, M. A., Zink, D. L., Tsipouras, A., Shoop, W. L., Slayton, L., Dombrowski, A. W., Polishook, J. D., Ostlind, D. A., Tsou, N. N., Ball, R. G. and Singh, S. B. (1997). Nodulisporic acid A, a novel and potent insecticide from a *Nodulisporium* sp. Isolation, structure determination, and chemical transformations. *Journal of The American Chemical Society*, **119**(38), 8809–8816.

Oxford, A. E., Raistrick, H. and Simonart, P. (1939). Studies in the biochemistry of micro-organisms: griseofulvin, $C_{17}H_{17}O_6Cl$, a metabolic product of *Penicillium griseo-fulvum* Dierckx. *Biochemical Journal*, **33**(2), 240–248.

Padmaja, P., Reddy, B. V. S., Jain, N., Mutheneni, S. R., Bollepelli, P., Pollepalli, S., Rambabu, G. and Reddy, P. N. (2016). Synthesis, molecular docking and in vitro antiproliferative activity of novel pyrano [3,2-*c*] carbazole derivatives. *New Journal of Chemistry*, **40**(10), 8305–8315.

Paeshuyse, J., Kaul, A., Clercq, E. D., Rosenwirth, B., Dumont, J. -M., Scalfaro, P., Bartenschlager, R. and Neyts, J. (2006). The non-immunosuppressive cyclosporin DEBIO-025 is a potent inhibitor of hepatitis C virus replication in vitro. *Hepatology*, **43**(4), 761–770.

Pan, R., Bai, X., Chen, J., Zhang, H. and Wang, H. (2019). Exploring structural diversity of microbe secondary metabolites using OSMAC strategy: a literature review. *Frontiers in Microbiology*, **10**, 294.

Paranagama, P. A., Wijeratne, E. M. K. and Gunatilaka, A. A. L. (2007). Uncovering biosynthetic potential of plant-associated fungi: effect of culture conditions on metabolite production by *Paraphaeosphaeria quadriseptata* and *Chaetomium chiversii*. *Journal of Natural Products*, **70**(12), 1939–1945.

Pendleton, J. N., Gorman, S. P. and Gilmore, B. F. (2013). Clinical relevance of the ESKAPE pathogens. *Expert Review of Anti-infective Therapy*, **11**(3), 297–308.

Petersen, A. B., Rønnest, M. H., Larsen, T. O. and Clausen, M. H. (2014). The chemistry of griseofulvin. *Chemical Reviews*, **114**(24), 12088–12107.

Pfannenstiel, B. T. and Keller, N. P. (2019). On top of biosynthetic gene clusters: how epigenetic machinery influences secondary metabolism in fungi. *Biotechnology Advances*, **37**, 107345

Priti, V., Ramesha, B. T., Singh, S., Ravikanth, G., Ganeshaiah, K. N., Suryanarayanan, T. S. and Shaanker, R. U. (2009). How promising are endophytic fungi as alternative sources of plant secondary metabolites? *Current Science*, **97**(4), 477–478.

Puri, S. C., Nasir, A., Chawla, R., Arora, R., Riyaz-ul-Hasan, S., Amna, T., Ahmed, B., Verma, V., Singh, S., Sagar, R., Sharma, A., Kumar, R., Sharma, R. K. and Qazi, G. N. (2006). The endophytic fungus *Trametes hirsuta* as a novel alternative source of podophyllotoxin and related aryl tetralin lignans. *Journal of Biotechnology*, **122**(4), 494–510.

Puri, S. C., Verma, V., Amna, T., Qazi, G. N. and Spiteller, M. (2005). An endophytic fungus from *Nothapodytes foetida* that produces camptothecin. *Journal of Natural Products*, **68**(12), 1717–1719.

Qi, X., Li, X., Zhao, J., He, N., Li, Y., Zhang, T., Wang, S., Yu, L. and Xie, Y. (2019). GKK1032C, a new alkaloid compound from the endophytic fungus *Penicillium* sp. CPCC 400817 with activity against methicillin-resistant *S. aureus*. *The Journal of Antibiotics*, **72**(4), 237–240.

Rathinasamy, K., Jindal, B., Asthana, J., Singh, P., Balaji, P. V. and Panda, D. (2010). Griseofulvin stabilizes microtubule dynamics, activates p53 and inhibits the proliferation of MCF-7 cells synergistically with vinblastine. *BMC Cancer*, **10**(1), 213.

Reddy, P., Guthridge, K., Vassiliadis, S., Hemsworth, J., Hettiarachchige, I., Spangenberg, G. and Rochfort, S. (2019). Tremorgenic mycotoxins: structure diversity and biological activity. *Toxins*, **11**(5), 302.

Rønnest, M. H., Raab, M. S., Anderhub, S., Boesen, S., Krämer, A., Larsen, T. O. and Clausen, M. H. (2012). Disparate SAR data of griseofulvin analogues for the dermatophytes *Trichophyton mentagrophytes*, *T. rubrum*, and MDA-MB-231 cancer cells. *Journal of Medicinal Chemistry*, **55**(2), 652–660.

Saikia, S., Nicholson, M. J., Young, C., Parker, E. J. and Scott, B. (2008). The genetic basis for indole-diterpene chemical diversity in filamentous fungi. *Mycological Research*, **112**(2), 184–199.

Sallam, A. A., Ayoub, N. M., Foudah, A. I., Gissendanner, C. R., Meyer, S. A. and El Sayed, K. A. (2013). Indole diterpene alkaloids as novel inhibitors of the Wnt/*β*-catenin pathway in breast cancer cells. *European Journal of Medicinal Chemistry*, **70**, 594–606.

Sallam, A. A., Houssen, W. E., Gissendanner, C. R., Orabi, K. Y., Foudah, A. I. and El Sayed, K. A. (2013). Bioguided discovery and pharmacophore modeling of the mycotoxic indole diterpene alkaloids penitrems as breast cancer proliferation, migration, and invasion inhibitors. *MedChemComm*, **4**(10), 1360–1369.

Santajit, S. and Indrawattana, N. (2016). Mechanisms of antimicrobial resistance in ESKAPE pathogens. *BioMed Research International*, **2016**,1–8

Scherlach, K. and Hertweck, C. (2009). Triggering cryptic natural product biosynthesis in microorganisms. *Organic and Biomolecular Chemistry*, **7**(9), 1753–1760.

Scott, B., Young, C. A., Saikia, S., McMillan, L. K., Monahan, B. J., Koulman, A., Astin, J., Eaton, C. J., Bryant, A., Wrenn, R. E., Finch, S. C., Tapper, B. A., Parker, E. J. and Jameson, G. B. (2013). Deletion and gene expression analyses define the paxilline biosynthetic gene cluster in *Penicillium paxilli*. *Toxins*, **5**(8), 1422–1446.

Sena, A., Pedrosa, R. and Morais, M. G. (2003). Therapeutic potential of lovastatin in multiple sclerosis. *Journal of Neurology*, **250**(6), 754–755.

Stierle, A., Strobel, G. and Stierle, D. (1993). Taxol and taxane production by *Taxomyces andreanae*, an endophytic fungus of Pacific yew. *Science*, **260**(5105), 214–216.

Strobel, G. (2018). The emergence of endophytic microbes and their biological promise. *Journal of Fungi*, **4**(2), 57.

Strobel, G., Daisy, B., Castillo, U. and Harper, J. (2004). Natural products from endophytic microorganisms. *Journal of Natural Products*, **67**(2), 257–268.

Strobel, G. A., Miller, R. V., Martinez-Miller, C., Condron, M. M., Teplow, D. B. and Hess, W. M. (1999). Cryptocandin, a potent antimycotic from the endophytic fungus *Cryptosporiopsis cf. quercina*. *Microbiology*, **145**(8), 1919–1926.

Tacconelli, E., Carrara, E., Savoldi, A., Harbarth, S., Mendelson, M., Monnet, D. L., Pulcini, C., Kahlmeter, G., Kluytmans, J., Carmeli, Y., Ouellette, M., Outterson, K., Patel, J., Cavaleri, M., Cox, E. M., Houchens, C. R., Grayson, M. L., Hansen, P., Singh, N., Theuretzbacher, U., Magrini, N. and the WHO Pathogens Priority List Working Group (2018). Discovery, research, and development of new antibiotics: the WHO priority list of antibiotic-resistant bacteria and tuberculosis. *The Lancet Infectious Diseases*, **18**(3), 318–327.

TePaske, M. R., Gloer, J. B., Wicklow, D. T. and Dowd, P. F. (1989). The structure of tubingensin B: A cytotoxic carbazole alkaloid from the sclerotia of *Aspergillus tubingensis*. *Tetrahedron Letters*, **30**(44), 5965–5968.

TePaske, M. R., Gloer, J. B., Wicklow, D. T. and Dowd, P. F. (1989). Tubingensin A: an antiviral carbazole alkaloid from the sclerotia of *Aspergillus tubingensis*. *The Journal of Organic Chemistry*, **54**(20), 4743–4746.

TePaske, M. R., Gloer, J. B., Wicklow, D. T. and Dowd, P. F. (1990). Aflavazole: a new antiinsectan carbazole metabolite from the sclerotia of *Aspergillus flavus*. *The Journal of Organic Chemistry*, **55**(18), 5299–5301.

Tobert, J. A. (2003). Lovastatin and beyond: the history of the HMG-CoA reductase inhibitors. *Nature Reviews Drug Discovery*, **2**(7), 517–526.

Tomm, H. A., Ucciferri, L. and Ross, A. C. (2019). Advances in microbial culturing conditions to activate silent biosynthetic gene clusters for novel metabolite production. *Journal of Industrial Microbiology and Biotechnology*, 1–20.

Tudzynski, B. (2014). Nitrogen regulation of fungal secondary metabolism in fungi. *Frontiers in Microbiology*, **5**, 656.

Uhlig, S., Botha, C. J., Vralstad, T., Rolen, E. and Miles, C. O. (2009). Indole-diterpenes and ergot alkaloids in *Cynodon dactylon* (Bermuda Grass) infected with *Claviceps cynodontis* from an outbreak of tremors in cattle. *Journal of Agricultural and Food Chemistry*, **57**(23), 11112–11119.

van Dijk, J. W. A. and Wang, C. C. C. (2018). Expanding the chemical space of nonribosomal peptide synthetase-like enzymes by domain and tailoring enzyme recombination. *Organic Letters*, **20**(17), 5082–5085.

Wakefield, J., Hassan, H. M., Jaspars, M., Ebel, R. and Rateb, M. E. (2017). Dual induction of new microbial secondary metabolites by fungal bacterial co-cultivation. *Frontiers in Microbiology*, **8**, 1284.

Wang, W. -J., Li, D. -Y., Li, Y. -C., Hua, H. -M., Ma, E. -L. and Li, Z. -L. (2014). Caryophyllene sesquiterpenes from the marine-derived fungus *Ascotricha* sp. ZJ-M-5 by the one strain-many compounds strategy. *Journal of Natural Products*, **77**(6), 1367–1371.

Wang, X., Filho, J. G. S., Hoover, A. R., King, J. B., Ellis, T. K., Powell, D. R. and Cichewicz, R. H. (2010). Chemical epigenetics alters the secondary metabolite composition of guttate excreted by an atlantic-forest-soil-derived *Penicillium citreonigrum*. *Journal of Natural Products*, **73**(5), 942–948.

Wichmann, C. F., Liesch, J. M. and Schwartz, R. E. (1989). L-671,329, A new antifungal agent. *The Journal of Antibiotics*, **42**(2), 163–167.

Wijeratne, E. M. K., He, H., Franzblau, S. G., Hoffman, A. M. and Gunatilaka, A. A. L. (2013). Phomapyrrolidones A–C, antitubercular alkaloids from the endophytic fungus *Phoma* sp. NRRL 46751. *Journal of Natural Products*, **76**(10), 1860–1865.

Yang, Y., Zhao, H., Barrero, R. A., Zhang, B., Sun, G., Wilson, I. W., Xie, F., Walker, K. D., Parks, J. W., Bruce, R., Guo, G., Chen, L., Zhang, Y., Huang, X., Tang, Q., Liu, H., Bellgard, M. I., Qiu, D., Lai, J. and Hoffman, A. (2014). Genome sequencing and analysis of the paclitaxel-producing endophytic fungus *Penicillium aurantiogriseum* NRRL 62431. *BMC Genomics*, **15**(1), 69.

List of abbreviations

$[\alpha]_D$	Specific rotation at the sodium D-line
5-AC	5-Azacytidine
Å	Angström
amu	Atomic mass unit
BGCs	Biosynthetic gene clusters
br	Broad
CD_3OD	Deuterated methanol
$CDCl_3$	Deuterated chloroform
CEs	Cotton effects
CH_2Cl_2, DCM	Dichloromethane
CH_3COOH	Formic acid
COSY	Correlation spectroscopy
$CuCl_2$	Copper (II) chloride
$CuSO_4$	Copper (II) sulfate
d	Doublet signal
dd	Doublet of doublet signal
ddd	Doublet of doublet of doublet signal
dt	Doublet of triplet signal
1D	One dimensional
2D	Two dimensional
DAD	Diode array detector
DFT	Density functional theory
DMAPP	Dimethylallyl pyrophosphate
DMSO	Dimethyl sulfoxide
DNA	Deoxyribonucleic acid
DNMT	DNA methyltransferase
DNPs	Dictionary of natural products
ECD	Electronic circular dichroism
e.g.	Exempli gratia (for the sake of example)
et al.	Et altera (and others)
EtOAc	Ethyl acetate
ESKAPE	*Enterococcus faecium*, *Staphylococcus aureus*, *Klebsiella pneumoniae*, *Acinetobacter baumannii*, *Pseudomonas aeruginosa,* and *Enterobacter* spp.
FDA	Food and drug administration (United States)
$FeSO_4$	Iron (II) sulfate
g	Gram
GABA	γ-Aminobutyric acid
h	Hour (s)
HCV	Hepatitis C virus
HDAC	Histone deacetylase
HIV-1	Human immunodeficiency virus type 1
HMBC	Heteronuclear multiple bond connectivity
HMG-CoA	3-Hydroxy-3-methylglutaryl coenzyme A
HPLC	High-performance liquid chromatography
HRESIMS	High-resolution electrospray ionization mass spectrometry
HSQC	Heteronuclear single quantum coherence
Hz	Hertz
IC_{50}	Half maximal inhibitory concentration

IPP	Isopentenyl pyrophosphate
ITS	Internal transcribed spacer
L	Liter
LC-ESIMS	Liquid chromatography-electrospray ionization mass spectrometry
LPS	Lipopolysaccharide
m	Multiplet signal
M	Molar
m/z	Mass per charge
MeCN	Acetonitrile
MeOH	Methanol
mg	Milligram
$MgCl_2$	Magnesium chloride
$MgSO_4$	Magnesium sulfate
MHz	Megahertz
MIC	Minimum inhibitory concentration
min	Minute (s)
mL	Milliliter
mm	Millimeter
MMFF	Merck molecular force field
MRSA	Methicillin-resistant *Staphylococcus aureus*
MS	Mass spectrometry
(*R*)-MTPA-Cl	(*R*)-(-)-α-Methoxy-α-(trifluoromethyl)phenylacetyl chloride
(*S*)-MTPA-Cl	(*S*)-(+)-α-Methoxy-α-(trifluoromethyl)phenylacetyl chloride
MTT	3-(4,5-Dimethylthiazol-2-yl)-2,5-diphenyltetrazolium bromide
MW	Molecular weight
NaCl	Sodium chloride
NAD^+	Nicotinamide adenine dinucleotide (oxidized form)
NaF	Sodium fluoride
NaI	Sodium iodide
$NaNO_3$	Sodium nitrate
NaOH	Sodium hydroxide
NCEs	New chemical entities
NFκB	Nuclear factor-κB
$(NH_4)_2SO_4$	Ammonium sulfate
nm	Nanometer
NMR	Nuclear magnetic resonance
NOE	Nuclear overhauser effect
NOESY	Nuclear overhauser effect spectroscopy
NRPs	Non-ribosomal peptides
OSMAC	One Strain MAny Compounds
ov	Overlapped signals
p	Pentet signal
PBPs	Penicillin-binding proteins
PDA	Photodiode array detector
PDB	Potato-dextrose broth
PKSs	Polyketide synthases
ppm	Parts per million
qd	Quartet of doublet signal
ROESY	Rotating frame overhauser effect spectroscopy
RP 18	Reverse phase C_{18}
s	Singlet signal

SAHA	Suberoylanilide hydroxamic acid
SAR	Structure-activity relationship
SBHA	Suberoyl bishydroxamic acid
SI	Selectivity index
sp.	Species
t	Triplet signal
TDDFT-ECD	Time-dependent density functional theory-electronic circular dichroism
TFA	Trifluoroacetic acid
TLC	Thin-layer chromatography
TNBC	Triple-negative breast cancer
UV	Ultra-violet
VLC	Vacuum liquid chromatography
μM	Micromolar
$ZnSO_4$	Zinc sulfate

Acknowledgements

I would like to express my sincere appreciation to Prof. Dr. Dres. h.c. Peter Proksch for giving me the precious opportunity to pursue my doctoral study on secondary metabolites from endophytic fungi, in the excellent working conditions and facilities at the Institute of Pharmaceutical Biology and Biotechnology, Heinrich Heine University, Düsseldorf. I wish to express my gratitude for his kind supervision, valuable guidance, fruitful discussions, constant encouragement and remarkable support during my study.

I wish to express my sincere appreciation and gratitude to Prof. Dr. Rainer Kalscheuer (Institute of Pharmaceutical Biology and Biotechnology, Heinrich Heine University, Düsseldorf) for evaluating my doctoral study as the second referee and his remarkable support in the antibacterial assays.

I would like to convey my cordial thanks to Dr. Chaidir (Center for Pharmaceutical and Medical Technology, Agency for the Assessment and Application Technology, Indonesia) for introducing me to Prof. Dr. Dres. h.c. Peter Proksch and his advises during my study.

I am deeply indebted to Dr. Georgios Daletos for his kind help since I came to Germany in 2016, his valuable advises and assistance in the structure elucidations, as well as preparation of manuscripts. I wish to thank Dr. Elena Ancheeva for fruitful discussions during my experimental work and her scientific guidance in the preparation of manuscripts. I would like to extend my special thanks to Dr. Zhen Liu for his precious help and suggestions on structure elucidations and the preparation of manuscripts. I am heavily indebted to Dr. Marian Frank for his scientific guidance since the first month of my study till the end, fruitful discussions, his kind help on German translation of my abstract and preparation of manuscripts.

I wish to appreciate the help of Prof. Dr. Matthias U. Kassack and Ms. Chenyin Wang (Institute of Pharmaceutical and Medicinal Chemistry, Heinrich Heine University, Düsseldorf), Prof. Dr. Sebastian Wesselborg and Mr. Fabian Stuhldreier (Institute of Molecular Medicine I, Medical Faculty, Heinrich Heine University, Düsseldorf) and Prof. Dr. W.E.G Müller (Institute

for Physiological Chemistry, University Medical Center of the Johannes Gutenberg University Mainz) for their collaboration in the cytotoxicity assays.

I would like to appreciate Prof. Dr. Nicole Teusch and Ms. Irene Reimche (Department of Biomedical Sciences, Faculty of Human Sciences, University of Osnabrück) for their collaboration in the cytotoxicity and NFκB reporter gene assays.

I wish to express my appreciation to Prof. Dr. Christoph Janiak, Mr. Tim-O. Knedel and Mr. Simon-Patrick Höfert (Institute of Inorganic Chemistry and Structural Chemistry, Heinrich Heine University, Düsseldorf) for their collaboration on X-ray crystallography analysis.

I cordially thank Prof. Dr. Wenhan Lin (National Research Laboratories of Natural and Biomimetic Drugs, Peking University, Health Science Center) for fruitful discussions and constructive advises on my Ph.D. research projects. My sincere appreciation to Prof. Dr. Bingui Wang (Laboratory of Experimental Marine Biology, Institute of Oceanology, Chinese Academy of Science) for pleasant discussions and advises.

I would like to express my sincere gratitude to Prof. Dr. Tibor Kurtán and Dr. Attila Mándi (Department of Organic Chemistry, University of Debrecen, Hungary) for helping in ECD measurement and calculation.

I truly appreciate Prof. Dr. Clauss Passreiter (Institute of Pharmaceutical Biology and Biotechnology, Henrich Heine University, Düsseldorf) for his safety introduction in the laboratory work.

My sincere appreciation to Dr. Rudolf Hartmann and Dr. Kevin Bochinsky (Institute of Complex Systems (ICS-6), Forschungszentrum Jülich GmbH) for measuring NMR and nice discussions on the structure elucidation of my compounds.

I want to express my sincere gratitude to Ms. Claudia Eckelskemper for her hospitality and generous help on administration issues, to Mrs. Waltraud Schlag, Mrs. Simone Miljanovic, Mrs. Heike Goldbach-Gecke, Mrs. Katja Friedrich, Mrs. Eva Müller, Mrs. Simone Mönninghoff-Pützer, Ms. Linda Weigand and Mrs. Maryam Masrouri, for their generous help

and support. I extend my appreciation to Dr. Peter Tommes, Mr. Ralf Bürgel and Ms. Maria Beuer, for their help in the ESI/HRESIMS and NMR measurements, respectively.

My sincere thanks to all former postdocs at the Institute, Dr. Daowan Lai, Dr. Ramsay Kadeem, Dr. Sergi Herve Akone, Dr. Weaam Ebrahim and Dr. Yang Liu, for sharing expertise and nice discussions. I would like to profound my sincere thanks to my colleagues and friends, Dr. Amin Mokhlesi, Ms. Arta Kuci, Ms. Blessing Umeokoli, Dr. Catalina Perez Hemphill, Ms. Dina Elkashef, Mr. Feng Pan, Mr. Ferhat Oezkaya, Dr. Festus Okoye, Mr. Haiqian Yu, Prof. Han Xiao, Mr. Harwoko, Ms. Kim Thao Lee, Mr. Lei Wang, Mr. Lin Wang, Ms. Mariam Moussa, Ms. Miada Sakr, Ms. Nada Mohamed, Mr. Nam Michael Tran-Cong, Ms. Nihal Aktas, Dr. Peter Eze, Dr. Rini Muharini, Dr. Shuai Liu, Mr. Tino Seidemann, Ms. Xiaoqin Yu and Ms. Ying Gao, for discussions and sharing nice time together in the Institute. I would like to extend my sincere thanks to Mr. Dieter Meier and Ms. Yvonne Gröner, for their help in the antibacterial assay.

My special thanks to all my colleagues in the Faculty of Mathematics and Natural Sciences, Udayana University, Bali, for their kind help and support with regard to the administration issues during my study.

I am grateful for the doctoral scholarship from the German Academic Exchange Service (DAAD) under the Program Biodiversity and Health, that financially support my study.

My heartfelt thanks to my beloved parents, I Made Phastera and Ni Nyoman Sukasih, for their continuous support and encouragement. I wish to extend my deep thanks to my parents in law, I Made Suarmodin and Ni Nyoman Suladri, for spiritual support. I would like to express my deepest appreciation and gratitude to my dear husband, I Putu Budha Sugira, B.Eng. for his continuous support, encouragement and always be my side in any kind of condition. Finally, I would like to dedicate this accomplishment to my angel, I Gede Andhika Pratama, who is continuously motivating me in my study.

Curriculum vitae

Name	: Ni Putu Ariantari
Nationality	: Indonesian
Address	: Heinrich Heine University Düsseldorf, Universitätstraße 1 40225 Düsseldorf
Email	: Ni.Putu.Ariantari@hhu.de; putu_ariantari@unud.ac.id

Educational backgrounds

10. 2016 – present	: Ph.D. student in Pharmacy at the Institute of Pharmaceutical Biology and Biotechnology, Heinrich Heine University, Düsseldorf, Germany. Supervisor: Prof. Dr. Dres. h.c. Peter Proksch.
09. 2007 – 08. 2009	: Master of Pharmaceutical Sciences, Pharmaceutical Science at Faculty of Pharmacy, Airlangga University, Surabaya, Indonesia. Supervisor: Dr. Aty Widyawaruyanti.
08. 2003 – 08. 2004	: Pharmacist (Apotheker), Faculty of Pharmacy, Gadjah Mada University, Yogyakarta, Indonesia.
08. 1999 – 08. 2003	: Bachelor of Science in Pharmacy, Faculty of Pharmacy, Gadjah Mada University, Yogyakarta, Indonesia. Supervisor: Prof. Dr. Zullies Ikawati.

Employment record

2005 – present	Department of Pharmacy, Faculty of Mathematics and Natural Sciences, Udayana University, 80361 Bali, Indonesia.

Publications:

1. **Ni P. Ariantari**, Elena Ancheeva, Chenyin Wang, Attila Mándi, Tim-O. Knedel, Tibor Kurtán, Chaidir Chaidir, Werner E. G. Müller, Matthias U. Kassack, Christoph Janiak, Georgios Daletos, Peter Proksch. Indole diterpenoids from an endophytic *Penicillium* sp. *Journal of Natural Products*, 2019, **82**, 1412−1423.

2. **Ni P. Ariantari**, Georgios Daletos, Attila Mándi, Tibor Kurtán, Werner E. G. Müller, Wenhan Lin, Elena Ancheeva, Peter Proksch. Expanding the chemical diversity of an endophytic fungus *Bulgaria inquinans*, an ascomycete associated with mistletoe, through an OSMAC approach. *RSC Advances*, 2019, **9**, 25119–25132.

3. **Ni P. Ariantari**, Elena Ancheeva, Marian Frank, Fabian Stuhldreier, Dieter Meier, Yvonne Gröner, Irene Reimche, Nicole Teusch, Sebastian Wesselborg, Werner E. G. Müller, Rainer Kalscheuer, Zhen Liu, Peter Proksch. Didymellanosine, A New Decahydrofluorene Analogue, and Ascolactone C from *Didymella* sp. IEA-3B.1, an Endophyte of *Terminalia catappa*. *RSC Advances (submitted)*.